

# NSTX Research Program Five Year Plan for 2009-2013



Supported by



Office of  
Science



*This page intentionally left blank*

# **NSTX Research Program Five Year Plan for 2009-2013**

## *Table of Contents*

<i>Chapter 1 – Overview.....</i>	<i>5</i>
<i>Chapter 2 – Macroscopic Stability.....</i>	<i>53</i>
<i>Chapter 3 – Transport and Turbulence.....</i>	<i>139</i>
<i>Chapter 4 – Waves and Energetic Particles.....</i>	<i>183</i>
<i>Chapter 5 – Boundary Physics.....</i>	<i>237</i>
<i>Chapter 6 – Plasma Formation and Sustainment.....</i>	<i>289</i>
<i>Chapter 7 – Facility Status and Upgrades.....</i>	<i>351</i>
<i>Appendix – NSTX Collaboration Research Plans.....</i>	<i>399</i>

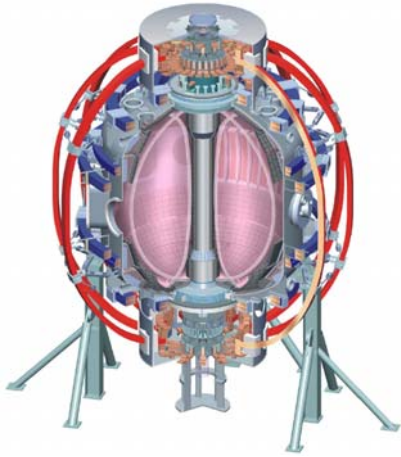
*This page intentionally left blank*

## **Chapter 1 - Overview of the NSTX Research Program Plan for 2009-2013**

1.1 Introduction.....	1.1
1.2 Unique Parameter Regimes Accessed by NSTX.....	1.5
1.2.1 Macroscopic Stability.....	1.5
1.2.2 Transport and Turbulence.....	1.7
1.2.3 Waves and Energetic Particles.....	1.9
1.2.4 Boundary Physics.....	1.13
1.2.5 Plasma Formation and Sustainment.....	1.15
1.3 Contributions to tokamak physics and ITER.....	1.17
1.3.1 International Tokamak Physics Activity (ITPA) .....	1.17
1.3.2 ITER design.....	1.18
1.4 Fusion Energy Science Applications of the ST.....	1.21
1.4.1 Overview.....	1.21
1.4.2 Mission, design concept, and operating parameters for NHTX.....	1.24
1.4.3 Mission, design concept, and operating parameters for ST-CTF.....	1.26
1.4.4 Design concept and operating parameters for an ST reactor.....	1.28
1.5 Gaps between present and future STs.....	1.29
1.6 Research Goals and Opportunities in NSTX.....	1.32
1.6.1 Overview.....	1.32
1.6.2 Opportunities in Macroscopic Stability Research.....	1.33
1.6.3 Opportunities in Transport and Turbulence Research.....	1.35
1.6.4 Opportunities in Energetic Particle Research.....	1.36
1.6.5 Opportunities in Boundary Physics Research.....	1.38
1.6.6 Opportunities in Plasma Formation and Sustainment Research.....	1.40
1.7 NSTX long-term goals.....	1.43
1.8 NSTX scientific organizational structure.....	1.44

*This page intentionally left blank*

# Chapter 1



## Overview of the NSTX Research Program Plan for 2009-2013

### 1.1 Introduction

The Spherical Torus (ST) concept is a low-aspect-ratio tokamak magnetic configuration characterized by strong intrinsic plasma shaping and enhanced stabilizing magnetic field line curvature. These characteristics are shown pictorially in Figure 1.1.1. These unique ST characteristics enable the achievement of a high plasma pressure relative to the applied magnetic field and provide access to an expanded range of plasma parameters and operating regimes relative to the standard aspect ratio tokamak. NSTX has demonstrated that ST's can access a very wide range of dimensionless plasma parameter space with toroidal beta  $\beta_t$  up to 40% (local  $\beta \sim 1$ ), normalized beta  $\beta_N$  up to 7, plasma elongation  $\kappa$  up to 3, normalized fast-ion speed

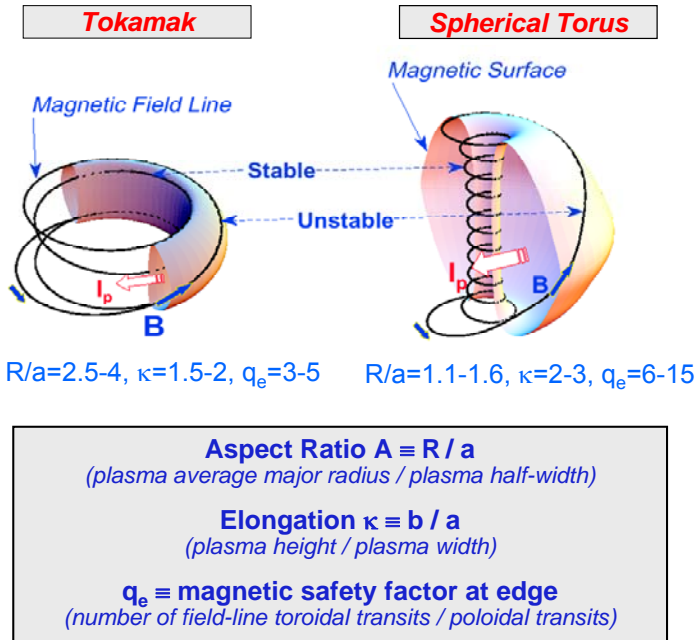


Figure 1.1.1: Comparison of magnetic field-line trajectories, aspect ratio, elongation, and safety factor parameters for a tokamak (left) and spherical torus (right).

$V_{\text{fast}}/V_{\text{Alfvén}}$  up to 5, Alfvén Mach number  $M_A = V_{\text{rotation}}/V_{\text{Alfvén}}$  up to 0.5, and trapped-particle fraction up to 90% at the plasma edge. All of these parameters are well beyond that accessible in conventional tokamaks, and these parameters approach those achievable in other high- $\beta$  alternative concepts. These characteristics therefore allow ST research to complement and extend standard aspect-ratio tokamak science while providing low-collisionality, long pulse-duration, and well-diagnosed plasmas to address fundamental plasma science issues – including

burning plasma physics in ITER. The ST addresses fundamental issues in magnetic fusion energy science in the areas of: macroscopic stability, turbulence and transport, wave-particle interactions, boundary physics, and solenoid-free current formation and sustainment. For fusion applications, the high  $\beta$ , compact geometry, accessibility, modularity, and simplified magnets of the ST are potential advantages for plasma material interaction studies at high heat flux, nuclear component testing, and for a fusion power reactor.

NSTX is the world’s highest performance ST research facility and is the centerpiece of the U.S. ST national research program. As illustrated below in Figure 1.1.2, NSTX is an essential element in the program to advance the understanding and development of the ST concept while also complementing and accelerating the development of all DEMO concepts.



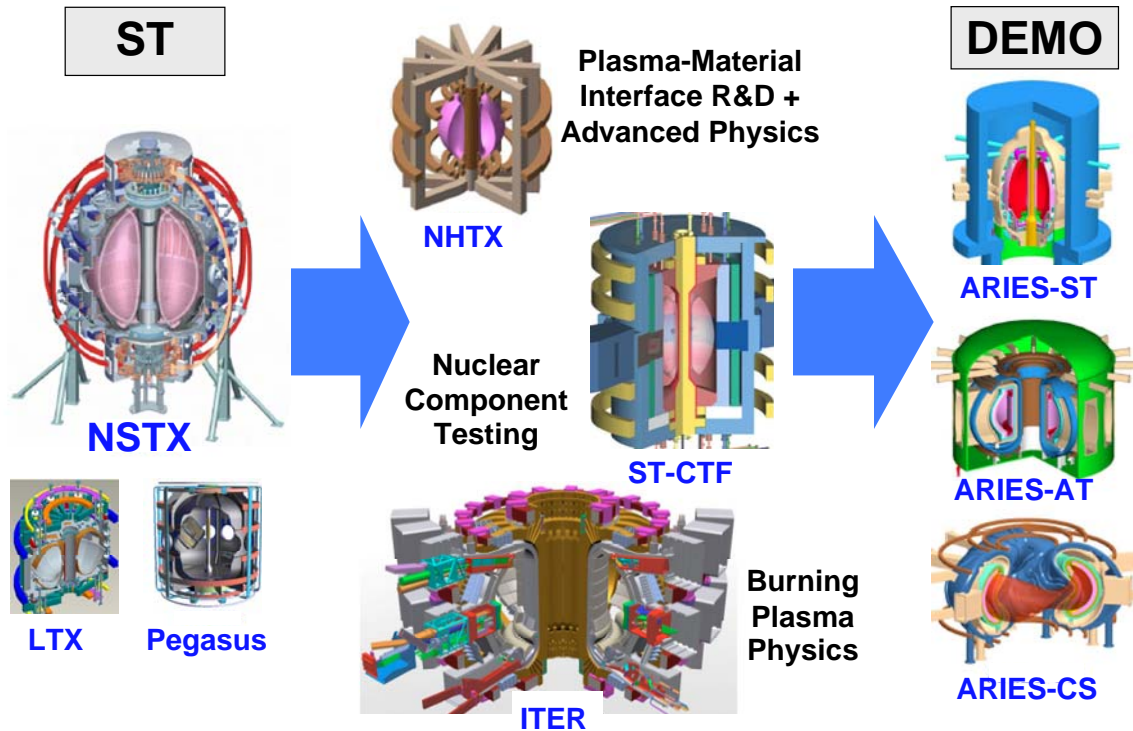


Figure 1.1.2: (left) U.S. ST research facilities, (middle) next-step STs to complement tokamaks and ITER burning plasma research by addressing key PMI and neutron fluence gaps between ITER and DEMO, and (right) spherical torus (ST), advanced tokamak (AT), and compact stellarator (CS) DEMO/reactor concepts developed by the ARIES reactor studies group (<http://www-ferp.ucsd.edu/aries/>).

The three overarching mission elements of the NSTX research program for 2009-2013 are:

- (1) Determine the physics properties of the ST - utilizing its low aspect-ratio ( $A \sim 1.5$ ) and very high ratio of plasma pressure to magnetic pressure (up to order-unity beta) - to advance toroidal plasma science.
- (2) Provide unique ST data to the tokamak knowledge-base in support of ITER final design activities and preparation for burning plasma research in ITER through participation in the International Tokamak Physics Activity (ITPA) and U.S. Burning Plasma Organization (USBPO), while also benefiting from tokamak and ITER R & D.

(3) Develop the ST knowledge-base and attractive ST operating scenarios and configurations to enable the ST to narrow key gaps between expected ITER performance and the fusion environment expected in a demonstration fusion power plant (DEMO) – including an ST-DEMO. In particular, NSTX research aims to enable the ST to be utilized to:

*a) Integrate DEMO-relevant Plasma Material Interface (PMI) solutions with high plasma performance (mission of the National High-power advanced-Torus eXperiment - NHTX).*

*b) Produce DEMO-relevant neutron flux and fluence at high duty-factor in an ST-based Component Test Facility (ST-CTF).*

Mission (3) above (“Develop the ST knowledge-base and attractive ST operating scenarios...”) is the highest priority mission of the NSTX research program for 2009-2013, and mission (1) provides the scientific underpinning for missions (2) and (3). Developing the knowledge-base and performance for addressing missions 3a) and 3b) above would also greatly enhance the prospects for developing an ST-based DEMO.

The remainder of this chapter first describes the unique parameter regimes accessed in NSTX (Section 1.2) to provide context for understanding NSTX contributions to tokamak physics and ITER (Section 1.3) and, most importantly, for motivating fusion energy science applications of the ST (Section 1.4) and identifying scientific gaps (Section 1.5) and opportunities (Section 1.6). Section 1.7 briefly summarizes the NSTX 10 year scientific research objectives, and Section 1.8 describes the scientific organizational structure of the NSTX national research team.

## 1.2 Unique Parameter Regimes Accessed by NSTX

### 1.2.1 Macroscopic Stability

The fundamental fusion advantage and scientific opportunity enabled by low aspect ratio  $A \equiv R/a$  (see Figure 1.1.1) is stable access to high plasma beta. The most commonly used definition of beta for tokamaks is the toroidal beta  $= \beta_T \equiv 2\mu_0\langle p \rangle / B_T^2$  where  $\langle p \rangle$  is the volume-averaged pressure and  $B_T$  is the vacuum toroidal field at the plasma geometric center. Since the fusion power density of a tokamak scales as  $\beta_T^2 B_T^4$ , achieving high  $\beta_T$  is clearly advantageous. The reduced aspect ratio of NSTX increases the plasma current  $I_p$  accessible for a given plasma minor radius  $a$ , toroidal field  $B_T$ , and magnetic safety factor. As shown in Figure 1.2.1.1, the maximum normalized current  $I_N \equiv I_p/aB_T$  achievable in NSTX is a factor of 2 to 3 higher than in

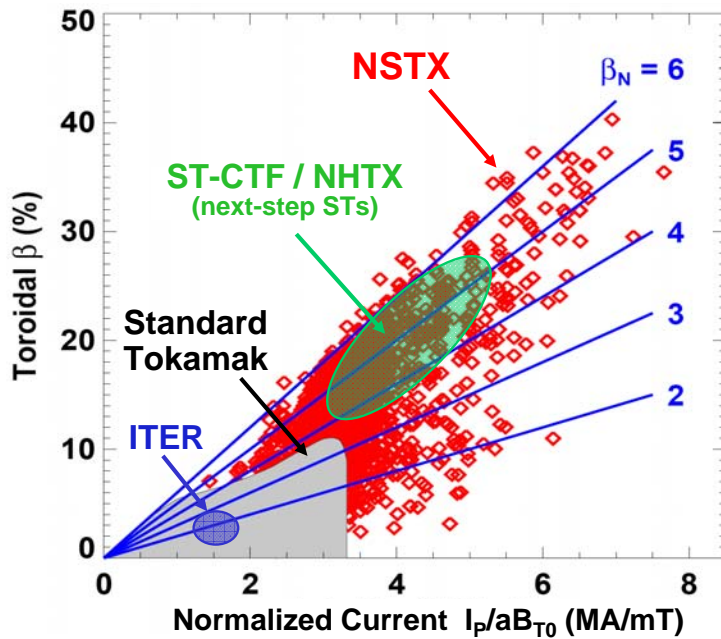


Figure 1.2.1.1: Troyon diagram showing toroidal beta achieved/expected versus normalized current  $I_p/aB_T$  for ITER, present standard aspect ratio ( $A \sim 3$ ) tokamaks, NSTX, and next-step STs NHTX and ST-CTF.

a standard aspect ratio tokamak. Experimental results largely confirm ideal MHD theoretical predictions that the maximum achievable  $\beta_T$  is proportional to the normalized current. The proportionality coefficient relating  $\beta_T$  to  $I_N$  is the normalized  $\beta = \beta_N \equiv \beta_T(\%) / I_N$  (MA/mT). As shown in Figure 1.2.1.1, the maximum  $\beta_N$  achieved in NSTX is also significantly higher (up to a factor of 1.7 at high  $I_N$ ) than is achievable at higher  $A$ .

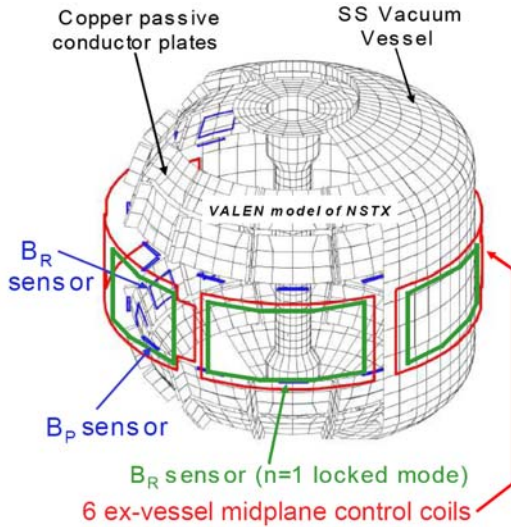


Figure 1.2.1.2: Vacuum vessel, passive conducting structures, non-axisymmetric field sensors, and ex-vessel mid-plane MHD mode control coils of NSTX.

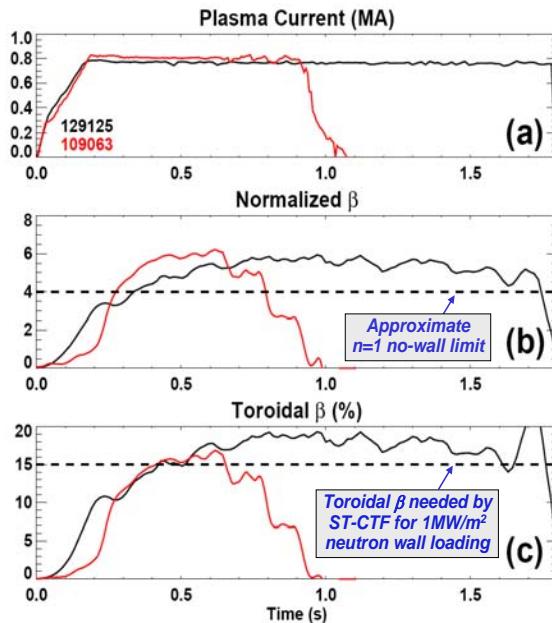


Figure 1.2.1.2: Since 2002 NSTX has (a) doubled the flat-top duration, (b) increased the duration of operation above the  $n=1$  no-wall limit by a factor of 2.5, and (c) increased the duration of  $\beta_T > 15\%$  (needed for ST-CTF) by a factor of 4. For reference, the energy confinement time  $\tau_E \approx 30\text{-}50\text{ms}$  and current redistribution time  $\tau_{CR} \approx 0.3\text{-}0.4\text{s}$  in these plasmas.

Rotational stabilization of the resistive wall mode (RWM) made possible by rapid rotation generated by strong tangential NBI heating is an essential element in achieving these high beta values far above the  $n=1$  no-wall kink instability limit ( $\beta_N \approx 4$  in NSTX). Access to very high  $\beta$  values made possible by low aspect ratio and wall stabilization from rapid toroidal rotation is a unique capability in the world program that impacts all science areas in NSTX research and improves understanding of tokamak MHD equilibrium and stability physics.

NSTX has progressed far beyond passive stabilization of the resistive wall mode and presently has the most advanced mode control system of any ST in the world program. As shown in Figure 1.2.1.2 and discussed in Chapter 2, NSTX has an extensive array of non-axisymmetric field sensors and 6 external mid-plane active control coils. These sensors and active control coils have been utilized to correct intrinsic error fields and maintain high plasma

rotation to passively stabilize the resistive wall mode, to actively stabilize resistive wall modes when the plasma rotation is insufficient to passively stabilize the RWM, and to controllably modify the toroidal rotation profile by damping toroidal flow with 3D fields. As shown in Figure 1.2.1.3, the duration of sustained high- $\beta$  has increased significantly during the last 5 years. This has been achieved through a combination of increased plasma shaping, control of error fields, resistive wall mode control, and conditioning the plasma facing components with lithium. The equilibrium and stability control tools of NSTX (described in Chapter 2) have played a major role making NSTX the highest performance ST in the world program, and the planned major upgrades of NSTX will further advance the understanding and achievement of sustained high  $\beta$  operation for STs and tokamaks.

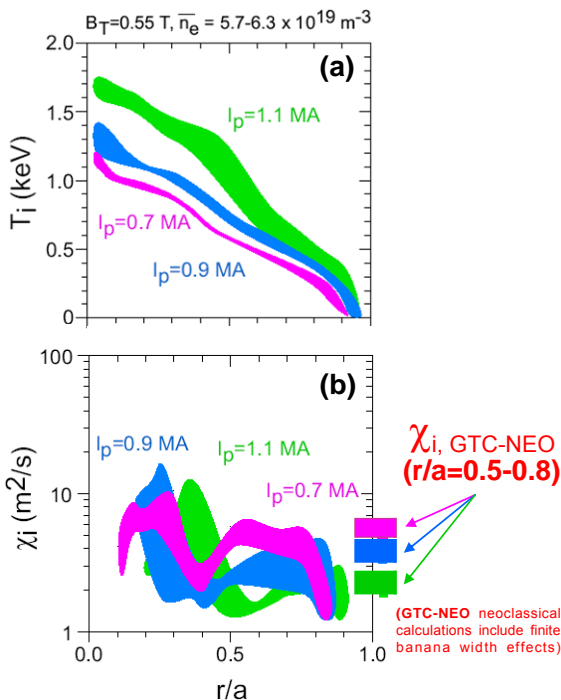


Figure 1.2.2.1: (a) Illustration of nearly linear dependence of ion temperature on  $I_p$ , and (b) consistency between measured ion thermal diffusivities and neoclassical predictions of the GTC-Neo code.

## 1.2.2 Transport and Turbulence

Just as the enhanced toroidicity (low aspect ratio) and increased natural shaping of NSTX plasmas can suppress macroscopic instabilities, these ST characteristics are also expected to reduce microturbulence levels, and thus reduce the transport associated with the microturbulence. Enhanced toroidicity also results in higher trapped particle fractions, which can influence Trapped Electron Mode (TEM) turbulence. Furthermore, the low toroidal field and near sonic toroidal flow yield large values of the  $E \times B$  shearing rates expected to be important for the suppression of long wavelength micro-turbulence and its associated transport. Consistent with such suppression,

Figure 1.2.2.1 shows examples of H-mode plasmas with high flow velocities (and  $E \times B$  shearing rates) which exhibit neoclassical thermal transport over most of the outer plasma minor radius for a range of scanned plasma current values at fixed toroidal field and density. As described in Chapter 3, this unique regime of apparently suppressed ion turbulence enables studies of electron transport with reduced influence of long-wavelength turbulence, thereby potentially enabling isolation and determination of the modes responsible for anomalous electron transport.

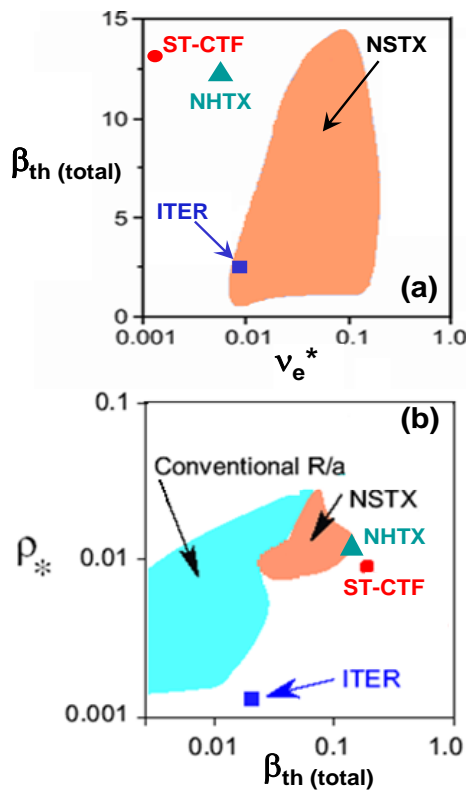
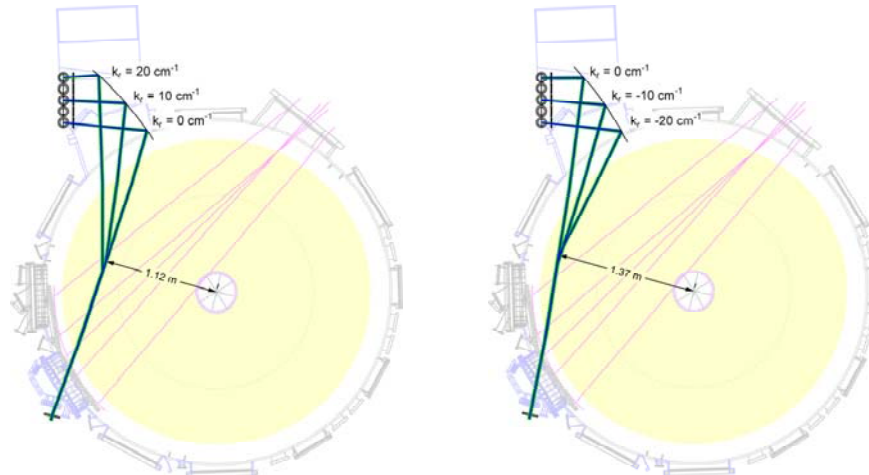


Figure 1.2.2.2: (a) Range of thermal  $\beta$  accessible in NSTX versus electron collisionality with comparison to ITER, NHTX, and ST-CTF, and (b)  $\rho_*$  vs.  $\beta_{th}$ .

Further, as shown in Figure 1.2.2.2, NSTX can operate in regimes with plasma collisionality similar to that of conventional aspect ratio tokamaks including ITER, but in which both the thermal plasma beta  $\beta_{th}$  and normalized ion gyro-radius  $\rho_* \equiv \rho_i / a$  respectively, can be up to a factor of 10 greater than those at higher toroidal field and aspect ratio. The high  $\beta$  (up to 40%) enables NSTX to explore electromagnetic and stochastic magnetic effects that may influence transport, and the large electron gyro-radius (0.1 mm) has already enabled direct and unique measurements of spatially-resolved electron-scale turbulence using the tangential microwave scattering diagnostic shown in Figure 1.2.2.3. High- $k$  fluctuations consistent with Electron Temperature Gradient (ETG) turbulence have been measured with this diagnostic, and the possible link between ETG turbulence and anomalous electron transport is

actively being investigated as described in Chapter 3. Such research is important for understanding magnetic confinement generally, since the underlying cause(s) of electron transport remain elusive, and electron confinement could determine the burning plasma performance of ITER and the performance of future STs.



- $k_r=2$  (upper ITG/TEM) to  $\sim 24$  (ETG)  $\text{cm}^{-1}$  ( $\rho_e \sim 0.01 \text{ cm}$ )
- $\Delta r \sim 6 \text{ cm}$ ,  $\Delta k \sim 1 \text{ cm}^{-1}$
- Can vary scattering volume location (axis to near edge)

Figure 1.2.2.3: High-k microwave scattering diagnostic beam trajectories and measurement capabilities.

### 1.2.3 Waves and Energetic Particles

Spherical torus (ST) plasmas, such as those in NSTX, provide a unique opportunity for studying wave-particle interactions in plasma at high  $\beta$  and high dielectric constant  $\epsilon \equiv \omega_{pe}^2 / \Omega_{ce}^2 \sim 10-100$ . The over-dense plasma conditions of the ST make plasmas inaccessible to lower hybrid (LH) and electron cyclotron (EC) waves. As a result, waves that can propagate in over-dense plasma conditions are required for the ST, and the two leading candidates are the high harmonic fast wave (HHFW) with  $\omega/\Omega_D=8-16$  and electron Bernstein wave (EBW) with  $\omega/\Omega_e = 1-3$ . These waves are being developed and explored in NSTX to assist non-inductive plasma startup, plasma current ramp-up, and sustained plasma operation at high  $\beta$ . The most challenging aspect of exploiting these waves for fusion applications is efficient coupling of these waves from the edge to the hot plasma core.

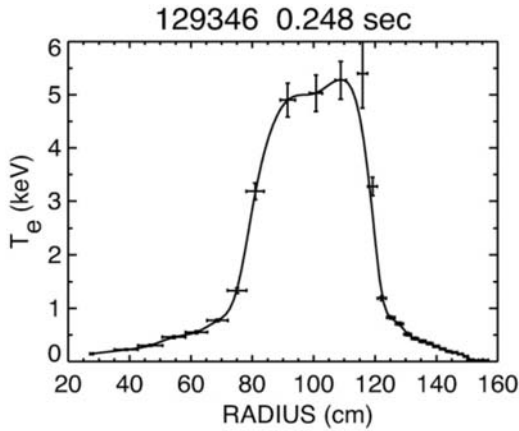


Figure 1.2.3.1: The highest electron temperature  $T_e \approx 5\text{keV}$  produced in an ST has been achieved with 3MW of HHFW heating in NSTX in a target plasma with  $I_p = 600\text{kA}$ ,  $B_T(0) = 5.1\text{kG}$ ,  $n_e(0) = 1.3 \times 10^{19}\text{m}^{-3}$ , and  $\beta_e(0) \approx 10\%$ .

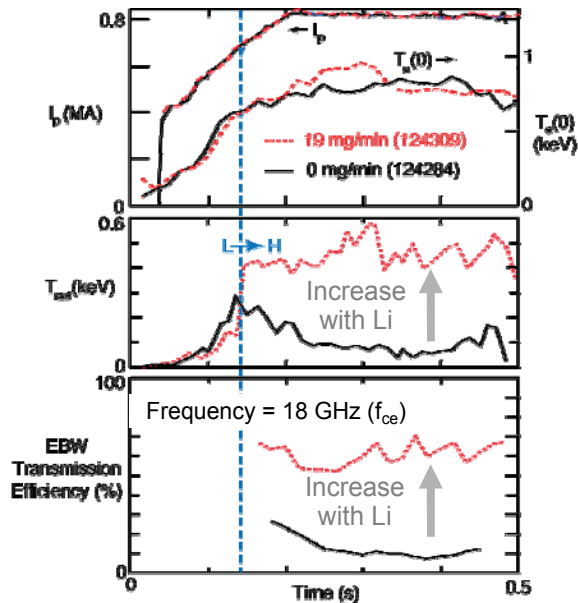


Figure 1.2.3.2: EBW radiation temperature (middle) and transmission efficiency (bottom) as a function of lithium evaporation rate which influences  $T_e$  at the mode conversion layer in the scrape-off-layer.

For the HHFW, research in NSTX has shown that edge effects including the excitation of parametric decay instabilities and surface waves can significantly damp wave power at the plasma edge reducing coupling efficiency to the plasma core. As described in Chapter 4, increased TF, reduced plasma density near the RF antenna, and lower wave phase velocities all reduce HHFW edge losses. Up to 90% HHFW coupling efficiency has now been demonstrated, and as shown in Figure 1.2.3.1, the highest electron temperatures attained in NSTX have been achieved with HHFW. With this improved understanding of coupling and heating, the HHFW has become a powerful tool for probing core electron transport physics and is poised to become a reliable auxiliary heating and current drive tool for the ST. Further, as described in Chapter 4, the coupling issues encountered for HHFW on NSTX are also relevant to ICRF heating schemes planned for ITER.

While the HHFW is launched as a radially evanescent wave that must tunnel through a cutoff determined by the plasma density profile in front of the antenna, the EBW is typically

launched as a radially propagating electromagnetic wave in vacuum that must undergo multiple mode conversion process (O-mode to X-mode to Bernstein  $\rightarrow$  O-X-B) to transition into an electrostatic wave that can propagate freely in an over-dense plasma and be absorbed at an



electron cyclotron resonance. Thus, the EBW is especially sensitive to plasma conditions at the mode-conversion layer(s). For present ST experimental conditions the EBW mode conversion layer commonly resides near or in the edge scrape-off-layer (SOL). A key finding from NSTX experiments is that collisional damping of the EBW at the mode conversion layer strongly influences the EBW coupling efficiency.

EBW emission (B-X-O) measurements in NSTX indicate that the electron temperature at the mode conversion layer is a critical parameter, and strong damping is observed for  $T_e < 20\text{eV}$ . As discussed in Chapter 4 and shown in Figure 1.2.3.2, evaporated lithium has been shown to increase  $T_e$  from 10 to 30eV at the mode conversion layer and increase the transmission efficiency from 10% to 65% at 18 GHz ( $f_{ce}$ ) and from 10% to 50% at 28 GHz ( $2f_{ce}$ ). These are the highest EBW transmission efficiencies observed to-date in ST H-mode plasmas, and further optimization is possible to increase the EBW coupling efficiency for wave heating and current-drive applications in NSTX, future STs, and alternative concepts with over-dense plasmas.

Beyond waves that are excited by external means, fast ions produced during neutral beam

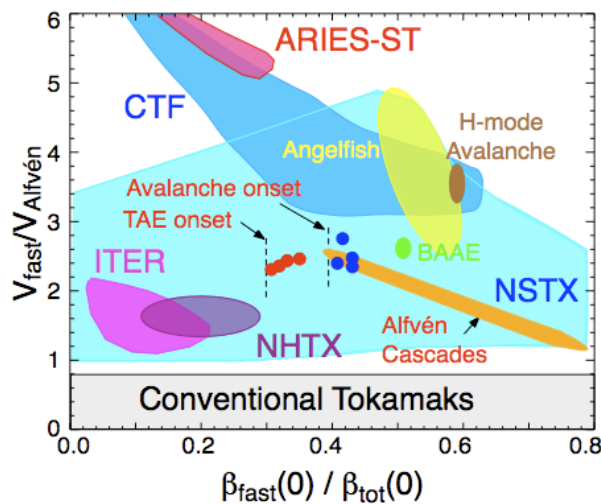


Figure 1.2.3.3: Normalized fast-ion velocity and  $\beta$  accessible in NSTX with NBI heating compared to ITER (with only  $\alpha$ 's included) and future ST devices: NHTX (NBI), ST-CTF (NBI+ $\alpha$ 's), and ARIES-ST reactor ( $\alpha$ 's).

injection in NSTX have velocities that exceed the Alfvén speed and can consequently resonate strongly with a wide variety of Alfvén waves and destabilize them. Further, the fraction of fast ion beta relative to the total beta accessible in NSTX can be large and is also important in determining the instability drive. As shown in Figure 1.2.3.3 the ratio of NBI fast-ion speed normalized to the Alfvén speed can approach 5 in NSTX, and the fast-ion to total central beta ratio can reach up to 80%. As seen in the figure, NSTX can access the

fast-ion instability drive regime expected in ITER (shown for  $\alpha$ -particles only - not including NBI fast-ions) and NHTX (NBI fast-ions only), has significant overlap with the fast ion regime expected in an ST-CTF (NBI+ $\alpha$ -particles), and can approach the parameter regime of an ST reactor (ARIES-ST).

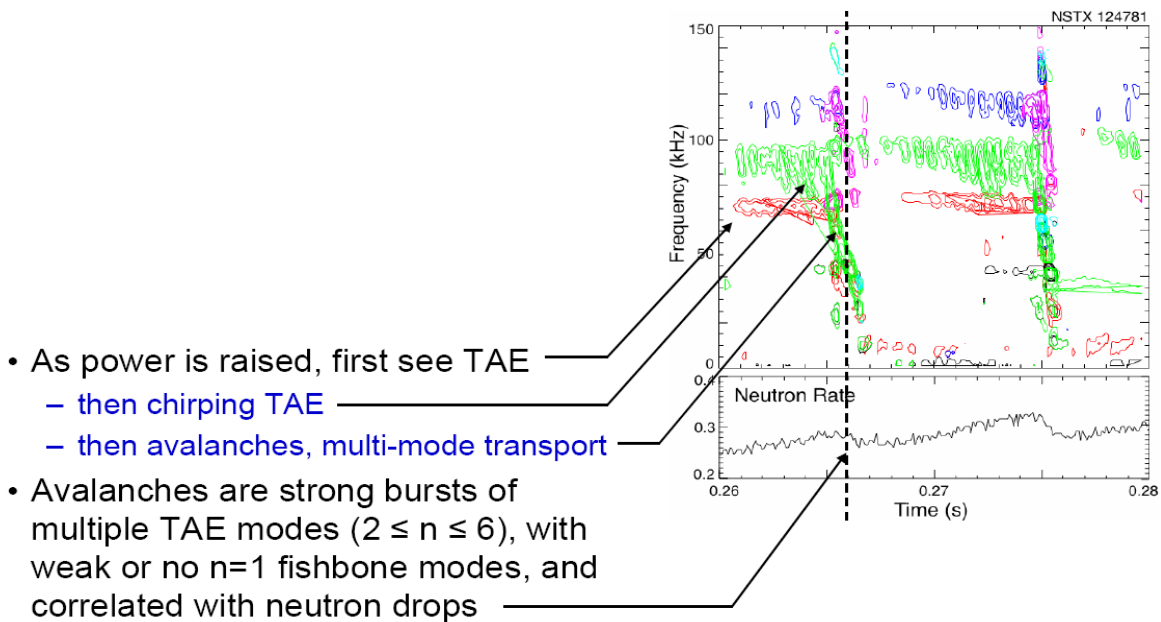


Figure 1.2.3.4: Time evolution of mode activity (top) and neutron rate (lower) for TAE avalanche events.

Importantly, as described in Chapter 4, the high normalized fast ion velocity and pressure accessible in NSTX can excite Toroidal Alfvén Eigenmode (TAE) avalanches in which multiple interacting TAE modes are excited simultaneously potentially leading to significant fast-ion transport and/or loss. ITER with  $\alpha$ -particles and NBI is expected to be unstable to such TAE instabilities and may exhibit avalanches, and ST-CTF is likely strongly in the avalanche regime. The time evolution of mode activity associated with an avalanche event is shown in Figure 1.2.3.4 which shows how multiple modes interact and lead a significant (up to 15%) decrease in the neutron rate indicating significant fast ion transport and/or loss from the plasma core. As

described in Chapter 4, NSTX has unique access to and diagnosis of this TAE avalanche regime including MSE  $q$  profile measurements at very low  $B_T = 0.35\text{-}0.55\text{T}$  and fast ion distribution function and fast-ion loss diagnostics. NSTX research has yielded additional research results including the discovery of CAE/GAE (Compressional/Global AE), Alfvén-acoustic modes, and a new understanding of chirping modes. These experimental results have helped advance theoretical modeling and have significant implications for future burning plasma devices.

### 1.2.4 Boundary Physics:

The plasma boundary is especially influenced by the unique magnetic geometry and compactness of the ST. As described in Chapter 5, the high global magnetic shear, large fraction of trapped

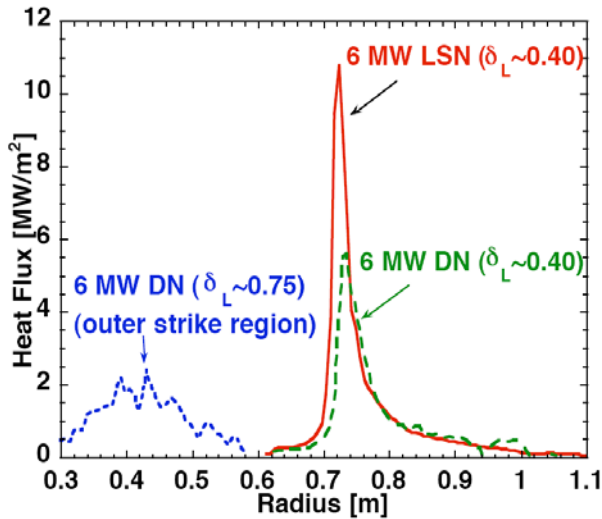


Figure 1.2.4.1: Divertor heat flux profiles for low triangularity lower-single null (LSN) (red), double-null (DN) (green), and high triangularity DN plasmas at fixed NBI heating power = 6MW.

particles, and reduced connection length impact edge transport and stability in both the closed-field-line edge confinement region and on the open magnetic field lines in the scrape-off layer (SOL). For example, as shown in Figure 1.2.4.1, the compactness of the ST can result in very high heat fluxes up to  $10\text{MW/m}^2$  at the divertor in lower-single-null diverted plasmas at reduced triangularity. Such heat fluxes are comparable to those expected in ITER and enable research on heat-flux mitigation strategies such as

enhanced divertor radiation and poloidal flux expansion. As seen in the figure, operating in a double-null configuration can reduce the peak heat flux by nearly  $\frac{1}{2}$ , and increasing the triangularity and exhausting at smaller major radius actually reduces the peak heat flux through a combination of flux expansion and increased radiation. Access to, diagnosis of, and mitigation

of these very high heat fluxes is a unique capability of NSTX and opens the possibility of using the ST as a test-bed for developing heat flux solutions not only for the ST but for all DEMO configurations.

NSTX is also unique in the world program for investigating the impact of lithium plasma facing components (PFCs) on diverted H-mode plasmas. As discussed in Chapter 5, lithium has been shown to offer several potential benefits in NSTX plasmas including particle pumping, enhanced thermal confinement, and the suppression of edge localized modes (ELMs). ELM reduction and/or suppression is a vital research area in the world program, since large ELMs must be avoided in next-step devices such as ITER to avoid ablating and/or melting divertor PFCs. As shown in Figure 1.2.4.2, unlike some tokamak experiments which have demonstrated ELM

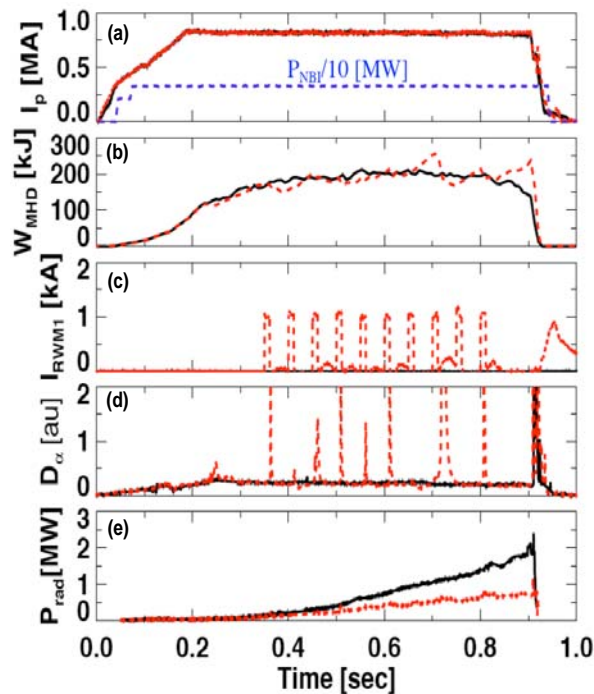


Figure 1.2.4.2: (a) Plasma current and NBI power, (b) plasma stored energy, (c) RMP coil current, (d) divertor  $D_\alpha$  light, and (e) radiated power in an ELM-free discharge (black) and with Type-I ELMs triggered by RMP fields (red).

suppression (DIII-D) and/or reduction (JET) using resonant magnetic perturbations (RMPs) at the plasma edge, NSTX experiments have thus far exhibited ELM *destabilization* and/or ELM enlargement/enhancement with the application of RMP fields. Understanding of the causes of these differences is required to confidently extrapolate RMP effects to ITER. ELM destabilization by RMP is presently being exploited in NSTX to reduce impurity accumulation in otherwise ELM-free plasmas (made ELM-free using lithium wall coatings) by controllably applying RMP pulses to induce ELMs and expel impurities. As shown in Figure 1.2.4.2, preliminary tests have already demonstrated a factor of two reduction in radiated power with this pulsed-RMP technique,

and further optimization of ELM size and frequency is possible. The unique plasma boundary regimes accessible by NSTX are enabling improved understanding of the complex interplay between wall conditions and materials, pedestal stability and transport, 3D edge magnetic fields, and power and particle exhaust to the divertor.

### **1.2.5 Plasma Formation and Sustainment:**

In present ST devices, the compact geometry of the ST leaves little room for the central solenoid normally used for inductive current drive in a tokamak. In future nuclear-capable ST devices, in order to maintain low aspect ratio, the shielding of the central column must be minimized. However, with this level of shielding, the insulation of multi-turn coils is likely damaged by fusion neutrons, and future ST-based nuclear facilities are therefore envisioned to operate with little or no central solenoid. As a result, techniques for plasma current start-up, ramp-up, and sustainment must be developed for next-step STs and would also greatly benefit tokamak reactors. Because these techniques are ultimately essential to the ST concept, ST research takes the leading role in the development of non-inductive startup and ramp-up techniques for STs and tokamaks.

On NSTX, the Coaxial Helicity Injection (CHI) plasma start-up technique has generated up to 20% of the nominal high-performance operating current, and CHI has recently been coupled to inductive operation in NSTX. As shown in Figure 1.2.5.1, up to 160kA of closed-flux current has been produced in NSTX using CHI, and as discussed in Chapter 6, a record high current multiplication factor of 60 was achieved in these plasmas. NSTX is presently the only device in the world program studying CHI, and these experiments clearly indicate that high closed-flux plasma currents can be produced. However, additional effort is needed to further heat these plasmas to achieve impurity burn-through and to raise the electron temperature so that the HHFW can be absorbed to enable plasma current ramp-up using current over-drive.

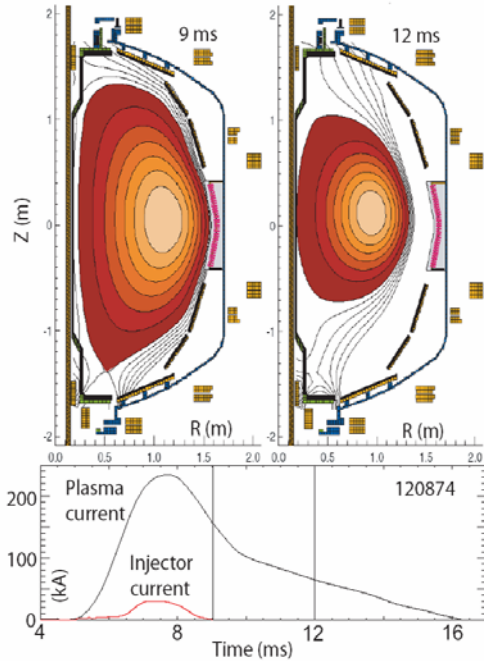


Figure 1.2.5.1: (Top) Equilibrium reconstructions show the shape evolution of the CHI-produced plasma in response to decaying current. (Bottom) Up to 160kA of closed-flux plasma current has been produced by CHI.

discussed in Chapter 6, HHFW heating has driven up to 85% of the plasma current at low plasma current with bootstrap (BS) current in high-confinement-mode (H-mode) plasmas in NSTX – the highest bootstrap fraction achieved in any ST to-date. However, additional current-drive from either BS or other means (such as HHFW-CD or NBI-CD) is needed to achieve plasma current ramp-up to high plasma current.

With regard to sustained high-performance scenarios, NSTX has sustained up to 70% of the plasma current at high plasma performance with a combination of pressure-gradient-driven “bootstrap” current and neutral beam injection current drive (NBI-CD). As discussed in Chapter 6, this high fraction of non-inductive current drive is achieved at high beta ( $\beta_T = 15-20\%$  and  $\beta_N = 5.5-6$ ) and simultaneously has high pressure-gradient-driven current fraction ( $f_{\nabla p} = 55\%$ ) comparable to that assumed for ST-CTF. Thus, based on NSTX results, fully non-inductive current drive appears within reach for the ST. The largest gap in achieving completely solenoid-free ST operation is arguably the plasma-current ramp-up phase between plasma start-up and plasma sustainment. As

## Contributions to tokamak physics and ITER

**1.3.1 - ITPA:** The unique parameter regimes accessible by NSTX described in Section 1.2 provide new insight into the underlying plasma physics relevant to tokamaks of all aspect ratios and for future burning plasma experiments. As a result, NSTX data is increasingly being sought out to clarify aspect ratio, beta, fast-ion, and other dependences in tokamak physics. Since 2005, NSTX has become increasingly engaged in the **International Tokamak Physics Activity (ITPA)** and has participated in many joint experiments involving participation by NSTX researchers and/or contributions of experimental data to international databases – for example databases for H-mode confinement (Chapter 3) and disruption current quench-rate (Chapter 2). For the H-mode confinement scaling example, NSTX confinement exhibits a relatively weak confinement degradation with  $\beta$  relative to the ITER 98(y,2) scaling, but is consistent with dedicated JET and DIII-D scans. NSTX experiments have shown that variability in the confinement dependence on  $\beta$  is likely related to differences in plasma shaping and/or ELM type. For the disruption current quench-rate example, the lower aspect ratio of the ST decreases the normalized external inductance and increases the current quench rate. However, when the aspect ratio dependence of the inductance is accounted for, the normalized quench rates of NSTX are comparable to those observed in tokamaks. This indicates that the plasma temperature during the quench is weakly dependent on aspect ratio and is consistent with processes in which impurity radiation dominates the dissipation of plasma inductive energy during the current-quench.

Participation in ITPA activities also benefits the ST by aiding in the understanding of the impact of higher beta and reduced aspect ratio on a variety of physics issues for next-step ST design. As of June 2008, NSTX was actively involved in 17 joint ITPA experiments and is contributing to a total of 24. As shown in Table 1.3.1, the contributions of NSTX to ITPA research extend across all topical science areas described in Section 1.2, and selected ITPA-related results are also discussed in Chapters 2-6.

**Boundary Physics**

- PEP-6 Pedestal structure and ELM stability in DN
- PEP-9 NSTX/MAST/DIII-D pedestal similarity
- PEP-16 C-MOD/NSTX/MAST small ELM regime comparison
- DSOL-15 Inter-machine comparison of blob characteristics
- DSOL-17 Cross-machine comparison of pulse-by-pulse deposition

**Macroscopic stability**

- MDC-2 Joint experiments on resistive wall mode physics
- MDC-3 Joint experiments on neoclassical tearing modes including error field effects
- MDC-12 Non-resonant magnetic braking
- MDC-13: NTM stability at low rotation

**Transport and Turbulence**

- CDB-2 Confinement scaling in ELMy H-modes:  $\beta$  degradation
- CDB-6 Improving the condition of global ELMy H-mode and pedestal databases: Low A
- CDB-9 Density profiles at low collisionality
- TP-6.3 NBI-driven momentum transport study
- TP-9 H-mode aspect ratio comparison

**Wave Particle Interactions**

- MDC-11 Fast ion losses and redistribution from localized Alfvén Eigenmodes

**Advanced Scenarios and Control**

- SSO-2.2 MHD in hybrid scenarios and effects on q-profile
- MDC-14: Vertical Stability Physics and Performance Limits in Tokamaks with Highly Elongated Plasmas

*Table 1.4.1 - International Tokamak Physics Activity (ITPA) joint experiments involving participation by NSTX researchers and/or contributions of NSTX experimental data as of June 2008.*

**1.3.2 – ITER Design:** During 2007, several ITER design issues were identified to be of critical importance because they potentially impact the ability of ITER to achieve its stated missions of achieving  $Q=10$  at 500MW sustained for 400s and fully non-inductive operation at  $Q=5$ . As described in Section 1.2.4, a critical issue for all ITER scenarios is the mitigation of ELMs. Several dedicated RMP ELM control experiments were conducted in NSTX for ITER in FY2008, and a subset of these results are described in Chapter 5. A key issue in understanding RMP ELM mitigation is the plasma response to the applied field. As described in Chapter 2, the Ideal Perturbed Equilibrium Code (IPEC) has been developed to better model tokamak plasma response to 3D fields. This code was initially developed to better understand locked-mode threshold scalings and error-field effects on NSTX, and has since been applied to DIII-D and ITER as well. Of particular importance to ELM mitigation using RMP is the avoidance of the



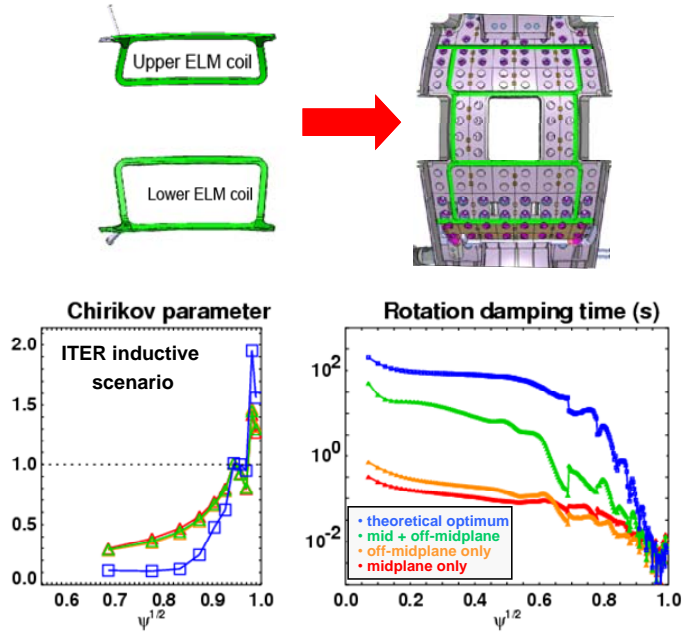


Figure 1.3.2.1: (Top) Non-axisymmetric control coils under consideration for ITER shown in green, (bottom left) Chirikov parameter vs. minor radius for the optimum coil current distribution computed by IPEC, and (bottom right) NTV rotation damping time computed by IPEC.

excitation of core resonant radial field perturbations (to minimize island excitation) and the minimization of both resonant and non-resonant rotation damping. By linking IPEC to Neoclassical Toroidal Viscosity (NTV) calculations (see Chapter 2), the optimal applied external field can be computed to ergodize the edge (i.e. satisfy the Chirikov overlap parameter in the H-mode pedestal) while minimizing core island formation and NTV flow damping. As shown in Figure 1.3.2.1, the ELM control coils under consideration for ITER are computed to be capable of ergodizing

the plasma edge while providing Chirikov  $\ll 1$  in the plasma core. This figure also shows that the combination of midplane and off-midplane coils is up to 2 orders magnitudes more effective at minimizing rotation damping relative to mid-plane or off-mid-plane coils alone. The combination of the mid-plane and off-midplane coils approaches the theoretical optimum (shown in blue) for coil placement (i.e. normal field distribution on the plasma boundary) unconstrained by engineering considerations.

The coils shown in Figure 1.3.2.1 also appear attractive for fast vertical control and resistive wall mode control applications. A key issue for ITER is the maximum tolerable displacement of the plasma vertical position (typically caused by an MHD-induced perturbation to  $I_i$  and/or  $\beta_p$ ) that is allowable before the vertical position control system fails to recover and a vertical displacement event (VDE) occurs leading a plasma current disruption. Dedicated experiments on NSTX with

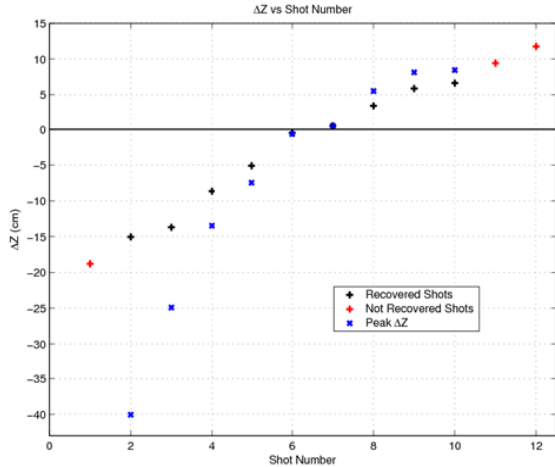


Figure 1.3.2.2: Recovered (black) and non-recovered (red) shots vs. vertical position displacement  $\Delta Z$  from vertical control experiments in NSTX for ITER.

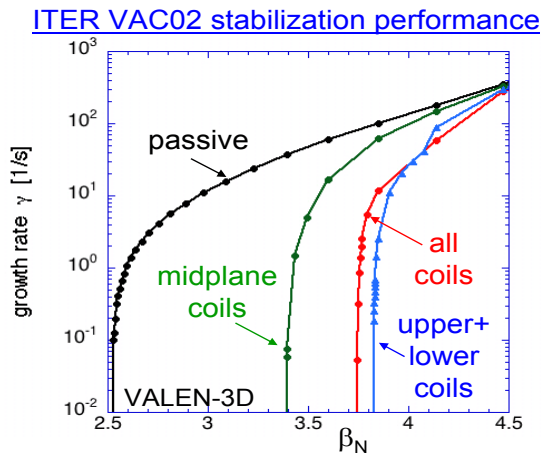


Figure 1.3.2.3: VALEN calculations of  $n=1$  RWM control capabilities for different coil combinations for the proposed ITER 3D coils shown in Figure 1.3.2.1.

As shown in Figure 1.3.2.3, VALEN calculations (validated with NSTX RWM control data as discussed in Chapter 2) indicate that the internal 3D coils proposed for ITER are sufficient to stabilize the  $n=1$  RWM up to  $\beta_N = 3.7$ . The operating  $\beta_N \approx 3$  is therefore less than 50% of the separation between the no-wall and RWM control limits and should provide sufficient margin for robust RWM control in ITER advanced scenarios.

plasma elongation and internal inductance similar to ITER values have been performed and observed a maximum recoverable displacement  $\Delta Z_{MAX}/a < 10\%$ . This value is consistent with results at higher aspect ratio  $A \approx 3$  and further confirms the potential inadequacy of the original ITER vertical control system for providing robust control of large vertical excursions. This finding further motivates the usage of the coils shown in Figure 1.3.2.1 for more robust vertical control. A further potentially important finding of NSTX is shown in Figure 1.3.2.2 which indicates that the maximum recoverable displacement depends on the direction of displacement and is likely the result of up/down asymmetries in the vessel conducting structure of NSTX (up/down asymmetries in vessel conducting structure are also present in ITER).

Finally, in addition to sufficient ELM and vertical control, ITER will also require  $n=1$  RWM control to operate stably in the proposed fully non-inductive scenario with  $Q=5$  (ITER

## 1.4 Fusion Energy Science Applications of the ST

### 1.4.1 Overview

Beyond the contributions of the NSTX to tokamak physics and ITER development, the ST is also attractive for a range of fusion energy science applications as shown previously in Figure 1.1.2. The ST offers high normalized pressure (i.e. high  $\beta$ ), a very compact geometry resulting from low-A, and simplified normally conducting magnets with significantly reduced coil stress on the outboard low-field side. As shown in ARIES and CTF design studies, the ST also offers the possibility of a single-turn demountable central conducting rod for the toroidal field coil and ease of maintenance, accessibility, and change-out of components.

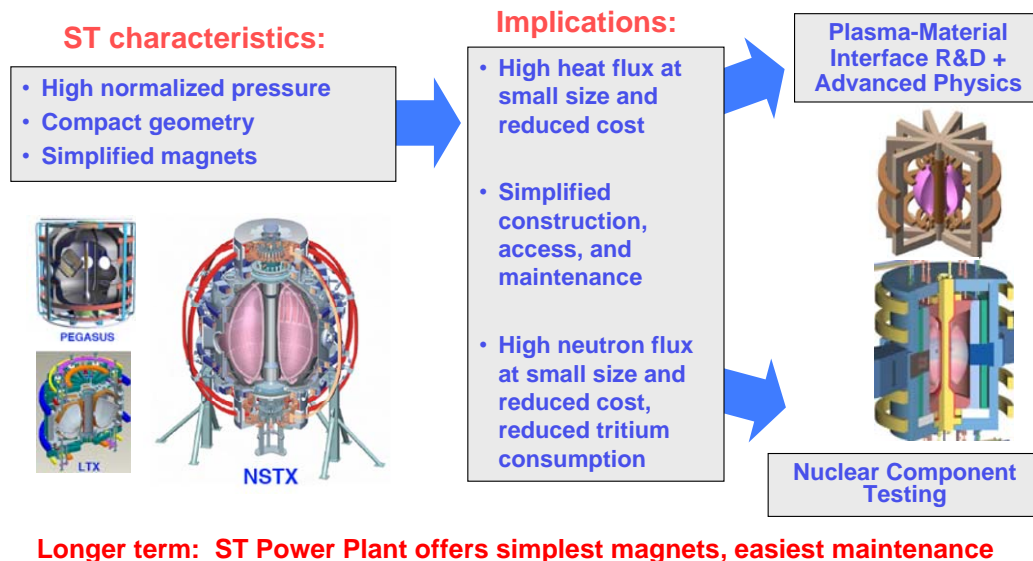


Figure 1.4.1.1: The characteristics of the ST relevant to fusion energy, their implications, and resulting near-term and long-term applications of the ST.

As shown graphically in Figure 1.4.1.1, the intrinsic ST characteristics described above have several implications. First, the compactness of the ST results in very high heat fluxes to the Plasma Material Interfaces (PMI) – namely the divertor. High plasma exhaust heat flux is common to all fusion DEMO concepts based on the ST, tokamak, or compact stellarator, but the

issue is most severe for the ST. Empirically, the measured power scrape-off width (projected from the divertor back to the outboard midplane) does not vary strongly with machine size, the divertor heat-flux challenge can be approximately parameterized by the ratio  $P_{\text{heat}}/R$  where  $R$  is the average plasma major radius. The ratio  $P_{\text{heat}}/S$  (where  $S$  is the wall surface area) is also

Device	R (m)	a (m)	$P_{\text{heat}}$ (MW)	$P_{\text{heat}}/R$ (MW/m)	$P_{\text{heat}}/S$ (MW/m <sup>2</sup> )	Pulse (sec)	$I_p$ (MA)	Species	Comments
<b>Planned Long-Pulse Experiments</b>									
EAST	1.70	0.40	24	14	0.55	1000	1.0	H (D)	Upgrade capability
JT-60SA	3.01	1.14	41	14	0.21	100	3.0	D	JA-EU Collaboration
KSTAR	1.80	0.50	29	16	0.52	300	2.0	H (D)	Upgrade Capability
LHD	3.90	0.60	10	3	0.11	10,000	–	H	Upgrade capability
SST-1	1.10	0.20	3	3	0.23	1000	0.2	H (D)	Initial heating
W7-X	5.50	0.53	10	2	0.09	1800	–	H	30MW for 10sec
<b>NHTX</b>	<b>1.00</b>	<b>0.55</b>	<b>50</b>	<b>50</b>	<b>1.13</b>	<b>1000</b>	<b>3.5</b>	<b>D (DT)</b>	<b>Initial heating</b>
ITER	6.20	2.00	150	24	0.21	400-3000	15.0	DT	Not for divertor testing
<b>Component Test Facility Designs</b>									
<b>CTF (A=1.5)</b>	<b>1.20</b>	<b>0.80</b>	<b>58</b>	<b>48</b>	<b>0.64</b>	<b>Weeks</b>	<b>12.3</b>	<b>DT</b>	<b>2 MW/m<sup>2</sup> neutron flux</b>
FDF (A=3.5)	2.49	0.71	108	43	1.61	Weeks	7.0	DT	2 MW/m <sup>2</sup> neutron flux
<b>Demonstration Power Plant Designs</b>									
ARIES-RS	5.52	1.38	514	93	1.23	Months	11.3	DT	US Advanced Tokamak
ARIES-AT	5.20	1.30	387	74	0.85	Months	12.8	DT	US Advanced Technology
<b>ARIES-ST</b>	<b>3.20</b>	<b>2.00</b>	<b>624</b>	<b>195</b>	<b>0.99</b>	<b>Months</b>	<b>29.0</b>	<b>DT</b>	<b>US Spherical Torus</b>
ARIES-CS	7.75	1.70	471	61	0.91	Months	3.2	DT	US Compact Stellarator
ITER-like	6.20	2.00	600	97	0.84	Months	15.0	DT	ITER @ higher power, Q
EU A	9.55	3.18	1246	130	0.74	Months	30.0	DT	EU "modest extrapolation"
EU B	8.60	2.87	990	115	0.73	Months	28.0	DT	EU
EU C	7.50	2.50	794	106	0.71	Months	20.1	DT	EU
EU D	6.10	2.03	577	95	0.78	Months	14.1	DT	EU Advanced
SlimCS	5.50	2.12	650	118	0.90	Months	16.7	DT	JA

Table 1.4.1.1: Comparison of the accessible normalized heat-flux (highlighted in yellow) and other parameters of planned long-pulse experiments, Component Test Facility (CTF) design points, and demonstration power plant (DEMO) designs. ST concepts: NHTX, ST-CTF, and ARIES-ST are highlighted in green.

important for parameterizing the expected wall heat loading challenge. As shown in Table 1.4.1.1, NHTX could access normalized heat fluxes twice those of ITER with values comparable to those of CTF designs and with a P/S value similar to all DEMO design concepts. With magnetic flux compression, NHTX should also be able to access heat flux values of tokamak-based reactor designs, but accessing and mitigating ST reactor-level heat fluxes would be more challenging. The heat flux challenge must be resolved to achieve a successful ST-DEMO, and PMI solutions developed in ST research benefit not only the ST path but also all other DEMO concepts shown in Table 1.4.1.1.

The compactness of the ST can also potentially create very high neutron wall loading ( $1\text{-}2\text{MW/m}^2$ ) in a device not much larger (20-50% in major radius) than present mega-ampere-class STs. Using the ST as a volume neutron source (VNS) to test nuclear components in a high fusion neutron irradiation environment with neutron fluences  $10\times$  those of ITER and approaching DEMO-level fluences could reduce the usage of tritium and also the risks of proceeding directly from ITER to DEMO. For both PMI and VNS uses of the ST, the simplified construction, access, and maintenance are significant potential advantages for rapidly testing new materials, components, and techniques, in an environment of high heat, particle, and neutron flux sustained for long durations.

The 2007 FESAC panel report entitled “Priorities, Gaps and Opportunities: Towards a Long Range Strategic Plan for Magnetic Fusion Energy” identified plasma facing components and materials (i.e. the PMI) as the most challenging gaps to close between ITER and DEMO. The ST appears particularly well suited to address the related highest priority FESAC panel “theme” of “Taming the Plasma Material Interface” (Theme B) which encompasses: plasma-wall interactions, plasma facing components, RF antennae, launching structures and other internal components. The ST also appears particularly well suited to address the FESAC panel theme of “Harnessing Fusion Power” (Theme C) which encompasses: fusion fuel cycle, power extraction, materials science in the fusion environment, safety, reliability, availability, maintainability, and inspectability. As described in section 1.4.2 below, the proposed NHTX device could address Theme B in a non-nuclear environment (operating with D-D and very limited D-T capability) including prototyping of PMI solutions for ST-CTF and testing the PMI applicability of neutron-irradiated materials from the International Fusion Materials Irradiation Facility (IFMIF). ST-CTF could strongly address the neutron irradiation implications of Theme B issues on a much larger scale while also strongly addressing Theme C.

A third theme of “Creating predictable high-performance steady-state plasmas” (Theme A) was identified by FESAC encompassing: measurement, performance integration, validated theory

and predictive modeling, control, disruptions, control auxiliary systems, and magnets. Significant research and development is expected to be performed in ITER steady-state scenarios and in the long-pulse superconducting tokamak program utilizing the EAST, KSTAR, and JT-60SA devices. Since the normalized plasma stability requirements of an ST-DEMO are similar to those of an AT-DEMO, the ST can leverage expected future progress in advanced tokamak physics research. However, the confinement (and other) properties of the ST may be sufficiently different from the tokamak that high-performance steady-state plasmas must also be demonstrated in the ST prior to proceeding to an ST-DEMO. Normally conducting magnets in a nuclear environment are the most important and unique technology aspect of the ST with respect to Theme A, and the ST community has identified critical issues for the ST-CTF center post:

- 1) Materials interface and design to ensure uniform current distribution over large area high current possibly sliding joints and feeders
- 2) Replaceable vacuum seal located near the TF sliding joints
- 3) Requirements for remote handled assembly and replacement of such center posts
- 4) Manufacturability of the TF center post using radiation tolerant normal conductors
- 5) Center post water cooling capability and management of activated corrosion products

These design issues are also directly relevant to an ST-DEMO, and ST-CTF would therefore contribute strongly to developing the magnet technology for ST-DEMO. More detailed information on the goals and operating parameters for NHTX, ST-CTF, and an ST reactor are provided below for reference.

#### **1.4.2. Mission, design concept, and operating parameters for NHTX**

As described in Section 1.4.1, the 2007 FESAC panel identified “Taming the Plasma Material Interface” as the highest priority gap that must be addressed to progress from ITER burning plasmas to an electricity producing DEMO. PMI solutions must also be compatible with sustained high plasma performance to be relevant to DEMO, and this challenge motivates the proposed scientific mission of the National High-power advanced Torus eXperiment (NHTX).

***NHTX mission: “Integration of a fusion-relevant plasma-material interface with stable, sustained, high-performance plasma operation”***

The NHTX mission aims to integrate the following PMI and plasma performance goals:

1. Access and diagnose DEMO-relevant heat-fluxes
2. Perform rapid testing of new PMI concepts, including comparing solid vs. liquid PFCs and testing novel divertor concepts (X, Super-X, snow-flake divertor, etc.)
3. Perform PMI research at DEMO-relevant  $T_{\text{wall}} \sim 600^{\circ}\text{C}$
4. Access pulse durations sufficient to achieve plasma-wall equilibration:  $\tau_{\text{pulse}} \sim 200\text{-}1000\text{s}$
5. Develop methods to avoid tritium retention
6. Demonstrate the compatibility of PMI solutions with high plasma performance:
  - a. High confinement will tolerable or no ELMs
  - b. High beta without disruptions
  - c. Steady-state with full non-inductive current drive
7. Test advanced performance regimes (high  $\beta_N$  and  $f_{\text{BS}}$ ) for ST-DEMO and ST-CTF, test  $I_P$  start-up/ramp-up techniques for ST-CTF at similar size, toroidal field, and  $P_{\text{AUX}}$ .

The NHTX device geometry, parameters, and possible plasma and divertor configurations to be studied are shown in Figure 1.4.2.1, and NSTX and future ST divertor and plasma exhaust issues are discussed in much more detail in Chapter 5.

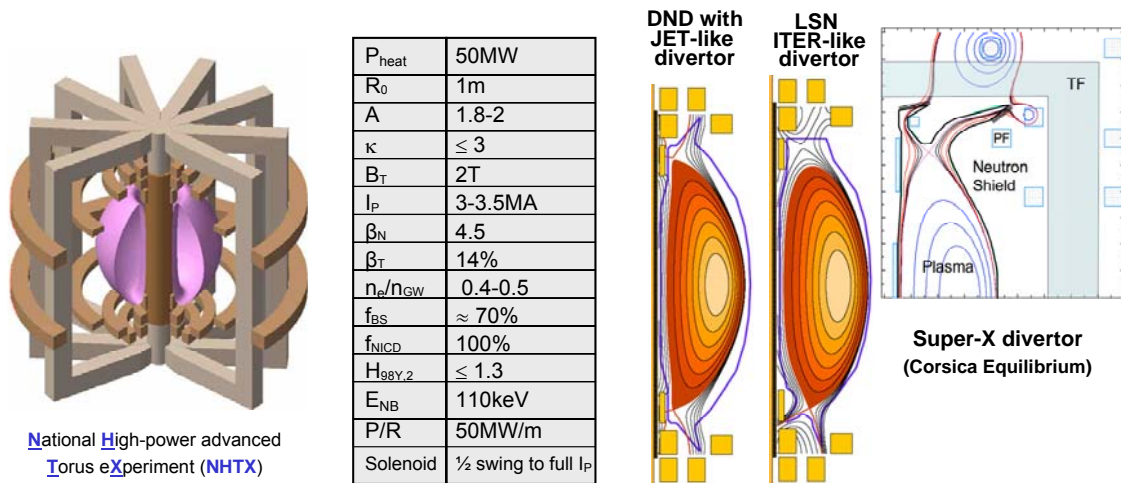


Figure 1.4.2.1: (Left) 3D cut-away of NHTX coils and plasma, (middle) device parameters for the base-line operating scenario, and (right) examples of plasma shapes and divertor configurations that could be accessed in NHTX including a JET-like, ITER-like, and “Super-X” divertor.

### 1.4.3. Mission, design concept, and operating parameters for ST-CTF

As described in Section 1.4.1, the ST is potentially very well suited to address FESAC panel Theme C, “Harnessing Fusion Power” – a critical gap that must be addressed to progress from ITER burning plasmas to an electricity producing DEMO. The goal of performing component testing with nuclear conditions relevant to DEMO with potentially significantly reduced risk, cost, and tritium consumption as compared to performing the same R&D in DEMO itself motivates the mission of the (ST-based) CTF program, namely:

***“Create a lowered-risk, reduced-cost approach to a fusion environment beyond the ITER level, and utilize it to test, discover, innovate, and develop the remaining needed engineering science and technology knowledge base for Demo.”***

*(From “Bridging Engineering Science and Technology Gaps From ITER to DEMO” – M. Peng et al., APS-DPP meeting Nov. 12-16, 2007)*

This mission aims to exploit the following potential advantages of the ST for component testing:

1. Compact device and high- $\beta$  operation
2. Reduced device cost
3. Reduced operating cost ( $P_{\text{electric}}$ )
4. Reduced T consumption
5. Simplified vessel and magnets
6. Fully modularized core components
7. Fully remote assembly and disassembly

The ST-CTF design concept geometry, parameters, and an example of how device modularity could facilitate assembly/disassembly and maintainability are shown in Figure 1.4.3.1.



**ST-based Component Test Facility (ST-CTF)**

Performance metrics	ITER	Required Conditions	Demo Goals
Continuous operation	~hour	weeks	~months
14-MeV neutron flux on module (MW/m <sup>2</sup> )	~0.8	1.0-2.0	~3
Total neutron fluence goal (MW-yr/m <sup>2</sup> )	~0.3	6	~6-15
Duty factor goal	~1%	30%	~80%
Tritium self-sufficiency goal (%)	~0	~100	≥100

W <sub>L</sub> [MW/m <sup>2</sup> ]	0.1	1.0	2.0
R0 [m]	1.20		
A	1.50		
kappa	3.07		
q <sub>cyl</sub>	4.6	3.7	3.0
Bt [T]	1.13	2.18	
I <sub>p</sub> [MA]	3.4	8.2	10.1
Beta <sub>N</sub>	3.8		5.9
Beta <sub>T</sub>	0.14	0.18	0.28
n <sub>e</sub> [10 <sup>20</sup> /m <sup>3</sup> ]	0.43	1.05	1.28
f <sub>BS</sub>	0.58	0.49	0.50
T <sub>avg1</sub> [keV]	5.4	10.3	13.3
T <sub>avg2</sub> [keV]	3.1	6.8	8.1
HH98	1.5		
Q	0.50	2.5	3.5
P <sub>aux-CD</sub> [MW]	15	31	43
E <sub>ND</sub> [keV]	100	239	294
P <sub>Fusion</sub> [MW]	7.5	75	150
T M height [m]	1.64		
T M area [m <sup>2</sup> ]	14		
Blanket A [m <sup>2</sup> ]	66		
F <sub>n-capture</sub>	0.76		
P/R [MW/m]	14	38	61
<b>Solenoid</b>	Small iron core or mineral insulated transformer for startup		

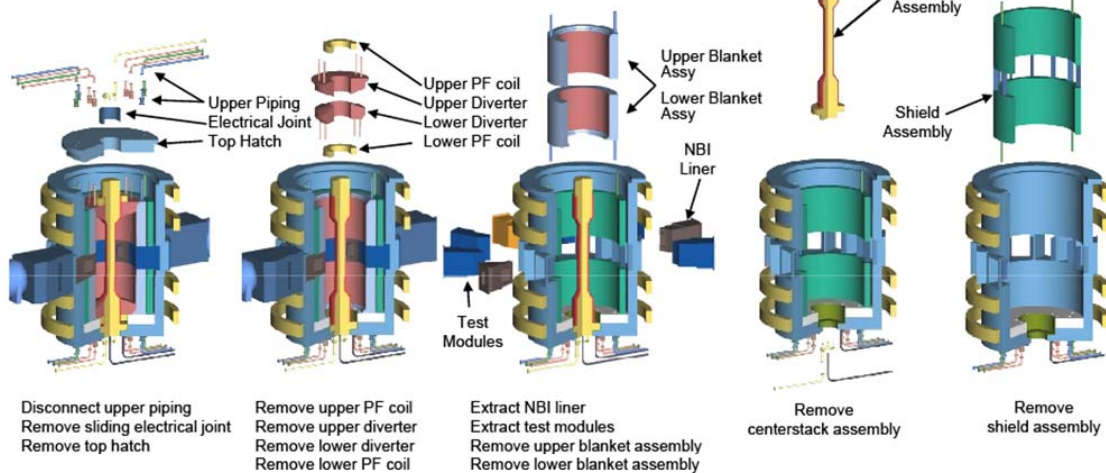
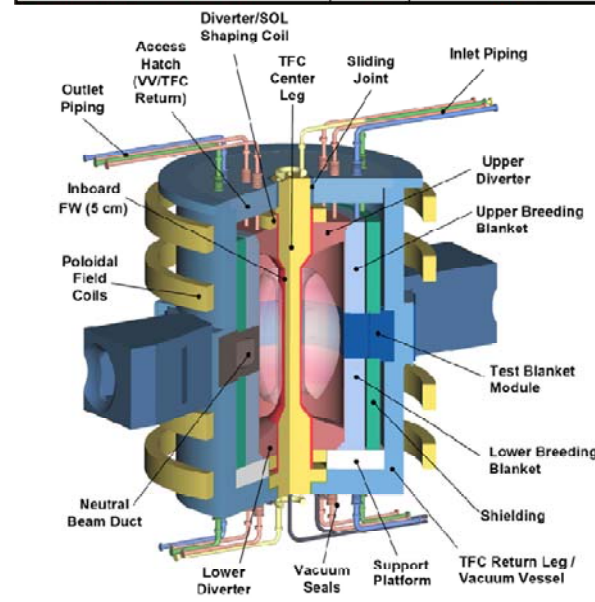


Figure 1.4.3.1: (Top left) Required performance and nuclear conditions for a CTF mission and for DEMO goals, (middle left) ST-CTF design concept, (right top) table of parameters for ST-CTF, and (bottom) example of how an ST CTF device with modular design could facilitate assembly/disassembly and maintenance.

### 1.4.4. Design concept and operating parameters for an ST reactor

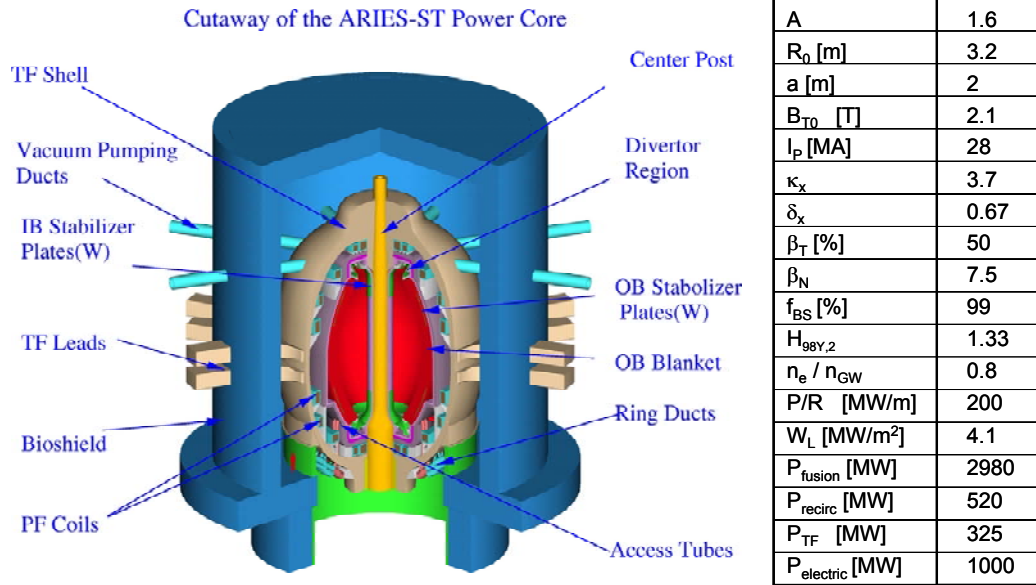


Figure 1.4.4.1: (Left) ARIES-ST design concept and (right) table ARIES-ST parameters.

The design requirements to optimize a tokamak, ST, or stellarator-based power reactor have been studied extensively by the ARIES reactor studies group (<http://www-ferp.ucsd.edu/aries/>). The design concept and plasma and fusion parameters for an ST-based reactor (ARIES-ST) are shown in Figure 1.4.4.1. As for ST-CTF, there is a single-turn central TF bundle and the vacuum vessel provides the current return for the TF current. Similar to advanced tokamak reactor concepts, ARIES-ST relies heavily on operation far above the no-wall stability limit (i.e.  $\beta_N = 7.5 = 90\%$  of ideal-wall  $\beta_N$  limit = 8.3), nearly all the plasma current is provided by the bootstrap current, and the elongation is maximized ( $\kappa_x$  up to 3.7 in ARIES-ST) to maximize the toroidal beta at high bootstrap fraction. One issue for the ST-based reactor is the relatively high resistive power dissipation ( $\approx 300$  MW) in the TF coil which reduces the overall plant efficiency. However, the cost of electricity (COE) is driven primarily by the plant capital cost. The COE of ARIES-ST (78 mill per  $kW_e$  h in 1992 dollars) is very close to that computed for superconducting tokamaks such as ARIES-RS (76 mill/ $kW_e$ h) using design assumptions from the mid-to-late 1990's. For the more recent ARIES-AT studies, improvements in technology

including higher thermal conversion efficiency blankets (59% thermal conversion efficiency vs. 45% assumed for ARIES-ST) and other cost reductions account for a significant reduction of COE to 50 mill/kW<sub>e</sub>h. The low COE of ARIES-AT is attractive because it is competitive with present electricity costs adjusted for inflation. Preliminary estimates indicate that if ARIES-ST could utilize higher efficiency blankets and operate near ~1.5GW<sub>e</sub>, COE values much closer to those of ARIES-AT values are achievable. However, more detailed design studies are needed to assess if such design modifications and COE reductions are possible for ST-based reactors.

## 1.5 Gaps Between Present and Future STs

All of the future ST concepts described in Section 1.4 require advances in plasma performance and understanding to achieve their stated missions. Present MA-class ST experiments (NSTX and MAST) have progressed significantly in the last decade – particularly in sustaining high normalized performance as described in Chapter 6. However, as shown quantitatively in Table 1.5.1, several gaps between present and future ST performance remain.

For the NHTX and ST-CTF device concepts, NSTX already achieves bootstrap fraction and elongation values comparable those assumed, and achieves  $\beta_N$  values above those assumed. However, significant increases in NBI current drive are needed to achieve fully non-inductive current drive. Much of this increased current drive can be achieved via reduced electron collisionality as a result of increased electron temperature and/or reduced normalized density. In order to maximize NBI current drive, ST-CTF is projected to operate at  $n_e/n_{\text{Greenwald}} = 0.25-0.3$  which is approximately 1/3 of the normalized density presently achieved in H-mode (without active pumping). ST-CTF is also projected to require up to 50% higher H-factor  $H_{98-IPB(y,2)}$  than presently achieved in order to minimize device size and power requirements. While NHTX is designed to include a solenoid for ramp-up to  $I_p$  flat-top, ST-CTF is designed to have minimal (or no) central solenoid, so plasma current start-up and ramp-up to high plasma current (up to

Present high $\beta_N$ & $f_{NICD}$	NSTX	NSTX-U	NHTX	ST-CTF	ARIES-ST
A	1.53	1.65	1.8	1.5	1.6
$\kappa$	2.6-2.7	2.6-2.8	2.8	3.1	3.7
$\beta_T$ [%]	14	10-16	12-16	18-28	50
$\beta_N$ [%-mT/MA]	5.7	5.1-6.2	4.5-5	4-6	7.5
$f_{NICD}$	0.65	1.0	1.0	1.0	1.0
$f_{BS+PS+Diam}$	0.54	0.6-0.8	0.65-0.75	0.45-0.5	0.99
$f_{NBI-CD}$	0.11	0.2-0.4	0.25-0.35	0.5-0.55	0.01
$f_{Greenwald}$	0.8-1.0	0.6-0.8	0.4-0.5	0.25-0.3	0.8
$H_{98y2}$	1.1	1.15-1.25	1.3	1.5	1.3
<b>Dimensional/Device Parameters:</b>					
<b>Solenoid Capability</b>	Ramp+flat-top	Ramp+flat-top	Ramp to full $I_p$	No/partial	No
$I_p$ [MA]	0.72	1.0	3-3.5	8-10	28
$B_T$ [T]	0.52	0.75-1.0	2.0	2.5	2.1
$R_0$ [m]	0.86	0.92	1.0	1.2	3.2
a [m]	0.56	0.56	0.55	0.8	2.0
$I_p / aB_{T0}$ [MA/mT]	2.5	1.8-2.4	2.7-3.2	4-5	6.7

Table 1.5.1: Comparison of key dimensionless and dimensional parameters of present high non-inductive current fraction scenarios in NSTX, and those proposed for NSTX-Upgrade, NHTX, ST-CTF, ARIES-ST.

8MA) are required. Thus, high priority NSTX research goals for 2009-13 include access to reduced density and collisionality, improved thermal confinement and improved understanding of thermal confinement to reliably project to future ST devices, and a demonstration of non-inductive plasma current ramp-up from low (~200kA) to intermediate (~400kA) current values.

For the ST-DEMO device concept, a significant increase in bootstrap current (from  $f_{vp} \approx 55\% \rightarrow 100\%$ ) is required relative to presently achieved values at high  $\beta_T$ . As described in Chapter 6, HHFW-heated plasmas at low current have achieved up to 85% bootstrap fraction at  $\beta_N \approx 4$ , but with  $\beta_T < 4\%$ . Increased  $\kappa$  and  $\beta_N$  are required to access higher  $\beta_T$  at high  $f_{BS}$ . As described in Chapter 2, NSTX has stably achieved  $\kappa=3$  and has sustained  $\kappa = 2.7-2.8$ . At present, for  $q_{min} = 1.2-1.5$ , the predicted and experimentally measured ideal-wall limit for the n=1 external kink is  $\beta_N \approx 6$ . Elevated  $q_{min} > 2.2-2.4$  is projected to increase the n=1 ideal-wall limit to  $\beta_N \approx 7-8$ . Thus, a major NSTX performance goal for 2009-13 is to access high  $\beta_N > 6$  plasmas at high  $\kappa$  up to 3 with elevated  $q_{min} > 2$  to increase the bootstrap fraction toward ST reactor values.

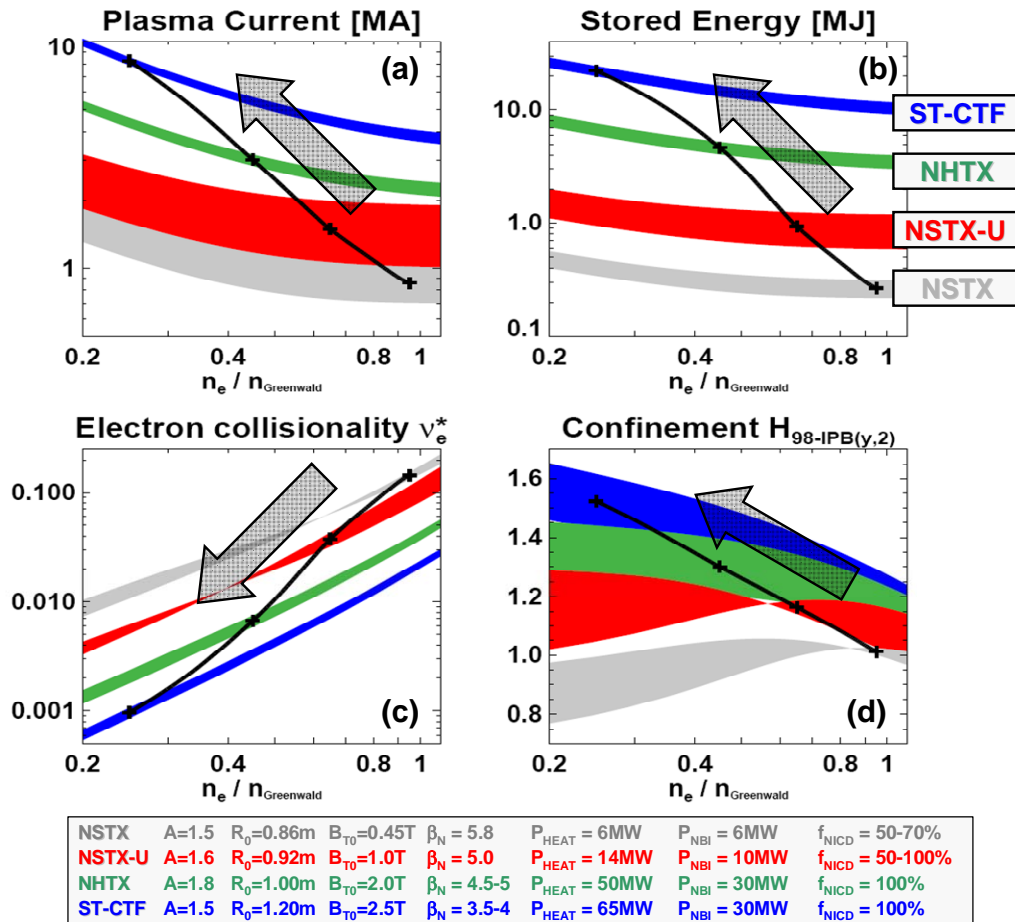


Figure 1.5.1: Progression of (a) plasma current, (b) stored energy, (c) normalized electron collisionality, and (d) H-mode confinement enhancement vs. normalized density for proposed NSTX, NSTX-Upgrade and possible future ST devices. Note that NSTX and NSTX-U operate with a range of non-inductive fractions, whereas NHTX and ST-CTF curves assume fully non-inductive operation.

An ITER-era (20 year) goal under consideration by the U.S. ST community is to develop the ST knowledge-base to enable design and begin construction of an ST-CTF device. As shown in Figure 1.5.1, achieving ST-CTF conditions requires an extrapolation of 1 order of magnitude in current and 2 orders of magnitude in stored energy in a device only 40% larger in major radius than NSTX. In terms of dimensionless parameters, this entails a 2 order of magnitude decrease in collisionality and a seemingly modest H-mode confinement enhancement of 1.5. However, the strong power degradation of H-mode confinement implies that a roughly 3-fold increase in heating power would be required to compensate for an inability to increase  $H_{98}$  from 1.0 to 1.5.

## 1.6 Research Goals and Opportunities in NSTX

### 1.6.1 Overview

As discussed in Section 1.5, the dimensionless parameter most significantly altered along the ST-path from NSTX to ST-CTF is the normalized electron (and ion) collisionality. As shown in Figure 1.5.1, the first factor of 4 decrease in collisionality along this path can be accessed and diagnosed with upgrades to NSTX (i.e. NSTX-Upgrade = NSTX-U) – in particular a new center-stack to double the magnetic field and plasma current, a liquid lithium divertor (LLD) for density control, a range of advanced profile and turbulence diagnostics, and a 2<sup>nd</sup> more tangential NBI system for increased heating power, non-inductive current drive efficiency, and current drive flexibility. More detailed timelines for facility and diagnostic upgrades for the next 5 years are provided in Chapter 7. As described in Chapter 3, reductions in collisionality can be achieved by operating at lower density and reduced  $q$ , and NSTX-U can in principle achieve the electron collisionality of NHTX to within a factor of 2. As described in Chapters 2-6, reduced collisionality has the potential to impact a wide range of physics issues in ST plasmas including:

- Macroscopic Stability
  - RWM critical rotation and neoclassical viscous torques may increase at lower  $v_i$
- Transport & Turbulence
  - Underlying instabilities (micro-tearing, TEM, and ETG) scale differently versus  $v^*$ . Micro-tearing modes are expected to be stabilized at reduced collisionality, and reduced collisionality can be stabilizing for dissipative-TEM or de-stabilizing for collisionless-TEM.
  - If  $T_e(r)$  is set by a critical  $\nabla T_e$ , H-mode confinement may be reduced at reduced  $n_e$
- Boundary Physics
  - ELM  $\Delta W_{ped}$  increases at lower  $v_e^*$  - could impact confinement, plasma purity, divertor
  - ELM stability may improve at lower  $v_e^*$  due to second-stability access

- Detachment for heat flux reduction will be more challenging at reduced SOL density
- Wave-Particle Interaction
  - AE avalanches may be more easily triggered at reduced  $n_e$  due to increased fast-ion pressure fraction resulting in possible fast-ion redistribution and/or loss
- Current Start-up and Ramp-up
  - NBI-CD and RF-CD efficiency for ramp-up are increased at reduced  $n_e$ , increased  $T_e$
- Current Sustainment
  - Steady-state scenarios rely on reduced  $n_e$  and increased  $T_e$  to increase NBI current drive efficiency to achieve 100% non-inductive current fraction.

While understanding the role of decreased collisionality is clearly important in future ST research, additional research questions and opportunities exist for all NSTX topical science areas. These questions and opportunities are described in much greater detail in Chapters 2-6, but highlights are provided below. In the descriptions below, key scientific questions for the ST (and tokamaks) are described and motivate the proposed major upgrades to NSTX.

### 1.6.2 Opportunities in Macroscopic Stability Research

As described in Chapter 2, advanced operating scenarios of the ST and tokamak require high normalized plasma pressures, and are therefore susceptible to dangerous large-scale instabilities. Such instabilities can lead to complete loss of confinement of the plasma and damage to the plasma facing components in next-step devices. Stabilizing these modes requires a nearby conducting wall and a combination of plasma rotation and/or active control coils. Experiments on NSTX have already provided data on stabilization physics in a conductor and coil geometry similar to that of ITER, but in a unique regime of rotation, collisionality, and toroidicity parameter space as described in Section 1.2.

NSTX has demonstrated passive stabilization of large-scale modes, and has also demonstrated active feedback control at ITER-relevant low plasma rotation. However, many questions remain

regarding the physics of stabilization by plasma rotation and/or active control. In particular, the reduction of plasma collisionality by up to an order of magnitude will provide access to a new collisionality regime ( $\nu$ -regime vs. present  $1/\nu$  regime) in NSTX to fully test the theory of Neoclassical Toroidal Viscosity (NTV) rotation damping in conditions closer to those of next-step STs and ITER while also clarifying the important effects of tokamak plasma response to 3D fields. Access to reduced collisionality will enable the determination of the relative importance of collisional versus collisionless/kinetic dissipation in resistive wall mode (RWM) stabilization for STs and for ITER. Further, the ability to vary the magnetic field and current over a large factor will clarify the relative roles of Alfvén and ion thermal effects in RWM rotational stabilization. By enabling up to a factor of three variation in magnetic field and current and factor of ten variation in collisionality, the major upgrades of NSTX will provide unique and definitive data on large-scale mode instability thresholds and the physics of rotation drag by 3D fields. This unique NSTX data coupled with advanced linear and non-linear stability and feedback control codes will greatly aid the development of a predictive capability for sustaining very high plasma pressures.

Further, there is the opportunity to assess the stability of advanced ST operating regimes in NSTX. As described in Chapter 6, NSTX-U (higher TF and 2<sup>nd</sup> NBI) is predicted to be capable of sustaining fully non-inductively-driven plasmas with  $q_{\min} > 2$ . Such scenarios are predicted to have ideal-wall  $\beta_N$  limits of 7-8, and these high  $\beta_N$  states are particularly relevant to ST-DEMO. In such plasmas, multiple RWMs of different toroidal mode number may be unstable, and the proposed Non-axisymmetric Control Coils (NCC) may be required to stabilize very high  $\beta_N$  plasmas in NSTX in addition to their potential use for controlling ELMs. Demonstrating fully-non-inductive and sustained operation at high- $\beta_N$  in NSTX-U and NHTX would also improve the prospects for increased neutron flux ( $W_L = 1\text{MW/m}^2 \rightarrow 2\text{MW/m}^2$ ) and fluence in ST-CTF.



### 1.6.3 Opportunities in Transport and Turbulence Research

As described in Chapter 3, in present spherical torus experiments, ion transport in neutral-beam heated H-modes is commonly measured to be near neoclassical levels – consistent with ion turbulence being suppressed by large shear in the plasma flow. In contrast, electron energy transport is observed to be anomalous, and commonly dominates the overall energy loss. In the ST, electron and ion transport scale differently with magnetic field and plasma current than they do in a conventional tokamak. This difference provides a unique opportunity to understand the underlying physics of electron transport. NSTX data exhibits a strong (nearly linear) scaling of electron confinement with magnetic field at larger minor radius in regions where  $\nabla T_e$  is largest. This is also the region in which the measured high-k fluctuations have turbulence characteristics consistent with ETG and correlate most strongly with the measured electron thermal diffusivity.

In NSTX, at least four instabilities are potentially responsible for anomalous electron transport: micro-tearing modes (electromagnetic), collisionless trapped electron modes – CTEM (electrostatic), electron temperature gradient modes – ETG (electrostatic), and Global Alfvén Eigenmodes – GAE (Alfvénic). Micro-tearing, ETG, and GAE modes have been correlated in a preliminary way with anomalous electron transport in NSTX. Multiple instabilities may be present simultaneously, and isolating the effects of individual instabilities can be difficult. Higher magnetic field and current will provide access to much lower collisionality allowing suppression of micro-tearing modes. Higher magnetic field will also provide access to reduced fast-ion instability drive and enable the reduction (possibly suppression) of GAE modes. Thus, access to higher magnetic field will enable the ability to control the onset of electromagnetic and Alfvénic modes and to separate the impact of these modes from electrostatic modes.

As described in Chapter 3, higher field and current will also reduce neoclassical ion transport by at least a factor of 3 (due to smaller orbit sizes and reduced collisionality) thereby enabling investigations of the extent to which shear-stabilization will suppress anomalous ion transport in future ST devices. This capability will also provide new insight into the underlying causes of

anomalous momentum transport (most likely ITG and/or CTEM) and the flow-shear suppression of ion turbulence in the ST. Reduced/suppressed ion turbulence is especially important for achieving a “hot-ion” H-mode regime for high fusion gain in ST-CTF.

Overall, the planned major upgrades of NSTX will greatly enhance the ability to isolate the roles of different micro-instabilities in anomalous electron and ion transport by doubling the achievable toroidal magnetic field and thereby increasing the range of magnetic field variation from a factor of 1.5 to a factor of 3. Importantly, the minimum collisionality made accessible by the major upgrades will approach (to within a factor of two) the collisionality values expected of NHTX at comparable Greenwald density fraction. Existing high-k diagnostics and planned low-k diagnostics (BES) will provide the ability to distinguish between the electrostatic CTEM and ETG modes, and BES and high-k may also be capable of measuring GAE fluctuations. Understanding the physics of electron and ion thermal transport is key to reliably predicting the performance of an ST-CTF.

#### **1.6.4 Opportunities in Energetic Particle Research**

As described in Chapter 4, an area of major importance to STs and ITER is the confinement of both injected energetic particles and fusion-produced  $\alpha$ -particles. At present, while the modes responsible for fast-ion transport have largely been identified, there is no quantitative predictive capability for the transport of fast ions by fast-ion-driven instabilities. Because of its low magnetic field and higher fraction of fast-particle pressure, an ST can be unstable to a variety of instabilities driven by energetic particles. These instabilities can lead to significant redistribution or loss of fast ions from the plasma. This results in degraded self-heating of the plasma and increased flux of fast particles to localized regions of the plasma facing components. Next-step ST devices are expected to rely heavily on auxiliary heating and current drive from injected fast ions, so understanding and minimizing (possibly even controlling) the redistribution and/or loss of fast ions by instabilities is a very important issue. Further, experiments in an ST can simulate

and diagnose the complex multimode interactions expected in ITER and next-step devices more closely than can experiments in other configurations.

The fast-ion instabilities thought to influence fast-ion transport most strongly are high frequency modes existing at a fraction of the fundamental cyclotron frequency (sub-cyclotron), and lower frequency modes near the Alfvén frequency. Higher magnetic field will decrease the ratio of fast ion speed to Alfvén speed ( $v_{\text{fast}}/v_{\text{Alfvén}}$ ) and is expected to be stabilizing for both the Compressional Alfvén Eigenmode (CAE) and Global Alfvén Eigenmode (GAE) sub-cyclotron modes. In contrast, the lower frequency Toroidal Alfvén Eigenmode (TAE) and Reverse Shear Alfvén Eigenmode (RSAE) are expected to remain unstable at higher magnetic field, primarily because the velocity space instability drive increases as  $v_{\text{fast}}/v_{\text{Alfvén}}$  decreases toward the most unstable value of  $\approx 2$ . This destabilizing effect is expected to dominate the overall stability provided the fast-ion beta is not strongly reduced by increased magnetic field. Further, as the magnetic field is increased, the fast-ion orbit size is reduced by the same factor and moves closer to the regimes of next-step STs and ITER. Both the number of modes and the most unstable mode number are expected to increase linearly with magnetic field strength, and this will enable studies of avalanche physics in a regime where quasi-linear theory is expected to be more applicable, is more readily compared to non-linear kinetic MHD simulations, and is more similar to ITER conditions.

Overall, access to higher magnetic field in NSTX will enable control of the onset of high frequency Alfvén Eigenmodes and thereby enable a determination of the relative importance of low versus high frequency modes on fast-ion transport, and test the quasi-linear treatment of fast-ion transport. The doubling of the magnetic field strength in an upgraded NSTX will greatly enhance the ability to isolate and understand the roles of different Alfvénic modes on the transport of energetic ions in fusion plasmas.

In addition to the strong effects of magnetic field, the pitch angle distribution of the fast particles is an important determinant of low-frequency \*AE stability. More tangential injection of fast ions is expected to be destabilizing to TAE modes, and this increased drive is expected to lead to stronger bursting/chirping mode behavior and to increased fast-ion transport. The combination of increased toroidal field and more tangential injection will dramatically widen the parameter space over which the transition from single-mode to multi-mode interactions responsible for increased fast-ion transport could be studied and understood. The planned NSTX upgrades will provide access to this widened parameter space, and in combination with advanced non-linear simulations will greatly aid the development of a predictive capability for the transport of fast ions by instabilities excited by fast ions in future STs and in ITER.

### **1.6.5 Opportunities in Boundary Physics Research**

As described in Chapter 5, the performance of the plasma-material interface is a critical issue for future ST devices, for ITER, and especially DEMO, as all will operate with higher heat fluxes and longer pulse lengths than existing tokamak facilities. The situation at the plasma-material interface is exacerbated by an instability known as an Edge Localized Mode (ELM), which can lead to very high transient heat loads and can damage the plasma facing components. Predictive understanding and control of both the steady-state and transient heat fluxes are essential. As highlighted in Section 1.4.1, because of the compact geometry of the ST, future ST devices are expected to operate with heat fluxes beyond those of ITER and approach (or reach) DEMO-level edge conditions. Thus, NSTX and next-step ST devices provide excellent environments to understand these plasma-material interactions and to develop the heat-flux mitigation techniques needed for magnetic fusion reactors.

A fundamental issue in tokamak and ST boundary research related to power exhaust is the understanding of transport of heat from the main plasma into the scrape-off-layer (SOL) to the plasma material interface (PMI) – specifically the divertor. The SOL transport properties determine the peak heat flux at the divertor and have major implications for the design of next-

step devices. While progress has been made at understanding parallel heat transport in the SOL, at present, even a rudimentary understanding of the scaling of the cross-field thermal transport (and corresponding peak divertor divertor heat-flux) remains elusive in both tokamaks and STs. However, the plasma collisionality and beta (or beta gradient) are thought to potentially play important roles in SOL cross-field transport. Increased magnetic field and power will enable tests of the collisionality and beta dependence of the SOL transport over a much broader parameter range, produce experimental SOL conditions and divertor heat-loads much closer to those of next-step ST devices, and provide unique data for comparison to edge turbulence models of SOL cross-field transport. Recent heat flux scaling studies in NSTX over a limited range of plasma current (700kA to 1MA) indicate a rapid narrowing of the divertor heat-flux width as the plasma current is increased. These scalings need to be developed over a much wider parameter range to improve their utility in projecting to future ST devices of much higher current (3-10MA). For example, using these scalings, very narrow midplane SOL profile widths (few mm) and high divertor heat-fluxes (10's of MW/m<sup>2</sup>) beyond ITER values are projected to be possible at higher field and heating power in NSTX-U. The proposed major upgrades of NSTX enabling access to higher magnetic field, current, and power will greatly enhance the ability to understand SOL transport physics and to better project divertor performance to future devices.

Given the seriousness of the divertor heat flux problem, NSTX is actively investigating potential heat flux mitigation techniques, including large expansion of magnetic flux and enhanced divertor radiation. NSTX has shown that lithium coating of plasma facing components can stabilize ELMs and improve confinement. This illustrates the complex role of the edge in affecting core turbulence and confinement. A liquid lithium divertor (LLD) module - a unique capability in the world fusion program - will be tested as a means to extend these benefits to new regimes while also providing particle control. Enhanced pumping capability from the LLD will expand the range of accessible edge collisionality to lower values, which in turn could strongly influence ELM stability. Pumping is required to control the core plasma density to achieve high current drive efficiency to enable fully non-inductive current drive. A long-pulse divertor

capability is also needed to support long-pulse plasma operation with stationary plasma conditions. While an LLD does not by itself reduce the peak divertor heat flux, an LLD may enable efficient pumping compatible with high flux expansion since the LLD is expected to provide pumping over its entire surface area. Further, active-cooling, flowing liquid lithium, and evaporative cooling could ultimately provide a means of steady-state heat removal from an LLD. As described in Chapters 5 and 6, an upgraded LLD combined with very high flux expansion (an X-divertor configuration) will be tested to assess the compatibility of an LLD with high heat flux, particle pumping, and sustained high-performance operation. A “Super-X” configuration for further peak divertor heat flux reduction is under consideration as a longer-term upgrade option. Such upgrades will provide the needed characterization and understanding of these potentially revolutionary divertor technologies for use in NHTX and ST-CTF.

### **1.6.6 Opportunities in Plasma Formation and Sustainment Research**

As described in Section 1.2.5 and Chapter 6, techniques for plasma current start-up, ramp-up, and sustainment must be developed for next-step STs and could be beneficial for tokamak reactors. On NSTX, plasma start-up techniques such as Coaxial Helicity Injection (CHI) have generated up to 20% of the nominal high-performance operating current, and CHI has recently been coupled to inductive operation in NSTX. NSTX has also sustained up to 70% of the plasma current at high plasma performance with a combination of pressure-gradient-driven “bootstrap” current and neutral beam injection current drive (NBI-CD). Thus, the largest gap in achieving completely solenoid-free ST operation is arguably the plasma-current ramp-up phase between plasma start-up and plasma sustainment.

As described in Chapters 4 and 6, fast Alfvén waves with frequencies at high multiples of the ion-cyclotron frequency (High-Harmonic Fast-Waves - HHFW) have driven up to 85% of the plasma current at low plasma current with bootstrap (BS) current in high-confinement-mode (H-mode) plasmas in NSTX. Increased plasma ramp-up current can be obtained with additional bootstrap current and/or RF current drive. Increased RF heating power could increase the

plasma pressure and bootstrap current, and higher toroidal field would increase the magnetic safety factor and lower the normalized beta by a similar factor (at fixed poloidal beta), thereby improving the plasma stability of high bootstrap fraction over-driven plasmas. Higher toroidal field should also largely eliminate parasitic surface wave losses of the HHFW for high phase velocity current-drive phasing, thus enabling RFCD during the ramp-up phase. Quantitatively, the planned doubling of the toroidal field and doubling of the HHFW heating power (made possible by antenna upgrades) are projected to enable demonstration of non-inductive plasma current ramp-up from low (~200-250kA) to intermediate (~400-500kA) current values.

In next-step ST devices, neutral beam injection (NBI) will very likely provide the majority of auxiliary heating power and a significant fraction (30-50%) of the steady-state current drive. Thus, NBI heating and current drive will also very likely be the preferred method of plasma current ramp-up. However, in present ST devices, NBI current ramp-up is difficult to test because neutral-beam injected fast ions are poorly confined at currents only 30% (approximately) below the nominal operating current. Higher plasma current and NBI power are required to test NBI current ramp-up physics. In particular, the complex interplay between the beam-driven current and instabilities commonly triggered by the evolving current and pressure profiles (both thermal and fast-ion) requires much more extensive investigation. The major upgrades of NSTX to higher field, current, and NBI power with more tangential injection will enable assessments of NBI current drive efficiency (and possibly NBI-driven plasma current ramp-up) under conditions similar to the early ramp-up phase of an ST-CTF.

As described in Chapter 6, demonstrating and understanding full non-inductive sustainment is also essential for the ST concept. Efficient off-axis current drive is needed to sustain a fully non-inductive current profile with a minimum  $q \sim 1.2$  to 1.5 to avoid deleterious core MHD activity. More tangential beam injection can increase the current drive efficiency relative to present NBI injection geometries while also driving current off-axis. Higher toroidal field in combination with more tangential injection should enable tests of fully non-inductive scenarios operating far

from disruptive limits as envisioned for robust ST-CTF operation. Fully non-inductive scenarios with minimum  $q > 2$  will also become accessible at high plasma confinement. These scenarios are much more likely to be inherently free of low- $n$  neoclassical tearing modes (NTMs) and could largely eliminate the need for active NTM control in future ST devices. Accessing this physical regime and understanding its properties are very important for an ST-CTF, and would provide key data for understanding similar regimes that must be developed at higher aspect ratio for fully non-inductive operation of ITER. The proposed doubling of the toroidal field and more efficient off-axis current drive from a 2<sup>nd</sup> NBI in an upgraded NSTX will provide the means for achieving, sustaining, and understanding fully non-inductive operation in NSTX, next-step STs, and beyond.



## 1.7 NSTX Long-term Goals

As described in Section 1.1, the highest priority of the NSTX research program for 2009-2013 is to develop the ST knowledge-base and to develop attractive ST operating scenarios and configurations to enable the ST to be utilized as a next-step facility in support of DEMO. Major upgrades to NSTX are proposed within the next 5 year period to strongly address these objectives, and research utilizing these upgrades will extend into the next 5 year (2014-2018) period. Shown in Figure 1.7.1 are the major upgrades and scientific objectives of the NSTX 10 year research plan consistent with achieving the highest priority objectives. More detailed timelines for facility and diagnostic upgrades for the next 5 years are provided in Chapter 7, and detailed research plans are provided in Chapters 2-6.

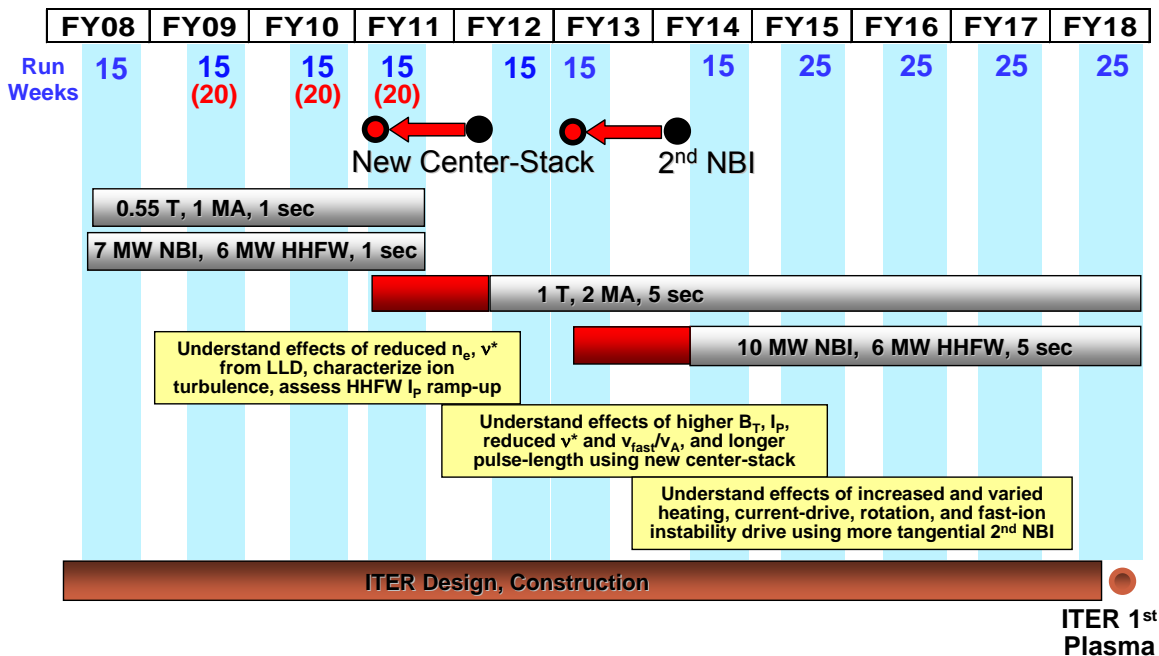


Figure 1.7.1: NSTX 10 year research timeline highlighting the timing of the proposed major upgrades and the roles of the major upgrades in research as summarized in the yellow boxes. The “base” research plan assumes a 15% increment over FY08 funding levels, and the “incremental” research plan shown in red assumes a 25% increment over FY08 funding levels. The incremental plan enables acceleration of the major upgrades by 1 year, provides additional run-time, and enhances (not shown) divertor, diagnostic, and EBW capabilities.

## 1.8 NSTX Scientific Organizational Structure

The NSTX scientific organizational structure is organized by topical science area into “Topical Science Groups” (TSGs). These groups have been formed to sustain scientific and programmatic focus beyond the annual milestones, and as such, tenure for the leadership team of a TSG is expected to be 2 years, but this leadership is both flexible and renewable. The TSG leaders are expected to share responsibilities among the team members and to try to achieve consensus on priorities from all members involved in a particular topical science area. The TSG leadership structure has one TSG leader, one deputy leader (typically both experimentalists), and a third leader for theory and modeling support of the experiments. The inclusion of theory and modeling in the leadership structure is designed to enhance the scientific coupling between theory and experiment in NSTX research. The TSG leadership responsibilities include:

1. Determine and address the highest priority scientific issues within a topical area through group discussion and consensus and including the NSTX team in TSG meetings
2. Organize the NSTX Research Forum guided by (but not limited to) these priorities
3. Define draft scientific/performance milestones utilizing expertise of the TSG
4. Organize, propose, and execute experiments to achieve milestones and address priorities
5. Define facility and theory resources required to achieve research goals
6. Aid dissemination of results (help Physics Analysis & Simulation Division)
  - a. Journal publications, seminars, colloquia, invited talks, conferences, ITPA, BPO
7. Provide brief summaries of TSG scientific progress at NSTX monthly team meetings and other venues to promote discussion
8. Assist and report to the NSTX Program and Project directors

The run coordination and topical science group structure (as of July 2008) is shown in Table 1.8.1 below. The NSTX five year plan chapters of this document are organized with a similar structure and were coordinated and/or written in large part by members of the TSG leadership. As described in the plan Appendix, NSTX collaborators play an essential role in leading the NSTX scientific program. As shown in Table 1.8.1, nearly half of the combined topical science group leadership, deputy leadership, and run coordination is provided by non-PPPL researchers.

### NSTX Scientific Organization for FY2008 Run

	<b>Coordinator</b>	<b>Deputy</b>	
<b>Run coordination</b>	Michael Bell	Roger Raman (Univ. Washington)	

<b>Topical Science Group</b>	<b>Leader</b>	<b>Deputy Leader</b>	<b>Theory / Modeling</b>
<b>Macroscopic Stability</b>	Steve Sabbagh (Columbia Univ.)	Stefan Gerhardt	Josh Breslau
<b>Transport and Turbulence</b>	Stan Kaye	Kevin Tritz (Johns Hopkins Univ.)	Taik-Soo Hahn
<b>Boundary Physics</b>	Vlad Soukhanovskii (LLNL)	Rajesh Maingi (ORNL)	Daren Stotler
<b>Wave-Particle Interactions</b>	Gary Taylor	Eric Fredrickson	Nikolai Gorelenkov
<b>Advanced Scenarios and Control</b>	David Gates	Jon Menard	Charles Kessel
<b>Solenoid-free Start-up and Ramp-up</b>	Roger Raman (Univ. Washington)	Dennis Mueller	Steve Jardin

*Table 1.8.1: NSTX scientific organizational structure for Run Coordination and Topical Science Group leadership as of July 2008.*

*This page intentionally left blank*

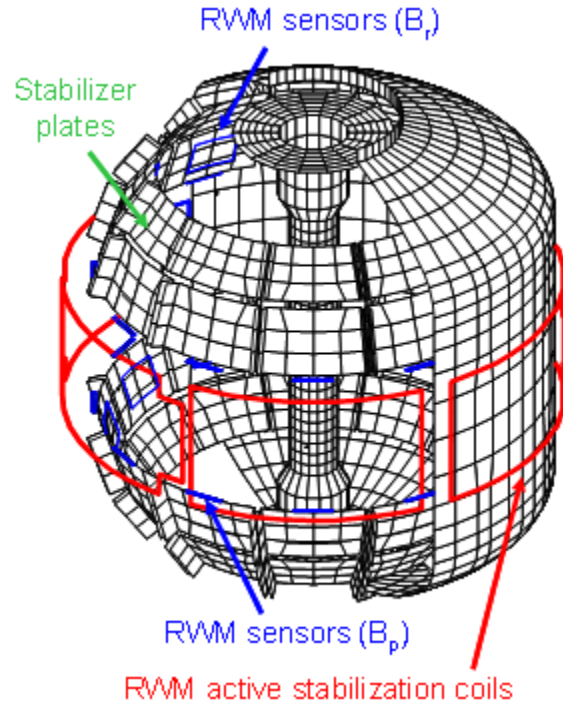
# Chapter 2: Macroscopic Stability

## Table of Contents

2	Macroscopic Stability.....	2
2.1	Maintaining High Beta Macroscopic Stability in the Spherical Torus.....	2
2.2	Overview of Research Plans for FY2009-2013.....	6
2.2.1	Long-term Research Goal .....	7
2.2.2	General Objectives of Macroscopic Stability Research.....	7
2.2.3	Top-level Research Goals by Topical Area .....	8
2.2.4	Overview of Major Device Upgrades Supporting Planned Research .....	10
2.2.5	Guidance for Macroscopic Stability Research Goals.....	11
2.3	Macroscopic Stability Results and Plans by Topical Area.....	12
2.3.1	High plasma shaping sustainment and global stability .....	12
2.3.2	Resistive wall mode control and stabilization physics.....	18
2.3.2.1	Active feedback control.....	18
2.3.2.2	Passive stabilization physics.....	36
2.3.3	Dynamic error field correction.....	45
2.3.4	Tearing mode / NTM physics.....	52
2.3.5	Plasma rotation and non-axisymmetric field-induced viscosity.....	62
2.3.6	Disruption physics, consequences, avoidance, and prediction.....	72
2.4	Timeline for Research Goals FY2009-2013.....	81
2.5	References .....	82

*This page intentionally left blank*

# Chapter 2



## 2 Macroscopic Stability

### 2.1 Maintaining High Beta Macroscopic Stability in the Spherical Torus

Economically attractive operation of a thermonuclear fusion reactor based on the tokamak magnetic confinement concept requires that the burning plasma maintain stability at high ratio of the plasma pressure to that of the confining magnetic field. Therefore, an important figure of merit for tokamak operation is the toroidal beta  $\beta_t \equiv 2\mu_0\langle p\rangle/B_{t0}^2$  where  $\langle p\rangle$  is the volume-averaged pressure and  $B_{t0}$  is the vacuum toroidal field at the plasma geometric center.

Stable high beta operation alone is insufficient for the tokamak design to yield an efficient steady-state reactor. Superior plasma equilibria will self-generate most, or all, of the plasma current via the pressure gradient driven neoclassical bootstrap effect, decreasing the auxiliary current drive power requirements. Since the bootstrap current is naturally driven closer to the plasma edge than the core, it creates broad

current profiles, and therefore equilibria with low plasma internal inductance,  $l_i$ . This leads to an apparent conflict of optimizing constraints, as tokamak experiments have shown that ideal magnetohydrodynamic (MHD) stability of large scale global modes with vacuum boundary (“no-wall”) conditions decreases with decreasing  $l_i$  [1,2,3]. This beta limit is typically characterized by the normalized beta  $\beta_N \equiv \beta_i(\%)a(m)B_0(T)/I_P(MA)$ . Since  $\beta_i \propto \beta_N^2$  at fixed bootstrap fraction and since fusion power output  $P_{fus} \propto \beta_i^2 \propto \beta_N^4$ , maximizing  $\beta_N$  is especially significant.

Tokamak research has shown that the inclusion of conducting wall (“wall-stabilized”) boundary conditions can lead to stabilization of global MHD modes [4,5] with especially high values of  $\beta_N$  and  $\beta_N/l_i$  predicted by ideal MHD theory [6] for tokamak designs with low aspect ratio – the spherical torus (ST) [7]. However, reactor design studies show that the favorable promise of stable high  $\beta_N$  and low  $l_i$  ST equilibria must be a reality to create an efficient steady-state ST reactor [8]. Therefore, it was critical that such conditions first be demonstrated, with subsequent demonstration that the conditions be maintained.

NSTX has demonstrated the promise of advanced tokamak operation in a mega-Ampere class spherical torus, and in present and future research moves forward to demonstrate the reliable *maintenance* of these conditions. An illustration of the evolution to the high  $\beta_N$  and  $\beta_N/l_i$  wall stabilized state is shown in Figure 2.1-1 and Figure 2.2.1-2. Accessing this operational state was a long-term plan that was defined during the conceptual design of the device. A milestone in the process was reaching the ideal “no-wall” limit, which was achieved after neutral beam heating was installed on the device, as illustrated in Figure 2.1-1 (further detail published in Ref. 9). The figure as published illustrated the planned paths to higher  $\beta_N$  operation in the device; this path was successfully executed with NSTX wall-stabilized plasmas now having reached  $\beta_N > 7$  and  $\beta_N/l_i > 11$ , as well as  $\beta_i > 39\%$  - significant low aspect ratio advanced tokamak equilibria (Figure 2.2.1-2). Three key practical elements to this success were the reduction of the static error fields in the device, the routine access to broad pressure profiles via H-mode operation, and maintaining the minimum  $q$  value greater than unity [10]. Maintenance of sufficient plasma rotation was also found to be important to this success, and the impact of the rotation profile on MHD stability remains a subject of active research.



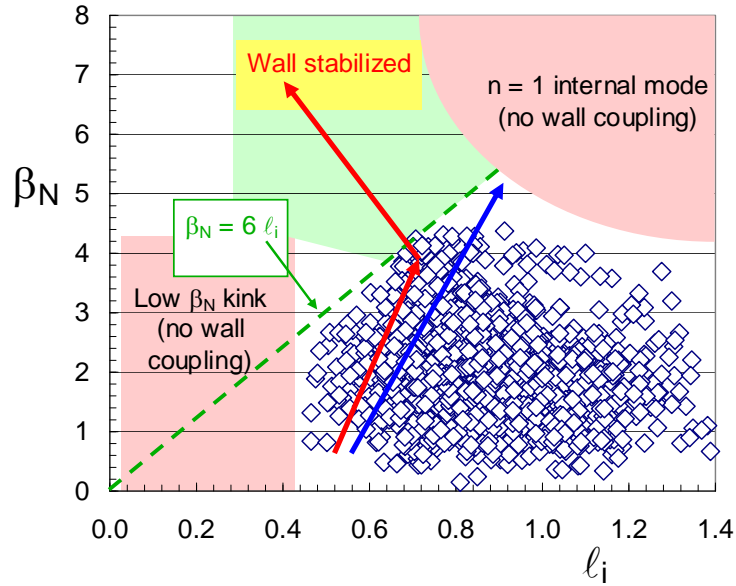


Figure 2.2.1-1 Early ( $l_i, \beta_N$ ) stability space operational diagram for NSTX (from Sabbagh, et al., Phys. Plasmas 2002).

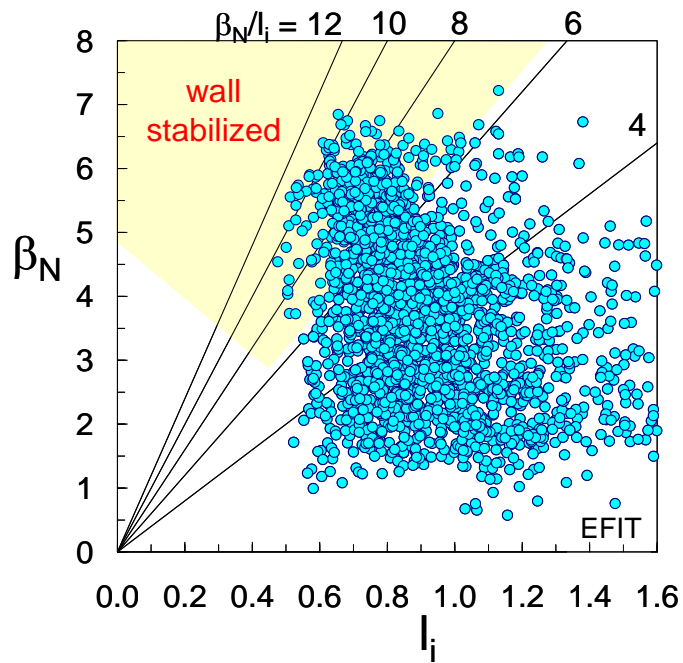


Figure 2.2.1-2 Wall-stabilized operation in NSTX at high  $\beta_N > 7$ ,  $\beta_N/l_i > 11$ .

The high beta, low  $l_i$  equilibria created to date on NSTX are significant advances, especially because any one of several factors might have led to a failure to reach these operational states required for successful and efficient ST reactor or CTF operation. For example, the low  $l_i$ , high bootstrap fraction equilibria produced may not have been wall stabilized, or H-mode pressure profiles may not have been sufficiently broad to allow the high  $\beta_N$  operation shown in Figure 2.2.1-2. The NSTX research shows that the original theoretical plan came to pass experimentally. The stability challenges faced so far have been met, and have created important understanding in several areas including kink/ballooning and resistive wall mode (RWM) stabilization, the behavior of the  $n=1/m=1$  mode, and long pulse operation including maintenance of  $q > 1$  [2,9,11,12].

The overarching goal for MHD research in the 2009 – 2013 period – reliable maintenance of the highest beta conditions – is a key step to ST development, leads to a knowledge base of advanced tokamak research at all device aspect ratios, and naturally follows from the present NSTX database. Plasma shaping research has produced high beta and confinement performance in plasmas with high bootstrap current fraction. Both kink/ballooning stabilization and passive resistive wall mode stabilization have been demonstrated producing plasmas at least 50% above no-wall limit,  $\beta_N^{no-wall}$ . Accessing higher elongation (up to 3) and shaping factors has also required plasmas with lower  $l_i$  to maintain vertical stability. Sustained operation of high  $\beta_N$  in such plasmas in the next five years is expected to extend stabilization to higher ratios of  $\beta_N / \beta_N^{no-wall}$ . Understanding when and how such stabilization fails is now of paramount importance, including the role of plasma rotation magnitude and profile, Alfvén frequency, ion collisionality,  $v_i$ , and aspect ratio. Active RWM stabilization has just begun on the device, with the key focus now on maintaining this stabilization indefinitely. Dynamic error field correction (DEFC) has shown sufficient effectiveness to maintain or slightly increase stabilizing plasma rotation, and will continue to be developed to maintain or increase plasma beta and confinement performance. The occurrence and impact of neoclassical tearing modes in low aspect ratio geometry will be investigated, including the dependence of mode onset on rotation, rotation shear, and bootstrap drive, the source of NTM triggering when  $q_{min} > 1$ , and fast particle redistribution. First-principles understanding of plasma rotation damping achieved in the last five years on NSTX will be tested further, examining for example the dependence on ion collisionality. This understanding can be used to generate the new techniques for maintenance or increase of plasma rotation that are proposed for the coming five year period. Disruption

studies will also be expanded in NSTX, examining important technical detail such as halo current generation, thermal and current quench studies, and first wall power distribution for future burning plasma devices.

It is expected that the planned NSTX MHD research for the 2009 – 2013 period in all of the areas proposed and roughly outlined above will benefit significantly from joint experiments with toroidal magnetic confinement experiments including MAST and DIII-D. The strength in joint MAST / NSTX experiments hinges on the uniqueness of the ST operating space (e.g. ultra-high beta approaching unity in the core plasma) while examining differences due to machine configurations. For example, comparison of global mode stability in MAST and NSTX will lead to further understanding the role of the conducting wall and plasma rotation in stabilization. A joint experiment to study neoclassical toroidal viscosity has been proposed to be run in 2008. The strength in joint experiments between NSTX and DIII-D hinge upon the complementarity of the devices. Examples of this include the large difference in Alfvén frequency (applicable to RWM stability theory) and the explicit aspect ratio dependence that appears in most neoclassical effects including NTM stabilization, RWM stability theory, and non-resonant plasma viscosity theory. Joint experiments have already been conducted between NSTX and DIII-D in the RWM topical area [13], and experiments in the 2007 and 2008 run periods have started joint research in the NTM area.

Note that MHD research during the 2009 – 2013 period in the important area of energetic particle modes will be covered in Chapter 4 of this document “Waves and Energetic Particles” and ELM stability will be covered in Chapter 5 “Boundary Physics”.

## *2.2 Overview of Research Plans for FY2009-2013*

MHD research on NSTX has produced high beta plasmas yielding several classes of beta-limiting instabilities. With transient beta goals established, and RMW/kink instabilities observed and documented, the natural emphasis of MHD research turns to (i) the physical understanding of beta-limiting and other deleterious modes and methods of stabilizing them and (ii) controlling these modes either directly or indirectly, while understanding the physics explaining this control. Another important approach to understanding and producing mode stabilization is through control of the underlying equilibrium profiles.

Two such areas to be addressed further in the coming five year period are the control of the plasma rotation and  $q$  profiles. This research applies to the ST development path toward future burning plasma devices and has direct application to the understanding of tokamak mode stabilization in general. The research utilizes the unique and complementary aspects of the advanced tokamak equilibrium produced in NSTX, including very high beta, low aspect ratio, and low  $l_i$  to leverage the validation of physical theories of key phenomena.

### 2.2.1 Long-term Research Goal

*Demonstrate high reliability, sustained operation of high confinement, high beta low aspect ratio tokamak plasmas operating near the computed ideal, with-wall  $\beta_N$  limit by gaining an understanding of the underlying mode stabilization physics and implementing appropriate control techniques.*

### 2.2.2 General Objectives of Macroscopic Stability Research

NSTX Macroscopic Stability research comprises two general objectives that support the long-term goal:

*(OBJECTIVE 1) advancement of the physics understanding of low aspect ratio, high beta tokamak plasma devices in support of a development path to sustained fusion generation in future devices*

NSTX has pioneered the operation of low aspect ratio, high beta plasma equilibria in a mega-ampere class device and has demonstrated ultra-high beta operation with high energy confinement. Several crucial and favorable physics results have resulted in a successful proof-of-principle demonstration of the low aspect ratio spherical torus concept as the baseline for a next-step device. The generation of relatively broad pressure profiles in H-mode operation increases MHD stability limits. The broad current profiles (low  $l_i$ ) of high performance equilibria yield superior alignment of the bootstrap current profile and open a large conducting wall-stabilized operating space. Sufficient plasma rotation induced by neutral beam injection affords passive RWM stabilization, allowing operation of the device at maximum  $\beta_t$  and  $\beta_N$ . The plasmas created to date in NSTX are advanced tokamak equilibria that were only envisioned (and highly desired) theoretically during the past period of conventional tokamak operation. CTF designs based on the ST can

expect with greater confidence the ability to operate at pressure and confinement levels required to meet fusion performance goals. The 2009 – 2013 research period in NSTX aims at solving key issues related to reliable long-pulse operation of these high beta equilibria, including operation at ultra high elongation (~ 3), RWM stabilization, NTM physics, maintenance of stabilizing plasma rotation, and an improved understanding of disruption physics, prediction, and mitigation techniques.

*(OBJECTIVE 2) applied stability physics understanding applicable to tokamaks in general, leveraged by the unique low aspect ratio and high beta operational regime of the device*

The key to successful extrapolation of techniques used in present tokamak experiments to future burning plasma devices is a first-principles understanding of the underlying physics. A powerful tool in this endeavor is the ability to test physics hypotheses in significant and different operational regimes. NSTX offers the ability for researchers to fully test key physics hypotheses in an operational space not accessible in other devices, for example in the important scaling parameters of beta and aspect ratio, which appear prominently in MHD stability theory and neoclassical transport theory. Having this unique and complementary ability to test key theories allows greater confidence in extrapolating theory to future devices, thereby reducing both risk and development time in the goal of fusion energy development.

### 2.2.3 Top-level Research Goals by Topical Area

- *High plasma elongation sustainment and global stability*  
*Goal: sustain stable, high beta operation at very high plasma elongation ~ 3 as a proof-of-principle for ST development and to confirm MHD stability theory in this operating space.*
- *Resistive wall mode control and stabilization physics*  
*Goal: Determine the physics of RWM stabilization, by both passive and active means, and apply this understanding to optimize and increase reliability of active stabilization in low aspect ratio plasmas. Use this information to provide greater confidence in models used to extrapolate RWM stabilization performance to future tokamaks including burning, and driven-burn plasma devices such as ITER and ST-CTF.*

- *Dynamic error field correction*

*Goal: Determine sources of dynamically changing error field due to inherent asymmetries in the device and the plasma physics responsible for amplification of these sources. Apply techniques that will dynamically cancel these fields to maintain plasma rotation and stability.*

- *Tearing Mode / NTM physics*

*Goal: Study neoclassical and classical tearing modes in the unique low aspect ratio, high beta, and large ion gyro-radius plasmas available in NSTX, in order to both extrapolate our understanding to future ST devices and provide data complementary to that from conventional aspect ratio tokamaks. Investigate the impact of these modes on plasma beta, rotation, fast particle redistribution, and the potential of low aspect ratio operation as being theoretically favorable for NTM stability. Determine scenarios that allow operation without these deleterious instabilities.*

- *Plasma rotation and non-axisymmetric field-induced viscosity*

*Goal: Continue to develop quantitative, first-principles physics models of non-axisymmetric field induced plasma viscosity for both resonant and non-resonant field, and apply results to create new techniques for imparting significant toroidal momentum to the plasma.*

- *Disruption physics, consequences, avoidance, and prediction*

*Goal: Characterize the effects of disruptions at low aspect ratio and high beta by measuring halo currents, and thermal and current quench characteristics. Develop methods to predict disruptions and mitigate their impact.*

### 2.2.4 Overview of Major Device Upgrades Supporting Planned Research

Several device upgrades (See Chapter 7) to NSTX will strongly support the goal of reliably sustained high beta operation with physics understanding for confident extrapolation toward a driven-burn ST-CTF. As discussed throughout this chapter, a critical element for testing stabilization physics of all beta-limiting modes and plasma rotation damping is operation at lower  $v_i$ . This will be afforded by an upgrade to the device center column that will allow a doubling of the toroidal field to the typical high field operational value of 0.5 T to 1.0 T and an increase in plasma current from a typical value of 1 MA to 2 MA. As the energy confinement time in NSTX scales favorably with both  $B_t$  and  $I_p$ , plasma stored energy could quadruple, exceeding 1 MJ, and  $v_i$  could decrease by an order of magnitude (Figure 2.2.4-1), to within a factor of 2 of the proposed NHTX (Section 1.4.1) device. This is especially important as neoclassical effects are expected to be amplified in this transition region from weakly to strongly collisionless operation. For example, the dependence of RWM stabilization (Section 2.3.2) and neoclassical toroidal viscosity on  $v_i$  (Section 2.3.5) can be tested at levels closer to an ST-CTF.

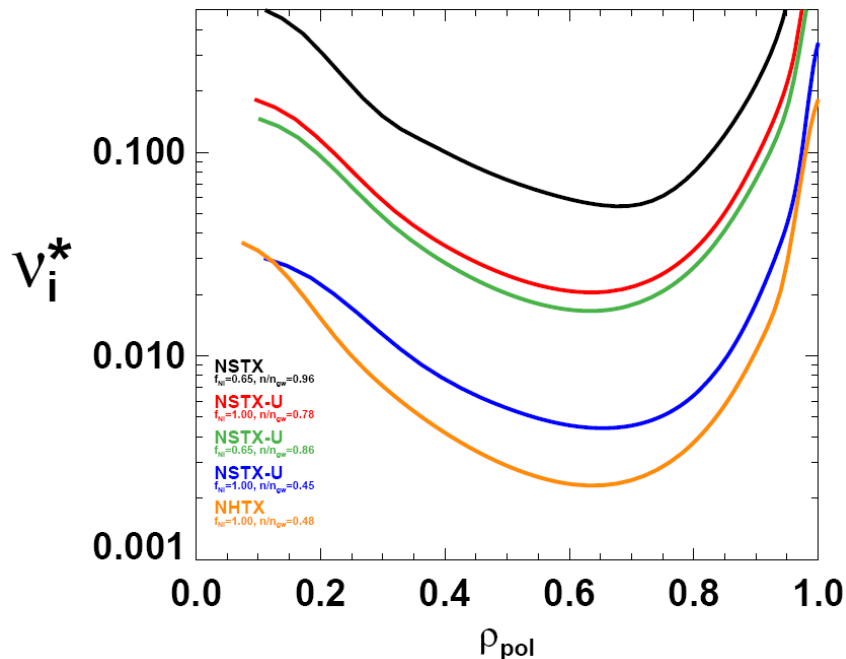


Figure 2.2.4-1 Profiles of the ion collisionality to bounce frequency ratio from TRANSP for an existing NSTX plasma (116313) compared to significantly reduced levels predicted for NSTX-U and NHTX at various non-inductive current fractions and Greenwald density ratios.

The addition of a second neutral beam source, planned for operation at the end of the five year plan period, will provide critical capabilities including alteration of the  $q$  profile to study the effects on MHD modes, especially NTMs, with a goal of stabilizing deleterious modes at elevated  $q > 2$  (see Section 6.3.2 and Figure 6.3.3 for  $q$  profile calculations for the upgrade). It will also provide greater ability to produce highly non-inductive high  $\beta$  plasmas that will be sustained for several seconds – suitable targets to demonstrate suppression or control of instabilities. A set of off-midplane non-axisymmetric control coils (NCC) are also planned (with incremental funding) to supplement the existing midplane control coils (see Section 2.3.2.1). These coils will serve several roles on NSTX including ELM and RWM control, and would provide important supporting research for ITER as the envisioned coil geometry closely resembles the present ITER VAC02 coil design (endorsed by the ITER Science and Technical Advisory Committee). Finally, very recent operation of NSTX with lithium evaporation on plasma facing components has demonstrated suppression of ELMs and mitigation of NTMs – a remarkable result for which the stability physics is yet to be understood. A phased plan of liquid lithium divertors (LLD - starting in 2009) has therefore become an important tool to better understand the underlying physical cause of MHD mode stabilization and to determine if the LLD is more or less effective in this role compared to the present lithium deposition system (LITER). Suppression of ELMs and NTMs eliminates energy dissipation by these modes, making them more susceptible to both resonant field amplification (RFA) by stable RWMs, and unstable RWMs, emphasizing the need for reliable feedback control of these modes in these conditions.

### *2.2.5 Guidance for Macroscopic Stability Research Goals*

Guidance for NSTX MHD research has always been closely linked to the needs of the ST development and general tokamak objectives as embodied in directives set by major US and world advisory committees. The 5 year plan for 2004-2008 followed IPPA guidelines. At present, the major research topical areas defined by the Fusion Energy Science Advisory Committee (FESAC) are followed. In 2008 the FESAC Toroidal Alternates Panel was formed and recently, with input from the ST community and the DOE Spherical Torus Coordinating Committee (STCC), has formulated a U.S. ST mission to “develop a compact, high beta, burning plasma capability for fusion energy”, and an ITER-era (20 year)



goal “to establish the ST knowledge base to construct a low aspect-ratio fusion component testing facility that provides high heat flux, neutron flux, and duty factor needed to inform the design of a demonstration fusion power plant”.

The long term research goal and objectives stated in Sections 2.2.1 and 2.2.2 directly support this mission and goal, as CTF designs show that producing sufficient levels of fusion neutron fluence requires high  $\beta_N$  operation approaching or above the ideal no-wall beta limit, and high duty factor requires steady high  $\beta_N$  operation with few or no disruptions. Specific, detailed guidance is provided to the NSTX Research Team in several ways, and at the yearly NSTX Research Forum, the team defines the prioritized research experiments for a run period consistent with U.S. fusion program goals. Experiments receiving the highest run priority in 2007 - 2008 addressed the largest subset of the following guidelines:

- 1) NSTX DOE milestones
- 2) ST physics – research to directly support the development of the ST
- 3) ITPA / BPO – research that serves stated ITPA joint experiments and USBPO initiatives
- 4) ITER issue cards – research supporting ITER issue cards (for 2007)
- 5) Joint experiments with other US facilities

### *2.3 Macroscopic Stability Results and Plans by Topical Area*

The balance of the document states present research results and plans by topical area stating (i) the goal of the research, (ii) present results of stability physics and control, (iii) research plans for the upcoming 5 year period, and (iv) a summarized timeline of the 5 year research plan.

#### *2.3.1 High plasma shaping sustainment and global stability*

**Goal:** *sustain stable, high beta operation at very high plasma elongation ( $\kappa \sim 3$ ) and shaping as a proof-of-principle for ST development and to confirm MHD stability theory in this operating space.*

##### **(i) physics and control - results**

The compact device size of an ST fusion reactor [14] or Component Test Facility [15] makes these devices attractive as it leads to a relatively low cost device compared to higher aspect ratio tokamaks. To optimize the efficiency of the system, it is crucial to run the device with high bootstrap current fraction  $f_{bs}$  and high  $\beta_t$ . Maximizing these parameters is equivalent to maximizing  $\beta_N$  and the plasma shaping parameter  $S_I \equiv q_{95}(I_p/aBt)$  since  $f_{bs}\beta_t \sim S_I\beta_N^2$  [16].

During the past five year period, a plan was executed to expand the initial equilibria created in the device [17] toward higher elongation and  $S_I$  [18]. The plasma control system (PCS) response time was improved to better control vertical instability, a substantial upgrade to the magnetic field sensors in the divertor region was made, real-time plasma boundary shape reconstruction (rtEFIT) was implemented to enable more accurate control of plasmas with higher  $S_I$ , and the center stack shaping coil PF1A was modified to allow the creation of high triangularity,  $\delta$ , simultaneous with high elongation,  $\kappa$ . The combined increase of these two parameters is required to produce the greatest increase in ideal MHD stability. Also,  $\delta$  has a much stronger effect on  $S_I$  at low aspect ratio than at high aspect ratio [19]. The PF1A coil modification is illustrated in Figure 2.3.1-1.

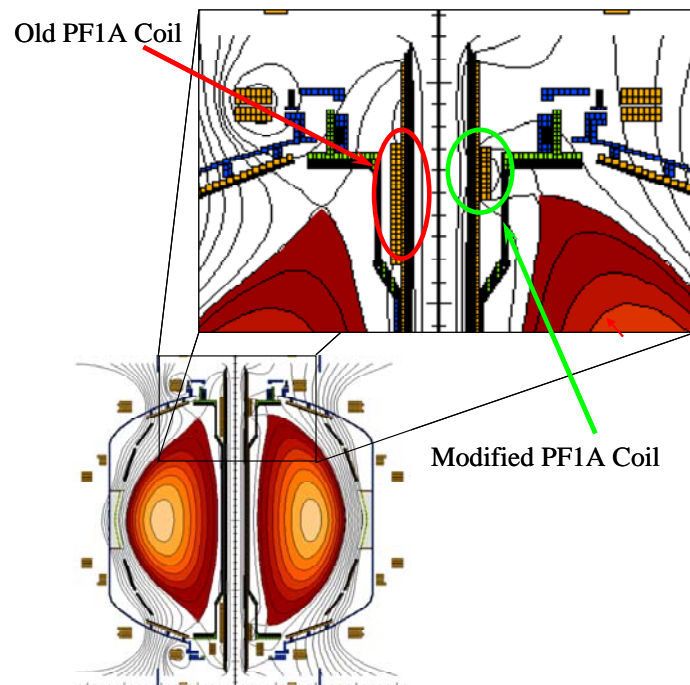


**Figure 2.3.1-1 Upgrade of PF1A coil has enabled simultaneous achievement of high  $\kappa$  and  $\delta$**

The successful expansion of the NSTX operating space in  $\kappa$  and  $\delta$  due to these improvements is summarized in Figure 2.3.1-2. Shots shown in the 2001 – 2003 period pre-date the improvements described above. As shown, the operating space was limited to  $\kappa \sim 2.2$ , with a small decrease from this value at the highest  $\delta \sim 0.85$ . The reduced latency of the PCS in 2004 led to a substantial increase in  $\kappa$  at intermediate  $\delta \sim 0.6$ . Finally, the PF1A coil upgrade (2005 – 2006 period shown) allowed access to high  $\kappa > 2.5$  and high  $\delta > 0.8$  simultaneously. Poloidal flux contours from equilibrium reconstructions illustrating this evolution and the increase in  $S_l$  attained are shown in Figure 2.3.1-3.

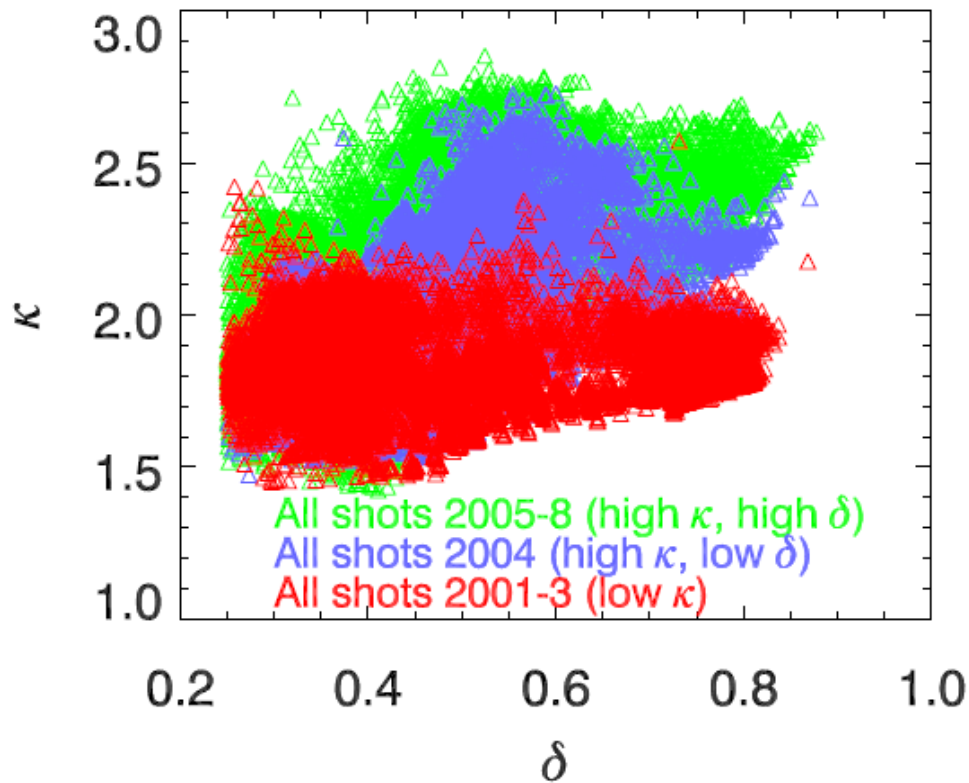
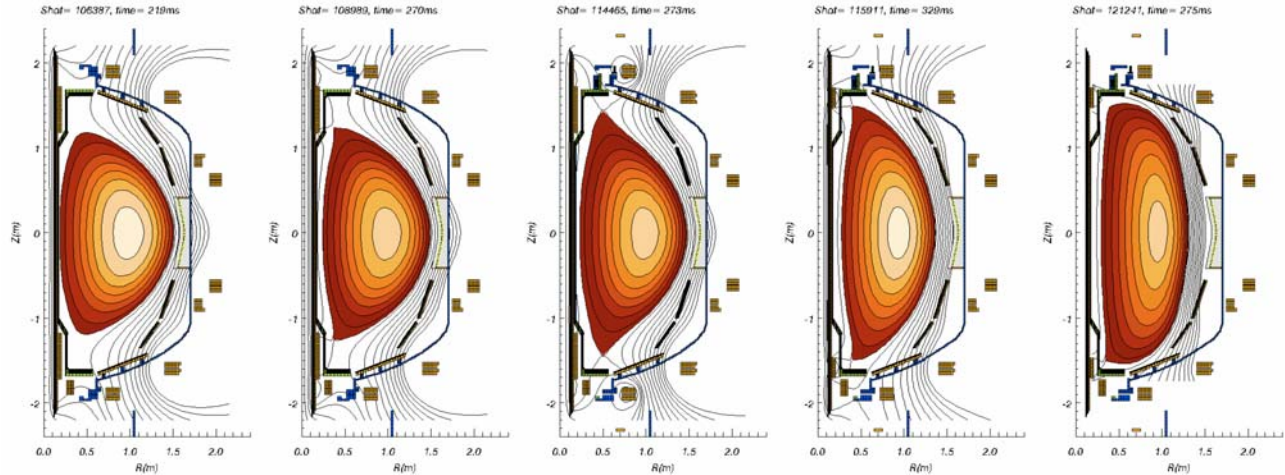


Figure 2.3.1-2 Expansion of NSTX operating space in  $\kappa$  and  $\delta$  due to improvements made in the last five year period. Each point represents an EFIT equilibrium reconstruction. Data span the entire NSTX database and are filtered to avoid equilibria exhibiting rapid plasma motion.



**Figure 2.3.1-3 Evolution of plasma shaping capability in NSTX in the last five year years. From left to right (initial device capabilities 2001:  $\kappa = 1.8$ ,  $\delta = 0.6$ ,  $S_I \sim 22$ ; 2002-3:  $\kappa = 2.0$ ,  $\delta = 0.8$ ,  $S_I \sim 23$ ; PCS latency reduced 2004:  $\kappa = 2.3$ ,  $\delta = 0.6$ ,  $S_I \sim 27$ ; PF1A modification 2005:  $\kappa = 2.75$ ,  $\delta = 0.8$ ,  $S_I \sim 37$ ; 2006:  $\kappa = 3$ ,  $\delta = 0.8$ ,  $S_I \sim 41$ .)**

While the high  $S_I$  equilibria have now been produced in NSTX, the initial plasmas somewhat unexpectedly displayed  $\beta_N$  limits close to the computed ideal MHD no-wall stability limits  $\beta_N \sim 4$ , rather than the values reached in wall-stabilized plasmas  $\beta_N \sim 6.5$ . This finding naturally called out the possibility that these plasmas have somehow lost passive kink/ballooning stabilization [18]. One possibility at sufficiently low  $I_i$ , as shown in Figure 2.2.1-2, is the destabilization of the purely current-driven kink mode, which eventually becomes unstable for all  $\beta_N$  when the edge current instability drive is sufficiently large. Investigating this possibility may lead to further understanding of the physics of passive stabilization of these modes. Another possibility is that the resistive wall mode (RWM) is destabilized in the high  $S_I$  plasmas since their larger size moves them closer to the conducting wall, and the RWM becomes *less* stable as the plasma is brought closer to the wall [20]. Another hypothesis being considered is the possibility of impurity-driven tearing modes.

### ***Extension of high $S_I$ plasmas to high $\beta_N$***

Generating stable high  $S_I$  plasmas at high  $\beta_N$  is an important goal toward demonstrating that future devices such as an ST-CTF have sufficient margin against instability and the ability of sustaining plasma current non-inductively with a high fraction of bootstrap current. As such, these plasmas are of high

interest to several topical areas including MHD, which research will focus on access to, and maintenance of the wall-stabilized state with  $\beta_N > 6$ .

Recent experiments in this regard were conducted in June 2008 after lithium was deposited in the device and utilizing both active  $n = 1$  RWM control and  $n = 3$  DC error field correction. High elongation plasmas were created that have now reached  $\beta_N$  up to 6. These plasmas have low  $l_i$ ,  $\sim 0.4 - 0.5$  and may have significantly reduced core current (current holes). Further analysis of these recent experiments and comparison to the 2007 database is underway to determine the underlying physics responsible for accessing high  $\beta_N$ . Kink/ballooning and RWM stability will be investigated for these equilibria, especially the comparison of passive stabilization in these plasmas as compared to plasma with lower  $S_l$  and the reduced  $\beta_N$ . Potential differences in equilibrium profile shape including rotation will be examined.

## (ii) physics and control - plans

### *Plasma control system upgrades*

The general plan for upgrading the control capability of NSTX in the 2009 – 2013 period is substantial ( $\beta$  control upgrade, ELM mitigation/control upgrade, RWM stabilization/DEFC system upgrade, plasma rotation control upgrade,  $q$  profile alteration by second NBI). The upgrades for plasma boundary shaping are relatively minor, involving hardware changes required to support the center stack upgrade and associated software tasks. A new set of PCS control computers were successfully tested at the end of the 2007 run and used in 2008 with the upgrades to PCS software including more flexible  $n = 1$  feedback system control. These computers run a LINUX operating system and have reduced the system latency by a factor of 2 compared to that in 2006 & 2007. Interfaces for planned  $\beta$  feedback control using real-time EFIT computation of  $\beta_N$  and NBI power for control were installed in 2008. Testing of this system will occur over the next year using an imposed target-beta specifications. A more sophisticated option for stability limit detection is real-time, low frequency MHD spectroscopy [21]. Another important upgrade of the shaping control system will be to provide greater accuracy and reliability in strike point control for the new liquid lithium divertor to be installed. More details regarding these control upgrades can be found in chapter 7.

The overall goal of the 2009 – 2013 period hinges on research enabling the reliability and control of high beta ST plasmas. Real-time measurement of plasma rotation from charge exchange recombination spectroscopy (CHERS) for rotation control and real-time motional Stark effect data for real-time evaluation of the safety factor are planned. The latter would be used in real-time EFIT, allowing greater flexibility in the reconstructed current profile basis function set and evaluation for future  $q$  profile control. Alteration of the  $q$  profile will be possible with the addition of the second neutral beam line, with transport code predictions showing a large variation in core  $q$  values and  $q_{min}$  exceeding 3 (see Section 6.3.2 and Figure 6.3.3). The use of diagnostic and control algorithm upgrades to evaluate and/or allow feedback control of various plasma parameters for MHD studies are discussed further in the appropriate sections of this document. Examples of these include real-time rotation measurements using CHERS (section 2.3.5), LQG controllers for resistive wall mode stabilization (section 2.3.2), soft X-ray detection of RWMs for future use in the active control system (section 2.3.2), and implementation of disruption prediction/mitigation measures (section 2.3.6).

## SUMMARY OF RESEARCH PLANS AND TIMELINE

- FY2009-10      Test  $\beta$  feedback control real-time EFIT and NBI power for control. Conduct experiments to extend high  $S_I$  plasmas into wall-stabilized, high  $\beta_N > 6$  operating space.
- FY2010-12      Implement strike point control for liquid Li divertor experiments. Implement real-time measurement of plasma rotation. Begin initial rotation profile control experiments.
- FY2012-13      Implement real-time MSE for evaluation of  $q$ . Attempt  $q_0$  control with either HHFW current drive or second NBI (depending on hardware availability). Attempt beta feedback using simple  $(\beta_N, l_b, F_p)$  models and evaluate more sophisticated models. Demonstrate sustained high  $\beta_N \sim 6$  in high elongation, highly shaped plasmas with newly upgraded center stack.

### 2.3.2 Resistive wall mode control and stabilization physics

**Goal:** Determine the physics of RWM stabilization, by both passive and active means, and apply this understanding to optimize and increase reliability of active stabilization in low aspect ratio plasmas. Use this information to provide greater confidence in models used to extrapolate RWM stabilization performance to future tokamaks including burning, and driven-burn plasma devices such as ITER and ST-CTF.

#### 2.3.2.1 Active feedback control

##### (i) physics and control - results

###### *Mode detection and control coils*

Resistive wall modes are kink/ballooning modes whose growth is slowed by stabilizing conducting structures which allow control of the modes. Resistive wall modes are deleterious to sustaining plasma beta, in that unstable modes cause rapid  $\beta$ -collapses, loss of H-mode, and eventual plasma disruption. Weakly damped stable modes can cause resonant field amplification that can also facilitate disruptions by reducing plasma rotation, causing the plasma to be more susceptible to tearing mode locking.

Significant progress has been made regarding RWM stabilization physics and mode control in NSTX. Key to this success was the addition of new hardware capability to both diagnose and actively stabilize the RWM, and to alter the plasma rotation magnitude and profile. NSTX is equipped with 48 toroidally segmented copper conducting plates, covered with plasma facing carbon tiles, to provide kink-ballooning mode stabilization (**Figure 2.3.2-1**). These plates are arranged symmetrically in four toroidal rings, two above and two below the device midplane. The segments are independently connected to the stainless steel vacuum vessel by high resistance supports. Detection of the RWM is primarily made by magnetic loops measuring the radial,  $B_r$ , and poloidal,  $B_p$ , flux located at each of the plates closest to the midplane.

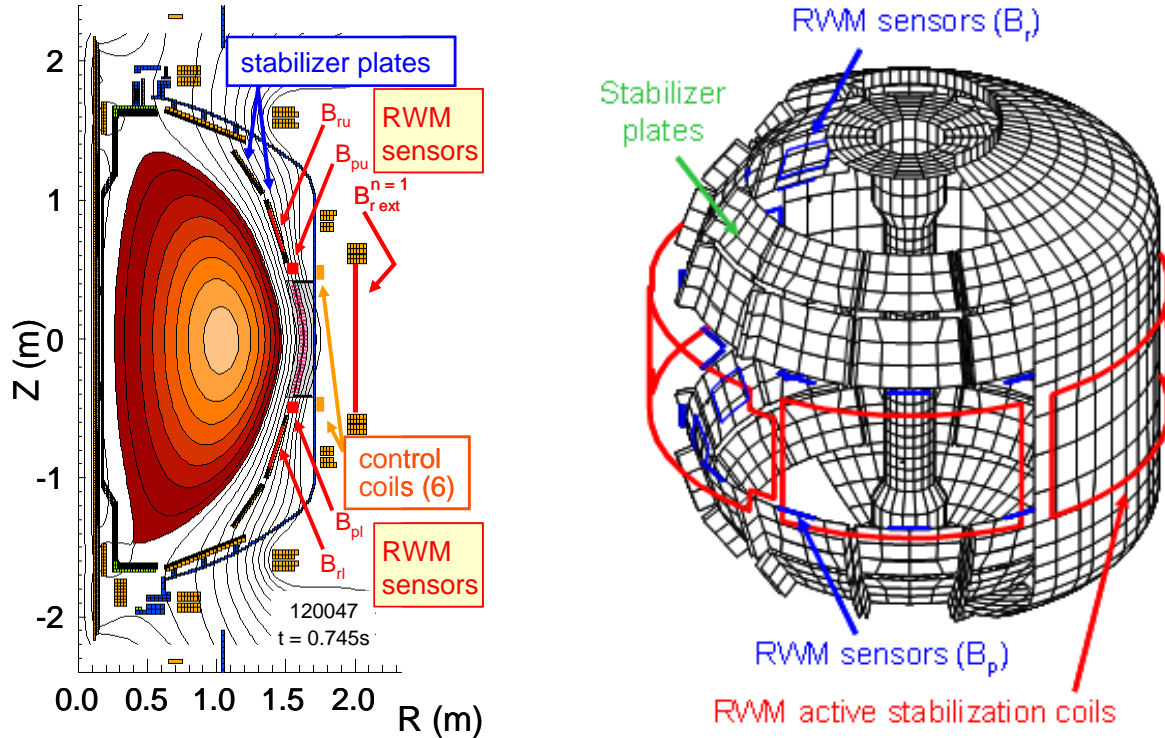


**Figure 2.3.2-1** Diagram of NSTX conducting structure showing internal  $B_r$  and  $B_p$  sensors, passive stabilizing plates, and ex-vessel non-axisymmetric (RWM) control coils.

The  $B_r$  sensors are mounted between the carbon tiles and the copper shells, and the  $B_p$  sensors are mounted a few centimeters below each plate. The sensors are instrumented to detect modes with frequencies up to 2.5 kHz, sufficient to detect RWM growth and rotation frequencies in NSTX ( $1/\tau_w \sim 200$  Hz). The signals are processed to measure toroidal mode number,  $n$ , up to 3. The non-axisymmetric coil set, known as the RWM coil set, is comprised of six control coils located at the outboard midplane (**Figure 2.3.2-1**). Each coil has two turns, spans approximately 60 degrees of toroidal angle, and is located outside, but closely coupled to the device vacuum vessel. These coils have been primarily connected in diametrically-opposed, anti-series pairs that allow generation of odd parity  $n = 1$  and 3 magnetic fields. Each coil pair is powered by an independent switching power amplifier capable of operation up to 3.3 kA at 7.5 kHz. This current corresponds to 10-15 G of  $n = 1$  midplane radial field at the  $q = 2$  surface. The fields generated by these coils can be used to reduce or amplify static and dynamic error fields, control  $\omega_\phi$ , and actively control the RWM.



### *Stabilization performance, resonant field amplification, and $n > 1$ observation*

At the start of the last five year period, the  $n = 1$  RWM had been identified as a discharge-terminating instability in the device [10]. The presence of large error fields resulted in unstable RWM growth soon after  $\beta_N$  exceeded  $\beta_N^{no-wall}$ , indicating reduced passive stabilization in this condition. In the last five year period, error field reduction and the increased maintenance of sufficient plasma rotation resulted in a much larger stabilized operating space, with  $\beta_N/\beta_N^{no-wall}$  up to 1.5, producing the highest  $\beta_N$  achieved in the device [22]. The proximity of the plasma  $\beta_N$  to  $\beta_N^{no-wall}$  was computed for the entire plasma discharge as desired with the DCON code [23] using reconstructed plasma equilibria that included kinetic profile data. This capability was available between shots in the NSTX control room. Maintaining high toroidal rotation across the entire profile produced passive RWM stabilization for long durations exceeding the eddy current decay time of the stabilizing plates of the device by at least a factor of 50 [24]. Pressure-driven amplification of applied non-axisymmetric fields was identified as resonant field amplification (RFA) [25] as had been identified in DIII-D [26,27]. The dependence of RFA on  $n = 1$  applied field frequency and propagation direction with respect to the toroidal plasma rotation in NSTX showed the RFA to be due to weakly damped RWMs [22]. The RWM sensor system on NSTX was outfitted to discriminate both amplitude and phase of RWM mode activity with toroidal mode number between 1 – 3, and for the first time in a tokamak, the unstable RWM with  $n > 1$  was observed [22] (Figure 2.3.2-2). The ideal MHD eigenfunctions with  $n = 1 - 3$  were computed using the DCON code using reconstructed equilibria from this plasma discharge. By using the measured  $n = 1 - 3$  mode amplitudes and phases, these eigenfunctions were scaled and summed in the proper phase to reconstruct the RWM field perturbation. This reconstruction is shown in Figure 2.3.2-3 Visible light emission (a) and DCON computed normal perturbed field (b,c) for the unstable RWM shown in Figure 2.3.2-2. (discharge 114147) at  $t = 0.268$ s. Along with the visible light observed from the plasma during the unstable RWM.

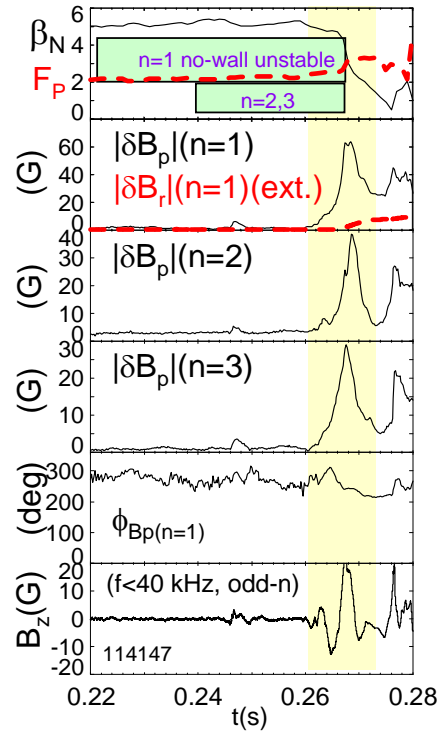


Figure 2.3.2-2 RWM toroidal mode spectrum and dynamics. The evolution of  $\beta_N$ , pressure peaking factor,  $F_p$  (dashed line), amplitude of  $n = 1-3$  components of mode-generated  $B_p$  (internal to vacuum vessel),  $n=1$   $B_r$  (external to vacuum vessel; dashed line), phase of  $n = 1$  mode-generated  $B_p$ , and integrated pickup loop data measuring the vertical field,  $B_z$ , for odd- $n$  MHD modes are shown. The computed ideal MHD no-wall stability for  $n = 1-3$  is also shown.

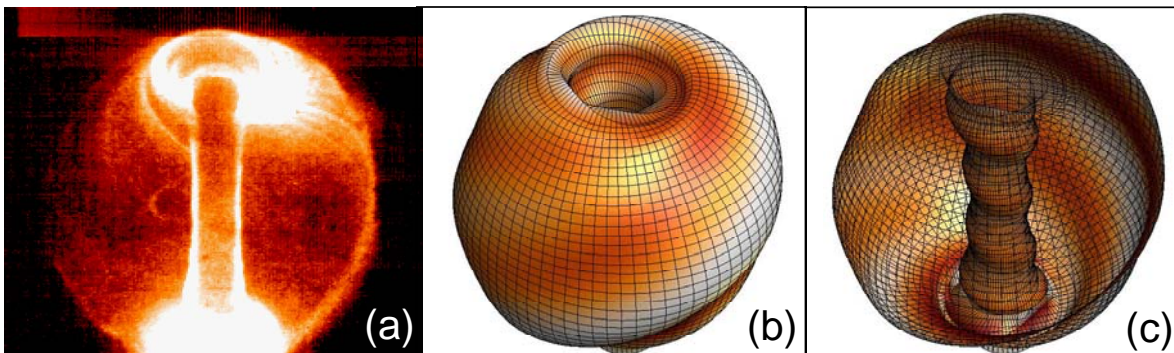
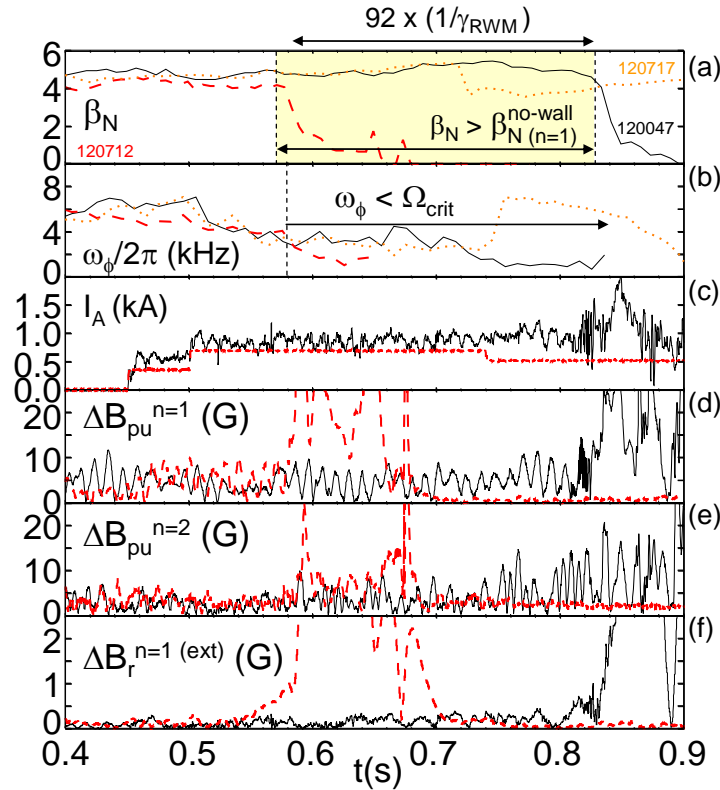


Figure 2.3.2-3 Visible light emission (a) and DCON computed normal perturbed field (b,c) for the unstable RWM shown in Figure 2.3.2-2. (discharge 114147) at  $t = 0.268$ s.

### Active stabilization

Successful operation of the RWM active control system has demonstrated for the first time active stabilization of the pressure-driven RWM in high beta, low aspect ratio tokamak plasmas, with  $\omega_\phi$  significantly below the experimentally determined critical rotation profile for the chosen target plasma. A comparison of high  $\beta_N$  plasmas with and without RWM active stabilization is shown in Figure 2.3.2-4. The plasma without active stabilization has  $\beta_N = 4.1$  as  $\omega_\phi/2\pi$  at major radial position  $R = 1.323\text{m}$  (near the  $q = 2$  flux surface) drops to below 4 kHz. At this time, RWM passive stabilization becomes insufficient and the  $n = 1$  RWM becomes unstable, indicated by poloidal and radial field sensors ( $\Delta B_p$ ,  $\Delta B_{r-ext}$ ), and  $\beta_N$  collapses. With active stabilization turned off, the current in one of three control coil pairs,  $I_A$ , is the pre-programmed  $n = 3$  braking field current (Figure 2.3.2-4(c)). The experimentally fitted  $n = 1$  RWM growth rate is between  $0.5 - 0.25 \text{ s}^{-1}$ . This agrees well with the theoretical growth rate  $\gamma_{\text{RWM}} = 0.37 \text{ s}^{-1}$  as computed by the VALEN code [28], using experimental equilibrium reconstructions [17] including internal magnetic field pitch angle constraints from a motional Stark effect diagnostic. In contrast, the plasma with active stabilization does not suffer an unstable RWM and continues to increase in  $\beta_N$  up to 5.6 and  $\beta$ , up to 19.4%, as  $\omega_\phi$  continues to decrease to  $\omega_\phi/\Omega_{crit} = 0.2$  near  $q = 2$ . The RWM is actively stabilized above  $\beta_N^{no-wall}$ , as computed by the DCON MHD stability code [29], and below  $\Omega_{crit}$  for a significantly long duration exceeding  $90/\gamma_{\text{RWM}}$  and seven  $\tau_E$ . The control coil current is now the superposition of  $n = 3$  braking field current and  $n = 1$  active feedback stabilization current, determined from the measured  $n = 1$  RWM amplitude and phase. This amplitude,  $\Delta B_{pu}^{n=1}$  is measured by an array of 12 poloidal field sensors above the device midplane. The amplitude modulation shown in Figure 2.3.2-4(d) is attributed to the interaction of the mode and eddy current fields, and the field generated by the RWM control coils is subtracted from  $\Delta B_{pu}^{n=1}$ . The  $\Delta B_{pu}^{n=1}$  is larger in the non-stabilized plasma as the  $n = 1$  RWM becomes unstable, and in the stabilized plasma is controlled at an average level of about 5 G. During  $n = 1$  stabilization, the  $n = 2$  RWM does not become unstable, although  $\Delta B_{pu}^{n=2}$  becomes larger than  $\Delta B_{pu}^{n=1}$  at the lowest values of  $\omega_\phi$  and highest values of  $\beta_N$  (Figure 2.3.2-4(e)). The actively stabilized, low  $\omega_\phi$  plasmas can suffer partial  $\beta_N$  collapse due to largely internal modes, which do not disrupt  $I_p$ , allowing  $\beta_N$  to recover. An example is shown by the dotted curves in Figure 2.3.2-4 (a) & (b). DCON stability calculations show that  $\beta_N > \beta_{N(n=2, no-wall)}$  and are consistent with the identification of this mode as an  $n = 2$  internal MHD instability.



**Figure 2.3.2-4 RWM active feedback stabilization in low rotation plasmas. Solid curves: actively stabilized plasma at  $\omega_\phi$  significantly below  $\Omega_{crit}$ , dashed curves: RWM unstable plasma at  $\omega_\phi/\Omega_{crit} = 1$  with active feedback turned off, dotted curves: (upper two frames) actively stabilized plasma suffering a beta collapse from an internal  $n = 2$  plasma mode. Shown are the evolution of (a)  $\beta_N$ , (b)  $\omega_\phi$  near  $q = 2$ , (c) current in representative non-axisymmetric control coil, (d) and (e) mode amplitude of  $n = 1$  and  $2$  field components measured by the upper  $B_p$  sensor array, and (f) mode amplitude of  $n = 1$  field component at the midplane, external to the vacuum vessel.**

The measured  $n = 1$  and  $2$  RWM amplitude and phase, along with chord integrated soft X-ray (SXR) measurements spanning from the plasma core to the edge [30] are shown in Figure 2.3.2-5. Without active control, the  $n = 1$  RWM becomes unstable. At early times in the figure,  $\phi_{B_{pu}^{n=1}}$  appears to wobble between 150 and 300 degrees, eventually settling to the lower end of this range, and as  $\Delta B_{pu}^{n=1}$  grows exponentially,  $\phi_{B_{pu}^{n=1}}$  shows mode rotation in the direction of plasma rotation, as expected by theory.

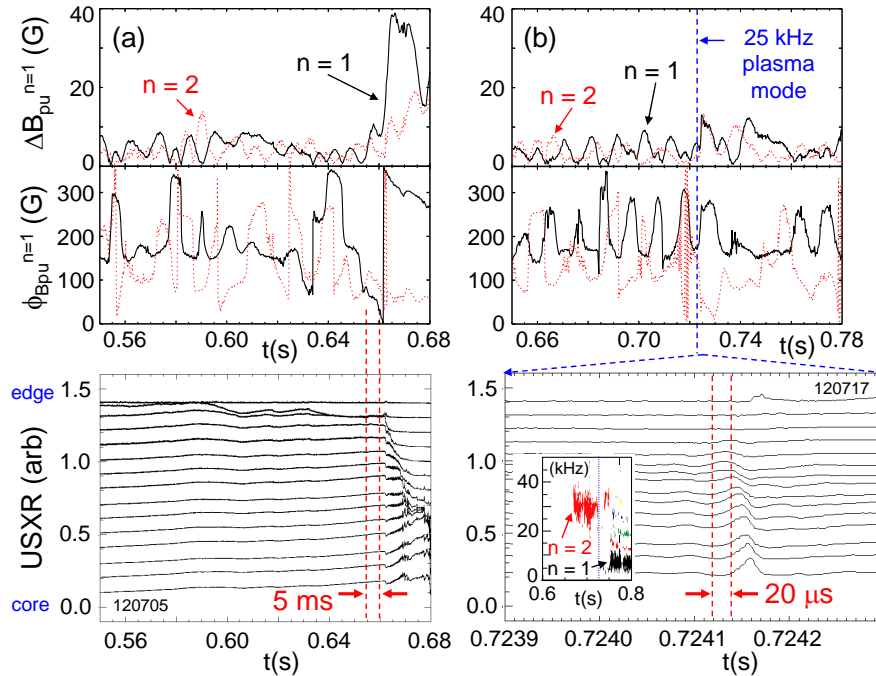


**Figure 2.3.2-5 Mode activity in plasmas with and without active stabilization. Frames from top down show upper  $B_p$  sensor amplitude, phase, and ultra-soft X-ray emission spanning from the plasma core to edge vs. time. Solid lines:  $n = 1$ , dotted:  $n = 2$ . Column (a) discharge with active feedback off, column (b) RWM actively stabilized plasma with internal  $n = 2$  plasma mode. Lower frame inset:  $n$  spectrum from midplane toroidal magnetic pickup coil array.**

SXR data shows the mode amplitude largest in the outer region of the plasma, propagating toward the core during mode growth. The  $n = 2$  RWM amplitude shows periods when  $\Delta B_{pu}^{n=2} > \Delta B_{pu}^{n=1}$ , but the  $n = 2$  mode growth that eventually occurs, although strong, is subsidiary to  $n = 1$  mode growth. Figure 2.3.2-5(b) shows analogous detail for the actively stabilized plasma suffering a largely internal mode shown in Figure 2.3.2-4. Both  $n = 1$  and 2 RWM activity are stable, with  $\phi_{Bpu}^{n=1,2}$  wobbling within some range. SXR data shows mode growth on an ideal MHD timescale, much faster than  $\tau_w$ , is largely internal, and the measured 25 kHz frequency indicates that the mode is  $n = 2$ , since it appears in a region of the plasma with  $\omega_\phi/2\pi \sim 12 - 15$  kHz. The  $n$  spectrum measured by a toroidal array of magnetic pickup loops also shows  $n = 2$  mode activity at this frequency and time.

RWM stabilization can fail due to a change in the poloidal form of the mode. An example is shown in Figure 2.3.2-6, where the  $n = 1$  components of both upper and lower  $B_p$  and  $B_r$  sensors, and  $\Delta B_{r-ext}^{n=1}$  sensor signals are shown. Note that since the latter sensor is outside the vacuum vessel, the signal lags those of the internal sensors by  $\sim O(\tau_w) \sim 6$  ms for  $n = 1$ . Approaching the time of  $\beta_N$  collapse,  $\Delta B_{pu}^{n=1}$  and  $\Delta B_{pl}^{n=1}$  first decrease to near zero, as the radial field sensors increase by a small amount. Then,  $\Delta B_{pu}^{n=1}$  increases strongly, while  $\Delta B_{pl}^{n=1}$  lags, and the ratio  $\Delta B_{pl}^{n=1} / \Delta B_{pu}^{n=1}$  never gets above 0.5. There is also a strong increase in  $\Delta B_{r-ext}^{n=1}$  while  $\Delta B_{ru}^{n=1}$  and  $\Delta B_{rl}^{n=1}$  decrease, indicating that the mode is bulging through the midplane gap in the stabilizing plates and decreasing in amplitude in front of the plates. This observation may indicate a lack of “mode rigidity”, normally assumed theoretically and observed experimentally [31].

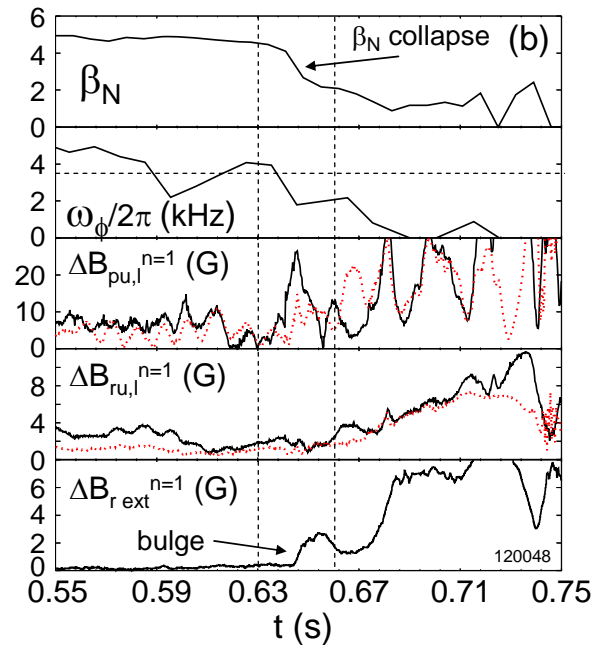


**Figure 2.3.2-6 Poloidal deformation and mode destabilization during RWM active stabilization. Sensors are distinguished by solid (upper sensors) and dotted (lower sensors) lines.**

This poloidal deformation appears to occur when large RWM coil currents are requested and sometimes when the central  $q$  is near unity. These conditions may lead to nearby stable  $n = 1$  MHD modes becoming important in the mode dynamics, causing the RWM eigenfunction to apparently change poloidal

structure. The hypothesis of other weakly damped eigenfunctions causing the deformation in this way requires further study. Initial analysis of reconstructed equilibria shows the ideal energy functional for the *second* least stable  $n = 1$  eigenfunction becoming sufficiently small for the mode to enter the dynamics when  $\beta_N$  exceeds  $\sim 5.5$ . The RWM stability code NMA [32] (Normal Mode Analysis) allows up-down symmetric, 2-D calculations that include more than a single rigid mode and is presently being tested against experimental results from DIII-D and NSTX. The VALEN code has been upgraded to include multiple modes in 3-D geometry and is presently being tested on NSTX, DIII-D, and HBT-EP equilibria.

In experiments through 2008, RWM active stabilization research continued by examining stabilization using a greater array of RWM sensors in the feedback loop (2006 experiments used  $\Delta B_{pu}^{n=1}$ ; 2007-2008 experiments added different combinations of  $\Delta B_{pl}^{n=1}$ ,  $\Delta B_{ru}^{n=1}$  and  $\Delta B_{rl}^{n=1}$  for feedback.). Development of the active  $n = 1$  control system has reached the point where non-RWM experiments are now using it as a routine tool to control RWMs and for dynamic error field correction. More than 10 experiments have used the system in 2008, with more than 200 shots taken so far with  $n = 1$  feedback control on. The system is widely used in the 2008 run campaign because unstable RWMs have been observed at intermediate levels of rotation, showing that stability at low plasma rotation does not insure stability at higher rotation. This result contradicts simple threshold models of RWM “critical rotation”, and will be considered in the next section sub-section on passive stabilization physics. Discharges at intermediate plasma rotation with and without active  $n = 1$  feedback and  $n = 3$  DC error field correction (see section 2.3.3 for  $n = 3$  correction) are compared in Figure 2.3.2-7. Analysis of the present data will lead to further optimization of the present feedback system in the near term, with focus on mode dynamics during stabilization.

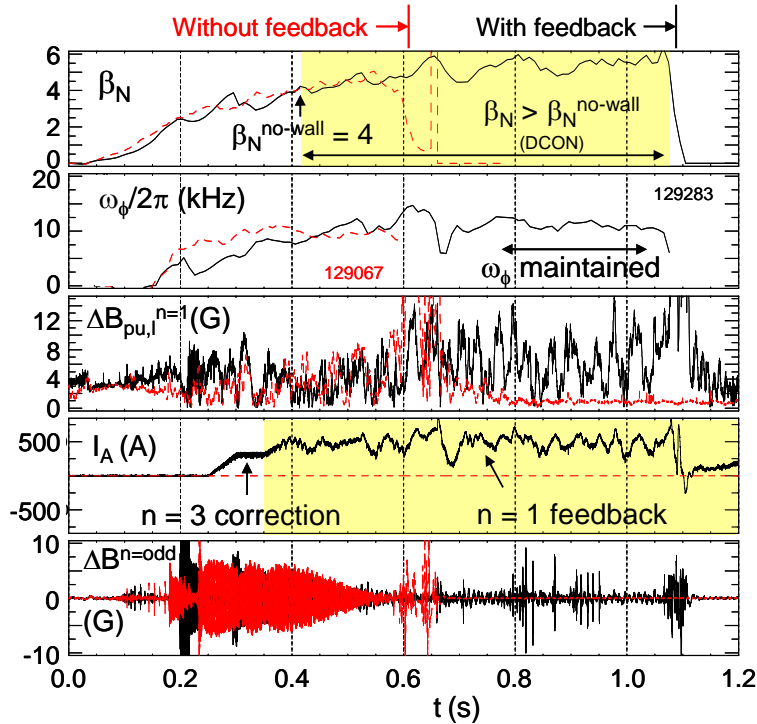


Figure 2.3.2-7: Comparison of discharge encountering RWM instability at intermediate plasma rotation, leading to disruption without  $n = 1$  active feedback and  $n = 3$  DC error field correction (red dashed lines) vs. mode control and resulting long pulse length when RWM control and error field correction are enabled.

(i) physics and control – upgrades and plans

Expanded machine capability in several areas will aid in the RWM research task, and will allow advanced experimentation and comparison to theory. The new capabilities will also expand the applicability of the research to future devices including ITER. The key capabilities planned in the 2009-2013 timeframe are:

- (i) Implementation of an additional non-axisymmetric control coil set (NCC)
- (ii) Alteration of stabilizing plate material and electrical connections
- (iii) Non-magnetic detection of resistive wall mode using soft X-rays
- (iv) Measurement of scrape-off layer currents
- (v) Advanced active feedback stabilization control algorithms



These capabilities are discussed below in the context of the appropriate RWM stabilization physics to be explored. A timeline summary of the proposed research will complete this section.

### *Addition of new non-axisymmetric control coil set*

In the 2009 – 2013 period, a new non-axisymmetric control coil (NCC) set is proposed (with incremental funding) to serve research functions synergistically across topical groups including RWM stabilization, ELM mitigation, and plasma rotation control. Each research area is covered in this document, with the first and last covered in this MHD chapter, and ELM mitigation via resonant magnetic perturbations discussed in Chapter 5.

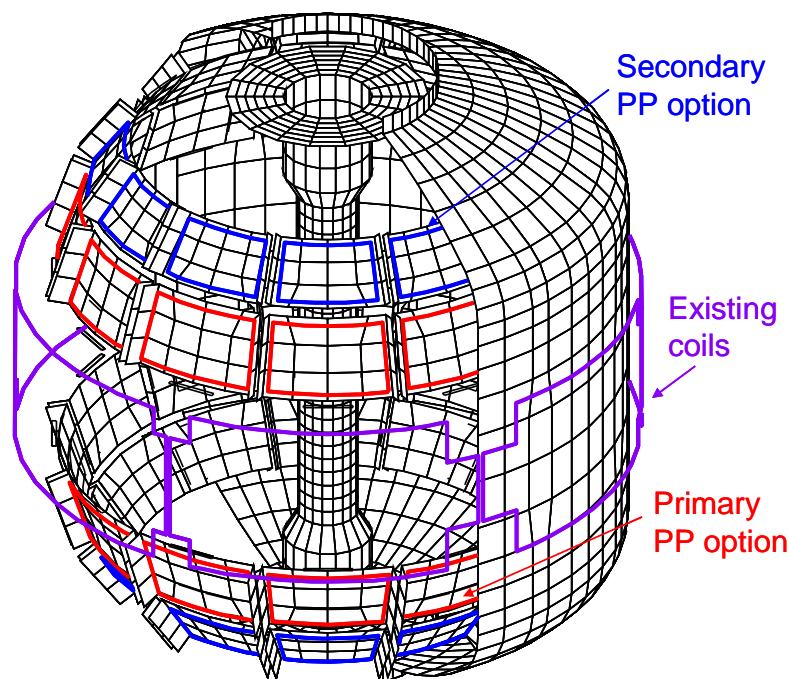


**Figure 2.3.2-8** Initial configurations considered for supplemental RWM stabilization coils, which will also be used for ELM mitigation, and plasma rotation control research in the 2009 – 2013 time frame.

The physics design for optimal NCC configurations is presently underway. All research considerations are being considered in this joint design effort, and at present it is agreed that an off-midplane coil set that

is internal to the machine vacuum vessel is desired for all roles. Here, we consider an initial physics design study for RWM stabilization using the VALEN code, analogous to the study performed for the existing RWM stabilization coil on NSTX [10], but with just two simple, non-optimized coil configurations (illustrated in Figure 2.3.2-8).

The present designs consider a total of 24 coils, with two sets of 12 coils each located above and below the device midplane. The large number of coils is primarily desirable for greater  $n$  spectrum generation for ELM mitigation and plasma rotation control, but could also be used for future  $n > 1$  RWM stabilization. There is ample free space in the vessel in the region behind the primary and secondary passive plates to consider several variations for coil optimization. At present, we consider the following variations: (i) coils behind the primary passive plates and separately (ii) coils behind the secondary passive plates. These coil options have significant overlap with KSTAR and the present ITER VAC02 coil design, and directly support present KSTAR and ITER RWM stabilization and rotation control design efforts by the U.S. In the initial NSTX configurations, the coils are chosen to be parallel to the plates, which is not necessarily an optimal orientation. In the VALEN studies, we also consider changing the present copper passive plate material to stainless steel. The performance of these two coil options are shown in Figure 3.3.2-9 (a) for the present copper passive plate material, and Figure 3.3.2-9(b) for modified stainless steel plate options, displaying mode growth rate at near optimal active stabilization using simple proportional gain. Also shown on the plots are the growth rate curves for the present midplane coil RWM stabilization system on NSTX, passive stabilization growth rate curves, and the with-wall beta limit. The results show that the initial coil geometries chosen in this study should improve control performance only if more resistive plate material such as stainless steel is used. Please note that these are initial, unoptimized coils and plate configurations. Further designs are now being considered to improve control system performance, with the goal of reaching operation at  $\beta_N$  up to the ideal no-wall limit.

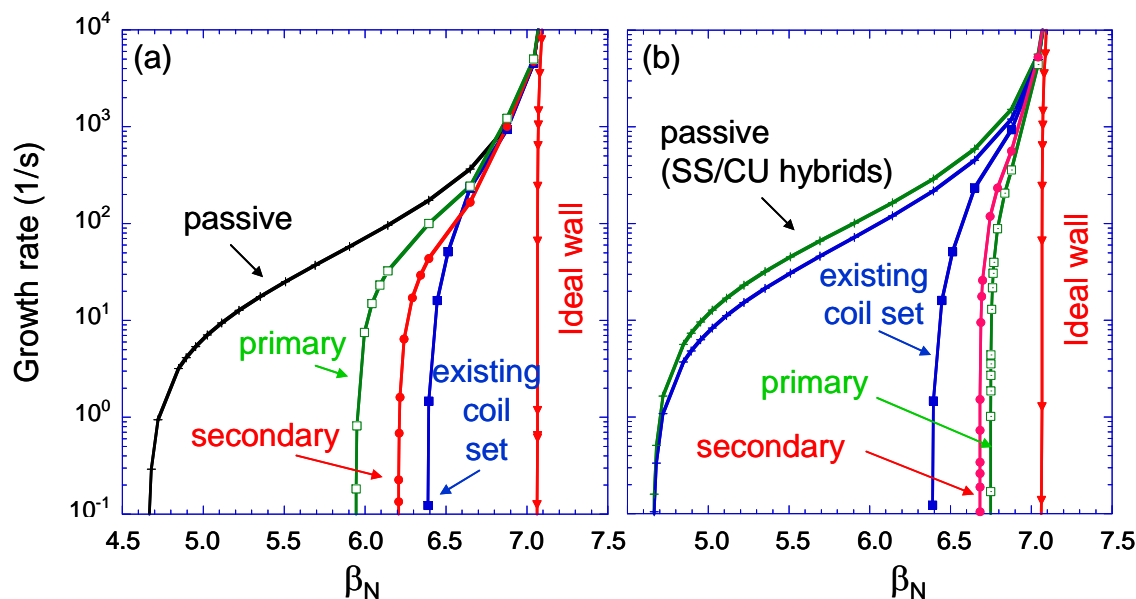


**Figure 2.3.2-9 Active RWM stabilization performance of NCC system coil options, (a) for the present copper passive plate material, and (b) for modified stainless steel plate options. Also shown is the growth rate curve for the present external midplane RWM stabilization coil, and the with-wall  $\beta_N$  limit curve. The two passive curves in frame (b) correspond to two possible combinations of primary/secondary passive plates made of copper/stainless steel.**

In addition to the increased ability for the internal NCC (behind stainless passive plates) to stabilize the NSTX plasma at higher  $\beta_N$  than the present external RWM stabilization coil, the NCC will allow stabilization of the RWM above/below the plasma midplane, independent of the present external coil at the midplane. Also, if funding is sufficient to allow power supplies to independently power the upper and lower NCC arrays, the stabilization system could be set up to independently respond to the RWM amplitude measured in the upper/lower/midplane  $n = 1$  sensors. This configuration would allow a complete study of RWMs displaying poloidal deformation.

The NCC would also allow experiments that would support the use of similar coils for RWM control in ITER. The recent VAC02 coil design for ITER, shown in Figure 2.3.2-10, resembles the coil geometry considered for the NCC, with three rows of toroidal coils, each partially shielded from the plasma by conducting structure (analogous to the ITER blanket modules). VALEN code calculations show that a

substantial increase in  $\beta_N$  is possible in ITER Scenario 4 using this coil ( $\beta_N$  up to 3.8 with active control vs. 2.5 without). Research on the impact and solution of mode deformation and the effect of shielding conducting structure on RWM feedback system performance would prepare for operation of this ITER coil system for RWM stabilization.

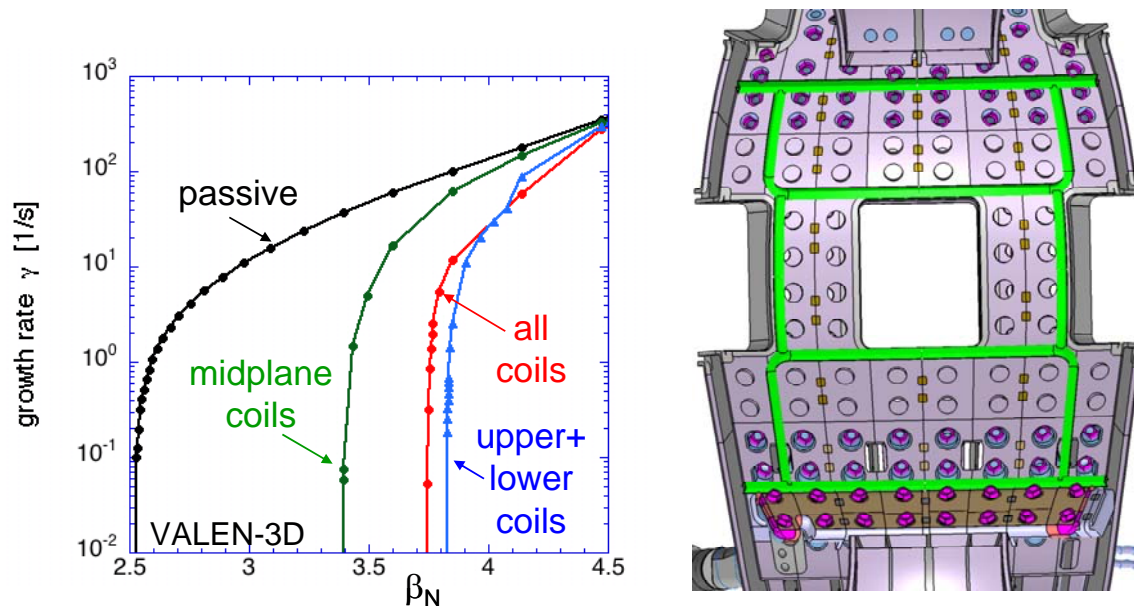


Figure 2.3.2-10 ITER VAC02 non-axisymmetric coil design (40 degree toroidal sector) and computed stabilization system performance.

*Alteration of stabilizing plate material and electrical connections*

As shown in the active stabilization performance diagrams computed using VALEN, changing the passive plate material from copper to stainless steel in front of the planned coil positions increases the active feedback performance. In addition to this potential change, the VALEN code will be used to determine the optimal way to electrically connect the passive plates. Conceptual design studies conducted before NSTX was built showed that the originally planned  $n = 1$  configuration of electrical jumpers led to a substantial error field during plasma start-up. The present lack of connections leads to an  $n = 12$  configuration. While eddy currents with an  $n = 1$  pattern can be set up in this configuration, it is possible

that an  $n = 6$  jumper configuration could yield superior passive stabilization performance. Such configurations will be considered in the NCC design.

### *Non-magnetic detection of resistive wall mode using soft X-rays*

While magnetic sensors are a simple and logical choice for RWM detection and have been used exclusively in RWM feedback stabilization systems in tokamak and RFPs to date [33,34,35], they have several disadvantages. Magnetic pickup from sources other than the RWM sought to be stabilized needs to be subtracted from the measured signals in real-time. While in many cases this can be done for known sources, such as the applied control field, it is difficult or impossible to eliminate all non-desirable field sources by subtraction or filtering techniques (e.g. fields due to currents in significant conducting structures, such as the passive stabilizing plates). Eliminating non-RWM coherent mode activity in the RWM frequency range (e.g. ELMs) is an active area of research [36]. Additional significant issues arise in long pulse burning plasma devices such as ITER or CTF, where long-pulse operation combined with the presence of the electrically-conducting thick metallic blankets and a strong radiation field will make control with conventional magnetic sensors difficult.

NSTX provides an excellent laboratory to research and implement non-magnetic detection of the RWM, partially because such research would serve an immediate practical purpose to both understand and eliminate unwanted field sources due to uncompensated currents picked up by the present magnetic detection system. A possible indication of unmeasured fields in RWM detection in NSTX is the observed amplitude modulation observed in the poloidal field RWM sensors during RFA or RWM activity, which may be caused by the superposition of weakly damped stable RWMs, or unmeasured currents in the closely coupled passive conducting plates or scrape-off layer. The amplitude modulation observed in the present magnetic sensors during stable RWM/RFA activity (Figure 2.3.2-4(d)) appears to be supported by the present multi-energy soft X-ray (ME-SXR) sensor data from the same plasma discharge (Figure 2.3.2-11). As shown in Figure 2.3.2-11a) during the RWM evolution both the poloidal field perturbation amplitude and the high energy ( $E > 2$  keV) peripheral SXR signals exhibit an oscillation with  $\approx 100$  Hz characteristic frequency, showing that there is a plasma component in the frequency range of the magnetic signal modulation. Spatially inverted SXR data in Figure 2.3.2-11b) shows that this oscillation occurs near the plasma boundary, around  $R_{tan} \approx 1.45$ m.

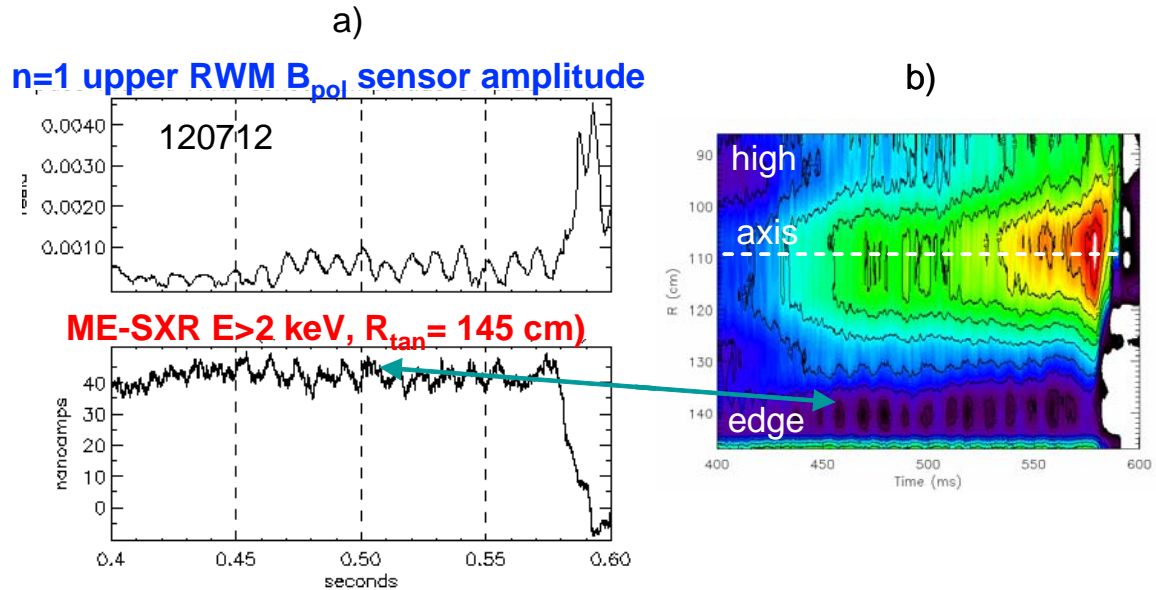


**Figure 2.3.2-11 a) Comparison between time history of  $n = 1$  RWM  $B_p$  sensor amplitude and that of high energy ME-SXR emission from the NSTX pedestal, b) Intensity contour plots of Abel inverted SXR emissivity at high energy.**

A dedicated set of ME-SXR sensors will be designed and implemented in the 2009 – 2013 period to both compare magnetic and non-magnetic RWM detection techniques and would be an option for input to the RWM active control system. The ME-SXR system used for RWM detection will comprise a dedicated set of sensors arranged toroidally to best discriminate  $n = 1$  (and perhaps  $n = 2$ ) mode activity. The system will aim at detecting with high sensitivity and accuracy the RWM toroidal  $T_e$  perturbation of the boundary plasma. ‘Gradient’ ME-SXR sensors, measuring the sharpness of the H-mode pedestal could also be deployed in order to facilitate discrimination between the RWM and the ELM perturbations. The ME-SXR technique is already used as part of the general SXR detection system on NSTX developed by the Johns-Hopkins University collaboration. In addition to the advantages over magnetic sensors mentioned above, ME-SXR sensors also potentially offer much larger signal-to-noise ratio.

### *Measurement of scrape-off layer currents*

The behavior of scrape-off layer currents (SOLC) may be an important component for understanding the diagnosis and behavior of RWMs, as well as ELMs and edge magnetic islands. With measurement of the SOLC, their importance can be evaluated. The potential modification of these currents during use of the present midplane RWM control system and/or with the proposed NCC set can determine how the SOLC affects finite- $n$  feedback. The SOLC flows along an open field lines that terminate at the surface of divertor plates and other structural elements in tokamaks. The return current of a SOLC circuit may flow along another open field line and/or through vacuum vessel wall and other structures. The SOLC has been observed during MHD activity, including ELMs on DIII-D. [37] However, the efficacy of a non-axisymmetric SOLC in creating a non-axisymmetric field, and hence also the question of whether or not the SOLC can play a causal role in the MHD stability, depend importantly on the SOLC's spatial structure, both toroidal and radial. During the 2009-2013 period, NSTX will be outfitted to measure the SOLC using tile current sensor arrays and upgraded Langmuir probe arrays (more detail is given in Section 2.3.6). If found to be important, the VALEN, IPEC, (see Section 2.3.3) and M3D codes can be used to model the effects of the SOLC on RWM stability, dynamic error field amplification or screening, and ELMs.

The version of M3D developed for ELM studies has the capability to extend the usual M3D equilibrium from a closed flux surface out beyond the separatrix and to a possibly resistive wall, treating the vacuum region as a low-density, highly resistive plasma. By imposing a moderate- $m$  helical current perturbation in the SOL in this region, supported by a matching source term, the effects of SOLC on the stability properties of MHD modes can be studied. With sufficient measurement and modeling of the SOLC, an investigation can be made as to whether the SOLC could be controlled to suppress or mitigate plasma instabilities. This investigation naturally couples to NSTX experience with RWM control and stabilization physics. If the SOLC can be controlled in ways beneficial to the RWM and/or other low frequency MHD modes, it might allow advantages to present mode stabilization with magnetic coils in future devices with high neutron fluence.

### *Advanced active feedback stabilization control algorithms*

The present RWM active stabilization system on NSTX utilizes simple proportional gain. The physics design of the present stabilization hardware and control system software shows a maximum capability of stabilization up to 74% of the ideal with-wall stability limit [10]. The theoretical inability to reach higher stable  $\beta_N$  is due to the control coil being outside of the vacuum vessel. The geometry is similar to either the baseline EFCC coils or newly proposed RWM control coils in ITER, which will be shielded to various extent by the blanket modules. However, with more advanced software control algorithms, greater stabilization capability in ITER, and in general, is possible [38]. Evaluation of such algorithms has essential importance for RWM stabilization in ITER, as such control algorithms are being considered in the ITER design, yet they have not yet been tested and evaluated in present active RWM stabilization experiments.

Evaluation of algorithms such as the LQG controller [38] is presently underway on NSTX using existing active RWM stabilization data. In the 2009-2013 period, an advanced algorithm for RWM stabilization will be implemented on NSTX to determine the performance of the algorithm compared to simple proportional gain. This research will provide the required experimental verification of advanced algorithms for future devices such as ITER.

### *Additional potential applications of new capabilities to RWM physics research*

The observation of  $n > 1$  RWMs during passive stabilization in NSTX,  $n = 2$  internal kink modes during  $n = 1$  RWM active stabilization, and the ability to violate the  $n = 2$  ideal no-wall beta limit indicate that the  $n = 2$  RWM may be driven unstable at higher  $\beta_N$  than has been actively stabilized at present. If this occurs during the next 5 year research period, perhaps in conjunction with the addition of the second neutral beam, the NCC set could be configured to stabilize the  $n = 2$  RWM while the present external RWM coil is used to stabilize the  $n = 1$  RWM. VALEN would be used to determine the capability of stabilizing the  $n = 2$  RWM with the NCC. M3D can be used to model the presently observed  $n = 2$  internal link during RWM stabilization. Plasmas with stabilized  $n = 1$  RWMs can be modeled by generating suitable stable equilibria with ideal wall boundary conditions as an approximation to  $n = 1$  stabilization. A small  $n=2$



perturbation can then be added to the poloidal flow field in the presence of an arbitrary toroidal rotation profile, following which M3D will be run in its linear mode to find unstable eigenmodes, if any, and their growth rates.

The soft X-ray system upgrade is being proposed to have complete poloidal coverage at two toroidal positions. This upgrade will restore prior SXR diagnostic capability that was used to clearly distinguish the  $n = 1$  RWM from  $n = 0$  perturbations [22], and to expand that capability to greater plasma coverage. Additionally, the use of ME-SXR arrays will enable a direct measurement of the toroidal and poloidal displacement of  $T_e$  iso-surfaces.

### 2.3.2.2 *Passive stabilization physics*

While passive stabilization has been established with great effect in NSTX (Figure 2.2.1-2) [22], and even simple models of the RWM go far in describing RWM dynamics in general [39], a full understanding of the stabilization mechanism, first-principles or otherwise, remains elusive. Attaining this understanding is a critical milestone in RWM research, particularly for the purpose of confident extrapolation to future devices.

The rotation at the  $q = 2$  surface has been used for the past decade as a key parameter to define the critical plasma rotation,  $\Omega_{crit}$ , required for passive RWM stabilization. RWM research in NSTX has questioned this hypothesis of a scalar critical rotation value for several years [9], and showed success in defining a critical rotation *profile*  $\Omega_{crit}/\omega_A = 1(4q^2)$  based on analytic theory by Bondeson and Chu [22] (Figure 2.3.2-12(a)). Subsequently,  $n = 3$  non-resonant magnetic braking was used on NSTX to reduce the plasma rotation to zero on low-order rational surfaces with  $q > 2$  to show that rotation on these surfaces was not required for stability [24] (Figure 2.3.2-12(b)). This result appeared to contradict conclusions made based on DIII-D research highlighting the importance of plasma rotation on outer flux surfaces.

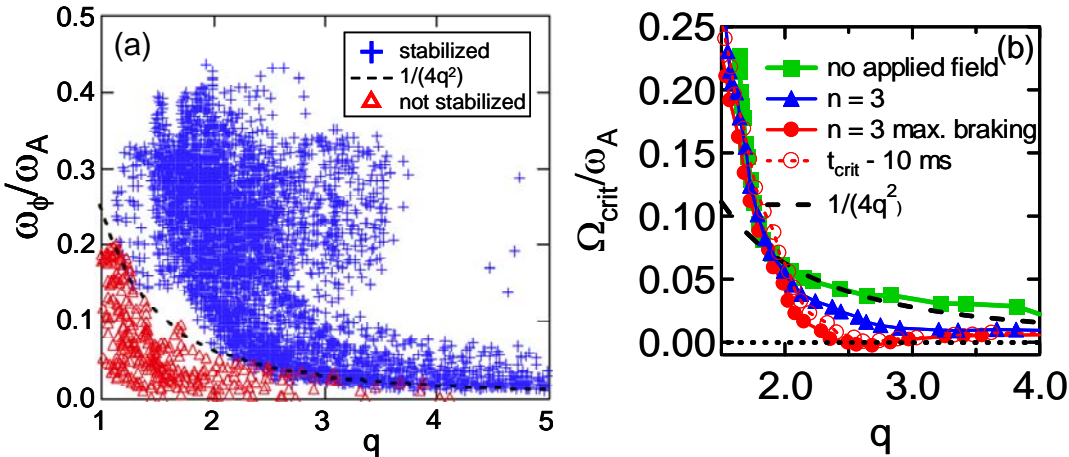


Figure 2.3.2-12 Observed kink/RWM stability vs. local  $\omega_\phi/\omega_A$ , parameterized by local  $q$  value (no applied fields - frame (a)), and variation of marginally stable profile shape using applied non-resonant  $n = 3$  magnetic braking (frame (b)).

Recent results using balanced NBI in DIII-D further call into question the concept of a scalar critical rotation frequency for RWM stabilization [40]. The importance of the Alfvén frequency in describing the stability criteria is also called into question, as extremely low values  $\sim 0.3\%$  are quoted for stabilization at the  $q = 2$  surface. The large difference in Alfvén frequencies, due to the large difference in toroidal field magnitude between NSTX and DIII-D, may help to distinguish the important plasma parameters and underlying physics for RWM passive stabilization by conducting further joint experiments aimed at this topic. If, for example, the Alfvén frequency normalization is eliminated, the “critical rotation” for RWM stabilization would be comparable in NSTX and DIII-D, indicating that physics leading to this normalization may not be important. Also it has been noted that ion Landau damping is greatly reduced when toroidicity is included in the calculation [41]. This was a key motivation to examine the role of toroidal inertia enhancement, as described in Ref. 41, for RWM stabilization in NSTX [22].

The effect of resonant  $n = 1$  error fields on past RWM critical rotation experiments in DIII-D has been examined, with the conclusion that application of such fields to slow the plasma rotation may explain the higher previously quoted values of  $\Omega_{crit}/\omega_A$  in DIII-D compared to the far lower values in more recent balanced NBI experiments [42]; this was explained using a model of toroidal torque balance [43] similar

to that used to explain tearing mode locking [44]. This past quoted “critical rotation” explanation in DIII-D does not explain the presently observed RWM critical rotation profile in NSTX where  $n = 3$  non-resonant magnetic braking is used to slow the plasma rotation and alter the profile shape [24]. As shown in Figure 2.3.2-13, NSTX data does not follow the critical rotation criteria based on the equilibrium plasma rotation frequency  $\omega_0$  shown in DIII-D, indicated by the dashed line in the figure.

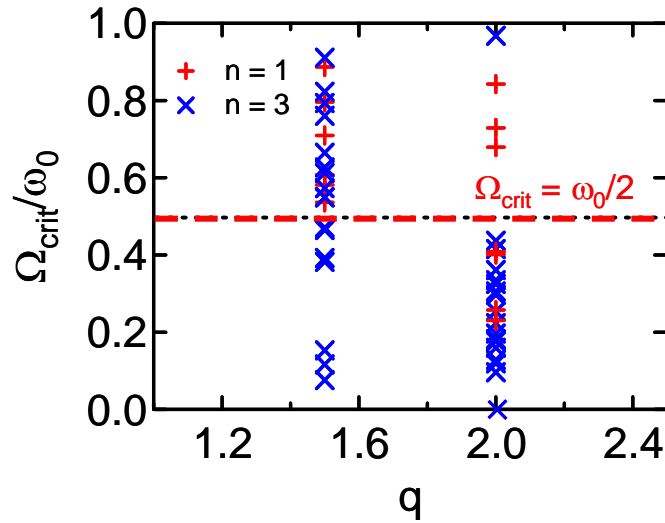


Figure 2.3.2-13  $\Omega_{crit}/\omega_0$  at  $q = 1.5$  and  $2$  showing wide distribution of values with stable discharges down to  $\Omega_{crit}/\omega_0 \sim 0.0$ . The dashed line indicates a proposed critical threshold value for toroidal torque balance to be maintained, which does not apply to NSTX.

Ion collisionality appears to be an important parameter for RWM passive stabilization in NSTX. Shaing’s modification of the Fitzpatrick “simple” RWM model [39] includes neoclassical viscosity [45] and introduces a dependence on the ion collisionality to the critical plasma rotation for RWM stabilization. This can be seen by solving for the critical rotation in the high dissipation limit of Shaing’s theory, analogous to Equation (26) of Ref. [45], but expanding the solution of the dispersion relation to first order in  $(\gamma/\mu_1)$  rather than zeroth order. The result is

$$|\Omega_{crit}| > ((1 - d/d_c)/4 + (1 - d/d_c)^2/\eta^2)^{1/2}, \quad (1)$$

where  $d$  is related to the radius of the resistive wall and  $d_c$  is related to the maximum radius of wall that will stabilize the external kink mode (the critical wall radius) and  $\eta \equiv 1/\mu$ , where  $\mu$  is defined in Equation (24) of Ref. [45]. In the high dissipation limit, the viscous dissipation  $\eta$  scales linearly with  $v_i$ , yielding an inverse dependence of  $\Omega_{crit}$  on  $v_i$ . Here,  $v_i$  is given by  $v_i = 4.8 \times 10^{-8} Z^A m_i^{-1/2} n_i \ln \Lambda T_i^{-3/2} \text{ sec}^{-1}$ . Therefore, increased  $v_i$  is theoretically stabilizing and yields lower  $\Omega_{crit}$ . A series of experiments were performed to qualitatively examine the variation in  $\Omega_{crit}$  with  $v_i$ . The plasma current and toroidal field were scanned together to create a series of discharges with similar shapes,  $q$  profiles, and Alfvén speed  $(v_A)_L$  profiles. The density was allowed to vary and a wide variation of  $v_i$  was achieved. Comparing discharges with similar  $v_A$ , but varying  $v_i$  indeed shows that increased ion collisionality leads to lower  $\Omega_{crit}$ . Experiments performed in 2008 using lithium evaporation to change  $v_i$  showed a similar result.

Experiments run through the 2008 campaign show greater complexity of the RWM marginal stability condition and do not support simple models of critical plasma rotation. In particular, intermediate levels of plasma rotation are found to be experimentally unstable, while lower levels of plasma rotation can be stable. Initial results from the kinetic stability model of Hu and Betti [46] show the general behavior required to reproduce experiments. The model contains several resonance effects that modify the ideal fluid energy functional  $\delta W$ . Both rotation and collisionality affect stability by physical processes different than viscous dissipation models in fluid theories. The modified RWM growth rate is expressed as

$$\gamma \tau_w = - \frac{\delta W_\infty + \delta W_K}{\delta W_b + \delta W_K}$$

Where  $\delta W_\infty$  is  $\delta W$  computed with no stabilizing conducting structure,  $\delta W_b$  is computed with a model of the experimental stabilizing conducting structure, and  $\delta W_K$  is the kinetic modification to  $\delta W$ . The effects of trapped ions and electrons, circulating ions, hot particles, and Alfvén resonances are included.

Examining the modification of  $\delta W_K$  due to trapped ion shows the influence of rotation and collisionality on stability. From Reference [47], Equation 6 we have

$$\begin{aligned} \delta W_K^{ti} = & \int_0^{\Psi_a} d\Psi \left( \frac{p_s}{1 + \frac{T_e}{T_i}} \right) \left( 2\sqrt{\pi} \frac{r}{v} \right) \sum_{l=-\infty}^{\infty} \int_{B_0/B_{max}}^{B_0/B_{min}} d\Lambda \left( \frac{\hat{r}_b}{2} \right) \\ & \times \int_0^{\infty} \left[ \frac{\omega_{*N} + \left( \hat{\epsilon} - \frac{3}{2} \right) \omega_{*T} + \omega_E - \omega}{\langle \omega_D \rangle + l\omega_b - i\nu_{eff} + \omega_E - \omega} \right] \hat{\epsilon}^{5/2} e^{-\hat{\epsilon}} d\hat{\epsilon} \\ & \times \left| \left\langle \left( 2 - 3 \frac{\Lambda}{B_0/B} \right) (\kappa \cdot \xi_{\perp}) - \left( \frac{\Lambda}{B_0/B} \right) (\nabla \cdot \xi_{\perp}) \right\rangle \right|^2 \end{aligned}$$

with full definitions found in the reference. The first integration is over flux surface, the second over pitch angle, and the third over particle energy. The integrand of this term shows resonances with the trapped ion precession drift,  $\langle \omega_D \rangle$ , bounce frequency,  $\omega_b$ , the effective ion collisionality,  $\nu_{eff}$ , and the plasma rotation, which enters the integrand through the ExB frequency  $\omega_E$ . The integration allows a more complex trajectory through stability space as a function of the rotation profile, which can in NSTX vary from Alfvén Mach  $\sim 0.5$  in the plasma core with no magnetic braking, to levels at or below that attained in DIII-D balanced NBI experiments [40] when non-resonant magnetic braking is used.

This model is starting to be tested against the existing RWM marginal equilibrium database for NSTX. As an example, Figure 2.3.2-14 shows contours of normalized RWM growth rate,  $\gamma_{\tau_w}$ , from the Hu-Betti-Manickam code [47], in terms of the real and imaginary parts of  $\delta W_K$ , using input from an NSTX discharge that becomes unstable at relatively high plasma rotation. Varying plasma rotation from high to low in theory (Frame (a)) shows the plasma move from a region of stability into the unstable region, then return to stability at reduced plasma rotation. This occurs as the different levels of plasma rotation, yielding kinetic resonances of varying strengths (varying energy dissipation). Frame (b) illustrates the dependence of the physics model on ion collisionality, parameterized by variation in  $Z_{eff}$ , for another plasma reconstruction. Greater stabilization is found at lower ion collisionality, which is due to the kinetic stabilization effects being more prominent at lower  $\nu_i$ . This result counters those typically found in simpler fluid viscous models which have increased dissipation at higher collisionality.

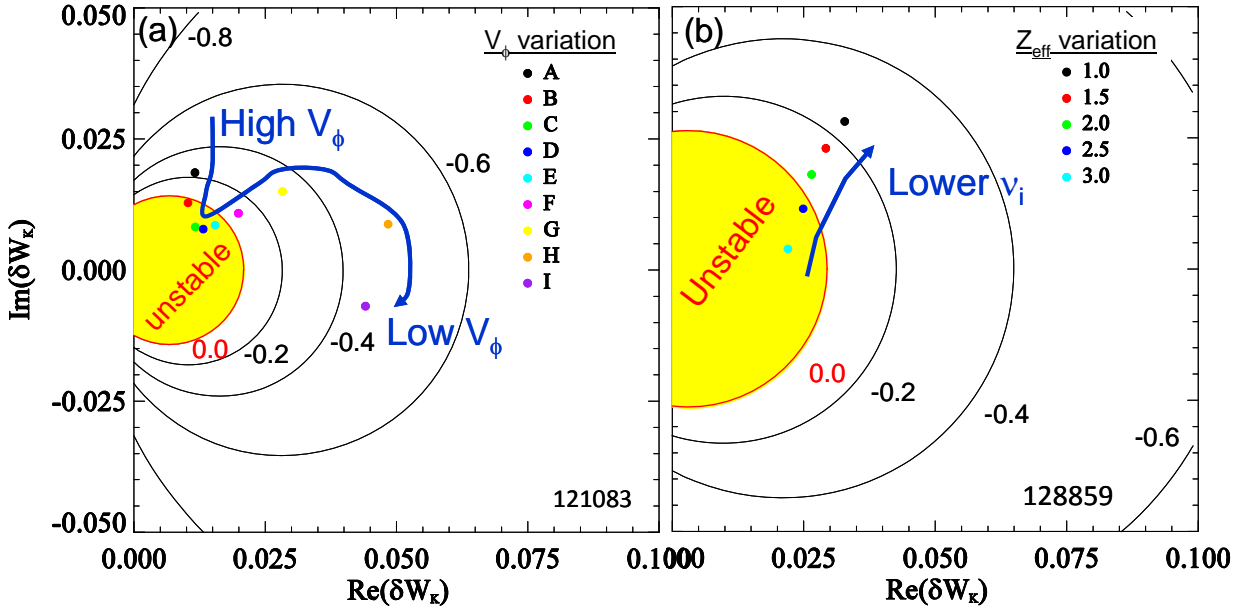


Figure 2.3.2-14: Contours of  $\gamma\tau_w$  computed for an NSTX plasma that becomes RWM unstable at an intermediate level of plasma rotation (Frame (a)) and for a plasma used to test stability variation versus ion collisionality (Frame (b)). The measured marginally stable experimental rotation profile best matches the rotation profile variation from fastest (case A) to slowest (case I) at case B or C, in agreement with the computed crossing point into the unstable region.

The kinetic model result is also qualitatively inconsistent with NSTX experiments performed in the past two years, including recent (2008) experiments. These initial results form the basis of further study of the kinetic model to explain RWM marginal stability more generally and to understand the mode stabilization physics. Understanding the physical role of plasma rotation and ion collisionality is key to this study in order to have greater confidence in extrapolations to next-step ST devices. Specific experiments in 2008 will provide further tests, and in the 2009 – 2013 time frame the center stack and rotation control upgrades will go further to both test the physics, and to determine robustly stable rotation profiles to maintain high  $\beta_N$  for long pulse duration.

## (ii) physics and control - plans

Planned research to meet the RWM stabilization physics and control goals in the 2009 – 2013 timescale follows two general approaches:

- (i) understanding of active stabilization physics and demonstration of reliability at all levels of plasma rotation.
- (ii) development and experimental verification of an expanded passive stabilization physics model

Research in the next five years will address key issues to bridge the present gap in both RWM passive and active stabilization physics understanding and system performance. Understanding the role of poloidal mode deformation,  $n > 1$  mode activity during  $n = 1$  active stabilization, and understanding and implementing improvements to the present active feedback system are important components of RWM active stabilization study. The investigation of using both upper and lower radial and/or poloidal field RWM sensors for mode detection during feedback will continue using the initial experimentation in 2007-2008 to define the next steps. We envision that key physics experiments can be conducted with the present active feedback system for the next few years, and outline several specific upgrades to NSTX capability and diagnostics to take the research into further advanced topics. These upgrade plans and associated studies will be discussed in the balance of this section.

The general plan for RWM passive stabilization research in the 2009-2013 follows from present experimental results from NSTX and DIII-D, but will seek out a new physics paradigm for RWM stabilization that can reproduce the observations of present experiments in NSTX and other tokamaks. One key departure from present theory will be to abandon both the assumption of a single “critical rotation frequency” and most likely the existence of a single critical rotation profile for RWM stabilization. Data to date supports this approach, as new data suggests that the RWM can be destabilized at intermediate to high rotation frequencies, while plasmas with zero rotation at the  $q = 2$  surface can remain stable at high  $\beta_N$ . A potential hypothesis that departs least from the existing physics models is one where multiple dissipation mechanisms apply at different levels of rotation and with differing radial localization. The introduction of stabilizing dissipation due to resonance with trapped particle precession

drifts (Hu-Betti theory) may aid in this understanding. Since the kinetic model depends on aspect ratio,  $\nu_i$ , and rotation profile, NSTX data is important to determine if this physics can be responsible for mode destabilization at high rotation and mode stabilization at low rotation. The new center stack upgrade will expand this study to strongly collisionless plasmas with an order of magnitude lower  $\nu_i$ . This physics is additionally important to non-ST devices as it should apply to RWM stabilization at plasma rotation levels expected in ITER. Accessing the important range of rotation frequency where trapped particle precession effects become important (similar to the low levels reached in DIII-D balanced NBI experiments) has been demonstrated on NSTX using non-resonant  $n = 3$  magnetic braking, and this technique will continued to be used in future studies.

## SUMMARIZED RESEARCH PLANS AND TIMELINE

### (i) ACTIVE FEEDBACK CONTROL

- FY2009-11      Use active RWM feedback as a standard tool for mode stabilization in experiments as desired by session leaders. Continue optimization of the RWM active feedback system at various plasma rotation speeds and profiles by determining the best combinations and relative spatial phase of RWM sensors to be used for feedback, setting of feedback phase (difference between measured mode phase and applied field phase) and other control settings.
- FY2009-11      Investigate underlying RWM active control physics, and methods of decreasing the possibility of poloidal deformation of the mode and loss of stabilization. Begin investigation of multiple modes in RWM stabilization and the role of SOLC as additional measurements become available. Determine role of boundary conditions in RWM stability analysis, and the role of plasma response in stabilization using the IPEC code (see section 2.3.3)
- FY2009-10      Complete design studies for the proposed NCC, modifications to passive stabilizing structure, and non-magnetic detection of RWMs. Continue analysis of advanced active feedback stabilization control algorithms using present NSTX data and define a



specification for the implementation of these algorithms for RWM feedback control enhancement.

- FY2010-13 Implement non-magnetic detection of RWM using soft X-rays, measure RWM activity, and determine how to best process data for future interface to the plasma control system. Determine the role of  $n > 1$  RWM activity during  $n = 1$  stabilization and expand study when additional NBI power capability becomes available. Examine the role of measured SOLC in stability analysis.
- FY2011-13 Implement improvements to passive stabilizing structure and new NCC control coils (incremental). Conduct initial RWM stabilization experiments using the NCC (incremental). Compare stabilization performance with design expectations. Examine the role of  $n > 1$  instabilities with second neutral beam. Determine effectiveness of active control in low collisionality plasmas with new center stack.
- FY2013 Conduct advanced RWM stabilization experiments using the midplane and new NCC coils (incremental) to produce high reliability of RWM stabilization at the highest  $\beta_N$  possible. Experiments would include prevention of poloidal deformation of mode,  $n > 1$  control, high  $\beta_N$  sustainment with active mode control,  $V_\phi$  control, and initial  $q_0$  control.

#### (ii) PASSIVE STABILIZATION PHYSICS

- FY2009-11 Continue research to determine the physics of RWM passive stabilization (a 2009 NSTX milestone) including proposals for joint experimentation with DIII-D. Further examine the role of the rotation profile, Alfvén frequency, sound frequency, ion collisionality, applied resonant and non-resonant fields, and kinetic resonances (e.g. trapped particle precession resonance) in RWM passive stabilization.

- FY2011-12 Examine passive stabilization in low collisionality plasmas created with the new center stack, and with greater rotation profile variation under  $V_\phi$  control and with new non-resonant magnetic braking torque profile using the NCC. Compare to theory.
- FY2012-13 Determine a reliable physics model to confidently predict RWM stabilization as a function of rotation and ion collisionality. Test this model against equilibria created with the second neutral beam (further variation of  $V_\phi$  and  $q$  profiles).

### 2.3.3 Dynamic error field correction

**Goal:** Determine sources of dynamically changing error field due to inherent asymmetries in the device and the plasma physics responsible for amplification of these sources. Apply techniques that will dynamically cancel these fields to maintain plasma rotation and stability.

#### (i) physics and control - results

Dynamic error field correction (DEFC) involves the detection and correction of non-axisymmetric fields generated during evolution of the plasma discharge. In a low beta plasma, this basically involves correction of static error fields and alteration of those fields based on movement of device components during the discharge evolution. In addition, plasmas of sufficiently high beta will alter these fields, typically amplifying them, while plasma rotation will shield them. The creation of resonant field amplification closely couples DEFC research to RWM research, since RFA is theoretically due to weakly damped (stable) RWMs. [25] At high beta, DEFC is basically the correction of beta-dependent RFA and so is in essence RWM control. A standard distinction between active RWM stabilization or control and DEFC is timescale: “RWM control” is typically used to describe control of unstable modes (up to a few times the RWM inverse growth rate) and “DEFC” is typically used to describe control of stable modes (timescale of changes in  $\beta_N$ , therefore  $\tau_E$ ). When the RWM growth rate is slowed to  $O(1/\tau_E)$ , the distinction is not clear, nor is highly important. In general, DEFC is critical for reliable, high performance plasma operation, aiming to reduce low beta locked mode density thresholds as well as minimizing drag due to non-axisymmetric fields, maintaining plasma rotation and maximum  $\beta_N$ .

Dynamic error field correction has played a significant role in allowing the highest performance plasmas in NSTX, and the correction of  $n > 1$  fields (specifically,  $n = 3$ ) was found to be important. Initially, open-loop correction of the low beta dynamic error field due to movement of components such as the center stack leg of the toroidal field coil was addressed, with good success during the plasma startup through the plasma current flat top. Utilization of the closed-loop  $n = 1$  feedback system was subsequently used, providing correction over the full pulse including the high  $\beta_N$  phase of the discharge, yielding the longest pulses and maintenance of plasma rotation.

The method utilized for training the feedback system for  $n=1$  DEFC is illustrated in Fig. 2.3.3-1. A reference discharge with no current in the RWM coils is shown in black; it achieves  $\beta_N \sim 4.5$ , above the no-wall  $\beta$  limits for these class of plasmas. The next case, in red, has a pre-programmed  $n=1$  field, but with the feedback turned off. The applied error field is amplified by the RFA response of the plasma, resulting in increased rotation damping, and an eventual RWM followed by a rotation and  $\beta$  collapse. The two cases in green and blue have the same pre-programmed  $n=1$  error field, but feedback proportional gains of 0.5 and 0.7 respectively. Importantly, the direct coupling of the RWM coils to the in-vessel sensors is removed by the realtime software before the mode decomposition is calculated and the feedback requests generated; the system is thus feeding back on only the measured RFA response. The feedback system produces current requests that attempt to cancel the applied error field, and increasing the gain leads to improved cancellation. The key step is to then to turn off the applied error field, but retain the optimized feedback settings.

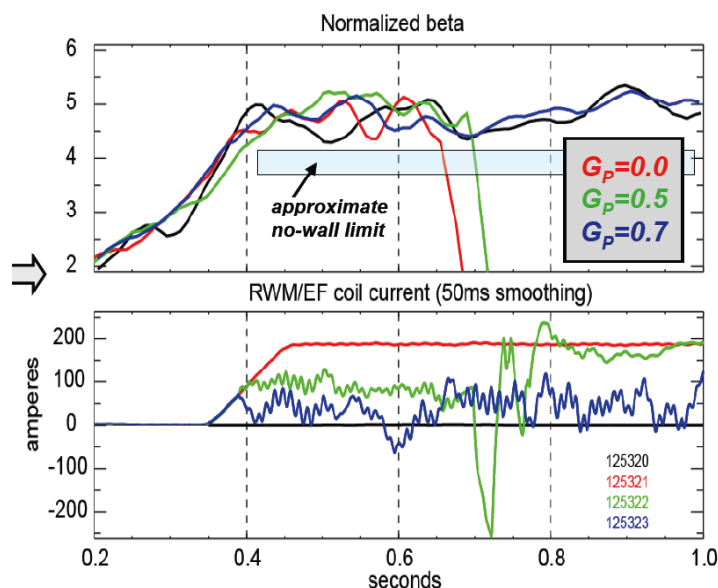


**FIG 2.3.3-1: Optimization of the feedback system for dynamic error field correction. The top frame shows the  $\beta_N$  traces while the bottom shows the current in a representative RWM coil. The feedback proportional gain and approximate no-wall limit are shown in the top frame.**

In 2007, it was found that discharge pulse length depended on the polarity of an applied  $n = 3$  field, which is typically used for non-resonant magnetic braking (see section 2.3.5). Figures 2.3.3-2 a) and b) show the plasma current and  $\beta_N$  for cases where different levels of  $n=3$  braking, shown in frame c), were applied. There is a clear extension of the high-beta phase and pulse length with  $n=3$  fields of favorable phase. The peak rotation and pulse lengths occur at approximately 300A of  $n=3$  current in the favorable phase. This is significantly lower than the 0.8 – 1.0 kA level of current typically used to control plasma rotation in NSTX by  $n = 3$  magnetic braking.

Further experiments in 2008 have indicated that the required  $n=3$  correction level is likely tied to the PF5 coil current. This is consistent with the measured shape of the coil, which is predicted to produce a predominantly  $n=3$  field. A future upgrade will be to tie this  $n=3$  correction to the PF5 current in the realtime system, allowing more accurate  $n=3$  correction over a range of plasma conditions. In 2008,  $n = 2$  fields were generated using the RWM control coil for the first time in NSTX, and a dedicated experiment was not able to increase plasma rotation, indicating that  $n = 2$  error fields may not be significant.

However, applying the  $n = 2$  fields with only six coils also generated a significant  $n = 4$  component, which may complicate the analysis.

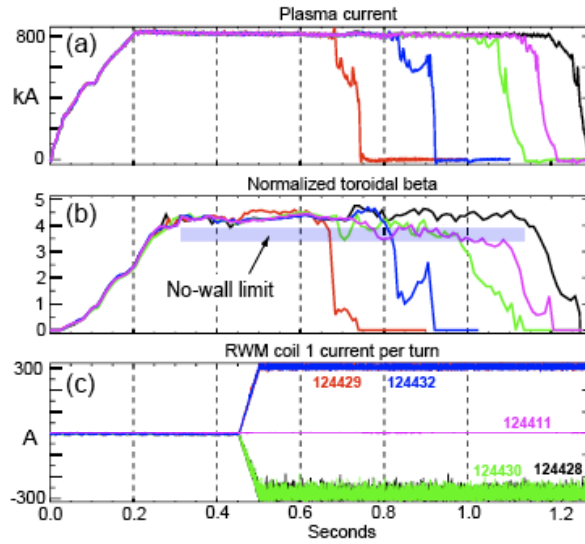


**Figure 2.3.3-2 Increased pulse length observed with  $n = 3$  applied field with favorable phase, as evidenced by the pulse length (a) and sustainment of the high- $\beta$  state (b). The RWM coil current, applying a pure  $n=3$  spectrum, is shown in (c).**

These error-field correction techniques have been utilized to develop long pulse discharges with sustained high values of  $\beta_N$  and rotation. An example is shown in Fig 2.3.3-3, where the dynamic error field correction was accomplished by preprogrammed  $n=3$  correction and optimized  $n=1$  feedback based on the combined upper and lower  $\Delta B_p^{n=1}$  sensors. This discharge had superior discharge characteristics, including a very long period free of rotating MHD modes and a steady *increase* of the edge rotation, compared to the typical decrease observed without DEFC. Note that this class of discharges has been further improved through the use of lithium conditioning.

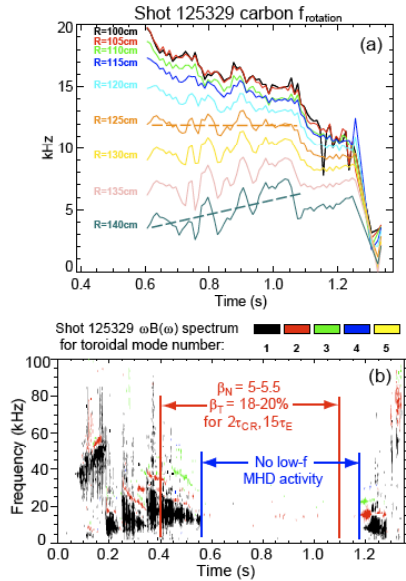


**Figure 2.3.3-3 Plasma rotation evolution (top), and MHD activity (bottom), for a long-pulse discharge facilitated by DEFC. This class of discharges has been further improved by lithium conditioning.**

These favorable results motivate further study to increase the effectiveness of DEFC in producing plasmas with greater pulse duration, maintaining high  $\beta_N$  and plasma rotation for as long as device limitations (OH flux consumption, coil heating) will allow. Plasmas already produced with pulse durations greater than one second typically allow sufficient time to conduct desired experiments and allow a ramp-down of the plasma current in a controlled manner.

**(ii) physics and control - plans**

DEFC research is an essential part of bridging the present operation of NSTX to the long-term 5 year goal of demonstrating sustained operation of high confinement, high beta plasmas with high reliability, and so will remain an active area of study in the 2009 – 2013 period. It will remain closely coupled to RWM stabilization research, as the studies and control hardware and software are highly complementary. As high levels of plasma rotation generally appear favorable for both confinement and stability and will likely lead to passive stabilization in future NBI-driven devices such as CTF, understanding the physics regarding the effect of error fields in high beta NSTX plasmas is key to future extrapolations.

Research in this regard will utilize the Ideal Perturbed Equilibrium Code (IPEC), [48] which has been used to evaluate the plasma response to error fields in DIII-D and NSTX, allowing their accurate correction. [49] IPEC finds 3D perturbed scalar pressure equilibria with shielded islands in tokamaks. Given a 2D tokamak equilibrium and an external perturbation, an ideal perturbed equilibrium can be determined by solving the force balance  $\bar{\nabla} \delta p = \bar{\mathbf{j}} \times \delta \bar{\mathbf{B}} + \delta \bar{\mathbf{j}} \times \bar{\mathbf{B}}$  with boundary conditions set by external coils while preserving the pressure  $p(\psi)$  and the safety factor  $q(\psi)$  profiles in the plasma. IPEC augments DCON and VACUUM stability codes to solve the force balance given a set of perturbed field  $\delta \bar{\mathbf{B}} \cdot \bar{\mathbf{n}}_b$  on the plasma boundary, and uses virtual surface currents on the boundary to match the set of  $\delta \bar{\mathbf{B}} \cdot \bar{\mathbf{n}}_b$  with a set of externally given field  $\delta \bar{\mathbf{B}}^x \cdot \bar{\mathbf{n}}_b$ . The total field  $\delta \bar{\mathbf{B}} \cdot \bar{\mathbf{n}}_b$  and the external field  $\delta \bar{\mathbf{B}}^x \cdot \bar{\mathbf{n}}_b$  are linearly related to  $\delta \bar{\mathbf{B}} \cdot \bar{\mathbf{n}}_b = \hat{P} [\delta \bar{\mathbf{B}}^x \cdot \bar{\mathbf{n}}_b]$  by a permeability operator P on the plasma boundary. The perturbed field and displacement found by IPEC includes the effects by perturbed currents in the plasma (plasma response effects) as well as the externally given field. These effects can substantially change the perturbed field and displacement in tokamak. A comparison of two-dimensional equilibrium flux surfaces for NSTX, and corresponding IPEC perturbed flux surfaces formed by an applied  $n = 1$  field configuration are shown in Fig 2.3.3-4 (a) and (b). It can be seen that the flux surfaces inside the plasma boundary are only deformed in the IPEC equilibrium. Macroscopic stability physics involving ideal flux surface perturbations, such as RWM deformation and correction (Section 2.3.2.1), and associated neoclassical toroidal viscosity causing plasma rotation damping (Section 2.3.5) can be studied using IPEC.

The present form of IPEC has the limitation of not including the currents associated with anisotropic tensor pressures. The tensor pressure IPEC is the next step of the research, which could be completed within a couple of years, will allow a more complete evaluation of shielding currents and may provide greater insight into RWM control by plasma rotation. Also, IPEC can be modified to allow islands at one or multiple rational surfaces. An example of such an equilibrium is shown in Fig 2.3.3-4(c), without the plasma response, but the modified IPEC with islands will include the perturbed plasma currents. This relaxed IPEC can allow the study of the interactions of external perturbations with neoclassical tearing modes as another important application.

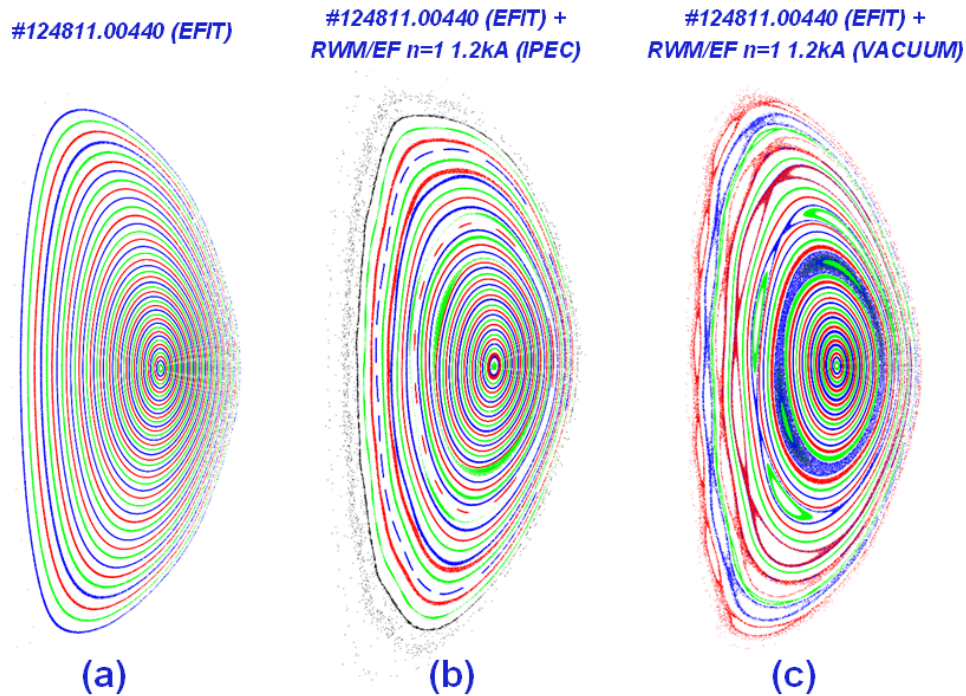


**Figure 2.3.3-4** The reconstructed (a) 2D equilibrium, (b) IPEC perturbed equilibrium, and (c) perturbed equilibrium with superposed vacuum field, in NSTX with an  $n=1$  perturbation generated by the midplane non-axisymmetric coils.

DEFC research and practical correction of the field in real-time will benefit from the installation of the upgraded non-axisymmetric control coil (NCC). Simultaneous correction of  $n = 1, 2$  and  $3$  fields would be possible with significantly improved flexibility in the 2009-2013 period with the NCC. The design of this system for most effective DEFC will be analyzed using IPEC and VALEN. With the coil upgrade and additional power supplies,  $n > 1$  fields could be made to toroidally propagate to better match the error field evolution, and the poloidal spectrum of the dynamic error field could be significantly better matched (the present midplane coil does not allow a significant change in the poloidal spectrum of the correcting field). In general, upgrades to the RWM active control system discussed directly transfer for use in DEFC.



## SUMMARY OF RESEARCH PLANS AND TIMELINE

- FY2009-11 Continue DEFC studies experimentally and with IPEC to further investigate sources of dynamic error field and implementing methods of correction. Develop calculation of tensor pressure equilibria in IPEC. Experimental data will provide field amplification and shielding data as needed to validate IPEC tensor-pressure predictions.
- FY2011-12 Evaluate changes to DEFC required to optimize plasmas created with new center stack. Modify IPEC to allow the formation of magnetic islands at one or multiple rational surfaces. Compare to experiments involving the interaction of external magnetic perturbations and tearing modes.
- FY2011-13 Utilize the NCC (incremental) to expand the flexibility and capability of DEFC (correction of  $n$  number up to 6) to reliably sustained high  $\beta_N$  plasma operation. Develop self-consistent theory of flow-damping by intrinsic error fields and 3D externally applied fields to calculate optimal correction of error fields at high beta. Compare to NSTX experimental data and utilize in real-time error-field control algorithms as applicable.

### 2.3.4 Tearing mode / NTM physics

*Goal: Study neoclassical and classical tearing modes in the unique low aspect ratio, high beta, and large ion gyro-radius plasmas available in NSTX, in order to both extrapolate our understanding to future ST devices and provide data complementary to that from conventional aspect ratio tokamaks. Investigate the impact of these modes on plasma beta, rotation, fast particle redistribution, and the potential of low aspect ratio operation as being theoretically favorable for NTM stability. Determine scenarios that allow operation without these deleterious instabilities.*

#### (i) physics – results and plans

The neoclassical tearing mode (NTM) is a magnetic island driven by a hole in the bootstrap current. These modes are a likely problem for any high-performance tokamak, leading to confinement degradation (soft  $\beta$  limit) in the case of the  $m/n=4/3$  and  $3/2$  modes, and potential mode-locking and disruption for the  $2/1$  NTM [50]. These modes were studied in early NSTX [51] research, and have been observed in MAST [52]. We plan a renewed focus on NTM physics in the coming research period. Important areas for proposed NTM research include i) investigation of the onset- $\beta$  and marginal island widths as functions of kinetic parameters and plasma rotation ii) studies of the NTM triggers in  $q_0 > 1$  regimes, iii), modeling these modes in low-aspect ratio geometry including the effects of flow and flow shear, and iv) studies of the interaction of NTMs with fast particles, including particle redistribution during mode activity.

The degrading effects of an  $m/n=2/1$  NTM on a high performance discharge are shown in Fig 2.3.4-1. The mode amplitude is shown in frame a), with the mode striking at  $t=0.56$  and maintaining its saturated state until  $t=0.71$ , when it locks; the plasma then disrupts at  $t=0.75$ . Frames b) and c) show that  $\beta_N$  continually drops during the period of the mode, as does the energy confinement time (both determined by the EFIT code with partial kinetic constraints). The mode has a profound effect on the rotation profile: an immediate collapse of the core rotation and transition to rigid-body rotation. Indeed, it is likely that both the short-circuiting of the magnetic surfaces [53] and the reduction of rotation and rotation shear contribute to the severe confinement degradation. It is clear that in NSTX as well as conventional tokamaks, these modes must be avoided in order to maintain the desired high- $\beta$  state.

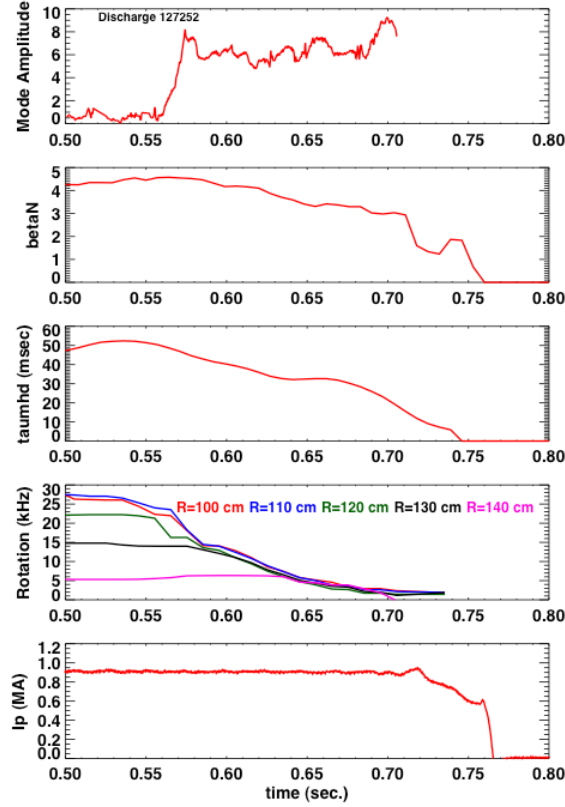


Figure 2.3.4-1: Illustration of the effects of a 2/1 NTM on discharge confinement. From top to bottom are the mode amplitude,  $\beta_N$ ,  $\tau_E$ , the rotation frequency at five radii, and the plasma current.

The Modified Rutherford equation (MRE) provides a convenient basic framework to consider for the NTM studies described below:

$$\frac{\tau_R}{r_s} \frac{dw}{dt} = r_s \Delta' - \frac{6r_s D_R w}{w^2 + w_d^2} + \sqrt{\frac{r_s}{R}} \frac{L_q}{L_p} \beta_p r_s \left( \frac{w}{w^2 + w_d^2} - \frac{w_{pol}^2}{w^3} \right) \quad (1)$$

This equation describes the evolution of the full island width ( $w$ ), including classical tearing stability ( $\Delta'$ ), neoclassical drive due to the bootstrap current missing inside the island ( $\propto \beta_p/w$ ), stabilizing terms due to toroidal geometry ( $D_R/w \propto \beta/w$ , the “Glasser, Greene and Johnson” term), and threshold effects (the transport threshold manifested by  $w_d$  [54] and the polarization threshold manifested through  $w_{pol}$  [55]) which are important for small islands. Given that  $\beta$  can begin to approach  $\beta_p$  in NSTX, the GGJ term is expected to be strongly stabilizing [56], an effect to be examined as these studies move forward.

Additional terms can be added to this equation, such as those associated with stabilizing electron cyclotron current drive (ECCD) [57].

Equation 1 predicts that for saturated island sizes larger than  $w_d$  and  $w_{pol}$ , the island width should be proportional to  $\beta_p$ . This trend is indeed observed, as illustrated in Fig. 2.3.4-2, where the square root of the  $m/n=2/1$  magnetic fluctuation amplitude at the wall ( $\propto$  to the island width), is plotted against the global  $\beta_p$  for four discharges where NBI power ramp downs occurred. The linear relationship is clear. This observation, coupled to the close frequency match between the magnetic fluctuations and the  $q=2$  rotation frequencies and the observation of flat spots at  $q=2$  in the electron temperature profile, confirms that the observed mode is indeed a neoclassical island. Similar observations have been made for the  $3/2$  NTM as well, and the physics discussed above and below is typically relevant to both modes.

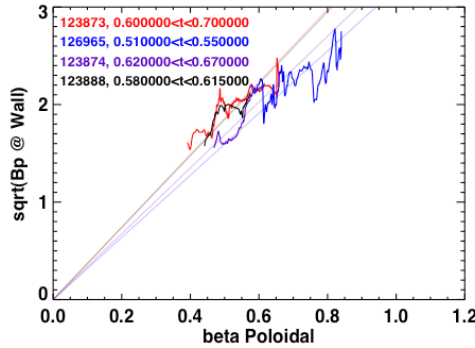


**Fig 2.3.4-2: The measured  $m/n=2/1$  island width ( $\propto \tilde{B}_{p,wall}$ ) is proportional to  $\beta_p$ , as expected for a saturated NTM.**

The small island terms in (1),  $w_d$  and  $w_{pol}$ , prevent NTM growth for arbitrarily small islands when classical tearing is stable ( $\Delta' < 0$ ). Instead, a seed island must be formed whose width exceeds some threshold value. For the  $3/2$  NTM, this seed-island is typically provided by sawteeth in conventional aspect ratio tokamaks; ELMs have been suggested to play a similar role for the  $2/1$  NTM in DIII-D and JET. In NSTX, rapid changes in the beam timing have been observed to trigger the  $3/2$  NTM. The NSTX discharge illustrated in Fig. 2.3.4-3, however, shows a large  $2/1$  NTM growing with no observable trigger. The spectrogram from a single Mirnov coil in the top frame shows the mode growing at  $t=0.83$ , with no precursor; this smooth growth is clearly indicated in the mode amplitude plot in the frame below. Neither

the  $H_\alpha$  nor the edge and core USXR signals show a precursor. The NTM eventually locks at  $t=0.95$ , as evidenced by the rapid drop of the edge USXR signal and spike in  $H_\alpha$ , followed by a disruption. It is possible that cases like these begin as classical tearing modes, which transition to neoclassically driven modes when the island width exceeds the critical island width [58]. This classical physics can be especially important for high- $\beta$  plasmas, where a pole in  $\Delta'$  occurs at the ideal kink limit [59]. This discharge had  $\beta_N=4.3$  when the mode struck, near to if not exceeding the no-wall limit. Understanding this triggering will be an important part of NSTX research.

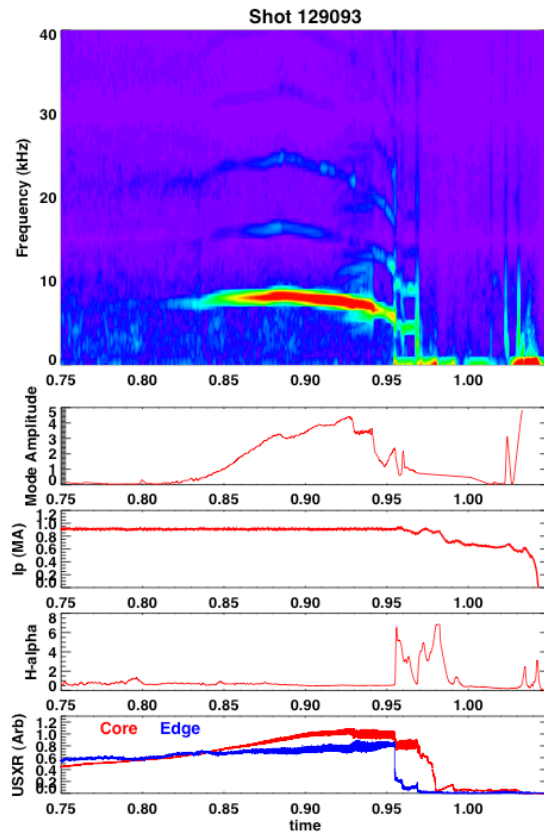


Fig 2.3.4-3: Example of an  $m/n=2/1$  NTM with no clear trigger.

The marginal island width, i.e. the island width where  $dw/dt=0$  for the smallest  $\beta_p$  where NTMs are still metastable, is a key parameter for understanding the relevant small island physics ( $w_d$  and  $w_{pol}$ ) and extrapolating to larger and hotter plasmas. Experiments at conventional aspect ratio in DIII-D [60], JET [61] and ASDEX-U [62] suggest that the marginal island width scales empirically with the poloidal

gyroradius. Verifying this empirical scaling at low aspect ratio is particularly important, as it predicts that an ST reactor or CTF (or indeed, ITER) will be very susceptible to NTM destabilization, and that NTM control techniques must be implemented.  $\beta_p$  ramp down experiments will be conducted to establish the marginal island widths for both the 3/2 and 2/1 NTMs, as a function of parameters such as rotation and poloidal gyroradius. It is planned to make a first complete set of marginal island-width experiments in the FY09-FY11 time-frame. However, the extended field and current capabilities of the upgraded NSTX will expand the parameter regime in quantities like poloidal gyroradius, collisionality,  $q_{\min}$  and q-shear, providing greater a wider range of applicability for the results.

Plasma rotation and rotation shear enter the eqn. 1 in a number of places, for instance through the polarization threshold term and through modifications to  $\Delta'$ , as well as through mechanisms outside of the MRE, such as modifications to the coupling between the rational surface and the surface where triggering instabilities occur. Given that the momentum input to a future reactor is likely to be much reduced compared to present experiments, there has been recent interest in how rotation and rotation shear experimentally impact the onset and saturation of NTMs. Experiments in JET and DIII-D demonstrated the importance of rotation in increasing the NTM threshold [63]. For the 3/2 NTM, this effect may be associated with dynamic rotation shielding between the NTM resonant surface and the  $q=1$  surface, where the seed perturbation originates. Experiments in DIII-D have also demonstrated a reduction in the onset  $\beta$  for 2/1 modes when the co-injection beam torque is reduced to and beyond zero [64].

Experiments in NSTX have begun to study the dependence of the 2/1 mode onset on rotation shear. We have observed a ~20% reduction in onset global  $\beta_N$  as the rotation at  $q=2$  is reduced. However, given that the NTM evolution in eqn. (1) is determined by local parameters, we have undertaken more systematic studies in terms of local bootstrap drive and rotation shear. Fig. 2.3.4-4 shows the local

neoclassical island drive at mode onset,  $\mu_0 \langle J \cdot B \rangle L_q / \sqrt{\langle B_p^2 \rangle}$ , where  $\langle J \cdot B \rangle$  is determined for the Sauter

model for the bootstrap current, as a function of the normalized rotation shear at  $q=2$ ,  $\left( \frac{d\Omega}{dR} \right) \tau_A L_s$ . The

discharges in the scan were chosen from a wide variety of experiments which utilized  $n=3$  braking and NBI torque to vary the rotation. All were high- $\kappa$ , high- $\delta$  plasmas with  $I_p=1\text{MA}$  and  $B_T=0.45\text{T}$ , typical of

high-performance regimes in NSTX. There is a clear offset-linear dependence of the bootstrap-drive on rotation shear when the mode strikes, implying the importance of rotation shear in allowing higher- $\beta$  operation. Importantly, this is the first ever correlation of the local NTM properties with local rotation shear, expanding on the previous DIII-D work.

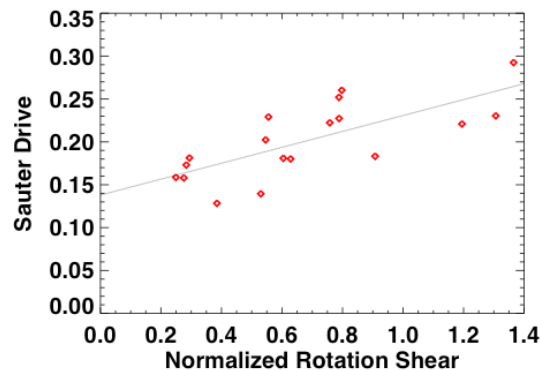


**Figure 2.3.4-4 Local bootstrap drive and a function of rotation shear at  $q=2$ , for discharges high- $\kappa$ , high- $\delta$  discharge. Both  $n=3$  braking and variations on the NBI are used to vary the rotation shear.**

There may, however, be NTM physics outside the direct purview of eqn (1). For instance, the tearing modes in TFTR [65], AUG [66], and possibly other major tokamaks, are commonly coupled to core kink-like modes. As these internal kink-like modes resemble the fishbone instability, it is reasonable to view this as a mechanism through which NTMs are coupled to the fast ion distribution. Evidence for such coupling, e.g., strong frequency chirping, has not been seen as yet in NSTX, though it has been observed in AUG [67] and TFTR. However, NSTX presently operates in a fast ion regime far from typical operating regimes of present large aspect ratio tokamaks. The upgrade to the center stack will allow higher field operation, bringing NSTX fast ion parameters more in line with those of conventional tokamaks. This will allow experiments to study the interactions of fast ions, including potential drive mechanism, with NTMs.

These experimental tasks will be executed in parallel with modeling and simulations of NTM dynamics at low aspect ratio. A three part modeling effort is planned in this regard, involving the linear dispersion relation describing the threshold for onset of the mode, the quasilinear island evolution equation for

intuitive study of the effects of low aspect ratio, and the simulation of mode onset and evolution with initial value codes. The presence of toroidal flow shear introduces a number of physics issues into these analyses, which are critical to understanding the experimental outcome. Experimental discharges that exemplify the physics of flow shear effects on the onset and evolution of these resistive MHD instabilities will be compared to theoretical predictions.

The effect of a sheared flow field on the coupling between modes can be described by the solution to the dispersion relation  $\det(D' - D(Q)) = 0$  where  $D'$  includes both tearing ( $\Delta'$ ) and interchange parities,  $D(Q)$  is the solution vector inside of the resonant layer, and  $Q$  is the normalized growth rate. With flow shear,  $Q$  becomes complex in the sense that the growth rate now has both real and imaginary parts in the inner layer  $Q \equiv Q_r + iQ_i$  where  $Q_r = k \cdot V_\phi$  (ignoring poloidal precession from  $\omega_*$  effects) represents the toroidal angular frequency at the rational surface, and  $Q_i$  represents the mode growth rate. This directly affects the coupling between modes in toroidal geometry, as addressed at length in [68] and recently published in Ref. [69] as well as the local stability via the inner layer physics, as described in [70], among several others.

In this research plan, we intend to compute the tearing and interchange solutions for multiple rational surfaces using the PEST-III code, and compute the inner layer solutions using the code described in Ref. [71] to solve the dispersion relation. The individual effects can then be examined and compared with a similar approach using the NIMROD code.

A further step will be to implement solutions of the MRE (equation 1) in full low aspect ratio geometry. These studies were begun in the work by [72], where PEST-III was used to calculate  $\Delta'$ , and routines from NIMROD were used to calculate the bootstrap drive and  $D_R$ . These steps will allow full calculations of the island growth and decay rates, as well as the saturated island eigenfunctions, for comparison with the experimental measurements described above. A primary goal of these efforts will be to assess the impact of the GGJ term in the context of experimental measurements.

A more advanced modeling step will be to utilize initial value codes such as M3D and NIMROD to simulate the non-linear evolution of NTMs. Compared to the approach in equation (1), these methods are



far more advanced in their treatment of heat conduction around the island, the effects of rotation shear, and self consistent current profile and island width evolution.

A thorough theoretical and computational analysis of the effects that low aspect ratio will have on the resistive stability will be complimentary to the results from the experiment. Also, a comparison with results from the high aspect ratio experiments will give us insight to further develop our theoretical description of the physics of these instabilities.

Our ability to meet these scientific goals will be augmented through improved diagnostic coverage during this research period. NSTX plasmas are overdense, preventing traditional measurements of island widths via electron cyclotron emission (ECE); measurements to date have relied on edge magnetics and USXR emission to constrain the island size and location. However, the BES system currently under construction will allow core fluctuation measurements with high frequency and spatial resolution. The CIF-MSE system also has the ability to measure spatially localized fast magnetic fluctuations at NTM relevant frequencies. This measurement, combined with USXR emission and edge magnetics, should allow detailed studies of the island eigenfunction, including the coupling to internal kink-like modes if present.

## **(ii) NTM Control**

The results in Fig. 2.1.1-1 illustrate that 2/1 NTMs must be avoided in order to maintain optimal performance in NSTX. Experiments in DIII-D, JT-60, and AUG have demonstrated the ability to suppress both the 2/1 and 3/2 NTM with ECCD replacing the missing bootstrap current. This method is not available in the overdense NSTX plasma. Hence, passive control techniques will be employed in the planned research period.

To date, the most successful means of mitigating the 2/1 NTM has been through the use of combined lithium conditioning and dynamic error field correction. This is illustrated in Fig. 2.3.4-5, where the mode activity is compared between discharges with and without lithium evaporation; the rotation frequency in the core and at  $q=2$  are also shown, based on CHERS data and equilibrium reconstruction. Both discharges show a period of MHD activity during and immediately after the current ramp, as the  $q$ -profile evolves.

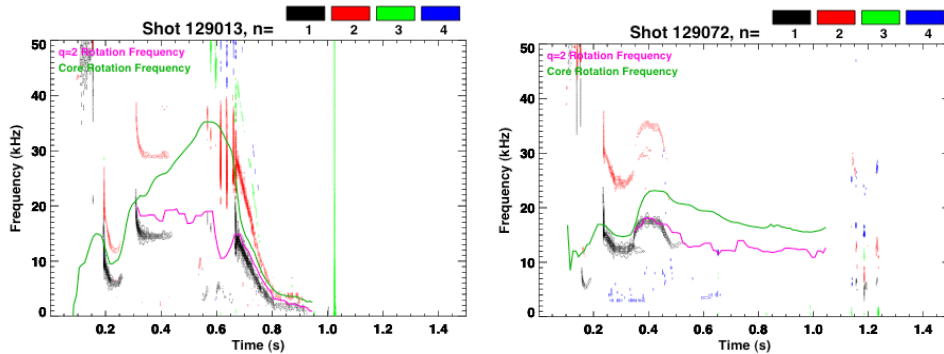


**Figure 2.3.4-5: Comparison of low-frequency mode activity in shots without (129013) and with (129072) with lithium evaporation. Also shown are the core (green) and  $q=2$  (magenta) rotation frequencies. The two discharges, designed to determine the effect of lithium evaporation on plasma performance, have all other controlled parameters the same.**

The control shot 129013 then develops the large  $2/1$  mode, the plasma rotation is dramatically reduced, and the shot ultimately disrupts at  $t=1$  sec. after the mode locks. The discharge with DEFC and lithium evaporation shows no sign of the later rotating instability, and ultimately succumbs to a fast-growing external mode, likely a resistive wall mode, at  $t=1.3$  seconds.

The stabilization noted in the above figure was achieved with both lithium evaporation and DEFC; in other more rare cases, one of these two ingredients is sufficient to suppress the mode for the duration of the discharge. A high priority for near-term studies is to understand how the current and rotation profiles with lithium and DEFC change the mode stability, including changes in mode triggering. The studies offer exciting prospects for NTM control, as the liquid lithium divertor and improved dynamic error field correction should allow a significant extension of these high performance discharge regimes.

In the five-year period starting in FY2014, an additional 3 sources will be added to the NSTX NBI system. As discussed in Chapter 6, this upgrade should allow access to fully non-inductive equilibria with  $q_{min} > 2$ . This scenario would have the effect of eliminating the pernicious  $m/n = 2/1$  and  $3/2$  resonances from the plasma. The effect of higher order NTMs, such as  $m/n=3/1$  and  $5/2$ , can then be studied. Additionally, the current profile control allowed with the more tangential beams may allow stabilization or mitigation of the NTM through modifications to  $\Delta'$ , in a fashion similar to what was achieved in COMPASS-D [73] with lower-hybrid current drive.

## SUMMARY OF RESEARCH PLANS AND TIMELINE

- FY2009-11 Complete characterization of NTM onset, including triggering physics and the role of rotation, rotation shear, and small island effects.
- FY2009-11 Utilize  $\beta_P$  ramp down experiments to characterize the dependencies of the small island physics on kinetic parameters at low aspect ratio
- FY2009-11 Utilize PEST-III for accurate calculations of  $\Delta'$  in NSTX geometry. Develop solutions to (1) utilizing low-aspect ratio solutions for all terms. Assess merits of low-A for NTM stability
- FY2010-12 Implement nonlinear initial value simulations of NTMs with NIMROD and M3D. Compare measured island seeding and evolution to simulations.
- FY2012-13 Utilize upgraded NSTX to look for interactions of NTM with fast particles
- FY2012-13 Utilize previously developed knowledge base and new tools to develop routine high- $\beta$  discharges with no deleterious island activity.

### 2.3.5 Plasma rotation and non-axisymmetric field-induced viscosity

**Goal:** Continue to develop quantitative, first-principles physics models of non-axisymmetric field induced plasma viscosity for both resonant and non-resonant fields, and apply results to create new techniques for imparting significant toroidal momentum to the plasma.

#### (i) physics and control - results

Plasma rotation can contribute to the stabilization of MHD instabilities by shielding static, three-dimensional error fields and by dissipating free energy available to the instabilities [39, 74]. Sufficient toroidal plasma rotation is required for passive RWM stabilization in NSTX and allows access to the highest  $\beta_N$  operation and the longest pulses in the device. Recent balanced NBI experiments in DIII-D have also shown an increase in energy confinement with increasing plasma rotation [75].

Because of the significant beneficial effects of plasma rotation in tokamaks, it is desirable to maintain plasma rotation in tokamak devices, including ITER, which will have a relatively low source of external momentum input. However, plasma rotation typically slows down in tokamaks during the discharge, likely due to the presence of non-axisymmetric fields from error fields or mode activity. For instance, resonant electromagnetic (EM) torque due to the interaction of device error fields with tearing modes [44, 76] causes the plasma rotation to slow, and magnetic islands to lock, leading to a significant loss in confinement or plasma termination. In addition, non-resonant, non-axisymmetric fields can also lead to substantial rotation damping caused by neoclassical toroidal viscosity (NTV) [77]. This effect was correlated with RWM activity [9,10] and was subsequently verified by quantitative comparison of theory to experiment in NSTX during the past five year period [78].

The plasma rotation profile evolution due to tearing modes is distinct from NTV-induced rotation damping so their lack of influence on rotation drag could be verified. This is illustrated in Figure 2.3.5-1, where the rotation damping observed during application of a non-axisymmetric magnetic field (Figure 2.3.5-1a) is contrasted with rotation damping due to  $T_{\times B}$  on a rotating island (Figure 2.3.5-1b). The damping due to NTV is relatively rapid, global, and the rotation profile decays in a self-similar fashion. In contrast, the damping due to EM drag is initially localized near the island, and diffusive from this radius, leading to a local flattening of the toroidal plasma rotation frequency,  $\Omega_\phi$ , and a distinctive momentum transfer across the rational surface from smaller to larger  $R$  as expected by theory [44, 81].

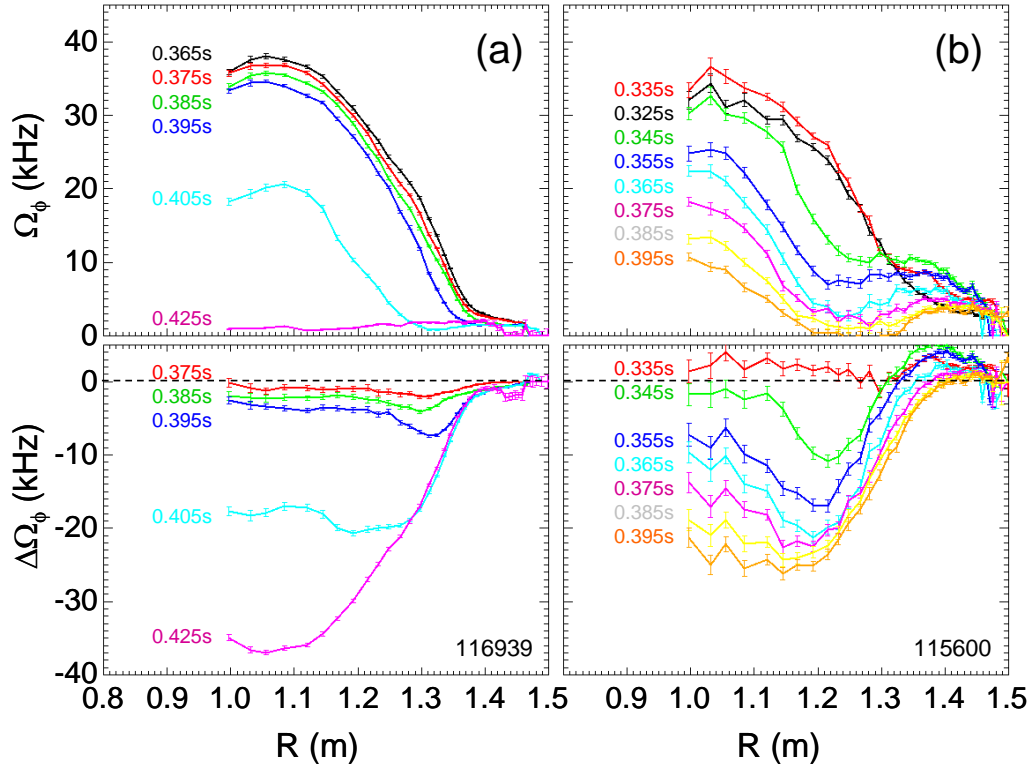


**Figure 2.3.5-1 Toroidal plasma rotation profile vs. major radius, and difference between initial profile and subsequent profiles for rotation damping (a) during application of non-axisymmetric field, and (b) during excitation of rotating tearing instability.**

Neoclassical toroidal viscosity is caused by the interaction of the plasma with magnetic field components that break the toroidal symmetry of the magnetic confinement field in a tokamak. Using a fluid model, NTV drag can be described as the force on the plasma fluid as it flows through the non-axisymmetric field perturbation. Using a particle model, the drag can be described in a relatively collisional plasma as a toroidal force caused by a radial non-ambipolar flux of particles drifting due to the non-axisymmetric field. In a sufficiently collisionless plasma, the effect is dominated by trapped particle drifts. While the full formulation used for comparison to NSTX experiments can be found in Ref. [78], the dominant flux surface-average force for the present NSTX range of ion collisionality is given by

$$\left\langle \hat{\mathbf{e}}_t \cdot \vec{\nabla} \cdot \vec{\Pi} \right\rangle_{(1/\nu)} = B_t R \left\langle \frac{1}{B_t} \right\rangle \left\langle \frac{1}{R^2} \right\rangle \frac{\lambda_{li} P_i}{\pi^{3/2} v_i} (\Omega_\phi - \Omega_{NC}) I_\lambda \quad (1)$$

where

$$I_\lambda = \frac{\varepsilon^{3/2}}{\sqrt{2}} \left[ \int_0^1 d\kappa^2 [E(\kappa) - (1 - \kappa^2)K(\kappa)]^{-1} \sum_n n^2 \left\{ \left[ \oint d\theta (\kappa^2 - \sin^2(\theta/2))^{1/2} A_n \right]^2 + \left[ \oint d\theta (\kappa^2 - \sin^2(\theta/2))^{1/2} B_n \right]^2 \right\} \right] \quad (2)$$

$\varepsilon \equiv r/R_0$ , and  $\lambda_{li} \equiv 13.708$ . The independent integration variable  $\kappa$  is a normalized pitch angle parameter defined in Ref. 79. The functions  $K(\kappa)$  and  $E(\kappa)$  are the complete elliptic integrals of the first and second kind, respectively, and the Fourier coefficients  $A_n, B_n$  for the magnetic field  $B$  as defined in Equation (6) of Ref. 78, and  $\Omega_{NC}$  is the neoclassical toroidal flow velocity [80]. Dedicated NSTX experiments found good quantitative agreement, i.e.  $\sim O(1)$ , between the measured change in the plasma angular momentum profile during periods of increased non-axisymmetric fields generated by  $n = 1$  and  $n = 3$  applied fields,  $n = 1$  RFA, and the  $n = 1$  RWM. As an example, a comparison of the measured dissipation of plasma angular momentum caused by the externally-applied non-axisymmetric fields with the theoretical NTV torque profile is shown in Figure 2.3.5-2 for an  $n = 3$  applied field configuration. The measured value of  $d(I\Omega_p)/dt$  includes error bars that take into account the uncertainty in the measured plasma rotation and mass density.

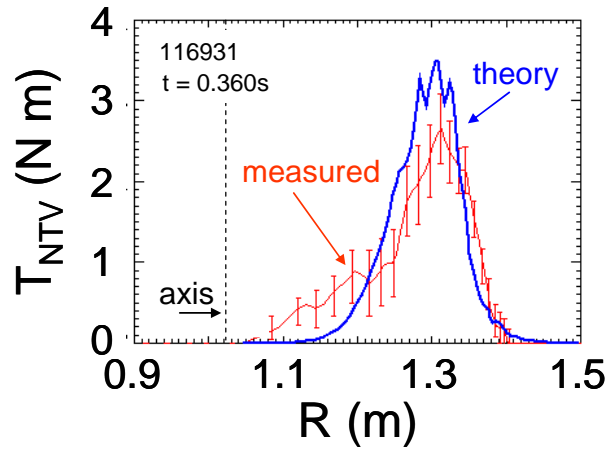


Figure 2.3.5-2 Comparison of measured  $d(I\Omega_p)/dt$  profile to theoretical integrated NTV torque for an  $n = 3$  applied field configuration (from Zhu, et al PRL 2006).

The dependence of Equation (1) above on  $v_i$  is expected to saturate as the value becomes much smaller than the trapped ion ExB precession frequency,  $\omega_D$ . Testing the dependence of NTV torque on  $v_i$  at high beta and low aspect ratio is an important goal to be addressed at the reduced collisionality made possible by the center stack upgrade. This is discussed in the subsection on NTV research plans given below.

Non-resonant  $n = 3$  braking has been developed sufficiently to be used as a control tool to reduce toroidal plasma rotation in many NSTX experiments spanning most topical research areas. Although restricted to rotation reduction, this capability has been very useful since co-directed NBI in the device doesn't allow for rotation control with NBI alone. Also, braking with higher- $n$  fields is convenient because small changes in applied current can change the plasma rotation by small, predictable amounts, and leads to only a modest reduction to energy confinement, typically less than 10%. Cyclic braking and spin-up of the plasma rotation has been demonstrated by pulsing the braking field (Figure 2.3.5-3).

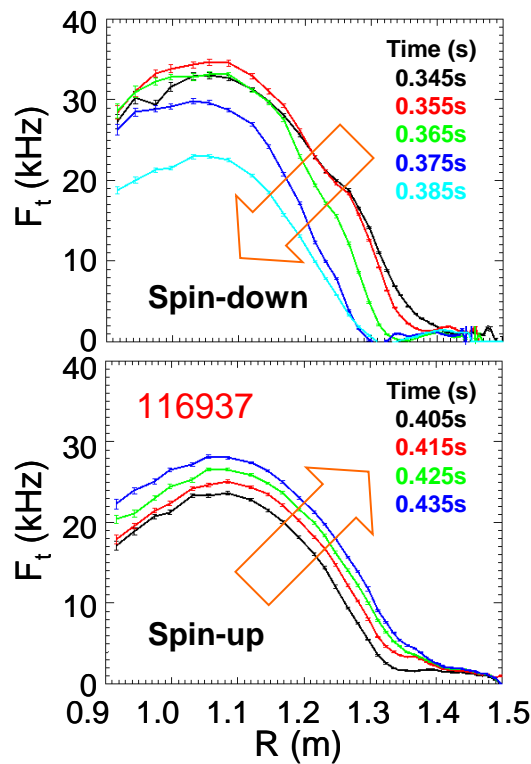


Figure 2.3.5-3 Plasma rotation damping as  $n = 3$  braking is applied, and subsequent plasma spin-up when the braking is released.

To date, the only tool available in NSTX to increase plasma rotation other than the significant toroidal momentum input by neutral beam injection has been dynamic error field correction afforded by the  $n = 1$  RWM feedback stabilization system, or open-loop feedback techniques. The observed increases in plasma rotation have been small, but maintenance of plasma rotation can yield significant improvements in plasma pulse length (e.g see Figure 2.3.3-3). However, the success of non-resonant  $n = 3$  braking and its understanding as being generated by NTV opens up the possibility of maintaining or increasing plasma rotation via this physics. This control technique is proposed below for the 2009 – 2013 research period.

## (ii) physics and control - plans

### *First-principles physics understanding of viscosity due to non-axisymmetric fields*

It is important to understand the physics of both resonant and non-resonant sources of drag torques to form reliable, first-principle models for future burning plasma and other tokamak experiments. The theory of electromagnetic drag on tearing modes from error fields and NTV drag from non-resonant fields is established, but key questions remain in extrapolation to burning plasma regimes such as in ITER. While the qualitative picture of electromagnetic drag torque fits observations of plasma rotation damping in the presence of tearing modes, there is little first-principle theoretical modeling [81] in toroidal geometry with quantitative comparison to experiment. Therefore, it is unclear whether or not other effects contribute significantly to the torque. For example, the theory of neoclassical toroidal viscosity in the near-field of the island [82] (island NTV, or INTV) might play a significant role in the rotation damping of tearing modes. Since EM, NTV, and INTV drag have different dependencies on plasma parameters (EM scales as  $\delta B_{resonant}^2$ , NTV scales as  $\delta B^2(p_i/v_i)\varepsilon^{-1.5}$ , and INTV scales as  $\delta B$  (more strongly than NTV) with a more complex dependence on  $v_i$ , understanding each quantitatively is important when scaling to ITER and other future devices. Another important consideration, especially for ITER, is the NTV  $1/v_i$  scaling. (the so-called “ $1/\nu$  regime”) as shown in Equation (1), which is appropriate for present NSTX plasmas where the trapped particles are becoming collisionless,  $q\omega_E < v_i/\varepsilon < \varepsilon^{0.5}\omega_{Ti}$  [80]. Theoretically, NTV is expected to saturate as the ion collisionality drops further, i.e. to significantly below the trapped ion ExB precession frequency. In this regime, which is appropriate for ITER, the  $1/v_i$  scaling is



theoretically expected to become  $v_i/(v_i^2 + \omega_E^2)$ , but this has not been experimentally demonstrated. Experiments conducted in the 2009 – 2013 period will investigate the key scalings of the important physical mechanisms described above that lead to plasma rotation damping, with particular emphasis on the dependence of NTV torques on ion collisionality once the center stack upgrade is made. The IPEC code will be an important tool for this study, determining the impact of non-axisymmetric field amplification or shielding on the perturbed field used in the NTV torque calculations.

### *Toroidal momentum input from propagating, non-resonant fields*

The present physics understanding of NTV may allow a new practical tool for maintaining or increasing plasma rotation by means other than neutral beam momentum input, without exciting strong tearing modes and/or leading to a reduction in energy confinement. The application is of critical importance to future devices with low toroidal momentum input (e.g. burning plasma devices such as ITER) that could benefit from increased rotational stabilization of MHD modes and may synergistically aid ELM mitigation. Quantitative agreement between NTV theory and experiment on NSTX to date supports the idea of controlling the plasma toroidal rotation by applying toroidally phased fields with  $n > 1$  and relying on the NTV from the propagating, non-resonant field components to apply positive momentum to the plasma, enabling the plasma to be spun-up as well as spun down.

The technique of using propagating field-driven NTV for robust maintenance of plasma rotation via non-resonant rotating fields has many advantages. The technique can be applied in principle to any toroidal device in which NTV is significant (relatively low collisionality plasmas), including future burning plasma experiments such as ITER. The technique is relatively simple – a toroidally propagating, non-resonant field is applied to the plasma, and NTV drags the plasma in which the field penetrates up to the rotation speed of the applied field. The most basic implementation does not require feedback or a sophisticated control system.

In NSTX, the newly proposed NCC can do triple-duty by supplying the propagating non-resonant field for this research. With 12 internal toroidal coils,  $n = 2$  or  $n = 3$  fields can be made to propagate. With  $n > 1$ , the most deleterious  $n = 1$  resonant modes, both tearing modes and RWMs, will not be excited. This has been demonstrated in NSTX already in that  $n = 3$  fields used for slowing the plasma do not directly excite these modes. If magnetic islands form in the region of the applied field, the NTV torque will supplement the NBI torque in counteracting the tendency of the mode to lock. Also, the radial footprint of the NTV torque is radially wider than electromagnetic torques caused by propagating resonant fields. Although the technique is not specific to NSTX, the device is an excellent facility to run the research since the applied torque scales as  $(1/A)^{1.5}$  (see Equation (1)). Low-cost audio amplifiers may be sufficient to generate the field amplitude and propagation frequencies needed. Having the ability of at least maintaining 5 kHz rotation speeds near the  $q = 2$  surface should yield a sufficient proof-of-principle and give reasonable flexibility to conduct physics research (of course, a higher frequency  $\sim 10$  kHz would be even better). A full design study is required, but this should be possible with  $n = 2$  fields, and the desired  $n = 3$  may also be possible. The system would also allow research using the resonant  $n = 1$  field, so that the effects of resonant fields could be evaluated, and also to make important comparisons with the existing tokamak research in this area. For instance, TEXTOR has demonstrated spin up of  $n = 1$  tearing modes using  $n = 1$  fields up to 3.75 kHz [83,84] and JFT-2M has demonstrated a local increase in plasma rotation due to the EM transfer of momentum from the  $n = 1$  field to an  $m = 2$ ,  $n = 1$  magnetic island [85].

Application of NTV momentum input to the plasma, while relatively simple in principle, requires that a practical system be designed, constructed and demonstrated to determine if certain potential issues can be addressed. Propagating  $n > 1$  fields requires higher frequency,  $f$ , to generate the same phase velocity, since toroidal phase velocity  $\sim f/n$ . The need to use higher frequencies presents issues with field penetration. Also, the higher  $n$  sideband fields won't propagate unidirectionally, therefore higher order  $n$  sidebands should be kept small. For the present RWM coil on NSTX, the NTV due to  $n \neq 3$  is relatively small, with the  $n = 9$  being the largest sideband. An NCC design with 12 coils should place the majority of the NTV torque into the  $n = 2$  and  $n = 3$  component. This will be evaluated during the physics design of the system.

### *Real-time control of plasma rotation*

Real-time control of plasma rotation will be useful in NSTX, as well as in other future devices envisioning solely high plasma rotation due to co-directed NBI (KSTAR, CTF). With the new NCC, the following directly controlled sources and sinks of plasma toroidal momentum on NSTX will be:

Sources:

- 1) Neutral beam injection
- 2) Resonant field propagation momentum (NCC)
- 3) Non-resonant field propagation (NCC)

Sinks:

- 1) Static resonant field (NCC, external RWM coils)
- 2) Static non-resonant field (NCC, external RWM coils)

In the nearer term, the plan calls for a 2<sup>nd</sup> SPA in FY11. This will allow n=1 DEFC/RWM feedback at the same time as n=2 & 3 fields are utilized for rotation control. Given that the n=2 and 3 fields from the RWM coils yield different radial profiles of damping (due to the different radial variations of the fields), this should allow some localization of the damping, and hence basic rotation control. This feature, i.e. simultaneous and independent n=1,2,&3 fields, is thus useful for both RMP (chapter 5) and rotation control.

The design of the NCC will then aim at producing a field spectrum that yields a different radial footprint of non-resonant NTV than that produced by the existing external RWM coils. Therefore, rotation profile control will be possible by using both sets of coils.

These sources and sinks can be used in a feedback loop to control the plasma rotation magnitude and profile. Such control can be used to examine a greater range of rotation profiles for future MHD stability studies.

Real-time charge exchange recombination spectroscopy (CHERS) will be implemented as the primary sensor for such a system at two or three radial positions in the 2009 – 2013 time frame. After successful interface of these measurements with the PCS, control system software will be developed that will allow control of the sources and sinks of toroidal plasma momentum. Basic capability of this system is envisioned in the next five years, which is planned to include NBI for source control, and the external RWM coil for sink control. The sources and sinks due to the NCC will be implemented as they are tested, but are not envisioned to be implemented in the feedback loop in the 2009 – 2013 period.

#### SUMMARY OF RESEARCH PLANS AND TIMELINE

- FY2009-11      Expand physics understanding of plasma viscosity induced by resonant and non-resonant field sources (applied fields and MHD modes), determining the plasma response with experimental data and IPEC. Focus on examining key parameters for future tokamak devices such as ion collisionality,  $q$ , and  $\beta_N$ . Test NTV theory quantitatively using  $n = 2$  applied field. Perform design study of NCC for use as source and sink of toroidal momentum.
- FY2010-12      Utilize reduced collisionality plasmas using new center stack to controllably access  $1/\nu$  and lower collisionality regimes of NTV theory. Compare to NTV theory including more consistent collisionality connection formulae and kinetic simulations of NTV flow-damping.
- FY2011-12      Demonstrate  $n=2$  & 3 NTV for rotation magnitude and profile
- FY2011-12      Demonstrate the use of the NCC (incremental) as a momentum sink using both resonant and non-resonant static field and quantitatively compare to NTV theory for verification. Subsequently, attempt use of the NCC as a momentum source using both resonant and non-resonant fields as suitable power supplies become available.

- FY2011-12 Demonstrate real-time plasma rotation control using rtCHERS sensors and basic sources and sinks of plasma toroidal momentum input (NBI,  $n = 3$  non-resonant NTV drag using external RWM coil).
- FY2013 Demonstrate real-time plasma rotation control using full complement of toroidal momentum sources and sinks, including the NCC.

### 2.3.6 *Disruption physics, consequences, avoidance, and prediction.*

*Goal: Characterize the effects of disruptions at low aspect ratio and high beta by measuring halo currents and thermal and current quench characteristics. Develop methods to predict disruptions and mitigate their impact.*

#### **(i) Understanding the consequences of disruptions in an ST plasma**

Disruptions can quickly eliminate the entire thermal energy and quench the total plasma current in a tokamak/ST facility like NSTX, resulting in impulsive heat loads to plasma facing components and large forces on in-vessel structures. While disruptions do not generally have operational consequences in NSTX for the present parameters, the device represents a unique environment for the study of disruption physics. These studies began in earnest in the 2007, with the initiation of a detailed examination of existing NSTX data for disruption characteristics, particularly the dynamics of the plasma current quench [86], and continued into 2008 with the installation of a devoted halo current detection system. Studies in the coming research period will continue this effort, with a particular focus on the dynamics of the thermal quench and halo currents. This data will provide valuable contributions to the updated ITPA disruption database [87], and provided critical design data for future low aspect ratio devices such as NHTX or a CTF. Disruption control will be addressed through the implementation of disruption prediction algorithms, and techniques to mitigate the effects of disruptions will be addressed.

The process leading up a disruption typically begins with some MHD mode or control failure [88]. This event typically leads to a degradation of confinement, often including loss of H-mode, for a period of time before the actual disruption. The energy loss during this precursor phase is of great importance, as energy lost slowly during this period will not be present to contribute to loading during the thermal quench [89]. Results from NSTX have demonstrated substantial energy loss in this pre-disruptions phase, as indicated by the histograms in Fig 2.3.6-1. This data was taken from a database of ~800 disruptions spanning the operational lifetime of the device, selected for having large quench rates, large values of stored energy before the disruption, or large halo currents. The blue curve shows a histogram for the maximum stored energy during the discharge; there are values at low stored energy, corresponding to disruptions during the current ramp or shots with low heating power, and at high stored energy, for instance in high- $\beta$  experiments. The distribution of pre-disruption energies is, however, weighted strongly to low energy, and there are no cases found with stored energy  $>250\text{kJ}$  immediately before the disruption. This result bodes well for future large ST devices, as it implies that the full flat-top stored energy will usually not be present for the thermal quench. The extension of the NSTX operating regime to higher fields, currents, and stored energy will be critical in establishing whether the trend will hold for larger devices.

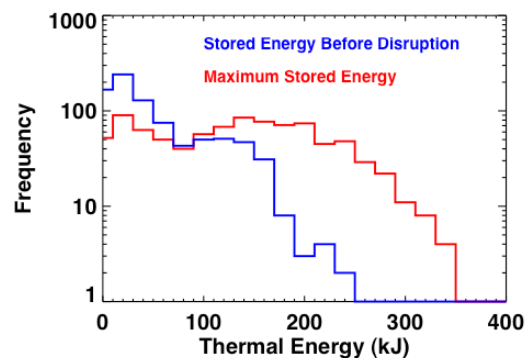


**Figure 2.3.6-1** *The area-normalized current quench time for discharges in the NSTX disruption database, as well as the suggested limit for ITER.*

Whatever thermal energy remains after this precursor phase is very rapidly lost to the wall during the thermal quench phase, either through radiation or conduction. This is of great concern in a burning plasma, where a significant fraction of the first wall material can be melted/ablated in each event [90]. There is not, however, general agreement regarding the broadening of the power deposition profile during

this phase: the ITER physics basis assumes a broadening of 1-10 times the equilibrium SOL heat deposition width, though results from, for instance, ASDEX upgrade [91] or JET [92] show substantially greater broadening of the SOL during a disruption. This creates significant uncertainty in extrapolation to divertor heat loading in larger devices. Indeed, the load in the divertor may be less than feared, but the loading of the first wall may be unacceptably large [92]. NSTX has not in the past had the diagnostics to address this issue. However, a fast IR camera was recently purchased for the study of transient power loading events, allowing this to be an important area of focus for future research. This camera, coupled to soft X-ray measurements, should allow an accurate assessment of the time-scale of the thermal quench and its associated heat pulse, as well as the spatial distribution of the lost energy. An important focus of these studies will be to understand which, if any, plasma configurations lead to disruptions with the largest heat loading.

The thermal quench is followed immediately by the current quench, often resulting in large eddy current induced forces and torques on nearby conducting structures [93]; this subject has been the focus of a recent study in NSTX [86]. A key finding of these studies, first identified in the context of ITPA Disruption Database Activities [ii], is that the maximum current quench rates in NSTX are, on an area normalized basis, up to four times faster than in conventional aspect ratio tokamaks. This is clearly demonstrated in Fig 2.3.6-2, where the NSTX disruption data implies a minimum quench time of 0.4 msec/m<sup>2</sup>, compared to the a suggested ITER limit of 1.7msec/m<sup>2</sup> [iii]. The faster quenches in NSTX, and STs in general, can likely be understood as an L/R decay effect, where L is the effective inductance of the plasma torus and R is the resistance of the cold plasma. Using an inductance  $L_p^{eff} = \mu_0 R_0 \left[ \ln \left( \frac{8}{\sqrt{\kappa \epsilon}} \right) - \frac{7}{4} \right]$

yields an area normalized decay time of

$$\frac{\tau_{L/R}}{S} = \frac{\mu_0}{2\pi\eta} \left[ \ln \left( \frac{8}{\sqrt{\kappa \epsilon}} \right) - \frac{7}{4} \right].$$

The term in brackets is 4-5 times smaller for a highly elongated ST than a conventional aspect ratio tokamak at moderate elongation, potentially explaining the difference in quench rates.

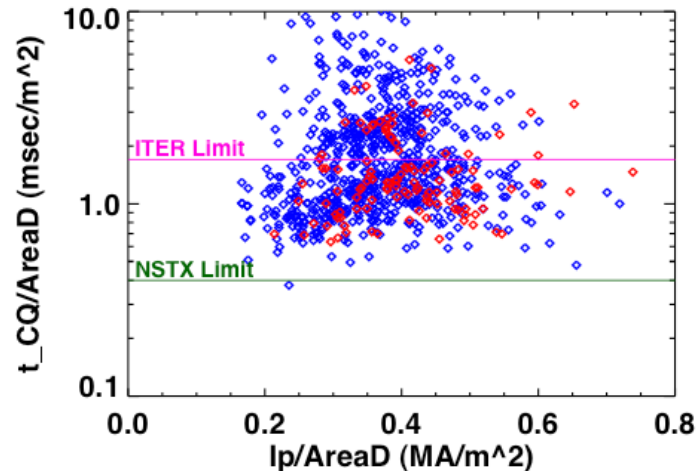


**Figure 2.3.6-2** *The area-normalized current quench time for discharges in the NSTX disruption database, as well as the suggested limit for ITER. Blue points correspond to discharges that disrupt during the  $I_p$  flat top or rampdown, and red points to those that disrupt during the current ramp.*

The process of disruption is often coupled to loss of vertical position control; this can happen in the period between the MHD precursor and the thermal quench, after the thermal quench itself, or when the loss of vertical control and subsequent plasma-vessel contact initiates the disruption. When contact is made between the plasma and plasma facing components, currents can flow that link both the plasma edge (the halo) and nearby PFCs. These “halo currents” can result in large forces on the in-vessel components [94]; they are, for instance, anticipated to be the dominant source of electromagnetic loading during slow current quenches in ITER [90]. In response to ITPA requests, and the anticipated design needs for future ST facilities, NSTX has begun a program to measure and understand halo currents.

This effort began with the implementation of a set of halo current detectors in the lower divertor for the FY08 research campaign. These are composed of two toroidal arrays of individual  $B_T$ , six sensors per array, functioning as sections of a partial Rogowski coil. They can measure both the magnitude and toroidal peaking of currents flowing in the lower vessel, and can be used to assess the net current flowing into the outboard divertor. These are complemented by previously installed lower center-column halo current measurements via Rogowski coils and measurements of the currents flowing from the inner to outer vessels through the torus grounding system.



These efforts during the FY08 physics campaign have proved highly successful, measuring halo currents that had previously gone unnoticed and revising upward estimates for halo current fractions in NSTX. A sample of this data is shown in Fig 2.3.6-3, which shows maximum halo currents, as a function of  $I_p^2/B_T$ , for four different current paths. The blue and red points, corresponding to the currents in the lower center-stack and busswork linking the inner and outer vessel respectively, show maximum halo currents of 40-50 kA. Similar data has existed for a few years and implied halo current fractions of ~5%, with little dependence on  $I_p$  or  $B_T$ . The newly available dark green and turquoise points, corresponding to the current flowing in the lower vessel near the CHI gap and the net current into the lower outboard divertor, show substantially larger halo currents, with a clear  $I_p^2/B_T$  scaling as noted on Alcator C-MOD [95]. The points nearest the bounding lines are for deliberate VDEs with  $I_p^2/B_T < 1.2 \text{ MA}^2/\text{T}$ , and represent a factor of ~5 increase in the measured halo current with the new instrumentation. Note that for the upgraded NSTX ( $I_p=2\text{MA}$ ,  $B_T=1\text{T}$ ), this scaling implies ~380kA of halo current flowing in the lower vessel and a factor of four increase in the expected halo current JxB loading of in-vessel components.

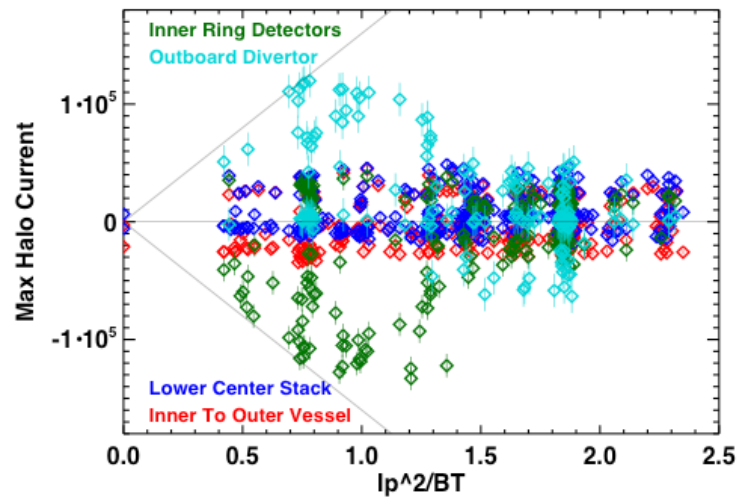
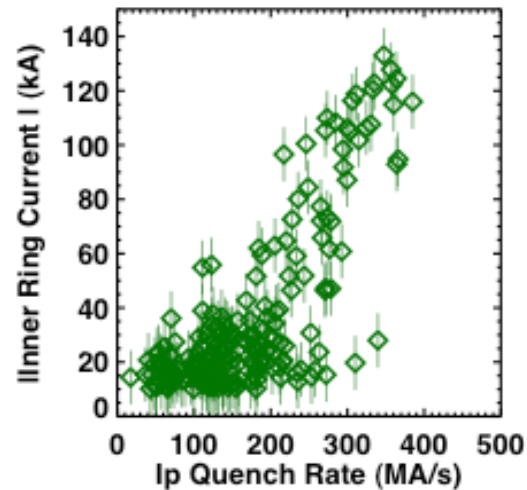


Figure 2.3.6-3: The maximum halo current, as a function of  $I_p^2/B_T$ , for different paths in the device.

One assumption in the ITER design is that the maximum halo current and eddy current load will not occur simultaneously; this is based on, for instance, JET results demonstrating the larger halo currents for discharges with slower quench rates [96]. The trend observed in NSTX is exactly the opposite: as shown in Fig. 2.3.6-4, the envelope of halo currents, in this case detected flowing in the vessel bottom near the

CHI gap, scales linearly with the  $I_p$  quench rate, in agreement with the notion that the voltage due to the toroidal and poloidal flux decay drives the halo current. This and similar information is critical in performing design tasks for next-step ST experiments.



**Figure 2.3.6-4: Halo current magnitude in the vessel near the CHI gap vs. the plasma quench rate. The largest halo currents often occur for the fastest quenches.**

While the present halo current detection upgrades have proven successful, they leave many questions open. In particular, this system measures only the net current flowing into the lower divertor; currents that flow into and then out of the lower divertor are not detected. In this sense, the measurements presented above are *lower bounds* on the halo current magnitude. In order to resolve the local currents in the divertor more clearly, the magnetic diagnostics for halo currents will be augmented by instrumented tiles during this research period [97]. The first set of these instrumented tiles will be installed on the outboard divertor during the fy09-fy11 period, as part of the upgrade for the liquid lithium divertor (LLD). These will likely include both toroidal and radial arrays of tiles. These will be supplemented with measurements of the currents flowing into the LLD segments. The machine modifications associated with the center-stack upgrade will then be utilized to install instrumented tiles on the inner divertor. These tiles arrays will allow the local halo current sources and sinks in the divertor to be accurately measured and provide greater spatial resolution for measurements of local peaking factors. More speculatively, the sensitive measurements allowed by the instrumented tiles may allow a connection to be drawn between SOLC

currents during pre-disruption mode growth and halo currents during disruption, potentially allowing more detailed understanding of the mode physics leading to halo current peaking [98]. Note that during the equilibrium phase of the discharge, these instrumented tiles will be utilized to measure equilibrium SOL currents, as described in section 2.3.2.

### **(ii) Disruption prediction, avoidance, and mitigation**

Disruption control has typically been addressed through three steps: i) avoiding the discharge configurations and underlying instabilities that lead to disruptions, ii) detecting the approach to a disruption, and iii) implementing a either soft-stop or fast shutdown procedure to mitigate the damaging effects. Substantial progress has been made in the last area via Massive Gas Injection (MGI) [99] in DIII-D and C-MOD, with results that should be broadly applicable to the ST as well.

The research presented in the other sections of this MHD chapter, and to a lesser extent in the control chapter, is largely devoted to understanding and controlling the MHD instabilities that lead to disruptions. By developing discharge designs and control techniques that avoid or mitigate instabilities like low-density locked modes, RWMs and NTMs, it should be possible to reduce disruptivity at high  $\beta_N$ . The implementation of NBI control for  $\beta_N$  feedback in FY09 should allow comfortable operation closer to limits, i.e. compensate for transients in confinement that otherwise would result in too-high values of beta. Continued improvements in DEFC and RWM feedback will allow better maintenance of stabilizing rotation in high- $\beta$  plasmas. Furthermore, the potential exists to use the RWM coils to generate traveling waves and the in-vessel sensors to detect the RFA plasma response in real time; this active MHD spectroscopy scheme would allow NBI control based on proximity to the no-wall  $\beta$  limit.

However, even with these planned improvements, disruptions will occur when expanding operation boundaries, as well as due to machine infrastructure malfunctions; this provides an opportunity to test methods that predict the onset of disruptions in an ST. NSTX has an ever-expanding set of real-time measurements that can be used to monitor and predict disruptive behavior. Present capabilities include real-time equilibrium reconstructions with rtEFIT, yielding quantities like  $\beta_N$ ,  $q_{95}$ ,  $I_i$  and accurate reconstructions of the plasma position, and real-time detection of resistive wall modes and locked modes.

These will be expanded during this research period to include real-time measurements of plasma rotation from CHERS and non-axisymmetric mode growth from dedicated USXR arrays. Specific additional real-time measurements, such as radiated power and detection of large rotating modes, can be easily added as the need arises.

These diagnostics and capabilities will be used in order to develop disruption prediction methods. Neural-net algorithms have proven successful in predicting impending disruptions in conventional aspect-ratio tokamaks [100], and are a likely method for disruption prediction in ITER [88]; these methods have never been implemented at low-A. However, other unique precursors can be studied in NSTX, including RFA growth from active MHD spectroscopy and non-magnetic detection of locked modes and RWMs. The relative merits of single-signal vs. neural net detection will be examined, and efforts will be made to determine the minimal set of precursor signals for reliable disruption prediction in a high- $\beta$  ST.

With the more aggressive parameter regime for the upgraded NSTX, it will likely be advantageous to attempt some mitigation techniques in order to reduce thermal and mechanical stresses on components. The previously mentioned disruption prediction research will then naturally lead to disruptions mitigation research. These will likely include simple techniques like deshaping of the plasma, reducing the heating power, and preemptively ramping down the plasma current, all of which can be relatively easily implemented with the flexible NSTX control system. More aggressive mitigation strategies, including noble gas injection, will be implemented if the physics program and engineering constraints mandate them.

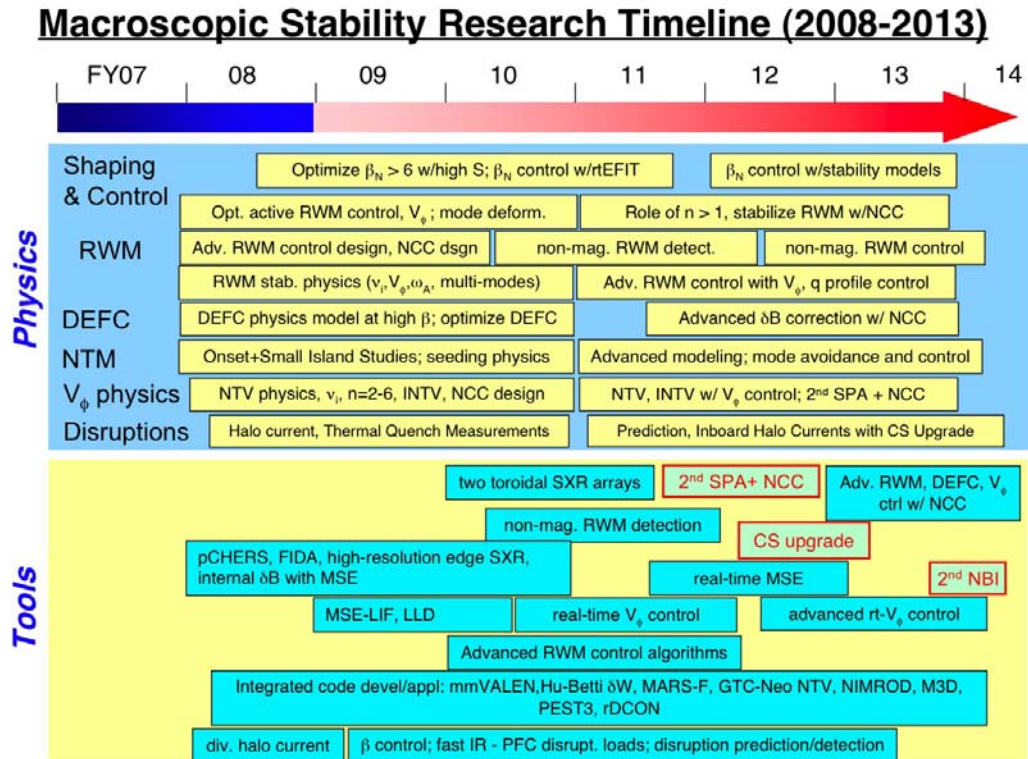
## SUMMARY OF RESEARCH PLANS AND TIMELINE

FY2009-11      Design and test prototype instrumented tiles in the outboard divertor, for SOL and halo current measurements. Install array on outboard divertors to enable complete assessment of halo current there

- FY2009-10      Implement fast IR camera for studies of PFC loading during the disruption thermal quench. Quantify the time-scale and heat distribution against relative plasma parameters and disruptions type, if possible.
- FY2010-11      Study techniques for the detection of impending disruptions, utilizing techniques such as neural nets, based on quantities measured in real-time on NSTX. Develop strategies to mitigate these disruptions.
- FY2011-12      Implement instrumented tiles on the inboard divertor as part of the center-stack upgrade. This should allow near complete measurements of halo currents in NSTX.
- FY2012-13      Test mitigation strategies in upgraded NSTX plasmas. Determine how previously measured disruption characteristics extrapolate to  $I_p=2\text{MA}$ ,  $B_T=2\text{T}$  configurations.

### 2.4 Timeline for Research Goals FY2009-2013

The proposed research program time line for macroscopic stability for 2009-2013 is shown below.



## 2.5 References

---

- [1] E. Strait, *Phys. Plasmas* **1**, 1415 (1994).
- [2] S.A. Sabbagh, *et al.*, *Phys. Fluids B* **3**, 2277 (1991).
- [3] Howl, W. *et al.*, *Phys. Fluids B* **4**, (1992) 1724.
- [4] Strait, E.J. *et al.*, *Phys. Rev. Lett.* **74**, (1995) 2483.
- [5] Turnbull, A.D. *et al.*, *Phys. Rev. Lett.* **74** (1995) 718.
- [6] Menard, J.E. *et al.*, *Nucl. Fusion* **37** (1997) 595.
- [7] Peng, Y.-K.M. and Strickler, D.J., *Nucl. Fusion* **26** (1986) 769.
- [8] Stambaugh, R.D. *et al.*, *Fusion Technology* **33** (1998) 1.
- [9] S.A. Sabbagh, *et al.*, *Phys. Plasmas* **9**, (2002) 2085.
- [10] S.A. Sabbagh, J.M. Bialek, R.E. Bell, *et al.*, *Nucl. Fusion* **44**, 560 (2004).
- [11] J.E. Menard, R.E. Bell, E.D. Fredrickson, *et al.*, *Nucl. Fusion* **45**, 539 (2005).
- [12] J.E. Menard, R.E. Bell, D.A. Gates, *et al.*, *Phys. Rev. Lett.* **97**, 095002 (2006).
- [13] H. Reimerdes, T.C. Hender, S.A. Sabbagh, *et al.*, *Phys. Plasmas* **13**, 056107 (2006).
- [14] F. Najmabadi and the ARIES Team, *Fus. Eng. Design* **65**, 143 (2003).
- [15] Y.-K. M. Peng, P.J. Fogarty, T.W. Burgess, *et al.*, *Plasma Phys. Controll. Fusion* **47**, B263 (2005).
- [16] T.K. Mau, S.C. Jardin, C.E. Kessel, *et al.* *Proc. 18th IEEE/NPSS Symp. on Fus. Eng.* (Albuquerque, NM) 1999 pp 45-48.
- [17] S.A. Sabbagh, *et al.*, *Nucl. Fusion* **41**, 1601 (2001).
- [18] D.A. Gates, J.E. Menard, R. Maingi, *et al.*, *Nucl. Fusion* **47**, 1376 (2007)
- [19] D.A. Gates, and the NSTX National Research Team, *Phys. Plasmas* **10**, 1659 (2003).
- [20] A. Bondeson and D.J. Ward, *Phys. Rev. Lett.* **72**, 2709 (1994).
- [21] H. Reimerdes, *et al.*, *Phys. Rev. Lett.* **93**, 135002 (2004).
- [22] Sabbagh, S.A., Sontag, A.C., Bialek, J.M., *et al.*, *Nucl. Fusion* **46**, 635 (2006).
- [23] Glasser, A.H. and Chance, M.C., *Bull. Am. Phys. Soc.* **42**, 1848 (1997).
- [24] Sontag, A.C., Sabbagh, S.A., Zhu, W., *et al.*, *Phys. Plasmas* **12**, 056112 (2005).
- [25] Boozer, A.H., *Phys. Rev. Lett.* **86**, 5059 (2001).
- [26] Garofalo, A.M., Jensen, T.H., and Strait, E.J., *Phys. Plasmas* **10**, 4776 (2003).
- [27] Reimerdes, H., Chu, M.S., Garofalo, A.M., *et al.*, *Phys. Rev. Lett.* **93**, 135002 (2004).

- 
- [28] J.M. Bialek , et al., *Phys. Plasmas* **8**, 2170 (2001).
- [29] A.H. Glasser and M.C. Chance, *Bull. Am. Phys. Soc.* **42**, 1848 (1997); W. Newcomb, *Ann. Phys.* **10**, 232 (1960).
- [30] D. Stutman, et al., *Rev. Sci. Instrum.* **74**, 1982 (2003).
- [31] M. Okabayashi, et al., *Phys. Plasmas* **8**, 2071 (2001).
- [32] M. Chu, et. al., *Nucl. Fusion*, **43**, (2003) 441.
- [33] E.J. Strait, et al, *Phys. Plasmas* **11**, 2505 (2004).
- [34] S.A. Sabbagh, R.E. Bell, J.E. Menard, et al., *Phys. Rev. Lett.* **97**, 045004 (2006).
- [35] P.R. Brunell, et al., *Plasma Phys. Control. Fusion* **47**, B25 (2005).
- [36] Y. In, J.S. Kim, D.H. Edgell, et al., *Phys. Plasmas* **13**, 062512 (2006).
- [37] H. Takahashi, E.D. Fredrickson, M.J. Schaffer, *Phys. Rev. Lett.* **100**, 205001 (2008).
- [38] O.N. Katsuro-Hopkins, J.M. Bialek, D.A. Maurer, et al., *Nucl. Fusion* **47**, 1157 (2007).
- [39] Fitzpatrick, R., *Phys. Plasmas* **9**, 3459 (2002).
- [40] H. Reimerdes, A.M. Garofalo, G.L. Jackson, et al., *Phys. Rev. Lett.* **98**, 055001 (2007).
- [41] A. Bondeson and M.S. Chu, *Phys. Plasmas* **3**, 3013 (1996).
- [42] A.M. Garofalo, G.L Jackson, R.J. LaHaye, et al., *Nucl. Fusion* **47**, 1121 (2007).
- [43] R. Fitzpatrick, *Nucl. Fusion* 2007.
- [44] R. Fitzpatrick, *Nucl. Fusion* **33**, 1049 (1993).
- [45] K.C. Shaing, *Phys. Plasmas* **11**, 5525 (2004).
- [46] B. Hu and R. Betti, *Phys. Rev. Lett.* **93**, 105002 (2004).
- [47] B. Hu, R. Betti, and J. Manickam, *Phys. Plasmas* **12**, 057301 (2005).
- [48] J.-K. Park, A. H. Boozer, and A. H. Glasser, *Phys. Plasmas* **14**, 052110 (2007).
- [49] J.-K. Park, M. J. Schaffer, J. E. Menard, and A. H. Boozer, *Phys. Rev. Lett.* **99**, 195003 (2007).
- [50] T.C. Hender et al., Progress on the ITER Physics Basis (Chapter 3), *Nucl. Fusion* **47**, S128 (2007).
- [51] D.A. Gates, et al., APS 2000 – NTM observation in NSTX reference.
- [52] R. Buttery, et al., *Phys. Rev. Lett* **88**, 125005 (2002).
- [53] Z. Chang and J.D. Callen, *Nuclear Fusion* **30**, 219 (1990).
- [54] R. Fitzpatrick, *Phys. Plasmas* **2**, 825 (1995).
- [55] F. L. Waelbroeck, J.W. Conner, and J.R. Wilson, *Phys. Rev. Lett.* **87**, 215003 (2001).
- [56] S. Kruger, C.C. Hegna, and J.D. Callen, *Phys. Plasmas* **5**, 455 (1998).



- 
- [57] R.J. La Haye, et al, Nuclear Fusion **46**, 451 (2006).
- [58] H. Reimerdes, Phys. Rev. Lett **88**, 105005 (2002).
- [59] D. Brennan, et al, Phys. Plasmas **10**, 1643 (2003).
- [60] R.J. La Haye, Phys. Plasmas **13**, 055501 (2006).
- [61] R.J. Buttery et al., *20th IAEA Fusion Energy Conference*, (Vilamoura, Portugal 2004), paper IAEA-CN-116/EX/7-1, Conference & Symposium Papers CD ROM, IAEA-CSP-25/CD, ISBN 92-0-100405-2, ISSN 1562-4153, IAEA Vienna (2005).
- [62] M. Maraschek, et al, Plasma Phys. Control Fusion **45**, 1369 (2003).
- [63] R. J. Buttery, et al, *Rotation and Shape dependence of Neoclassical Tearing Mode thresholds on JET*, 28<sup>th</sup> EPS Conference on Contr. Fusion and Plasma Phys. 2001.
- [64] R. Buttery, et al, Phys. Plasmas **15**, 056115 (2008).
- [65] E. Fredrickson, Phys. Plasmas **9**, 548 (2002).
- [66] A. Gude, S. Gunter, S. Sesnic, and the ASDEX upgrade Team, Nuclear Fusion **39**, 127 (1999).
- [67] S. Sesnic, et al, Phys. Plasmas **7**, 935 (2000).
- [68] S.E. Kruger, PhD Thesis, The University of Wisconsin - Madison (1999).
- [69] Chandra, Nucl. Fusion **45**, 524 (2005).
- [70] X.L. Chen and P.J. Morrison, Phys. Fluids B **4**, 845 (1992).
- [71] D.P. Brennan, A.D. Turnbull, M.S.Chu, R.J. La Haye, L.L. Lao, T.H. Osborne and S.A. Galkin, General Atomics Report A25648, Phys. Plasmas **14**, 056108 (2007).
- [72] A.L. Rosenberg, et al, Phys. Plasmas **9**, 4567 (2002).
- [73] C.D. Warrick, et al, Phys. Rev. Lett **85**, 574 (2000).
- [74] R. Betti and J.P. Friedberg, Phys. Rev. Lett. **74**, 2949 (1995).
- [75] W. Solomon, et al., Plasma Phys. Controll. Fusion **49** No 12B, B314 (2007).
- [76] E. Lazzaro, et al., Phys. Plasmas **9**, 3906 (2002).
- [77] K.C. Shaing, S.P. Hirschman, and J.D. Callen, Phys. Fluids **29**, 521 (1986).
- [78] W. Zhu, S.A. Sabbagh, R.E. Bell, et al., Phys. Rev. Lett. **96**, 225002 (2006).
- [79] K.C. Shaing, Phys. Plasmas **10**, 1443 (2003).
- [80] A.J. Cole, C.C. Hegna, J.D. Callen, Phys. Plasmas **15**, 056102 (2008).
- [81] M. Yokoyama, et al., Nucl. Fusion **36**, 1307 (1996).
- [82] K.C. Shaing, PRL **87**, 245003 (2001).

- 
- [83] R.C. Wolf, W. Biel, M.F.M. deBock, et al., *20th IAEA Fusion Energy Conference*, (Vilamoura, Portugal 2004), paper IAEA-CN-116/EX/6-5 Conference & Symposium Papers CD ROM, IAEA-CSP-25/CD, ISBN 92-0-100405-2, ISSN 1562-4153, IAEA Vienna (2005).
- [84] H.R. Koslowski, Y. Liang, A. Krämer-Flecken, et al., *Nucl. Fusion* **46**, L1 (2006).
- [85] K. Oasa, H. Aikawa, Y. Asahi, et al., *Proc. 15th Int. Conf. On Plasma Phys. and Controll. Nucl. Fusion Research* (Seville, Spain 1994) (IAEA) vol. 2 p. 279.
- [86] S. P. Gerhardt et al, “Characterizations of the plasma current quench during disruption in the National Spherical Torus Experiment”, submitted to *Nuclear Fusion*.
- [87] J.C. Wesley et al. , *21st IAEA Fusion Energy Conference* (Chengdu, China 2006), paper IT/PI-21.
- [88] T.C. Hender, et al., *Nuclear Fusion* **47**, S128 (2007).
- [89] V. Ricardo, A. Loarte, and the JET EFDA Collaborators, *Nuclear Fusion* **45**, 1427 (2005).
- [90] M. Sugihara et al., *Nucl. Fusion* **47**, 337 (2007).
- [91] G. Pautasso, et al., 31<sup>st</sup> European Physical Society Conference on Plasma Physics, London, 2004, Paper P-4.132.
- [92] G.F Mathews, et al, *Nuclear Fusion* **43**, 999 (2003).
- [93] M. Sugihara, V. Lukash, Y Kawano, R. Yoshino, Y. Gribov, R. Khayrutdinov, N. Miki, J. Ohmori, and M. Shimada, *J. Plasma Fusion Res.* **79**, 706 (2003).
- [94] V. Ricardo, S. Walker, and P. Noll, *Nucl. Fusion* **42**, 29 (2000).
- [95] R. S. Granetz, et. al., *Nuclear Fusion* **36**, 545 (1995).
- [96] V. Riccardo, et al, *Nuclear Fusion* **46**, 925 (2004).
- [97] M.J. Schaffer & B.J. Leikind, *Nuclear Fusion* **31**, 1750 (1991).
- [98] N. Pomphrey, et al., *Nucl. Fusion* **38**, 449 (1998).
- [99] R.S. Granetz et al., *Nucl. Fusion* **47**, 1086 (2007).
- [100] C.G. Windsor, et al., *Nucl. Fusion* **45**, 337 (2005).

## **Chapter 3 - Transport and Turbulence**

<i>3.1 Understanding and Optimizing Transport and Turbulence in the Spherical Torus.....</i>	<i>3.1</i>
<i>3.2 Overview of Research Plans for FY2009-2013.....</i>	<i>3.4</i>
<i>3.3 Transport and Turbulence Results and Plans by Topical Area.....</i>	<i>3.7</i>
<i>3.3.1 Energy Transport.....</i>	<i>3.7</i>
<i>3.3.1.1 Global Confinement.....</i>	<i>3.8</i>
<i>3.3.1.2 Ion Turbulence and Transport.....</i>	<i>3.14</i>
<i>3.3.1.3 Electron Turbulence and Transport.....</i>	<i>3.19</i>
<i>3.3.2 Momentum Transport.....</i>	<i>3.27</i>
<i>3.3.3 Particle Transport.....</i>	<i>3.31</i>
<i>3.4 Theoretical Tools and Modeling.....</i>	<i>3.35</i>
<i>3.5 Facility and Diagnostic Upgrades.....</i>	<i>3.37</i>
<i>3.6 Summary of Research Goals for FY2009-2013.....</i>	<i>3.39</i>
<i>Timeline for Transport and Turbulence Research.....</i>	<i>3.40</i>
<i>References.....</i>	<i>3.41</i>

*This page intentionally left blank*

## 3 Transport and Turbulence

### *3.1 Understanding and Optimizing Transport & Turbulence in the Spherical Torus*

The low toroidal field of NSTX, approximately a factor of five lower than that in conventional aspect ratio devices, leads to plasma operations in parameter regimes that are different than those at higher aspect ratio, which in turn lead to new opportunities to extend and benchmark theory and to make new diagnostic measurements. The enhanced toroidicity and natural shaping at low aspect ratio is predicted to lead to reduced microturbulence levels, and thus reduced transport associated with the microturbulence. Enhanced toroidicity also results in higher trapped particle fractions, which can influence Trapped Electron Mode (TEM) turbulence and zonal flow damping. Furthermore, the low toroidal field and near Mach flow yields large values of the ExB shearing rates, believed to be important for the suppression of long wavelength microturbulence and its associated transport. NSTX operates in regimes whose plasma collisionality is similar to that at conventional aspect ratio (and to that of ITER), but in which both the plasma beta,  $\beta_{th}$ , and the electron and ion gyroradii,  $\rho_e$ ,  $\rho_i$  respectively, can be up to a factor of 10 greater than those at higher toroidal field and aspect ratio. The high  $\beta$  (up to 40%) enables NSTX to explore electromagnetic and stochastic magnetic effects that may influence transport, and the large electron gyroradius (0.1 mm) allows for a direct measurement of spatially-resolved electron-scale turbulence.

Because of the expanded parameter regime in which NSTX operates, the results will naturally extend and challenge theory. The robustness of theories being used for extrapolation to future devices at higher aspect ratio will be tested by extending them into a wider operating regime at low aspect ratio. Thus, the validity of these theories will be assessed, and this will aid in identifying modifications and additions to improve their physics basis and make them more relevant to operational scenarios at all aspect ratio. Answers to these questions will necessarily

deepen our understanding of basic toroidal confinement physics, which will naturally lead to more confidence when extrapolating this physics to future devices.

Not only will the physics theories themselves be tested, but complex numerical calculations that will push the limits of present computational resources will be necessary to gain this understanding. For instance, the non-linear simulation of short-wavelength, electron-scale instabilities will require use of state-of-the-art computational tools, especially under circumstances where scale separation between electrons and ions (i.e, high and low-k) modes, is not possible. NSTX operation does offer some regimes where such scale separation may be possible, regimes in which anomalous ion transport is low and thus the ions can be treated adiabatically, but the difficult issue of turbulence spreading may require fully kinetic treatment of the ions.

These requirements, and the validity of the results of the calculations, will be determined through extensive benchmarking. This benchmarking procedure, which has been ongoing through the life of the NSTX project, and has recently been called out as Verification and Validation by the wider fusion community, will be a true test of the validity of the codes (Verification) and transport physics models (Validation). As the codes for simulating the plasma transport become more sophisticated, so too will the diagnostics for measuring this turbulence and its associated transport. This will offer the opportunity to test theory at all levels, from the specific fluctuating quantities to an overall level of transport. Agreement between actual measurements and those from synthetic diagnostics built into the codes at all these levels will give enhanced confidence in our understanding of the processes controlling the plasma transport.

The goal of this research is to develop a comprehensive picture of transport and turbulence in NSTX by combining and benchmarking results from measurement, analysis and theory, with an ultimate target of developing a fully predictive tool for energy, particle and momentum transport that can be used with confidence for predicting performance of future devices, both ST and non-

ST. NSTX research is critical to justifying, and perhaps modifying, key assumptions for achieving the performance objectives of future devices. In particular, for an ST-based Component Test Facility, crucial assumptions include those of achievable confinement enhancement factors and operation in the Hot-Ion H-mode regime. Global confinement and ion transport and turbulence research at high  $P_{\text{heat}}/P_{\text{LH}}$ , including understanding the role of ExB flow shear in suppressing ion-scale microturbulence, addresses these assumptions. Of overriding importance for both future ST and non-ST burning plasma devices is the optimization of neutron production and/or fusion gain, both of which are tied directly to understanding and optimizing electron transport, a task for which NSTX is ideally suited.

Laying the foundation for this comprehensive understanding and predictive capability will necessarily involve coordinated research with other major devices both in the U.S. and internationally, and will allow for discharge scenario development in NSTX and in future devices such as a possible NSTX follow-on (NHTX), an ST-based Component Test Facility, and longer-range targets such as an ARIES-ST prototype reactor. Such an understanding will allow for

- a) confident extrapolations of transport and turbulence properties to ensure that confinement requirements can be satisfied at high input powers (greater than the L-H threshold power) and high power density divertors (e.g., P/R),
- b) understanding and extrapolating momentum transport to assure adequate rotation and ExB shear for the suppression of microturbulence and MHD modes,
- c) determining regimes in which plasma profiles for current drive and fusion production are optimized.

Further, the detailed physics understanding gained from this coordinated effort will aid in the prediction of performance of confidence for success of future devices at conventional aspect ratio, such as ITER.

### *3.2 Overview of Research Plans for FY2009-2013*

The unique operating regime of NSTX will allow exploration of the transport and turbulence properties that govern toroidal confinement. Both as a complement to conventional aspect ratio tokamaks and as a confinement concept in its own right, NSTX will move in a direction to identify and control the fundamental physics mechanisms that are most important in determining energy, particle and momentum transport. The key transport goals for the period from 2009 to 2013 are:

- To verify global scaling trends in an expanded parameter space and to establish the dependence of confinement on aspect ratio,
- To establish conditions for neoclassical ion transport through coupling low-k turbulence measurements to results of non-linear gyrokinetic simulations addressing both neoclassical and turbulence physics,
- To determine the role of both low-k and high-k turbulence, through measurement and non-linear theory, in setting the level of anomalous electron transport,
- To understand momentum transport and to determine the source of the plasma rotation/radial electric field and its influence on both low- and high-k turbulence,
- To understand the relation of particle and impurity transport throughout the plasma to measurements and simulations of microturbulence, ultimately to
- To participate in national and international efforts to develop a validated, fully-predictive tool for developing confinement-optimized discharge scenarios for both NSTX and future ST and non-ST devices.

A summary of the key physics results and issues, what is needed in order to gain a better understanding of them, and how NSTX upgrades will allow this is as follows. In present spherical torus experiments, the energy confinement time in neutral-beam heated H-modes has different parametric dependences than it does at higher aspect ratio, scaling almost linearly with



$B_T$  ( $B_T^{0.9}$ ), but more weakly with plasma current ( $I_p^{0.4}$ ). The ion transport is typically inferred to be near neoclassical levels, and the ion turbulence is apparently suppressed by large shear in the plasma flow. In contrast, electron energy transport is observed to be anomalous, and it dominates the overall energy loss.

At least four micro-instabilities could play a role in anomalous electron transport in tokamaks and STs: micro-tearing modes (electromagnetic), collisionless trapped electron modes – CTEM (electrostatic), electron temperature gradient modes – ETG (electrostatic), and Global Alfvén Eigenmodes – GAE (Alfvénic). Micro-tearing, ETG, and GAE modes have been correlated in a preliminary way with anomalous electron transport under different discharge conditions. Multiple instabilities may be present simultaneously, and isolating the effects of individual instabilities is difficult. The baseline approach for developing an understanding of the source of anomalous electron transport in the ST is to increase the operating toroidal field and plasma current, and, along with Lithium conditioning, reduce the collisionality by up to an order of magnitude. The lower collisionality can result in suppression of micro-tearing modes. Higher magnetic field would provide access to reduced fast-ion instability drive and enable the reduction (possibly suppression) of GAE modes. Thus, access to higher magnetic field would provide control of the onset of electromagnetic and Alfvénic modes, and separate the impact of these modes from electrostatic modes.

Higher field and current will also reduce neoclassical ion transport by up to an order of magnitude (due to smaller orbit sizes and reduced collisionality) thereby enhancing the relative importance of anomalous ion transport in the overall ion transport. This capability would also provide new insight into the underlying causes of anomalous momentum transport (most likely ITG and/or CTEM) and the flow-shear suppression of ion turbulence in the ST. Reduced/suppressed ion turbulence is especially important for achieving a “hot-ion” H-mode regime for high fusion gain in next-step ST-based CTF devices.

Overall, the planned major upgrades of NSTX, which include replacing the center stacks in both experiments and the installation of a Liquid Lithium Divertor, would greatly enhance the ability

to isolate the roles of different micro-instabilities in anomalous electron and ion transport by doubling the achievable toroidal magnetic field and thereby increasing the accessible range of magnetic field variation to over a factor of three and expanding the range of collisionality by up to an order of magnitude. Importantly, the minimum collisionality made accessible by the major upgrades would approach (to within a factor of two) the collisionality values expected of next-step STs assuming comparable Greenwald density fractions. Existing high-k diagnostics and planned low-k diagnostics (BES) will provide the ability to distinguish between the electrostatic CTEM and ETG modes, and BES and high-k may also be capable of measuring GAE fluctuations. In parallel, and coupled to the fluctuation and transport measurements, theory model validation will permit extrapolation to future devices.

Detailed results and plans follow.

### *3.3 Transport and Turbulence Results and Plans by Topical Area*

#### *3.3.1 Energy Transport*

Understanding and ultimately being able to control the sources of ion and electron transport is critical to the success of creating high performance plasmas in present day experiments. Furthermore, it is equally critical for being able to extrapolate to future device operation through high-confidence predictions. One of the goals of NSTX is to develop a comprehensive picture of energy transport for both electrons and ions. This can be done using a multi-faceted approach whose elements include:

- Detailed profile measurements
- Transport analysis resulting in energy, momentum and particle fluxes and transport coefficients
- Measurements of turbulence spectra
- Turbulence code predictions of fluxes and turbulence spectra from synthetic diagnostics, using the measured profiles as input.

Of particular importance in this area of research is the study of electron transport, which, in NSTX, is anomalous and dominant in all operational regimes. NSTX is particularly suited to study the electron turbulence and transport physics, since in many regimes the ion transport is at or near neoclassical levels, leading to an electron-transport dominated operating regime. Because of the high neutral beam injection energy relative to the electron temperature in NSTX, the electrons are preferentially heated, by a 2:1 ratio, emulating the dominant electron heating in ITER as well as in possible future ST devices. Furthermore, the low toroidal field in NSTX leads to electron gyroradius scale-lengths that are approximately 0.1 mm, meaning that microturbulence on these scales is readily measurable with high spatial resolution using microwave scattering technology. These attributes, coupled with state-of-the-art computational tools, make NSTX an excellent laboratory in which to study electron transport.

A major part of the transport research will be the use of both linear and non-linear gyrokinetic calculations. These calculations will cover the range of neoclassical transport of ions, impurities and momentum using a kinetic (i.e., finite banana width and ultimately multiple species and full Larmor radius effects) approach, to a determination of the unstable microinstabilities and their characteristics. An important part of these calculations will be detailed benchmarking of codes and physics models with respect to one another and with respect to measured quantities. This Verification and Validation has been ongoing, but more sophisticated approaches will allow for more detailed benchmarking on a variety of levels. For instance, synthetic diagnostics will be built into the various simulation codes, and these will allow us to make direct comparisons with equivalent measured data such as the plasma density fluctuations. Comparisons will be made between the measured and simulated primary characteristics of the fluctuation spectra, such as  $\delta n$  and cross-phase, as well as secondary characteristics, including Zonal Flows, and wavenumber and frequency spectra. At a higher level, local heat fluxes or thermal diffusivities calculated by the codes will be compared to those inferred from experiment. Ultimately, a physically valid and relevant model will yield agreement with measurements at those levels and at the highest level, which is a predication of global trends (i.e., the parametric dependence of confinement scaling). A successful Verification & Validation procedure will lead to a high confidence predictive tool for extrapolation to future devices.

Since transport and turbulence are inexorably related, they will be integrated into a single, coherent plan.

### *3.3.1.1 Global Confinement*

#### **Results**

Dedicated global confinement studies that have been carried out over the last several years have focused on several issues: to establish the basic parametric dependences of the L-H threshold

power and energy confinement at high heating power, and to address global confinement issues of particular importance to ITER and for which NSTX is particularly suited.

Early studies of the L-H threshold in NSTX have indicated an apparent dependence of the threshold power on  $I_p$  (Fig. 1), unlike at higher aspect ratio, and that the L-H transition occurred

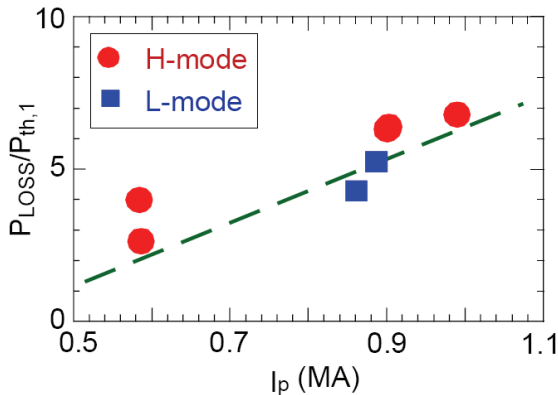


Fig. 1 L-H power threshold normalized to the ITER-scaling value [1] as a function of plasma current. There is a clear plasma current dependence in the threshold power that is not reflected in the scaling.

at lower powers with high-field-side gas fueling. It was also found that plasma shape affected the threshold power, most notably triangularity, X-point height and configuration.

Dedicated confinement scans to elucidate the basic parametric dependences, such as the  $I_p$  and  $B_T$  scaling, were carried out in H-mode plasmas with elongation  $\kappa$  of 2.1 and triangularity  $\delta$  of 0.6 at fixed beam power ( $P_{\text{input}}=4$  MW) and at similar densities. These dedicated studies have revealed confinement trends that differ from those at conventional

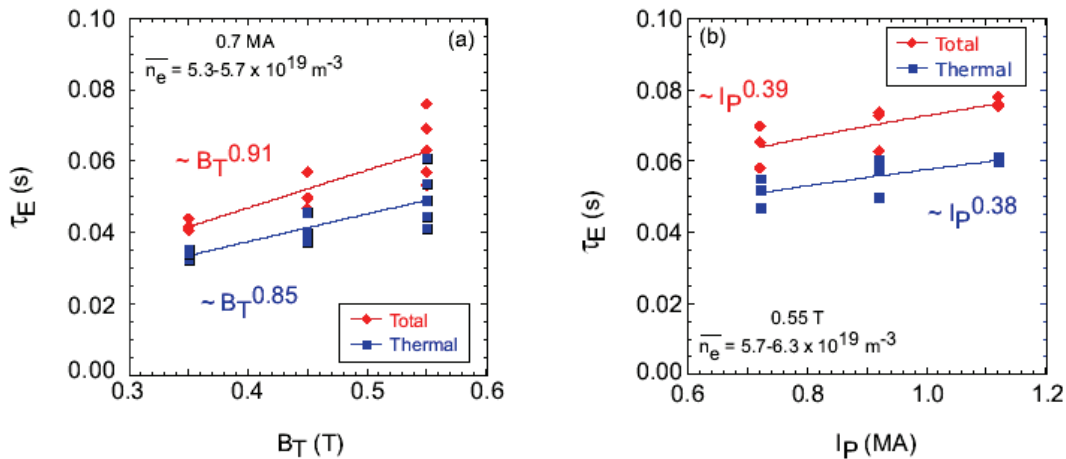


Fig. 2 Thermal and global confinement time scalings as a function of (a)  $B_T$  and (b)  $I_p$  from dedicated scans at constant injected beam power, 4 MW, and density.

aspect ratio, as is illustrated in Fig. 2, where the results of the  $B_T$  and  $I_p$  scans at constant  $I_p$  and  $B_T$  respectively are shown. Unlike at conventional aspect ratio, where the dependence of  $\tau_E$  on  $B_T$  is weak ( $\tau_E \sim B_T^{0.15}$  in the ITER98(y,2) scaling [2]), the dependence on  $B_T$  in NSTX is stronger, with  $\tau_E \sim B_T^{0.9}$  for both thermal and global confinement time. Alternatively, the dependence on plasma current is much weaker than what is observed at conventional aspect ratio, with  $\tau_E \sim I_p^{0.4}$  as compared to  $I_p^{0.9}$  for ITER98(y,2). The results of these dedicated scans [3, 4] verify trends that were extracted from earlier data by statistical means [5].

The results of the dedicated scaling experiments also showed a very strong dependence of confinement on collisionality, as is seen in Fig. 3. The scan was conducted at constant  $\rho_e$ ,  $\beta$  and  $q$ , with the variation in  $v_e^*$  being associated with the variation in  $I_p$  and  $B_T$  at constant  $I_p/B_T$ . The normalized confinement is seen to scale essentially inversely with  $v_e^*$ . The thermal transport in

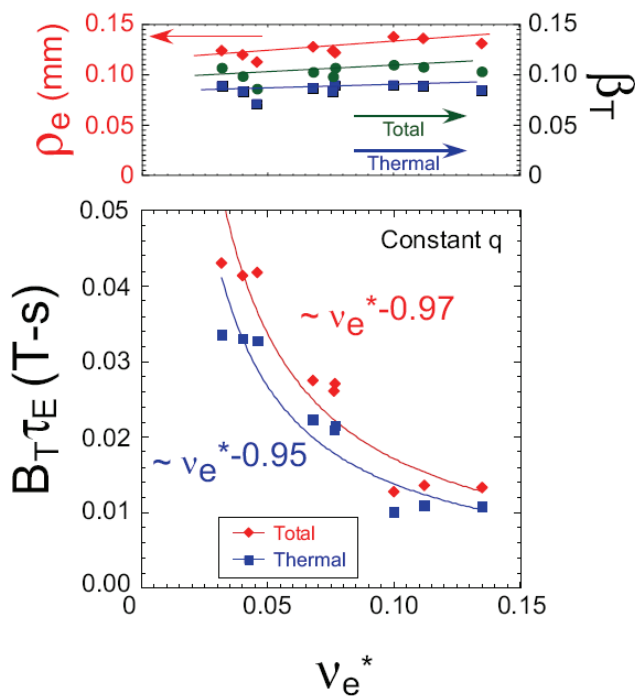


Fig. 3 Results of collisionality scan at fixed  $\rho_e$ ,  $\beta$  and  $q$  ( $I_p/B_T$ ).

both the electron and ion improves as collisionality is reduced. If this scaling holds at even lower collisionality values, large increases in the global confinement could be realized.

The confinement experiments have focused also on studying the dependence of confinement on plasma  $\beta$ , an issue that is critical to assessing the potential for success of the ITER Advanced Tokamak scenario, which will operate at higher  $\beta$  than the standard target. Key to this is whether there is the degree of degradation (if any) of confinement with plasma beta. The results from standard aspect ratio

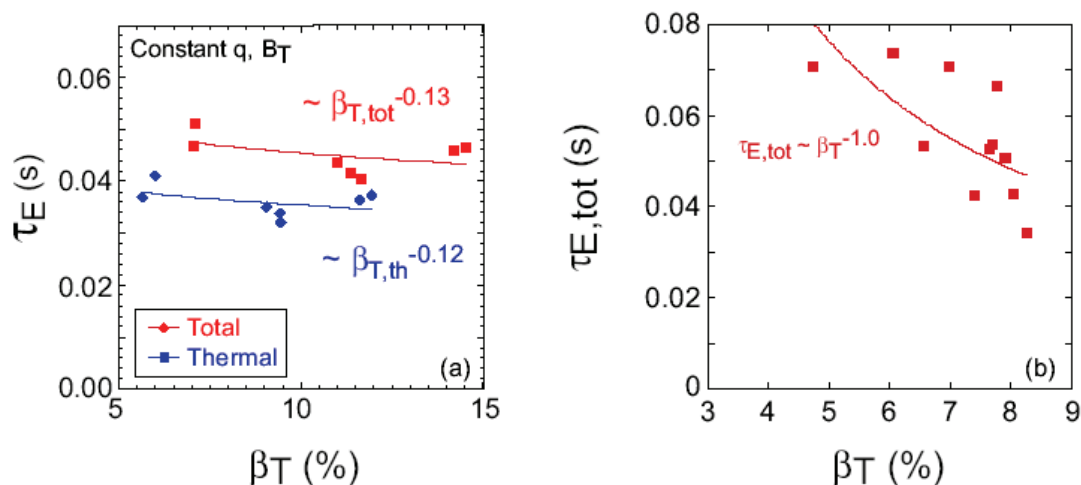


Fig. 4 Scaling of H-mode confinement with  $\beta$  at fixed  $B_T$ ,  $I_p$  for a plasma with (a)  $\kappa=2.1$ ,  $\delta=0.6$  and (b)  $\kappa=1.85$ ,  $\delta=0.4$

tokamaks are mixed; while JET and DIII-D experiments [6,7] have shown no degradation of  $\tau_E$  on  $\beta$ , experiments run by JT-60U and ASDEX-U [8,9] have shown degradation that is similar to what is predicted by the ITER98(y,2) scaling, where  $B\tau_E \sim \beta^{-0.9}$ . One difference between the two sets of scans is that the results showing the strong degradation were from discharges that had lower  $\kappa$  and  $\delta$ . NSTX is particularly well-suited to address this problem, in that not only can a large range of  $\beta$  be covered in a scan, but shape comparisons can be performed within the NSTX device itself. The results of the scans are shown in Fig. 4, where the  $\beta$  scan was performed by varying power at fixed  $I_p$  and  $B_T$ . Across this range of power and beta, other dimensionless variables such as  $v^*$  and  $\rho^*$  were held constant to within 20%. In the case with strong shaping,  $\kappa=2.1$  and  $\delta=0.6$ , the confinement time showed no degradation with  $\beta$ , while in the more weakly shaped plasmas, with  $\kappa=1.8-1.9$  and  $\delta=0.4$ , the confinement time was seen to degrade with  $\beta$  rather strongly, with  $\tau_E \sim \beta^{-1.0}$ .

One of the key results of the scan showing the degradation is the variability of the edge stability, as reflected by the variability of the ELM severity. In the high elongation/triangularity discharges, only small, Type V ELMs were observed for all powers, while in the lower  $\kappa/\delta$

scans, the ELM type varied from Type III at low power to Type I at high power. In order to assess better the dependence of confinement on  $\beta$ , it is necessary to compare plasmas which similar ELM characteristics. Lithium evaporation and LLD provide a means to do this.

Significant increases in plasma confinement were seen with Lithium evaporation. An example of this is shown in Fig. 5, which compares a 4 MW discharge with no Lithium to 2 and 3 MW discharges with Lithium evaporation. The stored energies in the 2 MW Lithium and 4 MW no Lithium cases were essentially the same, indicating a near doubling of the energy confinement

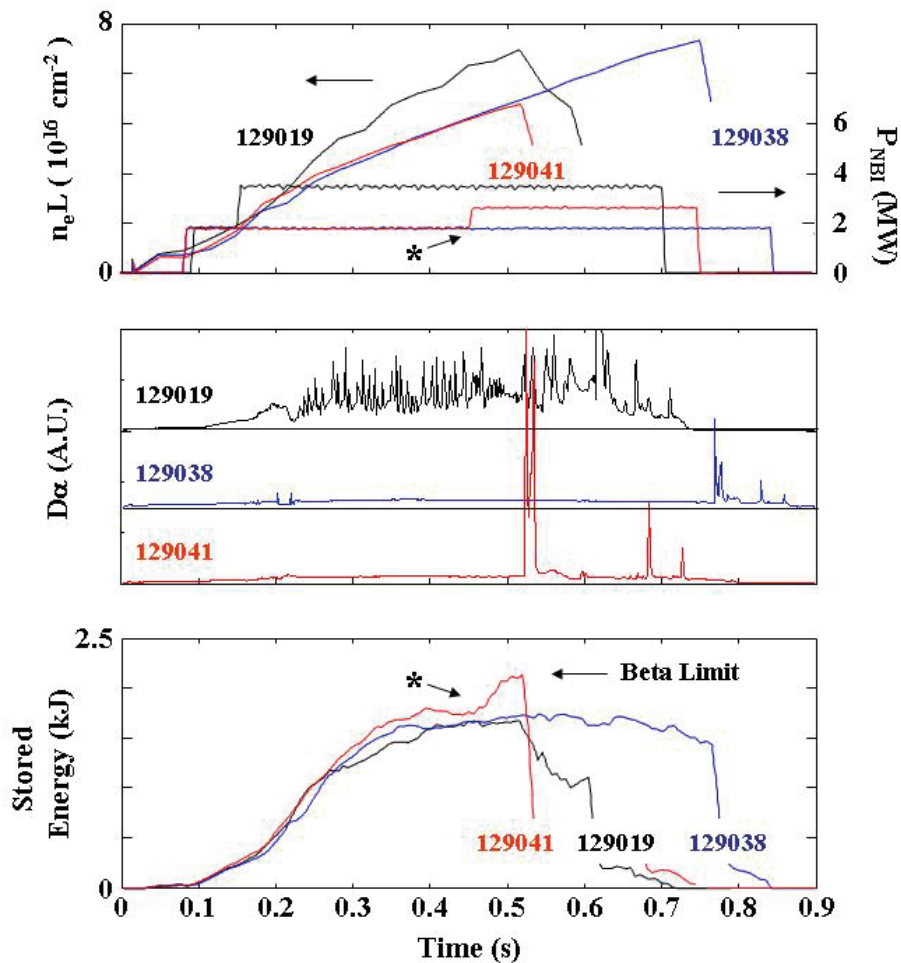


Fig. 5 Comparison of 4 MW no Lithium discharge to 2 and 3 MW discharges with Lithium evaporation.



time. This confinement improvement is reflected by an increase in the  $H_{98y,2}$  enhancement factor from 0.85 in the no Lithium discharge to 1.30 in the Lithium discharge. The 3 MW Lithium discharge is  $\beta$ -limited at this relatively low power. Lithium evaporation also was seen to suppress ELMs during the H-mode phase. The Lithium evaporation and Liquid Lithium Divertor provide a set of tools for studying the L-H threshold and the ramifications of ELM stability. In particular, these tools will allow for an assessment of the  $\beta$ -dependence of confinement (as described above) in lower  $\kappa/\delta$  discharges that are ELM-free due to the Li conditioning.

### Plans

A key question that needs to be answered is whether the  $B_T$  and  $I_p$  scalings observed in NSTX, which differ from those at higher aspect ratio, are due to the relatively low  $B_T$  and  $I_p$  in the present operating space, or does confinement at low aspect ratio continue to scale in the present manner at higher  $B_T$  and  $I_p$ ? Are there other dependences, such as with  $\beta$  and  $v^*$ , that affect the confinement scalings?  $v^*$  will be reduced by up to an order of magnitude with the new centerstack and LLD, bringing the operating space in this parameter closer to that of NHTX and ST-CTF. L-H studies are important for NHTX and ST-CTF, which need to operate well above the L-H threshold to allow large radiated power. NSTX needs to determine how the L-H threshold power continues to scale with  $B_T$ ,  $I_p$  and configuration.

#### 2009-2011:

Studies will be carried out which will determine the quantitative dependence of the L-H threshold power on  $I_p$ ,  $B_T$  and plasma shape. In addition, the effect of rotation on the L-H threshold will be studied using  $n=3$  magnetic braking and HHFW. Experiments will be carried out to determine the dependence of confinement on aspect ratio, both within NSTX and in conjunction with conventional aspect ratio devices (e.g., an NSTX/DIII-D similarity experiment) in order to optimize NHTX and ST-CTF designs. The effect of lower collisionality and recycling in the presence of Lithium PFCs on the L-H threshold and confinement will be established

through global and local studies. Finally, the source of the variation of  $\beta$  degradation of confinement will be explored in both strongly and weakly shaped plasmas while using Lithium evaporation and the LLD to suppress ELMs, to understand whether it is plasma shape or edge stability that results in the varied scaling results with this parameter.

#### 2012-2013:

The new centerstack will be installed and operational during this time period, giving a factor of two increase in the achievable range and magnitude of both  $B_T$  and  $I_p$ . Operation at higher  $B_T$  and  $I_p$  will allow for determining whether the difference in the  $B_T$  and  $I_p$  dependences between NSTX and conventional aspect ratio tokamaks is due to differences in  $B_T$ ,  $\beta_T$ ,  $v^*$  or whether it is due to differences in aspect ratio. The higher  $T_e$  expected at higher  $B_T$ , coupled with operation with Lithium PFCs, will allow exploration of confinement trends at collisionalities reduced by up to an order of magnitude to a regime that is closer to that expected for NHTX and ST-CTF. This will allow an assessment of the confinement scaling with collisionality in this regime. Also during this period, L-H threshold studies will be carried out to determine whether the threshold power continues to scale with  $I_p$  in this expanded parameter range. additional divertor diagnostics will enable evaluation of the role of the X-point position in determining the L-H power threshold. Experiments with the 2<sup>nd</sup> NBI (incremental budget) will be carried out to study trends at higher power and with different heating deposition profiles.

### *3.3.1.2 Ion Turbulence and Transport*

#### **Results**

Ion transport in NSTX H-mode plasmas has been determined to be at or near neoclassical levels in the gradient region (e.g.,  $r/a=0.3-0.7$ ) of well-controlled and relatively MHD-quiet H-mode plasmas. It was found further, that while the ion transport did not exhibit much variation with  $B_T$ , it was this channel, and, in fact, the variation of the neoclassical transport that was

predominantly responsible for the scaling of global confinement with plasma current [3]. The variation of the ion thermal diffusivity profiles with  $I_p$  and  $B_T$  from these dedicated scans are shown in Fig. 6. As can be seen, while the ion thermal diffusivity outside of  $r/a=0.5$  did not vary much at different values of  $B_T$  for fixed  $I_p$ , there was a much stronger variation in the  $I_p$  scan, with  $\chi_i$  decreasing with increasing plasma current. Also shown in the figure is the range of neoclassical transport, given by the cross-hatched rectangular region for the  $B_T$  scan, and by the solid, color-coded rectangles for the  $I_p$  scan. For this latter scan, the rectangles indicate the neoclassical levels in the region from  $r/a=0.4$  to  $0.7$ . For both scans, the neoclassical levels were determined by the GTC-NEO code [10], which performs a gyrokinetic calculation based on measured plasma and impurity profiles, and which includes non-local effects, such as those due to the finite banana-width, to determine neoclassical levels.

A picture in which the ion transport is near the neoclassical level during the H-phase of the NSTX discharges, dropping from an anomalous level during the L-phase, is supported by both linear and non-linear gyrokinetic calculations. Shown in Fig. 7 are results from linear GS2 flux-

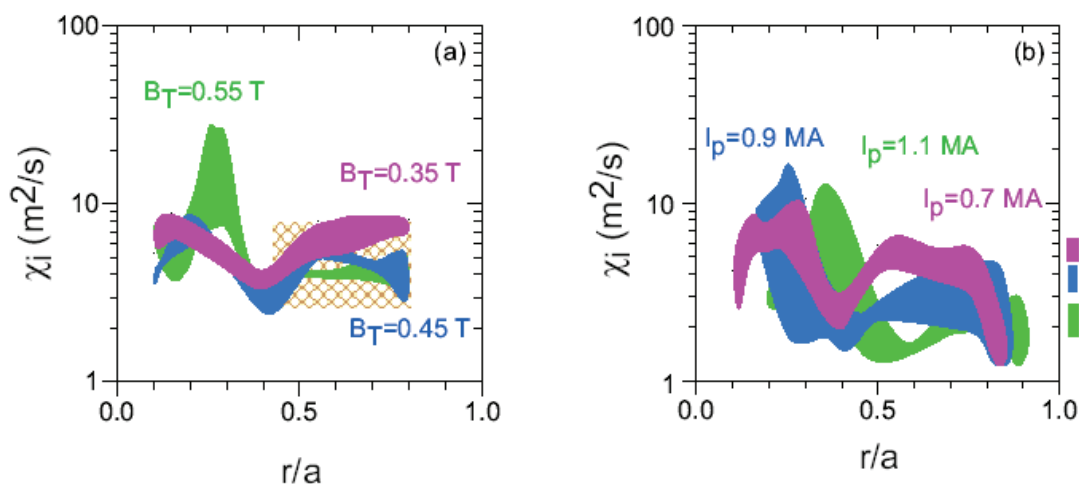


Fig. 6 Ion thermal diffusivity at fixed heating power and density as a function of (a)  $B_T$  at fixed  $I_p$  (b)  $I_p$  at fixed  $B_T$ . The cross hatched box in (a) and the color coded rectangular boxes in (b) indicate levels of neoclassical transport as determined by GTC-NEO.

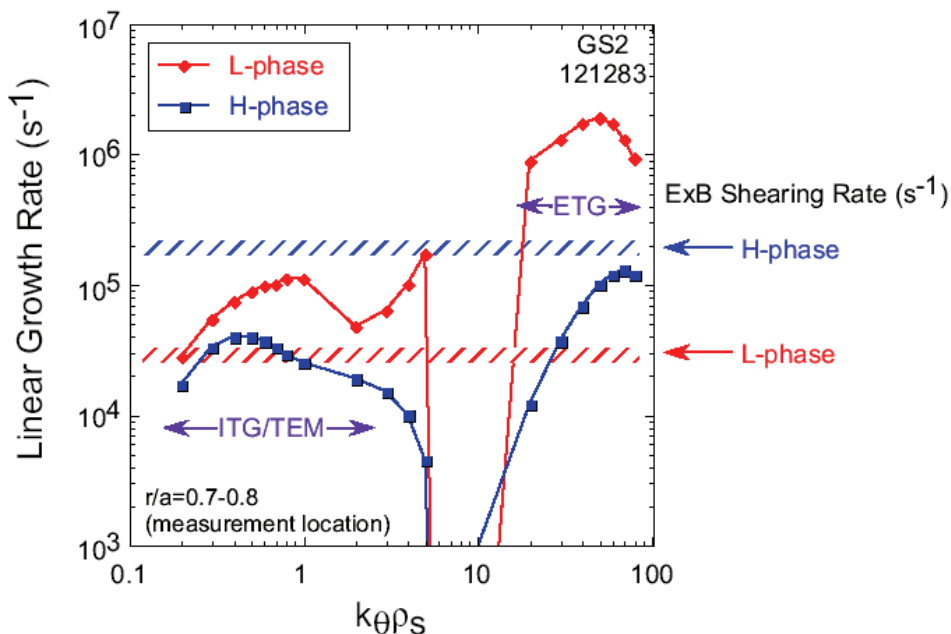


Fig. 7 Linear growth rates as a function of  $k\theta\rho_s$  for an L-mode phase and a subsequent H-mode phase. Also shown are the ExB shearing rates for both phases.

tube calculations, showing much larger growth rates for low-k modes during the L-phase than during the H-phase of a selected discharge. Non-linear, global GTS calculations indeed show that the neoclassical ion heat flux is greater than the turbulence-driven flux during the H-phase of these discharges. Also adding to the suppression of these low-k modes during the H-phase is an increased level of ExB shearing rate, reaching values of up to five times the linear growth rate during the H-phase (see Fig. 6). Furthermore, the magnetic shear is seen to have a profound effect on the ion transport as well in L-mode plasmas, with the transport being anomalous in low magnetic shear or monotonically increasing q plasmas, while the transport drops to near the neoclassical level in reversed magnetic shear plasmas, giving rise to ion Internal Transport Barriers in RS plasmas [4, 11-12].

Ion transport barrier physics has been studied further in the Enhanced Pedestal H-mode plasmas, plasmas exhibiting much higher pedestal ion and electron temperatures than in standard H-modes, where very strong  $T_i$  gradients are observed in regions of zero toroidal and zero poloidal

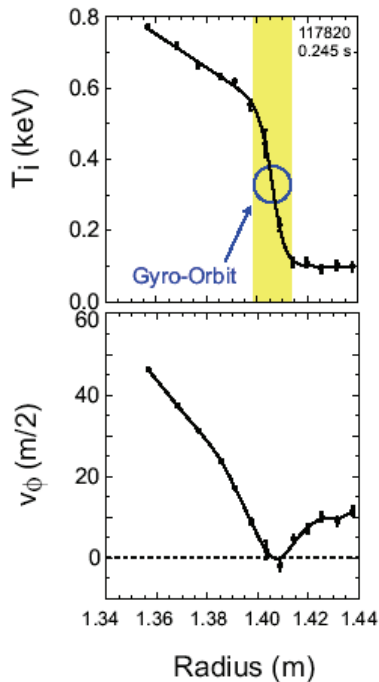


Fig. 8 Ion temperature gradient and toroidal velocity near plasma edge during an Enhanced Pedestal H-mode plasma

velocity (Fig. 8). The gradients are so strong that their scale lengths are of order the ion gyroradius ( $\sim 1$  cm). Standard neoclassical theory would suggest gradients to be limited to scales of order the banana width, and thus the smaller gradient scale lengths seen in NSTX may be indicative of neoclassical banana orbit squeezing [13]. Analysis to test this theory is underway, as is determining the effect that these strong gradients would have on destabilization of low-k microturbulence (e.g., ITG modes).

### Plans

An important goal of ion transport research on NSTX is to determine whether a future ST such as NHTX or an ST-CTF will operate in the ion neoclassical regime. Operation at higher  $B_T$ ,  $I_p$  and lower  $v^*$  will be in a regime in which  $\chi_{i,neo}$  is predicted to be reduced by up to an order of magnitude from the range in present operating regimes. Further, ITG and this could make neoclassical transport sub-dominant to turbulent transport. Operation with the new center-stack readily allow a test of this possible transition between the neoclassical- and turbulence-dominated regimes.

### 2009-2011:

The study of ion energy transport will continue to determine the conditions under which ions are governed by neoclassical transport vs either electrostatic or electromagnetic turbulent transport. This will be done experimentally by actively changing the  $T_i/T_e$  driving/damping terms for ITG/TEM turbulence in L- and H-mode using RF injection into NBI discharges. The ExB shear damping term of ITG turbulence will be controlled through  $n=3$  magnetic braking using the Non-

Resonant Magnetic Perturbations (NRMP) in fine steps to slow the plasma down, and determine the ExB level at which the ITG is sustained and ion transport becomes anomalous. Low-k turbulence measurements will be made using a Beam Emission Spectroscopy diagnostic, implemented in 2009, and the turbulence will be compared to ion transport and predictions of microturbulence levels and transport from non-linear gyrokinetic codes, for both neoclassical and turbulent driven transport. BES and Doppler reflectometry will be used to assess the role of Zonal Flows in the plasma core and at the edge. All these results will be coupled to results from non-linear gyrokinetic calculations, an input to which will be the full radial electric field determined from  $v_\phi$ ,  $v_\theta$  and  $\nabla p$  measurements. This will allow a preliminary validation of neoclassical and low-k turbulent transport theories. Ion Internal Transport Barrier studies will continue, focusing both on the potential for improved core fusion performance, and on regimes of strong  $T_i$  gradients and their relation to zonal flows, current profile and low-order rational  $q$ -values. The strong  $T_i$  gradient regions and possible orbit squeezing effects will allow validation of neoclassical theory at low aspect ratio.

#### 2012-2013:

The higher  $B_T$  and  $I_p$ , and the lower collisionality operation with the new centerstack will allow for an extension of the study of  $\chi_i$  to determine whether neoclassical transport still dominates over turbulence-induced transport in the H-mode in this extended parameter regime. In particular, will  $\chi_{i,neo}$  be low enough at the lower  $v^*$  for turbulent transport to become dominant? Will the reduction in ion-scale turbulence by ExB shear still be expected at the higher  $B_T$  and  $I_p$  and lower collisionality? This is coupled to the important area of momentum transport, which will be discussed in a later section, and the determination of whether the source of ion transport changes as the parameter regime is extended will be addressed also by direct measurement of the ion-scale turbulence by BES. The relation of inferred ion diffusivity to low-k fluctuations will be assessed in more detail using the low-k BES diagnostic, and this, coupled with results from non-linear gyrokinetic calculations, will allow for a very high-level test of neoclassical and ITG theory in the NSTX plasmas. Zonal flow measurements by BES will be made both near the core

and edge, which will enable a test of the possible  $q$  dependence. Studies of ion transport barrier physics will continue, with new information over a range of  $B_T$  and  $I_p$  measured by BES. Neoclassical theory that takes into account multiple species and full Larmor radius effects will be developed during this period. Internal control coils will be used for finer control of magnetic braking to determine the role of  $E \times B$  for suppressing low- $k$  modes and affecting ion transport (incremental budget). These comparisons will allow us to draw definitive conclusions regarding the source of ion transport under various operating conditions, and they will also allow for an assessment of the non-local nature of turbulence due to the large  $\rho^*$ . These more comprehensive studies will help establish a predictive understanding of the transition between neoclassical and turbulent ion transport, and how to predict ion transport in future devices with higher confidence.

### 3.3.1.3 Electron Turbulence and Transport

#### Results

NSTX operates in an electron-transport loss dominated regime in both L- and H-modes. It was

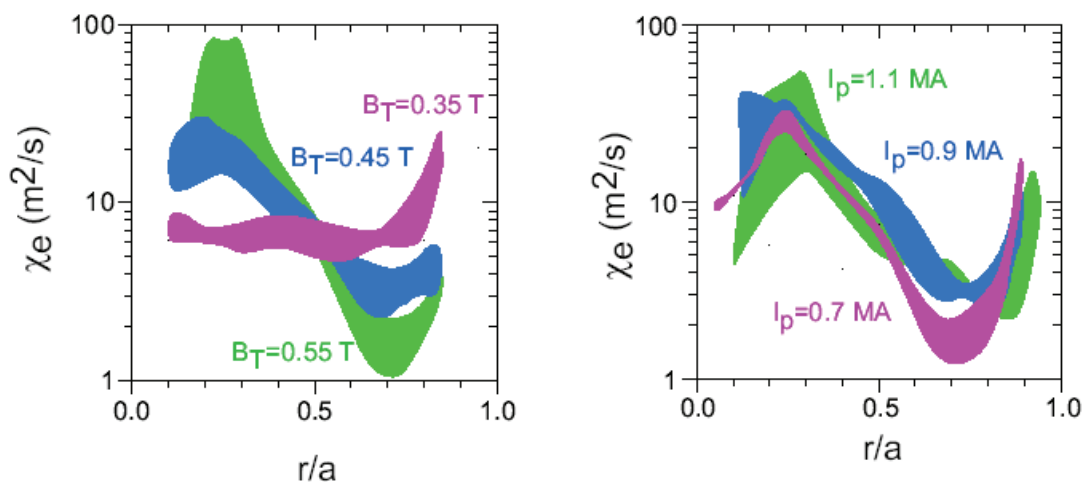


Fig. 9 Electron thermal diffusivity at fixed heating power and density as a function of (a)  $B_T$  at fixed  $I_p$  (0.7 MA) (b)  $I_p$  at fixed  $B_T$  (0.55 T).

the variation of electron transport that was found to govern the  $B_T$  scaling in the H-mode, as can be seen in Fig. 9. Seen in this figure is a strong decrease in  $\chi_e$  outside of  $r/a=0.5$  with increasing  $B_T$  that led to a broadening of the electron temperature profiles. Inside of this radius, the  $\chi_e$  increases with increasing  $B_T$ , although the temperatures in this region are comparable for all values of the toroidal field. Thus, the increase in  $\chi_e$  within  $r/a=0.5$ , where the total plasma volume is relatively small, does not significantly impact the overall improvement of electron and global confinement with increasing toroidal field. The change in electron thermal diffusivity in these two regions of the plasma is qualitatively consistent with the change in the measured high- $k$  fluctuation levels with toroidal field at these two locations, as is seen in Fig. 10. Shown in this figure are results from the microwave scattering diagnostic, which reveals a higher fluctuation level at higher  $B_T$  in the core of the plasma ( $r/a\sim 0.25$ ), while the fluctuation levels are lower at the higher field at  $r/a\sim 0.75$ . Furthermore, linear and non-linear theory simulations indicate that ETG modes with the development of radial streamers are unstable in the outer part of the plasma ( $r/a>0.5$ ) for the lowest toroidal field (Fig. 11), but not for higher toroidal fields. For both the low and high-field cases, the measured electron temperature gradients are within 15% of the calculated critical gradients for ETG modes. Non-linear saturated heat fluxes calculated from ETG/radial streamer theory

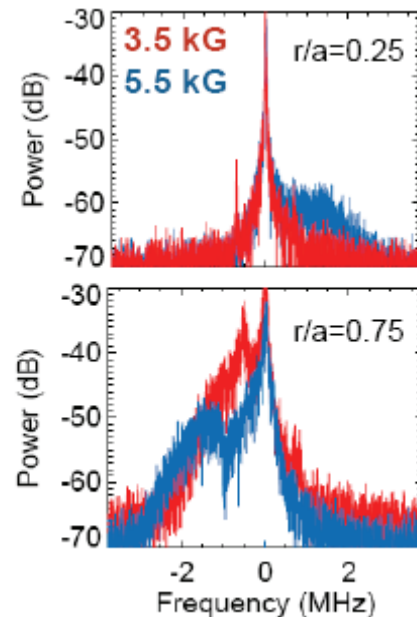


Fig. 10 High  $k$ -fluctuation ( $k_{\theta}\rho_e\sim 0.18$ ) spectra for 0.35 T (red) and 0.55 T (blue) for the core,  $r/a=0.25$  (top panel), and farther out,  $r/a=0.75$  (bottom panel).



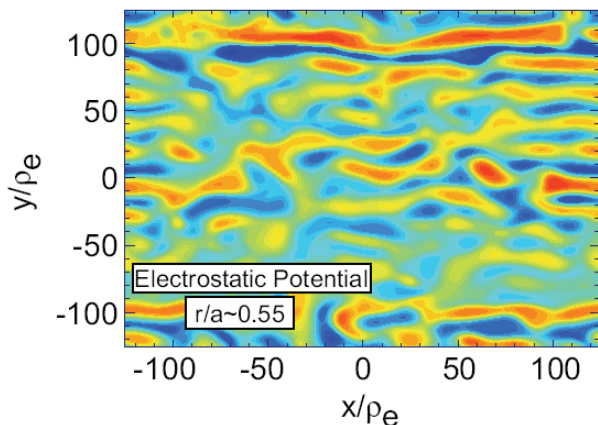


Fig. 11 Results of non-linear calculation showing the formation of radial streamers from ETG modes at  $B_T=0.35 T$

[14] are comparable to those inferred from the TRANSP transport analysis. Just as the ion transport in L-mode plasmas improves with reversed magnetic shear, so to does electron transport, leading to electron Internal Transport Barriers (Fig. 12). While ETG modes are expected to be unstable outside the reversed shear region, and non-linear GYRO calculations predict electron heat fluxes that are consistent with those inferred from TRANSP analysis (Fig. 13), the reduction in electron transport in the reversed-shear core region may be in fact due to a suppression of the high-k ETG and low-k microtearing modes. Microtearing modes, which are calculated to be important in NSTX [15] are low- k, electromagnetic modes extended along field lines that are important in the collisionality range within which NSTX operates. The instability of these modes is also dependent on magnetic shear profiles, and it is found that accompanying the reduction in transport with reversed magnetic shear is a narrowing of the wavenumber range over which microtearing modes are unstable. Calculations of the electron thermal diffusivity predicted by the magnetic stochasticization due to microtearing modes in the core region of

with those inferred from TRANSP analysis (Fig. 13), the reduction in electron transport in the reversed-shear core region may be in fact due to a suppression of the high-k ETG and low-k microtearing modes. Microtearing modes, which are calculated to be important in NSTX [15] are low- k, electromagnetic modes extended along field lines that are important in the collisionality range within which NSTX operates. The instability of these modes is also dependent on magnetic shear profiles, and it is found that accompanying the reduction in transport with reversed magnetic shear is a narrowing of the wavenumber range over which microtearing modes are unstable.

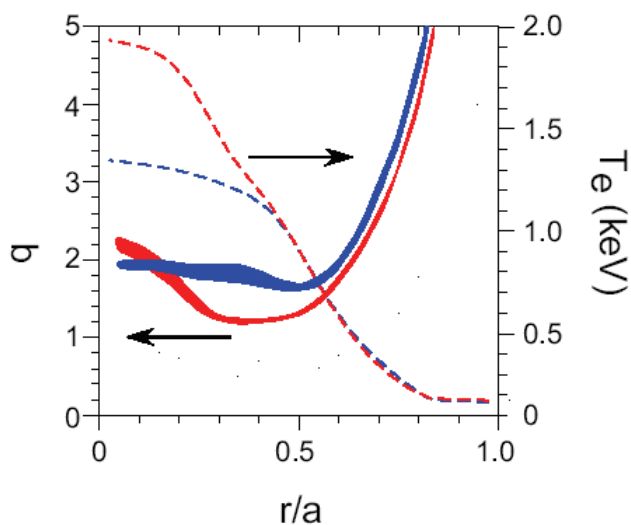


Fig. 12 Electron temperature and q-profiles showing the development of an electron Internal Transport Barrier with reversed magnetic shear.

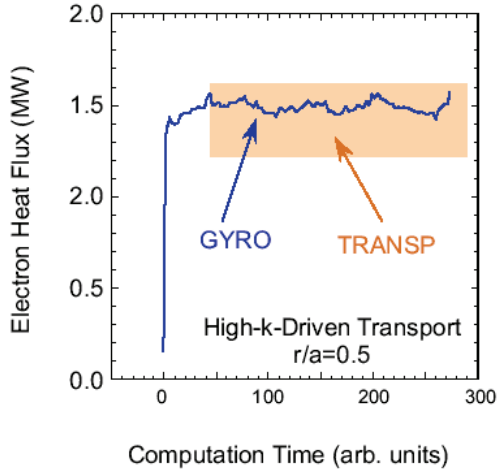


Fig. 13 Electron heat flux outside the region of reversed magnetic shear calculated by non-linear GYRO simulations and inferred from TRANSP

diagnostic. An example of this is shown in Fig. 15. Seen in the figure is a strong peaking of the  $T_e$  profile as the RF heating is applied (Fig. 15a). The high-k fluctuations grow and are the strongest when the experimental  $R/L_{Te}$  exceeds the critical value for ETG growth, as estimated by an empirical formula [16]. Linear gyrokinetic calculations confirm that ETG modes in the wavenumber range covered by the high-k scattering diagnostic are expected to be unstable for these  $R/L_{Te}$ .

“hybrid” NSTX plasmas show agreement to within a factor of two to that inferred from transport analysis (Fig. 14). It is clear from these and the ETG results that there may be multiple instabilities across a range of wavenumbers that control electron transport. Experiments to determine the critical electron temperature of the transport-inducing modes have just begun. These experiments make use of High Harmonic Fast Wave heating to change the electron temperature gradient, and the change in high-k fluctuations accompanying the change in the mode driving term is measured by the microwave scattering

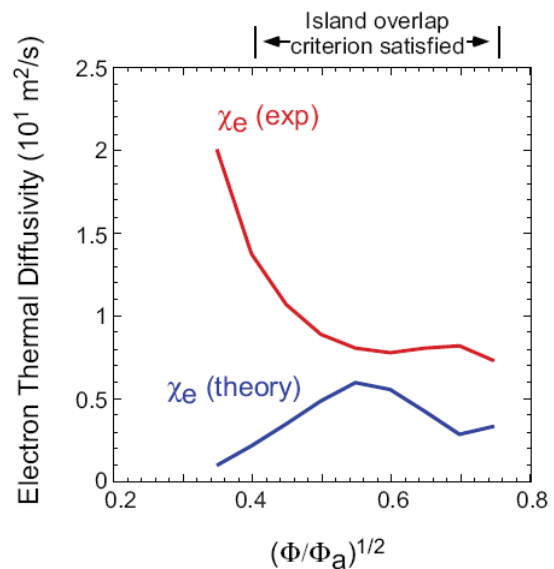


Fig. 14 Experimental  $\chi_e$  inferred from TRANSP (red) compared to  $\chi_e$  predicted by microtearing theory (blue)

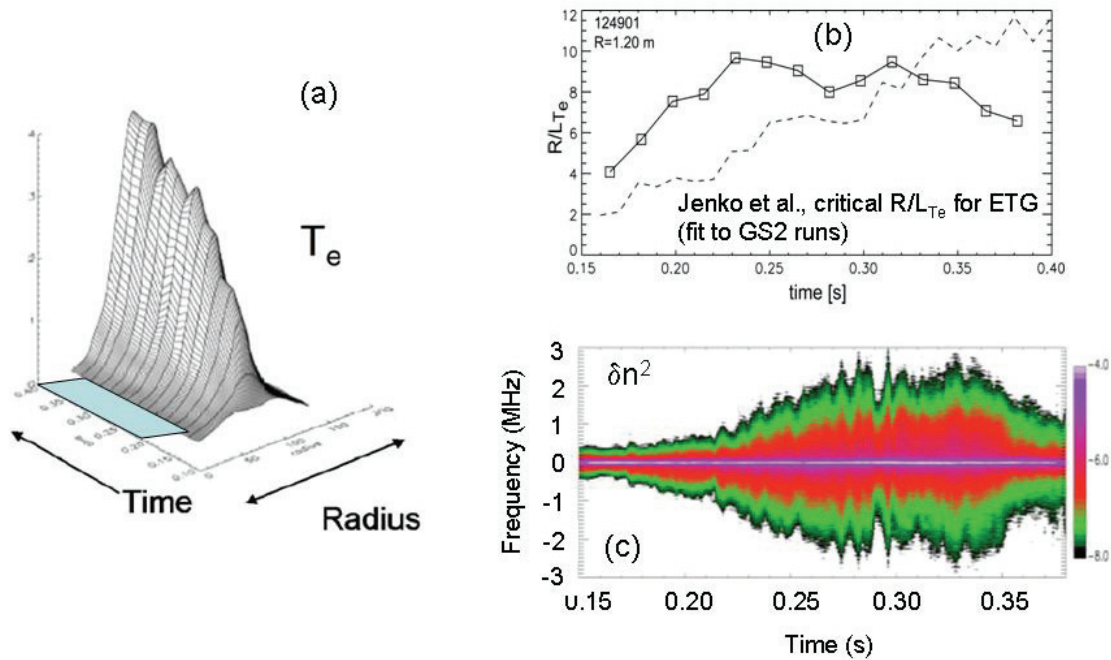


Fig. 15 (a)  $T_e$  profile as a function of time and radius with HHFW injection (b) Measured  $R/L_{T_e}$  (solid line) and  $R/L_{T_e}$  from a fit to GS2 runs (dashed line) as a function of time (c) high-k scattering signal at  $14 \text{ cm}^{-1}$  as a function of time

One of the outstanding questions in electron transport for all aspect ratio devices is what drives transport in flat temperature regimes, where the microinstability drive is absent since  $\nabla T_e \sim 0$ ? Recent observations on NSTX have shown a relation between the strength of core, fast ion-driven Global Alfvén Eigenmode activity in both L- and H-modes, and electron transport. Fig. 16 shows a series of L-mode discharges with increasing GAE activity associated with increasing neutral beam power. Associated with the higher level of GAE activity are flatter electron temperature profiles and higher inferred values of  $\chi_e$  in the core, where the GAE mode is predicted to exist. Preliminary theoretical estimates show that the measured GAE fluctuation levels can lead to core  $\chi_e$  values comparable to those inferred from transport analysis.

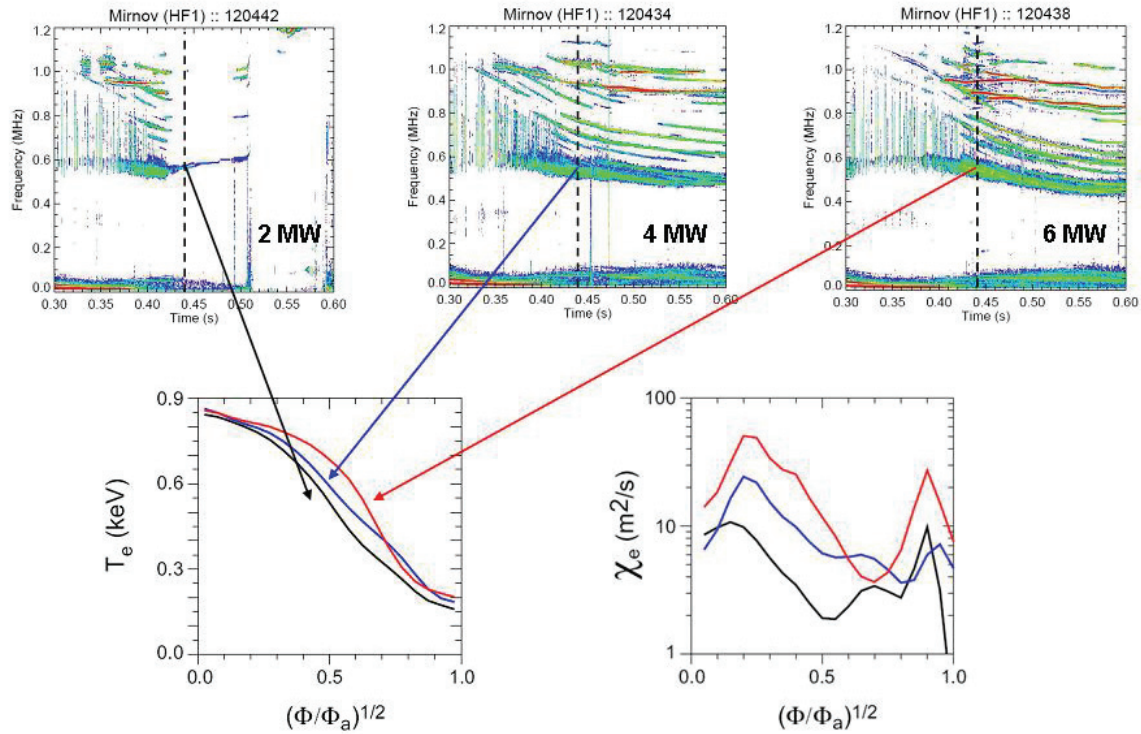


Fig. 16 Series of discharges showing increasing GAE activity with increasing beam power. The temperature profiles in the core are flatter and the central electron thermal diffusivities are higher with higher levels of GAE activity.

## Plans

NSTX is in an excellent position to study and understand the key areas of electron turbulence and critical gradient physics. This is the top priority in the Transport and Turbulence Five Year Plan. Because of the relatively large  $\rho_e$  at the low fields at which NSTX operates, electron scale length turbulence can be measured. The microwave scattering diagnostic on NSTX, which is radially scannable and which provides a highly localized ( $\pm 2.5$  cm)  $k_r$  measurement, is unique and particularly well-suited for measuring ETG and short wavelength TEM modes. Additionally, SXR arrays can be used to monitor fast changes in the electron temperature profiles due to turbulence. Since the turbulent-driven ion transport is subdominant to ion neoclassical transport

in H-modes, non-linear gyrokinetic ETG simulations with adiabatic ions and scale separation are possible. The ultimate goal is to develop a comprehensive picture of electron transport for developing a predictive capability for future STs.

2009-2011:

During this period, continued identification of TEM and ETG modes will be made using the present high-k scattering system. Collisionality scans, using HHFW and the LLD, will be made to differentiate modes. The critical gradient necessary for destabilizing high-k turbulence will be assessed experimentally using HHFW to change the  $R/L_{Te}$  in fine steps and at various collisionalities using the LLD. Once established experimentally, the critical gradient will be benchmarked against that predicted by gyrokinetic simulations to identify the responsible mode. Experimental studies of the roles of reversed magnetic shear and low order rational q surfaces in the development of electron Internal Transport Barriers will be carried out by varying key parameters that affect mode stability, such as the magnetic shear, density gradient,  $\nabla n_e$ ,  $\beta$ ,  $T_e/T_i$ , etc. Furthermore, the issue of whether the ST geometry, such as that which gives rise to precession reversal, reduces the TEM mode severity will be studied. The effect of ExB shear on the suppression of ETG modes will be explored. Microtearing modes will also be studied experimentally in order to determine their importance in driving electron transport by changing the driving terms such as  $\beta$  and collisionality, and by making initial measurements of internal B-field fluctuations possibly using MSE and polarimetry. It is expected that the sensitivity of these two diagnostics will be 5 to 10 G up to 100 kHz, the maximum frequency expected for microtearing. The first measurements will attempt to determine whether this sensitivity is low enough for measuring microtearing fluctuations.

Key to all these studies will be the direct connection and benchmarking against results from a suite of gyrokinetic simulations from different research groups at all levels. Synthetic diagnostics such as the high-k scattering and SXR and magnetic fluctuations will be built into the gyrokinetic codes for comparison with experiment. This could also help establish the importance of the high-k modes relative to the lower-k microtearing. Of importance is to determine the

source of electron transport in the core of plasmas where both the density and temperature profiles are too flat to destabilize the electrostatic instabilities such as ITG and ETG, as well as microtearing. The presence of high frequency magnetic fluctuations, such as those associated with the core-localized Global Alfvén Eigenmodes, as seen to be associated with high inferred levels of electron transport in flat  $T_e$  and  $n_e$  regions, and the causal relation between the two will be explored. The GAE mode structure may be measured with BES. Perturbed electron transport studies will investigate the cold pulse propagation from ELMs and pellets using high resolution measurements near the boundary with a multi-color soft X-ray array for fast  $T_e$ ,  $n_e$  and  $n_{imp}$  profile measurements. Finally, BES and Doppler reflectometry can be used to study the existence of Zonal Flows in the core and at the edge of the plasma in H-modes, and throughout the plasma in L-modes, and their effect on modes that are believed to drive electron transport.

#### 2012-2013:

The higher  $B_T$ ,  $I_p$  and lower collisionality will allow for a critical examination of which modes are responsible for electron transport and under what conditions. In particular, the higher field and lower collisionality can lead to a suppression of the GAE and microtearing modes respectively. The reduction of  $n^*$  at higher field and with LLD operation is expected to be up to an order of magnitude, which is sufficient to stabilize the microtearing modes for electron temperature gradients typical of present operation. Further, the high-frequency GAE activity is expected to be reduced with lower  $v_{fast}/v_{Alfvén}$  at the higher field. This would leave the TEM and ETG as the only candidates for causing turbulent-driven electron transport. The new centerstack and the LLD will provide this capability. Whether the electron transport continues to dominate the plasma energy loss at higher  $B_T$  and  $I_p$  will be studied during this operation period. Experimental identification of microtearing modes will also be pursued experimentally by assessing the extent of these modes along the field line using the low- $k$  diagnostic and from the internal B-field fluctuation measurements that may be obtained by MSE or polarimetry. Modification of the high- $k$  scattering system would enable measurements of the full range of medium-to-high  $k_r$  and  $k_\theta$  turbulence. This diagnostic will yield information on mode structure,

full frequency spectra and dispersion characteristics. Coupled with the BES measurements, the studies of microturbulence using the more detailed  $k_r$  and  $k_\theta$  information will allow for much more comprehensive validation of the gyrokinetic simulations across the full  $k$ -range. Included in this exercise will be the results of probing the structure of the higher- $k$  fluctuations. For instance, both TEM and ETG are strongly ballooning to the outside, and radial streamers may be expected from ETG. The existence or not of the radial streamers can be assessed with simultaneous measurements of  $k_r$  and  $k_\theta$  from the microwave scattering.

Electron transport and turbulence modification will be tested using local heating via local deposition of EBW at the multi-hundred kW level (incremental budget). This will include early application of EBW to modify the  $q$ -profile and possibly induce ITB formation. Turbulent spreading into the linearly stable region will be examined using the scannable high- $k$  diagnostic, and this spreading will be related to the ExB shear layer and variation in magnetic shear. Modulated EBW will be used to probe the local critical gradient physics and regions of good and bad transport along with the formation of Internal Transport Barriers, using a tangential optical soft X-ray system (TOSXR) with good signal-to-noise characteristics, and an upgraded MPTS. In order to use the MPTS for this, it will be necessary to combine several shots with different timing to get a complete evolution. The multi-hundreds of kW EBW system will be used for localized deposition and heating to probe critical gradient physics and turbulence spreading. These measurements, in turn, will be compared to output of similar synthetic diagnostics from gyrokinetic codes for a detailed assessment of the microturbulent sources of electron transport.

### 3.3.2 *Momentum Transport*

The rotation in NSTX has been observed to be quite high, with toroidal velocities up to 300 km/s in the core, and this leads to strong ExB shearing rates that can be up to five times greater than the linear growth rates of low- $k$  instabilities (Fig. 7). Thus, it is expected that the high rotation can effectively suppress these low- $k$  instabilities, and indeed non-linear gyrokinetic calculations

suggest that this is so. The rotation is important not only for suppressing the microturbulence, but also for suppression of both internal and external MHD modes and leading to achieving high performance goals both in NSTX and potentially in future devices. Consequently, it is important to understand the source of this rotation, how momentum diffusivity relates to electron and ion thermal and particle diffusivities, the effect of rotation and ExB shear on energy and particle confinement, and the source of intrinsic rotation on NSTX. In particular, will the ExB shear be high enough in future devices to suppress the low-k turbulence and maintain the ion energy transport at neoclassical levels?

## Results

In H-mode discharges, the momentum diffusivity was found to be highly anomalous relative to GTC-NEO neoclassical predictions, despite the fact that the ion thermal transport was close to neoclassical in these discharges. The momentum transport varied most strongly with  $B_T$ , showing very weak or no effect with  $I_p$ , which is more consistent with the observations of the electron thermal transport reported in [4]. However, over a wide database of plasma conditions, this correlation is not robust, with only a weak dependence on  $\chi_\phi$  on  $\chi_e$  emerging.

The lack of scaling of  $\chi_\phi$  with  $\chi_i$  seen in the dedicated scaling experiments is also clear statistically in the inner half of the plasma ( $\rho \leq 0.4$ ), where  $\rho$  is the square root of the normalized toroidal flux. In this region,  $\chi_i$  can be up to a factor of 30 greater than  $\chi_\phi$ . Farther out, at  $\rho \geq 0.65$ ,  $\chi_\phi$  is broadly seen to scale with  $\chi_i$ , more consistent with results from conventional aspect ratio tokamaks [17,18], although  $\chi_i$  still tends to be a factor of about 10 greater than  $\chi_\phi$ . The scaling, however, is not particularly tight, with approximately an order of magnitude scatter in the data.



Dedicated momentum confinement scaling experiments have been carried out in NSTX, making use of Non-Resonant Magnetic Perturbation (i.e., application of  $n=3$  error fields) to slow the plasma. The NRMP were applied for 50 ms, and a momentum confinement analysis was performed at the time when the NRMP was turned off, when NBI was the only known source of torque. This perturbative technique allowed for determination of  $\tau_\phi$ ,  $\chi_\phi$  and  $v_{\text{pinch}}$  through the plasma. Fig. 17 shows the results of this analysis for  $\chi_\phi$  and  $v_{\text{pinch}}$ . Consistent with the results from Fig. 17, both the global momentum balance and perturbative fit determination of the momentum confinement time indicates values in excess of 150 ms, and these values exceed the energy confinement time by a factor of approximately four to five. Additionally, the analysis

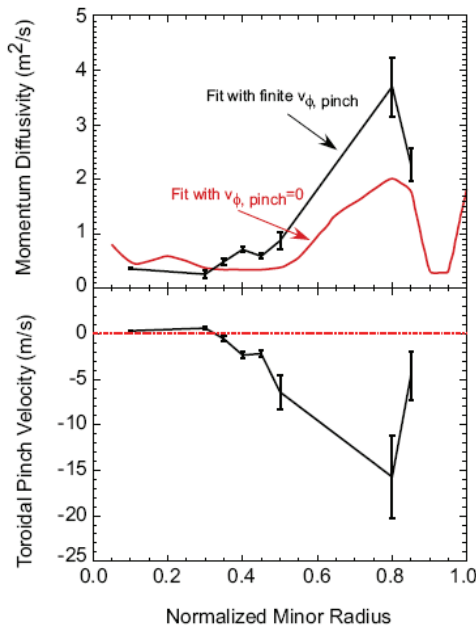


Fig. 17 Results of perturbative analysis to determine the momentum diffusivity and inward pinch velocity.

indicates a significant inward pinch velocity, with values reaching 40 m/s, and momentum diffusivities of order several  $\text{m}^2/\text{s}$ , which are closer to the values of  $\chi_i$  than are the  $\chi_\phi$ 's deduced from the global momentum balance. Furthermore, the inward pinch velocity is consistent with values predicted by the theories of Peeters et al. [19] and Hahm et al., [20], both theories predicated on low- $k$  turbulence induced momentum transport (Fig. 18). Previous work [21] has shown the change in angular momentum due to NRMP application is consistent with Neoclassical Toroidal Viscosity theory [22], and this will be used in the future as a basis for momentum confinement and transport studies during the NRMP application. Because of near-zero value of neoclassical momentum transport, the

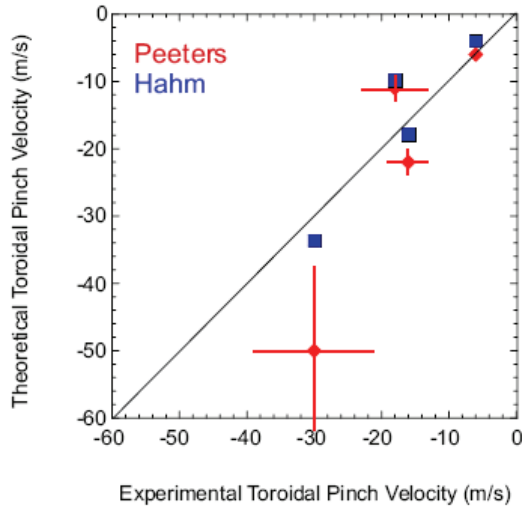


Fig. 18 Comparison of experimental and theoretical toroidal momentum pinch velocities.

observed momentum transport in NSTX will be a better probe of the effects of low-k turbulence than ion energy transport would be.

**Plans**

The essential questions to be addressed over the course of the Five Year Research Plan are “what is the source of momentum transport, and how does momentum transport couple to energy transport, and will the ExB shear be sufficient to suppress both low- and high-k turbulence?”

2009-2011:

Poloidal CHERS will be used to measure  $v_\theta$  under a variety of discharge conditions, and these measurements will be used to test the validity of neoclassical theory. Non-Resonant Magnetic Perturbation studies will continue in order to infer  $\tau_\phi$ ,  $\chi_\phi$  and  $v_{\text{pinch}}$  at NRMP turn-off under a variety of discharge conditions. Beam blips will be used to assess  $\tau_\phi$ ,  $\chi_\phi$  and  $v_{\text{pinch}}$  close to the plasma center. The inferred pinch velocities at different  $L_n$  will be used to differentiate between momentum pinch theories [19,20]. NTV theory will be used to estimate the torque due to the error field and thus the momentum transport properties during application of NRMP. These values will be compared to the post-NRMP values to check consistency and determine whether NTV theory provides a consistent picture that can be used for extrapolation to future devices and scenario development. The momentum transport will be compared in L- vs H- plasmas, with a focus on the relation between  $\chi_\phi$  and  $\chi_i$ ,  $\chi_e$ . Comparisons between momentum transport metrics and low-k measurements will be made.

2012-2013:

Higher  $B_T$ ,  $I_p$  and lower  $v^*$  provided by the new centerstack and LLD are the tools necessary not only to develop a further understanding momentum transport in this expanded parameter regime, but also to determine whether the ExB shear will be able to suppress low- and high-k microinstabilities in regimes close to those of future ST and non-ST devices. Rotation modulation studies will continue using NRMP. The low-k diagnostic will allow for a determination of the relation of low-k fluctuations to variations in momentum transport in both L- and H-modes. In particular, the  $v_\theta$  measurements will allow an assessment of the importance of neoclassical effects in this extended parameter regime, which will allow a closer coupling to the operational space expected for NHTX and an ST-CTF. This low-k diagnostic will also allow for Zonal Flow/GAM studies, and these will entail coupling of these large-scale flows to other microinstabilities at all k, bicoherence analysis to determine the most robust coupling of these flows and modes, and the effect of these large-scale flows on transport. Application of NRMP from off-axis internal coils will permit finer control of the magnetic braking for momentum diffusivity and pinch velocity determinations (incremental budget).

### *3.3.3 Particle Transport*

Particle transport, which is not well understood at present either at low or conventional aspect ratio, is a fertile area for study. Understanding particle transport is yet another level of validation of physics models describing microturbulent vs neoclassical transport, and it is complementary to energy transport studies. Another issue of importance is impurity transport in ion neoclassical plasmas and plasmas with Lithium. Helium transport studies in NSTX relate to the Helium ash issue in ST-CTF and ITER. Much of the necessary data for analysis already exists, and thus analysis can proceed immediately. Diagnostic and facility enhancements will, however, aid these studies. In addition, some of the unique features of NSTX add another dimension to the particle transport studies; these include the high mirror ratio in the Scrape-Off Layer (SOL) and thus a

high trapped particle fraction, and the ability to extend the ranges in collisionality,  $q$  and  $\beta$  for these studies.

## Results

To date, the particle transport studies in NSTX have focused on studies of impurity transport in beam-heated H-mode plasmas. These studies were carried out primarily using Neon injection into MHD quiescent plasmas. For these studies, the tangential array of Soft X-ray detectors with multi-foil capability for energy and thus radial discrimination was used to track the transport of the impurity. A synthetic SXR diagnostic with the multi-foil capability was built into the MIST code for comparison between simulated and measured impurity profile evolution. Fig. 19 shows this comparison, with very good agreement at this level of comparison between the measured

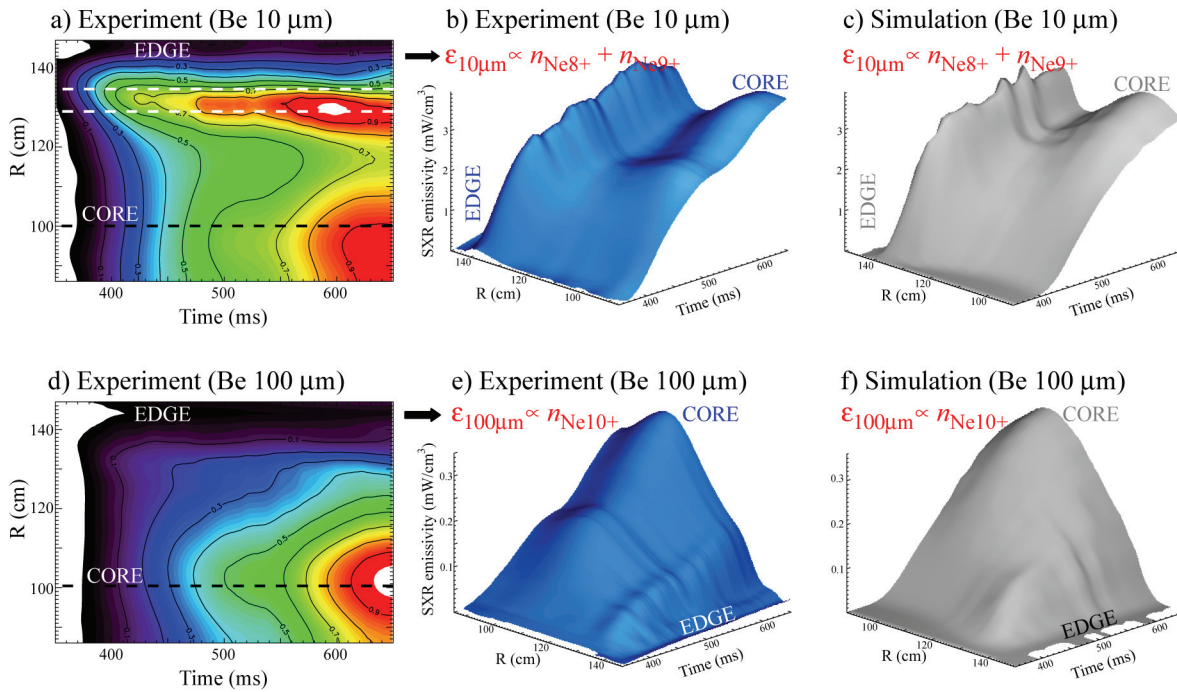


Fig. 19 Comparison of measured soft X-ray profile evolution for two different filters (left) with those from MIST simulations assuming neoclassical diffusivity for Neon. A small inward pinch is also required for agreement.

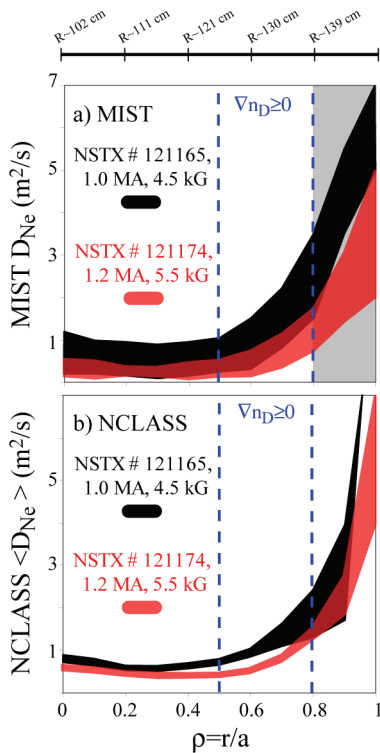


Fig. 20 Particle diffusivity values assumed in MIST for the Neon transport (upper panel) compared to the neoclassical values (lower panel).

and simulated profile evolution. In order to achieve this, a low core impurity particle diffusivity of  $D \sim 1 \text{ m}^2/\text{s}$  was required. This value of  $D$  is at the neoclassical transport level for the Neon impurity, as is shown in Fig. 20. This result complements those of the ion energy transport, which as described in a previous section, also suggests neoclassical levels of transport in these plasmas.

### Plans

What are the properties of particle and impurity transport, and how do they relate to energy transport and low- $k$  turbulence measurements? Does collisionality control the transport properties?

### 2009-2011:

The effect of low collisionality and recycling with Lithium evaporation and the Liquid Lithium Divertor on the particle and impurity transport will be established. Particle and impurity transport levels in the core, within the dominant NBI-fueling regime ( $r/a < 0.55$ ) will be studied using the TRANSP code. The fueling from NBI is dominant in this regime, and the particle source can be determined straightforwardly through the TRANSP beam Monte-Carlo calculation. The aim would be to understand the systematic variation of particle diffusivity with power, current, toroidal field, etc. from the pre-existing database. The relation of the particle to thermal diffusivities will be assessed to determine whether they have the same parametric dependences and what the differences are between L- and H-mode; are the particles driven by turbulent transport in high density L-modes as the thermal ion heat flux seems to be?

Density peaking studies and the effect of particle pinches, in conjunction with ITPA, will be carried out in order to determine the regimes in which fusion power production can be

maximized for devices such as ITER and ST-CTF. There is a clear trade-off between maximizing core reactivity (i.e., peaked profiles) and plasma stability.

Impurity transport will be assessed using high-Z impurity injection and TESPEL (Tracer Encapsulated Solid PELlet) injection at the edge in Lithium and no-Lithium plasmas. Tracking the impurities can be done with either the high-resolution edge/pedestal soft X-ray array or the CHERS diagnostic. The simultaneous inclusion of the multi-energy SXR array and the bolometer data, along with the time-dependent MIST modeling, puts a strong constraint in the determination of both  $D$  and  $v_{\text{pinch}}$  for  $r/a < 0.8$ . The possible relation between the particle pinch and the momentum pinch will be investigated.

#### 2012-2013:

The higher  $B_T$ ,  $I_p$  and operation with LLD will provide information on particle transport in lower collisionality plasmas. The effect of the LLD and Lithium wall conditioning on particle, impurity and Helium transport will be assessed; i.e., how do  $D$  and  $v_{\text{pinch}}$  change with changes in collisionality and recycling? The role of low- $k$  turbulence in controlling core particle transport will be assessed with the low- $k$  turbulence diagnostic in order to test particle transport models. The variation in density fluctuations will be studied as a function of  $D/D_{\text{neo}}$  in a variety of plasmas: L vs H over the full range of  $I_p$  and  $B_T$ , high vs low density (collisionality) and reversed magnetic shear vs low central shear ( $q$ -profile). Modulated core fueling studies with beam blips will be carried out, taking advantage of the upgraded MPTS diagnostic as well as higher beam power (incremental budget). The evolution of the density profile will have to be built up from numerous discharges in order to use amplitude and phase analysis to determine  $\tau_p^*$ . The modulated studies will also allow a separation of  $D$  and  $v_{\text{pinch}}$ , to be compared both to the steady-state particle balance value of  $D$  (i.e., from TRANSP) and to theory.

Edge particle transport studies will be performed with modulated fueling from the supersonic gas injector (SGI) and pellet fueling with a D pellet injector, again taking advantage of the upgraded MPTS. Outside of  $r/a=0.55$ , the fueling is dominated by wall fueling and recycling, and

estimating the source rate of the will be done using DEGAS2 and UEDGE. These neutral source profiles can be input to TRANSP for a determination of the particle diffusivities across the full plasma radius.

The understanding of Helium transport is needed for assessing the likelihood of success for integrated scenarios in future devices. Helium transport studies in NSTX can be carried out with either He puffing into deuterium discharges, or with Helium discharges themselves.

### *3.4 Theoretical Tools and Modeling*

The coupling of Theory and Modeling to experimental results is critical for developing a fundamental understanding of key physics issues and for helping develop a tool that will allow performance predictions with high confidence.

#### **Present Tools**

The international standard code, TRANSP, is and will continue to be used for steady-state energy, particle and momentum transport studies. A predictive tool under development that is based on codes from a number of research institutions, pTRANSP, is being used for predictive transport analysis and discharge scenario development. Low aspect ratio data will provide key tests of theory-based transport models; for instance, studies to validate the TGLF model [23] are underway.

Linear and non-linear gyrokinetic analysis is being done by a variety of codes. GTC-NEO takes into account finite banana width and thus non-local effects for determination of neoclassical transport. The GS2 flux tube code contains kinetic electron and ion, finite beta and generalized geometry descriptions, and it can be run in both linear and non-linear modes. However, for NSTX, global codes such as GTS, GYRO and GEM are required due to the large gyroradii of both electrons and ions. Verification of these codes using low aspect ratio data is underway.

## **Plans**

All available tools will be used, with a focus on Verification and Validation of codes and physics models developed by a number of research groups..

### 2009-2011:

A 2D/3D state-of-the-art neutrals package will be implemented in TRANSP to aid in particle transport studies. pTRANSP will be used to validate predictive models such as those given by TGLF [23]. GTC-NEO will be upgraded with multiple species and will be utilized to test neoclassical theory with  $v_\theta$  measurements. Non-linear GYRO simulations with synthetic diagnostics over the full range of  $k$  will be carried out. Non-linear GTS simulations with kinetic electrons and synthetic diagnostics for high- $k$  will begin. A multiple ion species capability will be implemented in GTS. Non-linear GEM simulations for low- $k$  microtearing modes will be carried out. A version of GEM with kinetic electron physics implemented will be developed and used. Results from GTC-NEO calculations and results from non-linear calculations (GYRO, GTS) will be used to evaluate the neoclassical and the non-diffusive turbulent flux (pinch and  $\nabla p$ -driven residual stress) for toroidal angular momentum transport. Comparisons between low- $k$  fluctuation measurements and results from synthetic diagnostics in non-linear gyrokinetic simulations will be made.

### 2012 - 2013:

More detailed and comprehensive comparisons between low- $k$  fluctuation measurements and results from synthetic diagnostics in non-linear gyrokinetic simulations will be made. The role of Zonal Flows and their relation and coupling to low- $k$  turbulence will be assessed. pTRANSP simulations will become more sophisticated as the plasma transport properties become more fully understood and the models become more physics-based. Tests of turbulence spreading using results from local EBW deposition experiments (incremental budget) will begin with comparisons to code predictions.



Predictions of ion and electron heat, particle and momentum transport profiles with respect to dimensionless variables will be made using gyrokinetic analysis with full features (i.e., collisions, turbulence spreading, etc). Transport codes such as TGLF will be used to predict full plasma profiles, and these will be compared to measured profiles as part of the Verification and Validation procedure.

Fully predictive transport simulation capabilities will be developed. These will be combined with other simulations (e.g., MHD) to form a fully integrated scenario package. This package will be used as a basis for developing actual experimental discharge scenarios in NSTX and in future devices.

### *3.5 Facility and Diagnostic Upgrades*

The facility upgrades, such as the new centerstack and LLD are crucial for testing the critical physics issues affecting the prediction of performance of future devices, both ST and non-ST.

#### 2009 - 2011:

A Liquid Lithium Divertor will be installed, allowing operation at lower collisionality than presently.

Additional MPTS channels will provide a more complete electron temperature and density profiles. The full complement of poloidal CHERS channels will be available for measuring the poloidal velocity. The full complement of FIDA channels and neutron collimators will be available for measuring beam deposition profiles necessary for higher confidence power balance calculations. A low-k fluctuation diagnostic (BES) will be implemented. The ability to use MSE and/or polarimetry to measure internal B-field fluctuations will be assessed. A modification of the high-k scattering system will provide  $k_{\theta}$  in addition to  $k_r$  information. A high resolution,

tangentially-viewing soft X-ray array for diagnosing the plasma edge/pedestal region will be implemented to support edge impurity and electron thermal transport studies.

Additional filters for CCD cameras will aid in Helium transport and recycling studies. Extra channels will become available for the Edge Rotation Diagnostic for measuring the edge toroidal and poloidal rotation.

2012 - 2013:

An upgraded centerstack, allowing for operation with  $I_p$  up to 2 MA and  $B_T$  up to 1 T. which will allow operation at even lower collisionality, will be installed and operational. Internal off-axis control coils and up to 700 MW of EBW are in the incremental budget.

MPTS will be upgraded to 45 channels and 100 Hz. The microwave scattering diagnostic will be modified to include  $k_\theta$  measurement. The core multi-color soft X-ray array, upgraded for high signal-to-noise, will provide better discrimination and faster profile measurements of small localized heat pulses for probing internal transport and barrier formation. A divertor Thomson Scattering system is in the incremental budget.

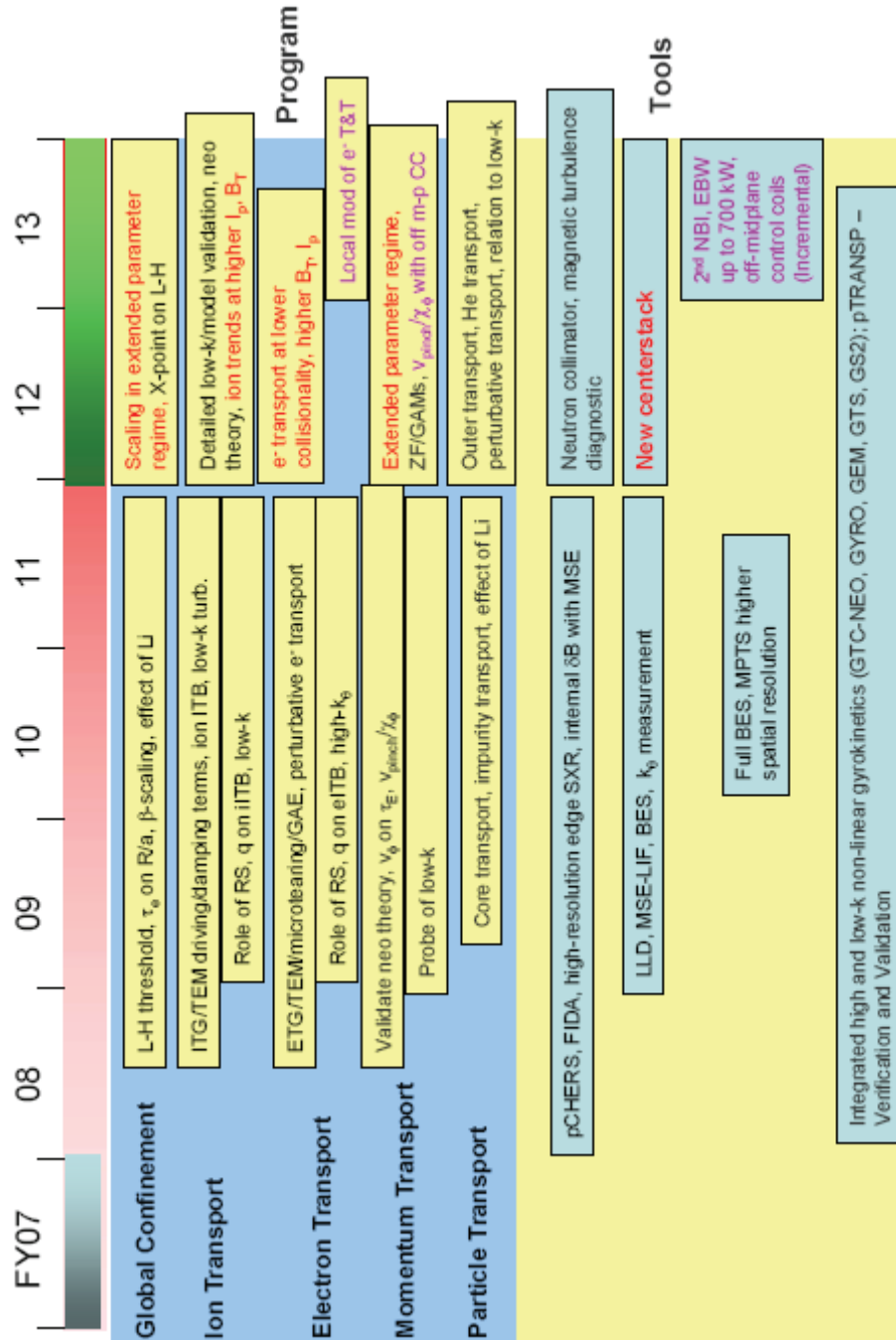
### 3.6 *Summary of Research Goals for FY2009-2013*

The major NSTX Transport and Turbulence research goals by topical area from section 3.2.3-4 are re-stated below to summarize the proposed research plan for the upcoming five-year period. The proposed research program time line is shown following these goals.

- To verify global scaling trends over an extended  $B_T$  and  $I_p$  range, and to establish the dependence of confinement on aspect ratio,
- To establish conditions for neoclassical ion transport through coupling low-k turbulence measurements to results of non-linear gyrokinetic simulations,
- To determine the role of both low-k and high-k turbulence through measurement and non-linear theory in setting the level of anomalous electron transport,
- To understand momentum transport and to determine the source of the plasma rotation/radial electric field and its influence on both low- and high-k turbulence,
- To understand the relation of particle and impurity transport throughout the plasma to measurements and simulations of microturbulence, ultimately to
- To participate in national and international efforts to develop a validated, fully-predictive tool for developing confinement-optimized discharge scenarios for both NSTX and future ST and non-ST devices.

The timeline for the research and tool development is shown on the next page.

# Transport and Turbulence Plans (2009-2013)



## References

- [1] Snipes, J. et al., 19<sup>th</sup> IAEA Fusion Energy Conference, Lyon, France, Oct. 2002, Paper CT/P-04
- [2] ITER Physics Basis, *Nuc. Fusion* **39** (1999) 2137.
- [3] Kaye, S.M. et al., *Phys. Rev. Lett.* **98** (2007) 175002.
- [4] Kaye, S.M. et al., *Nuc. Fusion* **47** (2007) 499.
- [5] Kaye, S.M. et al., *Nuc. Fusion* **46** (2006) 848.
- [6] McDonald, D.C. et al., *Plasma Phys. and Controlled Fusion* **46** (2004) A215.
- [7] Petty, C.C. et al., *Phys. Plasmas* **11** (2004) 2514.
- [8] Takizuka, T. et al., *Plasma Phys. and Controlled Fusion* **48** (2006) 799.
- [9] Vermare, L. et al., *Nuc. Fusion* **47** (2007) 490.
- [10] Wang, W. et al., *Comput. Phys. Commun.* **164** (2004) 178.
- [11] Stutman, D. et al., *Phys. Plasmas* **13** (2006) 092511.
- [12] Levinton, F.M. et al., *Phys. Plasmas* **14** (2007) 056119
- [13] Shaing, K.C. and M. Peng, *Phys. Plasmas* **11** (2004) 3726.
- [14] Horton, W. et al., *Nuc. Fusion* **45** (2005) 976.
- [15] Wong, K.L., et al., *Phys. Rev. Lett.* **99** (2007) 135003.
- [16] Jenko, F., W. Dorland and G. Hammett, *Phys. Plasmas* **8** (2001) 4096.
- [17] Scott, S.D. et al., *Phys. Rev. Lett.* **64** (1990) 531.
- [18] deGrassie, J. et al., *Nuclear Fusion* **43** (2003) 142.
- [19] Peeters, A.G. et al., *Phys. Rev. Lett.* **98** (2007) 265003.
- [20] Hahm, T.S. et al., *Phys. Plasmas* **14** (2007) 072302.
- [21] Zhu, W. et al., *Phys. Rev. Lett.* **96** (2006) 225002.
- [22] Shaing, K.C. et al., *Phys. Fluids* **29** (1986) 521.
- [23] Staebler, G., personal communication (2006).

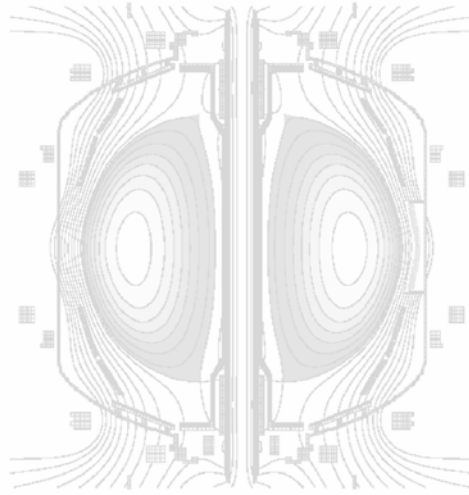
*This page intentionally left blank*

## Chapter 4 - Waves and Energetic Particles

4.1 Introduction.....	4.1
4.2 High Harmonic Fast Wave Physics.....	4.3
4.2.1 HHFW Research Goals.....	4.3
4.2.2 HHFW Physics.....	4.4
4.2.3 HHFW Heating System.....	4.8
4.2.4 Status of HHFW Research.....	4.10
4.2.5 HHFW Research Plan for 2009-2013.....	4.15
4.3 Electron Cyclotron and Bernstein Wave Physics.....	4.16
4.3.1 ECW/EBW Research Goals.....	4.16
4.3.2 EBW Physics.....	4.17
4.3.3 28GHz ECH/EBWH System.....	4.19
4.3.4 Status of EBW Research.....	4.19
4.3.5 ECW/EBW Research Plan for 2009-2013.....	4.24
4.4 Energetic Particle Physics.....	4.26
4.4.1 Energetic Particle Research Goals.....	4.26
4.4.2 Energetic Particle Physics.....	4.28
4.4.3 CAE Heating.....	4.30
4.4.4 Status of Energetic Particle Research.....	4.31
4.4.5 Energetic Particle Research Plan for 2009-2013.....	4.41
2009-2013 Timeline for HHFW/ECW/EBW Research.....	4.46
2009-2013 Timeline for Energetic Particle Research.....	4.47
References.....	4.48

*This page intentionally left blank*





## Chapter 4

# Waves and Energetic Particles

## 4.1 Introduction

Spherical torus (ST) discharges, such as those in NSTX, provide a unique opportunity for studying wave-particle interactions in plasma at high  $\beta$  and dielectric constant. In addition, fast ions produced during neutral beam injection in NSTX have velocities that exceed the Alfvén speed and can consequently resonate strongly with a wide variety of Alfvén waves. Controlling the distribution function of energetic ions through phase-space engineering is an important topic for spherical torus physics, as well as for ITER and tokamak research in general.

Scenarios that use high harmonic fast wave (HHFW), electron cyclotron wave (ECW) and electron Bernstein wave (EBW) heating and current drive are being developed and explored in NSTX to assist non-inductive plasma start-up, plasma current ramp-up and sustained plasma operation at high  $\beta$ , through the use of HHFW current drive to control  $q(0)$  and HHFW bulk heating. These scenarios will be discussed in detail in Chapter 6.

The 30 MHz HHFW heating and current drive system has been operational on NSTX since its inception. In recent years a deeper understanding of HHFW coupling physics has developed leading to significantly

improved coupling efficiency, with and without neutral beam heating, in L-mode plasmas. This improved coupling has resulted in the production of NSTX record core electron temperatures of over 5 keV with HHFW heating and the first direct measurement of on-axis HHFW current drive. These new results have led to several proposed improvements to the HHFW antenna that will support the 2009 - 2013 research program, and have important implications for future devices, including NHTX, the ST-CTF and ITER. Section 4.2 of this chapter discusses the status of HHFW research and plans for the NSTX HHFW program.

To date the ECW/EBW research program on NSTX has been focused on determining the EBW coupling efficiency for various plasma scenarios via the measurement of thermal EBW emission, and the theoretical modeling of EBW coupling, propagation, heating and current drive. With only baseline funding no EBW heating system is planned for NSTX during the time period covered by this five-year plan. However, a 28 GHz, 350 kW gyrotron is proposed for installation on NSTX in 2011 to support ECH-assisted plasma startup and, with additional incremental funding, installation of second 350 kW 28 GHz gyrotron is proposed in 2012. This 700 kW 28 GHz heating system, in combination with an EBW antenna, would allow the first high power EBW coupling and heating tests on NSTX. Section 4.3 presents the status of EBW research and plans for the NSTX ECW/EBW program.

Energetic particle research on NSTX has yielded important new results, including the discovery of CAE/GAE, Alfvén-acoustic modes, multi-mode transport and a new understanding of chirping modes. These experimental results have helped advance theoretical modeling and have significant implications for future burning plasma devices. Section 4.4 presents the status of energetic particle research and plans for the NSTX energetic particle program. One component of the energetic particle research plan is the study of wave-particle interactions through the use of active antenna excitation of various Alfvén eigenmodes observed in NSTX, which would lay the foundation for optimizing the performance of future fusion reactors, including the use of alpha channeling.

Plasma operation at toroidal magnetic fields up to 1 T, after installation of the new center-stack in 2011, will allow an assessment of HHFW physics in a regime where surface wave losses will be significantly reduced and at plasma parameters much closer to next-step STs. Operation at 1 T will also benefit the 28 GHz EBW research program by allowing fundamental resonance EBW heating, which has much better radial access than second harmonic heating. The higher field will also extend the range of  $V_{\text{fast}}/V_{\text{Alfvén}}$  and

$r^*$  for scaling studies of the \*AE activity, especially for the scaling of TAE avalanches closer to ITER parameters. The addition of the Liquid Lithium Divertor, in combination with the two existing LITER lithium injectors, will provide an important tool to enable improved HHFW and EBW coupling in H-mode plasmas.

## 4.2 High Harmonic Fast Wave Physics

### 4.2.1 HHFW Research Goals

The ultimate goals of the HHFW program on NSTX are to enable non-inductive plasma current ramp-up, and to provide  $q(0)$  control and bulk heating of H-mode plasmas to support very long pulse non-inductive plasma sustainment at high  $\beta$  [4.2.1]. Research to date has been directed toward understanding the HHFW coupling physics and improving the coupling efficiency for current drive phasing [4.2.2, 4.2.3] and, more recently, the exploration of HHFW current drive in L-mode plasmas [4.2.4]. Considerable improvement in coupling efficiency has been obtained in keeping with fast wave modeling by setting conditions to avoid fast wave propagation too close to the antenna/wall surfaces. It turns out that HHFW propagation is rather strongly directed close to the magnetic field direction, which favors propagation in the surface plasma and thus surface damping. Also, GENRAY [4.2.5] and AORSA [4.2.6] modeling show that the waves inside the plasma tend to be localized to the outer half of the plasma, potentially again favoring surface damping. This latter effect, which is particular to the HHFW regime, may also afford a means of localizing the HHFW power deposition off the axis of the plasma.

The HHFW research goals for 2009-10 will advance the physics basis established for L-mode plasmas to the plasma current ramp-up and H-mode regimes. These goals include:

1. Optimize heating and current drive in the H-mode and plasma ramp-up regime through the use of lithium injection and the Liquid Lithium Divertor to enhance HHFW coupling for plasma current ramp-up and discharge sustainment.
2. Increase the plasma-antenna gap to provide for less interaction of energetic neutral beam ions with the antenna and to permit optimization of the heating/current drive of H-mode plasmas by reducing edge density near the antenna to reduce edge power loss and avoiding arcing and edge MHD

3. Enhance coupled RF power by modifying the antenna to have two feedthroughs per strap and to have lower RF-induced electric fields
4. Include an ELM dump in the matching circuit to better couple to H-modes without arcing and use an electronic feedback system to avoid coupling power during ELMs

The HHFW research goals for 2011-13 support fully non-inductive plasmas with HHFW-assisted current ramp-up and very long pulse plasma operation with an upgraded antenna and HHFW controls that are integrated with the NSTX plasma control system (PCS). This research will benefit from improved coupling at the higher toroidal field that will be possible with the new center-stack in 2012-13. These goals include:

1. Optimizing HHFW heating and current drive in NBI deuterium H-mode conditioned with lithium.
2. Benchmarking current drive results against advanced RF codes.
3. Controlling  $q$  on-axis during very long pulse operation.
4. Combining HHFW coupling during current ramp-up with 28 GHz ECH-assisted CHI and PF-only plasma startup to provide fully non-inductive startup.

#### 4.2.2 HHFW Physics

HHFW coupling, propagation and damping physics are important areas of research on NSTX. Each must be understood to properly predict core vs. surface heating as well as the radial profile of the heating and current drive. Extensive theoretical and modeling studies have been and are being carried out to address these three critical areas for NSTX as well as for tokamaks generally. These studies, which are supported by the NSTX Project and by other DOE grants to the PSFC-MIT, CompX Corporation, and the RF SciDAC project, include the following efforts:

1) Analysis of the global 3D structure of the HHFW electric fields, energy flow, and power deposition is under way using both ray tracing [GENRAY] and full wave codes [AORSA, METS, and TORIC]. At the present time, these codes include both linear collisionless and collisional damping mechanisms. However, since experimental results indicate that significant damping may occur in the edge regions due to surface wave propagation, generalized boundary conditions that can treat edge dissipation due to the

formation of RF sheaths near the vacuum vessel wall and launcher are now being developed by the RF SciDAC group for inclusion in the full wave modeling codes.

2) Self-consistent simulations of the HHFW interactions with energetic ions are needed to accurately determine the power deposition and current drive that can be achieved in discharges with co-resonant neutral beam injection (NBI). Experimental observations indicate that the fast ions can interact strongly with HHFW, leading to significant modifications of the fast ion velocity distributions as well as the partitioning of the wave power among the various plasma species. To properly include the effects of these interactions, the wave propagation codes must be coupled with a Fokker-Planck treatment of the ion and electron distribution functions in ST geometry that includes effects of quasilinear diffusion at high cyclotron harmonics, collisions, trapped particle effects, and particle losses. Previously, the main focus of these studies was the GENRAY / CQL3D package, which was used to model the early combined HHFW and NBI experiments on NSTX [4.2.7]. More recently, the 1D and 2D full wave codes have all been generalized to include non-Maxwellian particle distributions in the plasma dielectric response modules. The CQL3D code has been integrated with the AORSA code, and work is currently underway to integrate it with the TORIC code. Since the power deposition and driven current profiles can change significantly as the resonant ion distributions evolve in time, the TORIC code has been integrated into the TRANSP analysis package, and work is currently underway to include CQL3D as well. Work is also underway in the RF SciDAC project to address the effects of finite drift orbit width on power deposition, an effect that may be important in both ST's as well as conventional tokamaks in which RF power damps on energetic ions.

3) In general, wave propagation and deposition codes have simplified models for the wave launcher: the codes assume that the amount of power that is coupled into the plasma is known. However, as the recent experiments on NSTX and previous results from other devices have shown, the core heating efficiency is strongly dependent on the launched wave spectrum as well as the other discharge characteristics. An analysis of the power coupled into the plasma that self-consistently includes the effect of the core absorption and wave propagation dynamics, rather than assuming a radiation boundary condition, is needed to understand the experimental observations on NSTX as well as on other tokamaks, including ITER. As a first step towards the development of this modeling capability, collaborators from the PSFC-

MIT and the RF SciDAC group have been developing an interface between the TOPICA 3D antenna module and the TORIC full wave code. This package, when complete, will be used to analyze the heating profiles in NSTX for various strap phasings on the NSTX launcher. Results from these studies should indicate regimes of operation in which the driven currents can be optimized for plasma start-up, ramp-up, or high performance sustainment phase.

4) The theoretical analysis tools for quantitative, or even semi-quantitative analysis of the parametric decay instability (PDI) phenomenon are not presently available. The AORSA1D all-orders full wave code

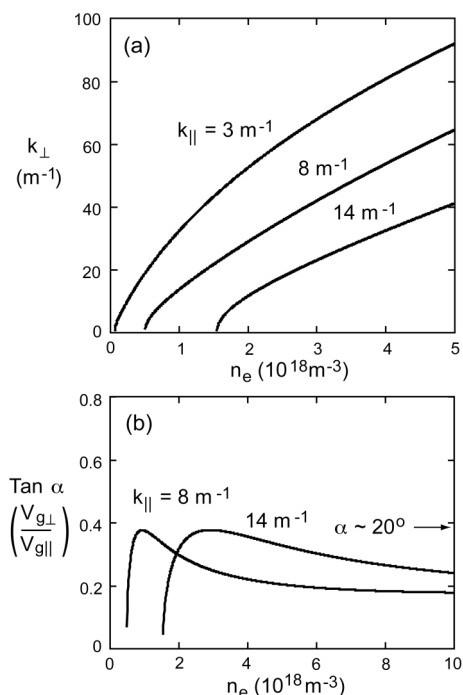


Figure 4.2.1: High harmonic fast wave propagation characteristics for total magnetic field  $B = 2.82 \text{ kG}$  at the antenna location on NSTX [toroidal field  $B_{\phi}(R_o) = 4.5 \text{ kG}$ , plasma current  $I_P = 0.6 \text{ MA}$ ]. (a) Perpendicular wavenumber  $k_{\perp}$  versus density for parallel wavenumbers  $k_{\parallel} = 3 \text{ m}^{-1}$ ,  $8 \text{ m}^{-1}$  and  $14 \text{ m}^{-1}$ . (b) The tangent of the propagation angle  $\alpha$  relative to the direction of  $B$  versus density. The onset density is  $\propto B * k_{\parallel}^2 / \omega$  and  $\alpha < 20^\circ$ .

is being modified to include resonant three-wave interactions. Because AORSA employs a spectral basis set, in essence a complete set of pseudo modes, this modification to account for so-called “extended pump” interactions should be straight forward to implement on a 1D model. This analysis should provide an understanding of PDI interactions on NSTX for HHFW, an ability to evaluate planned HHFW experiments for susceptibility to parasitic PDI losses, and approaches to minimizing these losses and optimizing the current drive efficiency.

The HHFW research to date on NSTX has been focused on how to optimize coupling of the HHFW power to the core plasma. It became clear in 2005 that heating for current drive phasing of the antenna ( $-90^\circ$  between adjacent antenna element currents) was about

$\frac{1}{2}$  as efficient as for heating phasing ( $180^\circ$ ) [4.2.8]. The plasma dispersion relation pointed to the onset of perpendicular propagation of the fast waves close to the antenna/wall surface as being a possible

contributor to the enhanced surface loss at the lower phasing values (longer wavelength) as shown in Fig. 4.2.1(a). Indeed, increasing the magnetic field and lowering the edge density in 2006 resulted in a heating efficiency at  $-90^\circ$  being equal to that at  $180^\circ$  [4.2.3]. Also, above onset the direction of the ray path in the HHFW regime is about  $20^\circ$  to the direction of the magnetic field, as opposed to the low harmonic case for which the angle increases with density into the plasma as shown in Fig. 4.2.1(b). This results in surface fast waves, especially for higher  $m$  modes, and for those waves entering the core of the plasma tends to keep the waves confined to the outer region of the plasma in major radius due to the up-shift in  $k_{\parallel}$  along the ray path. GENRAY analysis shows this effect for a single ray in Fig. 4.2.2 [4.2.9] and 3D AORSA modeling demonstrates this effect in the volume of the plasma in Fig. 4.2.3 [4.2.10].

The focus of the HHFW theory and modeling efforts during the five-year plan period will expand to

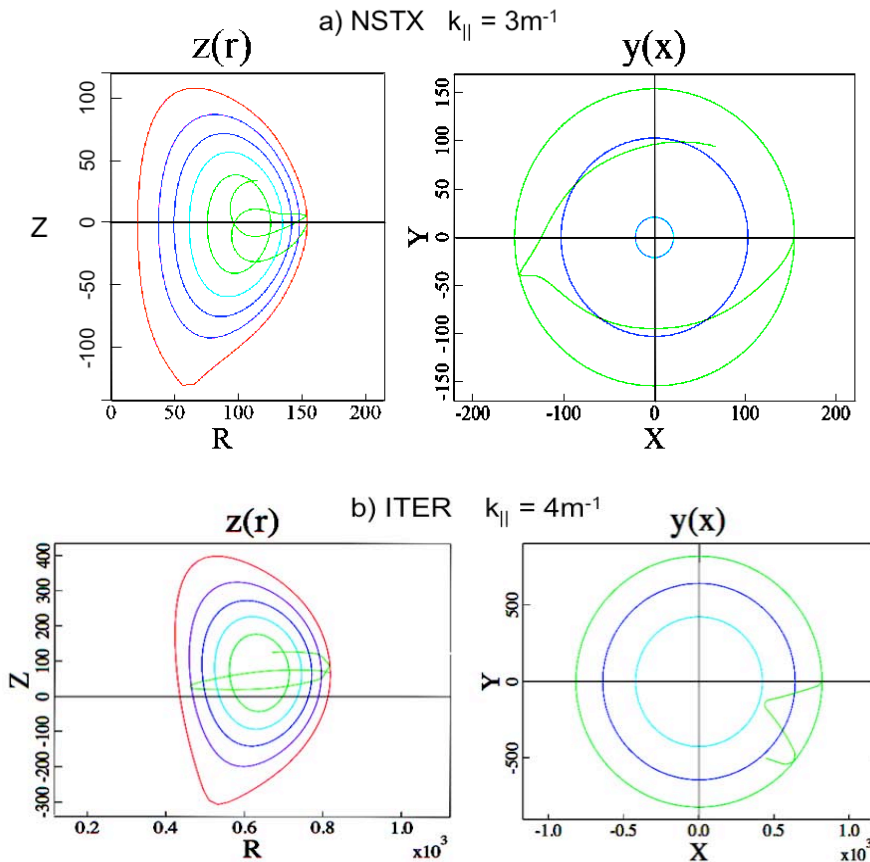


Figure 4.2.2: a) GENRAY modeling of ray path for NSTX conditions with  $k_{\parallel} = 3m^{-1}$ . Note that the ray does not go through the plasma core. b) Similar modeling for ITER conditions with  $k_{\parallel} = 4m^{-1}$ . Note that the ray propagates more radially and goes through the plasma core.

include other areas of importance including:

1. Mapping out propagation characteristics for L-Mode and H-mode plasmas:
  - Density versus magnetic field along the ray path can affect the path and hence the location of power deposition.
2. Understanding the fast wave damping mechanisms:
  - Core: Landau/Transit time magnetic pumping and short wavelength mode conversion effects.
  - Edge: Surface wave damping via collisions, sheaths, wall/antenna currents, and PDI heating.
3. Predicting conditions required to optimize plasma heating and current drive (CD):
  - Co vs counter CD
  - Can HHFW CD be used to help stabilize core MHD, e.g., by increasing reverse shear in the core with counter CD?

### 4.2.3 HHFW Heating System

The present HHFW system on NSTX [4.2.11] has 12 adjacent antenna straps which cover  $\sim 90^\circ$  of the torus toroidally as shown in

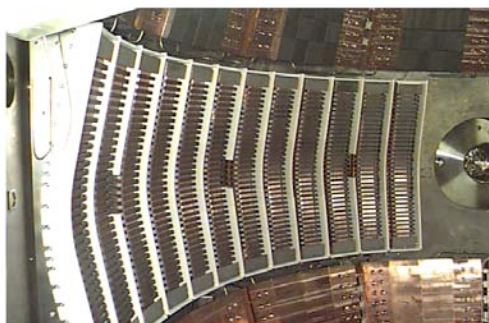


Figure 4.2.4: NSTX HHFW antenna

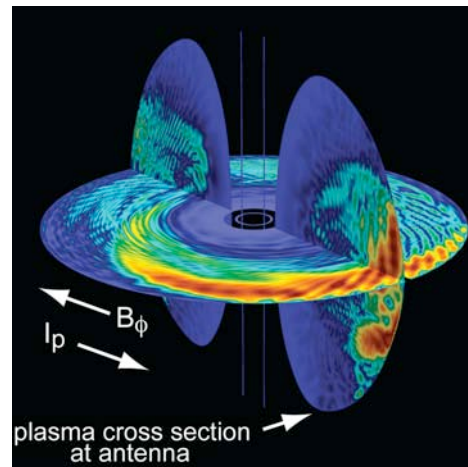


Figure 4.2.3: 3-D AORSA modeling shows propagation to be near the wall and primarily outside the major radius on NSTX ( $-90^\circ$  case, summed over 81 toroidal modes). The antenna is located on the right hand side of the figure.

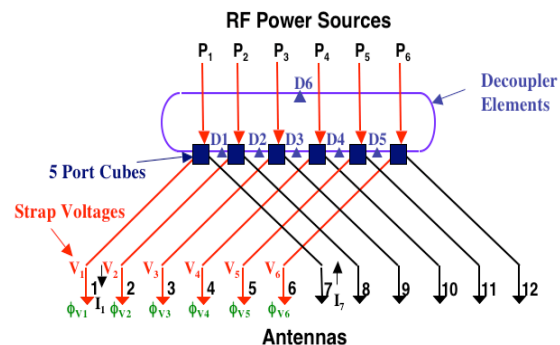


Figure 4.2.5: HHFW Antenna feed system



Fig. 4.2.4. Pairs of the straps are powered with six sources via a transmission/impedance matching system comprised of 6 long transmission lines, 6 phase shifters, 6 stubs, and 6 decoupling loops (Fig. 4.2.5). The system uses digital control of power and phase, and automated matching calculations to facilitate rapid changes in matching for desired phases. To meet the need for more HHFW power with a larger antenna-plasma gap to help avoid bombardment of the antenna, especially for H-mode operation at full beam power, a series of HHFW system upgrades are planned:

2008-09:

A major upgrade of the antenna will consist of providing two feedthroughs per antenna strap, as shown in Fig. 4.2.6. This should permit a threefold increase in power capability for the present antenna at the same RF voltage.

2010:

The HHFW antenna will be upgraded for resilience to ELMs during H-mode with the addition of an ELM dump.

2011-13:

Further improvements to voltage standoff (to minimize the RF-induced electric field) will be made.

Diagnosics planned for HHFW Research:

In addition to the diagnostics needed to operate and protect the HHFW antenna array (such as acoustic arc detectors in the pressurized transmission lines), information on the RF interaction with both the edge and the core plasma is needed to improve the HHFW performance and reliability. To make progress in modeling development, the codes need both accurate input parameters for their analyses and detailed measurements for output validation.

A wide array of edge diagnostics is presently employed in the study of power coupling/propagation and more will be deployed in the future. A fast ion gauge located behind the array is used to monitor the local neutral pressure. It is observed that the pressure increases with both RF power and with decreasing wavelength; this high neutral pressure can lead to increased collisional damping and breakdown in the

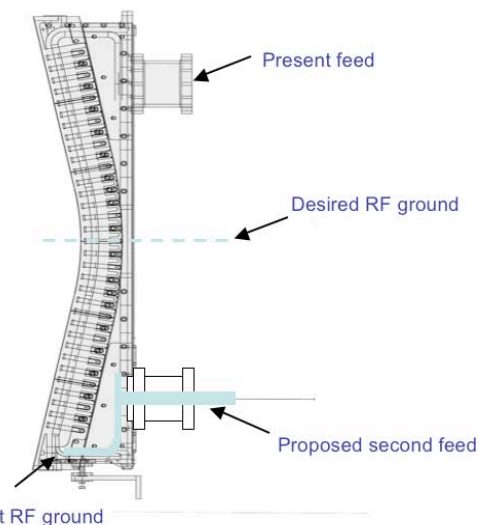


Figure 4.2.6: Planned HHFW antenna upgrade to two feedthroughs per strap

antenna. The heating of edge ions is measured with the Edge Rotation Diagnostic, which shows increased heating of edge ions as the wavelength is increased. Langmuir probes positioned between antenna boxes, in the shadow of the local limiter, have seen increases in the local plasma potential with decreasing wavelength. The characteristic spectrum of PDI, postulated as the mechanism for edge ion heating, is observed with both a Langmuir probe and a microwave reflectometer. B-dot probes that measure the RF fields near the wall have seen increased signal strength when plasma conditions and antenna phasing are expected to support surface wave propagation. A visible light camera looking at the Faraday shield has been able to identify hot spot formation as a precursor to some antenna arcs.

Light pipes will be added to the antenna enclosures during the opportunity presented by the HHFW antenna upgrade in 2008-9, giving the ability to look at impurity spectra and to identify internal arc locations. Additional B-dot probes will be added to study and to minimize the power loss associated with surface waves. The RF wave monitoring electronics in the edge density reflectometer will be upgraded for improved operation over a 2-50 MHz range, permitting observation of both the PDI daughter wave spectra (low frequency quasi-modes and higher frequency IBW modes). A dedicated IR camera could be used to study the plasma interaction with the front surface of the antenna.

HHFW power propagation and deposition in the core is inferred from traditional diagnostics such as Thomson scattering, soft x-ray arrays, and CHERS. Progress has been made in reducing the NBI perturbation on the plasma during RF operation, permitting MSE measurements to be made for HHFW current drive. More information is needed on the wave activity in the plasma core with regard to propagation and mode conversion. Direct observation of the RF wave structure in the core may be possible once the NSTX high-k scattering system is upgraded to detect 30 MHz frequencies in 2009. This capability is needed to make detailed comparisons to RF code predictions.

#### *4.2.4 Status of HHFW Research*

Significant progress in HHFW research has been made during the period covered by the previous five-year plan. In particular, efficient HHFW heating of L-mode plasmas was demonstrated in 2006-7 for heating and current drive antenna phasings, and demonstrated in 2007-8 in the presence of neutral beam heating. Also in 2007, analysis of MSE measurements of current drive has provided a quantitative

comparison to theoretical predictions of the current drive at RF power levels of  $\sim 2$  MW in L-mode plasmas. Optimization of heating and current drive at higher power should make very clear the appropriate conditions for applying HHFW to heat and drive current on NSTX and for applying HHFW to future ST devices.

HHFW Coupling Physics:

It has been demonstrated that keeping the edge density near the antenna low relative to the onset density

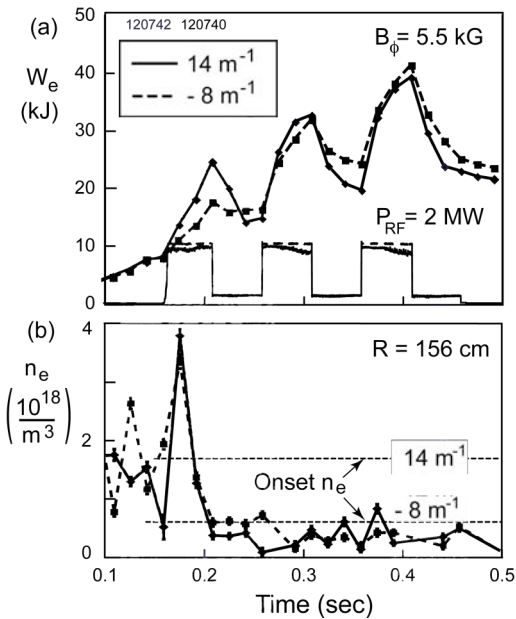


Figure 4.2.7: (a) Time dependence of electron stored energy ( $W_e$ ) with maximum modulated RF power of 2 MW, one with  $k_{||} = 14 \text{ m}^{-1}$  (solid curve) and the other with  $k_{||} = -8 \text{ m}^{-1}$  (dashed curve). (b) Edge electron density (2 cm in front of Faraday shield) versus time. The onset density for  $k_{||} = 14 \text{ m}^{-1}$  and  $k_{||} = -8 \text{ m}^{-1}$  perpendicular propagation indicated by horizontal dashed lines.

for perpendicular propagation ( $\propto B \times k_{||}^2 / \omega$ ) results in a substantial increase in coupling efficiency for current drive phasing  $k_{||} \approx -8 \text{ m}^{-1}$  ( $-90^\circ$ ) [4.2.3, 4.2.4]. This is demonstrated in Fig. 4.2.7 where it is shown that the efficiency at  $k_{||} \approx -8 \text{ m}^{-1}$  is equal to that for  $k_{||} \approx 14 \text{ m}^{-1}$  ( $180^\circ$ ) for the last two RF power pulses, when the density is at or below the onset

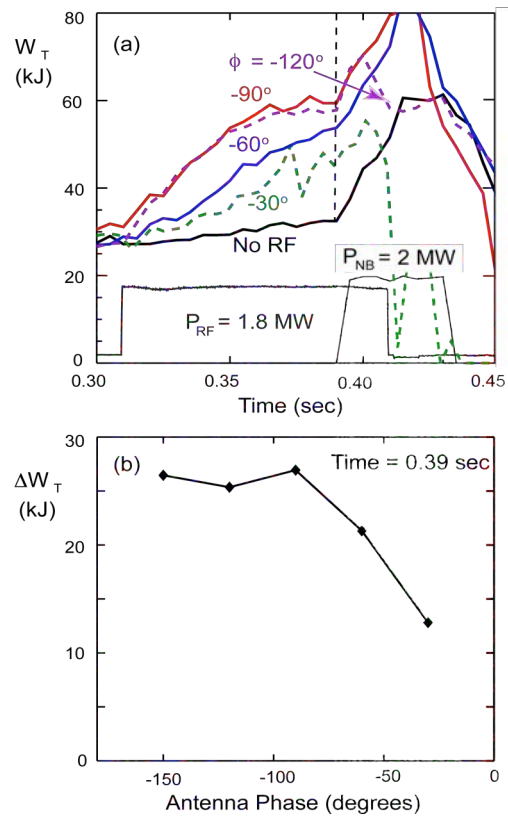


Figure 4.2.8: (a) Time dependence of total stored energy ( $W_T$ )  $P_{RF} = 1.8 \text{ MW}$  versus phase  $\phi$  between antenna straps (b) Change in total stored energy ( $\Delta W_T$ ) at time = 0.39 s showing the falloff of heating at longer wavelengths,  $|\phi| < 90^\circ$ . ( $B_{\phi} = 5.5 \text{ kG}$ ,  $I_p = 0.6 \text{ MA}$ ,

density 2 cm in front of the antenna. However, the efficiency for  $k_{\parallel} \approx -8 \text{ m}^{-1}$  during the first RF power pulse is half the  $k_{\parallel} \approx 14 \text{ m}^{-1}$  value where the density is  $\sim 3 \times$  the onset value for  $k_{\parallel} \approx -8 \text{ m}^{-1}$ .

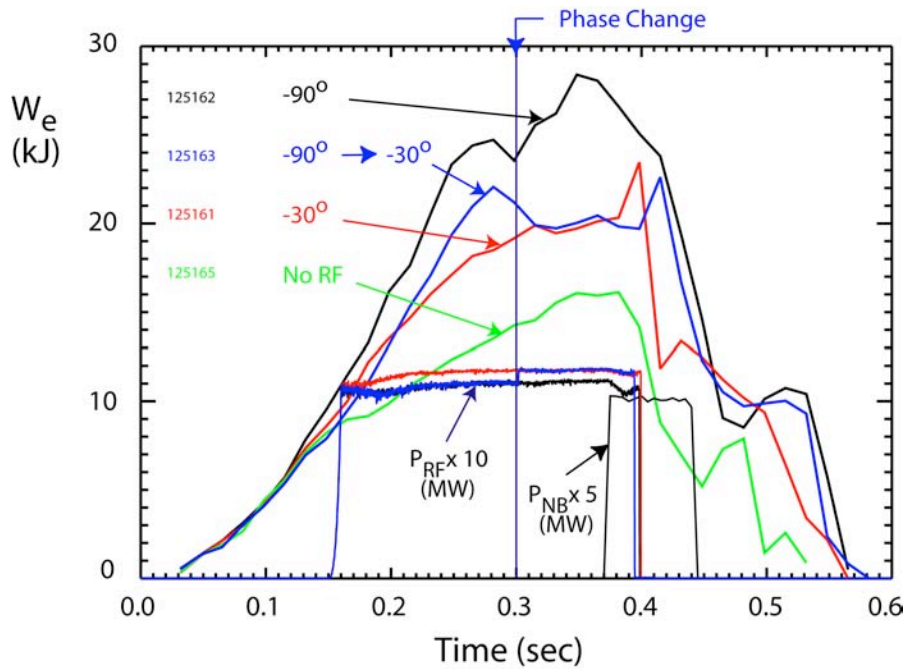


Figure 4.2.9: HHFW Heating at  $-30^\circ$  is  $\sim 1/2$  that at  $-90^\circ$

The fact that the placement of the perpendicular propagation onset is an important condition for determining surface wave losses is further illustrated in Fig. 4.2.8, where it is shown that at even longer wavelengths (lower  $k_{\parallel}$  or phase) the stored energy falls off with phase. Note that the onset density is proportional to  $k_{\parallel}^2$  and is pushed against the antenna/wall at the lower phases. Also, whereas the wavelength plays a dominant role in RF surface losses, the data of Fig. 4.2.8 suggests that the cancellation of reactive currents from near strap currents is not as important.

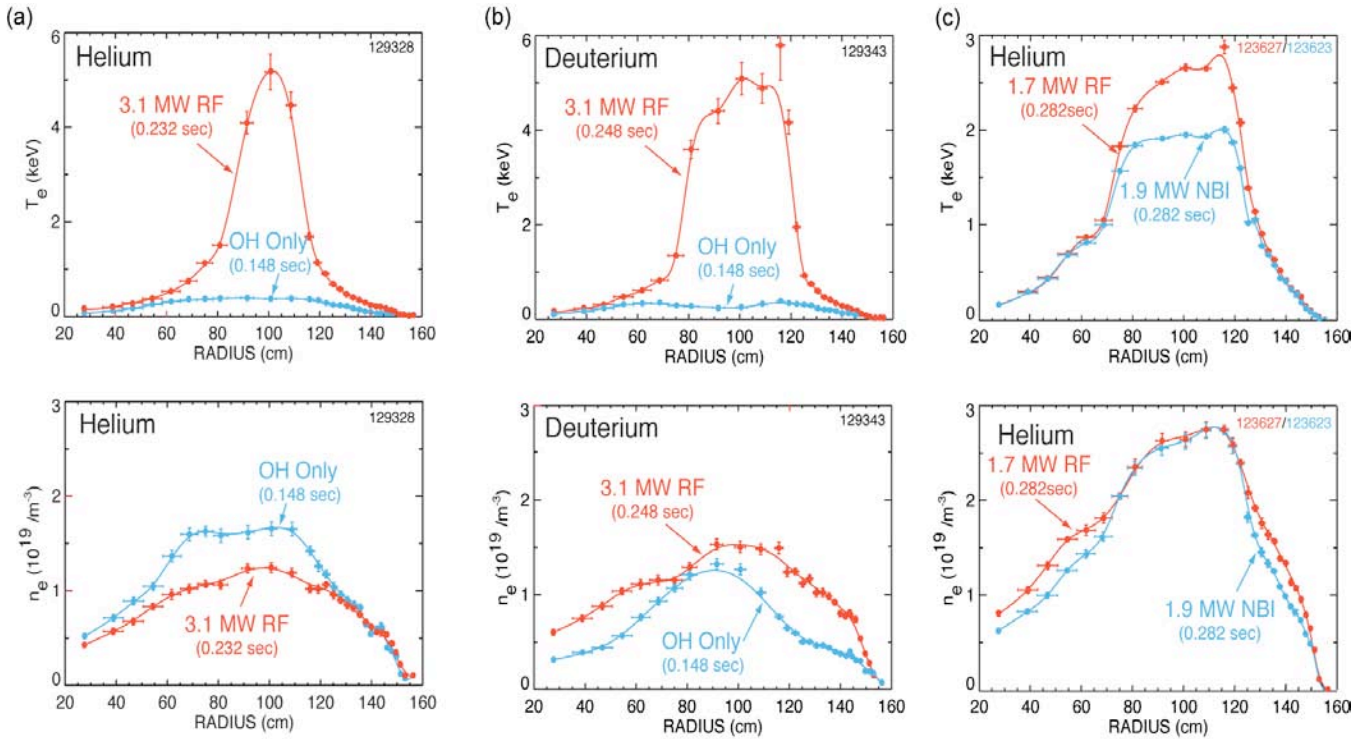


Figure 4.2.10:  $T_e$  and  $n_e$  profiles for high  $T_e(0)$  plasma heated with 3.1 MW of HHFW power coupled into (a) helium and (b) deuterium discharges with  $B_t(0) = 0.55$  T. c) Significant electron heating observed in the core of  $B_t(0) = 0.55$  T helium discharge when 1.7 MW of HHFW power is added to 1.9 MW of NBI power.

To further demonstrate the surface losses associated with having the onset density above the edge density at the antenna/wall, the core heating has been measured for a relatively long RF pulse during which the phase was changed from  $-90^\circ$  to  $-30^\circ$ . The results are compared to cases without the phase change and to the no RF case in Fig. 4.2.9. Again, this data shows that the wavelength plays a dominant role in RF surface losses and that these losses do not appear to be dependant on core damping (the increase in central temperature during the  $-90^\circ$  period did not result in better heating during the  $-30^\circ$  period).

Significant HHFW electron heating has been obtained with current drive phasing for L-mode helium and deuterium discharges with HHFW alone (Fig 4.2.10(a) and (b)) and in conjunction with neutral beam heating (Fig 4.2.10(c)). Promising results have also been obtained for HHFW coupling into low plasma current ( $I_p < 250$  kA) H-mode plasmas where bootstrap current fractions up to 85% have been generated

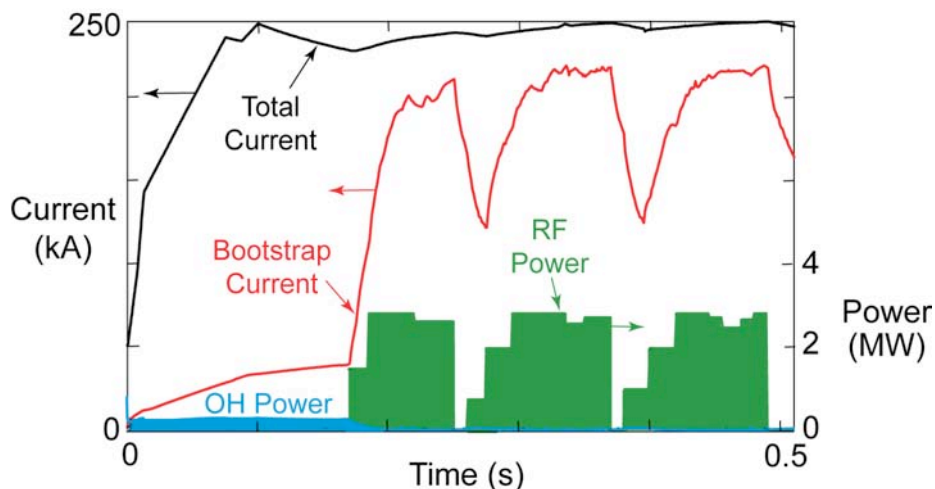


Figure 4.2.11: HHFW heating in low plasma current H-mode plasma generates 85% bootstrap fraction.

(Fig. 4.2.11). This result supports the use of HHFW for plasma current overdrive using bootstrap and HHFW current drive as a tool for ramping plasma current to  $I_p \sim 500$  kA, a level sufficient for effective NBI heating.

Initial motional Stark effect (MSE) measurements of the current profile in helium L-mode discharges (Fig. 4.2.12) show clear evidence of core HHFW current drive with  $-90^\circ$  phasing. The MSE RF-driven current profile measurements are consistent

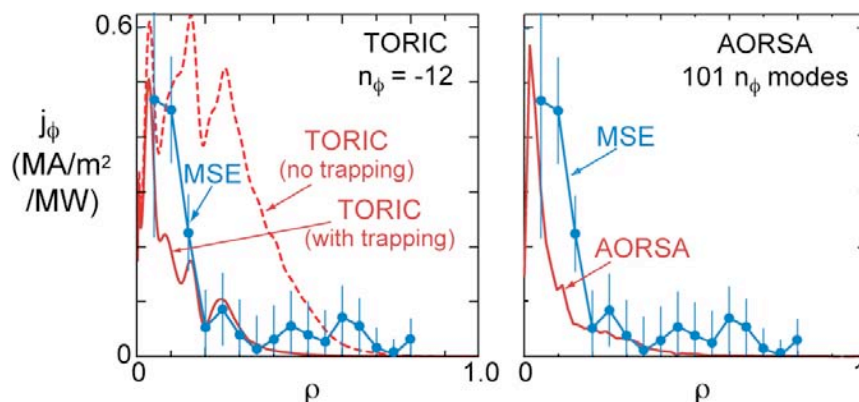


Figure 4.2.12: Measurement and simulations of rf-driven CD for  $-90^\circ$  phasing

with predictions from AORSA and TORIC full wave simulations, although the predicted profiles are narrower, perhaps because the simulations do not include radial transport.

#### *4.2.5 HHFW Research Plan for 2009-2013*

The HHFW research in 2009-10 will be directed toward extending the coupling and current drive studies to deuterium H-mode conditions. These experiments will be enabled by improvements in the HHFW antenna, including the double feed upgrade in 2008-9 and the ELM resilience system in 2009-10. In addition there will be some experiments in 2009-10 to couple HHFW into low temperature, low plasma current discharges to support the development of HHFW-assisted plasma ramp-up scenarios.

##### 2009-10:

- Optimize heating and current drive operation with NBI for L-mode and H-mode with the upgraded antenna and using guidance of modeling.
- Use larger plasma-antenna gap permitting greater stability and at higher power (more voltage standoff and greater power for same voltage). Also, faster feedback control of the plasma position would help to reduce the beam interaction with the antenna. An even larger gap will probably be required for operation with all three high-power NBI sources in the H-mode regime.
- HHFW-assisted startup/ramp-up plasmas using low  $T_e$ ,  $I_p$  ohmic plasmas

##### 2011:

- Optimize heating and current drive operation with NBI deuterium H-mode with fully upgraded HHFW antenna and lithium conditioning.
- Benchmark core current drive against advanced RF codes.
- Optimize HHFW-assisted ramp-up plasmas using low  $T_e$ ,  $I_p$  ohmic plasmas.
- Combine HHFW coupling into plasma ramp-up and 28 GHz ECH-assisted non-inductive startup.

##### 2012-13:

- Support very long pulse plasma scenario; integrate HHFW controls into NSTX PCS, control  $q$  on-axis and develop very long pulse, high power operation at toroidal fields up to 1 T.
- Support fully non-inductive startup and ramp-up, combining 28 GHz ECH-assisted CHI or PF-only startup and HHFW-assisted ramp-up.

## 4.3 Electron Cyclotron and Bernstein Wave Physics

### 4.3.1 ECW/EBW Research Goals

Off-axis radiofrequency-driven current is expected to be critical for stabilizing solenoid-free ST plasmas when  $\beta > 20\%$  [4.3.1]. For example, modeling predicts that adding 1 MA of off-axis EBW current drive (EBWCD) to the ST-CTF [4.3.2] would significantly improve the performance of the plasma (Fig. 4.3.1). The long-term research goal for the EBW research program on NSTX is to assess the viability of EBWCD as a tool for generating this critical stabilizing current. There are several intermediate research goals for the 2009-2013 research program that support solenoid-free ST research, they are:

1. Continue to optimize EBW coupling in H-mode through the use of EBW emission radiometry and a combination of lithium injection and the Liquid Lithium Divertor (2009-10)
2. Develop ECH-assisted plasma startup with 350 kW of 28 GHz power in order to increase  $T_e$  sufficiently for effective HHFW coupling (2011).
3. With additional incremental funding, study EBW coupling with up to 700 kW of 28 GHz power (2012-13).

If an EBW heating system is not installed on NSTX it may be possible to continue this research through collaboration on MAST where a 350 kW 28 GHz gyrotron is being installed this year in collaboration with Oak Ridge National Laboratory.

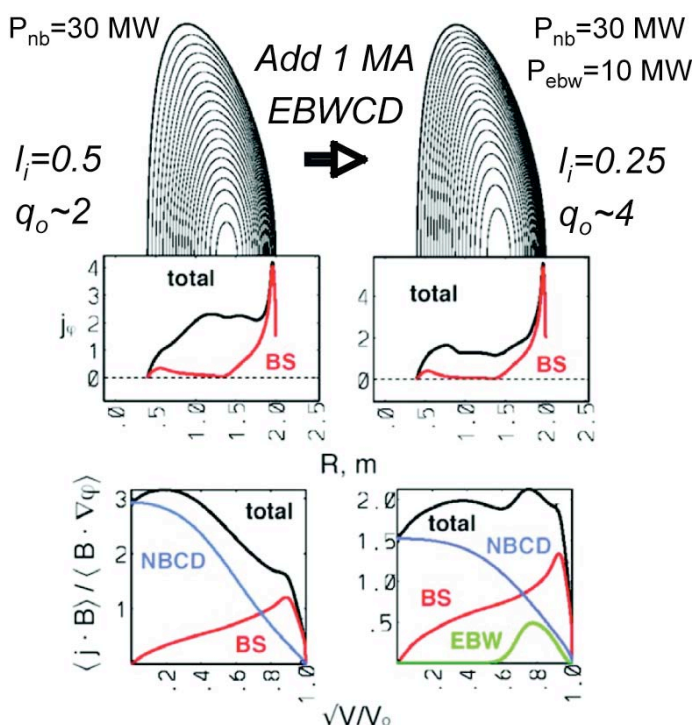


Figure 4.2.1: Adding 1 MA of off-axis EBWCD to CTF plasma generating wall loading of  $1 \text{ MW/m}^2$  can decrease  $l_i$  from 0.5 to 0.25 & increase  $q_o$  from  $\sim 2$  to  $\sim 4$ . As a result, the  $\beta_n$  limit increases from 4.1 to 6.1 and the  $\beta_t$  limit increases from 19% to 45%.



### 4.3.2 EBW Physics

When  $\omega_{pe} > 1.6 \omega_{ce}$ , where  $\omega_{pe}$  is the electron plasma frequency and  $\omega_{ce}$  is the electron cyclotron frequency, the electrostatic EBW [4.3.3] can propagate across the magnetic field. This regime is normally referred to as the overdense regime, and it is a regime that is not accessible to conventional ECH or ECCD. Except during plasma start-up and the initial stages of plasma current ramp-up, NSTX discharges operate well inside this overdense regime. EBWs are strongly absorbed at electron cyclotron resonances and have the potential to provide local electron heating (EBWH) and EBWCD. However, EBWs can only propagate inside the upper hybrid resonance (UHR) that surrounds overdense plasma, so EBWH and EBWCD systems that have microwave launchers external to the plasma, must employ a mode conversion

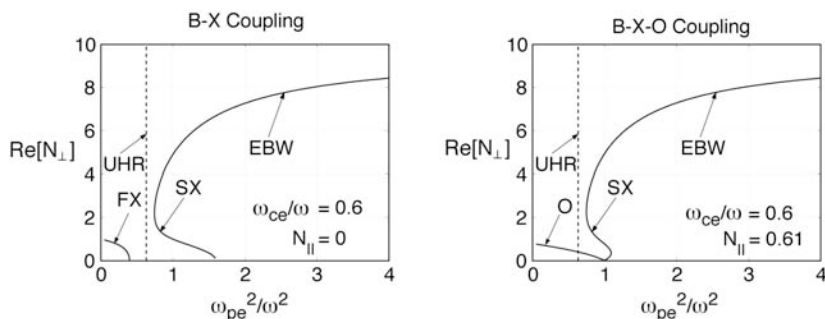


Figure 4.2.2: EBW and electron cyclotron wave roots of the real part of  $N_{\perp}$  as a function  $\omega_{pe}^2/\omega^2$  for two EBW coupling schemes have been studied on NSTX and other machines: (a) perpendicular ( $N_{\parallel} = 0$ ) X-B coupling where the fast X-mode (FX) tunnels to the slow X-mode (SX) and (b) oblique O-X-B coupling, where  $N_{\parallel} = N_{\parallel,opt} = 0.61$ .

process in the vicinity of the UHR to couple the microwave power to the EBWs. Electromagnetic radiation can couple to EBWs either by tunneling from the extraordinary mode to the EBW (X-B conversion) [4.3.4] or by mode conversion from the ordinary mode, via the slow

extraordinary mode, to the EBW (O-X-B conversion) [4.3.5]. For X-B conversion X-mode polarized microwave power is launched normal to the magnetic field (Fig. 4.3.2(a)). The left hand cutoff of the slow X-mode (SX), the UHR, and the right hand cutoff of the fast X-mode (FX) form a cutoff-resonance-cutoff triplet allowing the fast X-mode electromagnetic wave to tunnel through the UHR to the slow X-mode [4.3.4]. For O-X-B conversion (Fig. 4.3.2(b)) elliptically polarized microwave power is launched at an oblique angle to the magnetic field that is chosen to make the X-mode and O-mode cutoffs coincident [4.3.6, 4.3.7].

EBWs can exhibit large changes in refractive index after being launched. The change in the parallel

refractive index,  $N_{//}$ , is given by:

$$N_{//} \propto -\frac{1}{(k_{\perp} \rho_e)^2} \left| \frac{B_{\theta}}{B} \right| n_{\perp} \sin \theta \left( \frac{\Delta r}{R} \right),$$

where  $ck_{\perp}/\omega = N_{\perp}$ ,  $c$  is the speed of light,  $\omega$  is the wave angular frequency,  $\rho_e$  is the electron Larmor radius,  $B_{\theta}$  is the poloidal component of the magnetic field,  $|B|$  is the magnitude of the total magnetic field,  $\theta$  is the poloidal angle measured from the outboard side of the plasma midplane,  $\Delta r$  is the radial distance of propagation of the ray, and  $R$  is the major radius. For  $\theta \sim 0$  the shift in  $N_{//}$  is minimal. However, for EBWs launched above or below the plasma midplane the change in  $N_{//}$  can be large, since in the outboard edge region of the ST plasma the poloidal and toroidal magnetic field strengths are comparable. EBWs heat electrons and drive current at the Doppler shifted cyclotron resonance, given by:

$$\gamma \omega = k_{//} \frac{p_{//}}{m_e} + n \omega_{ce},$$

where  $\gamma$  is the Lorentz relativistic factor,  $p_{//}$  is the parallel momentum,  $m_e$  is the electron rest mass, and  $n$  is the harmonic number of the electron cyclotron resonance. So the location where electron heating and current drive occurs depends sensitively on  $N_{//}(=ck_{//}/\omega)$ , and therefore on where the EBW coupling occurs relative to the plasma midplane. Also, the direction of the driven current depends on whether the EBWs are launched above or below the midplane [4.3.8]. Current drive occurs via two mechanisms; *Fisch-Boozer* current drive [4.3.9], where EBWs predominantly heat electrons with one sign of  $v_{//}$ , creating an asymmetric resistivity, and *Ohkawa* current drive [4.3.10], where EBWs increase the  $v_{\perp}$  of passing electrons in one direction so that they become trapped, resulting in a net current being driven in the opposite direction. Normally in an ST both these current drive mechanisms are present, driving current in opposite directions. Fisch-Boozer current drive dominates near the magnetic axis and Ohkawa current drive dominates off-axis on the low field side, where there is a large trapped electron population in an ST.

### 4.3.3 28GHz ECH/EBWH System

A 28 GHz ECH system will be installed on NSTX in 2011 [Fig. 4.3.3]. This system will use a gyrotron with an output power of up to 350 kW. For the 2011 campaign, this system would employ a fixed horn antenna on the plasma midplane to launch X-mode microwave power to support second harmonic ECH-assisted plasma startup experiments at  $B_t(0) = 0.5$  T and fundamental O-mode ECH at  $B_t(0) = 1$  T. Unless

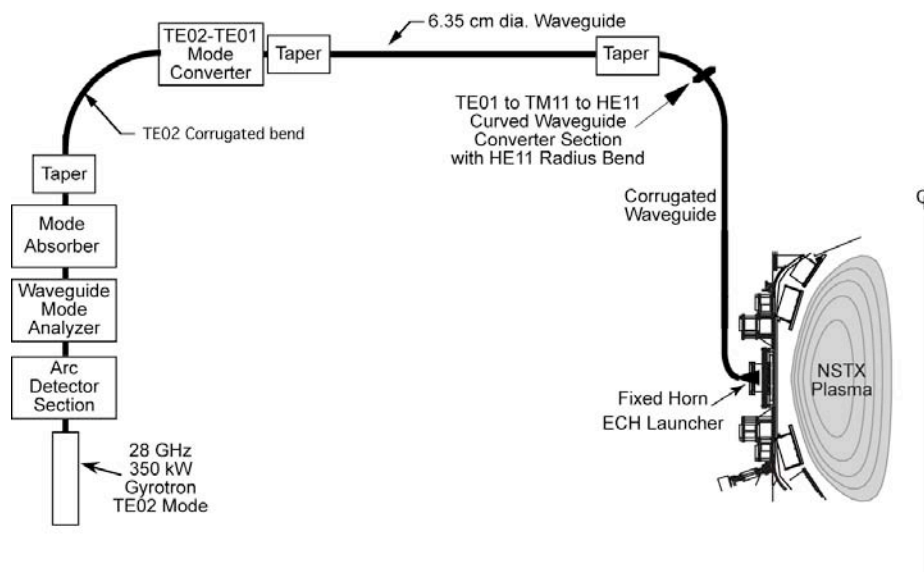


Figure 4.2.3: 350 kW, 28 GHz, 500 ms heating system proposed for installation on NSTX in 2011. With additional incremental funding the system would be upgraded to 700 kW in 2012.

incremental With incremental funding a second 350 kW 28 GHz gyrotron is proposed for 2012, increasing the total available RF power to 700 kW. With the installation of the new center-stack on NSTX in 2012 operation at 1 T will allow fundamental frequency 28 GHz EBWH which has significantly better radial access than second harmonic EBWH. MAST is planning to install a 350 kW 28 GHz ECH/EBWH system by the end of 2008, so if the proposed 28 GHz NSTX EBW heating system is not installed by 2012 it may be possible to conduct some of the proposed 28 GHz EBW research on MAST by upgrading their system.

### 4.3.4 Status of EBW Research

This section summarizes significant advances in EBW research on NSTX and other devices since the last NSTX 5-year research plan in 2003. High levels of EBW coupling efficiency have been measured via

thermal EBW emission from the magnetic axis of NSTX and Fokker-Planck modeling of NSTX discharges has predicted that efficient off-axis Ohkawa current drive is achievable in  $\beta > 20\%$  plasmas.

There have also been recent encouraging experimental results on MAST and TCV that show clear indications of O-X-B EBW heating, and recently efficient EBW heating of PF-only startup discharges in MAST has been measured at 28 GHz.

Status of NSTX Experimental EBW Research:

Except for power dependent effects like PDI, the O-X-B mode conversion process involved in coupling

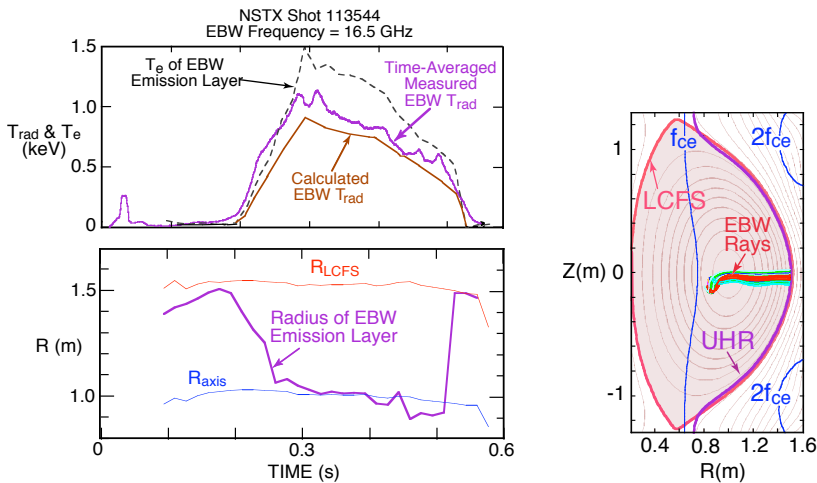


Figure 4.3.4: 80%  $f_{ce}$  B-X-O coupling measured in NSTX L-mode edge plasmas, consistent with modeling

microwaves to EBWs for EBWH and EBWCD is the reciprocal of the B-X-O mode conversion mechanism involved in coupling thermal EBW emission out of the plasma. So it is possible to study EBW coupling efficiency by measuring thermal EBW emission [4.3.11]. Initial B-X-O coupling studies on NSTX were performed in 2004 with a dual-channel, 8-18 GHz radiometer connected to a fixed, obliquely-viewing, quad-ridged antenna with its ridges aligned to simultaneously measure the radiation temperature of EBE polarized parallel ( $T_{||}$ ) and perpendicular ( $T_{\perp}$ ) to the magnetic field at the upper hybrid resonance (UHR) [4.3.12]. An example of data from this antenna is shown in Fig. 4.3.4, which shows the evolution of the EBW radiation temperature,  $T_{rad} = (T_{||} + T_{\perp})$ , for a L-mode plasma with  $B_T(0) = 4$  kG and a flattop current,  $I_p = 800$  kA between 0.27 and 0.46 s. The EBW coupling efficiency,  $T_{rad}/T_e$ , where  $T_e$  is the electron temperature of the EBW emitting layer, was measured to be  $80 \pm 20\%$  at 16.5 GHz, in good agreement with the  $\sim 65\%$  EBW coupling efficiency predicted by a model that includes a 1-D full wave calculation of the EBW mode conversion at the UHR, radiometer antenna pattern modeling and 3-D EBW ray tracing and deposition modeling [4.3.13]. Emission at 16.5 GHz was from the fundamental electron cyclotron

resonance at the plasma magnetic axis during the  $I_p$  flattop. The measured EBE polarization ratio,  $T_{//}/T_{\perp}$ , was also measured to be in reasonable good agreement with theoretical modeling.

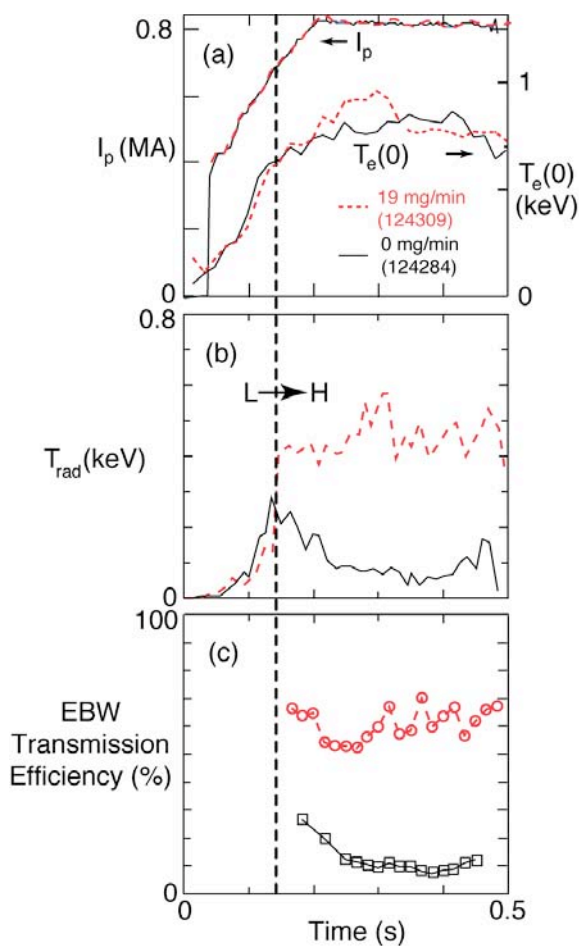


Figure 4.3.5: (a) Plasma current and central electron temperature evolution for two H-mode plasmas, one without lithium conditioning (black solid line) and one with lithium conditioning (red dashed line). (b) Time evolution of EBW radiation temperature for fundamental emission from the plasma core at 18 GHz and (c) EBW transmission efficiency from the core to the EBW radiometer antenna.

In 2005 a pair of remotely steered B-X-O antennas were installed on NSTX [4.3.14], allowing the B-X-O emission process to be studied in more detail. Results showed that the EBW coupling efficiency peaks at a poloidal and toroidal angle that is close to the direction predicted by theory [4.3.15]. Recent studies of B-X-O emission from H-mode plasmas in NSTX show a wide range of behavior; sometimes the coupling efficiency remains relatively high ( $\sim 50\%$ ) throughout the H-mode phase, sometimes it gradually decays, and sometimes the coupling efficiency collapses soon after the L to H transition. Measurements and modeling of EBW emission on NSTX are supportive of collisional damping of the EBW, prior to mode conversion, as being a possible major cause for the degradation of EBW emission in H-modes. Collisional damping is expected to become important when  $T_e$  near the EBW mode conversion layer is  $< 20$  eV. In NSTX H-mode plasmas, measured  $T_e$  in the B-X-O mode conversion region, particularly for  $f_{ce}$  emission, can be as low as 10 eV. During NSTX experiments in 2007 there was strong evidence

that Li conditioning can significantly enhance B-X-O emission from H-modes, either by changing the density scale length or increasing  $T_e$  in the conversion region [Fig. 4.3.5]. It is possible that EBW collisional damping may not be a problem for EBW heating of H-modes if the incident microwave power

can heat the EBW mode conversion region sufficiently to avoid EBW collisional loss.

Status of Experimental EBW Research on Other Devices:

Following the first demonstration of O-X-B EBWH in the W7-AS stellarator in 1997 [4.3.16] there have been several O-X-B heating experiments on other devices that show encouraging results. 60 GHz B-X-O EBW heating experiments conducted on the MAST ST used three plasma scenarios [4.3.17].

MAST was the first ST device to use O-X-B heating. The O-X-B coupling efficiency was at least 50% in high-density ELM-free H-mode discharges. In sawtoothing H-mode plasmas, a 10% increase of stored energy was measured during EBWH, and a 10% increase in  $T_e$  was measured in small ohmic H-mode plasmas [Fig 4.3.6]. Future plans on MAST call for the installation of a 1 MW 18 GHz O-X-B EBWH system. Recently, there have also been plasma startup experiments on MAST that employ a 28 GHz heating system. 90 kW of RF power generated 32 kA of plasma current, without using the central solenoid, in good agreement with modeling [4.3.18]. The resulting plasma had a  $T_e \sim 500$  eV and  $n_e \sim 10^{18} \text{ m}^{-3}$ . This result suggests the NSTX 350 kW, 28 GHz ECH system, that will be operational in 2011, should be able to heat the plasma sufficiently to allow effective HHFW heating.

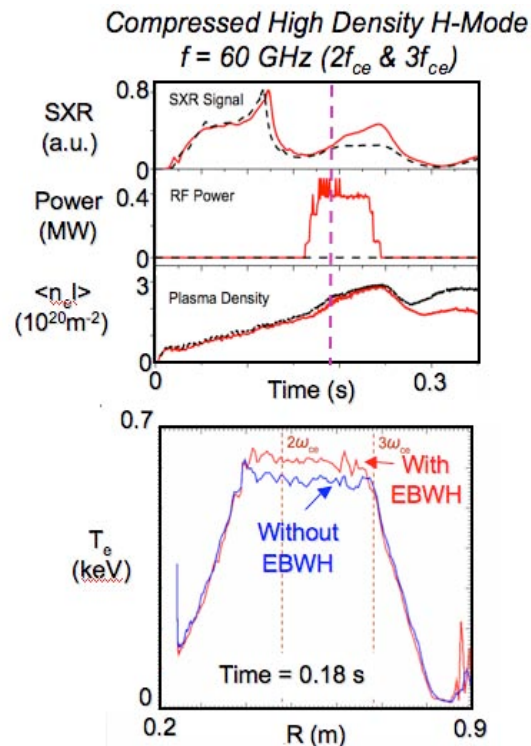


Figure 4.3.6: 60 GHz EBW heating via O-X-B coupling demonstrated on MAST.

The first demonstration of EBWH via O-X-B mode conversion in an overdense conventional aspect-ratio tokamak was achieved in the TCV device [4.3.19]. The central electron temperature evolution during 82.7 GHz EBWH was measured to increase by 80 eV when the RF power was increased from 1 to 2 MW [Fig. 4.3.7].

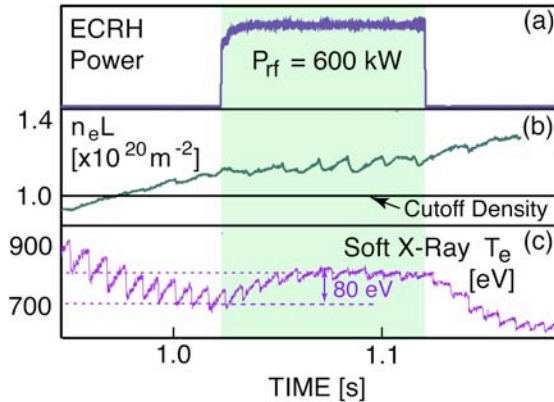


Figure 4.3.7: EBW heating via O-X-B coupling demonstrated on TCV. (a) 600 kW of 82.7 GHz power was coupled into (b) an overdense TCV plasma via O-X-B coupling. (c) At 60% of the RF power was absorbed by the plasma at  $r/a \sim 0.65$ , increasing  $T_e$ , as measured by soft X-rays, by 80 eV.

The optimum injection angle for O-X-B conversion was obtained experimentally by measuring the reflected microwave radiation during a two-dimensional angle scan. Ray tracing simulations yielded an optimum launch angle that was in good agreement with the measured angle. About 60% of the RF power was absorbed after conversion to EBWs.

Status of EBW Theory and Numerical Modeling:

The GENRAY numerical ray tracing code [4.3.8, 4.3.20] and the CQL3D Fokker-Planck code [4.3.21] have been used to model EBW

propagation, heating and current drive in NSTX discharges with  $\beta \geq 20\%$ . Efficient off-axis Ohkawa

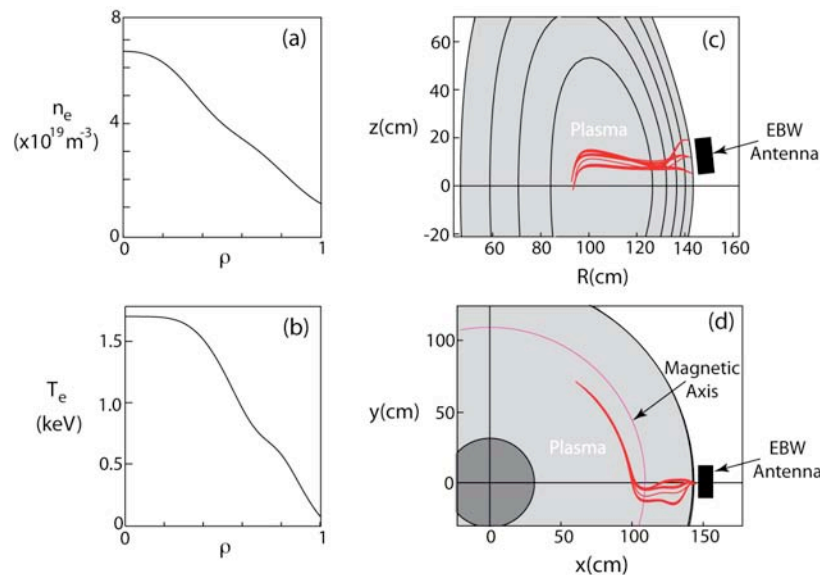


Figure 4.3.8: (a)  $n_e$  and (b)  $T_e$  profiles used to model 28 GHz EBW propagation and damping in a  $\beta = 20\%$ ,  $B_t(0) = 0.55$  T NSTX plasma. (c) Poloidal and (d) toroidal midplane projection of EBW rays calculated by GENRAY for a launched spectrum with  $N_{||} = -0.55 \pm 0.05$ . 28 GHz EBW power is absorbed near the magnetic axis.

current drive at a normalized minor radius,  $\rho \sim 0.7$ , and on-axis Fisch-Boozer current drive is predicted

[4.3.22] for a range of plasma and EBW launch scenarios. An example of 28 GHz EBW ray tracing results from the GENRAY for a  $\beta = 20\%$  NSTX plasma with a vacuum toroidal field,  $B_t(0) = 0.55$  T is shown in Fig. 4.3.8. EBW power is deposited near the magnetic axis. Figure 4.3.9 shows the EBW power deposition and EBW-driven current profile calculated by the CQL3. 85% of the EBW power is absorbed by at the Doppler-shifted  $2f_{ce}$  resonance, near  $\rho = 0.2$ , the remainder is absorbed at the Doppler-shifted  $3f_{ce}$  resonance, also near the axis. The total EBW-driven current, generated in this case via the Fisch-

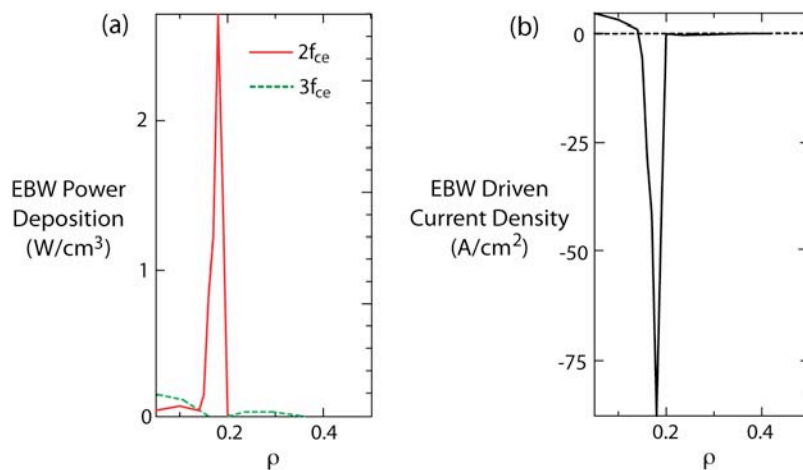


Figure 4.3.9 (a) EBW power deposition to electrons calculated by CQL3D for 750 kW of EBW power coupled into the plasma shown in Fig. 4.2.8. (b) EBW-driven current density calculated by CQL3D.

Boozer current drive mechanism is 29 kA, corresponding to a current drive efficiency of 39 kA/MW. Synergy between EBWCD and the current driven by the electron bootstrap effect has been calculated to be relatively weak, typically  $<10\%$ . However, the local bootstrap current density increases in proportion to increased plasma pressure, and this effect can significantly modify the radial

profile of the RF-driven current density [4.3.23]. Benchmarking between GENRAY/CQL3D and the European code BANDIT-3D [4.3.24] for a NSTX EBWCD case shows good agreement for the magnitude, direction and location of the EBW-driven current. A recent reviews of the most important theoretical and numerical modeling results for EBWs in ST's can be found in references 4.3.25 and 4.3.26.

#### 4.3.5 ECW/EBW Research Plan for 2009-2013

##### 2009-10:

EBW studies during this period will focus on emission from low-density plasmas that will use lithium injection and the Liquid Lithium Divertor to keep the EBW mode conversion layer inside the separatrix to



avoid EBW collisional damping and mode conversion efficiency fluctuations due to scrape off density turbulence.

2011:

A 350 kW, 28 GHz gyrotron will be installed on NSTX. This system will initially be used for second harmonic X-mode ECH to heat CHI and PF-only startup plasmas and increase the electron temperature sufficiently to allow efficient HHFW heating. A fixed horn antenna will be used for these ECH-assisted plasma startup experiments. Experiments will explore the transition from ECH-assisted startup to HHFW-assisted plasma current ramp up.

2012-13:

In 2012, with additional incremental funding, we propose to install a second 350 kW 28 GHz gyrotron on NSTX, bringing the total available 28 GHz source power to 700 kW. This upgraded ECH system would initially be used for ECH-assisted plasma start-up research, but could also be used later for experiments to study EBW coupling physics via an oblique O-X-B launch. Based on emission studies in 2006-7 we can reasonably expect 70% EBW coupling efficiency, or about 500 kW of EBW power for 750 kW of 28 GHz source power. 28 GHz EBW experiments would greatly benefit from the higher toroidal field that will be generated using the new center-stack. Operation at a toroidal field of 1 T will allow fundamental frequency 28 GHz EBW heating where there is much better radial access compared to second harmonic heating. Results from these heating experiments could be used to benchmark EBW simulation codes. If the proposed 28 GHz EBW heating system is not installed on NSTX it may be possible to conduct some of this research program on MAST.

## 4.4 Energetic Particle Physics

### 4.4.1 Energetic Particle Research Goals

An important goal of the present proof-of-principle spherical tokamaks (ST) is to evaluate the role of fast ion driven instabilities in fast ion transport and confinement. The results will be used to validate linear numerical codes, such as NOVA/ORBIT and nonlinear codes such as M3D, which are used to predict the effect of fast-ion driven instabilities on fast ion transport. The codes may then be used with greater confidence to predict fast ion confinement in either an advanced ST such as NHTX/CTF/ARIES-ST or for tokamak reactors such as ITER and, ultimately, DEMO. Spherical tokamaks have relatively low toroidal field so the fast-ion Larmor radius is large compared to the plasma minor radius ( $\rho_{fi} \approx 0.1 - 0.2 a_p$ ) and the fast-ion velocity is much greater than the Alfvén speed ( $V_{fi} \geq 2 V_{\text{Alfvén}}$ ), and overlaps the expected fast ion (fusion-alpha) parameters for either tokamak reactors (ITER) or advanced STs. This regime of large Larmor radius and low Alfvén speed is a regime in which fast ion driven instabilities are potentially virulent. Considerable progress was made during the last five year period of operation on NSTX in identifying the broad spectrum of observed fast ion driven modes, as well as the drive and damping mechanisms. The redistribution or loss of fast ions will impact the interpretation of thermal transport data, beam driven currents and momentum transport, as well as having a potentially direct impact on the design of plasma-facing components in a reactor (due to the potential for localized heating or ablation from lost fast-ions). Recently added diagnostics, as well as diagnostics planned for the near future, will allow for more detailed studies of the saturation amplitude, internal structure, and the effects on fast ion transport. The higher field and second beamline will extend the range of fast ion parameters, expanding the parameter range of the data to be used for code validation.

Good experimental measurements are required to validate the codes developed to predict the effect of fast-ion driven instabilities on transport of fast ions. It is not only necessary to have good measurements of the equilibrium parameters, but the stability thresholds and saturation amplitudes of the fast ion modes must also be measured. The impact of these modes on the fast ion distribution must be measured, as well. NSTX has accumulated a comprehensive suite of diagnostics for these studies. Redistribution of fast ions is now measured with the scanning Neutral Particle Analyzer (NPA), solid-state Neutral Particle Analyzer

(ssNPA) and the new Fast-Ion D-Alpha emission diagnostic. Losses of fast ions are detected with the scintillator Fast Lost Ion Probe (sFLIP), an array of Faraday cups for detecting lost fast-ions (iFLIP), as well as the fast neutron rate diagnostics. The planned addition of a neutron collimator diagnostic will complement these existing fast ion diagnostics by providing an additional measure of confined fast ion redistribution. The effect of loss or redistribution of fast ions on beam-driven currents, and interpretation of momentum and thermal transport can be documented with current profile evolution measurements based on Motional Stark Effect (MSE) diagnostic data (which is unique in providing q-profile measurements in fields as low as 3.5 kG), plasma rotation measurements with the toroidal and poloidal CHarge-Exchange-Recombination (CHERS) diagnostic and the complete complement of kinetic profile diagnostics.

Analysis of the data collected on fast ion instabilities is supported through an active theoretical program. The NOVA-k code calculates the linear eigenmode structure, as well as most of the damping and drive terms. While NOVA is a linear code, the saturated amplitudes of the individual modes will be directly measured and can be used to normalize the eigenfunctions calculated with NOVA. The resulting spectrum of eigenmodes, together with the unperturbed fast ion distribution calculated with the TRANSP code, is used as input to the ORBIT code. The ORBIT code follows the trajectories of many fast ions, in the presence of modes, and can predict the resulting loss or redistribution of fast ions. A fully non-linear code, M3D, is used to self-consistently predict saturated mode amplitudes and fast-ion transport for comparison with the measured values. M3D is a “ $\delta f$ ” code, where only the perturbed component of the fast ion distribution receives full kinetic treatment.

The presence of weakly damped plasma modes below the cyclotron frequency, revealed through excitation by beam fast ions, has suggested a unique heating method for spherical tokamaks. Although this method is different from the originally suggested alpha channeling [4.4.1] it serves the same goal of tokamak optimization by increasing its output power via minimizing electron heating and directing either auxiliary or fast ion produced power to heat thermal ions. A large amplitude wave at a fraction of the ion cyclotron frequency can stochastically heat thermal ions. The presence of weakly damped plasma modes in this frequency range suggests that excitation of these modes, with a driven antenna, to a sufficient amplitude would stochastically heat the thermal ions. The fundamental principles of stochastic heating

were developed in the late 1970's and early 1980's [4.4.2-4.4.6], and experiments validating the concept were done from the late 1980's to mid 1990's [4.4.7-4.4.11]. In the coming five years it is proposed to explore the possibility of using such a stochastic ion heating system on NSTX.

#### *4.4.2 Energetic Particle Physics*

The transport of fast ions can be greatly enhanced in the presence of multiple modes. This can mean either multiple modes of a similar type, for example several Toroidal Alfvén Eigenmodes (TAE), or, potentially, modes as disparate from TAE as Compressional Alfvén Eigenmodes (CAE) or fishbones. As the diffusive “step size” from interaction with fast ion instabilities tends to be proportional to the ion gyro-radius, fast ion losses in large, high field devices such as ITER are expected to be through the interaction of multiple modes [4.4.12]. The study of such multimode interactions will be a high priority in the next five years on NSTX. Strongly enhanced transport has been seen when multiple TAE modes interact, a process known as TAE avalanches [4.4.13-4.4.17]. Three-wave coupling of TAE, fishbones (kinks) and higher frequency Alfvén eigenmodes has also been seen [4.4.18], with some data suggesting that these modes may also interact through perturbations of the fast ion distribution.

The impact of these studies on future devices such as NHTX or ITER will be primarily through the numerical simulation code improvements needed to accurately model the NSTX data. The capability to predict stability thresholds for fast-ion driven instabilities in future fusion reactors is an important component of the design and identification of attractive operational regimes. The M3D-K code is a non-linear,  $\delta f$  code that can model the saturation amplitude of modes, frequency chirping and some forms of multimode coupling. Its future development will be within the recently approved energetic particle center lead by PPPL in collaboration with IFS and Colorado University. The much improved M3D-k code with the gyro-kinetic physics will be called GKM and will be able to model realistically the kinetic physics and the fast ion transport due to Alfvénic modes. The inclusion of gyro-kinetic physics is necessary for proper modeling of the coupling of Alfvén modes to kinetic Alfvén waves (KAW) where the eigenmodes enter the continuum, an important damping mechanism for TAE. The high-k scattering diagnostic on NSTX can directly measure the KAW waves, offering the exciting opportunity to study this physics.

An important part of the five year plan will be to utilize this capability to model well documented examples of Alfvénic instability induced fast ion losses. To supplement this effort, the NOVA-K and ORBIT codes will be used to simulate fast ion transport due to experimentally measured modes. NOVA-k calculates the linear mode eigenfunction, as well as drive and damping terms. The eigenfunctions calculated with NOVA can be normalized with experimental data and used in the particle tracking code, ORBIT, to calculate the affect on fast ion transport. These numerical simulations will then be compared to enhancements of fast ion transport as measured with FLIP, NPA and FIDA diagnostics.

A critical parameter of energetic particle-driven Alfvén modes is the normalized gyroradius of energetic particles. It is known that beam-driven Alfvén instability is maximized at  $k_{\theta} \cdot \rho_{\text{hot}} \sim 1$ . The stability threshold is also expected to be affected due to the change in the damping from the thermal plasma. More importantly, the number of unstable mode is expected to increase strongly with decreasing energetic particle gyroradius. This can in turn affect energetic particle transport due to the increased number of unstable modes. The doubling of magnetic field in the NSTX upgrade would allow a parameter scan in the beam gyro-radius over a factor of 3. With the upgrade to the center-stack, we can investigate experimentally the  $\rho_{\text{beam}}$  dependence of the stability threshold, unstable mode spectrum, and beam ion transport for beam-driven TAE/EPM modes predicted theoretically. The results of this experiment will help us to understand energetic particle transport in the presence of multiple modes and will provide critical data for validating nonlinear energetic particle simulation codes for predicting alpha particle transport in ITER.

On NSTX the electron thermal speed is only a little higher than the fast ion speed, e.g., at 1 keV the electron thermal speed is only 4.5 times the speed of a 90 kV deuterium beam ion. Thus, it is not surprising that some significant populations of thermal electrons have resonant interactions with fast-ion driven instabilities such as CAE or GAE. Such an interaction, leading to increased diffusivity for the electrons, is being considered as an explanation for anomalously large electron heat diffusivity seen in some regimes on NSTX, an explanation supported by simulations with the ORBIT code. The higher electron temperatures, which might be expected to accompany higher field operation, would separate the velocity scales and clarify the physics of this phenomenon.

### 4.4.3 CAE Heating

Stochastic heating of magnetized ions or electrons with large amplitude waves at frequencies just below the cyclotron frequency was proposed in the mid '70's to the early '80's for a variety of modes [4.4.2-4.4.6]. This work was, perhaps, an outgrowth of earlier experiments and theoretical work on heating of plasmas with stochastic waves [4.4.19-4.4.23]. An extensive experimental study of stochastic ion heating by a large amplitude wave was done on the ENCORE tokamak by Paul Bellan's group between 1986 and 1998 [4.4.7-4.4.11]. Stochastic heating of thermal ions was measured with a laser-induced fluorescence diagnostic. The wave was a large amplitude drift-Alfvén wave [4.4.24], probably driven by the plasma current. In a fairly extensive set of experiments, good agreement was found with the theory of stochastic heating. Recently, numerical studies of stochastic ion heating were done in the context of CAE [4.4.25-4.4.26]

The broad spectrum of CAE and Global Alfvén Eigenmodes (GAE) modes in the proper frequency range on NSTX offers an opportunity for stochastic thermal ion heating. These natural modes are weakly damped, as evidenced by the ease with which they are excited by the neutral beam fast ion population. Based on measurements of the mode damping rate and wave amplitude, and assumptions about the wave localization, only a few 10's of kW of power would be required to excite waves to the amplitudes that are seen. Numerical simulations have estimated that wave amplitudes 5 to 10 times higher than the peak so far observed would be necessary for stochastic ion heating. This power heats the electrons, as the damping is primarily electron Landau or continuum damping. A low linear damping rate means that relatively little power would be lost to the electrons by exciting the wave to the stochastic threshold amplitude, after which most of the additional heating power would be deposited in the thermal ion population. This thermal ion heating mechanism represents a form of alpha channeling [4.4.1] in that the GAE and CAE also take energy from the fast ion population and "channel" it to the thermal ion population, but with the additional possibility of some control via an externally excited antenna.

Experiments with a 5-10 kW, 0.1 - 1.5 MHz source to measure coupling to eigenmodes of the plasma would follow earlier experimental studies using antennas to launch Alfvén waves [4.4.27-4.4.29]. With 5 - 10 kW, it might also be possible to excite waves to the detection threshold of the microwave reflectometer systems on NSTX. The goal of these higher heating power experiments would be to further

understanding of the stochastic heating mechanism, rather than to see substantial ion heating. Further, excitation of Alfvén eigenmodes with a coil inside the vacuum vessel and a low power amplifier ( $\approx 5$  kW) is a valuable tool for the study of mode stability [4.4.30]. The spectrum of stable modes can be detected and the linear damping rate measured directly. This is very helpful information as stability codes must calculate both the sum of the damping and drive terms, the difference of which is the linear drive for the mode. Thus a direct measurement of the linear damping term also helps to interpret the experimentally determined linear growth rate.

The experiments would be supplemented with numerical calculations, as is done for other forms of RF heating. An effort has begun to develop the full-wave TORIC code [4.4.31] for simulations of wave excitation with the HHFW antenna at frequencies below or near the ion-cyclotron frequency. The TORIC full wave code can complement traditional stability codes, such as HYMN, GKM (gyrokinetic version of M3D) or NOVA-K. TORIC includes finite Larmor radius effects, finite  $\omega/\omega_{ci}$ , cyclotron resonances and a fast ion population. Further, TORIC can attain higher spatial resolution, although in a linear model. Initial simulations have found three waves near the cyclotron frequency, one of which may be a core-localized GAE.

#### *4.4.4 Status of Energetic Particle Research*

##### *Fishbones and EPMS:*

Bursting, chirping modes are seen in NSTX with frequencies starting at over 100 kHz and which can chirp down 10's of kHz on a millisecond timescale [4.4.32-4.4.40]. These modes can be present with  $q_{\min} \geq 1$  and with, sometimes multiple, toroidal mode numbers  $1 \leq n \leq 4$ . In plasmas where  $q_{\min} \approx 1$ , the modes typically have characteristics resembling the fishbone mode seen on conventional aspect ratio tokamaks. The modes are core-localized with a kink-like structure (no or small islands). Under conditions where  $q_{\min}$  is believed to be well above unity, the modes often have toroidal mode numbers greater than one. The modes still appear to be core localized and kink-like in nature. Some of these modes have been identified as bounce-precession resonance fishbone modes. They are expected to be unstable in high current, low shear discharges where the conventional precession-resonance drive is weak (due to low precession drift frequency) [4.4.33]. These plasmas have a significant population of trapped

particles with a large mean bounce angle, produced by near tangential beam injection into a small aspect ratio device.

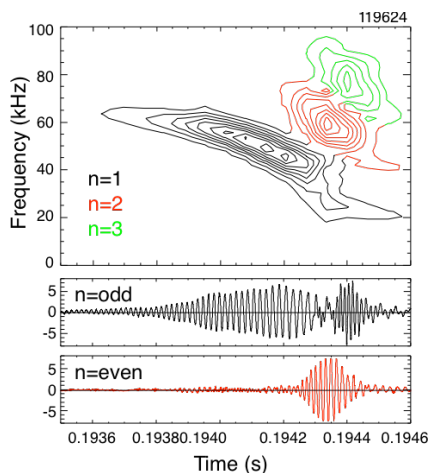


Figure 4.4.1: Fishbone mode showing multimode transport [4.3.38]

The strength of neutron drops (fast ion losses or transport) varies widely for these bursting, chirping modes. Those resembling the classical fishbone modes ( $n = 1$ ,  $q_{\min} \approx 1$ ) are most reliably correlated with neutron rate drops. However, many of the bursts involve multiple modes, and in some cases transient losses of fast ions (directly measured with the scintillator Fast Lost Ion Probe, sFLIP) are correlated with periods when multiple modes are present [4.4.40] (see Fig. 4.4.1).

Additional experimental studies of the mode structure, stability boundaries and resonant drive are necessary to develop the ability to predict their appearance and affect on fast ion confinement. At present, even though the mode eigenfunction is relatively well known, simulation of the fast ion losses has not been done.

Toroidal Alfvén Eigenmodes and Avalanches:

Multiple TAEs are commonly observed in beam heated NSTX discharges. However, evidence for significant fast ion transport or loss appears confined to instances of strong, multimode bursts (e.g., Fig. 4.4.2). Fast ion orbits are modified as they interact with the TAE, with those fast ions resonant with the wave becoming trapped in the wavefield, i.e., forming “phase-space islands”. As the mode amplitude increases, more fast ions will be trapped and the islands will become larger. It has been proposed that when the resonances from multiple modes are nearby in phase space, sufficiently large amplitude modes will cause the phase space islands to overlap. The orbits of the formerly trapped ions become

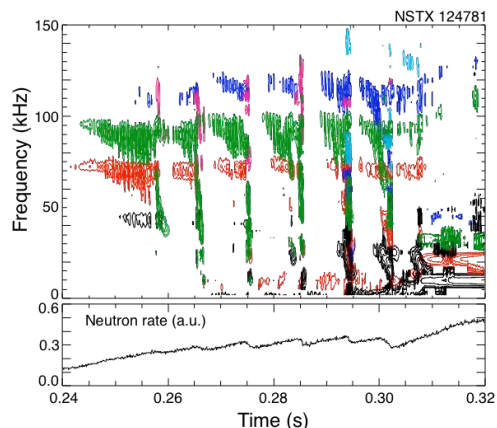


Figure 4.4.2: TAE avalanches and neutron drops indicating fast ion losses



stochastic and very rapid transport of fast ions may occur. Additionally, the ensuing modifications to the fast ion distribution function may result in otherwise stable modes being excited, ultimately leading to an “avalanche” effect which further enhances the transport of fast ions [4.4.13-4.4.17]. This mechanism of fast ion transport through an interaction of many modes could be important in ITER [4.4.12].

TAE avalanches, correlated with drops in the neutron rate suggesting fast ion losses, have been studied in NSTX. Recent experiments have documented the internal mode amplitudes, measured with the five-channel reflectometer system, together with MSE documentation of the current profile. These measurements provide the basis for numerical modeling of the island overlap threshold and enhanced fast ion transport. These experiments were necessarily carried out in L-mode plasmas to obtain reflectometer measurements of the internal structure. As with many of the studies of fast ion driven instabilities, it is important to extend these studies to the high performance, H-mode regimes, even at the expense of detailed measurements of the internal structure. The addition of the BES diagnostic will remove the requirement of L-mode density profiles for internal mode measurements, allowing Avalanche studies to be extended to the H-mode regime. The higher field available with the center-stack upgrade in 2012 will allow access to regimes with smaller  $V_{\text{fast}}/V_{\text{Alfvén}}$  and  $\rho^*$ , extending the experimental basis for scaling of the Avalanche physics.

Simulations of the fast ion redistribution due to interactions of multiple toroidal Alfvén eigenmodes have been done with the M3D-k code [4.4.41]. These simulations demonstrated both the synergistic interaction of multiple modes, giving a higher saturation amplitude, and the “overlap” of islands from individual modes in fast-ion phase-space responsible for the larger saturation amplitude. In parallel, simulations are being done with the NOVA and ORBIT codes, using the experimentally observed mode spectrum and amplitudes to compare with measurements of fast ion losses.

#### Beta-induced Alfvén Acoustic Eigenmodes:

New global MHD eigenmode solutions have been found numerically below the Geodesic Acoustic Mode (GAM) frequency in gaps in the low frequency Alfvén-acoustic continuum [4.4.42, 4.4.43]. These new eigenmodes can explain observations of modes with frequencies well below the TAE frequency (Fig. 4.4.3). These global eigenmodes, referred to here as Beta-induced Alfvén-Acoustic Eigenmodes (BAAE), exist in the low magnetic safety factor region near the extrema of the Alfvén-acoustic continuum. In

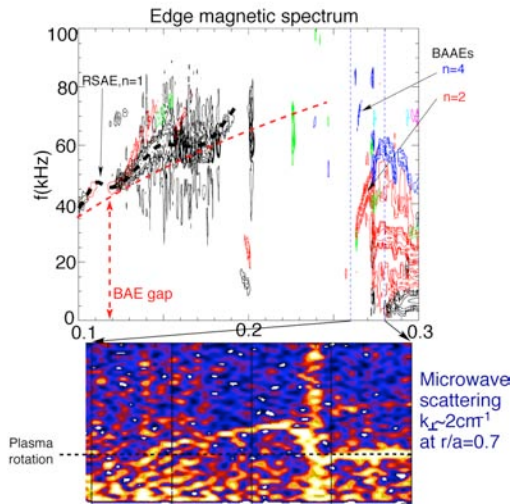


Figure 4.4.3: Beta-induced Alfvén Eigenmodes

accordance with the linear dispersion relation, the BAAE frequency increases as the safety factor,  $q$ , decreases. We show that BAAEs can be responsible for the observations of low frequency modes in relatively high  $\beta > 20\%$  NSTX plasmas. In contrast to the mostly electrostatic character of GAMs, the new global modes also contain an electromagnetic (magnetic field line bending) component due to the Alfvén coupling, leading to wave phase velocities along the field line that are large compared to the sonic speed. Initial measurements with the high- $k$  scattering diagnostics have found evidence of mode conversion to short wavelength kinetic Alfvén waves

as the BAAE enters the continuum. The ability to make these measurements will be valuable in the study of other Alfvén waves as well. Qualitative agreement between theoretical predictions and observations are found.

#### Beta Dependence of Alfvén Cascade Modes:

Alfvén Cascade Modes have been found in low density, low  $\beta$  NSTX plasmas (Fig. 4.4.4). An extension of the theory of Cascade modes, that includes the coupling to the GAM [4.4.44-4.4.46], is shown to imply their absence for typical ST  $\beta$ 's. A scan in  $\beta$  confirmed a threshold for suppression of Cascade modes in accord with theoretical predictions. Further, good agreement was found between the observed onset frequency and the frequency estimated from a simple dispersion relation for the GAM.

The time evolution of  $q_{\min}$  as calculated from the observed mode frequency sweeping was also found to be in good agreement with that found from equilibrium reconstructions using measurement of the equilibrium magnetic field pitch. This measurement was made with the MSE diagnostic.

Some limited measurements have been made of the internal structure of these modes. Future experiments will try to improve on these measurements, with a view, in particular, of detecting changes in the mode structure as the Alfvén Cascade modes saturate at the TAE gap. Because these modes occur in low  $\beta$ , thus low density plasmas, new diagnostics such as the BES are required for detailed measurements of the internal structure and amplitude.

These studies have been primarily done in L-mode plasmas. It remains to be seen whether a sufficiently low  $\beta$  H-mode plasma can be made such that Alfvén Cascade modes would be present. Finally, no strong evidence has been found to connect these modes to enhanced fast ion transport as has been reported elsewhere. Future experiments could take a closer look at this issue.

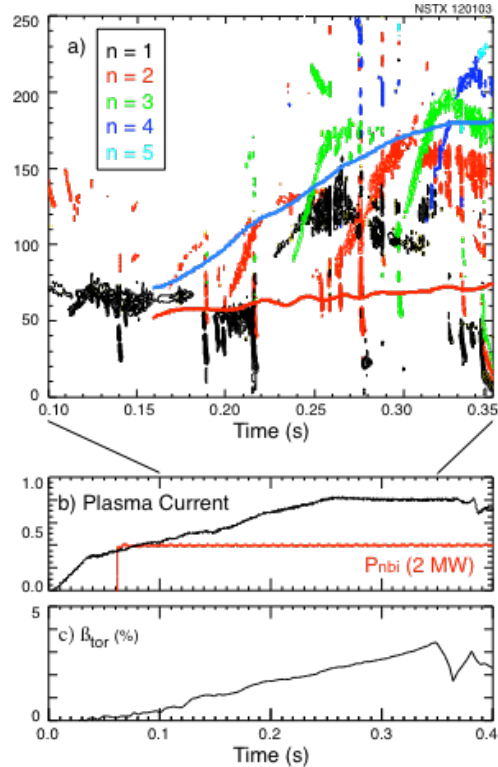


Figure 4.4.4: Alfvén Cascades

Compressional and Global Alfvén Eigenmodes and Angelfish (Hole-Clumps):

Neutral-beam-driven CAE at frequencies in the range  $0.2 \omega_{ci} \leq \omega \leq \omega_{ci}$  are commonly seen in NSTX plasmas [4.4.47-4.4.49]. The modes typically have a spectrum with multiple frequency peaks, sometimes equally spaced and with sequential toroidal mode numbers. The modes are counter-propagating for moderate mode numbers,  $3 \leq n \leq 6$ , and co-propagating for high mode numbers  $9 \leq n \leq 13$ . The frequency has a scaling with toroidal field and plasma density consistent with Alfvén waves. The modes have been observed with high bandwidth magnetic pick-up coils and with a reflectometer. The high- $k$  scattering system has again, in some instances, detected coherent modes with frequencies matching those seen on the Mirnov coils, suggesting continuum damping through mode-conversion to kinetic Alfvén waves.

Alfvénic Bursts (AB) of either compressional or global Alfvén eigenmodes, with strong frequency chirps

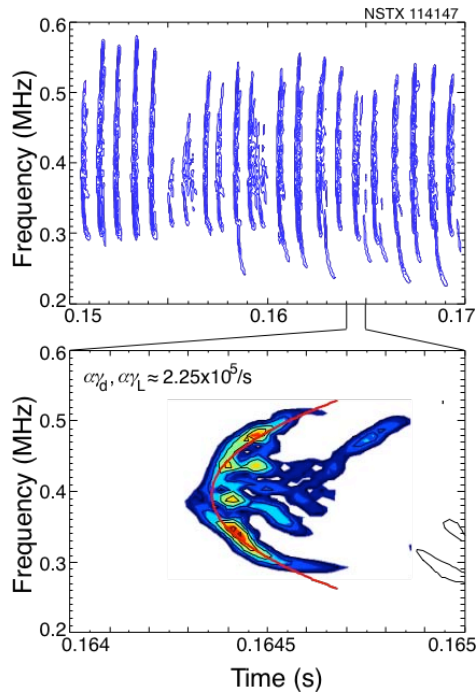


Figure 4.4.5: CAE hole-clumps (Angelfish)

have been observed in the early neutral beam-heating phase of discharges (Fig. 4.4.5). The bursts last for  $< 0.3 - 0.7$  ms, and the mode frequency chirps simultaneously up and down. The frequency evolution of the bursts is well described by the “Hole-clump pair” theory of Berk, Breizman, and Petviashvili, [4.4.50]. The AB arises from the generation of a hole in the particle distribution function, paired with a clump, and the non-linear interaction of the instability with the distribution function results in the propagation of the holes and clumps in phase space, which together with background damping, results in the simultaneous upward and downward frequency chirps of the mode. The hole-clump theory relates the rate of the frequency chirp to the linear damping rate of the mode. The damping rate determined by the frequency chirping is found to be in good agreement with predictions of the NOVA-k code.

There still remains ambiguity regarding the identification of these modes as GAE or CAE. Further numerical simulations and improvements in the measurement of the mode polarization, as well as internal structure with the multi-channel reflectometer system might help resolve this question. Likewise, additional work needs to be done to understand the extension of the hole-clump theoretical model to Doppler-shifted cyclotron resonance driven modes as these are believed to be.

Initial observations of sub-cyclotron frequency modes,  $0.2 \omega_{ci} \leq \omega \leq \omega_{ci}$ , were interpreted as CAE. Simulations with the HYM code, however, found that both CAE and GAE should be expected for the parameters of typical NSTX plasmas. Evidence for this second type of mode was soon found. The peaks in the frequency spectrum for these new instabilities intersect each other as plasma parameters evolve, whereas the CAE spectral peaks, which depend only upon density, tend to evolve parallel to each other.

The shear Alfvén dispersion,  $\omega \approx k_{\parallel} V_A$ ,  $k_{\parallel} = (m - nq)/qR$  allows for more complex behavior as the  $q$  profile and density are evolving independently during the discharge. A theory of localized CAEs and GAEs in low aspect ratio plasmas explains the observed high frequency instabilities [4.4.26,4.4.51-4.4.61]. Both classes of modes may be excited through the velocity space gradient of energetic super-Alfvénic beam ions via Doppler shifted cyclotron resonances (or, in the case of CAE, directly through a parallel bump-on-tail). CAE modes were also found on DIII-D in an aspect ratio scaling experiment motivated by the NSTX observations [4.4.62].

Non-linear, three-dimensional 3D hybrid simulations using the HYM code have been employed to study the excitation of both CAE and GAE by energetic ions in NSTX. The HYM simulations for typical NSTX parameters find that GAE are the most unstable modes, for low toroidal mode numbers,  $2 \leq n \leq 7$  at the large injection velocities of beam ions,  $V_b \approx 3V_A$ . The GAE are localized near the magnetic axis, and have large  $k_{\parallel}$ , so that  $\omega \approx k_{\parallel} V_{b\parallel} \approx \omega_{ci}/2$ . The perturbed plasma pressure in the poloidal cross-section of an NSTX plasma due to a GAE with  $n = 4$  and  $m = 2$  is shown in Fig. 4.4.6. These modes also have a significant compressional component,  $B_{\parallel} \approx B_{\perp}/3$ , due to strong coupling to the compressional Alfvén wave. In the HYM simulations for  $n_b/n_p \approx 3\%$ , the growth rates of the unstable GAEs are found to be of the order  $\gamma/\omega_{ci} \approx 0.002 - 0.01$  with frequencies  $\omega/\omega_{ci} \approx 0.3 - 0.5$ , where  $\omega_{ci}$  is evaluated at the magnetic axis.

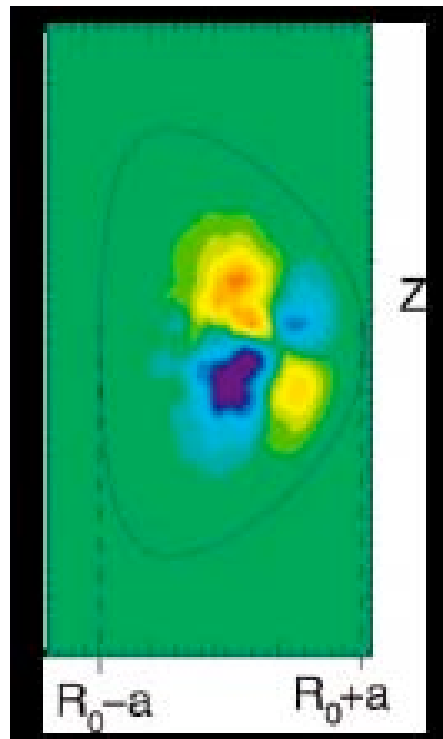


Figure 4.4.6: Color Contours of the fluid pressure perturbation of  $n = 4$ ,  $m = 2$  GAE mode plotted in the poloidal  $R, Z$  plane. Shown also is the last closed magnetic surface of the NSTX plasma. The red color regions indicate the high perturbed pressure, whereas dark blue ones correspond to the negative value of the pressure perturbation.

### Stochastic Ion Heating:

With strong neutral beam heating in NSTX a broad spectrum of fluctuations is observed in the frequency range from about 0.2 to 1.2 times the ion cyclotron frequency, demonstrating that there are many weakly damped eigenmodes present for stochastic ion heating. The modes have been identified as CAEs or GAEs. The linear damping rate has been determined from non-linear behavior of the mode frequency under some conditions, and calculated with NOVA-K and HYM.

We simulated this effect in a more complex toroidal geometry [see figure 4.4.7] than was reported previously [4.4.25, 4.4.26]. Stochastic domains at low energy corresponding to the plasma background ions occurs at a lower amplitude than in the slab plasma. The initial temperature profile of thermal ions is shown as a solid parabolic curve in figure 4.4.7. We used 21 CAEs to simulate the measured CAE spectrum by edge Mirnov probes in NSTX. Internal measurements of the rms amplitude of the perturbations is not available and was fixed at  $\delta B/B = 0.5 \times 10^{-3}$  in calculations with the collisional frequency  $\nu = 0.01\omega_c$ . Mode frequencies were in the range  $0.2 < \omega/\omega_{ci} < 0.8$ . Calculations indicate that the heating is proportional to the mode numbers if the amplitude is fixed. Stochastic multimode heating by CAEs could provide a way of direct energy channeling from beam ions (fusion alphas) to the thermal plasma ions.

### Non-linear Multi-mode Coupling:

Simultaneous bursts of Energetic Particle Mode (EPM) and TAE activity that correlate with significant fast-ion loss are observed in beam-heated plasmas. Three-wave interactions between these modes have been conclusively identified, indicating fixed phase relationships [4.4.18]. This nonlinear coupling concentrates the energy of the TAEs into a toroidally localized perturbation frozen in the frame of a rigid,

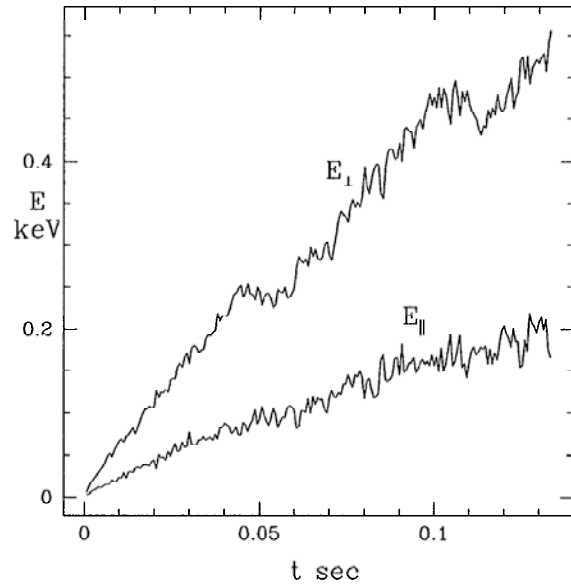


Figure 4.4.7: Ion energy in keV vs time, for  $\delta B_y/B = 6.0 \times 10^{-4}$ .

toroidally rotating structure formed by the EPMS. This redistribution of energy is significant because it will modify the effect of the TAEs on fast-ion loss.

Measurements of MHD-induced Energetic Ion Transport or Loss:

In quiescent or MHD-benign NSTX discharges, NPA measurements of the energetic beam ion distribution are consistent with classical behavior [4.4.63]. The appearance of strong, bursting or continuous MHD or Alfvénic activity can significantly affect the energetic ( $E \sim 10 - 100$  keV) deuterium ion population. Evidence of MHD-induced energetic ion transport or loss in NSTX relies primarily on neutron rate and charge exchange Neutral Particle Analyzer (NPA) [4.4.64] measurements. Neither the volume integrated neutron rate nor the line-integrated NPA efflux, however, can distinguish between transport or loss so additional diagnostics, such as sFLIP, FIRETIP and USXR are used to augment these measurements. sFLIP is able to identify ion loss while the others serve to spatially localize MHD-activity for the purpose of analysis using the time, space and energy dependent Anomalous Fast Ion Diffusion (AFID) model in TRANSP that is used to emulate MHD-driven transport or loss of energetic ions. Comparison of MSE-reconstructed toroidal current profiles with calculations taking into account AFID redistribution of NBI driven current helps to identify fast ion redistribution [4.4.65]. The AFID model is iterated to simultaneously match measurements of the neutron yield, NPA charge exchange efflux and MSE reconstructed current profiles with the TRANSP simulation.

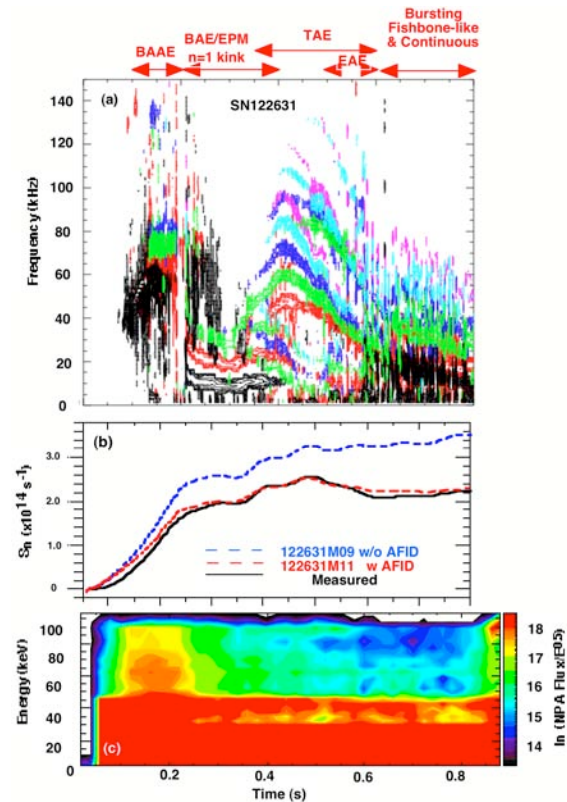


Figure 4.4.8: Mirnov MHD spectrogram, (a) measured and TRANSP-calculated neutron rates (b) and NPA energetic ion spectrum (c) for a typical H-mode discharge in NSTX.

Although redistribution or loss of energetic ions due to low-frequency ( $f \sim 10$  kHz) kink-type MHD activity has been reported previously [4.4.66], the primary goal of recent work [4.4.67] has been to contrast redistribution or loss due to continuous Energetic Particle Modes (EPM) and Toroidal Alfvén Eigenmode (TAE) activity ( $f \sim 20 - 150$  kHz) modes with the low- $f$  MHD modes, a topic that heretofore has not been investigated in detail for NSTX plasmas.

A NPA vertical scan was performed for a series of reproducible H-mode discharges, some characteristics of which are shown in Fig. 4.4.8. In panel (a), the Mirnov spectrogram shows robust activity in the low frequency range ( $f \sim 0 - 150$  kHz) where continuous  $f < 20$  kHz kink-type activity and bursting fishbone-like activity are intermingled with a ‘sea of Alfvénic modes’.

A tentative classification of the mode activity is presented in the header. Panel (b) illustrates the typical disparity in neutron yield for H-modes having strong MHD activity wherein the normal TRANSP-calculated rate (blue curve exceeds measurement (black curve), often by as much as  $50 \pm 20\%$ . The TRANSP-calculated rate using the AFID model (red curve) provides agreement with the measurement. Panel (c) shows a contour plot of the NPA efflux where it can be seen that energetic ion depletion above  $E > E_b/2$  starts around  $t \sim 150$  ms (coincident with onset of strong MHD activity) and grows throughout the discharge.

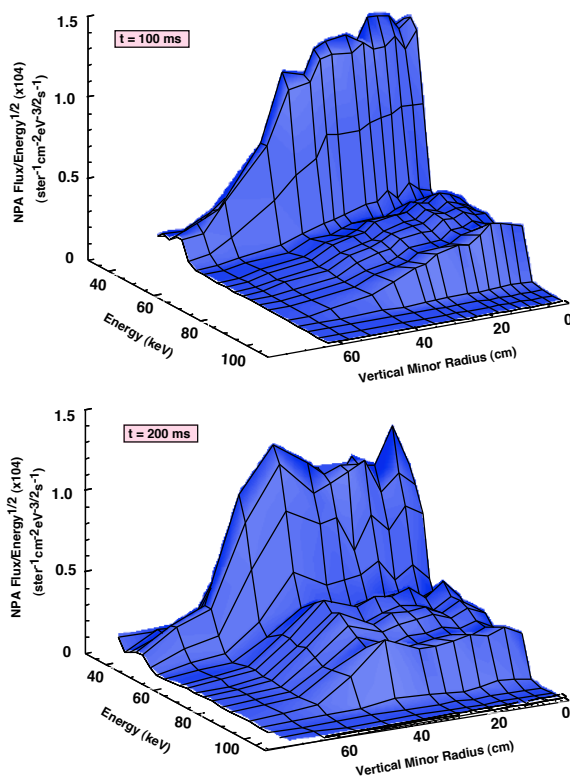


Figure 4.4.9: NPA vertical scan energetic ion spectra during MHD-quiescent (top panel) and MHD-active (bottom panel) discharge periods.

Selected NPA vertically scanning results are shown in Fig. 4.4.9 where the vertical minor radius axis is the distance along a vertical line centered at the intersection of the NPA sightline with the NB footprint (where the NPA efflux is



localized by charge exchange on the beam primary and halo neutrals). The NPA flux is displayed on a linear z-axis and the larger efflux at lower energy is the E/2 component of the neutral beam. The spectrum in the top panel corresponding to a MHD-quiescent period ( $\delta B \sim 10^{-2}$  Gauss) at  $t \sim 100$  ms shows a monotonically decreasing energetic ion distribution from the core outwards. By contrast, during strong MHD activity ( $\delta B \sim 10^{-1}$  Gauss) at  $t \sim 200$  ms the energetic ion distribution in the core region is depleted and the core ions are redistributed radially outwards to form a ‘shoulder’ on the measured distribution as evident in the bottom panel. Following this initial redistribution, the NPA spectra continue to exhibit depletion throughout the duration of the  $\sim 800$  ms discharge. This depletion is due in part to attenuation of the charge exchange neutral efflux with increasing plasma density and in part to MHD-induced energetic ion redistribution. TRANSP analysis is used to separate these contributions.

The sFLIP and FIRETIP signal activities (not shown) correlate with the Mirnov coil continuous low frequency ( $f < 20$  kHz) MHD activity (along with sporadic bursting fishbone-like activity). sFLIP energetic ion loss and FIRETIP  $\delta n_e/n_e$  core fluctuations are conspicuously absent during higher-frequency continuous TAE and CAE/GAE activity in the time interval  $t \sim 0.43 - 0.9$  s except possibly for MHD bursting activity at  $t \sim 0.78$  s and  $t \sim 0.83$  s. This leads to a tentative conclusion that both bursting fishbone-like and low-f kink-type MHD modes drive energetic ion loss whereas continuous TAE-like Alfvénic modes at most cause redistribution and the energetic ions remain confined [4.4.67].

So far, the role regarding energetic ion redistribution or loss of higher-frequency ( $f \sim 200 - 2000$  kHz) CAE/GAE activity that is omnipresent during NSTX H-mode discharges cannot be separated from the lower-frequency activity ( $f \sim 0 - 100$  kHz). Certainly they perturb the part of the fast ion distribution responsible for exciting them. While the typical amplitudes of the magnetic fluctuations are 1 – 2 orders of magnitude below those for the lower frequency fluctuations, the frequency may be an order of magnitude higher, so their role in fast ion redistribution remains to be verified.

#### *4.4.5 Energetic Particle Research Plan for 2009-2013*

The additional diagnostic capabilities and expanded parameter range (toroidal field up to 1 T) will greatly improve our understanding of the nature and impact of fast ion driven instabilities and our ability to validate numerical codes used to predict fast ion behavior in future devices.

New diagnostics include improvements to fast ion diagnostics such as the addition of the FIDA diagnostic to measure confined fast ion distributions and higher speed sFLIP data, either through a fast camera, or as a finite number of fast photomultiplier channels to improve correlation of losses with fast ion instabilities. In the post-2010 time frame, a neutron collimator could provide additional important measurements of fast ion redistribution. Improvements are planned for the reflectometer system, which is presently the basic diagnostic for internal measurements of mode structures and amplitudes. An upgrade to higher bandwidth is planned for the tangential interferometers, which could provide information on mode amplitudes in H-modes, something not possible with the reflectometers. A BES diagnostic, which could complement the reflectometer measurements will be added in 2009. The high-k scattering diagnostic has not been fully exploited for studies of kinetic Alfvén waves (KAWs), a result of continuum damping of Alfvén modes. In the following schedule we list some experimental goals that might optimistically be achieved in the experimental campaigns of 2009 and 2010

#### 2009:

In the 2009 campaign we propose experiments to continue studies of the wide range of energetic particle driven instabilities, with emphasis on their effect on beam driven current distributions. The FIDA diagnostic should be fully operational, and there may be some data available from the BES diagnostic. The MSE-LIF diagnostic may simplify experiments requiring measurement of the q-profile evolution as the restrictive requirement for beam source A at 90 kV to get MSE data will be lifted. The use of non-resonant magnetic field braking is a capability of NSTX that hasn't been fully exploited and could contribute to these experiments.

The highest priority will be to complete validation of numerical models for predicting fast ion transport as measured in studies of the TAE avalanches for present NSTX parameters (3.5 kG to 5.5 kG). Experiments will address the scaling of the onset thresholds with q-profile, fast ion distribution (pitch angle, energy) and  $V_{\text{fast}}/V_{\text{Alfvén}}$  through density and toroidal field scans. The neutral beam voltage and source dependence of TAE avalanches, a high priority in terms of impact on fast ion transport, would be investigated. An experiment will be dedicated to producing TAE modes and a search for continuum damping via coupling to KAW will be made using the high-k scattering diagnostic. Careful documentation of the current profile evolution will be done.

The study and modeling of the impact of EPMS on beam driven currents will begin in earnest with the improved diagnostic capability. The parametric dependencies of these modes on q-profile and beta will be investigated. The FIDA and BES diagnostics will be used to document the internal mode structure and redistribution of fast ions. The role of drift-reversal, assumed to be an important stabilizing effect for ITER, will be studied. Mode structure measurements will be used to validate the NOVA and PEST linear ideal codes as well as the M3D-K non-linear code. Predictions of fast ion transport with ORBIT and M3D-K will be compared with experimental data.

Documentation of the Alfvén Cascade eigenmode evolution to TAE modes will be completed. Density, toroidal field, and beam voltage scans will help to identify the parametric scaling of the GAM frequency from which the effective specific heat for the fast ion distribution can be determined. The data will provide important validation of the NOVA and M3D codes for plasmas with reversed core magnetic shear.

Complete documentation of internal mode structure and begin scaling of threshold parameters of the beta-induced Alfvén Acoustic mode (BAAE) will continue, utilizing the high-k scattering and BES diagnostics.

Finally, the first experiments to measure CAE/GAE coupling to an existing HHFW antenna strap will be done. This will provide useful information on the design of a dedicated CAE antenna.

#### 2010:

The fast Mirnov arrays will be upgraded for the 2010 campaign for increased bandwidth compatible with higher mode frequencies expected with the center stack upgrade and to provide additional spatial coverage. Additionally, the FIDA diagnostic to measure distributions of confined fast ions and the BES diagnostic for measurement of internal mode structure should be routinely available.

In this year the fast ion transport code validation emphasis will be extended to the study of Alfvén Cascade modes and to TAE avalanches in H-mode plasmas, utilizing the BES diagnostic for internal measurements of mode structure and amplitude. This is an important regime in which to understand the modes, and the flatter density profile could play an important role in the physics of the modes. The

addition of the BES diagnostic gives us the important ability to measure the internal mode amplitude and structure needed to validate numerical models.

The impact of fishbones on beam driven currents will be revisited with the improved diagnostic capability. The parametric dependencies of these modes on q-profile and beta will be investigated. The BES and FIDA (and other fast ion diagnostics) diagnostics will be used to document the internal mode structure and redistribution of fast ions. The role of drift-reversal, assumed to be an important stabilizing effect for ITER, will be studied.

There will be an experiment dedicated to the study of three-wave coupling between fishbone-like modes, TAE and the higher frequency GAE/CAE. Three wave coupling between these modes could affect instability thresholds as well as particle transport. Again, the BES system would contribute to this experiment. The FIDA diagnostic, together with sFLIP and NPA, will be used to look for fast ion redistribution correlated with three-wave coupling.

Additionally, the sensitivity of TAE avalanches to He-D concentration ratios will be studied. This may provide some insight into damping mechanisms for TAE modes. The switch from D to He both lowers the thermal ion speed as well as lowering the thermal ion beta (for fixed electron density), changing the ion Landau damping term for the TAE modes.

A number of the previous experiments, notably those on BAAEs and Alfvén Cascades, could benefit from the use of HHFW to control the electron temperature, thus altering the role of the Acoustic mode coupling for these modes.

The first low power coupling experiments to Alfvén waves will be done using an existing HHFW strap and a low power amplifier.

#### 2011-2013:

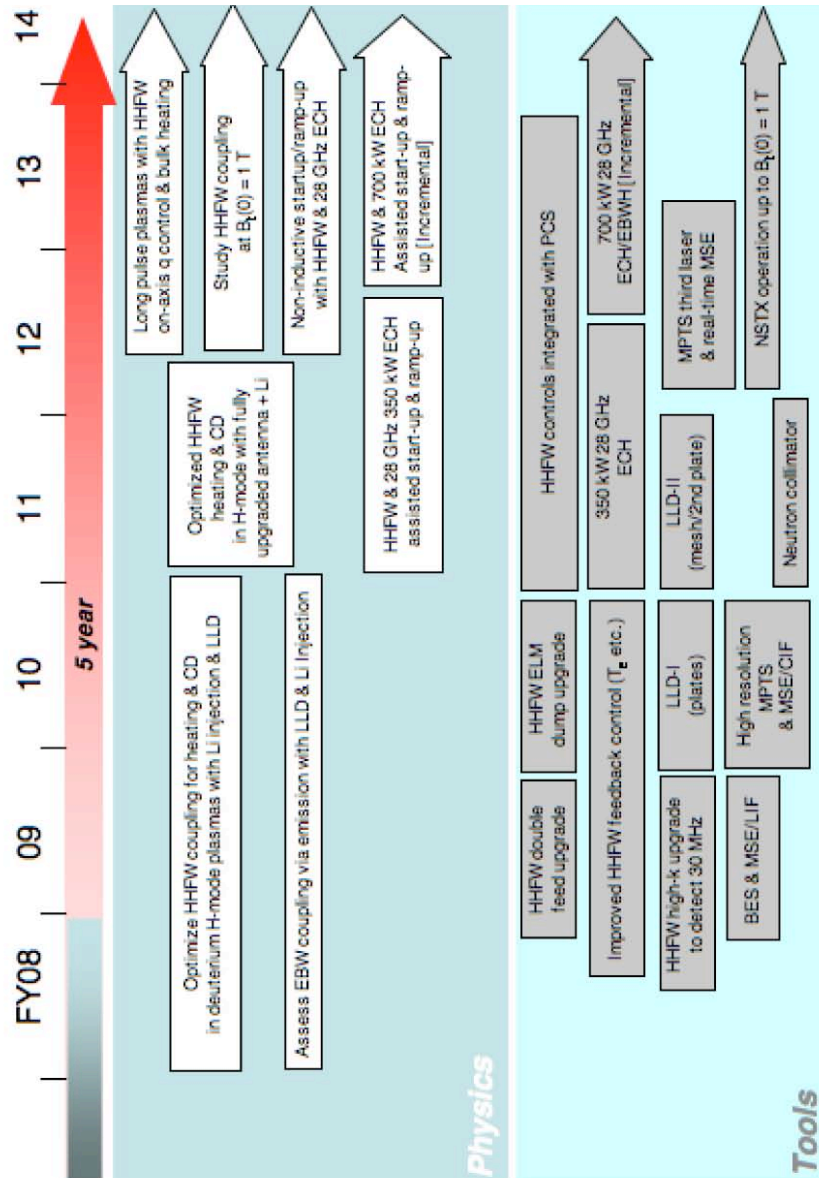
The upgrade to the center stack will allow operation to toroidal fields of up to 1 T, and plasma current up to 2 MA. The higher field extends the range of  $V_{\text{fast}}/V_{\text{Alfvén}}$  and  $\rho^*$  for scaling studies of the \*AE activity, especially for the scaling of TAE avalanches closer to ITER parameters. The higher field may allow use of the full voltage and power capability of the neutral beams, extending the energy of the fast ions up to  $\approx 110$  kV. The ability to explore lower  $V_{\text{fast}}/V_{\text{Alfvén}}$  is important as both present theoretical understanding

and experimental results suggest that the drive for TAE, and thus TAE avalanches, peaks for  $V_{\text{fast}}/V_{\text{Alfvén}} \approx 2$ . The increased range of  $\rho^*$  will extend the studies of TAE avalanches by changing the range of poloidal harmonics and number of interacting modes, providing better validation of the NOVA/ORBIT and M3D-K (GKM) codes. The new center stack will allow experiments to explore fast ion parameters ranging from those expected for the CTF-ST down to parameters expected for ITER and NHTX. These experiments will be used to validate the scalings developed in lower field operation. The increase in parameter regime will provide an important test of the predictive capability of numerical models.

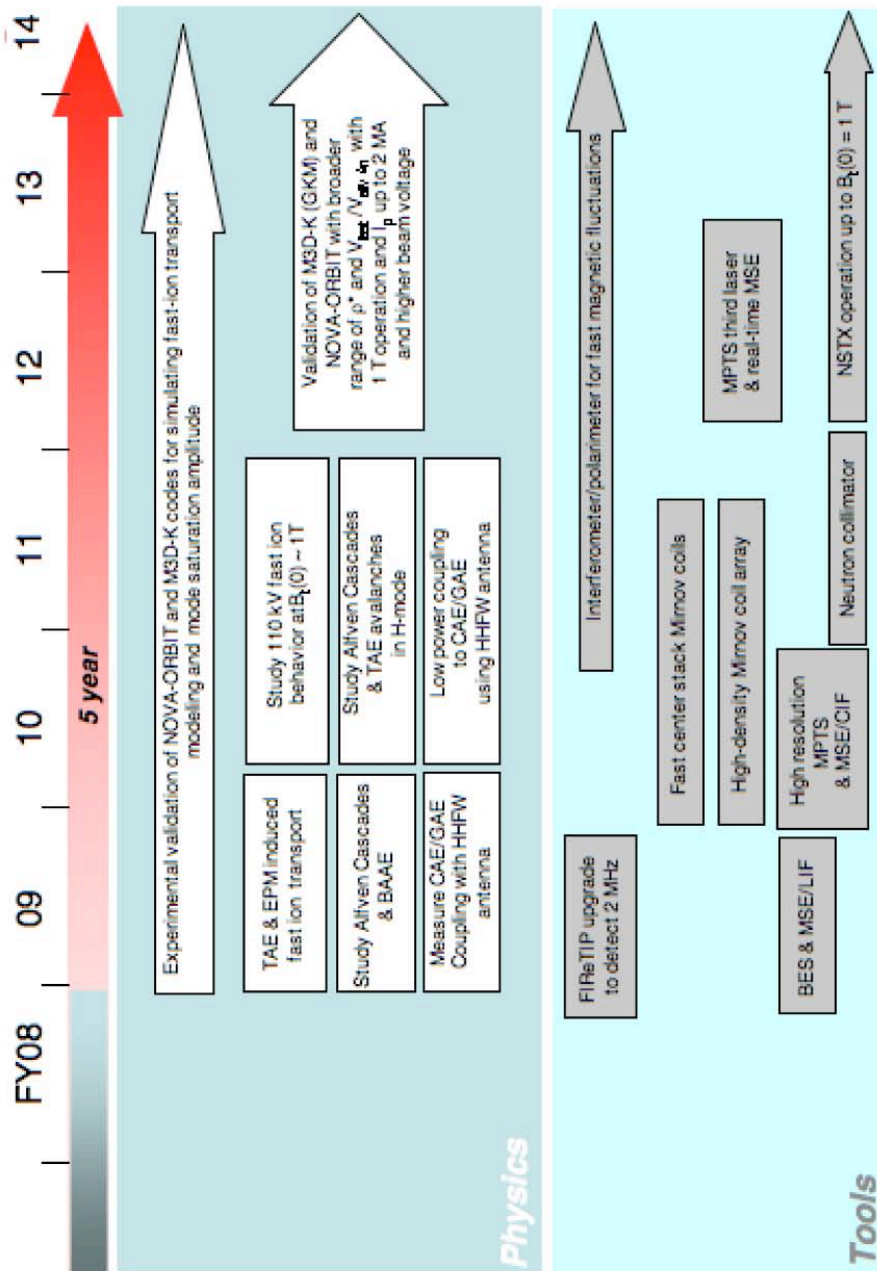
Compressional and Global Alfvén eigenmodes are predominantly excited through a Doppler-shifted ion cyclotron resonance,  $\omega \approx \omega_{ci} - k_{\parallel} V_{\parallel}$ , a form of drive for these modes probably unique to STs. The extension of  $V_{\text{fast}}/V_{\text{Alfvén}} \Rightarrow 1$  (relevant for ITER and NHTX) will open the possibility of the simpler resonant drive  $\omega \approx k_{\parallel} V_{\parallel}$ , tapping more fast-particle free energy. The higher field and current from the center stack upgrade will probably have little impact on stability of energetic particle modes (e.g., fishbones), but the additional beam line will allow for some control of the fast ion spatial and pitch-angle distributions.

The neutron collimator will provide additional high quality information on redistribution of fast ions by energetic particle driven instabilities. The second neutral beam line will greatly extend the range of fast ion anisotropies. The high frequency upgrade to Firetip should provide some internal mode amplitude and localization data for CAE/GAE frequency modes in H-mode plasmas. An experiment dedicated to the study of CAE/GAE hole-clumps, which provides important understanding of fast ion phase space transport, as well as tests present understanding of the non-linear behavior of energetic particle modes, will document the internal structure, as well as for the first time provide information on the poloidal localization of the modes and on the outboard local wavelength. Then an experiment will study the suppression of hole-clumps during HHFW heating to understand whether this reflects changes in the equilibrium plasma, or direct changes to the fast ion distribution. The BAAE modes will be revisited with the improved diagnostics to get better mode structure measurements and measurements of fast ion transport.

### 2009 – 2013 Timeline for HHFW/ECW/EBW Research



### 2009 – 2013 Timeline for Energetic Particle Research



## References

- 4.2.1 M. Ono, *Physics of Plasmas* **2**, 4075 (1995).
- 4.2.2 J. R. Wilson, *et al.*, *16<sup>th</sup> Topical Conf. on RF Power in Plasmas*, AIP Conf. Proc. **787**, 66 (2005).
- 4.2.3 J. Hosea, *et al.*, *17<sup>th</sup> Topical Conf. on RF Power in Plasma*, AIP Conf. Proc. **933**, 107 (2007).
- 4.2.4 J. Hosea, *et al.*, *Phys. Plasmas* **15**, 056104 (2008).
- 4.2.5 A. P. Smirnov and R. W. Harvey, *Bull. Amer. Phys. Soc.* **40**, 1837 (1995); CompX Report CompX-2000-01 (2001).
- 4.2.6 E. F. Jaeger, *et al.*, *Nucl. Fusion* **46**, S397 (2006).
- 4.2.7 A. L. Rosenberg, *et al.*, *Phys. Plasmas* **11**, 2441 (2004).
- 4.2.8 J. Hosea, *et al.*, *16<sup>th</sup> Topical Conf. on RF Power in Plasmas*, AIP Conf. Proc. **787**, 82 (2005).
- 4.2.9 J. B. Parker, *et al.*, *Bull. Amer. Phys. Soc.* **52**, 155 (2007)
- 4.2.10 P. T. Bonoli, *et al.*, *17<sup>th</sup> Topical Conf. on RF Power in Plasmas*, AIP Conf. Proc. **933**, 435 (2007).
- 4.2.11 P. M. Ryan, *et al.*, *Fusion Eng. and Design* **56-57**, 569 (2001).
- 4.3.1 C. E. Kessel, *et al.*, *Nucl. Fusion* **45**, 814 (2005).
- 4.3.2 Y-K. M. Peng, *et al.*, *Plasma Phys. Control. Fusion* **47**, B263 (2005).
- 4.3.3 I. B. Bernstein, *Phys. Rev.* **109**, 10 (1958).
- 4.3.4 A. K. Ram, and S.D. Schultz, *Phys. Plasmas* **7**, 4084 (2000).
- 4.3.5 J. Preinhaelter and V. Kopécky, *J. Plasma Phys.* **10**, 1 (1973).
- 4.3.6 E. Mjølhus, *J. Plasma Phys.* **31**, 7 (1984).
- 4.3.7 F. R. Hansen, *et al.*, *J. Plasma Phys.* **39**, 319 (1988).
- 4.3.8 C. B. Forest, *et al.*, *Phys. Plasmas* **7** 1352 (2000).
- 4.3.9 N. J. Fisch and A. Boozer, *Phys. Rev. Lett.* **45**, 720 (1980).
- 4.3.10 T. Ohkawa, National Technical Information Service Report No. PB2000-108008, 1976 and General Atomics Report No. GA-A13847, 1976].
- 4.3.11 A. K. Ram, A. Bers, and C. N. Lashmore-Davies, *Phys. Plasmas* **9**, 409 (2002)
- 4.3.12 G. Taylor, *et al.*, *Phys. Plasmas* **12**, 052511 (2005).
- 4.3.13 J. Preinhaelter, *et al.*, AIP Conf. Proc. **787**, 349 (2005).
- 4.3.14 S. J. Diem, *et al.*, *Rev. Sci. Instrum.* **77**, 10E919 (2006).
- 4.3.15 S. J. Diem, *et al.*, *17<sup>th</sup> Topical Conf. on RF Power in Plasma*, AIP Conf. Proc. **933**, 331 (2007).
- 4.3.16 H. P. Laqua *et al.*, *Phys. Rev. Lett.* **78**, 3467 (1997).



- 4.3.17 V. Schevchencko , *et al.*, Fusion Sci. Tech. **52**, 202 (2007).
- 4.3.18 V. Schevchencko , *et al.*, AIP Conf. Proc. **933**, 323 (2007).
- 4.3.19 A. Mueck, *et al.*, Fusion Sci. Tech. **52**, 221 (2007).
- 4.3.20 A.P. Smirnov, and R.W. Harvey, Bull. Am. Phys. Soc. **40**, 1837 (1995).
- 4.3.21 R.W. Harvey, and M.G. McCoy, *Proceedings of the IAEA Technical Committee on Advances in Simulation and Modeling of Thermonuclear Plasmas*, Montreal, Quebec (International Atomic Energy Agency, Vienna, 1993), p. 489; USDOC NTIS Doc. No. DE93002962.
- 4.3.22 G. Taylor, *et al.*, Phys. Plasmas **11**, 4733 (2004).
- 4.3.23 R.W. Harvey and G. Taylor, Phys. Plasmas **12**, 051509 (2005).
- 4.3.24 J. S. McKenzie, M.R. O'Brien and M. Cox, Comp.Phys.Comm. **66**, 194 (1991).
- 4.3.25 A. N. Saveliev, AIP Conf. Proc. **871**, 215 (2006).
- 4.3.26 A. K. Ram, J. Decker and Y. Peysson, *Proc. 14<sup>th</sup> Joint Workshop on ECE and ECRH*, (Santorini, Greece, May 2006) ed. Avrilios Lazaros (Heliotopos Conferences Ltd., Athens, Greece, 2006) p. 250.
- 4.4.1 N. J. Fisch and J.-M. Rax, Phys. Rev. Lett., **69**, 612 (1992)
- 4.4.2 G. R. Smith and A.N. Kaufman, Phys. Rev. Lett. **34**, 1613 (1975).
- 4.4.3 C. F. F. Karney and A. Bers, Phys. Rev. Lett. **39**, 550 (1977).
- 4.4.4 C. F. F. Karney, Phys. Fluids **21**, 1584 (1978).
- 4.4.5 J. Y. Hsu, K. Matsuda, M. S. Chu and T. H. Jensen, Phys. Rev. Lett. **43**, 203 (1979).
- 4.4.6 J. F. Drake and T. T. Lee, Phys. Fluids **24**, 1115 (1981).
- 4.4.7 J. M. McChesney, R. A. Stern, P. M. Bellan, Phys. Rev. Lett. **59** , 1436 (1987).
- 4.4.8 J. M. McChesney, P. M. Bellan and R. A. Stern, Phys. Fluids B **3** , 3363 (1991).
- 4.4.9 A. D. Bailey III, P. M. Bellan and R. A. Stern, Phys. Plasmas **2** , 2963 (1995).
- 4.4.10 A. D. Bailey III, R. A. Stern, and P. M. Bellan, Phys. Rev. Lett. **71**, 3123 (1993).
- 4.4.11 S. J. Sanders, P. M. Bellan, R A Stern, Phys. Plasmas **5** , 716 (1998).
- 4.4.12 N. N. Gorelenkov, H.L. Berk, and R.V. Budny, Nucl. Fusion **45**, 226 (2005).
- 4.4.13 E. D. Fredrickson, *et al.*, Nucl. Fusion **46**, s926 (2006).
- 4.4.14 H.L. Berk, B.N. Breizman and H. Ye, Phys. Lett. A **162**, 475 (1992).
- 4.4.15 H. L. Berk, B. N. Breizman, J. Fitzpatrick and H. V. Wong Nucl. Fusion **35**, 1661 (1995).
- 4.4.16 H. L. Berk, B. N. Breizman and M. Pekker, Nucl. Fusion **35**, 1713 (1995).
- 4.4.17 H. L. Berk, B. N. Breizman and M. Pekker, Phys. Rev. Lett. **76**, 1256 (1996).

- 4.4.18 N. A. Crocker, *et al.*, Phys. Rev. Lett. **97**, 045002 (2006).
- 4.4.19 T. H. Stix, Phys. Fluids **7**, 1960 (1964).
- 4.4.20 S. Puri, Phys. Fluids **9**, 2043 (1966).
- 4.4.21 S. Puri, D. A. Dunn, and K. I. Thomassen, Phys. Fluids **11**, 2728 (1968).
- 4.4.22 S. Q. Mah, H. M. Skaragard, and A. R. Strilchuk, Phys. Rev. Lett. **25** 1409 (1970).
- 4.4.23 A. Hirose, S. Q. Mah, H. M. Skarsgard, A. R. Strilchuk, Phys. Fluids **17**, 2147 (1974).
- 4.4.24 E. D. Fredrickson and P. M. Bellan, Phys. Fluids **28**, 1866 (1985).
- 4.4.25 D. Gates, R. White, and N. Gorelenkov, Phys. Rev. Lett. **87**, 205003 (2001).
- 4.4.26 N. N. Gorelenkov, *et al.*, Nucl. Fusion, **43**, 228 (2003).
- 4.4.27 G. Besson, *et al.*, Plasma Phys. and Cont. Fusion **28**, 1291(1986).
- 4.4.28 G. A. Collins, *et al.*, Phys. Fluids **29**, 2260 (1986).
- 4.4.29 A. B. Murphy, Plasma Physics and Cont. Fusion **31**, 21 (1989).
- 4.4.30 A Fasoli, *et al.*, Plasma Phys. Control. Fusion **44** (2002) B159–B172
- 4.4.31 M Brambilla, Plasma Phys. Control. Fusion **44** (2002) 2423.
- 4.4.32 E. D. Fredrickson, *et al.*, *Proc. of 29th EPS Conf. on Controlled Fusion and Plasma Physics*, Montreaux, 2002, (the European Physical Society, Geneva) ECA vol. 26B (2002), P-1.104.
- 4.4.33 E D Fredrickson, L. Chen, and R. B. White, Nucl. Fusion **43**, 1258 (2003).
- 4.4.34 E. D. Fredrickson, *et al.*, Phys. of Plasmas **10**, 2852 (2003).
- 4.4.35 S. Kaye, *et al.*, Phys. Plasmas **10**, 3953 (2003).
- 4.4.36 Ya. I Kolesnichenko, VS Marchenko and R B White, Phys. of Plasmas **13**, 052504 (2006).
- 4.4.37 W. W. Heidbrink, *et al.*, Plasma Phys. Control. Fusion **48**, 1347 (2006).
- 4.4.38 D. S. Darrow, *et al.*, *Proc. 19<sup>th</sup> IAEA Fusion Energy Conference, Lyon, France, 14-19 Oct 2002* (IAEA, Vienna)
- 4.4.39 H. L. Berk, *et al.*, Synopsis for 2006 IAEA meeting
- 4.4.40 D. Darrow, *et al.*, *Proc. 34<sup>th</sup> European Physical Society Conference on Plasma Physics* (Warsaw, Poland June 2-6, 2007), paper p1.117.
- 4.4.41 G-Y Fu, et al, " *Nonlinear Hybrid Simulations of Multiple Energetic Particle driven Alfvén Modes in Toroidal Plasmas*", 2007 APS DPP meeting, invited talk BI2/4.
- 4.4.42 N. N. Gorelenkov, *et al.*, *Proc. for the 34<sup>th</sup> European Physical Society Conference on Plasma Physics* (Warsaw, Poland June 2-6, 2007) paper I3.006.

- 4.4.43 N. N. Gorelenkov, *et al.*, submitted to Phys. Lett. A (2007).
- 4.4.44 B. N. Breizman and M. S. Pekker, Phys. Plasmas **12**, 112506 (2005).
- 4.4.45 E. D. Fredrickson, *et al.*, *Proc. for the 34<sup>th</sup> European Physical Society Conference on Plasma Physics* (Warsaw, Poland June 2-6, 2007) paper p1.106.
- 4.4.46 E. D. Fredrickson, *et al.*, “Beta suppression of Alfvén Cascade Modes in the National Spherical Torus Experiment” (accepted for Physics of Plasmas, 2007).
- 4.4.47 H. L. Berk, *et al.*, “Interpretation of Mode Frequency Sweeping in JET and NSTX”, *Synopsis for 2006 IAEA meeting*
- 4.4.48 E. D. Fredrickson, *et al.*, Phys. of Plasmas **13**, 056109 (2006).
- 4.4.49 E. D. Fredrickson, *et al.*, “Observation of Hole-Clump Pair Generation at Compressional and Global Alfvén Eigenmode Frequencies” (to be submitted to Physics of Plasmas, 2007)
- 4.4.50 H. L. Berk, B. N. Breizman and N. V. Petviashvili, Phys. Lett. A **234**, 213 (1997).
- 4.4.51 E. D. Fredrickson, *et al.*, Phys. Rev. Lett. **87**, 145001 (2001).
- 4.4.52 N. N. Gorelenkov, C Z Cheng, and E Fredrickson, Phys. Plasmas **9**, 3483 (2002).
- 4.4.53 E. D. Fredrickson, *et al.*, Phys. of Plasmas **9**, 2069 (2002).
- 4.4.54 N. N. Gorelenkov, *et al.*, Nucl. Fusion **42**, 977 (2002).
- 4.4.55 N. N. Gorelenkov, *et al.*, *Proc. 9<sup>th</sup> IAEA Fusion Energy Conference, Lyon, France, 14-19 Oct 2002* (IAEA, Vienna) paper IAEA-CN-94/TH/7-1 Ra
- 4.4.56 N. N. Gorelenkov, *et al.*, Nucl. Fusion, **43**, 228 (2003).
- 4.4.57 E. Belova, *et al.*, “Numerical Study of Instabilities Driven by Energetic Neutral Beam Ions in NSTX” in *Proc. of the 30<sup>th</sup> European Physical Society Conference on Controlled Fusion and Plasma Physics* (St. Petersburg, Russia, July 2003).
- 4.4.58 V. S. Belikov *et al.*, Phys. of Plasmas **10**, 4771 (2003).
- 4.4.59 E. D. Fredrickson, N. N. Gorelekov and J. Menard, Phys. of Plasmas **11**, 3663 (2004).
- 4.4.60 E. Hameiri, A. Ishizawa and A. Ishida, Phys. Plasmas **12**, 072109 (2005).
- 4.4.61 Ya. Kolesnichenko, R. B. White, and Yu. V Yakovenko, Phys.of Plasmas **13**, 122503 (2006).
- 4.4.62 W. W. Heidbrink, *et al.*, Nucl. Fusion **46**, 324 (2006).
- 4.4.63 W. W. Heidbrink and G. J. Sadler, Nucl. Fusion **34**, 535 (1994).
- 4.4.64 S. S. Medley and A. L. Roquemore, Rev. Sci. Instrum. **75**, 3625 (2004).

- 4.4.65 J. E. Menard, *et al.*, Phys. Rev. Lett. **97**, 095022 (2006).
- 4.4.66 S. S. Medley, *et al.*, Nucl. Fusion **44**, (2004) 1158
- 4.4.67 S. S. Medley, *et al.*, “*Status of Recent Experimental and Analytical Investigation of MHD-Induced Energetic Ion Redistribution or Loss in the National Spherical Torus Experiment*” Princeton Plasma Physics Laboratory Report, PPPL-4235 (2007)
- 4.4.68 S. S. Medley, *et al.*, “*Neutral Particle Analyzer Vertically Scanning Measurements of MHD-Induced Energetic Ion Redistribution or Loss in the National Spherical Torus Experiment*,” Princeton Plasma Physics Laboratory Report, PPPL-4270 (2007)

## Chapter 5 - Boundary Physics

5.1 Executive Summary.....	5.2
5.1.1 LLD program and fueling program.....	5.5
5.1.2. SOL turbulence and width program.....	5.15
5.1.3. ST divertor physics and heat flux control.....	5.23
5.2 H-mode pedestal, ELMs, and power threshold .....	5.33
5.2.1. H-mode Pedestal and ELM physics.....	5.33
5.2.2. L-H threshold physics.....	5.44
References.....	5.48

*This page intentionally left blank*

## Chapter 5 - NSTX Boundary Physics 5 year plan

NSTX Boundary Physics Group

### 5.1 Executive Summary

Boundary physics research in NSTX is geared toward 1) continued development and improvement of NSTX operational scenarios, 2) development of the physics basis for future STs, 3) contribution to toroidal confinement physics, e.g. by comparison with high aspect ratio tokamaks, and 4) direct contributions to ITER R & D needs. Nearly all of the main upgrades in this five-year plan represent opportunities to enhance our boundary physics understanding: 1) the Liquid Lithium divertor (LLD) and core fueling program represents a bold idea to control plasma-wall interactions; 2) the center stack upgrade with higher  $I_p$  and  $B_t$  will enable access to lower  $v_e^*$  than presently available; 3) enhancements to the EFCC/RWM capabilities enable extra flexibility to understand and control the H-mode pedestal and edge localized modes; and 4) the second NBI system (for which preparations are being made in this plan) enables studies of plasma-wall interactions at peak heat fluxes beyond ITER and toward DEMO.

The second NBI and the center stack upgrade represent not only opportunities but also responsibilities, in that the high levels of heat flux and intense plasma-wall interaction must be managed for time scales  $\sim 5$ sec, nearly tripling today's longest NSTX discharges of 1.8 sec. The combination of these facility enhancements will enable access to even lower  $v_{\square}^*$  (e.g. Fig. 5.0.1) and longer SOL connection length

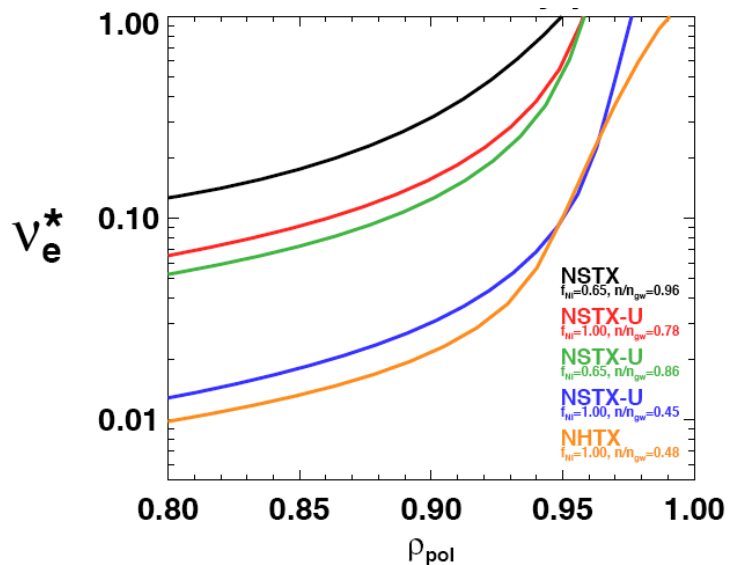


Fig. 5.0.1- Comparison of predicted edge electron collisionality  $v_e^*$  for present NSTX, NSTX-U (center stack + 2<sup>nd</sup> NBI) at two  $n/n_{GW}$  and NHTX.

for more detailed SOL width and heat flux management studies. Quantitatively the  $v_{\square}^*$  in the edge region is predicted to drop up to an order of magnitude, and within a factor of 2 of the level predicted for NHTX.

A new long pulse divertor will be designed to handle the longer pulse length enabled by the center stack and higher heating power provided by the 2<sup>nd</sup> NBI. The highest peak heat flux observed in NSTX is  $\sim 10 \text{ MW/m}^2$ , although up to  $15 \text{ MW/m}^2$  has been transiently seen. For the present outer divertor ATJ graphite tiles, this range of peak heat flux translates into a maximum pulse length of 2-3 sec. before a  $1200 \text{ }^\circ\text{C}$  administrative limit on PFC surface temperature would be exceeded. Moreover the scrape-off layer (SOL) heat flux width could well shrink at the lower  $v^*$  from higher  $I_p$ ,  $B_t$ , and  $P_{\text{NBI}}$  values, i.e. the peak heat flux could be even higher, necessitating a new divertor implementation. To manage these levels of heat flux, double-null configuration, large flux expansion, and detachment may all be needed, and novel divertor schemes (e.g. X-divertor, super X-divertor, or snowflake divertor) may also be required.

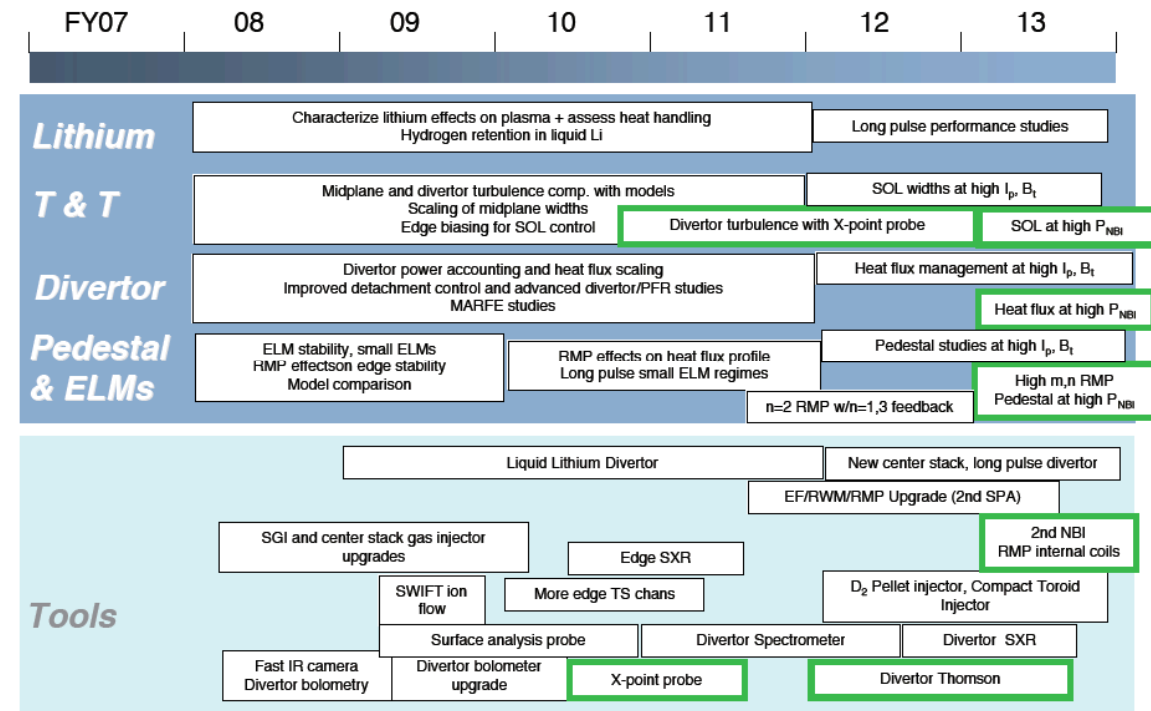
At the highest level, the boundary program has a SOL/divertor physics component and an H-mode physics component. The first area is discussed below in the context of several themes: lithium and fueling research, SOL transport and width research, and divertor physics research with an emphasis on heat flux management. The second area is discussed in the context of two themes: pedestal and ELM research, and H-mode operational window research, with an emphasis on power threshold studies. Progress in all of these areas relies both on the facility upgrades discussed above and a set of diagnostic upgrades, listed below and discussed in detail in the following sections:

1. LLD diagnostics in the toroidal gaps between LLD segments, including thermocouples, Langmuir probes, and a two-color IR measurement
2. A divertor bolometer upgrade
3. Additional Thomson channels near the pedestal and separatrix
4. A divertor spectrometer
5. A high-resolution edge soft X-ray system for fast  $T_e$  profiles
6. A Ly- $\alpha$  detector array
7. A DiMES-like surface analysis probe



8. A divertor soft X-ray system for fast  $T_e$  profiles
9. An X-point reciprocating probe (incremental)
10. A divertor Thomson scattering system (incremental)

The overall time-line of the boundary physics program is shown below.



\* incremental budget needed

## Sec. 5.1.1 – LLD program and fueling program

### 1. Introduction

High-performance, long-pulse NBI-heated small-ELM H-mode plasma discharges have been developed in NSTX as prototypes for confinement and current drive extrapolations to future spherical tori<sup>1</sup>, but these exhibit a secular density rise. A critical issue for the achievement of sustained non-inductive current drive H-mode plasmas is the control of this density rise and impurity influx. Lithium as a plasma-facing component (PFC) has potential for providing particle pumping because of its ability to pump hydrogen and reduce oxygen because of its high chemical reactivity. Given the preliminary success of lithium coatings for wall pumping, additional fueling mechanisms will be implemented to provide density control. Each of these elements: pumping and fueling, are described sequentially in this section.

Experiments to date have demonstrated improvements in plasma performance with lithium PFC's<sup>2-6</sup>, but they have primarily focused on limiter tokamak discharges in the low confinement mode (L-mode). However, future devices on the fusion energy development path such as ITER and DEMO are divertor machines. The efficacy of lithium as a PFC in divertor plasmas in the high confinement mode (H-mode) thus needs to be determined, and NSTX provides a unique opportunity for such research. The evaluation of lithium in NSTX has been conducted in a phased, three-part program to investigate density and impurity control through 1) lithium pellet injection, 2) evaporative lithium coatings on PFC's, and 3) a liquid lithium divertor. If successful, the achievement of low edge collisionality and improved confinement with lithium PFC's in NSTX would lead to a more thorough and favorable extrapolation to next-step STs and magnetic fusion energy devices in general.

Present options for fueling long pulse discharges include conventional gas puffing, high-velocity cryogenic fuel pellets, and compact toroids (CTs). Because of its technical simplicity, gas injection at the plasma edge is universally used for fueling of high-temperature plasmas in present day devices. As in high aspect ratio tokamaks, the gas fueling operating range in NSTX is defined by plasma operational limits and the injector poloidal location. The low density operational limit is determined by the onset of

a locked mode due to error fields or reconnection events, and by large type I ELMs in NBI-heated H-mode plasmas. The upper gas fueling limit is set by the onset of disruptive MHD modes, sawteeth, and confinement degradation. An additional operational constraint is H-mode access.

Gas fueling has well-known shortcomings: the low fueling efficiency (between 1 - 20%), and gas loading of in-vessel surfaces leading to uncontrolled fueling of plasma by out-gassing and recycling. Supersonic gas injection offers improved fuel control and enhanced fueling efficiency, as compared with standard gas puffing. Pellets are commonly used in present day devices for core fueling, while CTs have been tested with some success on a few devices.

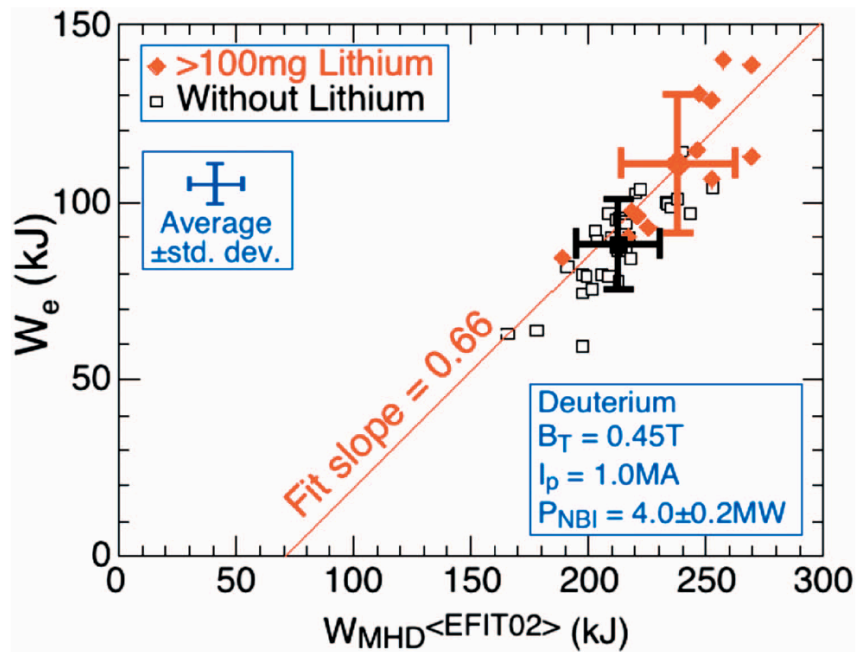


Fig. 5.1.1.1- L1 surface coatings improved plasma stored energy, mainly through electron channel.

## 2. Background and Results

### Lithium wall coating results

Recent NSTX experiments have shown significant and recurring benefits of lithium coatings on PFC's to the performance of divertor plasmas in both L- and H- mode confinement regimes heated by high-power neutral beams<sup>7</sup>. In 2005, a reduction in recycling was achieved in NSTX plasmas with lithium pellet injection (LPI). Low-Lithium pellets in the range of 2 to 5 mg were injected into both limiter and divertor plasmas. Measurements of the visible light emission from the plasma edge indicated that the injected lithium was deposited primarily in the vicinity of the discharge contact area. The first neutral beam-heated L-mode discharge that followed a discharge with LPI showed a reduction in the volume-average plasma density of about a factor 2 compared

with to a similar discharge prior to the introduction of lithium. This was also observed in higher density H-mode plasmas. While the reduction in density did not persist in subsequent discharges, there was enough of an effect to suggest that more coverage of PFC's with lithium might improve particle pumping.

During NSTX experiments in 2006 and 2007, lithium coatings were produced with a single oven mounted on the upper dome of the vacuum vessel<sup>7, 8</sup>. This LITHium EvaporatoR (or LITER) directed a collimated stream of lithium vapor downwards toward the graphite tiles of the lower center stack and divertor. In 2006, lithium deposition prior to a plasma shot decreased the plasma density, inductive flux consumption, and ELM frequency and increased the electron temperature, ion temperature, energy confinement time, and DD neutron rate. In addition, extended periods of MHD quiescence were observed.

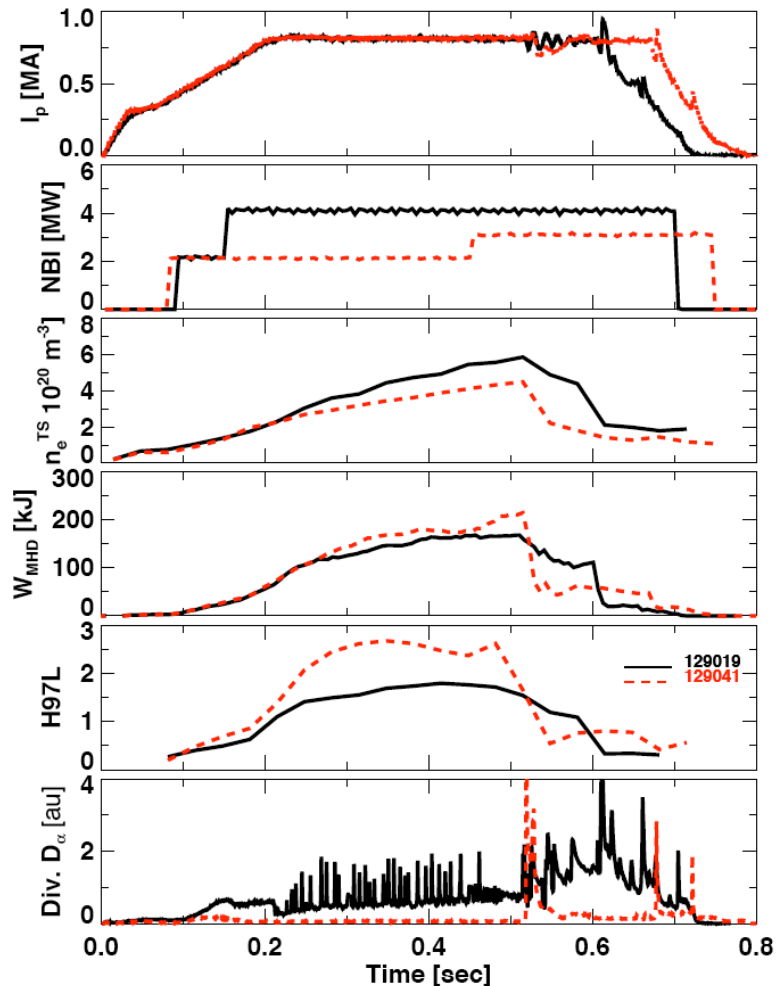


Fig. 5.1.1.2- Comparison of pre-(black) and post-LiTER(red) discharges with double LiTER system in 2008.

Measurements of the visible emission from the lower divertor also showed a reduction in the deuterium, carbon, and oxygen line emission. However, the improvements in plasma conditions were transient and performance reverted to the pre-lithium conditions by the following discharge unless the evaporation was resumed.

Erosion or passivation of the thin coating on the contact areas on the divertor by

plasma heat and particle fluxes and lithium reactions with the graphite substrate were possible explanations for the transient nature of the 2006 improvements. Such considerations motivated a LITER upgrade in 2007 to a larger diameter exit duct and improved heaters, and the re-aiming of the evaporator to increase the divertor target deposition rate by a factor of three. In addition, the 2007 LITER experiments involved continuous deposition between and during discharges. Generally both electron stored energy ( $W_e$ ) and total plasma stored energy ( $W_{MHD}$ ) increased following lithium deposition (Fig. 5.1.1.1). Although there is variability in the plasma performance, it is clear that both the best and the average confinement occurred after lithium and that the increase in  $W_{MHD}$  occurs mostly through an increase in  $W_e$ .

Other salient results with lithium evaporation included a broadening of the electron temperature profile, and changes in edge density gradients that benefited electron Bernstein wave coupling. Significant modifications to ELM behavior were also observed, as shown in Fig. 5.1.1.2. A reduction in ELM frequency and amplitude, followed by a period of complete ELM suppression, occurs in plasmas after lithium deposition<sup>8</sup>. There is a corresponding increase in  $W_{MHD}$  during the period when large ELMs are greatly reduced (0.3 - 0.5 s.). The power step from 2- $\rightarrow$ 3 MW in the post-LiTER discharge resulted in  $\beta_N > 5.5$ , i.e. the global  $\beta_N$  was exceeded. Keeping the NBI power fixed at 2 MW resulted in a longer discharge with a continuous increase in radiated power, owing to impurity accumulation in the ELM-free discharge.

#### Fueling program results

It has been demonstrated experimentally in both NSTX and MAST that H-mode plasmas fueled by a high field side (HFS) gas injector have much lower power thresholds and better reproducibility<sup>9, 10</sup>. It has been suggested that the effect could be

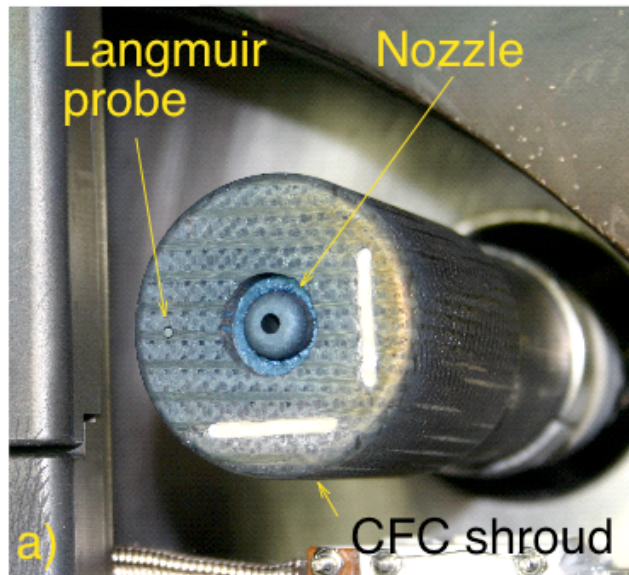


Fig. 5.1.1.3 - Photo of a supersonic gas injector inside NSTX

attributed to the charge-exchange viscous drag for neutral sources. The drag from LFS fueling is higher than from the HFS because the ions lost to charge exchange have the highest toroidal velocity at the outer midplane where the toroidal field is weakest. However the present HFS midplane injector on NSTX does not allow control of the gas flow duration, and as a result, the  $n_e$  typically increases continuously at a rate of  $dN_i/dt < 7 \times 10^{20} \text{ s}^{-1}$ . To address fueling efficiency and gas injection control issues, a supersonic gas injector was recently implemented.

The low field side supersonic gas injector (SGI) on NSTX consists of a small converging-diverging graphite Laval nozzle and a piezoelectric gas valve (Figure 5.1.1.3).

The nozzle is capable of producing a deuterium jet with Mach number  $M=4$ , estimated gas density at the nozzle exit  $n \sim 5 \times 10^{23} \text{ m}^{-3}$ , estimated temperature  $T < 70 \text{ K}$ , and flow velocity  $v = 2.4 \text{ km/s}^{11-13}$ . Despite the beneficial L-mode fueling experience with supersonic jets in limiter tokamaks, there is a limited experience with fueling of high-performance H-mode divertor discharges and the associated density, MHD stability, and MARFE limits<sup>14-16</sup>. In

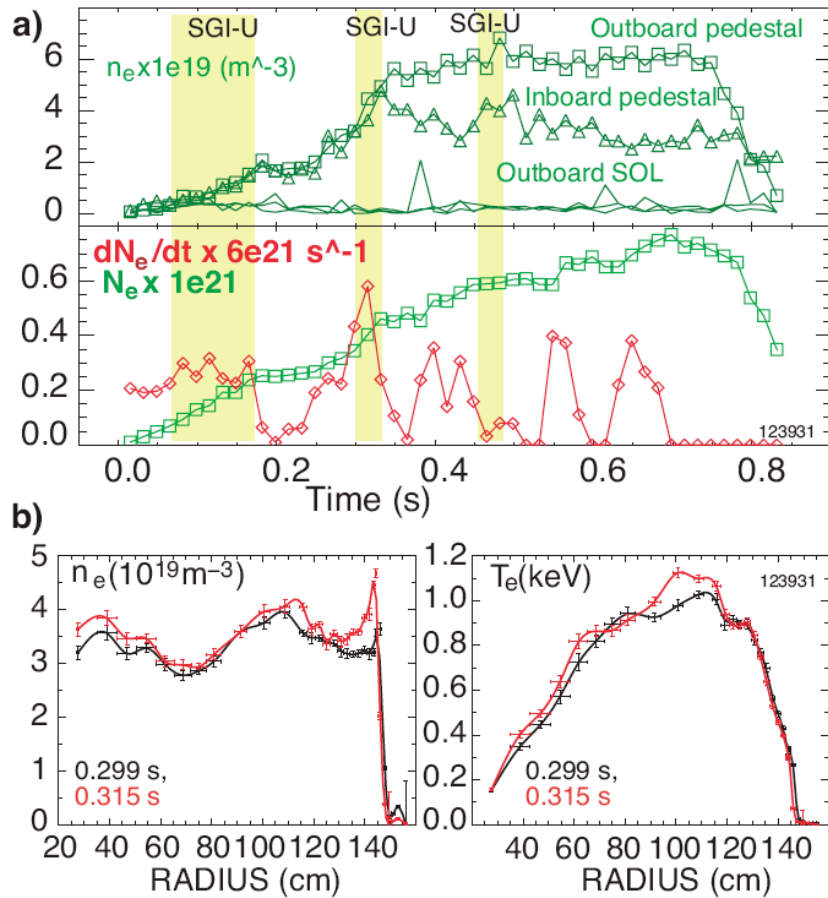


Fig. 5.1.1.4- discharge with SGI fueling: (a) inner and outer pedestal  $n_e$ , as well as outboard SOL density are shown, along with SGI pulses in yellow, and the evolution of electron inventory ( $N_e$ ) and  $dN_e/dt$ ; (b) profiles of  $n_e$  and  $T_e$  before and during an SGI pulse.

initial supersonic deuterium jet fueling experiments in NSTX, a reliable H-mode access, a low NBI power threshold,  $P_{LH} < 2$  MW, and a high fueling efficiency (0.1-0.4) have been demonstrated (e.g. Figure 5.1.1.4)<sup>17, 18</sup>. Progress has also been made toward a better control of the injected fueling gas by decreasing the uncontrolled high field side (HFS) injector fueling rate by up to 95 % and complementing it with the supersonic jet fueling<sup>19</sup>.

### 3. Plans (FY09-10)

The primary goal of lithium PFC research on NSTX in FY09-10 is to investigate the effects of a liquid lithium divertor (LLD) on plasma performance, e.g. its ability to provide density control through deuterium pumping, its effect on edge/ELM stability, and its effect on electron transport and global confinement. The LLD is about 20 cm wide, and will be located on the outboard divertor (OBD) about 5 cm outboard of the gap for coaxial helicity injection (CHI) between the OBD and the inboard divertor. (toroidal view shown schematically in Fig. 5.1.1.5). The location and dimensions of the LLD were

chosen so that the density would be reduced by 50-60% in low-triangularity plasmas, and 25-30% in high triangularity plasmas (poloidal cut shown schematically in Fig. 5.1.1.6). These density reduction estimates were obtained from 0-D modeling,

2-D data constrained pumping simulations have just begun<sup>20</sup>. Starting from a well documented H-mode discharge ( $I_p=0.8$

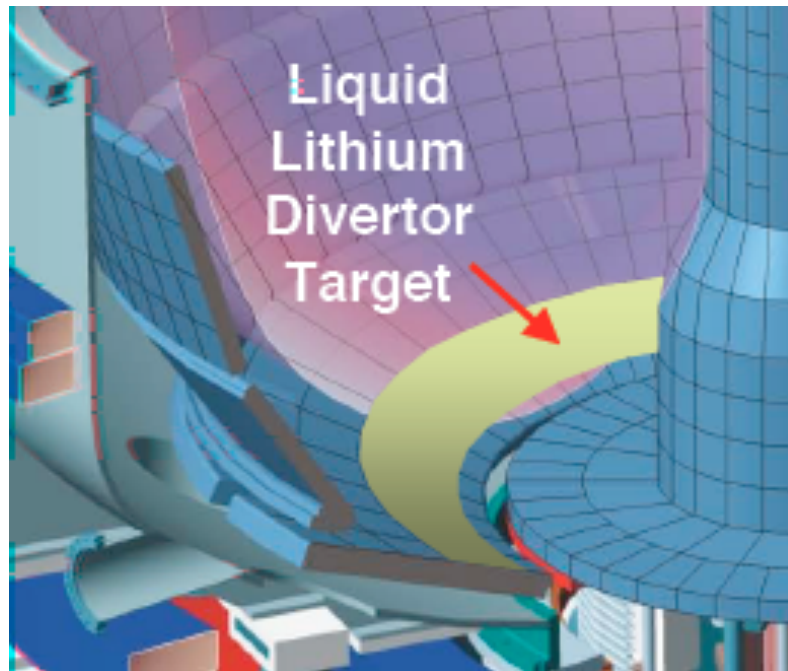


Fig. 5.1.1.5- LLD tray shown schematically as an annulus located physically on the outboard divertor. There are 4 toroidal breaks in the LLD for installation ease, and the tiles between the breaks contain many diagnostics.

MA,  $B_t=0.45$  T,  $P_{\text{NBI}}=1$  MW), the cross-field transport coefficients were varied to match available profiles. The recycling coefficient was then reduced to simulate the effect of lithium pumping. A strong increase in divertor  $T_e$ , decrease in divertor  $n_e$ , and a  $\sim 50\%$  increase in peak heat flux was predicted (see Fig. 5.1.1.7).

Initial plans are to coat the LLD surface with lithium using the LITER evaporators. A unique feature of the LLD is that it will have heaters to maintain its temperature between 200C and 400C. This is sufficient to keep the lithium on its surface molten and actively pumping, but not significantly evaporating. Built-in thermocouple arrays (toroidal and radial) will be used to confirm the LLD temperature. The plan is to install the LLD in time for the FY 2009 run. Details on the technical design aspects are given in the chapter 7 on facility enhancements.

The LLD is a temperature-controlled copper plate with a thin stainless steel layer to protect it from the lithium. A porous molybdenum coating will be plasma-sprayed onto the stainless steel. The characteristics of LLD for particle pumping and hydrogen retention will be determined during NSTX plasma operations in FY09. It may be possible to upgrade the LLD to a version with a mesh that allows a higher lithium inventory, if offline tests of the concept are successful.

The LLD will have four toroidal segments, with graphite tiles providing breaks between these segments. The four sets of graphite tiles will contain 1) a finely spaced Langmuir probe (4mm radial separation over

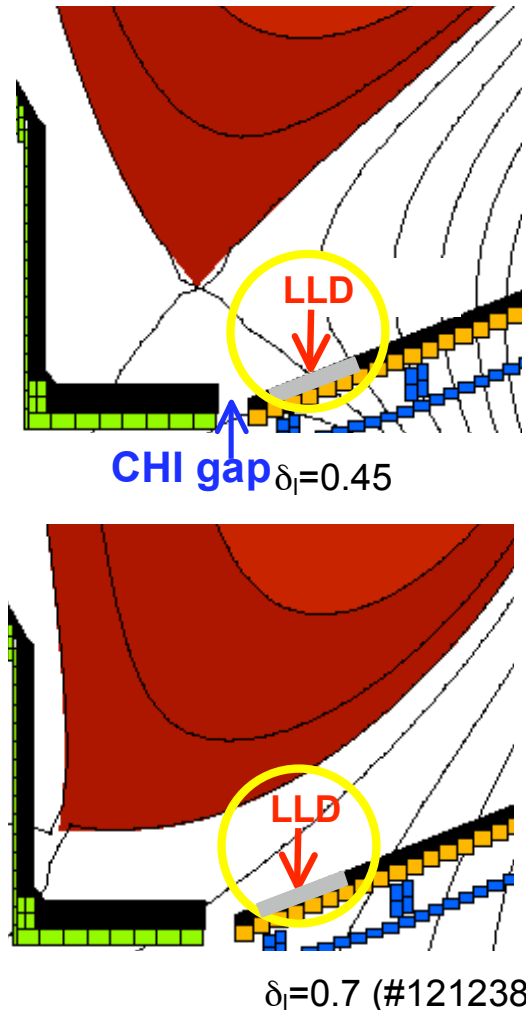


Fig. 5.1.1.6- Poloidal cut of LLD with high low  $\delta$  and high  $\delta$  equilibria. Calculations showed that the LLD would reduce density in these shapes by about 50% and 25%



a 10cm range), 2) magnetic probes for equilibrium reconstruction, and 3) two sets of electrodes for SOL biasing studies. In addition there will be top-down views for 1 slow IR camera (30 Hz), 1 fast IR camera (10 kHz), several 1-D linear arrays for recycling measurements, and several 2-D visible cameras to determine the impact of the LLD on divertor parameters.

LLD Plans for FY09-10 (more details given in section 5.1.3 plans):

- Install and characterize plate-based LLD operation
- Perform hydrogen retention and pumping efficiency studies, i.e. gas balance experiments
- Optimize efficiency of gas injector fueling
- Model pumping efficiency of LLD and effect on the edge and divertor plasma with DEGAS-2, SOLPS, UEDGE, and XGC codes.

*New tools:* LLD + diagnostics, upgraded supersonic gas injector, programmable center stack gas injector, CHERs capability to measure Li density and core concentration.

Fueling Plans for FY09-10:

Near-term plans on H-mode fueling optimization studies on NSTX include two efforts: one with HFS gas injection fueling, and one with the supersonic gas injector. Both efforts will be an integral part of the particle balance, fueling efficiency and density control studies with the LLD.

Initial work with the high field side injector in the upper corner of the machine (“shoulder”) demonstrated equally reliable H-mode access and low power threshold in shoulder-fueled H-modes in comparison with H-modes fueled from the HFS midplane

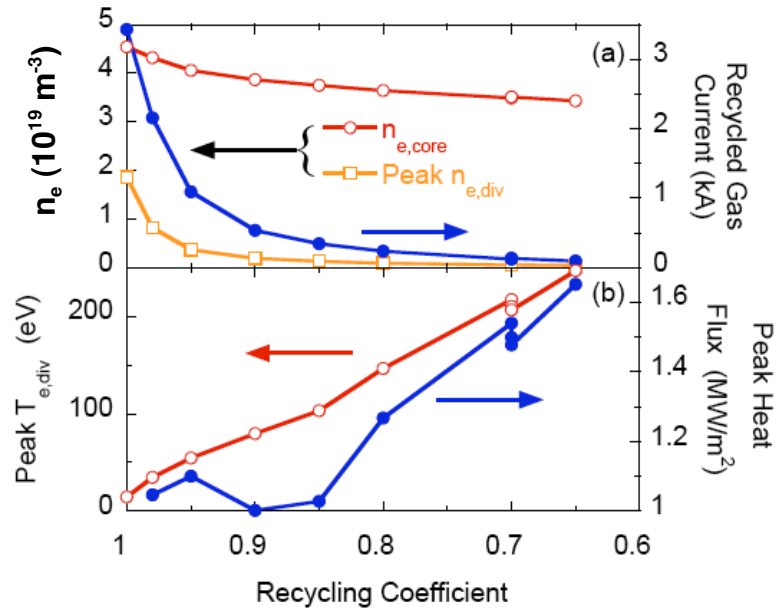


Fig. 5.1.1.7- Effect of reduced recycling coefficient on upstream ( $n_{e,core}$ ) and divertor  $n_e$ ,  $T_e$ , and  $q_{peak}$ , from a UEDGE simulation.

gas injector. We plan to implement a fully controllable shoulder gas injector, thus enabling the development of controlled HFS fueling scenarios – this is not possible for the HFS midplane injector because of limited space. Since the HFS fueling efficiency is fairly high, the goal of fueling optimization is to develop a reduced density H-mode with a possible feedback of density from the HFS shoulder injector. In addition, the supersonic gas jet is also viewed as a candidate for high-efficiency well-controlled gas fueling compatible with reliable H-mode access. The main effort will be the development of an SGI-fueled long-pulse high performance low-density H-mode plasma scenario with the locked mode correction and a density feedback algorithm with SGI.

Also, the fueling and penetration characteristics of the supersonic gas jet will be studied in detail. Specifically, we plan to carry out detailed measurements of penetration and fueling characteristics of the SGI with fast cameras, the upgraded multi-channel Far Infrared Tangential Interferometer / Polarimeter (FIRETIP) diagnostic, and the Langmuir probes. These measurements will be compared with the analytic neutral penetration model, and the DEGAS 2 neutral transport numerical model. We will try to improve the jet characteristics (density, collimation) with various supersonic nozzle designs, including the cryogenically cooled nozzle specially designed to achieve deuterium clustering. Laboratory tests will be carried out to characterize jets obtained with simple converging, conical nozzles and cryogenic nozzles. Finally, we plan to study the H-mode access and pedestal characteristics of the SGI-fueled H-modes. Specifically, the expected deeper penetration of the supersonic gas jet could change the pedestal characteristics (width, collisionality) beyond the limits defined by gas or recycling fueling.

#### **4. Plans (FY11-13)**

##### LLD Plans for FY11-13:

The objective for FY11-13 is to build on the operational experience with the LLD for long pulse experiments in NSTX. If the LLD provides the anticipated particle control, the fueling requirements for long pulse operation will be met with advanced capabilities such as pellet and compact toroid injection.

The LLD itself will be further upgraded for long pulse plasmas. The present LLD has been designed for particle pumping with static lithium surfaces; as such, it will have

limited heat removal capabilities. An upgrade to the LLD is envisioned during FY11-12, possibly consisting of a mesh-based system or technical improvements to the heaters, etc. Finally a long pulse divertor design will be needed around the time of the center stack and NBI upgrades. A flowing lithium system (LLD-Upgrade) is a candidate to handle the high heat fluxes and long pulses, depending on the success of the LLD. Experiments on CDX-U demonstrated that convection can play a major role in dissipating heat for liquid lithium<sup>21</sup>. By reducing the flow requirements for the liquid lithium, this has the potential of greatly simplifying the LLD-Upgrade design. IR cameras would be used to determine if convection is indeed occurring in such a system.

#### Fueling Plans for FY11-13:

While the near-term fueling plans focus on improvements and optimization of gas fueling, the longer-term goals are the implementation of a cryogenic pellet injector for central fueling, and a compact toroid injector for edge fueling and profile control. Pellets are a well-characterized core fueling option which would enable a range of additional studies, e.g. high density limits beyond Greenwald scaling, perturbative transport experiments, etc. The CT injector would provide not only efficient fueling, but also a possibility of ionization profile control and plasma profile control (including the momentum profile as the CT is a momentum source), both being attractive features for high-performance scenario optimization. Regarding this option, the CT injector previously used on the TdeV device is being stored on-site at PPPL. The cost of bringing the CT injector on-line would include retro-fitting it to NSTX and supporting a CT-centered fueling program. A programmatic decision on whether to install a pellet injector and/or the CT injector will be made in FY 2010, depending on the need for core fueling techniques with LLD operation. These tools would be available for the FY 2012 run.

## Sec. 5.1.2 – SOL turbulence and width program

### 1. Introduction

The ‘scrape-off layer’ (SOL) is the region of the boundary plasma just outside the magnetic separatrix or last-closed-flux surface (LCFS). Most of the heat and the particle flux which exits from the main plasma enters the SOL and then flows along and across the magnetic field to the first wall or divertor plates. The width of the SOL is a measure of the radial distance over which the plasma parameters decay by  $(1/e)$  outside the separatrix or LCFS. There are generally different widths for density  $\lambda_n$ , temperature  $\lambda_T$ , and total heat flux  $\lambda_q$ , and these can vary under different plasma conditions and at different places around the tokamak.

The importance of the SOL width is that it determines the local heat and particle fluxes to various parts of the wall and divertor. The local heat flux to the divertor plate must be kept below material damage limits, which becomes difficult to do if the heat SOL width is too small. Furthermore, the local particle flux must also be kept high enough to allow efficient exhaust of helium ash at the pumping port near the divertor plate. In addition, the heat and particle flux at other locations around the machine must also be low enough to avoid damage to those components, and the plasma density near some of the RF heating antennae must be high enough for good coupling. Besides these constraints on the SOL plasma itself, the SOL width may also indirectly affect several core plasma properties such as the impurity content, plasma rotation, and energy confinement. All of these interacting physics issues and potentially conflicting requirements make an understanding of the width of the SOL an interesting and important topic. The main proposed facility enhancements: 1) LLD, 2) larger center stack for higher  $I_p$ ,  $B_t$  and longer pulse, and 3) second NBI system will enhance the research in this area by enabling a larger  $\beta$  range, lower  $v^*$ , and higher  $P_{SOL}$ , extending physics studies closer to the parameter ranges for next step STs.

### 2. Background and results

Measurements have been made of tokamak SOL parameters and widths for many years with consistent results, e.g.  $\lambda_n \sim 1\text{-}3$  cm (see Ref. <sup>22</sup> for an early review, and Ref. <sup>23</sup>

for a recent review of JET results). These widths are the net result of the perpendicular transport across B over a timescale determined by the parallel transport to the divertor plates. Modern edge codes such as UEDGE<sup>24</sup> and B2-Eirene<sup>25</sup> still can not explain (or predict) these SOL widths from first principles due to an incomplete understanding of the physics that determines the perpendicular (and to some extent the parallel) transport. The goal of NSTX SOL research is help to provide such an understanding, from which it should eventually be possible to predict the SOL width in future tokamaks like ITER.

The parallel transport processes in the SOL are generally considered to be dominated by the classical heat and particle conduction along B. Recently NSTX has already made a significant contribution by testing this assumption experimentally. The upstream SOL widths for  $T_e$  and  $n_e$  as measured by the mid-plane fast reciprocating probe ( $z = -18\text{cm}$ ) were compared with the target heat flux ( $q_{\text{target}}$ ) width measured by IR camera. The use of an offset exponential for the profiles in the parallel conduction equation led to an additional factor to the theoretical relation between  $T_e$  and  $q_{\text{target}}$  SOL widths. The ratio of these two values showed an agreement between theory and experiment within  $\sim 20\%$ , implying that the parallel electron conduction for the near-SOL was consistent with the classical model<sup>26</sup>.

The perpendicular transport in the SOL is generally considered to be dominated by turbulence, including both diffusive and convective (intermittent or ‘blob’ transport) processes. NSTX has also made significant contributions to the measurement and understanding of these transport mechanisms. The gas puff imaging diagnostic (GPI)<sup>27</sup> was developed at NSTX to measure SOL turbulence and was used to characterize the

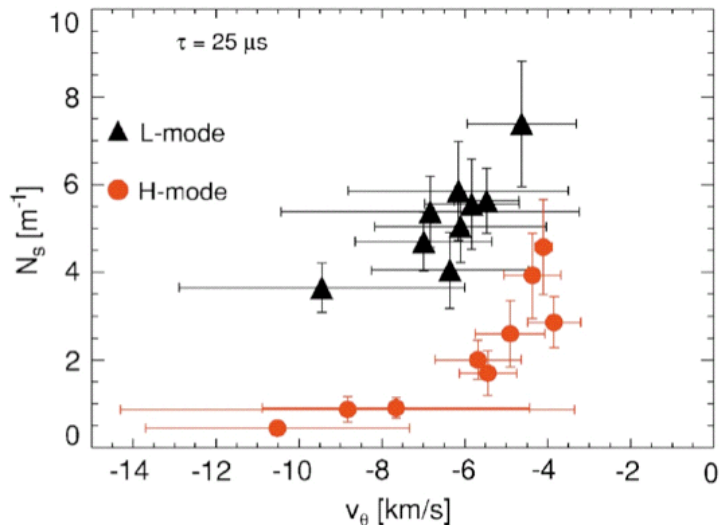


Fig. 5.1.2.1- Blob density vs/ poloidal propagation speed from GPI analysis.

structure of coherent filaments or ‘blobs’ in the SOL<sup>28, 29</sup>; for example, the linear density of blobs was seen to decrease significantly from L-mode to H-mode, as shown in Fig. 5.1.2.1. SOL profiles and turbulence characteristics were measured using Langmuir probes<sup>30</sup> and compared with the results from DIII-D. In the area of theory, initial studies have been carried out by the Lodestar group<sup>31, 32</sup>. It was found that the observed radial blob velocities in NSTX are bounded by theoretically predicted maximum and minimum velocities corresponding to the sheath-connected and resistive-ballooning regimes of blob transport (see Fig. 5.1.2.2)<sup>33</sup>.

### 3. Empirical studies and exploration (FY09-10 and FY11-13)

Given our present limited theoretical understanding of the SOL width, it is useful to continue empirical studies and scalings<sup>34, 35</sup>, and to explore new regimes and measurement techniques. In particular, empirical results on the comparison between carbon and lithium divertor surfaces will be a unique contribution from NSTX. These results will be especially valuable to help estimate SOL widths in future ST devices such as NHTX and ST-CTF.

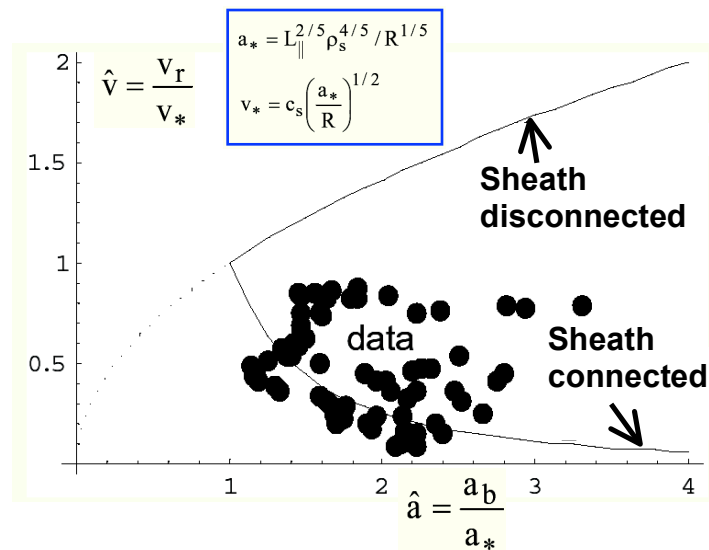


Fig. 5.1.2.2- Normalized blob speed vs. normalized blob radius from NSTX data.

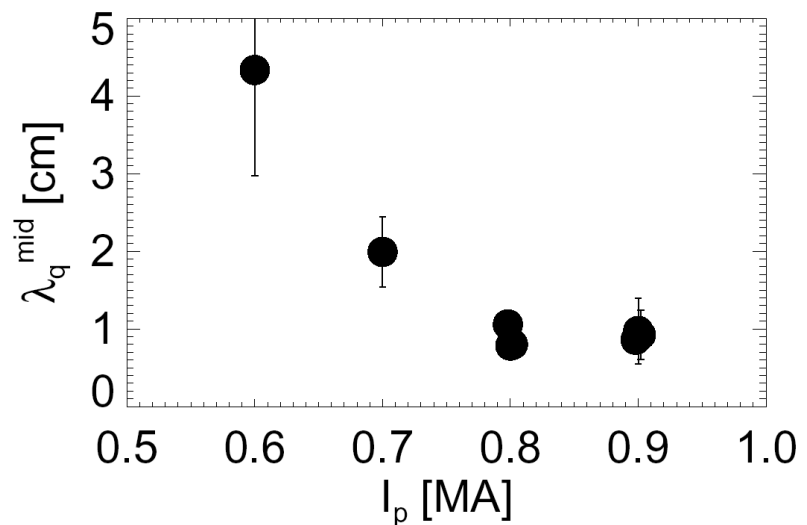


Fig. 5.1.2.3- Heat flux profile ( $\lambda_q^{\text{mid}}$ ) width decreased with plasma current ( $I_p$ )

Plans for FY2009-2010:

a) study of SOL widths:

Variation of the target IR heat flux SOL width as well as the fast probe mid-plane SOL widths ( $T_e$  and  $n_e$ ) as a function of plasma operation parameters will be experimentally investigated. Both the mid-plane and target profiles became narrower in the near SOL with increasing plasma current (Fig. 5.1.2.3) and experiments should be conducted to reveal the dependence on  $I_p$ ,  $\bar{n}_e$ , and input power in more detail. The SOL width data will be scaled with plasma operation parameters and the scaling law will be compared with analytical models. The simultaneous measurement of the SOL widths and blob characteristics will also allow a study of the link between the two. The LLD will enable access to lower  $v^*$ , closer to that envisioned for next step STs.

b) study of edge turbulence:

We plan to continue measurements of edge turbulence utilizing the existing GPI and Langmuir probe hardware to extend previous experience and results. We will study the process of the generation of intermittent filaments (blobs) from edge turbulence and the radial transport of the filaments in the midplane SOL, which very likely affects the SOL widths. We will also make new GPI measurements of the turbulence and filaments in the divertor region (including the private flux region), which may affect SOL of heat/particle flux at the divertor plate itself, and will measure the correlation between the midplane and divertor filament structures, such as shown in Fig. 5.1.2.4. All of these measurements will contribute to testing specific theoretical models for the SOL (see Sec. 4). An important upgrade of the NSTX Langmuir probe system to measure  $T_e$  fluctuations is planned.

Plans for FY2011-2013:

a) An additional reciprocating Langmuir probe located near the X-point would add an extremely valuable diagnostic capability to the study of the SOL width of NSTX. Specifically, this X-point probe would be useful to look at poloidal symmetries, X-point

physics (e.g. the resistive X-point instability), ELM dynamics and parallel heat transport issues.

b) The present NSTX GPI diagnostic utilizes two state-of-the-art fast framing digital cameras fielded by Nova Photonics Inc. These cameras, each capable of running at  $\sim 120000$  frames/s and with frame synchronization between the two cameras to within

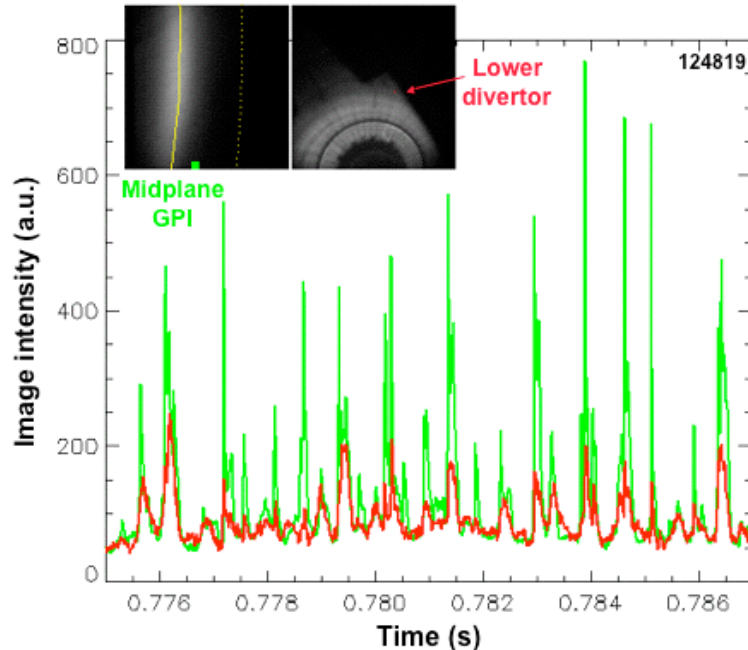


Fig. 5.1.2.4- Midplane GPI peaks (green) correlate in time with divertor GPI peaks (red).

0.25 ms, can image small sections of the plasma edge with high spatial resolution, thus providing unequal physics data well suited for the research indicated above. This capability will be improved during the period 2011-12 as the imaging technology is developed, thus providing further improvements in the diagnostic capabilities.

#### 4. Testing specific theoretical models (FY09-13)

At the present time the fundamental physics determining the SOL width and profiles is not well understood. In the next few years we will use NSTX data to test specific theoretical models and simulations to validate these models so that an eventual understanding of this physics can be obtained.

Plans for FY2009-2010:

a) The Lodestar group plans to carry out detailed validation/comparison studies between its newly developed SOLT (Scrape-Off-Layer Turbulence) code and the NSTX GPI and Langmuir probe data. NSTX will collaborate with the Lodestar group on these blob model validation studies to understand blob formation and intermittent transport; for example, a simulated GPI diagnostic capability has been added to SOLT in collaboration



with PPPL staff. In addition, the NSTX/Lodestar collaboration has proposed experimental tests to address (i) blob speed in disconnected/detached plasmas, (ii) parallel blob-filament structure in the presence of X-points, (iii) ICRF interaction with edge turbulence (see also Sec. 5).

b) The LLNL group is planning to conduct a systematic analysis of turbulence and transport in the SOL using both analytic models and the BOUT code, and to compare these results with NSTX data. In the BOUT model, the fluid turbulence determines the radial flux of particles and heat, and parallel fluid transport determines the average axisymmetric profiles. Due to the time scale separation between turbulence and transport it may not be practical to calculate self-consistent SOL profiles within a turbulence model. To overcome this difficulty one may resort to the projection-integration method developed for this class of problems<sup>36</sup>. This approach has been used, with coupling the turbulence code BOUT and edge transport code UEDGE. Some results with self-consistent edge were obtained<sup>37, 38</sup>, however for a more comprehensive study we are planning to revisit it in the near future.

c) The CPES group plans to use the XGC0 kinetic particle code to simulate the SOL plasma in NSTX, including the magnetic separatrix, X-point and material wall<sup>39</sup>. There will be a specified heat flux from the core plasma and particle source from neutral ionization, and the self-consistent radial electric will be evaluated. The only free parameter in the present model is the anomalous radial diffusion rate. We will study the sensitivity of the calculated scrape-off layer width to the wide range of pedestal plasma profiles, neutral recycling positions and rates, and assumed anomalous diffusion rates, and compare the results with experimentally measured heat deposition profiles on the divertor target plates of NSTX. Later versions of the code will include an edge turbulence model to calculate the SOL widths and profiles self-consistently.

Plans for FY2011-2013:

Each of these modeling and validation projects should be continued as the codes are developing and further validation experiments become feasible. This process can potentially continue using archived NSTX data if NSTX does not operate during this

period.

## 5. Methods to control the SOL (FY09-10 and FY11-13)

Even if a predictive theoretical understanding of the SOL width can be achieved, it is possible that the resulting widths will not be consistent with successful operation of future high powered tokamak devices such as ITER or NHTX. Therefore we need to develop methods to actively control these SOL widths, e.g. to increase them to reduce the peak heat flux at the divertor plate. These potential control methods can also be simulated using the models discussed in Sec. 4, and so provide interesting tests of these models.

Plans for FY2009-2010:

a) ‘blob’ detachment: Plasma detachment normally decreases the heat flux to the divertor by increasing the radiated power in the edge. The Lodestar group has proposed that the SOL width can also be increased by detaching these filaments from electrical contact with the divertor sheath using gas puffing in the divertor region, which will cause an increase in the filament’s ExB radial drift velocity. Initial tests of this idea will be made by measuring the radial filament speed with and without detachment using the GPI midplane and divertor systems.

b) convective cell generation: The LLNL group has proposed that the SOL can be increased by non-axisymmetric electrical biasing of the divertor plates to create small-scale convective cells<sup>40</sup>. Successful experimental tests of this idea have been made using a set of biased electrodes near the outer midplane of NSTX<sup>41</sup>. These experiments will be extended in FY2009-2010 to include biasing small electrodes mounted in divertor plate tiles between the LLD segments. The Lodestar group has also proposed that convective cells can be generated by RF sheaths and used to spread the heat load in the divertor<sup>42</sup>, and initial tests of this idea will be made using the HHFW antennas in NSTX.

Plans for FY2011-2013:

The SOL control methods described above do not require any significant hardware modifications to NSTX. Given additional time, we could potentially test

additional ideas that will require a significant modification to NSTX hardware. For example, if the small divertor tile biasing experiments in NSTX are successful in FY2009-2010, a system for larger-scale biasing of the divertor plates for SOL control might be installed and tested during FY2011-2013.

### 5.1.3 ST divertor physics and heat flux control

#### 1. Introduction

Steady-state mitigation of divertor heat flux and material erosion are critical issues for both the International Thermonuclear Experimental Reactor (ITER) and especially spherical torus (ST) based devices, which are designed to be high power density systems. Owing to their compact nature, spherical tori (ST) have the potential for high heat flux at divertor target plates because of the large ratio of  $P/R$ , where  $P$  is the heating power and  $R$  is the major radius of the device. One example: a Component Test Facility (CTF) design<sup>43</sup> based on the ST concept has a  $P/R$  of about 35, above the value for ITER, and it requires an 85% radiated power fraction to maintain target peak heat flux below 15 MW/m<sup>2</sup>. Furthermore, the combination of the high edge magnetic field line pitch, the short connection length, the high magnetic mirror ratio in certain configurations, and relatively low  $B_t$  can lead to a rather different divertor physics operational regime in NSTX.

At present, candidate heat flux mitigation techniques include use of radiative/detached divertors and/or divertor geometry optimization, including the deployment of novel divertors. Looking forward, heat flux control must be demonstrated in low-density Li-pumped discharges. The ultimate goal is to develop an experiment-based predictive capability of heat flux distribution and control for the next-step ST-based fusion devices.

#### 2. Background and results

In an ST magnetic geometry, access to the radiative divertor as well as its efficiency was predicted to be difficult because of the large  $P/R$ , and because of geometric features of the ST divertor - a small plasma volume, a small plasma-wetted area, a short parallel connection length, and a large inboard to outboard plasma surface asymmetry, as shown in Table 1. The ST effects, most notably, the geometric SOL structure, lead to observed differences in NSTX divertor operating regimes. Recent NSTX experiments have demonstrated both similarities and differences in the divertor regimes observed in NBI-

heated plasmas, as compared to conventional tokamak results. Divertor regimes have been characterized for both low  $\kappa$ ,  $\delta$  and high  $\kappa$ ,  $\delta$  configurations.

Table 1: comparison of geometric characteristics of NSTX and high aspect ratio tokamak, e.g. DIII-D

Quantity	NSTX low $\kappa \sim 2, \delta \sim 0.5$	NSTX high $\kappa \sim 2.3, \delta \sim 0.8$	Tokamak
Aspect ratio	1.3-1.4	1.4-1.5	2.7
In-out SOL area ratio	1:3	1:3	2:3
Midplane to target connection length $L_c$ (m)	10-12	8-10	30-80
X-point to target parallel length $L_x$ (m)	6-8	5-7	10-20
X-point to target poloidal length $L_p$ (m)	0.15-0.25	0.05-0.15	0.05-0.25
Poloidal magnetic flux expansion $f_m$ at OSP	3-4	16-24	3-15
Field angle at target (degree)	5-15	5-15	1-2

In NSTX, the typical H-mode operating scenario leads to a well-attached outer divertor leg with high peak heat flux, and a detached inner divertor leg with rather low heat flux<sup>44</sup>. The first detailed study on the dependence of outer divertor peak heat flux in H-mode on two key parameters,  $P_{\text{NBI}}$  and  $I_p$ , has been published, building on an earlier study of L-mode plasmas<sup>45</sup>. This study demonstrated that the peak heat flux increased monotonically with the power flowing in to the SOL ( $P_{\text{LOSS}}$ ), with a break in the slope

between 2 and 3 MW (Figure 5.1.3.1)<sup>46</sup>. To obtain insight into the experimental trends, these data were simulated with a two-point model of the SOL derived by K. Borass<sup>47</sup>. These simulations suggested that the break in the slope corresponded to a transition from a near detached regime through the high recycling regime (see Figure 10 blue, green, and red curves and the publication for details<sup>46</sup>).

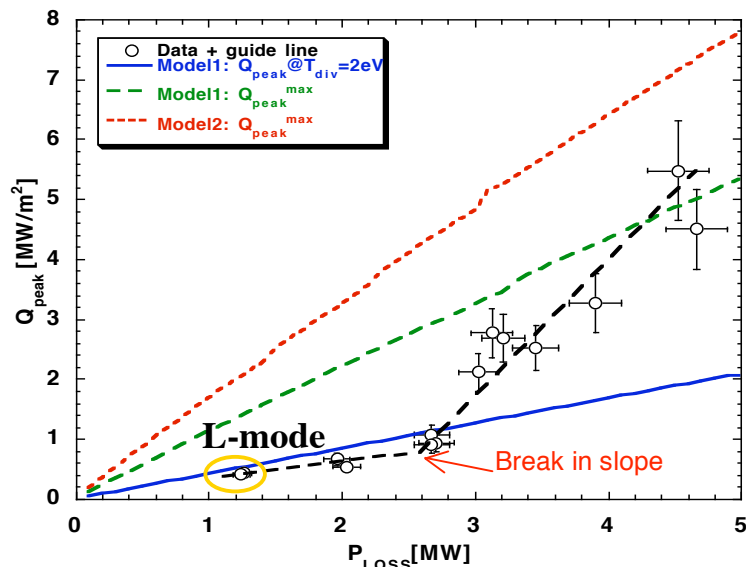


Fig. 5.1.3.1- Dependence of outer divertor peak heat flux ( $Q_{\text{peak}}$ ) on SOL loss power ( $P_{\text{LOSS}}$ ), and comparisons with Borass' 2-point model calculations of the NSTX SOL.

Even higher heat fluxes, up to  $10 \text{ MW/m}^2$ , have been measured in lower density plasmas<sup>48,49</sup>. The peak heat flux was also shown to increase rapidly with  $I_p$ , with a much stronger dependence than a simple connection length dependence observed in two-point models; the profile width also shrunk with  $I_p$ . Power accounting was not very good, i.e. up to 70 % of  $P_{in}$  could be accounted, with up to 10 % divertor radiation even at the highest densities<sup>50</sup>.

Several different techniques to mitigate the peak heat flux have been used. The simplest technique is by control of the boundary shape: it was shown that the peak flux was decreased by about 50% in comparing a LSN to a DN with otherwise similar shape parameters, and reduced again by 60% in comparing the standard DN to a high  $\delta$  DN with substantially increased flux expansion<sup>51</sup> (Figure 5.1.3.2). In that particular study, we note that the heat flux profile was rather broad, suggesting that partial detachment and radiation may have contributed to the heat flux reduction.

Dedicated radiative and detached divertor scenarios has also been investigated, the latter being differentiated by signs of volume recombination<sup>52-54</sup>. In low  $\delta$ , lower-single

null discharges, partial divertor detachment (PDD) and heat flux reduction by 60-80% was achieved. However, the PPD regime could be obtained only with high  $D_2$  injection rates that led to an X-point MARFE formation and confinement degradation. The limited access to detachment was found to be qualitatively consistent with predictions of zero-dimensional two point models and two-dimensional multi-fluid modeling with the

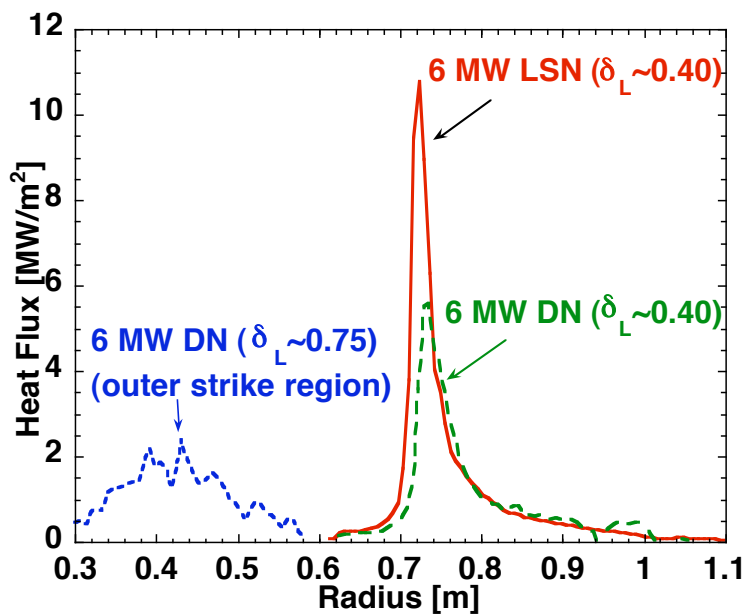


Fig. 5.1.3.2- Peak heat flux is reduced comparing in  $\delta \sim 0.45$  single-null (red) and double-null (green). It can be reduced further at high  $\delta \sim 0.8$  (blue), owing to higher flux expansion and relatively easier access to partial detachment.

b2.5 and UEDGE codes. The main conclusion was that it was difficult to maintain the adequate steady-state volumetric power and momentum losses required for detachment at high parallel heat flux  $q_k=30-50 \text{ MW/m}^2$  in the open geometry carbon divertor with a short parallel length and poor gas entrapment, typical of the lower-end  $\kappa, \delta$  configurations.

More promising results were obtained in high  $\delta$ , lower-single null discharges, in that similar levels of heat flux control were achieved without degradation of the energy confinement. These baseline discharges showed improved plasma performance approaching the performance level of CTF with high  $\beta_t = 15-25 \%$ , high  $\beta_N = 5.7$ , and a high bootstrap current fraction  $f_{BS} = 45-50 \%$  sustained for several current redistribution times. Higher plasma shaping factor also led to longer plasma pulses, and an H-mode regime with smaller ELMs, long with heat flux naturally reduced by 30-50 % because of higher flux expansion.

This high flux expansion divertor configuration has geometric properties facilitating access to detachment, because of a higher radiative volume, and a possible plasma "plugging" effect counterbalancing the openness of the NSTX divertor<sup>54</sup>. The PDD regime was obtained in NSTX in this configuration at several SOL power levels, corresponding to the highest  $q_{peak}$  values achieved with 4-6 MW NBI input power, and  $I_p = 0.8 - 1.0 \text{ MA}$  (Figure

5.1.3.3). The core stored energy and confinement time were practically unaffected. Divertor power and momentum losses measured in the PDD phase indicated similar trends with large aspect ratio tokamak experiments, e.g. a 30-60 % increase in divertor plasma radiation, a significant increase in neutral pressure

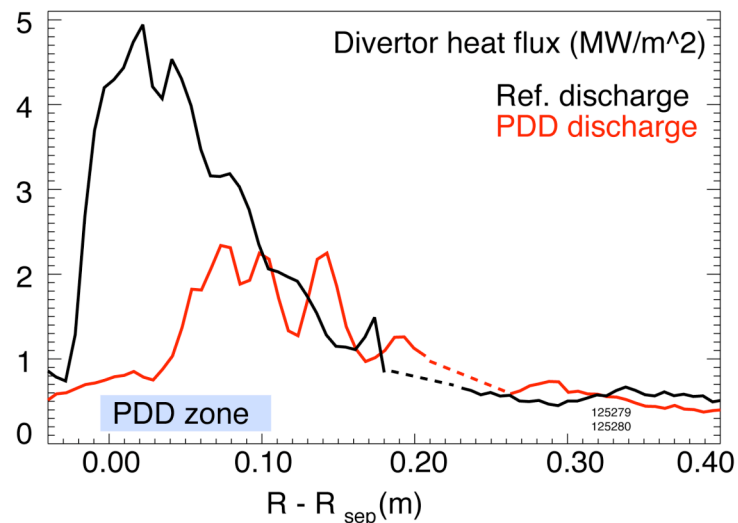


Fig. 5.1.3.3- Comparison of heat flux profiles in reference and partially detached (PDD) discharge in high  $\delta \sim 0.8$  configuration.

and recombination rate, and the peak heat flux reduction up to 60 %, measured in a  $\sim 0.1$  m radial zone. An analytic 1D five-region SOL transport model<sup>55</sup> with constant heat and particle sources and sinks predicted that large radiated power and/or momentum loss fractions were required to achieve detachment in the NSTX range of parallel SOL heat flux  $q_{\parallel} = 25\text{-}60 \text{ MW/m}^2$  and connection lengths  $l_{\parallel} = 6\text{-}10 \text{ m}$ <sup>54</sup>. This model is shown schematically in Fig. 5.1.3.4, along with the predicted  $n_e$  and  $T_e$  variation along field lines in the SOL in the high recycling and detached scenarios. In agreement with experiment, the model predicted that it was nearly impossible to reach the detachment by simply increasing plasma density in NSTX. However, increasing the fraction of neutral re-ionization in divertor by 50-90 %, thereby simulating a divertor gas injection, lead to a relaxation of the divertor radiated power fraction requirement to realistic  $P_{rad}$  levels (40-60 % of  $P_{in}$ ). An assessment of intrinsic carbon divertor radiation using a 1D SOL heat conduction model with

non-coronal carbon radiation indicated that it was marginally possible to reduce the parallel heat flux to low levels with realistic divertor carbon concentrations ( $c_{carbon} < 10 \%$ ). Thus, combined divertor geometry effects appeared to play

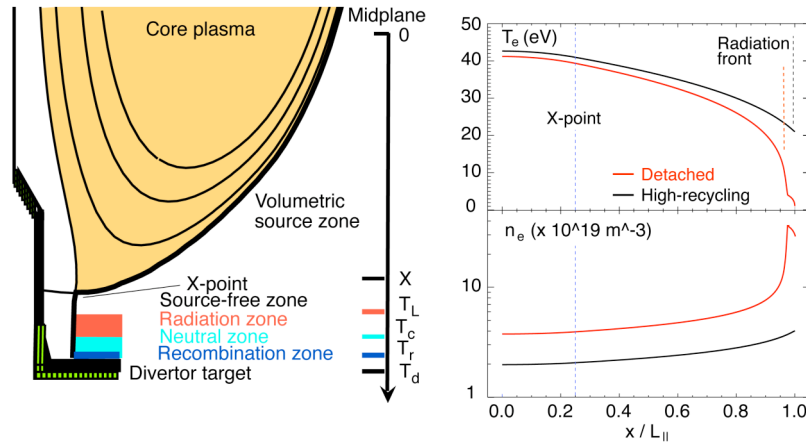


Fig. 5.1.3.4- 5-zone interpretive model showing variation of  $n_e$  and  $T_e$  along the field line for NSTX high recycling and detached cases.

a favorable role in promoting detachment in the high flux expansion open divertor configuration, showing much promise for future ST radiative divertor and novel high flux expansion divertor applications.

### 3. Plans

The goals for the next five-year period in the scrape-off layer and divertor research area on NSTX are three-fold. The near-term research (FY09-FY11) will focus on general



heat and particle transport studies in the ST, including the effect of liquid lithium divertor on edge plasma properties. In later years (FY12-FY13), we plan to enhance these studies with advanced diagnostics and analysis, and design a new divertor capable of handling the higher  $I_p$ ,  $B_t$ , and longer pulse length plasmas that will be enabled with the new center stack and solenoid. The new divertor would include advanced particle and power handling features, such as an upgraded liquid lithium module, new PFC target materials, a cryo-pump, and/or novel geometry (e.g., a “snowflake” divertor or an X-divertor).

### **Plans (FY09-11):**

#### ST SOL and divertor studies

The goal will be to characterize SOL and divertor heat and particle transport, improving our understanding of the ST impurity effects. This research will contribute to the general tokamak SOL and divertor studies, and improve experiment-based projections toward the future ST-based fusion devices. An increasingly important aspect of this work will be the coordinated efforts and collaboration with Alcator C-Mod and DIII-D scientists. This would help to separate the ST-specific magnetic geometry effects from the configuration-specific effects.

The following research efforts are planned for this period:

- A. Comparison of heat flux profiles and plasma parameters at the divertor and outer midplane with models to identify the thermal transport processes in the SOL
- B. Transient (ELM-induced) divertor heat and particle flux studies, including: 1) the interaction of ELMs with a detached or radiative divertor scenario; 2) parallel transport of ELMs on the open field lines; and 3) the 3-D structure of the ELMs
- C. Private-flux region characterization and transport studies
- D. Lower divertor power accountability and MARFE characterization studies with new diagnostics

These new diagnostics commissioned during this period will provide essential data for these studies:

- New IR cameras, including a fast IR camera for transient event analysis, and the use of two-color techniques, for divertor heat flux profile measurements
- New divertor bolometer system: 16 channels to reconstruct the 2-D radiated

- power profile
- Ion flow measurement of the edge and SOL flow
  - An X-point reciprocating Langmuir probe for local  $n_e$ ,  $T_e$  and fluctuations
  - Imaging divertor UV-VIS spectrometer for divertor  $T_i$ , impurity radiation, divertor  $n_e$  and  $T_e$  profiles
  - New “smart” tiles as part of the LLD program between LLD segments, with a dense Langmuir probe arrays, and thermo-couples, for divertor particle, heat flux,  $n_e$  and  $T_e$  profile measurements.

Data analysis and interpretation will include the application of 2D multi-fluid (UEDGE<sup>24</sup>, SOLPS<sup>25</sup>) and neutral (DEGAS-2<sup>56</sup>) numerical models, as well as reduced-dimension (2-point, 1D, onion-skin) models<sup>57</sup>.

#### Divertor properties with LLD (also summarized in section 5.1.1 plans)

As the LLD research is an important part of the NSTX program in FY09-FY11, the boundary physics effort will provide a comprehensive LLD characterization and cover dedicated experiments to clarify the impact of the LLD on edge plasma characteristics. The goal is to document the LLD module performance under various plasma conditions, and to investigate the pumping and heat flux handling capabilities of the LLD. The following topics will be addressed:

- A. LLD pumping characterization
- B. Divertor operating regimes with lithium pumping and strong lithium radiation, as functions of input power, density, impurity density
- C. Divertor heat flux handling, detachment operating space, and comparison of detachment and X-point MARFE onset with data from tokamak experiments
- D. Impurity sources, i.e., chemical and physical sputtering, in the presence of mixed target materials
- E. Role of molecular fluxes, since a number of D-, B- and Li- containing radicals are formed in the low temperature PFR plasmas

These studies will utilize a number of existing and newly commissioned diagnostics:

- New IR cameras, including a fast IR camera, and ones using two-color techniques, for divertor heat flux profile measurements

- New divertor bolometer system
- New Lyman- $\alpha$  diode arrays, to replace existing visible Balmer- $\alpha$  and Balmer- $\beta$  arrays, rendered inadequate in the presence of highly reflective lithium coatings
- Imaging divertor UV-VIS spectrometer, to provide divertor ion temperature, impurity, divertor  $n_e$  and  $T_e$  profiles
- New “smart” tiles, being a part of the LLD module design, will include dense Langmuir probe arrays, and thermo-couples, for divertor particle, heat flux,  $n_e$  and  $T_e$  profile measurements.

Data analysis and interpretation will include the application of codes mentioned above, as well as atomic data from ADAS database and collisional-radiative modeling. The emphasis will be on developing a comprehensive model of plasma-LLD interaction, which will utilize plasma and Monte Carlo neutral transport models, and the TRIM code and molecular dynamics calculations for plasma-lithium surface interaction.

#### Divertor heat flux mitigation studies

The heat flux control effort will continue to provide important answers for projections to the upgraded NSTX and future ST-based devices. In FY09-FY11, the emphasis will be on experimental studies of heat flux mitigation solutions with existing facility capabilities. The following research efforts are planned in this period:

- A. Optimization and control of partially detached divertor regime with impurity and deuterium injection at high input power and reduced density, integration with long-pulse H-mode scenarios, and in double-null configurations
- B. The use of resonant magnetic perturbations to split/sweep the strike point and reduce peak heat flux
- C. Development of heat flux mitigation solutions with novel flux expansion configurations with existing magnetic coils, e.g., the “snowflake” divertor<sup>58</sup>. While a pure snowflake divertor is thought to be topologically unstable, modest coil current variations can be used to create stable equilibria with high flux expansion. Preliminary calculations have suggested that a ‘snowflake-plus’ geometry can be achieved in NSTX with the existing coil set (Figure 5.1.3.5).

### Plans (FY12-13)

Between FY11 and FY 12, the center stack and central solenoid will be replaced in NSTX, with the goal of achieving 2 MA, 1 T discharges with pulse length up to 5sec. For NSTX ATJ divertor graphite tiles, a peak heat flux of  $\sim 6.5 \text{ MW/m}^2$  would result in exceeding the  $1200 \text{ }^\circ\text{C}$  administrative limit at the end of the 5 sec pulse. Peak heat fluxes of this magnitude are routinely encountered in LSN discharges with  $P_{\text{NBI}}=6 \text{ MW}$ . Moreover the use of Li (leading to ELM-free discharges) tends to reduce the SOL heat flux width by up to 50%, resulting in up to a 100% increase in peak heat flux. Thus a combination of heat flux mitigation schemes could well be required for this operation, including the use of DN geometry with high flux expansion, radiative/detached divertors (if compatible with low collisionality operation), and new divertor schemes. This need will be amplified with addition of the second NBI, the preparation for which is in FY112-13, and implementation would be FY 14.

In anticipation of these long pulse upgrades, a divertor geometry upgrade is planned, the precise details of which will be worked out over FY09-10. The likely candidate is installation of extra PF coils to create the X-divertor, or perhaps even multiple coils which would allow a Super X divertor geometry (Figure 5.1.3.6). In short, the X-divertor increases the poloidal flux

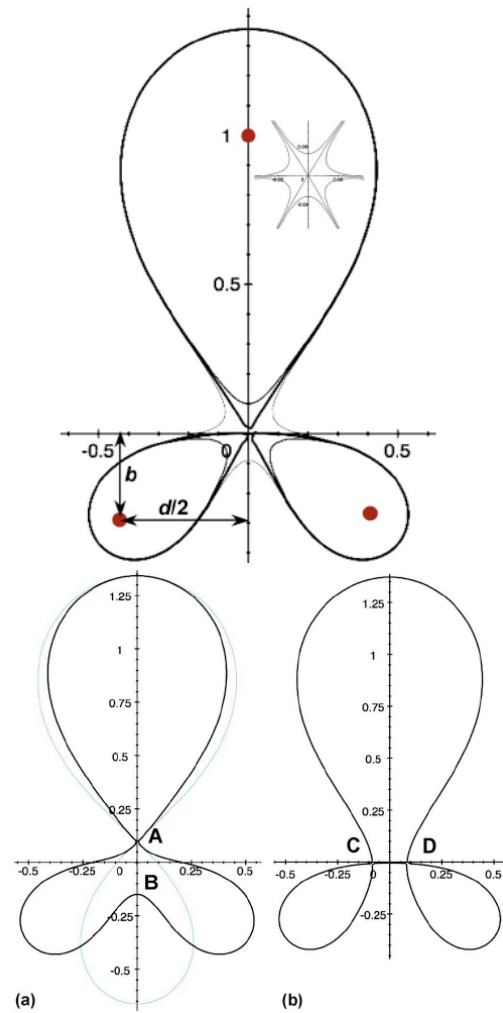


Fig. 5.1.3.5- Plot of separatrix in a snowflake divertor from ref. 58. Panels (a) and (b) represent  $\pm 5\%$  changes to coil currents to create a 'snowflake-plus' and a 'snowflake-minus', each of which have higher flux expansion than a standard X-point divertor.

expansion by adding a secondary X-point just outside the primary one, whereas the Super X-divertor also moves the outer strike point to large major radius to increase the plasma wetted area and the field line connection length/radiation volume. The Super-X divertor would also require modification of the secondary passive stabilizing plates and installation of a target near the vacuum vessel wall. It could be made compatible with Lithium coatings and/or a local cryopump for improved pumping.

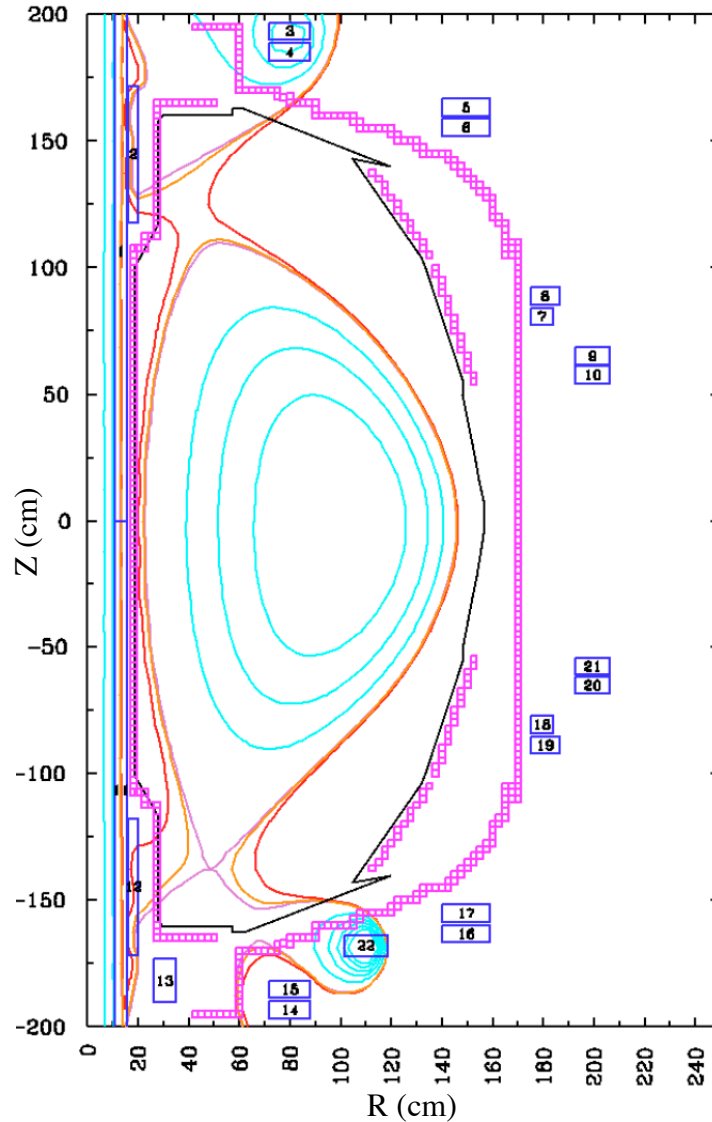


Fig. 5.1.3.6- Preliminary calculation of super-X divertor geometry possible with the addition of a single coil (#22) between PF2 (14, 15) and PF3 (16,17). Optimization of the geometry is in progress. Courtesy of P. Valanju, M. Kotschenreuther, and S. Mahajan (UT-Austin).

### 5.2.1 H-mode pedestal and ELM physics

#### 1. Introduction

The correlation between performance of the plasma core and the plasma temperature at the top of the H-mode pedestal has been established in tokamak experiments from the past decade. Studies examining many devices have shown<sup>59, 60</sup> that the highest pedestal temperature occurs at low pedestal collisionality, a region that is typically accompanied by large edge-localized modes (ELMs). Large or Type I ELMs result in a periodic exhaust of a substantial portion of the plasma stored energy to the plasma-facing components (PFCs). Localized melting of the PFCs would occur in the International Thermonuclear Experimental Reactor (ITER) if the ELM energy deposition were to exceed the PFC heat handling capability, which would effectively impose a limit on the ITER PFC lifetime<sup>61</sup>. Fig. 5.2.1.1 shows one multi-machine database of Type I ELM size vs. the parallel flow time in the SOL, thought to be one of the important physics parameter for

extrapolation. By this measure, estimation of ITER's ELM size is an interpolation within the existing data set, with a predicted pedestal fractional stored energy loss of about

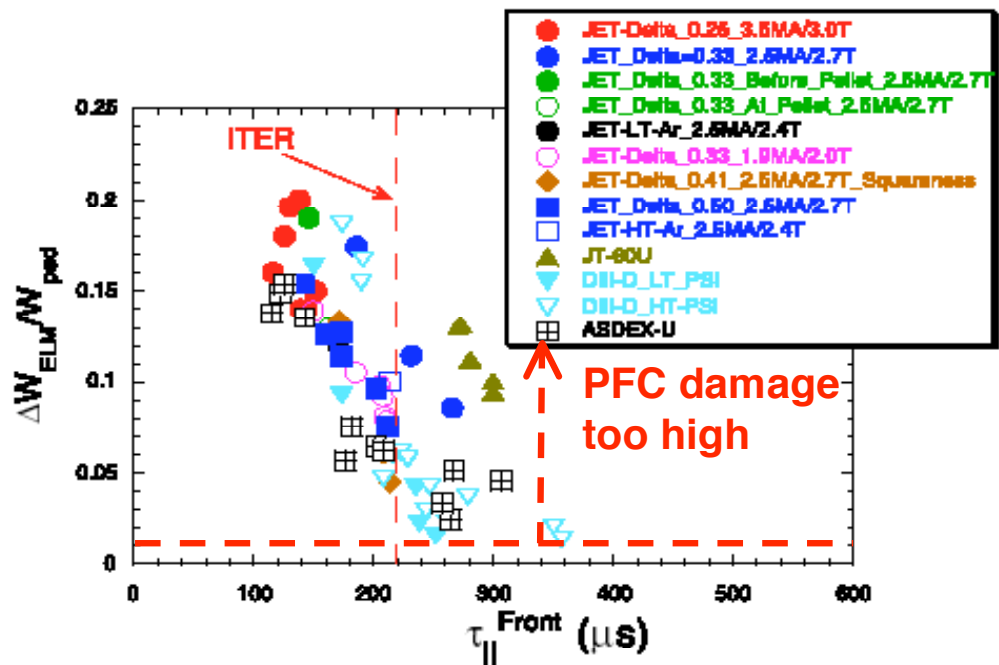


Fig. 5.2.1.1- International database of fraction pedestal energy loss per Type I ELM as a function of a parallel flow time from ref. 60. The ITER specification on  $\Delta W_{ELM}/W_{ped}$  was revised downward to 1%, i.e. Type 1 ELMs are unacceptable.

4%. This value compares with an acceptable pedestal stored energy loss per ELM of 1%. Other extrapolation models and scalings are less favorable, with the conclusion that repetitive Type I ELMs are unacceptable in ITER.

Accordingly the quest for high confinement regimes with no or small ELMs has received increasing priority in the fusion research community. Several promising regimes have been identified which maintain the H-mode transport barrier: small, Type II ELMs from shaping<sup>62-64</sup> or high density operation<sup>65, 66</sup>; grassy ELMs<sup>67</sup>; the Enhanced  $D_\alpha$  H-mode<sup>68</sup> and High Recycling Steady H-mode<sup>69</sup>; the Quiescent H-mode<sup>70</sup>; and the suppression of large ELMs with externally imposed edge resonant magnetic perturbations<sup>71</sup>. While the last one is the preferred ITER method for ELM suppression, many outstanding issues exist concerning the design of ELM control coils and the extrapolability of successful results from present day machines.

The H-mode pedestal is the region connecting the core plasma and the edge steep gradient and SOL plasma. A wide body of research has demonstrated the strong link between the core confinement and the H-mode pedestal parameters, owing to the existence of stiff transport. Thus an accurate prediction of H-mode pedestal parameters is integral for extrapolation to next step devices. In the simplest terms, the pedestal density, temperature, and pressure are represented as the product of a gradient and a width. In this manner, H-mode pedestal and ELM research is intricately linked because ELMS effectively set a limit to the edge pedestal pressure gradient. Substantial progress has been made on the identification of peeling and ballooning modes as the underlying instability responsible for large, Type I ELMs<sup>72</sup>. The physics responsible for setting the pedestal widths is not as well understood; as such a predictive model of the pedestal heights, as the product of width and gradient, requires further dedicated research. NSTX provides an important test-bed for such pedestal and ELM theories because aspect ratio is a leading order term in the stability calculations. Therefore, NSTX is actively participating in several pedestal/ELM related experiments sponsored by the International Tokamak Physics Activity (ITPA).

## 2. Background and results

ELM control research is an important element of the NSTX physics program, owing partly to the needs of long pulse operation and partly to the significance for ITER described above. Spherical tori such as NSTX have limited space for an ohmic transformer, leading to lower volt-second capabilities than higher aspect ratio tokamaks. Large ELMs can consume substantial flux in NSTX, leading to reduced pulse length<sup>73</sup>.

A wide variety of ELMs has been observed<sup>74, 75</sup> in NSTX, enabling a broad ELM research program and a straightforward connection to the studies from high aspect tokamaks. **Figure 5.2.1.2** shows several ELM types in NSTX: a large Type I ELM in panel (a), a medium-sized Type III ELM in panel (b), a small ELM discovered in NSTX

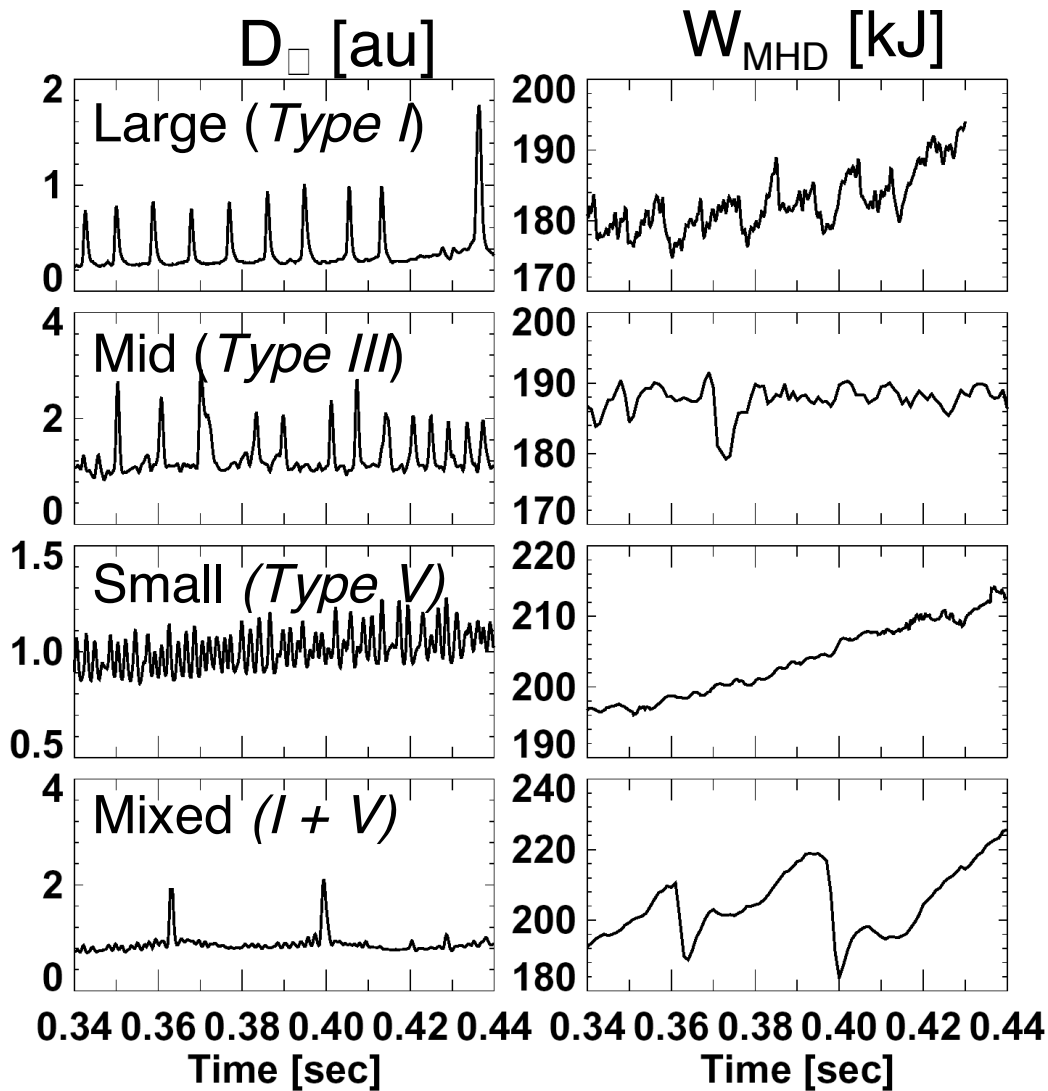


Fig. 5.2.1.2- Signature of different ELM regimes in NSTX, in divertor  $D_\alpha$  emission and stored energy drop. At the highest heating powers, a mixed Type I + V regime is encountered.



and labeled as Type V in panel (c), and a “mixed” regime with both Type I and Type V ELMs in panel (d)<sup>75</sup>. One measure of ELM severity is the reduction of the core plasma stored energy caused by the ELM. By this measure, Type I, III, and V ELMs typically result in a stored energy reduction of 3-15%, 1-5%, and  $\leq 1\%$  respectively, although reductions as high as 30% are occasionally observed for the largest Type I ELMs.

Because of the broad interest in small ELM regimes, studies of the small, Type V ELMs have received high priority<sup>73, 76</sup>. The main features of Type V ELMs are: 1) stored energy drop  $\leq 1\%$  per ELM, 2)  $n=1$  or  $n=2$  magnetic signature, propagating counter to  $I_p$  and NBI direction, 3)



Fig. 5.2.1.3- filamentary structure of Type V ELM on wide angle camera.

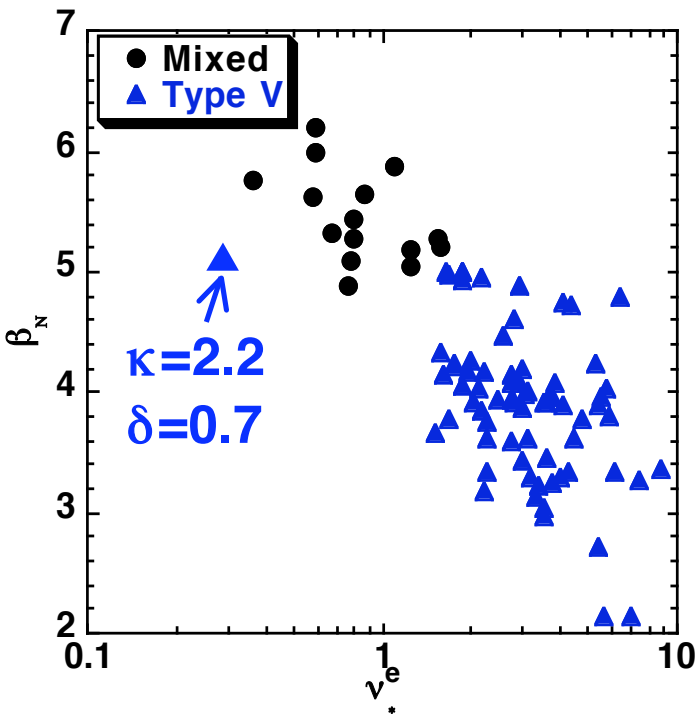


Fig. 5.2.1.4- Onset of mixed Type I + V ELM regime in normalized  $\beta$  and edge collisionality space for  $\kappa=2$ ,  $\delta=.45$ . The onset point is moved to lower collisionality with more shaping, i.e.  $\kappa =2.2$ ,  $\delta =.75$ .

characteristic single or double filamentary structure on various diagnostics (e.g. the visible camera image shown<sup>75</sup> in Figure 5.2.1.3), 4) existence only in plasmas with a dominant lower X-point, and 5) no poloidal beta threshold and no quasi-coherent edge MHD activity. At the upper end of the heating power available in NSTX, however, Type V ELMs appear inadequate for achievement of quasi-steady profiles, and thus Type I ELMs appear. The actual electron

collisionality  $\nu_*^e$  at the time of Type I ELM onset depends on the plasma boundary shape<sup>75</sup> (Figure 5.2.1.4).

Community-wide tokamak research over the past five years has connected the onset of ideal MHD instabilities with the occurrence of large, Type I ELMs. Specifically, the edge plasma normalized pressure gradient in DIII-D was shown to be unstable to intermediate-n peeling or ballooning modes just before the onset of a Type I ELM<sup>77</sup>. A similar calculation was used to predict that the pressure gradient limit should increase rapidly with inverse aspect ratio<sup>78</sup> (Figure 5.2.1.5). That study motivated an ITPA-sponsored experiment between NSTX, DIII-D and MAST to test the effect of aspect ratio on H-

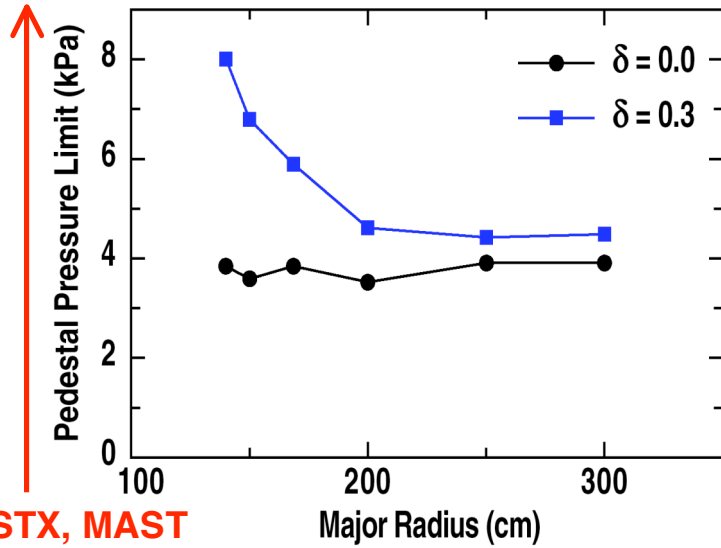


Fig. 5.2.1.5- Predicted pedestal pressure limit as a function of major radius at constant pedestal width, minor radius,  $I_p$ , and  $B_t$ , starting from a DIII-D equilibrium ( $R=167$  cm). The major radii of NSTX and MAST are 85cm.

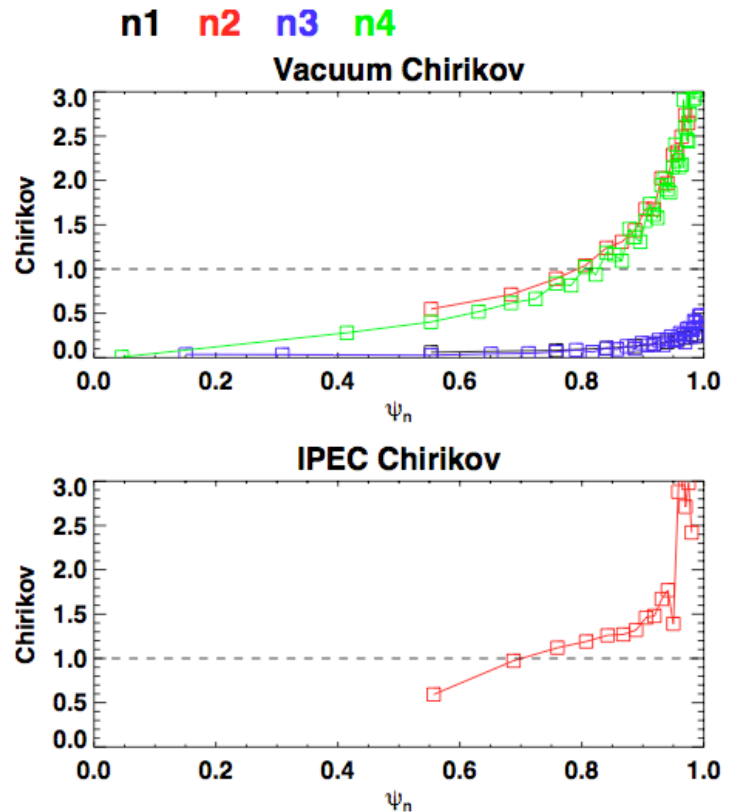


Fig. 5.2.1.6- Vacuum and IPEC-computed (i.e. including plasma response) Chirikov parameters for n=2+4 configuration.

mode pedestal heights, widths, and gradients. A common boundary shape was achieved<sup>79</sup> in all three devices while matching the pedestal normalized gyro-radius ( $\rho^*$ ) and  $v_*^e$ , and all three devices exhibited Type I ELMs. Stability analysis showed that the DIII-D and MAST discharges were at either the peeling or ballooning stability boundary, whereas the NSTX discharges were computed to be stable.

While characterization of ELMs provides insight to the instabilities, control of ELMs is the ultimate goal. As discussed above, the plasma boundary shape significantly affects the ELM characteristics in NSTX. Active control with externally

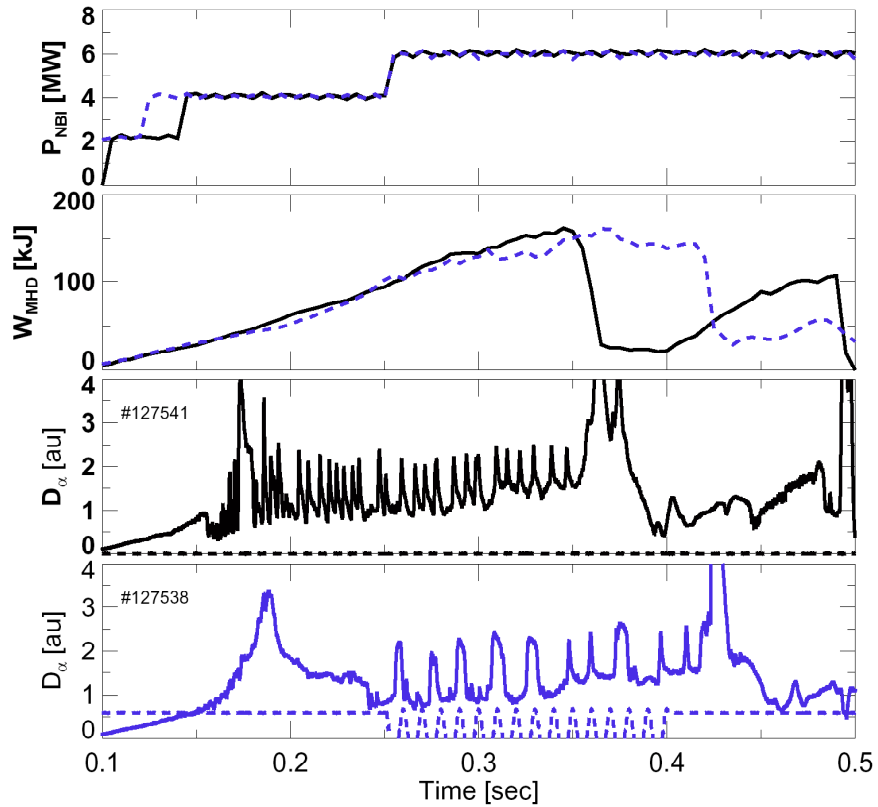


Fig. 5.2.1.7- Comparison of Type I ELMy discharges with (blue) and without n=3 3-D perturbation.

applied non-axisymmetric magnetic perturbations is being tested in NSTX, using a set of 6 midplane window-frame coils external to the vacuum vessel. The goal is to determine if these coils will allow ELM suppression as observed with internal coils in DIII-D<sup>71</sup>. Because internal coils could have a significant cost/schedule impact in next step devices, e.g. in ITER, experiments with external coils can help corroborate the need for such coils.

The NSTX coils allow a variety of spectra: pure n=1, pure n=3, mixed n=1+n=3, mixed n=2+n=3, or mixed n=2+n=4. The experimental studies to date have been guided by calculations of the island overlap from application of the 3-D field, both vacuum response and also including plasma response with the IPEC code<sup>80</sup>. Fig. 5.2.1.6 shows

that the Chirikov parameter was expected to exceed 1 for  $\psi_N > 0.7$ , i.e. for a large region of the edge plasma. This condition (Chirikov  $> 1$  for a large part of the edge plasma) is believed to be necessary for ELM suppression<sup>81</sup>. Two sets of studies have been completed: applying a variety of DC and AC fields to a plasma with reproducible, robust Type I ELMs, and applying  $n=3$  fields to a plasma with a long ELM-free phase. In the first set of studies, reproducible ELM modification (but not suppression) has been observed. Specifically the Type I ELM signature on  $D_\alpha$  is modified: the typical ELM duration of  $\sim 5$ ms duration was doubled to  $\sim 10$ ms, and the frequency was decreased. Data from soft X-rays and fast visible cameras shows that two or more large Type I ELMs are observed to occur within the single 10ms  $D_\alpha$  signature, indicating a change in the ELM stability. In the second set of studies,  $n=3$  magnetic perturbation was shown to reproducibly de-stabilize ELMs in an otherwise ELM-free period of the discharge, e.g. Fig. 5.2.1.7. In this case, the ELMs have similar signatures to normal Type I ELMs on

various NSTX diagnostics. Edge stability analysis on these discharges is underway. Finally this latter technique was very recently used in conjunction with ELM-free discharges (from Li evaporation), to trigger controlled ELMs (e.g. Fig. 5.2.1.8) and reduce the radiated power.

While ELM and pedestal research has clear overlap, H-mode pedestal studies have a broader goal of the

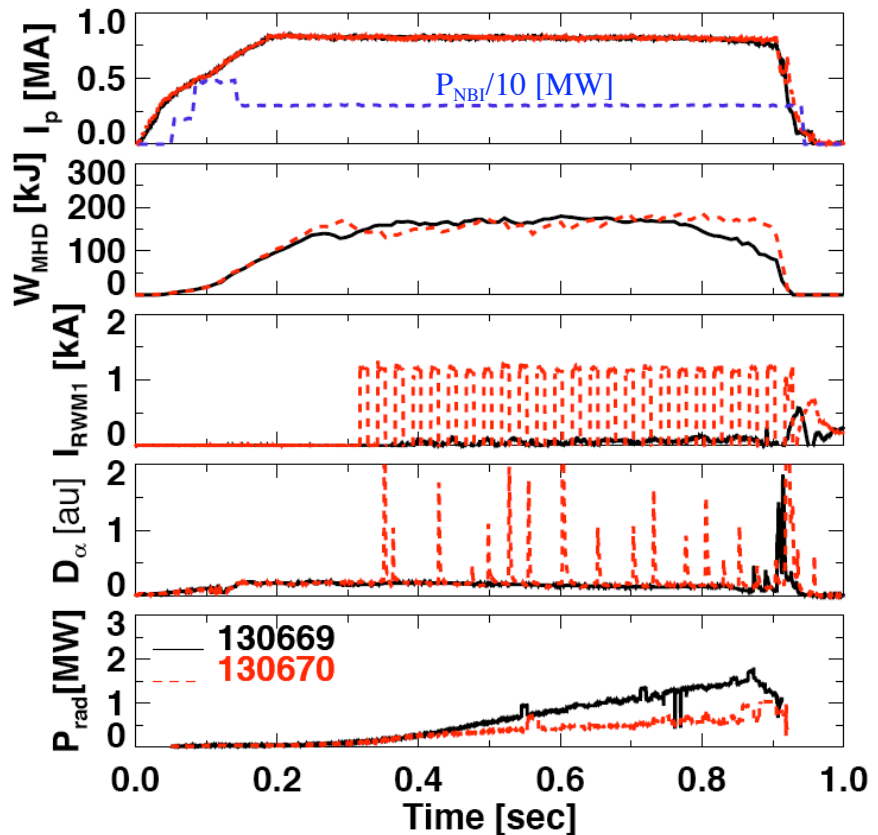


Fig. 5.2.1.8- Comparison of ELM-free discharges with/without  $n=3$  perturbation applied. ELMs are triggered by the  $n=3$  pulses, reducing the rate of increased in radiated power.

assessment of the dependence of pedestal properties on dimensional and dimensionless parameters. Over the past decade, an analysis technique has been developed to facilitate evaluation of the H-mode pedestal heights, widths and gradients for comparison across devices. The procedure involves fitting plasma density and temperature profiles to a mathematical function which includes a hyperbolic tangent term and a linear term<sup>82</sup>. Typically the NSTX pedestal  $n_e$ ,  $T_e$ , and  $P_e$  are in a range between 2 and  $5 \times 10^{19} \text{ m}^{-3}$ , 100 and 300 eV, and 1 and 3 kPa respectively<sup>75</sup>. The  $T_i$  profile is measured by a Charge Exchange Recombination Spectroscopy system; evaluation of the pedestal top is possible for  $T_i > 200 \text{ eV}$ , as the signal strength drops off strongly below this value. It can be stated that in quasi-steady conditions when both measurements are available, the pedestal  $T_i$  is very close to the pedestal  $T_e$ , i.e. in the range of a few hundred eV.

The use of lithium wall conditioning to reduce the density has indeed produced an increase in the edge  $T_e$  and  $T_i$ , as anticipated (see Fig. 5.2.1.9). Because the post-lithium discharges are ELM-free, the edge  $n_e$  is actually higher than in the pre-lithium discharges. This the edge pressure gradient increased. One theory for the ELM suppression is that this enhanced pressure gradient leads to higher edge bootstrap current density, which in turn

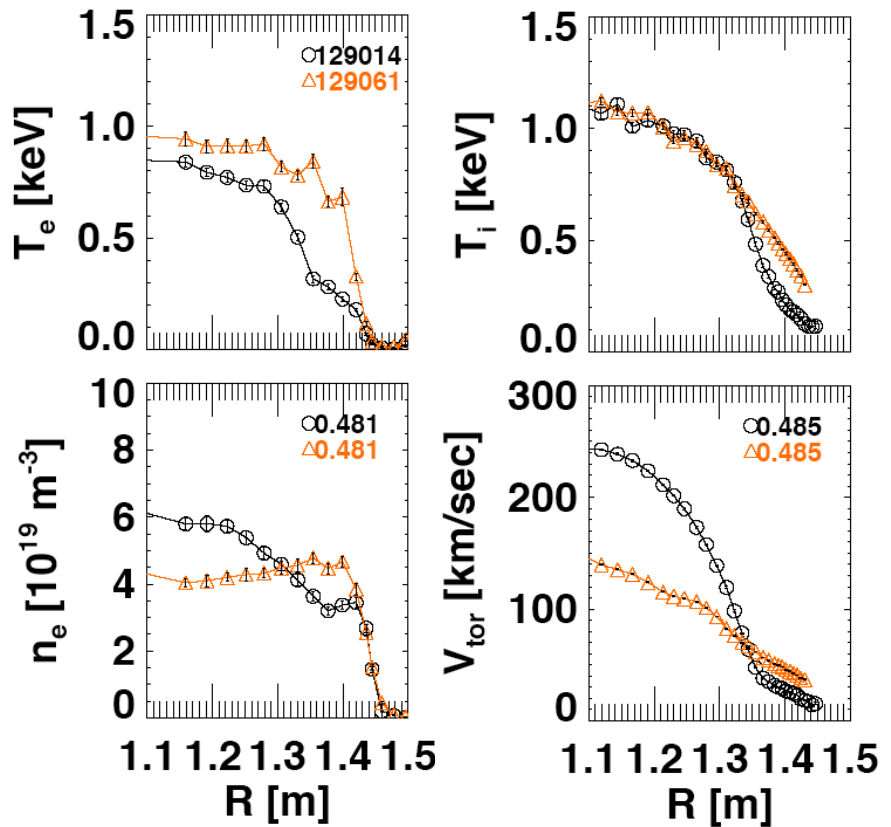


Fig. 5.2.1.9- Comparison of pre-(black) and post-LiTER(orange) discharges with double LiTER system in 2008:  $I_p=0.9 \text{ MA}$ ,  $B_t=0.45 \text{ T}$ ,  $P_{\text{NBI}}=4 \text{ MW}$ ,  $\delta=0.8$ ,  $\kappa=2.2$ . The drop in core toroidal rotation is not understood.

opens up access to second stability regimes. Tests of hypotheses such as these are in progress.

### 3. Plans

We plan to assess the edge stability in discharges with the different ELM types shown in [Figure 5.2.1.2](#). The first step in this assessment is to use all of the Thomson channels to constrain the equilibrium fits. The next step is to assess the edge stability with codes such as ELITE<sup>77</sup> or DCON<sup>83</sup>, and compare the prediction of the pressure gradient limit to the measured time-dependent pressure gradient. The present analysis is partly limited by 1) the spatial resolution of the  $n_e$  and  $T_e$  data from Thomson Scattering, 2) the difficulty in obtaining carbon-based charge exchange  $T_i$  profiles when  $T_i < 200$  eV, and 3) the transient nature of NSTX H-mode discharges which often exhibit a secular density ramp. These limitations will be reduced by enhancing diagnostic capability and improving control tools: 1) additional edge Thomson spatial channels will be added in FY 2009 and available for the F 2010 run, 2) the passive edge rotation diagnostic will be upgraded in both spatial and time resolution, 3) a high spatial resolution  $\sim 1$ ms time response edge Soft X-ray system will be implemented for  $n_e$  and  $T_e$  profile reconstruction, and 4) density control will improve as the Liquid Lithium Divertor is commissioned and fueling upgrades (high-field side fueling, supersonic gas injector) are implemented. In addition the availability of poloidal CHERs by the beginning of FY 2009 will allow an  $E_r$  correction to the edge MSE data to more effectively use it for equilibrium reconstructions used in the edge stability analysis.

The accessibility of the small, Type V ELM in NSTX has increased the NSTX pulse length and performance as compared with Type I ELMy discharges. We plan to continue this research line to answer outstanding questions, e.g.:

- 1) What is the underlying instability responsible for the Type V ELM? Is it an ideal or a resistive mode?
- 2) How far can the regime be extended in  $v_*^e$  space in NSTX, i.e. what is the dependence of the  $v_*^e$  threshold for Type V and Mixed regimes on  $\delta_r^{sep}$ ,  $\delta$ , and  $\kappa$ ?

- 3) What is the significance of the apparent threshold of the Mixed regime onset with the global parameter  $\beta_N$ ? Is the correlation actually with pedestal  $\beta$ , which probably scales with  $\beta_N$ ?
- 4) Has the regime been observed in other devices? If not, is the regime extensible to other devices?

Question #2 above is the subject of an ITPA experiment in which NSTX is participating, in collaboration with the MAST and ASDEX-Upgrade devices. Question #4 is the subject of a second collaborative experiment to assess the commonality of small ELM regimes between the NSTX, Alcator C-MOD, and MAST devices. We anticipate that these studies will be completed FY09-10. The new diagnostics described above will contribute to these studies by allowing a more quantitative assessment of the edge profiles as the different ELM regimes are encountered.

While suppression of ELMs with magnetic perturbations has not been achieved, the edge stability can clearly be altered. The path to ELM suppression may well require reduced collisionality, which is the goal of the LLD program, and/or a broader poloidal mode spectrum. Hence additional attempts at ELM suppression with the existing midplane coils will be made after reduced density discharges have been developed with the LLD. In addition, detailed experiments to understand the change in edge stability caused by these perturbations, including when ELMs are de-stabilized, will be completed.

The prospects of ELM stabilization (or de-stabilization as needed in ELM-free discharges from Li coatings) will be improved by the planned upgrade to the EFCC system. In the baseline budget, adding a second set of switching power amplifiers (SPAs) will allow feedback control for  $n=1$  and  $n=3$  modes *while applying* an  $n=2+4$  perturbation, which has shown the most promise for creating an ergodic edge region for ELM suppression studies. This capability is not possible with the present set of three SPAs. In the incremental budget, new internal non-axisymmetric control coils will allow imposition of up to pure  $n=6$  fields with more control over the poloidal mode spectrum. These coils will allow more precise localization of the perturbation to the edge, avoiding excessive rotation drag from lower- $n$  perturbations. The technical details of these upgrades are given in the facility chapter 7.

We also plan to characterize the H-mode pedestal in detail, in particular the dependence of the heights, widths, and gradients on 1) control parameters, such as  $I_p$ ,  $B_t$ ,  $P_{\text{NBI}}$ ,  $P_{\text{RF}}$ ,  $n_e$ , etc., and 2) dimensionless parameters, such as  $v_{\square}^*$  and  $\rho^*$ . Completion of the multi-machine experiment between NSTX, DIII-D, and MAST to determine the dependence of the pedestal on aspect ratio is a high priority item. Here the improved spatial resolution of the Thomson Scattering, the new high-resolution edge Soft X-ray system, and improved Edge Rotation Diagnostic are critical to an accurate experimental determination of the pedestal heights, widths and gradients.

Although there are presently few theory tools with which to compare these measurements, development of the XGC neoclassical transport code<sup>39</sup> will continue and we anticipate detailed comparisons with code predictions over the next few years. The present version (XGC-0) requires the stipulation of anomalous transport coefficients in addition to the neoclassical ones. The version in development (XGC-1) will compute the transport from an advanced turbulence model. The code predictions will be used not only to test pedestal dependencies on various parameters, but also how the pedestal evolves both between ELMs and leading up to the ELM crash.



## 5.2.2 H-mode transition physics

### 1. Introduction

H-mode discharges are important for the NSTX program because: 1) H-modes are characterized by broad pressure profiles, and therefore higher ideal stability limits; and 2) the edge pressure gradient drives bootstrap current, leading to a higher non-inductive current fraction, and therefore longer discharge pulse lengths. H-mode access is usually observed above a critical input power, known as the L-H power threshold ( $P_{LH}$ ). Development of models to predict  $P_{LH}$  for extrapolation has been an active research topic since the discovery<sup>84</sup> of the H-mode in the early 1980's. NSTX can contribute to H-mode transition physics in several critical ways. Here we discuss three areas: 1) dependence of  $P_{LH}$  on discharge boundary shape, 2) dependence of  $P_{LH}$  on heating mechanism, i.e. NBI vs. RF heating, and 3) dependence of  $P_{LH}$  on fueling location and mechanism.

Many details of the underlying physics of the H-mode transition have yet to be ascertained. External heating methods, e.g. NBI, complicate the determination of the fundamental physics because of the additional particle and momentum source, and so investigating L-H transitions with ohmic heating power alone provides additional insight. One important question is the level of change in core turbulence, which accompanies the development of the edge transport barrier. A simultaneous measurement of the edge and core fluctuations and correlation lengths can be obtained in ohmic H-modes because the density profile remains centrally peaked for a modest period of time after the transition. In NBI H-modes, the edge density rises quickly, preventing measurement of the core turbulence correlation length with reflectometry.

### 2. Background and results

Historical studies of the power threshold have identified the plasma surface area, the toroidal field, and the plasma density as the critical control parameters<sup>85</sup>. Recently, the role of boundary shape was re-investigated, and it was concluded that  $P_{LH}$  exhibited a minimum value in balanced double-null configuration in the MAST device<sup>86</sup>.

The shape experiment was repeated in NSTX, with participation from scientists from MAST. The results were rather similar: the  $P_{LH}$  with NBI fueling was lowest in a DN

shape, doubling in LSN shape and doubling again in USN shape<sup>87</sup> (e.g. Fig. 5.2.2.1). These results were extended further to plasmas with RF heating; the rationale was that whereas 1/3 of the NB heating goes directly to the ions, RF heats the electron population. In addition, NBI imparts momentum whereas RF does not. This comparison was intended to highlight the roles of electron/ion heat flux and rotation on  $P_{LH}$ .

It was found, however, that the  $P_{LH}$  local minimum in the DN shape was present with either heating method. Moreover,  $P_{LH}$  increased as the discharge shape was made to favor the lower divertor even more, i.e. when  $\delta_r^{sep}$  was reduced further. It was also found that  $P_{LH}$  was comparable with either RF or NBI heating. Note that the core plasma profiles differed substantially, but the edge profiles were nearly identical at constant density.

Other power threshold studies<sup>88</sup> have

suggested that neutrals and fueling play an important role in the actual value of  $P_{LH}$ . Further experiments highlighted a dependence on the gas fueling rate: discharges with low gas fueling and no NBI heating during the plasma current ramp showed comparable

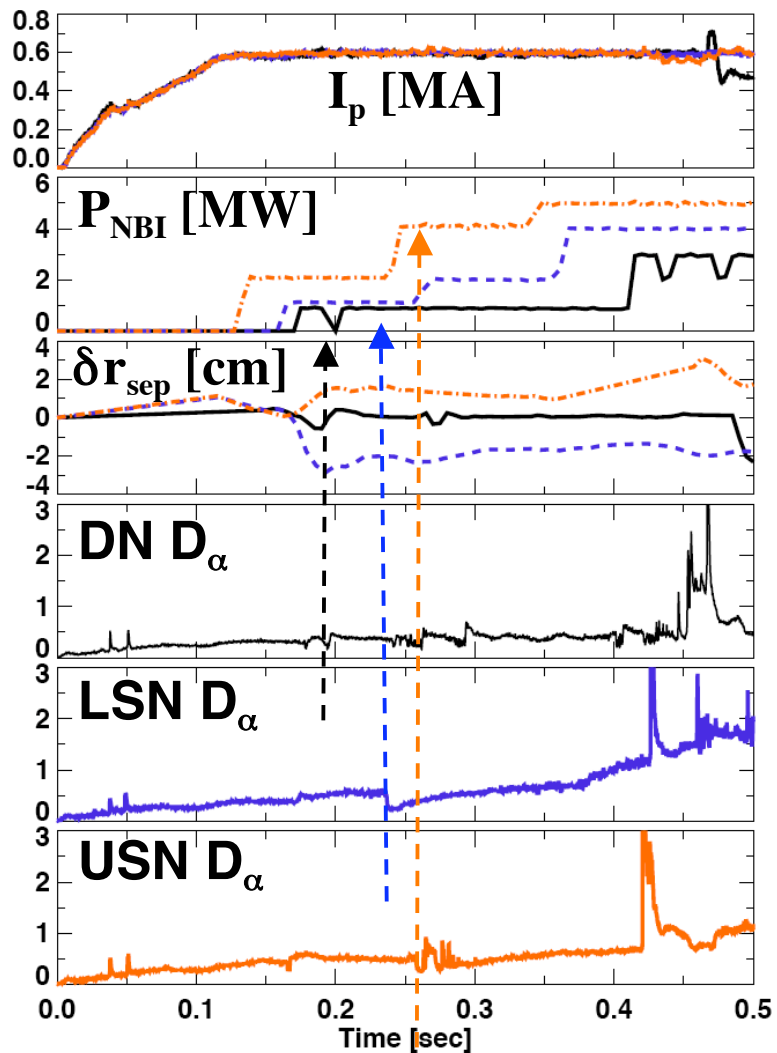


Fig. 5.2.2.1- Comparison of L-H power threshold for balanced double-null (black), lower single-null (blue) and upper single-null (orange).

L-H transition powers for HFS midplane and LFS midplane fueling<sup>75</sup>. Finally, research to date shows that the correlation length for turbulent density fluctuations in the core of ohmic plasmas to decrease 50-75% across the L-H transition<sup>89</sup>. In some cases there is a spontaneous spin up of both edge intrinsic poloidal and toroidal rotations prior to the transition itself.

There are few quantitative theories with which to compare these observations. Recently a new theory (the gyrocenter shift GCS theory) was developed to explain the mechanism of formation of the radial electric field ( $E_r$ ) at the tokamak boundary. The origin of  $E_r$  remains one of the most important problems in L-H transition physics. The basic concept behind GCS is that the neutral density radial gradient in the edge leads to a gradient in the charge exchange rate, hence a radial current and an  $E_r$  (see fig. 5.2.2.2). The validity of GCS theory was tested both in low temperature plasmas<sup>90</sup> and for NSTX directly<sup>91</sup>. This theory might clarify the physics of L-H transition by uncovering the mechanism behind a transition from turbulent flow to laminar flow<sup>92</sup>.

### 3. Plans

Thorough analysis of existing data is the first step. From the previously run L-H experiments, the discharges will be analyzed with the TRANSP code to obtain the heat flux in the separate and ion channels, to see if they

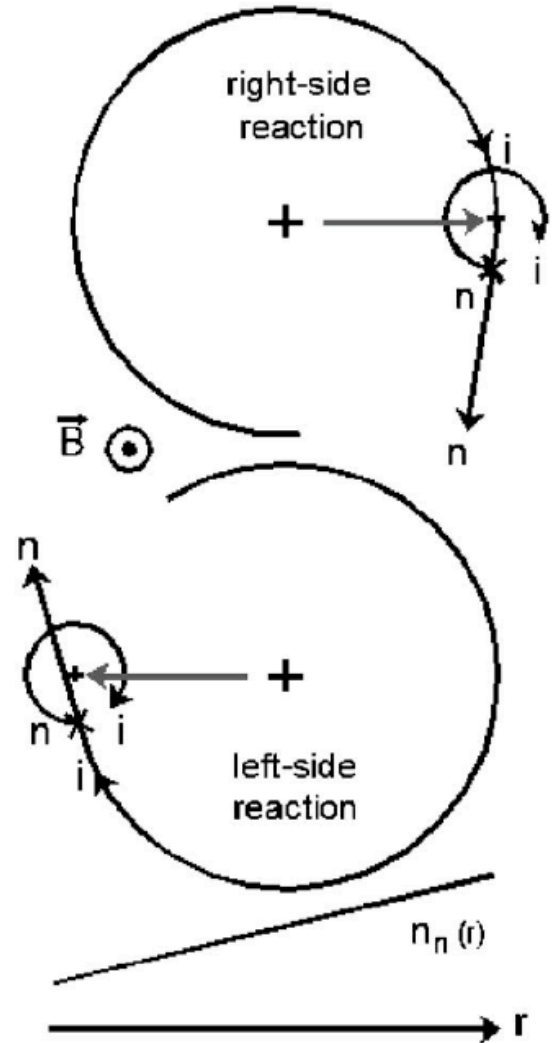


Fig. 5.2.2.2- Schematic of gyrocenter shift originating from charge exchange reactions. The charge exchange rate is higher on the right hand side than the left hand side because of the neutral density gradient, leading to a radial current and radial electric field ( $E_r$ ) buildup.

actually differed with RF and NBI heating. Although the core  $n_e$ ,  $T_e$ ,  $T_i$  and  $v_\phi$  differed in the RF and NBI discharges, collisional coupling may have forced the edge heat flux distribution between electrons and ions to be similar.

From 2009-2011, we plan to assess the dependence of the power threshold on other shape quantities as well, namely the  $\delta$  and  $\kappa$ , as discharges with variations in these two parameters have exhibited different H-mode access conditions in uncontrolled experiments. The effect of rotation on  $P_{LH}$  will also be measured, as ITER is expected to have low rotation speed. We also propose to complete the dependence of  $P_{LH}$  on external parameters, such as  $B_t$  and the fueling rate. We note that past power threshold experiments have been unable to test the E X B shear stabilization paradigm because one component in the radial force balance, the poloidal rotation  $v_\theta$ , was not measured by the existing CHERs system. A new poloidal CHERs system was recently installed on NSTX during 2007, and it will enable calculation of the  $E_r$  profiles to compare with the E X B shearing rate to further test the E X B paradigm.

We also plan to complete the previous study concerning the effect of the poloidal fueling location on  $P_{LH}$ . Several new capabilities have appeared since the last study: 1) a new supersonic gas injector, which allows reproducible H-mode access with LFS fueling in NSTX for the first time; 2) the availability of poloidal CHERs; and 3) continued improvement of the plasma control system, allowing improved position control for improved diagnostic measurements.

Following the center stack upgrade in 2011, we will extend the empirical scalings of  $P_{LH}$  to higher  $I_p$  and  $B_t$ , i.e. closer to next generation STs. Also in this longer term time frame, we plan to perform a more rigorous test of the GCS theory and its impact on the L-H transition and power threshold. Such a test requires a large number of diagnostics, and most of the required diagnostics<sup>93</sup> will be available during FY11-13. In particular, measurement of neutral density profile is one of the most important parameters in the gyrocenter shift theory, and techniques are being developed to make these measurements in the X-point region. We also plan to make comparisons with numerical simulations of these data with the XGC code.

## Chapter 5 References

- 1 J. E. Menard, et. al., *Nucl. Fusion* **47** (2007) 645.
- 2 D. K. Mansfield, et. al., *Nuclear Fusion* **41** (2001) 1823.
- 3 R. Budny, et. al., *J. Nucl. Materials* **196-198** (1992) 462.
- 4 S. V. Mirnov, et. al., *Fus. Eng. Des.* **65** (2003) 455.
- 5 V. Evitkin, et. al., *Fus. Eng. Des.* **56-57** (2001) 363.
- 6 R. Majeski, et. al., *Physical Review Letters* **97** (2006) #075002.
- 7 H. W. Kugel, et. al., *Physics of Plasmas* **15** (2008) #056118.
- 8 D. K. Mansfield, et. al., *J. Nucl. Materials* (2008) submitted.
- 9 R. Maingi, et. al., *Plasma Physics Controlled Fusion* **46** (2004) A305.
- 10 A. R. Field, et. al., *Plasma Physics Controlled Fusion* **46** (2004) 981.
- 11 V. A. Soukhanovskii, et. al., *Rev. Sci. Instrum.* **75** (2004) 4320.
- 12 V. A. Soukhanovskii, et. al., *Proc. 21st IEEE/NPSS Symposium on Fus. Eng., Knoxville, TN, Sep. 26-29* (2005) 2005.
- 13 V. A. Soukhanovskii, et. al., *Proc. 22nd IEEE Symposium on Fus. Eng., Albuquerque, NM June 17-21* (2007).
- 14 L. Yao, et. al., *Nucl. Fusion* **41** (2001) 817.
- 15 B. Pegourie, et. al., *J. Nucl. Materials* **313-316** (2003) 539.
- 16 P. T. Lang, et. al., *Plasma Phys. Contr. Fusion* **47** (2005) 1495.
- 17 V. A. Soukhanovskii, et. al., *Proc. 2008 Euro. Conf. on Plasma Phys. and Contr. Fusion, London, U.K.* **ECA 28G** (2004) paper P2.190.
- 18 V. A. Soukhanovskii, et. al., *Proc. 2006 Euro. Conf. on Plasma Phys. and Contr. Fusion, Roma, Italy* **ECA 30G** (2006).
- 19 V. A. Soukhanovskii, et. al., *Proc. 2008 Euro. Conf. on Plasma Phys. and Contr. Fusion, Crete, Greece* **ECA 32G** (2008).
- 20 D. P. Stotler, et. al., *J. Nucl. Mater.* (2008) submitted.
- 21 R. Kaita, et. al., *Physics of Plasmas* **14** (2007) #056111.
- 22 P. Staib, et. al., *J. Nucl. Materials* **111-112** (1982) 109.
- 23 W. Fundamenski, et. al., *Fusion Science Techn.* **53** (2006) 1023.
- 24 T. D. Rognlien, et. al., *Journal of Nuclear Materials* **196-198** (1992) 347.
- 25 R. Schneider, et. al., *Contrib. Plasma Physics* **46** (2006) 3.
- 26 J. W. Ahn, et. al., *Phys. Plasma* (2008) submitted.
- 27 R. J. Maqueda, et. al., *Review of Scientific Instruments* **72** (2001) 931.
- 28 S. J. Zweben, et. al., *Nuclear Fusion* **44** (2004) 134.
- 29 S. J. Zweben, et. al., *Physics of Plasmas* **13** (2006) 056114.
- 30 J. A. Boedo, et. al., *Plas. Phys. Contr. Nuclear Fusion Res.* (2006) paper EX/6.
- 31 J. R. Myra, et. al., *Phys. Plasma* **13** (2006) #092509.
- 32 J. R. Myra, et. al., *Plas. Phys. Contr. Nuclear Fusion Res.* (2006) paper TH/P6.
- 33 J. R. Myra, et. al., *Proc. 21st Fusion Energy Conference, Chengdu, China, Oct. 16-21, 2006* (2006) paper TH/P6.
- 34 R. Maingi, et. al., *J. Nucl. Materials* **363-365** (2007) 196.
- 35 R. Maingi, et. al., *Proc. 2007 Euro. Conf. on Plasma Phys. and Contr. Fusion, Warsaw, Poland, July 2-6, 2007* (2007) paper P2.020.
- 36 A. I. Shestakov, et. al., *J. Comput. Phys.* **85** (2003) 399.

- 37 T. D. Rognlien, et. al., *J. Nucl. Materials* **337-339** (2005) 327.  
38 T. D. Rognlien, et. al., *Contrib. Plasma Phys.* **44** (2004) 188.  
39 C. S. Chang, et. al., *Physics of Plasmas* **11** (2004) 2649.  
40 D. D. Ryutov, et. al., *Plasma Phys. Contr. Fusion* **43** (2001) 1399.  
41 S. J. Zweben, et. al., *J. Nucl. Materials* (2008) submitted.  
42 D. A. D'Ippolito, et. al., *Phys. Fluids B* **5** (1993) 3603.  
43 Y.-K. M. Peng, et. al., *Plasma Physics Controlled Fusion* **47** (2005) B263.  
44 V. A. Soukhanovskii, et. al., *J. Nucl. Materials* **337-339** (2005) 475.  
45 R. Maingi, et. al., *Journal of Nuclear Materials* **313-316** (2003) 1005.  
46 R. Maingi, et. al., *J. Nucl. Materials* **363-365** (2007) 196.  
47 K. Borass, et. al., *Nuclear Fusion* **31** (1991) 1035.  
48 R. Maingi, et. al., *Plasma Physics Controlled Fusion* **45** (2003) 657.  
49 R. Maingi, et. al., *Nuclear Fusion* **43** (2003) 969.  
50 S. F. Paul, et. al., *J. Nucl. Materials* **337-339** (2005) 251.  
51 D. A. Gates, et. al., *Physics of Plasmas* **13** (2006) #056122.  
52 V. A. Soukhanovskii, et. al., *J. Nucl. Materials* **363-365** (2007) 432.  
53 V. A. Soukhanovskii, et. al., *Proc. 21st Fusion Energy Conference, Chengdu, China, Oct. 16-21, 2006* (2006) paper EX/P4.  
54 V. A. Soukhanovskii, et. al., *Phys. Plasma* (2008) to be submitted.  
55 R. Goswami, et. al., *Phys. Plasma* **8** (2001) 857.  
56 D. P. Stotler, et al., et. al., *Contribution to Plasma Physics* **44** (2004) 294.  
57 P. C. Stangeby, *The Plasma Boundary of Magnetic Fusion Devices* (IoP, Toronto, 2000).  
58 D. D. Ryutov, et. al., *Phys. Plasma* **14** (2007) #064502.  
59 A. W. Leonard, et. al., *J. Nucl. Materials* **266-269** (1999) 109.  
60 A. Loarte, et. al., *Plasma Physics Controlled Fusion* **45** (2003) 1549.  
61 G. Federici, et. al., *J. Nucl. Materials* **313-316** (2003) 11.  
62 T. Ozeki, et al., et. al., *Nuclear Fusion* **30** (1990) 1425.  
63 J. Stober, et. al., *Nuclear Fusion* **41** (2001) 1123.  
64 G. Saibene, et. al., *Nuclear Fusion* **45** (2005) 297.  
65 A. W. Leonard, et. al., *J. Nucl. Materials* **290-293** (2001) 1097.  
66 G. Saibene, et. al., *Plasma Physics Controlled Fusion* **44** (2002) 1769.  
67 Y. Kamada, et. al., *Plasma Physics Controlled Fusion* **42** (2000) A247.  
68 Y. Takase, et. al., *Physics of Plasmas* **4** (1997) 1647.  
69 K. Kamiya, et. al., *Nuclear Fusion* **43** (2003) 1214.  
70 C. M. Greenfield, et. al., *Physical Review Letters* **86** (2001) 4544.  
71 T. E. Evans, et. al., *Physical Review Letters* **92** (2004) article #235003.  
72 P. B. Snyder, et. al., *Physics of Plasmas* **12** (2005) 056115.  
73 R. Maingi, et. al., *Physics of Plasmas* **13** (2006) #092510.  
74 R. Maingi, et. al., *J. Nucl. Materials* **337-339** (2005) 727.  
75 R. Maingi, et. al., *Nuclear Fusion* **45** (2005) 1066.  
76 R. Maingi, et. al., *Nuclear Fusion* **45** (2005) 264.  
77 P. B. Snyder, et. al., *Physics of Plasmas* **9** (2002) 2037.  
78 P. B. Snyder, et. al., *Plasma Physics Controlled Fusion* **46** (2004) A131.  
79 R. Maingi, et. al., *Proc. 21st Fusion Energy Conference, Chengdu, China, Oct. 16-21, 2006* (2006) paper IT/P1#12.

- 80 J.-K. Park, et. al., *Phys. Plasma* **14** (2007) #052110.  
81 M. E. Fenstermacher, et. al., *Phys. Plasma* **15** (2008) #056122.  
82 R. J. Groebner, et. al., *Plasma Physics Controlled Fusion* **40** (1998) 673.  
83 A. H. Glasser, et. al., *Bull. Am. Phys. Soc.* **42** (1997) 1848.  
84 F. Wagner, et. al., *Physical Review Letters* **49** (1982) 1408.  
85 J. A. Snipes, et. al., *Proc. of the 19th International Conference on Plasma Physics  
and Controlled Fusion, Lyon 2002 (IAEA, Vienna) (2002) paper CT/P#04.*  
86 H. Meyer, et. al., *Plasma Physics Controlled Fusion* **46** (2004) A291.  
87 T. M. Biewer, et. al., *Proc. 33rd EPS Conference on Plasma Physics and Contr.  
Fusion, Roma, Italy, June 19-23, 2006 (2006) Paper 5.112.*  
88 B. A. Carreras, et. al., *Physics of Plasmas* **5** (1998) 2623.  
89 C. E. Bush, et. al., *Presented at the 11th US-EU TTF Workshop, Marseille,  
France, Sept. 4-7, 2006 (2006).*  
90 K. C. Lee, et. al., *Phys. Plasma* **13** (2006) #062505.  
91 K. C. Lee, et. al., *Phys. Plasma* (2008) to be submitted.  
92 K. C. Lee, et. al., *Nucl. Fusion* (2008) to be submitted.  
93 K. C. Lee, et. al., *Rev. Sci. Instrum.* **77** (2006) 10F505.

*This page intentionally left blank*

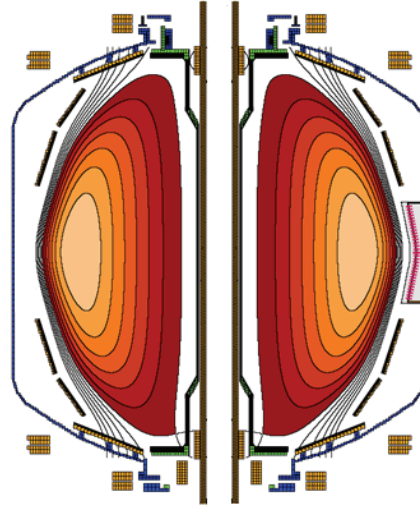


## **Chapter 6 – Plasma Formation and Sustainment**

6.1 Plasma start-up and sustainment overview.....	6.1
6.2 Plasma sustainment results.....	6.3
6. 3 Plasma sustainment plans .....	6.8
6.3.1 Overview .....	6.8
6.3.2 Near-term plans for improved plasma sustainment – FY2009-2011 .....	6.10
6.3.3 Longer-term plans for improved plasma sustainment – FY2012-2013.....	6.13
Timeline for Plasma Current Sustainment and Control Research.....	6.25
References for plasma sustainment.....	6.26
6. 4 Plasma startup results and plans.....	6.27
6.4.1 Coaxial Helicity Injection .....	6.27
6.4.2 Plasma Start-up Using Outer Poloidal Field Coils.....	6.44
6.4.3 Plasma Gun Startup.....	6.51
6.4.4 Plasma Current Ramp-up.....	6.54
Timeline for Plasma Current Start-up and Ramp-up Research.....	6.59
References for plasma formation.....	6.60

*This page intentionally left blank*

## Chapter 6



# Plasma formation and sustainment

## 6.1 Overview

The start-up, ramp-up, and sustainment of a tokamak plasma utilizing little or no induction from a central solenoid is a major challenge in magnetic fusion. The development of techniques to minimize or eliminate central solenoid action is critical to the design of compact electricity-producing fusion power plants based on the spherical torus/tokamak (ST) and could also benefit advanced tokamak (AT) reactors. For component testing applications of the ST, the central solenoid flux of ST-CTF is expected to be either zero or inadequate to ramp the plasma to full operating current. Thus, even if some inductive plasma start-up capability is available, non-inductive means of plasma current ramp-up and sustainment are required. Given the scientific and operational challenges of non-solenoidal formation and sustainment, the problem is best solved by dividing it into pieces and addressing issues individually while ensuring that the pieces are ultimately compatible and can be integrated.

This division of the start-up, ramp-up, and sustainment problem is shown schematically in Figure 6.1.1 below. As seen in the figure, four divisions and discharge phases are outlined, and each has received differing degrees of emphasis in NSTX. Coaxial Helicity Injection (CHI) has been the plasma start-up technique tested most extensively on NSTX as described in Section 6.4, and plasma guns, poloidal field

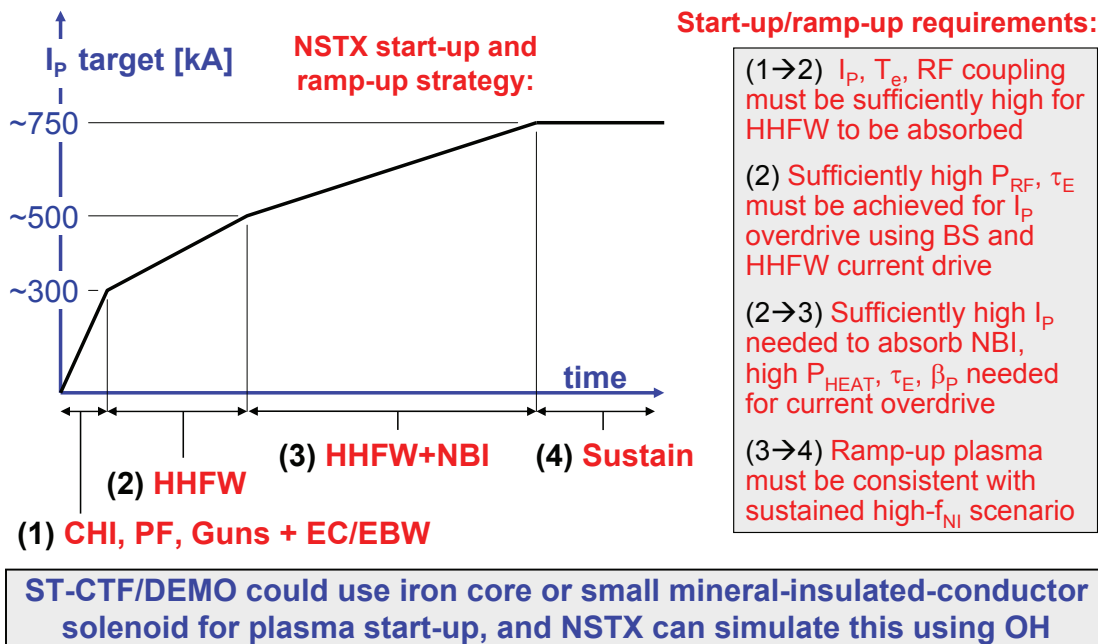


Figure 6.1.1: Division of plasma formation and sustainment problem into 4 distinct pieces as function of time and plasma current: (1) plasma start-up, (2) initial heating and over-drive ramp-up of start-up plasma, (3) additional heating and current drive for additional over-drive to full operating current, and (4) plasma sustainment phase.

start-up, and ECH/EBW start-up are planned to be tested in the five year plan. For plasma current ramp-up from low plasma current, high-harmonic fast-waves have heated 200kA H-mode plasmas to  $T_e > 1\text{keV}$  and generated high bootstrap fractions up to 85%. Increased heating power will be implemented to attempt to increase the bootstrap current  $> 100\%$  for plasma current ramp-up. For the present NBI sources, NBI power is only well absorbed for plasma currents above approximately 500kA in NSTX, so NBI ramp-up of the plasma current has been tested to only a very limited extent in NSTX. The combination of higher NBI power (from the 2<sup>nd</sup> neutral beam) and higher toroidal field will enable NBI plasma current ramp-up tests at higher plasma current for which the beam is better absorbed and higher NBI-CD is possible. Finally, for plasma sustainment, up to 70% of the plasma current has been sustained

non-inductively with NBI and BS current drive for plasma currents in the range of 700-800kA. With the major upgrades of NSTX (higher toroidal field and current, 2<sup>nd</sup> neutral beam for additional power and more tangential injection) combined with density reduction, fully non-inductive and controlled scenarios with plasma currents up to 1MA appear possible. In the sections that follow, progress and plans for plasma formation and sustainment for the 5 year period 2009-13 are provided. Since full non-inductive plasma sustainment is paramount to all next-step ST devices, plasma sustainment is treated first.

## 6.2 Plasma sustainment results

The NSTX five year goal for plasma sustainment is a demonstration of fully non-inductive current drive (NICD) in a regime consistent with high beta and high confinement that is extrapolable to next-step ST devices such as ST-CTF [1] and NHTX [2]. Next-step ST devices propose to achieve long-pulse/steady-state operation utilizing primarily bootstrap (BS) current and neutral beam injection (NBI) current drive. Other current-drive sources such as Electron Bernstein Wave (EBW) CD also appear promising for off-axis CD and profile control [3] in the over-dense plasmas of the ST and are under active investigation [4].

Fully non-inductive operation has not yet been demonstrated on any ST device, and full-NICD operation at or above the no-wall limit and with high confinement is extremely challenging for all tokamaks. DIII-D has transiently achieved fully non-inductive operation at high performance utilizing NBI + BS + ECCD, but with un-relaxed profiles [5]. As another example, a reasonably high level of non-inductive current drive (NICD) of approximately 70% has only recently been achieved on JET using NBI and BS [6], and only through operation above the no-wall stability limit [7] utilizing rotational stabilization of the RWM much like NSTX [8] and DIII-D [9]. As shown in Figure 6.2.1, NSTX has made significant progress operating far above the n=1 no-wall limit and near the n=1 ideal-wall limit and with H-mode confinement enhancement factor  $H_{98pby2}=1.0-1.1$  sustained for up to several current redistribution times [10,11]. In these plasmas, approximately 55% of current is provided by the bootstrap current, and 10-15% is provided by NBI-CD, resulting in 65-70% non-inductive current fraction. Also as shown in Figure 6.2.1, the predicted and reconstructed current profiles are in good agreement during periods when the discharges are MHD-quiescent, but there is also evidence that NBI fast-ions and the NBI current drive can be redistributed when large core MHD activity is present [12].

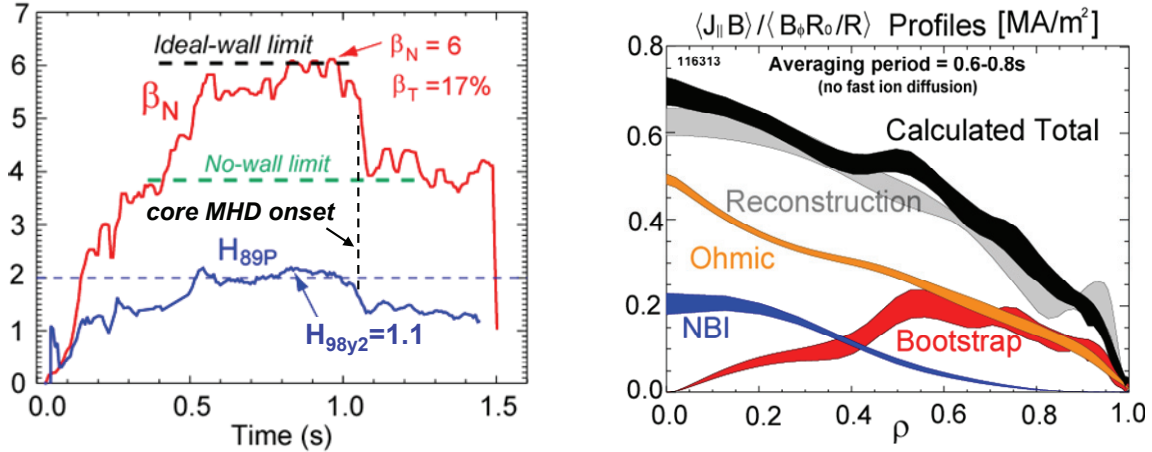


Figure 6.2.1: (Left) Example of integrated high performance discharge 116313 with  $\beta_N$  near the ideal wall limit,  $\beta_T = 15-20\%$ , and high confinement at or above the ITER-98y2 H-mode scaling projection. The high performance phase is sustained for 1.5-2 current redistribution times and 10-15 energy confinement times. The high performance phase is interrupted by core  $n=1$  kink/interchange activity triggered by the  $q$  profile evolving toward  $q_{min} = 1$  and repeated transient excursions above the ideal-wall limit. (Right) Demonstration of good agreement between predicted current profile (including inductive and non-inductive sources) and the reconstructed current profile constrained by the MSE data.

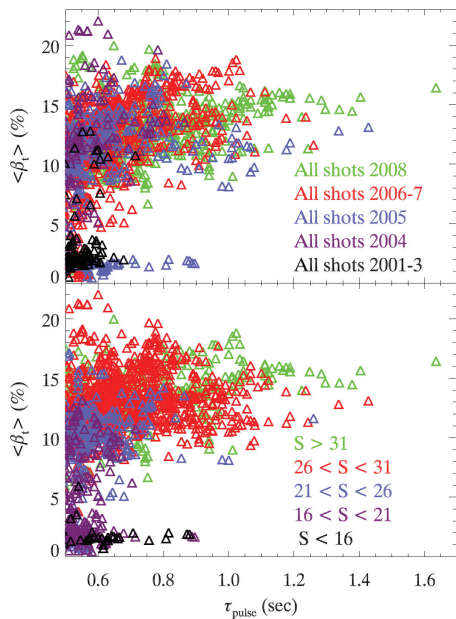


Figure 6.2.2: (Top) shot flat-top-average toroidal beta vs. flat-top duration sorted by year, (bottom) sorted by shaping factor  $S \equiv q_{95} a B_T / I_p [m \cdot T/MA]$ .

As described in Chapter 2 on NSTX Macroscopic Stability, the plasma shaping capability of NSTX has been systematically improved during the last five year period through the replacement of 2 divertor coils to increase the plasma triangularity at high elongation. The elongation has also been increased by taking advantage of reduced latency in the plasma control system, as described in Chapter 7.

As shown in Figure 6.2.2, plasma shaping factor is clearly important in increasing the duration of sustained high plasma beta. Strong plasma shaping can also play an important role in the early discharge evolution by modifying the current profile during the

plasma current ramp. In particular, increased elongation early in the discharge enables the plasma to be

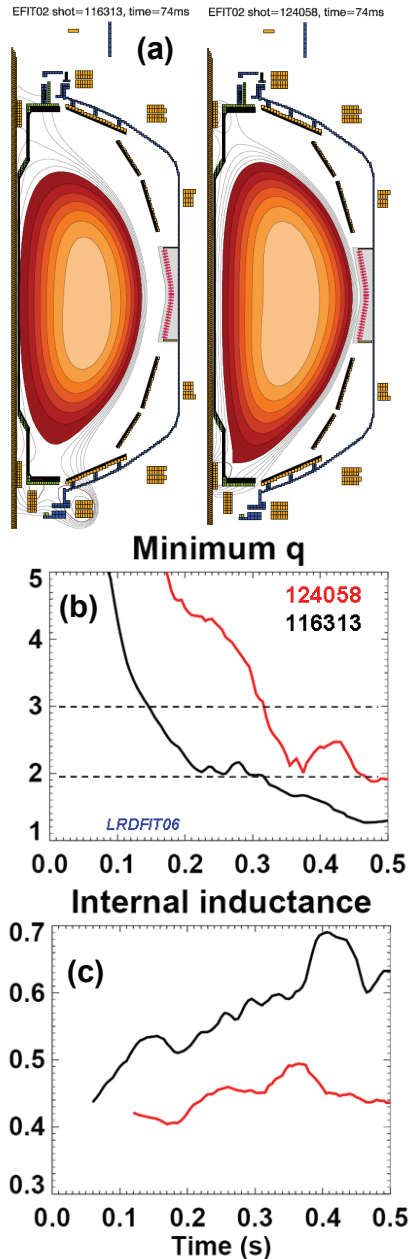


Figure 6.2.3: (a) Comparison of boundary shapes at  $t=74\text{ms}$  during the plasma current ramp without (left) and with (right) increased early elongation, and comparison of (b) minimum  $q$  and (c) internal inductance evolution.

diverted earlier. Increased elongation and triangularity at fixed current increase the magnetic safety factor, and early diverting can improve plasma confinement by enabling early H-mode access. As shown in Figure 6.2.3, increased early shaping ( $\kappa = 1.9 \rightarrow 2.2$  and  $\delta_L = 0.4 \rightarrow 0.8$ ) and early diverting can significantly increase the minimum  $q$  in the plasma and reduce the internal inductance by as much as 25%. By delaying the approach of  $q_{\text{min}}$  toward 1 with strong early shaping, deleterious MHD activity is reduced or avoided increasing discharge pulse-length and the duration of sustained high beta.

In 2006-2008, error field correction was also optimized and utilized routinely in an increasing number of discharge scenarios. In particular, it was found that both  $n=1$  and  $n=3$  error fields are present in NSTX. In the recently implemented EF correction system, the amplification of  $n=1$  error fields (resonant field amplification – RFA) is measured and compensated in real-time. The  $n=1$  RFA suppression algorithm is also effective at actively stabilizing resistive wall modes (RWM) when the plasma rotation is insufficient to stabilize the  $n=1$  RWM. The optimal  $n=3$  error field correction is presently pre-programmed and is apparently indicates the  $n=3$  intrinsic error field is proportional to the PF5 vertical field current. In 2007,  $n=3$  error field correction was shown to aid in the sustainment of high plasma rotation and high beta, and when combined with active  $n=1$  control, can aid

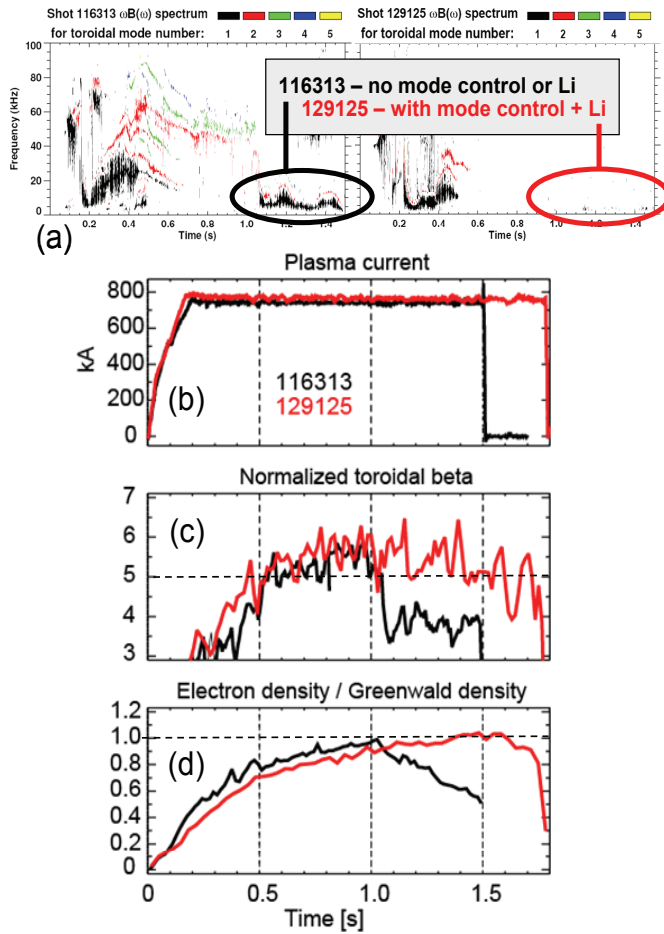


Figure 6.2.4: (a) Elimination of late  $n=1$  MHD mode activity by combination of  $n=1+n=3$  EF correction and lithiumization, (b) achievement of NSTX record pulse-length = 1.8s, (c) sustainment of  $\beta_N > 5$  for 1.1s = 3-4 current redistribution times – doubling the duration of the previous record, and (d) Greenwald density fraction evolution.

the sustainment of very high performance discharges in NSTX.

As shown in Figure 6.2.4, plasmas utilizing this multiple mode-number ( $n=1$  and  $n=3$ ) MHD control (in combination with the after-effects of evaporated lithium on the plasma facing components (PFCs)) have achieved record pulse-lengths in NSTX, and the duration of sustained high normalized beta has been doubled relative to that of Figure 6.2.1. For the record pulse-length discharge, Figure 6.2.5 shows that after  $t=0.8$ s the MSE pitch angle profile changes very little as a function of time. This result indicates that the current profile has reached a near-equilibrium state. The inductively-driven current fraction is estimated to be 35-45% in this discharge. Equilibrium reconstructions show that the minimum  $q$  value in the plasma is constant in time and in the range of 1.2-1.3 after  $t=0.8$ s – consistent with the absence of deleterious  $n=1$  MHD activity commonly observed when the minimum  $q$  is near or below 1.

Overall, improvements to the plasma start-up including early H-mode access [13,14] and early shaping combined with strong shaping in the flat-top, improved error field correction [15], and improved wall conditioning [16] have increased the pulse duration at high performance by a factor of 2 to 3 relative to the beginning of the previous 5 year plan which began in 2004.



From these results, it appears that most core plasma parameters of interest can achieve nearly steady-state

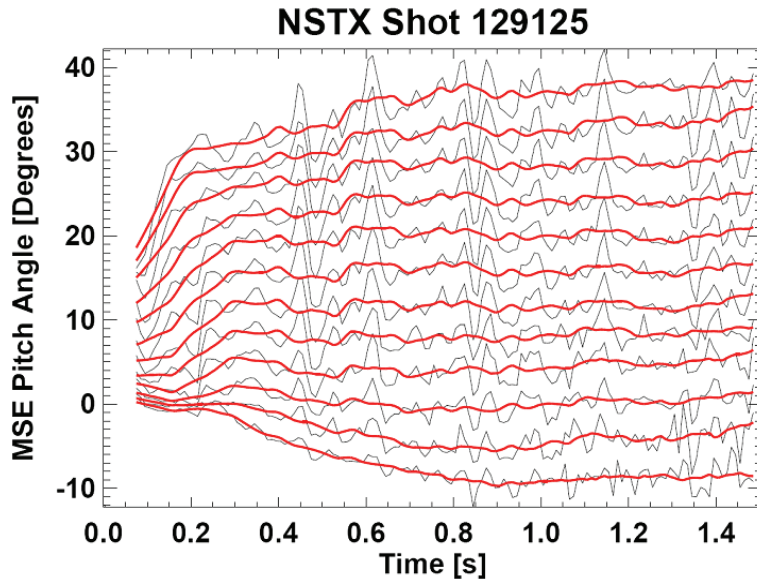


Figure 6.2.5: MSE pitch angle evolution of NSTX long-pulse discharge 129125 showing equilibration of the plasma current density profile after  $t=0.8s$ . Black is measured pitch angle (modulated by ELMs) and red is the time-smoothed pitch angle.

conditions in NSTX discharges.

However, Figure 6.2.4d shows that the plasma density does not reach steady-state conditions in this discharge, but rather continues to increase monotonically toward a Greenwald density ratio of approximately 1 by  $t=1.5s$ . Near this time, the high- $\beta$  phase of the discharge is interrupted by the onset of large ELMs and a reduction in confinement.

Similar density rises are observed in nearly all high performance H-

mode discharges in NSTX.

Improved density control would enable the achievement of more stationary plasma conditions, would enable controlled experiments as a function of density, and would increase the fraction of beam-driven current drive as proposed for next-step ST devices operating with 100% non-inductive current drive. As a result, achieving density control is major emphasis of the NSTX 2009-13 5 year plan. Furthermore, to achieve fully non-inductive current drive in NSTX, the inductive current-drive described above must be replaced by other non-inductive sources. During the next five year period, is not anticipated that sufficient EBW coupling efficiency and/or heating power will be available to provide bulk non-inductive current drive in NSTX. Because of this, and because of the heavy reliance of NBI-CD and BS-CD in the proposed operating scenarios of next-step ST devices, NSTX will focus on increasing the bootstrap and beam-driven currents by all available means.

## 6.3 Plasma sustainment plans

### 6.3.1 Overview

As described above, testing and demonstrating the viability of operating an ST-based magnetic confinement device without inductive current drive is a major goal for the next 5 years. Increased neutral beam and bootstrap current drive are the primary tools proposed for achieving this goal. A critical

**GOALS: reduce  $n_e$ , increase NBI-CD, increase thermal confinement**

Present high $\beta_N$ & $f_{NICD}$	NSTX	NHTX	ST-CTF
A	1.53	1.8	1.5
$\kappa$	2.6-2.7	2.8	3.1
$\beta_T$ [%]	14	12-16	18-28
$\beta_N$ [%-mT/MA]	5.7	4.5-5	4-6
$f_{NICD}$	0.65	1.0	1.0
$f_{BS+PS+Diam}$	0.54	0.65-0.75	0.45-0.5
$f_{NBI-CD}$	0.11	0.25-0.35	0.5-0.55
$f_{Greenwald}$	0.8-1.0	0.4-0.5	0.25-0.3
$H_{98y2}$	1.1	1.3	1.5
<b>Dimensional/Device Parameters:</b>			
<b>Solenoid Capability</b>	Ramp+flat-top	Ramp to full $I_p$	No/partial
$I_p$ [MA]	0.72	3-3.5	8-10
$B_T$ [T]	0.52	2.0	2.5
$R_0$ [m]	0.86	1.0	1.2
$a$ [m]	0.56	0.55	0.8
$I_p / aB_{T0}$ [MA/mT]	2.5	2.7-3.2	4-5

Table 6.3.1: Comparison of key dimensionless and dimensional parameters of present high non-inductive current fraction scenarios in NSTX, and those proposed for NHTX and ST-CTF.

element in making progress toward this goal is to identify and reduce the key operational and scientific gaps between present ST performance and the performance assumed in next-step ST device designs.

Table 6.3.1 shows a comparison of key dimensionless and dimensional parameters of present high non-inductive current fraction scenarios achieved in NSTX, and those proposed for NHTX and ST-CTF. This table shows that several parameters in next-step ST designs have been nearly achieved or even exceeded in NSTX plasmas – in particular the elongation, normalized beta, and bootstrap fraction. However, from this table, it is evident that the beam driven current fraction is lower than assumed in next-step ST designs

by a factor of 2 to 5, the normalized plasma density is higher than assumed by a factor of 2 to 3, and the H-mode confinement enhancement factor must be increased by up to 35%. Since NBI-CD efficiency is proportional to  $T_e / n_e$ , if the electron pressure remains constant as the electron density is varied, the NBI-CD efficiency would be proportional to  $1 / n_e^2$ . Thus, reduced electron density is projected to be a very important means of increasing the beam-driven current. However, if anomalous electron transport is determined by micro-instabilities with a critical gradient threshold for instability, the electron temperature profile may be stiff and may not increase as  $1 / n_e$  as the density is reduced. Thus, additional means of increasing beam current drive efficiency are warranted.

As discussed in Chapter 3, unlike the scaling observed in standard aspect ratio tokamaks, the electron energy confinement in STs scales nearly linearly with toroidal magnetic field. While the origin of this scaling remains unclear, this scaling does highlight the potential importance of increased toroidal field in increasing beam current drive by increasing the electron temperature. Another important means of increasing the beam-driven current is more tangential injection of the beams as has been proposed in the designs of next-step ST devices. As discussed below, for NSTX, more tangential injection ( $R_{TAN}$  up to 1.3m versus present  $R_{TAN} = 0.5$  to 0.7m) is computed to increase the beam current drive efficiency by up to a factor of 1.5 to 2 while also providing off-axis current drive to aid in sustaining  $q_{min} > 1$  to avoid deleterious core MHD activity. Thus, density reduction via pumping, higher toroidal field and current, and more tangential beam injection are the proposed means to increase the NBI current drive in NSTX.

Another key goal is increased thermal energy confinement. This is a very challenging goal, as transport is less directly controllable and improvable in general. Since electron transport is the dominant loss channel in NSTX high-performance H-modes, improvements in electron confinement are essential. Reduced electron thermal diffusivity has been observed in ST plasmas through modifications to the plasma safety factor profile – in particular shear reversal in the plasma core [17]. Utilizing the more tangentially injecting 2<sup>nd</sup> NBI proposed for NSTX, the degree of shear reversal can be controlled over a range of  $\Delta q = 0.5$  to 1, and this could in principle increase the core electron temperature and confinement while also increasing the beam current-drive efficiency. Lithium conditioning of the plasma facing components (PFCs) has also been demonstrated to increase thermal confinement in NSTX H-modes [11], and reduced recycling from liquid lithium PFCs has led to dramatic improvements in energy confinement in the CDX-U tokamak [18].

### 6.3.2 Near-term plans for improved plasma sustainment – FY2009-2011

Increased toroidal field capability from a new centerstack, and improved NBI current-drive efficiency and profiles from a 2<sup>nd</sup> NBI are longer-term major upgrade objectives of the NSTX research program. In the nearer term, NSTX research will focus on density reduction and understanding and utilizing the potential benefits of liquid lithium. Liquid lithium has been shown to be a very efficient pump of D, and this motivates an integrated approach to achieving the density control and confinement improvement goals of NSTX. In particular, NSTX will implement a Liquid Lithium Divertor (LLD) in 2009 as shown in Figure 6.3.1. This is a unique capability in the world program, as NSTX will be the only diverted H-mode tokamak using liquid lithium PFCs. More details of the design of the LLD are given in Chapter 7. The surface area of the LLD has been chosen to provide the needed pumping to reduce the electron density by 25% (for high triangularity  $\delta_{\text{Lower}} = 0.6-0.8$  shapes) to up to 50% (for lower triangularity shapes). This projected degree of density reduction is consistent with increasing the NBI-CD efficiency by a factor of 2 to 4, depending on whether the electron temperature is constant or increases with decreasing density.

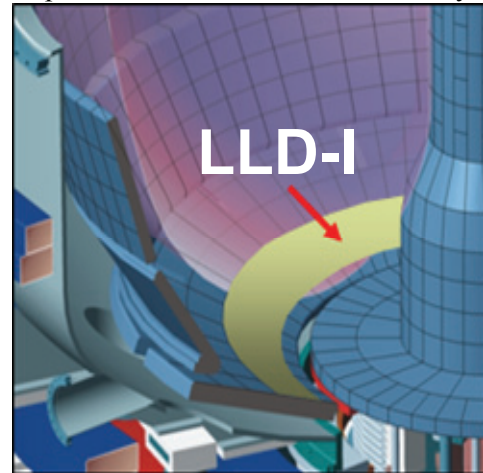


Figure 6.3.1: The NSTX liquid lithium divertor target plate – version 1 (LLD-I) will be located on the outboard divertor of NSTX and is planned to be operational during the FY2009 campaign.

Integrated modeling with the TSC code has been performed [19] to identify approaches to increasing the non-inductive current fraction with the tools presently available on NSTX. The parameters of the two approaches that appear most promising at the present time are summarized in Figure 6.3.2 below. Approach #1 (as described above) reduces the density to increase NBI-CD and thereby increases the non-inductive current fraction to up to 90%. However, because of the centrally peaked NBI-CD profile driven by the present NBI system, the resulting total current density profile is projected to be non-stationary and to reach an unstable equilibrium with  $q_{\text{min}} < 1$  unless the fast-ions are redistributed by MHD activity. Approach #2 utilizes an elevated core safety factor ( $q(0) = 1.4$  to  $2.4$ ) to increase the beta limit, and relies on higher confinement from LLD and/or heating power from HHFW to produce a high bootstrap fraction

plasma at electron density values below but comparable to those presently achieved. Thus, at the very least, both approaches require electron density reduction. Approach #1 with low density and high NBI-CD fraction is most similar to the proposed operating scenario of an ST-CTF, whereas approach #2 with increased bootstrap fraction is closer to the proposed operating scenario of NHTX.

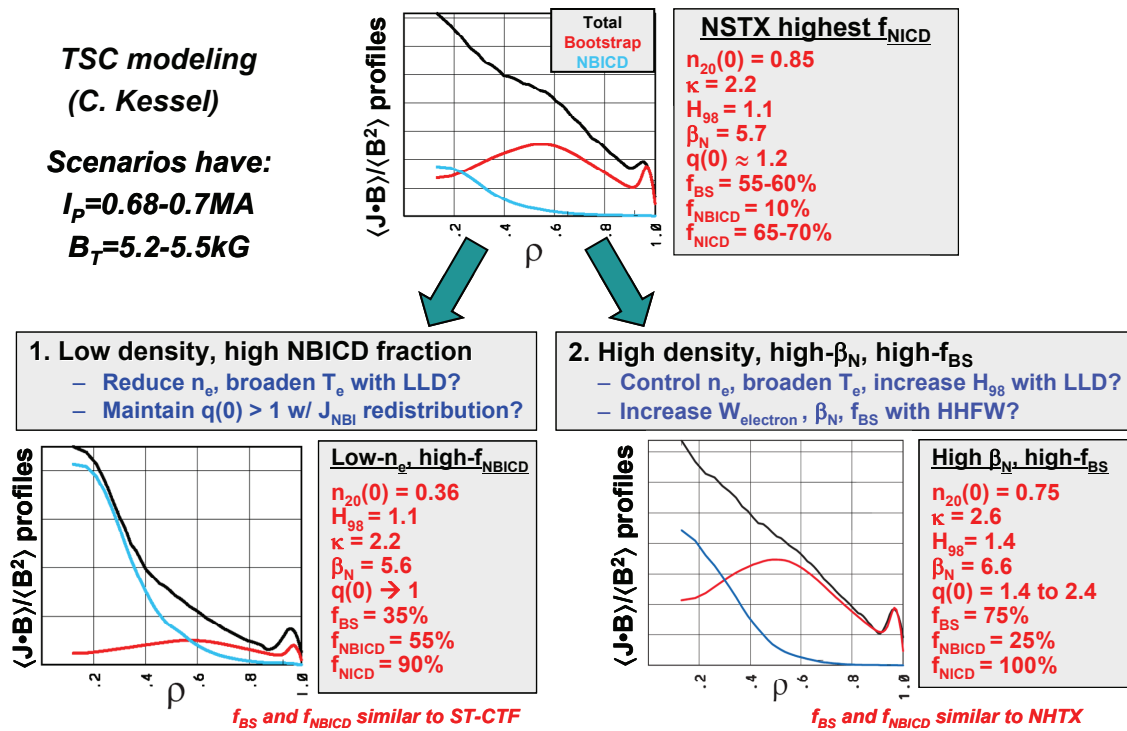


Figure 6.3.2: Comparison of key parameters and current profiles of present NSTX performance (top) and two operational scenarios proposed to increase the fraction of non-inductive current drive (bottom).

Unlike the ST-CTF and NHTX scenarios which are projected to operate near the no-wall stability limit, both NSTX approaches described here require operation above the no-wall stability limit and would rely on the MHD control techniques already developed successfully on NSTX. This difference in stability (i.e. normalized beta) results from NSTX scenarios targeting operation at toroidal beta values comparable to those of next-step STs but at lower normalized current  $I_p/aB_T$ . The lower normalized current operation of NSTX is due in part to the lower normalized NBI-CD efficiency resulting from the more perpendicular beam injection of NSTX, and is also due in part to operation at somewhat lower elongation in NSTX than is assumed in next-step STs. The plan for testing these two approaches is given below.

## 1) Plan for developing low density, high NBI-CD fraction scenario

**FY2008 results:** Characterized non-inductive current-drive fraction versus density, shaping, q

- i) Increased D pumping via more Li + more complete coverage using dual-LITER
- ii) Increased beta-poloidal from 1.5 to 1.8 by operating at higher  $\beta_N$  at high elongation
- iii) Improved fueling control using super-sonic gas injector (SGI) during  $I_p$  ramp phase

### b) FY2009-11 Plans

- i) Characterize D pumping with dual-LITER plus LLD-I and LLD-II
  - (1) Perform FY09 milestone on gas balance and particle retention
- ii) Study pedestal and ELM stability vs. pedestal collisionality and Lithium (FY10 milestone)
  - (1) Further test and understand ELM suppression observed with lithium from LITER
- iii) Characterize NBI  $J(r)$  redistribution from fast-ion and low-frequency MHD (FY09 milestone)

## 2) Plan for developing high normalized beta, high bootstrap fraction scenario

**FY2008 results:**

- i) Assessed confinement, ELM, thermal profile modifications from dual-LITER
- ii) Assessed HHFW heating in deuterium H-modes for advanced scenario applications
- iii) Incorporated n=1 RWM/RFA and n=3 EFC control into most operating scenarios

### b) FY2009-11 - GOAL: increase $f_{\text{NBI-CD}} = 65\text{-}70\% \rightarrow 80\text{-}90\%$ for $\tau \sim \tau_{\text{CR}}$

- i) Assess confinement, ELM, thermal profile modifications from LLD-I and LLD-II
- ii) Increase NBI-CD using lower density, higher/broader electron temperature from LLD
- iii) Use higher power HHFW heating with ELM resilience to increase electron stored energy, bootstrap fraction, and non-inductive current fraction in discharges with elevated q achieved via early H-mode and early strong shaping (see Figure 6.2.3).
- iv) Perform high-elongation wall-stabilized plasma operation – FY09 milestone

- (1) Conditions:  $\kappa$  up to 2.8,  $\tau \geq \tau_{CR}$ , low electron density for high NBI-CD fraction, high normalized beta for high bootstrap fraction
- (2) Integrate ELM reduction techniques into scenarios – use mid-plane coil RMP, or ELM stabilization from Lithium and ELM destabilization from RMP.
- (3) Utilize NBI beta feedback to controllably operate near ideal-wall limit

### 6.3.3 Longer-term plans for improved plasma sustainment – FY2012-2013

The two major upgrades to NSTX proposed to be operational in the FY2012-2013 time period are:

- (1) **2012**: A new centerstack (CS) with:
  - a. increased toroidal field: 0.55T  $\rightarrow$  1T
  - b. increased plasma current: 1MA  $\rightarrow$  2MA
  - c. increased pulse duration: 1s  $\rightarrow$  5s (at full TF)
- (2) **2013 (incremental)**: A 2<sup>nd</sup> NBI system with increased tangency radius for improved NBI current-drive efficiency, current profile control, and increased heating power.

#### Role of upgraded center-stack in fully non-inductive operation

These upgrades are presently planned to be staged, and the CS upgrade is planned to occur first, in part to enable access to higher toroidal field to more rapidly enable access to higher non-inductive current fraction. Higher toroidal field is advantageous for increasing the non-inductive fraction for several reasons. First, bootstrap fraction  $f_{BS} \propto \beta_p$ , where the poloidal beta  $\beta_p \propto \beta_N q^*$  where  $\beta_N$  is the normalized beta and  $q^*$  is the kink safety factor. Since  $q^* \propto B_T$ ,  $f_{BS}$  can be increased significantly without increasing the drive for pressure-driven instabilities, i.e. without increasing  $\beta_N$ . Or,  $\beta_N$  may be reduced to values further away from the ideal-wall limit without large sacrifices in bootstrap fraction. Second, as described in Chapter 3, the electron thermal confinement is proportional to  $B_T$ , so increased toroidal field is projected to increase the electron temperature and increase both the bootstrap fraction and the beam current-drive efficiency. Of course, if the total stored energy does not increase  $\propto B_T^2$  as the field is increased, the toroidal beta will decrease and could approach values that are less attractive for next-step ST applications. However, the 2<sup>nd</sup> NBI would double the available NBI heating power and provide

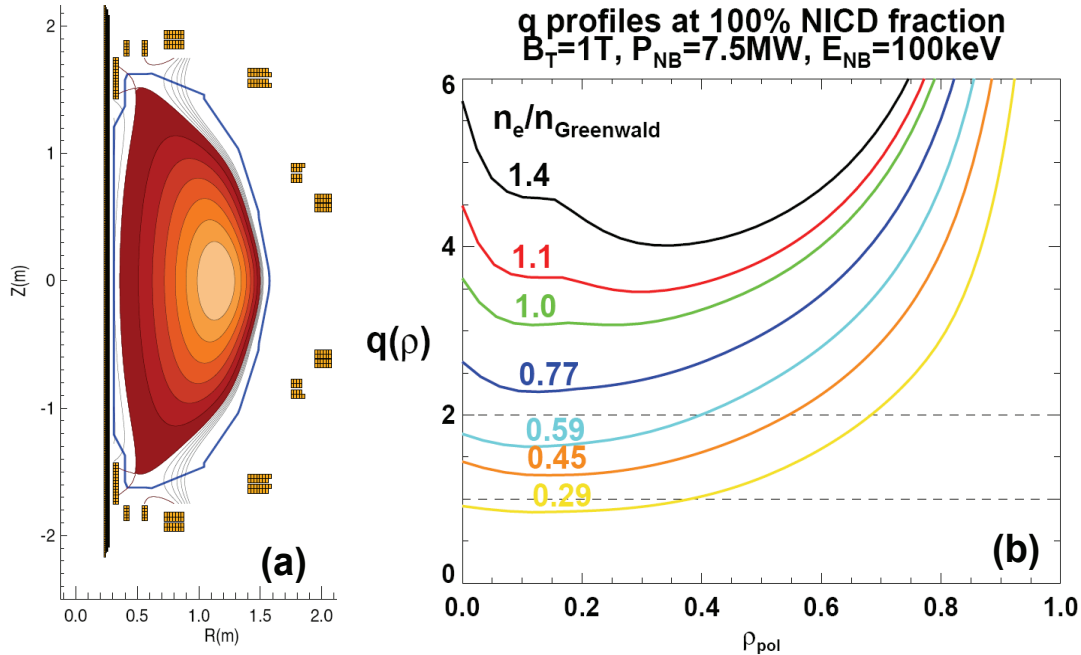


Figure 6.3.3: (a) Plasma equilibrium used in fully non-inductive profile calculations, and (b)  $q$  profile variation as the plasma density is varied between  $n_e/n_{Greenwald} = 0.3$  to 1.4 for fully non-inductive scenarios with  $B_T = 1T$  (utilizing the CS upgrade) and 7.5MW of injected NBI power using the existing 3 NBI sources.

additional plasma current, enabling recovery of access to high beta at high toroidal field if a single NBI source is insufficient to reach the beta limit at high field.

As shown in Figure 6.3.3a, the proposed new CS capable of high toroidal field = 1T operation supports strongly shaped diverted equilibria with  $A=1.6$ ,  $\kappa=2.7$ , and  $\delta=0.7$ . For the equilibrium shown, the divertor coils are designed and operated to generate very large poloidal flux expansion ( $|\nabla\psi_p|$  ratio of 20-40) while exhausting the outer SOL flux surfaces onto the outboard divertor where LLD will be located. For the new CS, additional divertor PF coils could prove quite important in controlling and optimizing the plasma exhaust to the divertor targets.

The broadened operating space enabled by a doubling of the toroidal field is very valuable for determining the optimal profiles and other parameters for achieving full non-inductive current drive in next-step STs. A key profile for stability and confinement optimization is the magnetic safety factor profile. As shown in Figure 6.3.3b, with increased toroidal field = 1T, fully non-inductive scenarios can be obtained for a wide range of  $q$  profiles with  $q_{min}$  ranging from 1 to 4 as the electron density is varied



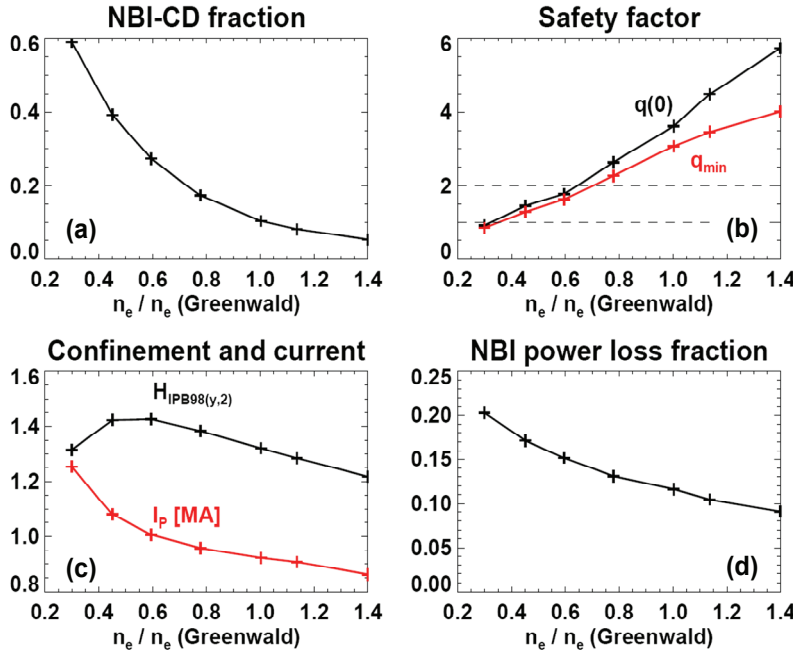


Figure 6.3.4: (a) Fraction of NBI CD, (b) central and minimum  $q$ , (c) H-mode confinement multiplier and plasma current, and (d) fraction of NBI power lost as a function of electron density ratio  $n_e / n_{\text{Greenwald}}$  for the fully non-inductive scenarios of Figure 6.3.3.

from a Greenwald fraction  $n_e / n_{\text{Greenwald}} = 0.3$  to 1.4. In these scans, the density is used to control the central NBI-CD efficiency which in turn controls  $q_{\text{min}}$ . Importantly, access to such a range of  $q$  profiles can be achieved at  $\beta_N = 4.5-5$  which is near the  $n=1$  no-wall limit. These profiles can be achieved using a combination of BS current and NBI current drive using the existing 3 NBI sources operated at 100keV and 7.5MW of total injected power plus an additional 4MW of HHFW heating power. For reference, the

density and temperature profiles used in the TRANSP calculations of these profiles are scaled versions of the experimental profiles from discharge 116313 discussed in Figure 6.2.1, and  $T_i/T_e$  is held fixed at 1.5. As is evident from the figure,  $q_{\text{min}} > 1$  is accessible for  $n_e / n_{\text{Greenwald}} > 0.35-0.4$ , and  $q_{\text{min}} > 3$  is accessible for  $n_e / n_{\text{Greenwald}} \approx 1$ . For these scenarios,  $\beta_T \approx 10\%$ , and higher  $\beta_T$  could be achieved from higher  $\beta_N$  or from higher current from increased NBI power from the 2<sup>nd</sup> NBI.

For these fully non-inductive scenarios at higher toroidal field = 1T, a key consideration is the plasma confinement required to support the plasma thermal energy and associated bootstrap current. To absorb most of the injected NBI power (more than 80%) over a wide range of plasma density variation, sufficient plasma current and density must be present. With only 7.5MW of auxiliary heating power from the existing 3 NBI sources,  $H_{\text{IPB98}(y,2)}$  factors of 1.5-1.7 would be required to support the plasma thermal energy to provide the bootstrap current and NBI-CD to support the equilibrium. These high values are beyond those assumed for next-step STs, and additional auxiliary heating power is required to reduce the required confinement closer to the assumed values. For this reason, an additional 4MW of HHFW

heating power is added to the scenarios above resulting in  $H_{IPB98(y,2)}$  values of 1.2-1.4 which are closer to presently achievable experimental values. Since 2MW of HHFW heating power can presently be coupled to NSTX H-mode discharges, the planned antenna upgrade to double the coupled power should provide sufficient margin to supplement the NBI heating power with up to 4MW of HHFW power. As shown in Figure 6.3.4, with this additional heating power, a wide range of NBI-CD fractions = 5 to 60%,  $q_{min}$  values = 1 to 4, and  $I_p = 0.85$  to 1.25MA are in principle accessible with at least 80% of the NBI power absorbed without exceeding  $H_{IPB98(y,2)} = 1.5$  which is the H-mode confinement enhancement value assumed for ST-CTF.

Should these levels of confinement not be achievable, additional heating power from the 2<sup>nd</sup> NBI (see Figure 6.3.8 below) could reduce the required  $H_{IPB98(y,2)}$  to values less than 1.2, i.e. values achievable in present experiments. Another possibility is to operate at lower plasma current (and  $\beta_T$ ) as shown for the TSC simulation of Figure 6.3.9.

### Role of 2<sup>nd</sup> NBI in fully non-inductive operation

As shown in Figure 6.3.5, the injection geometry of the proposed 2<sup>nd</sup> NBI is much more tangential than the present NBI system. The more tangential injection geometry is chosen to provide increased current drive efficiency while also providing for more variability in the driven current profile – ranging from centrally peaked to a profile broader than that obtain with any of the existing sources. As described below, this variability in the NBI-driven current profile can provide a means to modify and control the equilibrium  $q$  profile.

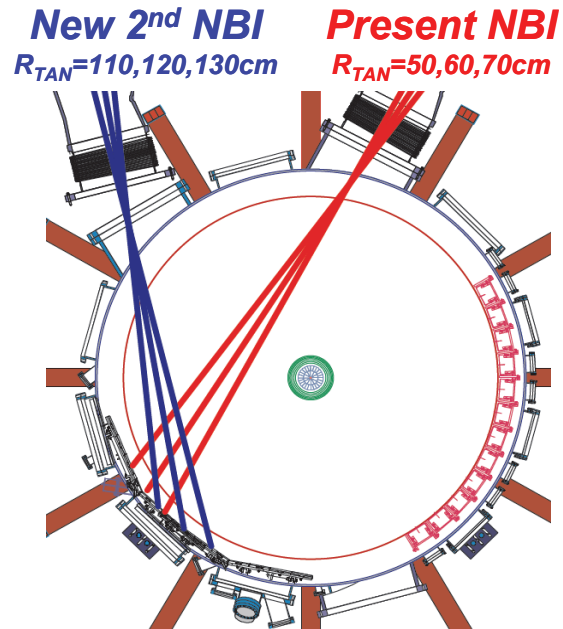


Figure 6.3.5: Injection geometry of present NBI (red) and proposed 2<sup>nd</sup> NBI (blue) with increased tangency radius of injection.

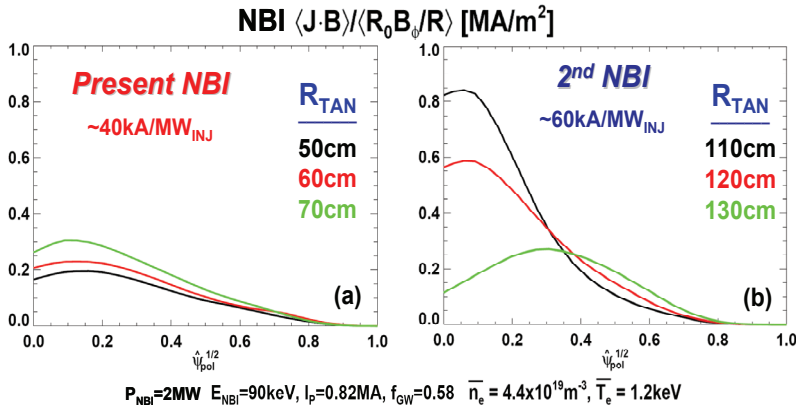


Figure 6.3.6: Comparison of the NBI-CD profiles for (a) the present NBI and (b) the proposed 2<sup>nd</sup> NBI with increased tangency radius.

As shown in Figure 6.3.6a, for the present NBI injection system, the profile shapes of the NBI-CD depend very little on the tangency radius of the source. The only significant difference among these sources is the 30% lower CD efficiency of the  $R_{\text{TAN}}=50\text{cm}$  source relative to the  $R_{\text{TAN}}=70\text{cm}$  source. In contrast, as shown in Figure 6.3.6b, the 2<sup>nd</sup> NBI source

with increased tangency radius provides up to a factor of 8 variation in driven central current drive, and all three sources offer higher current drive efficiency than the present NBI system by a factor of 1.5 to 2. The combination of the existing and 2<sup>nd</sup> NBI systems would provide a wide range of possible NBI-CD

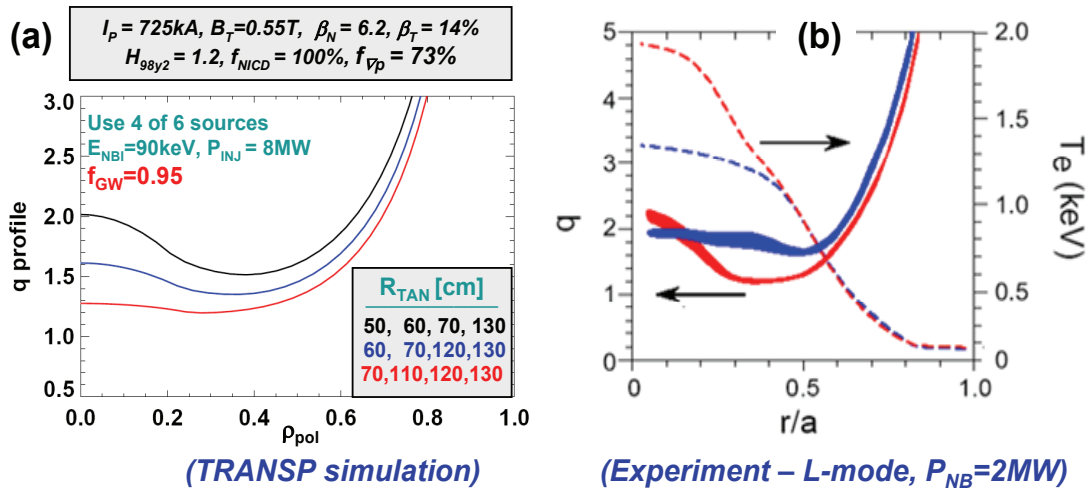


Figure 6.3.7: (a) Simulated  $q$  profiles for a mix of present and new NBI sources chosen to vary the degree of magnetic shear reversal while maintaining  $q_{\text{min}} > 1.2$ , and (b) experimentally observed variation of electron confinement with magnetic shear in L-mode.

profiles and resultant  $q$ -profiles while also providing increased heating power to increase the plasma stored energy to increase the bootstrap fraction at confinement and beta values comparable to those presently achieved. Figure 6.3.7a shows that even at the relatively low value of toroidal field of 0.55T of the present CS, fully non-inductive plasmas with  $q_{\text{min}} = 1.2$  to 1.5 can be obtained with  $\beta_N \approx 6$  and

$H_{IPB98(y,2)} = 1.2$  by operating at  $f_{GW} \approx 1$  – values comparable to those achieved in present experiments. Further, by varying the mix of available sources, the degree of shear reversal can be controlled.

As shown in Figure 6.3.7b, the magnetic shear is an important parameter in determining the electron transport in L-mode, and the influence of magnetic shear on electron transport presumably applies to H-mode scenarios as well. Thus, the  $q$  profile control enabled by the combination of the existing and 2<sup>nd</sup> NBI could provide a means of modifying and possibly controlling core electron transport. Control of the equilibrium  $q$  profile using NBI-CD could also be used to control and optimize MHD stability.

As shown in Figure 6.3.8, at higher  $B_T = 1T$  and with 4 NBI sources ( $P_{NB} = 10MW$ ),  $q$  profile control

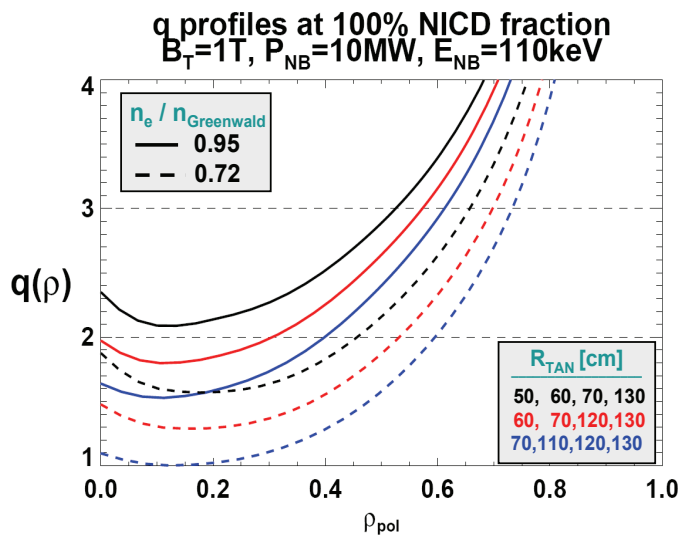


Figure 6.3.8: TRANSP simulations of full NICD  $q$  profiles vs. NBI source at  $B_T=1T, I_p=0.95MA, n_e / n_{Greenwald} = 0.72$  and  $0.95, H_{IPB98(y,2)} = 1.2, \beta_N=5, \beta_T=10\%, P_{NB}=10MW, P_{RF}=4MW$

with  $q_{min} = 1.0$  to  $2.2$  is possible by varying the mix of present and new sources in combination with electron density variation. This capability would enable controlled studies of NTM and low-n kink/RWM stability with and without a  $q=2$  surface in the plasma, and as a function of core magnetic shear. This research is highly relevant to next-step STs presently assumed to operate with  $q_{min} > 2$  to avoid low-n NTMs and thereby eliminate the requirement for active control techniques for stabilizing NTMs. Importantly, these results show that the combination of higher toroidal

field of the new CS and the additional NBI sources from 2<sup>nd</sup> NBI should enable the achievement of fully non-inductive scenarios with controllable core safety factor (including  $q_{min} > 2$ ) with normalized values of plasma density, confinement, and stability achieved in present experiments, namely:  $n_e / n_{Greenwald} = 0.72$  to  $0.95, H_{IPB98(y,2)} = 1.1$  to  $1.2$ , and  $\beta_N=5.1$ . Fully non-inductive solutions at lower  $B_{T0} = 0.75T$  also exist with  $I_p=1MA, \beta_T = 16\%, \beta_N = 6.1, n_e / n_{Greenwald} = 0.7, q_{min} \geq 1.3$ , and  $H_{IPB98(y,2)} = 1.25$ .

Finally, not only is HHFW heating power projected to be important for achieving fully non-inductive conditions with reduced thermal confinement requirements, but current drive from HHFW is also potentially useful as an on-axis current profile control tool. In particular, the HHFW-driven current density shown in Figure 4.1.1 of Chapter 4 scales to  $0.4\text{MW/m}^2$  at  $P_{\text{RF}}=4\text{MW}$  for the  $n_e / n_{\text{Greenwald}} = 0.72$  plasma scenario shown in Figure 6.3.8. This RF-driven current density is approximately 50% of the equilibrium current density at the magnetic axis, so HHFW-CD could in principle provide significant additional control of  $q(0)$ , and therefore of the magnetic shear in the plasma core by raising  $q(0)$  from 1.2-1.5 to values above 2.

### Pulse-length requirements for current profile equilibration

Sufficient flat-top duration (several current relaxation times) is required to achieve and demonstrate stationary fully-non-inductive current drive. Such a demonstration would significantly increase

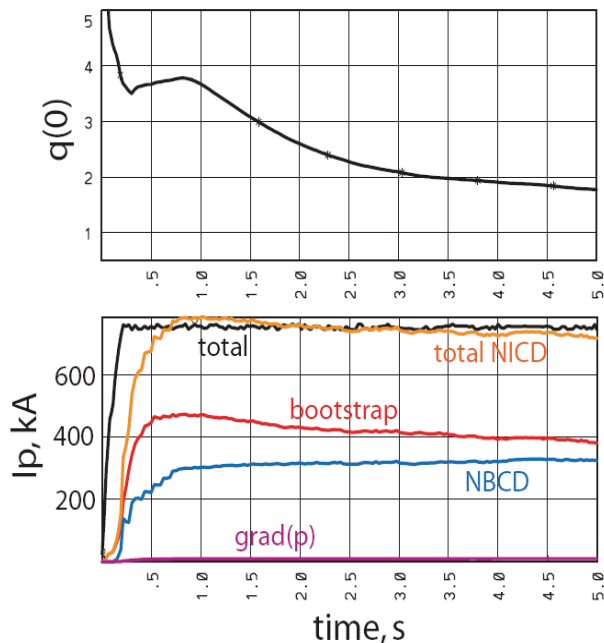


Figure 6.3.9: Preliminary TSC simulations indicating that nearly stationary fully non-inductive 1T, 750kA discharges are possible with upgraded TF and NBI capabilities.

confidence in extrapolating present understanding and control of non-inductive current drive sources to next-step ST devices. As described above, scenario modeling indicates that full non-inductive operation can most effectively be achieved at higher TF (i.e. at least 0.55T and preferably 0.8-1T). Since the proposed scenarios all operate at higher electron temperature than presently achieved in high density H-modes, the current redistribution time is expected to increase by up to a factor of 3 - from approximately 0.3s to up to 1s if the electron temperature doubles.

As seen in Figure 6.2.5 above, 2 to 3 current redistribution times are required for the current profile to reach a partially inductively-driven equilibrium, and an additional 2 to 3 current redistribution times are needed to measure the profiles as stationary. Thus, we also expect that toroidal field flat-top duration at least 3 times longer than presently achievable is required to achieve and measure

a stationary fully non-inductive current profile. The upgraded CS is designed to provide a 5s flat-top duration at full TF = 1T and is consistent with this requirement, and could operate for up to 8s at  $B_T = 0.8T$  if additional pulse-length is required at high toroidal field.

These simple estimates of the flat-top durations required to approach current profile equilibration with full non-inductive current drive are consistent with time-dependent simulations performed with the TSC code. Shown in Figure 6.3.9 is a TSC simulation result in which a 1T, 750kA fully non-inductive discharge is achieved at near stationary conditions using 6.15MW of absorbed neutral beam power with a Greenwald density fraction = 0.6 and  $H_{98}$  confinement factor of 1.15. By  $t=5s$  the central  $q$  is nearly independent of time with  $q(0) = 1.8$  and  $li(1) = 0.88$ . These results are consistent with the TRANSP simulation results of Figure 6.3.3 scaled to lower plasma current and H-mode confinement enhancement.

## **Additional capabilities needed to support long-pulse operation**

### Divertor heat flux mitigation

One key area of concern for the upgraded NSTX is the power handling capability of the plasma material interfaces. Recent heat flux scaling studies in NSTX over a limited range of plasma current (700kA to 1MA) indicate a very strong (faster than inverse) narrowing of the divertor heat-flux width as the plasma current is increased. These scalings need to be developed over a much wider parameter range to improve their utility in projecting to future ST devices, but using these scalings, very narrow midplane SOL profile widths (4-6 mm) and high divertor heat-fluxes ( $10^7$ 's of  $MW/m^2$ ) at or beyond ITER values are projected to be possible at higher field and heating power in NSTX. Further, recent results indicate that Li-conditioning of the plasma facing components using evaporated lithium can result in further narrowing of the SOL heat-flux width. Heat flux reduction from enhanced divertor radiation and partial outboard divertor detachment has already been demonstrated on NSTX [20] and has shown to be compatible with good plasma performance in H-mode at high density. Partial detachment can be further tested at higher heat flux and in reduced recycling conditions enabled by the LLD. The compatibility of radiative divertor solutions with reduced recycling and  $n_e$  control from LLD is a key question for the NSTX 5 year program.

To provide additional heat-flux reduction tools for NSTX, the enhanced divertor coil set shown in Figure 6.3.3 proposed for the upgraded CS would improved strike point control, enable strike point sweeping, and enable increased outboard divertor flux expansion as proposed for the “X-divertor” [21]. Finally, divertor heat fluxes in the range of  $10\text{MW/m}^2$  exhausted onto the LLD-I (cooled between shots) are expected to cause the LLD surface temperature to increase at a rate of  $0.35^\circ\text{C/ms}$  to  $0.5^\circ\text{C/ms}$ . Thus, the liquid lithium would reach evaporation temperatures on time-scales of order 1s and active cooling of the LLD would be required for compatibility of the LLD with long-pulse (5s) operation. It should also be noted that for similar heat fluxes, graphite PFC temperatures in the divertor are projected to reach an NSTX administrative limit of  $1200^\circ\text{C}$  within 2-3 seconds. Thus, for very high heat fluxes, active divertor cooling may be required for long-pulse operation independent of the type of divertor used in NSTX.

#### ELM and impurity control

Another potential concern is the impact of high transient heat loads from Edge Localized Modes (ELMs). While ELMs may not be problematic for the NSTX divertor, they could severely limit the lifetime of the divertor of ST-CTF. ELMs are also considered a major problem for ITER, and both pellet pacing and resonant magnetic perturbations (RMPs) are being considered to mitigate ELMs to limit the ELM energy density loss (to  $< 0.5\text{MJ/m}^2$ ) to avoid ablation/melting of C/metal divertor PFCs. Recognizing the importance of ELM mitigation to future ST devices and ITER, a high-n RMP coil set is part of the NSTX 5 year upgrade plan. As discussed in Chapter 2 on MHD stability, these non-axisymmetric control coils (NCC) also have a wide range of additional applications including control of rotation, error-fields, and resistive wall modes.

As described in Chapter 5, an important recent result from NSTX is that the existing mid-plane RMP coils (RWM/EF coils) have been shown to de-stabilize ELMs rather than stabilize them, despite having satisfied the Chirikov  $> 1$  criterion over most of the pedestal width as has been observed to be required for ELM mitigation in experiments on DIII-D [22]. The mechanisms for the observed ELM destabilization in NSTX plasmas are not yet understood. NSTX does not observe density pump-out during RMP as observed in other experiments, perhaps due to the lack of active pumping. One possible explanation of these results is that rotational shielding of the applied RMP fields may be limiting the degree of ergodization in NSTX RMP experiments, while the 3D RMP magnetic field perturbation modifies the

plasma rotation and/or the neoclassical or turbulent transport in the pedestal which in turn modifies the pedestal stability.

Despite the lack of success of suppressing ELMs with RMP fields in NSTX, Li-conditioning of the PFCs has succeeded in eliminating ELMs completely resulting in ELM-free H-mode. While this leads to significant and beneficial increases in thermal confinement, impurity accumulation and high radiation fractions are also observed in such conditions. Importantly, ELM destabilization from the mid-plane RMP coils has successfully triggered Type-I ELMs in these conditions and has reduced the impurity accumulation by a factor of two in initial experiments. Additional optimization is needed to reduce the ELM size and radiation levels further, but overall, the combination of Lithium with RMP fields appear very promising as a means of controlling ELMs and impurity accumulation. A significant issue with the present RMP coil set is the lack

of poloidal mode number spectral control and the resultant inability to strongly resonantly interact with the plasma edge at higher edge  $q$  values. Since the impact of RMPs on edge transport and stability remains poorly understood, and because a high degree of spectral flexibility is important to allow controlled RMP experiments, the NCC coil set shown in Figure 6.3.10 is high priority in the NSTX 5 year plan with incremental funding. Importantly, this proposed coil set in combination with the existing coil set would have a configuration very similar to that proposed for ITER, i.e. with coils above, at, and below the midplane with high- $n$  ( $n > 3$ ) capability. The high- $n$  (up to  $n=6$ ) NCC system would be a unique and important capability for understanding RMP and MHD physics in general. Further, this capability could be important for localizing field perturbations to the plasma edge to minimize core flow damping to aid rotational stabilization of resistive wall modes for stable long-pulse operation at high  $\beta_N$ .

**1) Plans for assessing impact of major upgrades on plasma performance and sustainment**

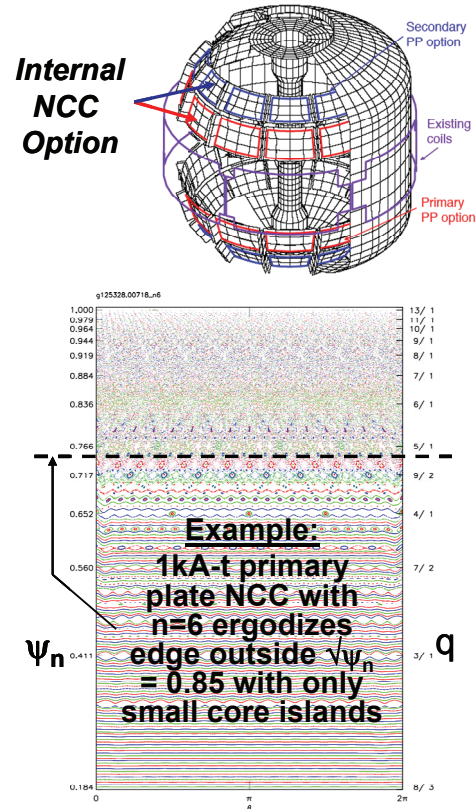


Figure 6.3.10: (top) NCC coils proposed for NSTX, (bottom) example of vacuum field calculation of localized ergodization of edge using  $n=6$  RMP.



**a) FY2012**

- i) Assess impact of higher A on vertical stability and  $n > 0$  no-wall and ideal-wall stability limits. Determine if sufficient power is available to reach  $n > 0$  stability limits at higher  $B_T$ .
- ii) Assess impact of higher  $B_T$  on energy confinement in general, and electron confinement in particular, and the impact of confinement on plasma sustainment.
- iii) Assess impact of higher  $B_T$  on non-inductive current drive sources
  - (1) Assess impact of higher  $B_T$  on bootstrap fraction through confinement modifications
  - (2) Assess impact of higher  $B_T$  on NBI-CD efficiency as a function of  $T_e$
  - (3) Assess impact of higher  $B_T$  on fast-ion-driven instabilities and possible redistribution of fast-ions and NBI-CD.
  - (4) Implement real-time MSE diagnostic for future current profile control
- iv) Assess impact of higher  $B_T$  and  $I_p$  on SOL and divertor heat-flux widths
- v) Assess impact of longer pulse-length on divertor temperature evolution, and develop operating scenarios that minimize peak heat flux as required.
- vi) Assess impact of NCC coils (incremental) on pedestal stability in long-pulse discharges.

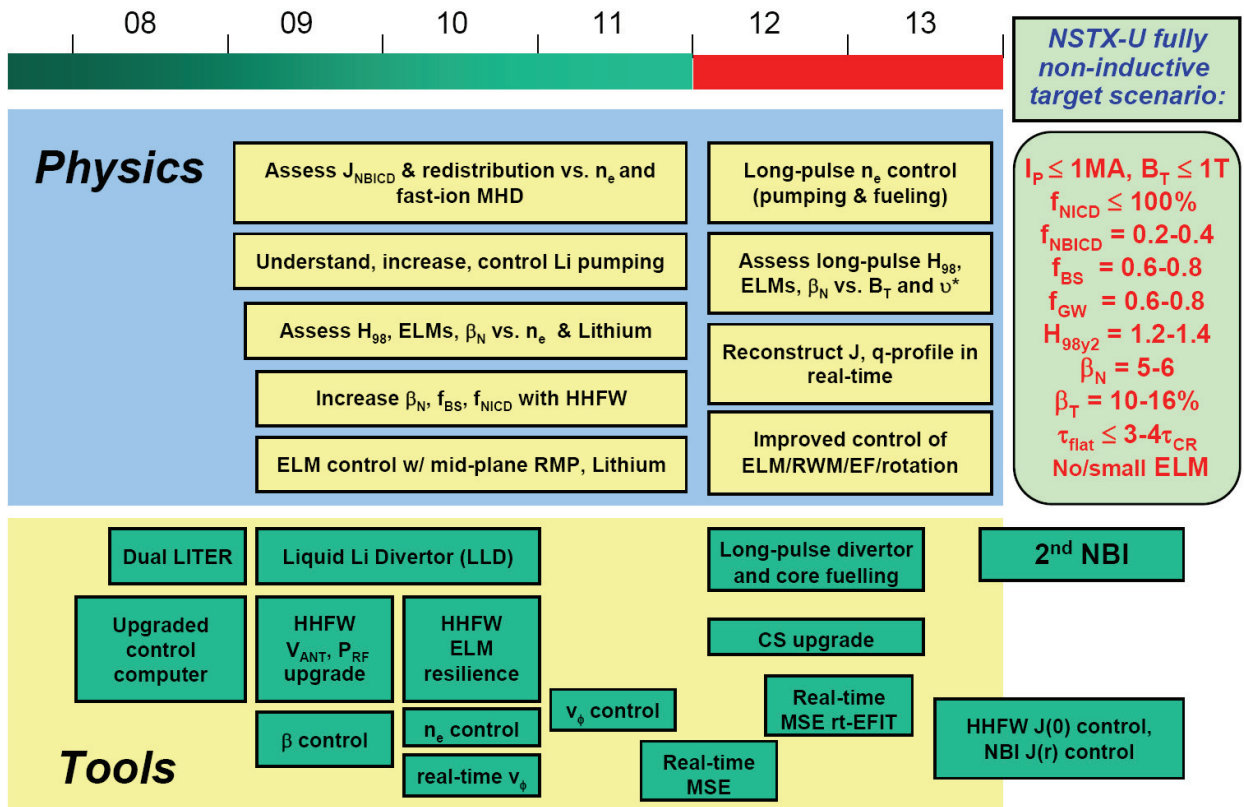
**b) FY2013**

- i) Assess HHFW coupling, heating, and CD at higher  $B_T$ 
  - (1) Vary central HHFW-CD to vary  $q(0)$ , assess impact on confinement and MHD stability
  - (2) Using real-time MSE, implement and assess algorithms for HHFW-based  $q(0)$  control
- ii) Assess impact of NCC coils (incremental) on rotation damping and SOL heat flux widths in sustained conditions.

**The additional research plans below assume the 2<sup>nd</sup> NBI is available during FY2013 (incremental):**

- iii) Assess impact of more tangential injection on fast-ion distribution function and on Alfvén eigenmode stability and resultant impact on driven current profile. Assess predicted vs. measured power deposition and current drive profiles from new NBI sources.
- iv) Assess impact of higher power and lower collisionality on SOL and divertor heat-flux widths and impact of divertor performance on plasma sustainment – for example impurity influx and accumulation.
- v) Assess impact of higher power and/or more tangential injection (and possible fast-ion losses) on divertor temperature evolution, and develop operating scenarios that minimize peak heat flux as required.
- vi) Vary mix of NBI sources to vary NBI-CD profile to modify  $q$  profile, and assess impact of global stability and confinement properties
  - (1) Using real-time MSE, implement and assess algorithms for NBI-based  $J$  profile control

### 2009 – 2013 Timeline for Plasma Current Sustainment and Control Research



## References (for Plasma Sustainment)

- [1] Y.-K. M. Peng, et al., Plasma Phys. Control. Fusion **47** (2005) B263–B283
- [2] J.E. Menard, et al., PPPL Report 4252
- [3] G. Taylor, et al., Phys. Plasmas **11**, (2004) 4733
- [4] S.J. Diem, et al., PPPL Report 4307
- [5] M. Murakami, et al., Phys. Plasmas **13**, 056106 (2006)
- [6] C.D. Challis, et al., EFDA Report EFD-C(07)03/29
- [7] M.P. Gryaznevich, et al., EFDA Report EFD-C(07)03/41
- [8] S.A. Sabbagh, et al., Nucl. Fusion **46**, (2006) 635–644
- [9] A.M. Garofalo, et al., Phys. Rev. Lett. **89**, (2002) 235001
- [10] D.A. Gates, et al., Nucl. Fusion **47**, (2007) 1376–1382
- [11] J.E. Menard, et al., Nucl. Fusion **47**, (2007) S645–S657
- [12] J.E. Menard, et al., Phys. Rev. Lett. **97**, 095002 (2006)
- [13] J.E. Menard, et al. Nucl. Fusion **45**, (2005) 539
- [14] D.A. Gates, et al., Nucl. Fusion **46**, (2006) S22–S28
- [15] J.E. Menard, et al., APS-DPP 2007, Invited talk UI1.00001
- [16] H.W. Kugel, et al., Phys. Plasmas **15**, 056118 (2008)
- [17] F. M. Levinton, et al., Phys. Plasmas **14**, 056119 (2007)
- [18] R. Majeski, Phys. Rev. Lett. **97**, 075002 (2006)
- [19] C.E. Kessel, et al., Phys. Plasmas **13**, 056108 (2006)
- [20] V.A. Soukhanovskii, et al., Journal of Nuclear Materials, Volumes 363-365, 432-436 (2007)
- [21] M. Kotschenreuther, et al., Phys. Plasmas **14**, 072502 (2007)
- [22] T.E. Evans, et al., Phys. Rev. Lett. **92**, 235003 (2004)

## 6.4 Plasma start-up and ramp-up results and plans

The Spherical Torus (ST) is capable of simultaneous operation at high beta and high bootstrap current fraction. These advantages of the ST configuration arise as a result of its small aspect ratio. At the low aspect ratios needed for an ST reactor, elimination of the central solenoid is necessary. Thus current generation methods that do not rely on the central solenoid are necessary for the viability of the ST concept. Elimination of the central solenoid could also lead to a more compact tokamak. Thus ST-based fusion systems including the CTF (Component Test Facility) and power plant designs (e.g., ARIES-ST) assume complete elimination of the ohmic solenoid. The investigation of plasma start-up without the ohmic solenoid is a major component of the NSTX research program. NSTX is exploring the technique known as Coaxial Helicity Injection (CHI) [1] and Outer Poloidal Field Start-up [2] as methods to produce the initial plasma and sufficient toroidal plasma current to allow other methods of non-inductive current drive and sustainment to be applied. Other new methods such as Plasma Gun Injection [3] will also be studied during the FY 2009 to 2013 period. Of the three US major magnetic fusion facilities (DIII-D, NSTX, C-Mod), at the present time NSTX is the only one actively conducting OH-solenoid-free start-up research. The goal of solenoid-free startup research in NSTX is to first generate high current discharges that do not rely on the central solenoid and then to ramp these up non-inductively to currents >800 kA using NBI and RF with minimal reliance on induction from the central solenoid.

### 6.4.1 Coaxial Helicity Injection

The CHI concept is an outgrowth of the spheromak research [4]. It has also been tried on DIII-D [5]. A number of smaller helicity injection experiments were performed with some success prior to introducing it on NSTX [6-9]. More recently, the HIT-II device has unambiguously demonstrated plasma start-up using this method [10]. The method has now also successfully produced 160kA of closed flux current in NSTX, which is a world record for non-inductively generated closed flux current [11,12]. As part of the proposed center stack upgrade to NSTX, the toroidal field in NSTX would be nearly doubled from present values. As described later, this now gives NSTX the potential to produce more than 500kA of CHI produced closed flux current, a level at which the realization for non-inductive startup, ramp-up and sustainment become much easier. The CHI research on NSTX has benefited greatly from a close

collaboration with the HIT-II experiment at the University of Washington. The CHI near term research goal is to improve the coupling of the CHI produced current to induction from the central solenoid and beyond that to other non inductive current drive methods.

CHI is a promising candidate for non-inductive current initiation and has, in addition, the potential to drive edge current during the sustained phase of a discharge for the purpose of controlling the edge current profile to improve plasma stability limits and to optimize the bootstrap current fraction. Other possible benefits include inducing edge plasma rotation for transport barrier sustainment and controlling edge SOL flows. The development of these methods would improve the prospects of the ST as a fusion reactor.

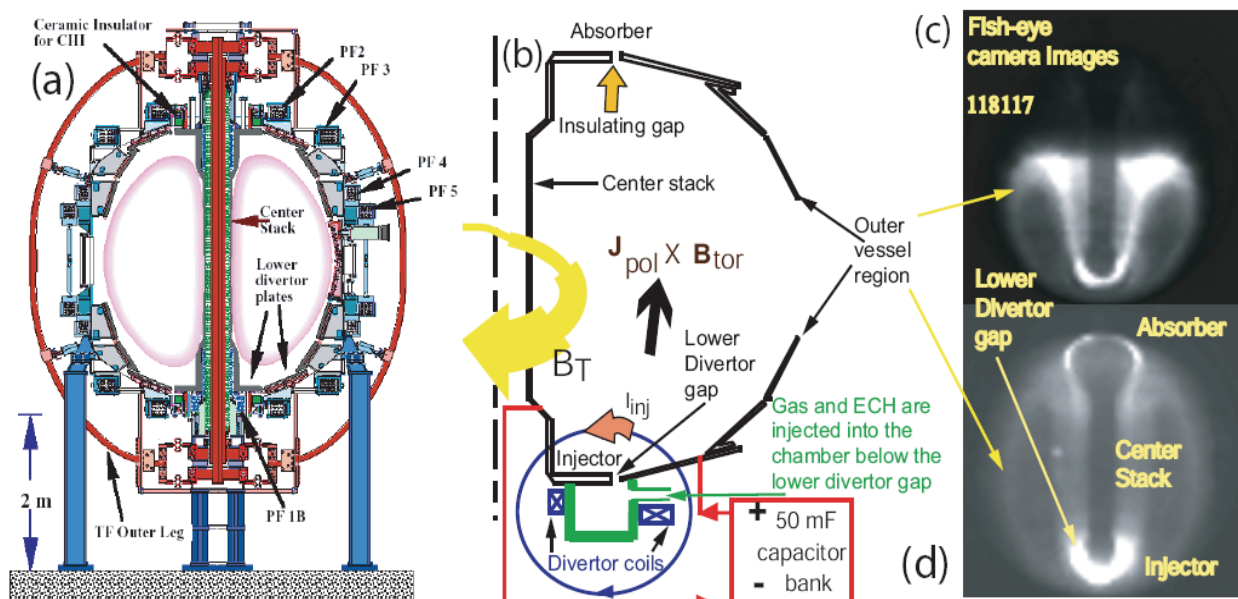


Figure 6.4.1: (a) The NSTX machine layout showing the location of the toroidal insulator and external poloidal field coils. Shown also are (b) the NSTX machine components used for CHI startup in NSTX and fast camera fish eye images showing (c) discharge evolution from near the injector region and (d) later during the discharge. Both gas and 18 GHz microwave power are injected in to a 100 Liter toroidal cavity beneath the lower divertor plates. The gas, which is ionized by the microwaves, emerges from the gap between the lower divertor plates, which eases the requirements for breakdown when the main capacitor bank discharge is initiated.

An important advantage of CHI start-up is that it could be used for closed flux plasma generation without any time variations in the PF coil currents as demonstrated on HIT-II [13]. Therefore, it is compatible

with future reactor system that would rely on superconducting PF coils, and PF coils located far away from the plasma.

**CHI implementation on NSTX** - In order to accommodate CHI, the stainless steel vacuum vessel (nominal major radius 0.85 m, volume 30 m<sup>3</sup>) has separate inner and outer sections, electrically isolated from each other by toroidal ceramic rings at the top and bottom which also act as vacuum seals. An alternate way to implement it is to insulate one of the lower divertor plates from the rest of the vessel as was done in D-III-D. This would avoid the need for a vacuum insulator. The inner divertor plate, which is part of the center stack assembly, is then electrically separated from the outer divertor plate, which is attached to the outer vessel. This is illustrated in Figure 6.4.1. For CHI, the poloidal field coils located beneath the lower insulated gap are used to produce poloidal flux connecting the lower inner and outer divertor plates, as indicated qualitatively by the circle in Figure 6.4.1b. When a small amount of deuterium gas is introduced into the chamber below the lower divertor plates and a voltage (typically 1 – 2 kV) is applied between the plates, a discharge forms with current flowing in the plasma from the outer divertor plate to the inner lower divertor plate, as shown by the arrow in Figure 6.4.1b. In the presence of a toroidal field, the plasma current, which essentially flows along field lines, develops a toroidal component. The bright region at the top of Figure 6.4.1c is the top of the CHI plasma that has extended to approximately the middle of the vessel at a time during the discharge when the plasma current is below the peak value. As the plasma current increases to near the peak value, the discharge further elongates vertically to fill the vessel as shown in Figure 6.4.1d. The bright ring shaped region at the top of this image is referred to as an absorber arc, a condition when part of the injector current bridges the upper divertor gap. We refer to the lower gap connected by the poloidal field as the injector and the complementary upper gap as the absorber because when voltage is applied toroidal flux flows out of the injector and into the absorber.

The toroidal plasma current produced by CHI initially flows on open field lines joining the electrodes. In order to produce toroidal plasma current on closed flux surfaces magnetic reconnection must occur. In steady state, this reconnection depends on the development of some form of non-axisymmetric plasma perturbation. In transient CHI, the initial poloidal field magnitude is chosen such that the plasma carrying the injected current rapidly expands into the chamber. When the injected current is rapidly decreased,

magnetic reconnection occurs near the injection electrodes, with the toroidal plasma current forming closed flux surfaces. The method of transient CHI has now been successfully used on NSTX producing an unambiguous demonstration of closed-flux current generation without the use of the central solenoid.

**Transient CHI Startup-** CHI can be applied in two ways. In both methods the toroidal plasma current produced by CHI initially flows on open field lines joining the electrodes. In order to produce toroidal plasma current on closed flux surfaces magnetic reconnection must occur. In the first approach referred to as *steady state* or *driven* CHI, closed flux current generation relies on the development of some form of non-axisymmetric plasma perturbation. This mode of CHI operation, in which the injector circuit is continuously driven for a time longer than the timescale for resistive decay of the toroidal current ( $t_{pulse} > \tau_{L/R}$ ) was initially studied in the early CHI experiments in NSTX [14, 15, 16]. However, for the purpose of initial plasma startup it was found in the HIT-II ST that a new mode of CHI operation in an ST, referred to as *transient* CHI [10], which involves only axisymmetric magnetic reconnection works very well and produces useful closed flux equilibrium. In transient CHI, the initial poloidal field configuration is chosen such that the plasma carrying the injected current rapidly expands into the chamber. When the injected current is rapidly decreased, magnetic reconnection occurs near the injection electrodes, with the toroidal plasma current forming closed flux surfaces. The method of transient CHI has now been successfully used on NSTX producing an unambiguous demonstration of closed-flux current generation without the use of the central solenoid [17]. The transient CHI method is therefore now being pursued as the preferred CHI method to start the NSTX discharge without the use of the solenoid.

There are two objectives for CHI research on NSTX. The primary objective is to start-up the NSTX plasma using CHI and to hand it off initially to inductive operation and then later to a non-inductive current drive system. The second objective is to provide edge current drive during sustained non-inductive operation, for the purpose of controlling the edge current profile and to modify the edge SOL flows.

For transient CHI, a 5-45 mF capacitor bank was used at up to 1.75kV to provide the injector current. The present operating condition for CHI in NSTX uses the inner vessel and inner divertor plates as the cathode while the outer divertor plates and vessel are the anode. The operational sequence for CHI



involves first energizing the toroidal field coils and the CHI injector coils to produce the desired flux conditions in the injector region. The CHI voltage is then applied to the inner and outer divertor plates and a pre-programmed amount of gas and 10kW of electron cyclotron waves at 18GHz are injected in an injector cavity below the lower divertor plates. This condition ensures that there is adequate energy in the capacitor bank for ionization and heating of the injected gas. The resulting current initially flows along helical magnetic field lines connecting the lower divertor plates. The large ratio of the applied toroidal field to the poloidal field causes the current in the plasma to develop a strong toroidal component, the beginning of the desired toroidal plasma current generation. If the injector current exceeds a threshold value, known as the bubble burst condition, the resulting  $\Delta B_{\text{tor}}^2$ , ( $J_{\text{pol}} \times B_{\text{tor}}$ ), stress across the current layer exceeds the field-line tension of the injector flux causing the helicity and plasma in the lower divertor region to expand into the main torus chamber. The initial poloidal field configuration is chosen such that the plasma rapidly expands into the chamber. When the injected current is then rapidly decreased, magnetic reconnection occurs near the injection electrodes, with the toroidal plasma current forming closed flux surfaces.

In Figure 6.4.2, we show traces for the toroidal plasma current, the injector current and fast camera images at two different times during the discharge. Note that the generated toroidal plasma current is about sixty times the injector current. The CHI capacitor bank discharge is initiated at 5ms. In these experiments the discharge rapidly grows to fill the vessel within about 2ms, then starting at about 9ms the discharge begins to detach from the injector electrodes. At 11ms, the injector current is zero and about 60kA of plasma current is still present. Note that at 13ms, the ring shaped plasma is clearly disconnected from both the injector and the upper divertor plate regions. As time progresses, the large bore plasma that fills the vessel gradually shrinks in size and after about  $t = 14\text{ms}$ , it evolves into a small diameter plasma ring, as seen in the 15ms time frame image. The formation of closed flux regions is clearly seen in the camera frames corresponding to 11ms and beyond as expected from a decaying closed magnetic flux configuration. For these discharges, circuit calculations show that only about 7kJ of capacitor bank energy is expended to generate 60kA of closed flux current. Electron pressure and temperature profiles from Thomson scattering show that profiles at later times are less hollow than at earlier times. This is consistent with the CHI startup process, since initially CHI drives current in the edge. After reconnection in the injector region, one expects the current profile to flatten, which should result in the profiles

becoming less hollow. The evolution of a hollow pressure profile into a peaked pressure profile is shown in Fig. 6.4.2c. The measured electron temperatures of about 20eV, combined with a plasma inductance of about  $0.5 - 1\mu\text{H}$ , should result in an e-folding current decay time on the order of about 8ms, which is consistent with the observed current persistence time after the injector current has been reduced to zero.

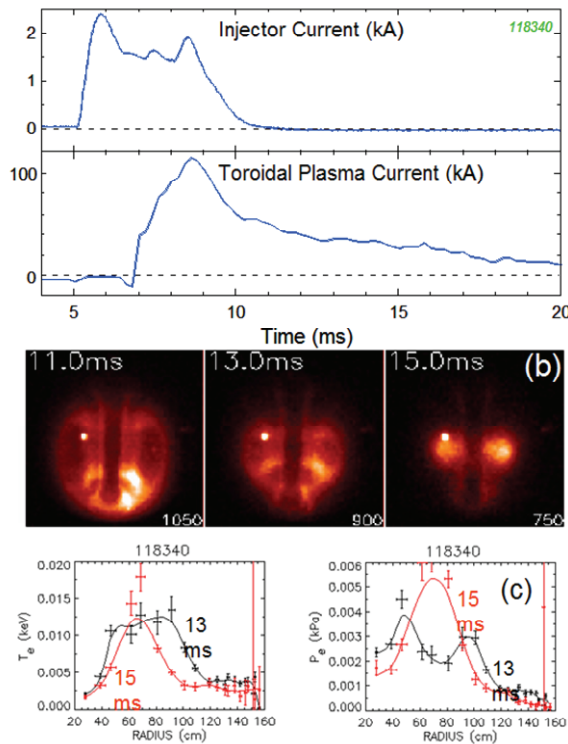


Figure 6.4.2: Shown are (a) Injector and plasma current traces (b) fast camera images and (c) the electron density and electron pressure profiles, at 13 and 15ms from a CHI discharge in NSTX. In this discharge about 2kA of injector current produces 120kA of toroidal current resulting in a current multiplication of 60. The best attained current multiplication (not shown here) was 70. During these discharges, the NSTX CS was disconnected from its power supply. The small bright glow is light from a tungsten filament. The images at 11 and 13ms show an elongated dark region, which is surrounded by a brighter region, like usual tokamak photos. It is useful to note that an absorber arc has not been produced in this discharge.

Equilibrium reconstructions from discharge 120874 are shown in Figure 6.4.3. The experimentally measured poloidal magnetic field, from 40 sensors, and poloidal flux, from 44 flux loops, are used in the computation of the Grad-Shafranov plasma equilibrium. While equilibrium reconstructions show the presence of closed flux for lower current discharges, such as for example, the data shown in Figure 6.4.2, equilibrium reconstructions for the higher current discharges such as for shot 120874, are much more robust and result in residuals similar to that in conventional inductive discharges. The  $\chi^2$ , which is a measure of the residual error, for the fit shown in Figure 6.4.3 is 50.

At the time  $I_{inj}$  is reduced to zero this discharge has 150kA of current, After  $t = 9\text{ms}$ , there is no  $I_{inj}$ , therefore there are no open field line currents. The only plausible explanation for the decaying current magnitude from 150kA to 70kA at 12ms is that it must result from decaying closed flux equilibrium, which is consistent with the equilibrium reconstructions. The LRDFIT

Grad-Shafranov equilibrium code, developed by J. Menard, which is now in routine use for NSTX

discharges, is used for these reconstructions. The code uses a circuit equation model of the plasma, vessel, and passive plate currents to better constrain the

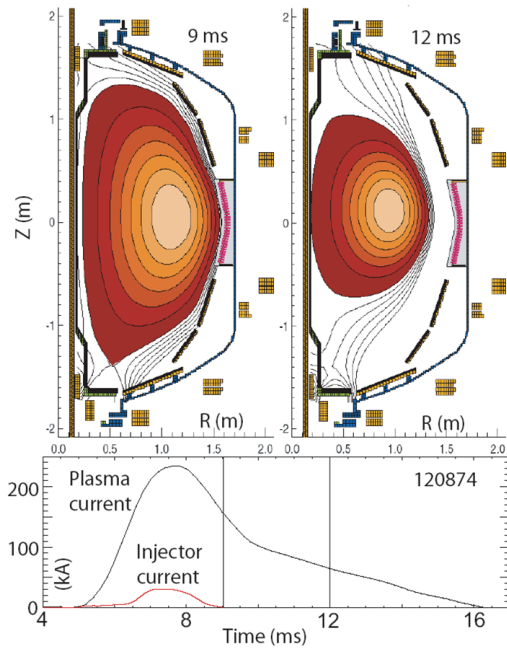


Figure 6.4.3: Equilibrium reconstructions show the shape evolution of the CHI produced plasma in response to decaying current, which is further evidence of decoupling from the injector leaving behind an inductively decaying plasma. In this discharge the increase in  $I_{inj}$  around 7.5ms is due to the presence of an absorber arc. Overdriving the injector by using a larger capacitor bank (45mF, charged to 1.8kV) caused a large amount of unused capacitor bank energy to be dissipated as an absorber arc, which probably contributed to an increase in the resistivity of these yet unoptimized discharges.

order of magnitude larger than the previous results on HIT-II. Experiments on the HIT-II device have shown that CHI discharges couple to and outperform inductive-only discharges, an example of which is shown in Figure 6.4.4.

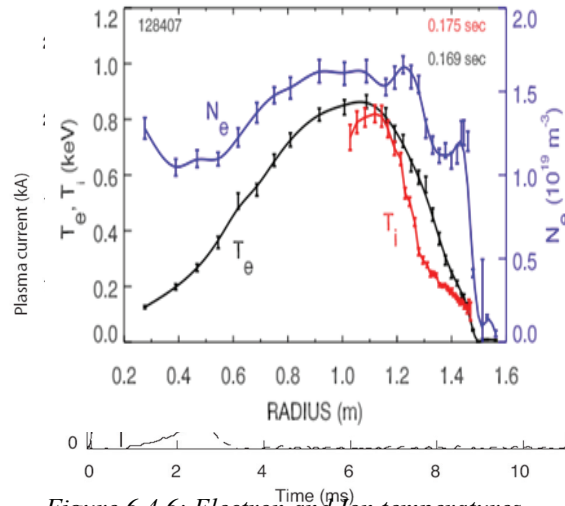


Figure 6.4.6: Electron and ion temperatures and the density profile of a CHI started discharge. The dashed trace is a CHI only discharge that was coupled to induction. The vertical dashed line shows the time at which the CHI injector current is reduced to zero. CHI current persistence beyond this time is due to the existence of a closed flux equilibrium. It is this closed flux plasma that is inductively driven in shot 30228. For comparison, an inductive only discharge, using the central solenoid, under identical pre-programmed loop voltage time history (total 30 mV s consumed) is also shown (shot 25999).

equilibrium fits at low  $I_p$ .

A result of particular importance for the extrapolation of this method to future machines is that the ratio of the generated plasma current to the injector current exceeds 60 for NSTX. This is an

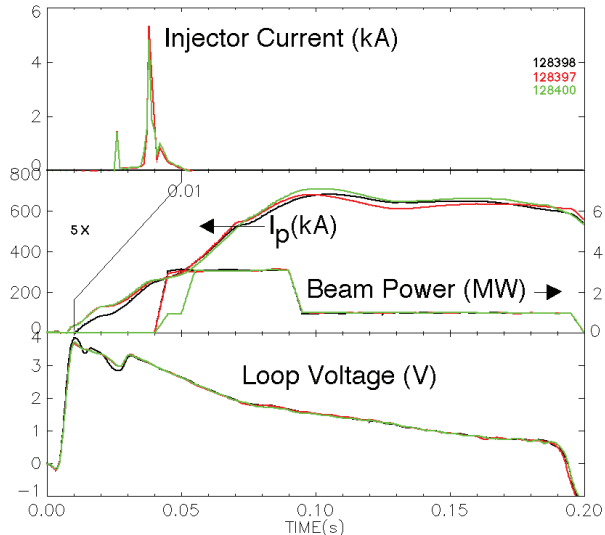


Fig. 6.4.5: Comparison of CHI initiated plasma (green and red curves) with an Ohmic initiated plasma (black curves). Note the expanded time in the top frame. All discharges used the same Ohmic coil current programming.

The Ohmic transformer has been applied in order to provide current drive to sustain and increase the current in CHI initiated discharges on NSTX. Fig. 6.4.5 compares discharges initiated with and without CHI and ramped up to over 600kA using the same ohmic transformer current programming and neutral beam injection heating. CHI initiated discharges can transition into H-Mode, reach electron temperatures of 800eV and have low inductance preferred for high-performance NSTX discharges. Figure 6.4.6 shows the electron density ( $n_e$ ), electron temperature ( $T_e$ ) and ion temperature ( $T_i$ ) profiles for a CHI-initiated, neutral-beam-heated

discharge after the transition into H-mode. However, the CHI discharges did not show the flux savings that was seen on HIT-II. The lack of flux savings is probably due to the influx of impurities with the CHI initiation. Earlier attempts to add the ohmic drive to CHI initiated discharge resulted in no increase in  $I_p$ , but there was a significant increase in the O-II emission measured by a filter scope [17]. It was not until further conditioning was performed in the form of  $D_2$  glow discharge cleaning (GDC) and electrode discharge conditioning that the plasma current was increased by the OH. Further evidence for the need to condition the walls and/or divertor plates is shown in Figure 6.4.7. Shots taken with 1, 2, and 3 capacitor banks in the CHI system differed primarily in the intensity of the low Z impurity emission and increased radiation measured by a bolometer viewing the injector region with only modest changes in the plasma current. The need for excellent vacuum conditions in order to successfully couple the CHI discharge to Ohmic drive was also found on HIT-II.

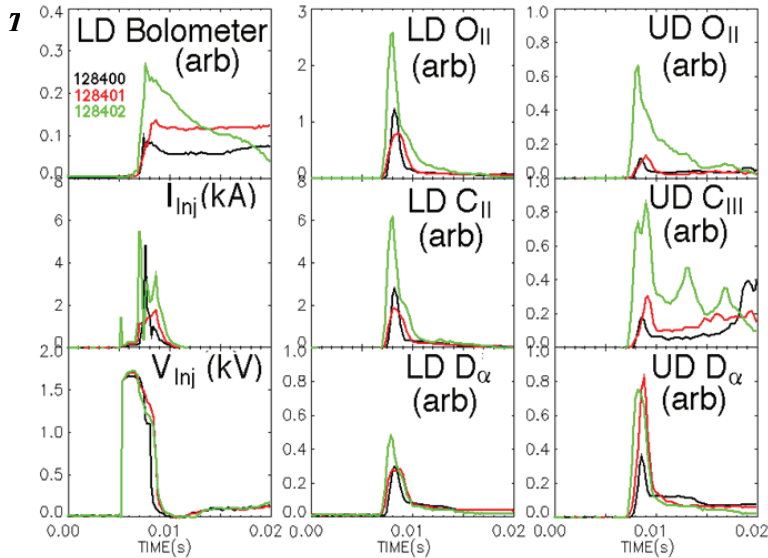


Figure 6.4.7: Discharges with larger capacitor power supplies show increased levels of line radiation and radiated power. Shot 128400 (5 mF bank), 128401 (10 mF), 128402 (15 mF).

## Improvements for CHI research

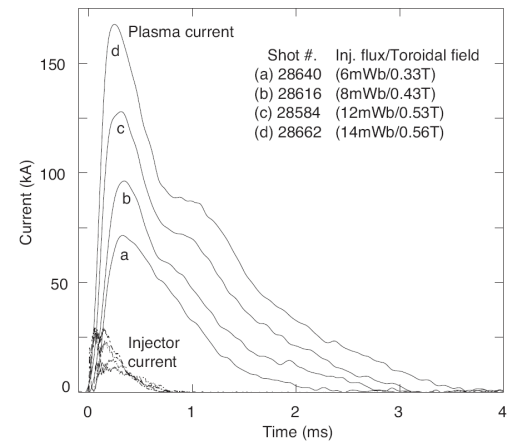


Figure 6.4.8: The amount of useful closed flux plasma current increases with the injector flux. The capacitor bank charge voltages for discharges (a) to (d) are 2.5, 2.7, 3.4 and 3.9 kV respectively. Note that the toroidal field is also increased as the injector flux is increased.

### 1. ECH Heating of CHI Produced discharges:

Results from the HIT-II experiment show that CHI produced discharges couple to induction only if the power radiated by the decaying CHI discharge is less than the input power from ohmic heating. At an applied loop voltage of about 3V, and at 100kA of plasma current, the ohmic input power is about 300kW. Present CHI discharges are observed to have an electron temperature in the range of 10 to 20eV at the start of the current decay phase. The radiated power from the best discharges is probably about 300kW. Because of the decreased sensitivity of the NSTX bolometers to emission below 20eV, the radiated power cannot be accurately estimated. During 2011, a 350kW ECH system is expected to be

available on NSTX. The ECH system will be used to increase the temperature of the CHI target to improve coupling to induction and to other non-inductive current drive methods.

1. Higher CHI voltage capability:

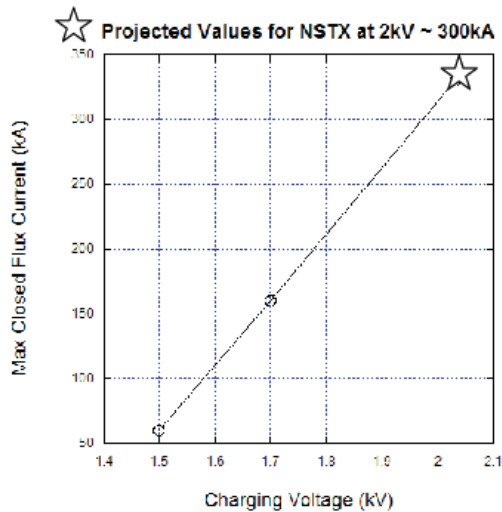


Figure 6.4.9: Projected closed flux current at a capacitor bank charging voltage of 2kV

Results from the HIT-II experiments show that by optimizing the injector voltage, injector flux and toroidal field, the extent of closed flux current can be increased. To increase the closed flux current more injector flux is needed. To reduce the injector current at higher levels of injector flux, the toroidal field needs to be increased. At higher toroidal field, the injector voltage needs to be increased. As a result of such an optimization, the magnitude of closed flux current in HIT-II was increased to 100kA. Figure 6.4.8 shows the results of this optimization.

At present in NSTX, such an optimization scan has not been conducted. At a capacitor bank charging voltage of 1.5kV used during FY 2005, 60kA of closed flux current was achieved. At 1.7kV used during FY 2006-8, 160kA was obtained. As indicated by Figure 6.4.9, at a capacitor bank charging voltage of 2kV closed flux current magnitude of 300kA should be possible. If the voltage could be increased to 2.5kV even higher levels of current should be attainable. If the lower divertor plates could be insulated from the rest of the vessel (similar to the ring electrode that was used on DIII-D), then it should be possible to bias the inner and outer vessel components with respect to this plate, which would allow the injector voltage to be increased to 4kV while maintaining the inner vessel voltage at 2kV. The present voltage snubbing system on the CHI system (the Metal Oxide Varistors) begins to significantly conduct at a voltage of 1.7kV. In order to extend the voltage to the full 2kV, new MOVs with a higher voltage rating are required. This upgrade is planned during 2009-10. In preparation for this, during the 2007 maintenance break, the CHI voltage monitors were improved to better assess the magnitude of the injector voltage transients.

### 3. Absorber field-null control

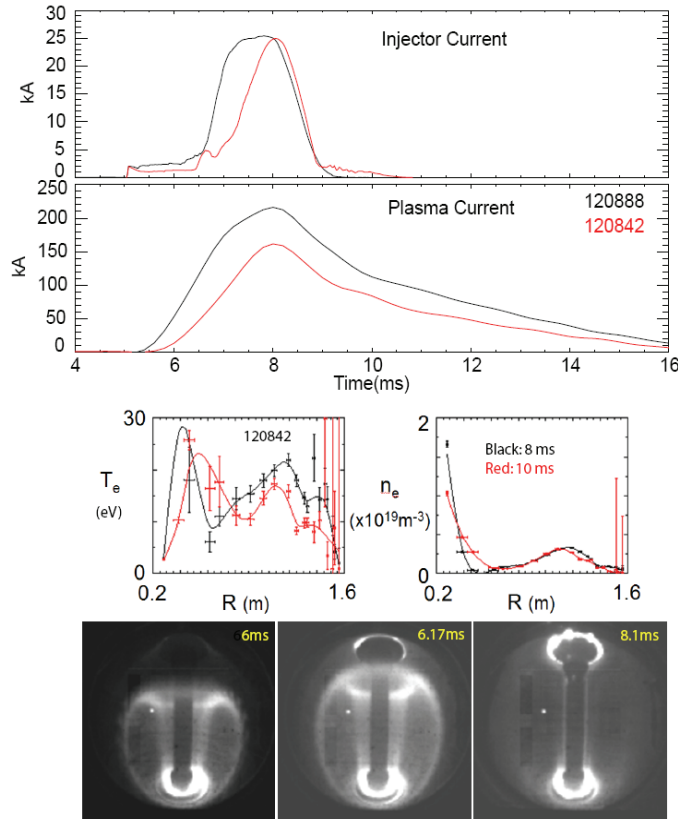


Figure 6.4.10: A discharge (120888) in which about 160 kA of persisting closed flux current is present after the injector current is reduced to zero. A lower current discharge (120842) is also shown along with electron temperature and electron density profiles at 8 and 10 ms. Shown are the injector current, the plasma current, Thomson scattering data (for 120842) and fast camera images for discharge 120888, which show the development of an absorber arc at 6.17 ms. The absorber arc is seen by the bright visible ring that is seen in the absorber region. The arc can be seen intensifying at 8.1 ms. For comparison, note that the images from Figure 6.4.2 do not show evidence for such a visible light emission in the upper divertor gap.

During CHI discharge initiation, the injected current flows along field lines connected to the lower divertor electrodes. As the magnitude of the injected current increases and the plasma grows to fill the vessel, an ionized region begins to form in the upper divertor region. Because of the presence of some poloidal magnetic field in this region (due to fringing fields from the PF5 and PF3U coils), these stray fields provide a conducting path between the upper divertor plates. If the impedance of this path becomes sufficiently low, such as when an ionized plasma front reaches this region due to an elongated plasma, then an alternate current path can develop along the upper divertor region. This is known as an absorber arc. An example of such an arc is shown in Figure 6.4.10. In NSTX, discharges with no absorber arcs typically draw about 2 – 4kA of injector current. Once the absorber arc initiates, the injector current increases to above 15kA, the maximum level dependent on the size of the capacitor bank. This additional arc current serves no useful purpose and could increase the impurity content in the CHI

discharge. On HIT-II, the absorber arcs are minimized by providing a region of poloidal field null in the absorber region. Absorber field control is very effective in minimizing or eliminating absorber arcs in

HIT-II. In preparation for this possibility two new absorber poloidal field coils were installed in NSTX. These coils can be driven using the same power supplies used to drive the Resistive Wall Mode coils in NSTX. Power feed cables from the CHI absorber coils to the RWM power supplies will be installed during the 2008 outage and the plasma control system revised to control these coils to provide a region of poloidal field null in the absorber region during the transient CHI discharge phase.

#### *4. Staged capacitor bank operation*

The CHI power supply consists of up to ten capacitors, each 5mF in size. Any number of these can be connected in parallel and discharged using a single ignitron. Adding two more ignitron switches that would allow two or three ganged up capacitors to discharge in sequence would provide an important control knob for discharge development. The immediate improvement would be that the size of the capacitor bank can be varied between shots without the need for a time consuming controlled access. The second benefit is that it would give greater control of absorber arcs as fewer capacitors could be used for injector flux conditions that require fewer capacitors. Under changing electrode conditions, such as when Lithium is deposited, having the capability to discharge three small banks separated in time by about 1ms, would allow the injector voltage to be maintained at a higher level for longer durations, as required for the transient CHI start-up process. This upgrade has now been completed and has significantly contributed to successful coupling of CHI started discharges to induction.

#### *5. Metal divertor plates*

Results from 2008 show low-z contamination of the CHI discharge to be a severe limitation for increasing the amount of CHI started current that can be coupled to induction . As shown in Figure 6.4.7, as the number of capacitors for initiating the CHI discharge are increased, the radiated power increases and there is increased line radiation from carbon and oxygen. This is a well known result from HIT-II, which shows decreased coupling to induction at increased levels of radiated power. Spheromaks operating with metal electrodes have shown electron temperatures of 500eV. The NSTX divertor plates are relatively easy to replace. For the 2009 campaign for a test of liquid Lithium divertor, part of the lower outer divertor plates would be metallic. Replacing the lower inner plates as well would significantly help CHI discharges by increasing the plasma electron temperature and allowing a high current CHI target to be generated at less



levels of radiated power. This hardware improvement in addition to the 350kW ECH system is very likely necessary to utilize the full potential of CHI in NSTX.

#### *6. Operation at higher toroidal field*

Results from HIT-II (Figure 6.4.8) clearly show that in order to maximize the closed flux current the toroidal field had to be increased. Although it is the injected poloidal flux that is responsible for increasing the closed flux current, the toroidal field plays a very significant role by reducing the magnitude of the injector current at which a given amount of poloidal flux could be injected. For reducing electrode erosion, the injector current needs to be reduced. Thus by operating at the highest possible toroidal field, the injector current could be reduced to the lowest possible value. However, as shown in Figure 6.4.8, some increases to the capacitor bank charging voltage are needed to compensate for the increased injector impedance. Thus, as part of the NSTX center stack upgrade, which would double the toroidal field, if metallic divertor plates could be used along with a small increase in the capacitor bank voltage, the total closed flux current that could be realized on NSTX could exceed 500kA. The PF1B coil which largely determines the magnitude of the injector flux is now typically operated at 5kA resulting in a closed flux current of 160kA. The maximum rating for this coil is 20kA, which means that closed flux currents in excess of 500kA should be possible in NSTX. At this current level, NBI can directly couple to the CHI produced current, thereby avoiding the intermediate step of a HHFW ramp to increase the current from 300kA to 500kA. Achieving 500kA startup currents in NSTX would make it much easier for NSTX to realize the goal of full solenoid-free start-up, ramp-up and sustainment.

#### *Plans for 2009 - 2013*

Start-up and sustainment: In this approach a transient CHI equilibrium will be produced and induction from the central solenoid will be added to this startup plasma to demonstrate compatibility of the CHI discharge with plasmas conventionally produced using the inductive method. In subsequent experiments, the CHI-started plasma will be driven inductively using a combination of outer poloidal field coils in conjunction with RF and NBI to ramp the initial startup current to a level where it can be non-inductively driven by neutral beams and by High Harmonic Fast Waves.

**Edge current drive:** The CHI process initially drives current in the edge, whereas other non-inductive methods drive current in the interior of the plasma. This unique capability of CHI will be used to drive steady-state current at the edge of a pre-formed inductive discharge in NSTX for the purpose of improving the edge current profile and controlling edge SOL flows for the purpose of altering the SOL density. Based on the results of these experiments, in dedicated experiments the physics of relaxation current drive may be studied as this has the potential of increasing the CHI produced current beyond what is possible using transient CHI.

**Coupling to OH:** Work conducted during 2008 in NSTX has conclusively demonstrated the coupling of CHI started discharges to inductive drive from the central solenoid. The remaining steps are (1) to increase the magnitude of this current to about 500kA, using higher voltage capability and higher TF of up to 1T (2) to heat the CHI started discharge with 350kW of ECH so that the electron temperature is increased above 200eV, 3) at this temperature, HHFW should be able to further increase the temperature to about 1keV, 4) At 500kA NBI should be able to ramp the current up to several hundred kA and to sustain it non-inductively.

**Coupling to a pre-charged OH coil:** During 2008, preliminary work with a pre-charged solenoid showed a CHI discharge could be initiated under conditions when the OH introduces fringing error fields. These discharges will be improved to enable start up under this condition.

**Edge current drive for a high beta NSTX discharge:** The goals are to determine the magnitude of edge current that can be added without confinement degradation and to alter the SOL flows to control the SOL plasma density. Since CHI current drive is applied to the edge region, it is possible that this current drive method can be used to modify the bootstrap current drive profile by providing current drive in regions where conventional methods cannot provide current drive. Initial experiments will use the transient CHI capacitor bank to apply voltage to the lower divertor legs of a reference inductive discharge. The purpose is to try to duplicate the experiments conducted on HIT-II, but with much improved diagnostics. If experiments with the capacitor bank are promising, then the applied current pulse would be extended using the DC power supply so that the duration of the edge current can be prolonged. Reducing the SOL density has the potential to increase the edge pedestal temperature during H-mode discharges. These experiments would be conducted after improved EMI noise suppression in the magnetic sensors and flux

loops used for plasma position control. If these, experiments are successful, relaxation current drive would be studied by using long-pulse high-current CHI discharge for initiating the plasma. Experimental data produced as part of this work is needed in conjunction with computational modeling work carried out by X. Tang of LANL and C. Sovenic of the University of Wisconsin to develop an understanding of relaxation current drive physics [18, 19]. Steady state CHI experiments thus far have succeed in attaining 390kA of CHI generated toroidal current in 330ms discharges using about 28kA of injector current. These discharges will provide data for a more complete understanding of dynamo current drive physics.

## **Timeline**

### **2009**

- Test heated metal outer divertor plate as cathode (reverse TF)
- Use the CHI Absorber coils to reduce the intensity of absorber arcs
- Test use of liquid Li for performance improvement

### **2010**

- Consider 2kV capability to increase the magnitude of the CHI started currents
- Test edge current drive

### **2011**

- Use 10ms, 350kW ECH to heat CHI plasma for coupling to HHFW
- Consider full metal divertor plates to improve CHI current startup capability
- Test relaxation current drive.

### **2012**

- Operate at 1T to maximize CHI startup currents
- Maximize startup currents using synergism with outer PF coil startup

### **2013**

- Use CHI startup for full integration with nearly full non-inductive operation, which includes startup with CHI, reaching  $I_p \sim 500\text{kA}$  followed by ramp-up with HHFW and NBI to current levels where it is non-inductively sustained.

**Conclusions and Discussions** – The CHI program plan on NSTX consists of two parts. For solenoid-free plasma startup, the transient CHI approach will be used. This method was demonstrated on HIT-II, and on HIT-II CHI started discharges are more robust than inductive only discharges, and they couple to and improve the performance of inductive only plasmas. Using this method, thus far 160kA of closed flux current has been produced in NSTX, which is a world record for non-inductive closed flux current generation. In addition, CHI started discharges have now successfully coupled to induction, transitioning to an H-mode and clearly demonstrating the capability of this startup method with high performance plasma operation.

Much of the needed technical development and hardware improvements needed to correctly implement this method on NSTX has been completed. A few remaining hardware upgrades remain. These are: (a) The use of metal divertor plates to reduce low-z impurity radiation during startup, (2) operation at 1T and at higher voltage to increase the magnitude of the plasma startup currents, and (3) test of synergism between CHI and outer PF startup to maximize the magnitude of startup currents.

Scaling to future devices is attractive. A number of particular importance is the injected current multiplication factor. The attained plasma current is directly proportional to this factor. It can be shown [1] that the attained plasma current in CHI discharges is given by the relation  $I_p = I_{inj}[\psi_{Tor}/\psi_{Pol}]$ . Here  $I_{inj}$  is the injector current,  $\psi_{Tor}$  is the toroidal flux that is inside the separatrix and  $\psi_{Pol}$  is the injector poloidal flux. For a given value of the injector flux, by increasing the toroidal flux (through increased  $B_T$ ), the current multiplication factor is increased. Thus operating CHI at higher  $B_T$  is easier. The remarkable benefit of the external toroidal field can be realized by comparing CHI discharges in STs and in Spheromaks. In Spheromaks (where  $B_T$  is small) the typical current multiplication factor is about 2 to 3, which means that the injector current is nearly half the value of the plasma current. On HIT-II this ratio was increased to 6 and on NSTX it increased to a remarkable 60. HIT-II has consistently operated at an injector current of 30kA and produced CHI discharges that coupled to and improved the performance of inductive discharges. For a machine such as CTF, a similar level of current density as on HIT-II would allow the injector to be operated at 250kA of injector current. The toroidal flux in CTF is about five times that in the present NSTX, which means that the current multiplication factor would be at least that achieved on NSTX. At a conservative value of the injector current of 50kA and current multiplication factor of 50, CTF should be able to realize plasma startup currents in excess of 2MA.

## 6.4.2 Plasma Start-up Using Outer Poloidal Field Coils

Because of the criticality of the OH-solenoid-free start-up issue for ST research, the NSTX PAC has urged the NSTX team to pursue alternate methods of OH-solenoid-free start-up. This method uses the external poloidal field coils to induce a toroidal electric field. It has been successfully used on the START and MAST devices [20]. In both these devices the poloidal field coils are located inside the vacuum vessel. NSTX will conduct these experiments in a configuration in which the PF coils are located outside the vacuum vessel. Initial results are promising and the potential for the generation of up to 500kA of toroidal current exists in NSTX [21-23]. This method could also work with an initial CHI or Plasma-Gun produced plasma to further boost the level of solenoid-free current generation.

**Introduction** - In addition to CHI, NSTX will investigate a concept for solenoid-free inductive plasma startup utilizing only the outer poloidal-field coils. We describe an experimental setup for generating up to 500 hundred kilo amperes of plasma current in NSTX by this method. Such plasma would provide a suitable starting point for the non-inductive current ramp-up experiments. If successful, this concept is applicable as a possible start-up method for the NHTX (Next Step ST) device [24], and will provide a crucial element for future ST-based nuclear facilities, such as the Component Test Facility (CTF) [25].

The MAST experiment routinely uses poloidal field coils at a larger major radius than the plasma but still inside the vacuum chamber to initiate the plasma; however, to be able to extrapolate the technique to future experiments, and fusion energy systems, it would be advantageous to use only the poloidal field coils located outside the vacuum vessel wall for startup.

**Basic Concept of the Plasma-Start-Up with Outer Poloidal Coil System** - Using only the outer PF coils of NSTX, we are able to satisfy the conditions for plasma start-up which have been established by many previous experiments using a conventional central solenoid. There are three important conditions which need to be satisfied for inductive startup:

1. A region of low poloidal magnetic field must be created over a sufficiently large region of the vacuum vessel poloidal cross-section to allow the ionization avalanche to develop in the applied toroidal electric field. The condition for highly reliable breakdown can be expressed as  $E_T \cdot B_T / B_p > \sim 1$  kV/m, where  $E_T$  is the induced toroidal electric field,  $B_T$  is the toroidal magnetic field and  $B_p$  is the

average poloidal (*i.e.* transverse) magnetic field. However, the application of suitable rf waves to break down the gas can relax this condition. For example, on DIII-D, operating at  $B_T = 2$  T, with high-power ECH pre-ionization ( $\sim 800$  kW), start-up was achieved at  $E_T = 0.3$  V/m with  $B_p > 5$  mT over most of the vessel cross-section [19]. This represents a value of  $E_T \cdot B_T / B_p \approx 0.12$  kV/m. The benefit of pre-ionization with even a very small ECH power ( $\sim 20$  kW) has been shown on NSTX (and also on other ST devices including CDX-U, START, MAST, and PEGASUS) [20]. The proposed configuration for NSTX startup achieves  $E_T \cdot B_T / B_p \sim 0.12$  kV/m, comparable to the value achieved on DIII-D.

2. The field null, which is produced transiently by the combined effects of currents in the PF coils and the induced currents in the machine structure, must be maintained for a sufficient duration  $\sim 3$  milliseconds to develop the avalanche. DIII-D experiment found that the time required increased as the loop voltage was reduced. However, high power ECH pre-ionization ( $\sim 800$  kW) was able to shorten this process on DIII-D to  $\sim 2$  msec even at low loop voltage. The field null is maintained in the proposed NSTX startup configuration for 3 msec.
3. After breakdown, the poloidal field coils must provide both fields to maintain plasma equilibrium and sufficient flux change for the current to ramp up to the desired level. The change in the vertical field required for equilibrium produces additional flux during the current ramp-up. These requirements are met in the proposed configuration.

**Outer Poloidal Field Start-Up Configuration on NSTX** – We propose to utilize the existing poloidal coil sets and available power supplies on NSTX for solenoid-free start-up. In Figure 6.4.11 (a) the poloidal coils installed on NSTX are shown. The required current levels in Figure 6.4.11 (a) are consistent with the current rating of the coils and power supplies for the short durations needed for this experiment. The mid-plane vertical field generated by the combination of PFs 2, 3, and 5 is compared with that generated by PF 4 in Figure 6.4.11 (b). The combined field is shown in Figure 6.4.11 (c); the field null is created around  $R = 1.4$  m. In Figure 6.4.12 (a), the resulting two dimensional poloidal field contours are shown. As can be seen in Figure 6.4.12 (a), a high quality field null is created. From Figure 6.4.12 (b), one can see that about 0.16 Wb (at  $R =$

1.0 m) is available for the current ramp up for this particular set of coil currents. In NSTX, under an optimized condition, about 0.3 Wb from the solenoid can produce a 1 MA discharge. Thus, the 0.16 Wb flux swing available from this scenario at  $R \approx 1.0$  m could, in principle, produce plasma currents of order 0.5 MA.

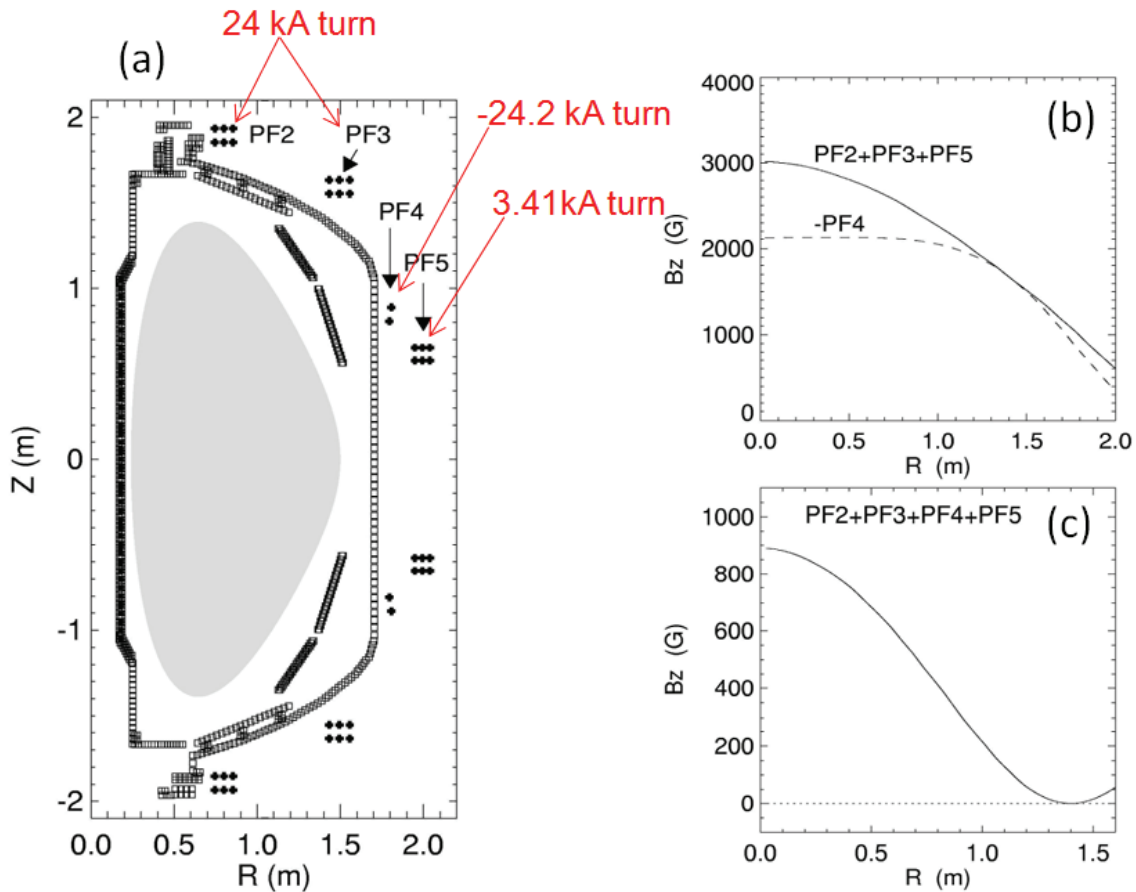


Figure 6.4.11: NSTX Configuration. (a) A schematic of the NSTX poloidal field coil set up. The required coil currents are indicated. (b) The mid-plane vertical field for the combination of PFs #2, #3 and #5 and PF #4. (c) The mid-plane vertical field generated by PFs 2, 3, 4, and 5

**Pre-ionization** – On NSTX, start-up has been routinely achieved for a relatively low loop voltage of  $\sim 2$  V with ECH pre-ionization. For the outer-PF-only start-up scenario, we expect to be able to generate a loop voltage up to 6 V transiently, corresponding to a toroidal electric field of 0.7 V/m at the radius of the field null,  $R = 1.4$  m. The toroidal field there is up to 0.35 T. Within the broad region where the poloidal field is  $< 20$  G, the value of  $E_T \cdot B_T / B_p$  is above 0.12 kV/m. Since DIII-D was able to initiate the plasma for  $E_T \cdot B_T / B_p$  as low as this value with strong ECH pre-ionization, start-up should be also feasible in NSTX if adequate pre-ionization is provided. For NSTX, with a combination of ECH ( $\sim 20$  kW) and HHFW ( $\sim 1$  MW), a favorable pre-ionization condition may be created. On CDX-U, this combined ECH-HHFW technique was indeed shown to be effective in creating relatively robust preionized plasmas [27].

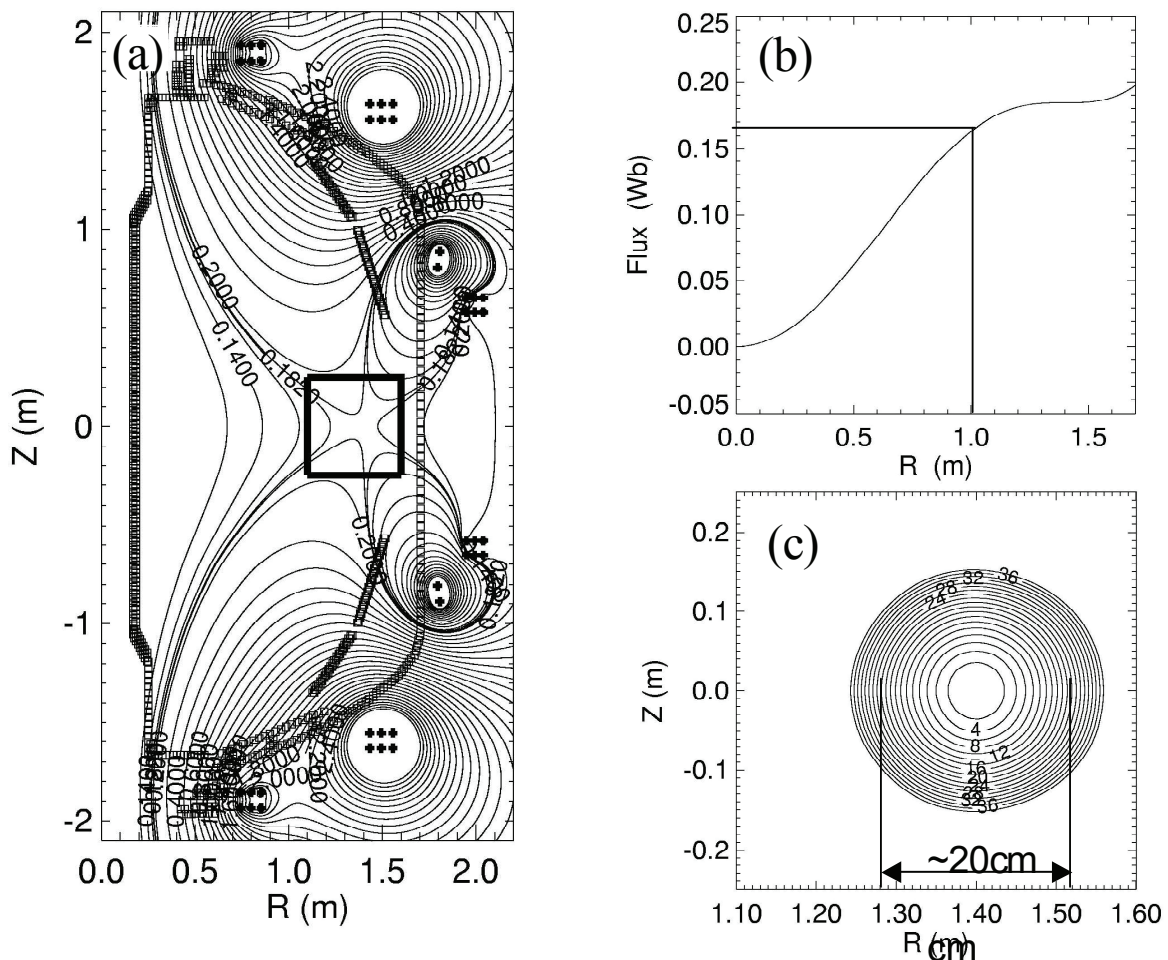


Figure 6.4.12: The NSTX null-field configurations. (a) Flux contours. (b) Flux radial profile. (c) Mod-B surfaces of the field null region



This preionization can be further developed and its effectiveness tested in the near term on NSTX using the existing ECH and multi-MW HHFW system. An initial test using these pre-ionization methods allowed the production of up to 20 kA of plasma current, as shown in Figure 6.4.13. The primary findings are that the 20 kW of ECH is too small and that HHFW is not a good pre-ionizing system. The experiment will be attempted again in 2009 using CHI for preionization and in 2011 after the installation of the 350 kW ECH system. In addition to this a washer plasma gun source will be installed for 2010. This may inject adequate amounts of ionized plasma into the field null region, which should facilitate easier breakdown of the remaining neutral gas. A Compact Toroid (CT) injector is also being considered for Advanced Fuelling experiments. This has the potential to inject all of the required plasma directly into the field null region, and is a possibility for experiments beyond 2012.

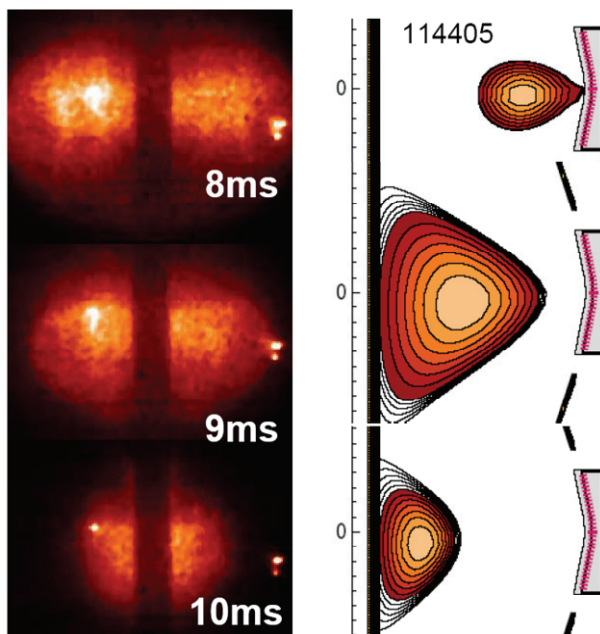


Figure 6.4.13: Shown on the left are fast camera fish eye visible images of a discharge produced using outer PF start-up. A small bore plasma is formed in the outer region as show by LRDFIT reconstruction at 8ms (top right), that subsequently moves to the inner wall and decays over several 10s of ms. Up to 20kA of plasma current was generated.

**Maintenance of Field Null** – During the initiation, it is important to maintain the field null for about 3 ms to create the avalanche. Since the poloidal field is changing rapidly during this period and inducing significant vacuum vessel eddy currents, a dynamic modeling code to include the vacuum vessel eddy currents has been implemented. This analysis shows that it is indeed possible to maintain the field null for about 3 ms, which should be long enough to initiate the avalanche process with the aid of sufficient pre-ionization as described above. The plasma stability with the presence of the eddy currents is an issue that needs to be further investigated. The presence of the nearby passive plates in NSTX should aid the vertical stability.

#### Hardware and Modeling Requirements

### for Outer PF startup

The current ramp up will require PF 5 to provide much of the equilibrium vertical field. However, for the initial test of the concept, the crucial initial breakdown and avalanche process was tested by reversing the PF 5 connection to its existing power supply. The bi-polar capability will be implemented after further tests. Once the plasma initiation is successful, feedback control must be introduced to maintain the plasma equilibrium and shape during the current ramp-up. The TSC code [28] will be utilized for the development of suitable current ramp-up scenarios to guide the development of control algorithms.

### Plans for 2009 – 2013

#### *2008: Preparatory work scopes:*

- Continue the basic start-up calculations including the wall eddy currents
- Assess basic power supply reconfigurations
- Analyze electro-magnetic forces and needs (if any) for further bracing of PF coils.

#### *2009: Initial Plasma Initiation Experiments with CHI*

- Develop effective pre-ionization capability using the CHI system with some assist from the central solenoid.
- Conduct initial breakdown and current initiation experiment up to ~ 100 kA with using the existing uni-polar supply for PF 5.
- After confirming successful breakdown, implement needed hardware changes including the bi-polar capability of PF 5.
- Develop optimized current ramp-up scenarios using TSC.
- Develop required magnetic sensors and control algorithms based on the TSC simulation.

#### *2010: Initial Plasma Initiation Experiments with plasma guns*

- Develop effective pre-ionization capability using the washer gun plasma sources with some assist from the central solenoid.

*2011: Start-up Demonstration Experiments with ECH*

- Establish a few hundred ( $I_p \sim 300 - 500$  kA) plasma discharges without use of the OH solenoid and higher power HHFW after using the newly installed ECH system for pre-ionization.
- Apply HHFW and/or NBI to achieve high beta poloidal discharges without the OH solenoid.
- Develop comprehensive understanding and predictive capabilities of the outer poloidal field coil plasma start-up concept for future devices including NHTX.

*2012-13: Assist the non-inductive research as a tool for ohmic-solenoid-free start-up.*

- Using a combination of CHI start-up and outer PF start up or Plasma Gun start-up and outer PF start-up, ramp-up to a high beta target.

**Conclusions and Discussions** – A plasma start-up concept using only the outer PF coils has been introduced. This method appears capable of generating in NSTX a solenoid-free start-up current of a few hundred kilo amperes, comparable to that produced by CHI. Once a significant level of plasma current is established, it should be possible to use other means of non-inductive current drive such as the bootstrap over-drive, and/or NBI / RF current drive to further ramp up and maintain the current. The outer PF coil start-up concept can be implemented relatively quickly with minimal facility modifications and, if successful, can play an important role in the non-inductive research phase of NSTX as described in this Five-Year plan. The concept scales favorably toward larger and higher field devices, such as NHTX, since the higher field tends to ease the breakdown requirements and the amount of available flux scales with the square of the major radius and linearly with the field. If successful, it will give us a method for the ohmic-solenoid-free start-up of future ST devices to a significant level of plasma current.

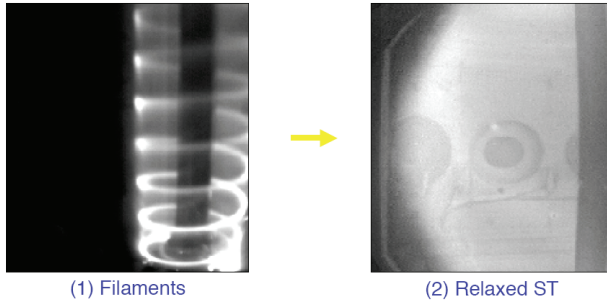
### 6.4.3 Plasma Gun Startup

In this method an electron beam is driven along magnetic filaments using a washer gun plasma source [3]. The method was first tried on the CDX-U machine [29] with some success. More recently the method has been further developed on the PEGASUS ST [30]. On Pegasus 30 kA of gun generated toroidal current was produced and ramped up to 80 kA after coupling to induction. The method has the advantage that it could be easily implemented in a reactor as the gun sources could be withdrawn after current generation. NSTX will test the viability of this concept in a large ST [31].

**Introduction** - In this method, an electron beam is created by biasing a washer gun plasma source negative with respect to the external vessel or a floating probe inserted into the vacuum chamber. An appropriate vacuum magnetic field pattern is setup so that the combination of poloidal and toroidal fields creates a spiraling field line configuration. The electrons released by the gun then follow these field lines. This method now adopted by PEGASUS is an improvement over the early experiments on CDX-U [30], in that CDX-U used a heated Lanthanum Hexaboride cathode, which from a cleanliness point of view is probably less cleaner than the plasma gun sources. In the Plasma gun sources, by choosing the appropriate bias voltages, the ions released by the gun can be made to preferentially fall back into the gun cavity, thereby reducing impurity influx into the vessel. These plasma gun sources typically operate for about 10 ms, which is about the time needed to couple it to induction from the outer PF coils.

#### **Results from Pegasus**

At present two different experiments have been performed on Pegasus. In the initial experiment, the gun source was located near the lower divertor region. It was then biased with respect to a floating component positioned below the upper divertor, so that an electron beam was driven up as shown in Figure 6.4.14. At sufficient low values of the toroidal field the spiraling electron beam channel relaxed and merged to a diffuse current channel that filled the entire vessel as shown in right portion of Figure 6.4.14. In these experiments up to 50 kA of toroidal current was generated using 4 kA of gun current. For representative cases, the toroidal field was about 0.01 T and the vertical field was 0.005 T.



(1) Filaments (2) Relaxed ST  
 Figure 6.4.14: Visible images of the current channel prior to and after relaxation in Pegasus Washer Gun experiments.

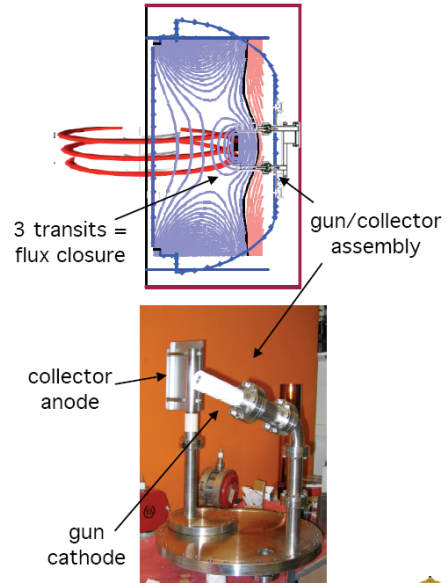


Figure 6.4.15: Layout of the mid-plane gun injection system in Pegasus

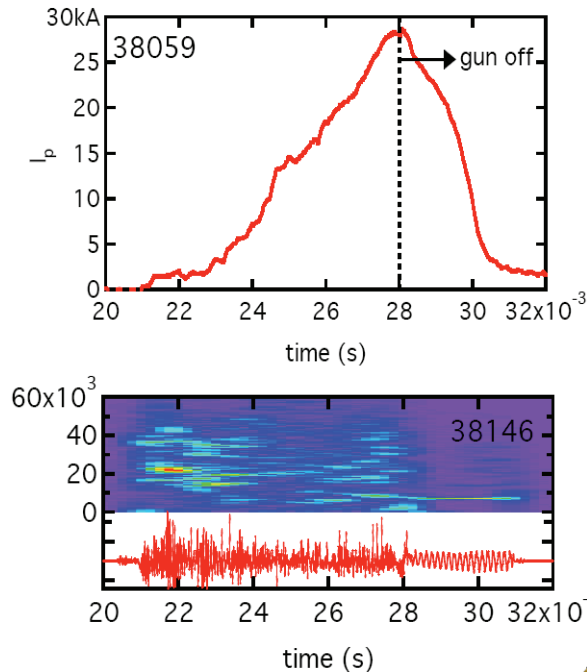


Figure 6.4.16: Plasma current and MHD activity of a discharge during mid-plane gun injection experiments in Pegasus.

In more recent experiments of perhaps more relevance to NSTX, the gun and a collector assembly was mounted in the outer midplane as shown in Figure 6.4.15. The driven electron channel now occupied the outer midplane of the vessel. In these experiments at relatively higher values of the toroidal field, up to 25 kA of toroidal current was generated using 1.5 kA of gun current as shown in Figure 6.4.16. After the guns were turned off, the current persisted for 2 ms and was accompanied by coherent MHD activity indicative of the generation of closed

flux. When this discharge was coupled to induction from the central solenoid, the current ramped up beyond what was possible using induction alone showing coupling to induction, as seen in Figure 6.4.17.

## Implementation of the method in NSTX

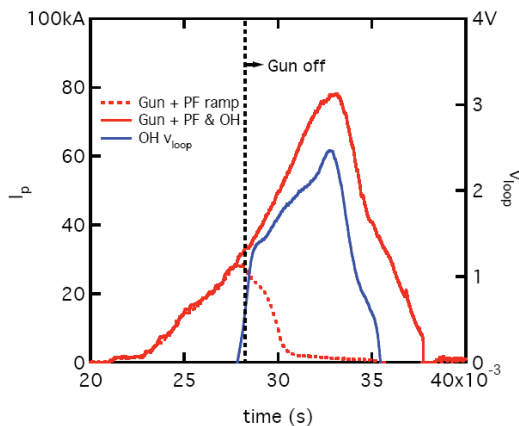


Figure 6.4.17: Shown are in blue an OH only discharge and in red, the same preprogrammed loop voltage applied to a mid-plane gun generated plasma.

The method will be implemented on NSTX in a manner similar to the Pegasus mid-plane experiments. A design of the conceptual design is now underway by the Pegasus group.

### Schedule (2009 to 2013)

**2008-09:** Conduct supporting experiments on Pegasus to understand scaling to larger current levels. Design the system for NSTX, including identifying hardware components and installation details.

**2010:** Installation on NSTX and commissioning tests. Support outer PF start-up experiments, by injecting ionized plasma into the region of field null. Test to see

if the startup loop voltage on NSTX can be reduced as a result of gun injected pre-ionized plasma.

**2011:** Test of plasma startup using the guns installed in the gap region between the primary and secondary passive plates.

**2012-2013:** Based on 2011 results, upgrade the system to produce higher current levels.

### Conclusion and Remarks:

The method is simple in concept and could be easily adapted to larger machines as the gun sources could be withdrawn after plasma startup. Initial results from Pegasus are encouraging. NSTX will test the concept on a larger scale. The method is compatible with outer PF startup and will assist the outer PF startup experiments by providing a pre-ionized source of plasma.

## 6.4.4 Plasma Current Ramp-up

Non-solenoidal initiation and current ramp-up is a critical goal of the ST program since its attractiveness is directly tied to eliminating or minimizing the inductive central solenoid on the inboard side of the device and allowing access to compact geometry. Since none of the proposed solenoid-free current start-up methods are expected to generate the full magnitude of the nominal value of the steady-state plasma current of a device like ST-CTF, successful demonstration of methods for non-inductive current ramp-up are essential to meet the goals of the ST program. As previously described, a discharge to achieve this goal can be divided into three phases; the breakdown and startup with coaxial helicity injection or the outer poloidal field PF coils or Plasma Gun startup as described in sections 6.4.1 to 6.4.3. The second phase is the current ramp-up phase. During this phase the current magnitude is non-inductively increased to the levels needed for steady-state operation. For NSTX plasmas, the early plasma current ramp-up and heating would be achieved with HHFW, and the later plasma current ramp-up and heating would be achieved using both HHFW and NBI [32]. In next-step devices it might in principle be possible to perform the ramp-up with NBI alone, but sufficient plasma current and density are required to avoid fast-ion loss and shine-through, respectively, so wave heating may remain useful or even necessary in next-steps. It is useful to note that the requirements on the non-inductive current ramp-up systems could be reduced if the initial current produced during the start-up phase is increased. During the final sustainment phase, a combination of bootstrap current drive, neutral beam and RF current drive are expected to maintain the current at steady state values. The time scales required for non-inductive current ramp-up are long compared to those required with inductive current ramp-up, since the inductive ramp rate is limited by the current redistribution time at the plasma edge whereas the non-inductive current ramp rate is limited by the current redistribution time at the plasma center [33].

To understand the requirements of current ramp-up, the TSC code has been used to establish the requirements of HHFW and NBI power and energy and the required target plasma conditions (density, temperature, current and magnetic field levels) and the simulations discussed below are described more extensively in Reference 32. The simulations assume that the plasma starts the non-inductive ramp-up at  $I_p=100$  kA, provided by the initiation phase, which is treated in the code as inductive current. HHFW is the heating and current drive source in this low  $I_p$  and low  $T_e$  phase, and NBI is added in the higher  $I_p$  phase when the  $I_p$  rate of increase is slowing down. The toroidal field is 0.45 T allowing a maximum of 1.8s of pulse length. In the low  $I_p$  phase the HHFW power is ramped slowly to avoid current hole formation, whereas the density is ramped to keep the temperature sufficiently low to access short core

current redistribution time scales. In order to keep the temperature from increasing too fast in this phase the plasma is limited on the inboard wall to avoid transition to H mode. The peak electron temperature reaches 1.3keV, whereas the density ramps up to  $0.3 \times 10^{20} \text{m}^{-3}$  over 0.3s. Around 0.3–0.4s the plasma is diverted, allowing an improvement in global confinement. Then beginning at 0.5s 6MW of NBI power is

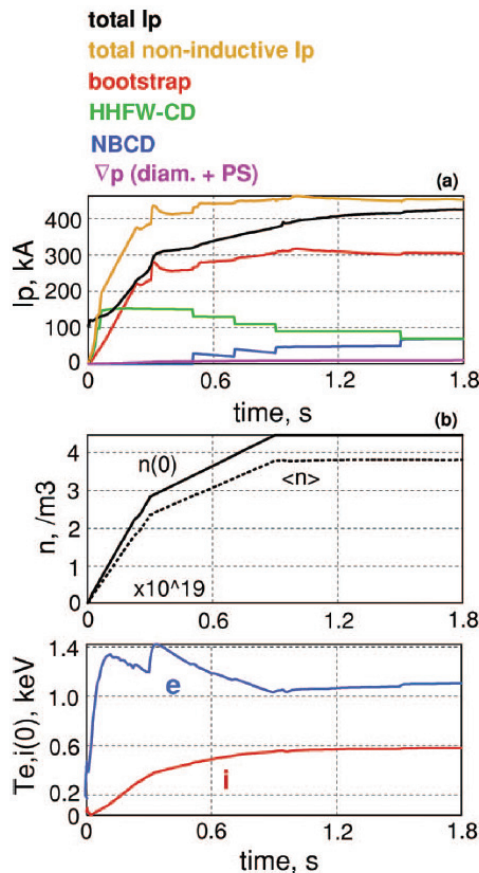


Figure 6.4.18: (a) Time histories of the plasma current (black), the total non-inductive current (yellow), and the contributions to the plasma current from bootstrap (red), HHFW CD (green), and NBCD (blue). (b) The peak electron and ion temperatures, and electron density for the non-solenoidal  $I_p$  ramp-up simulation for NSTX at  $B_T=0.45T$ .

injected in steps, accounting for the poor beam fast ion confinement at these lower plasma currents. The NB power absorbed and subsequent driven current is based on the beam confinement observed in the  $I_p$  ramp-up in discharge 109070 from TRANSP. The heating and driven current from the beam continue to improve as the plasma current increases, but the slow current rise keeps the absorbed power low in these simulations, only reaching 2–3MW for 6MW of injected power. The poloidal beta reaches 2.8, the toroidal beta reaches about 5.0,  $li(1)$  drops to 0.47, and the central safety factor remains above 4.0 during the discharge simulation. The bootstrap current reaches 300kA, and the HHFW driven current maximizes at 150kA in the early phase and decreases when the density rises and NB fast ions are present to absorb HHFW power calculated by CURRAY. The HHFW phase is  $7\text{m}^{-1}$  co-CD (same direction as the plasma current) and up to 6 MW are injected. By 1.8s the total plasma current has reached just over 420kA. As the beam ions are not well confined, at these low plasma currents a significant HHFW current persists, in spite of parasitic absorption of HHFW power on fast NB ions. These results are shown in Fig. 6.4.18 giving the contributions to the plasma current, density and electron

and ion peak temperatures as a function of time. The present NSTX does not have sufficient pulse length to reach a plasma current of at least 800kA to connect to a high performance plasma configuration, but can demonstrate the critical features of the non-inductive ramp-up.



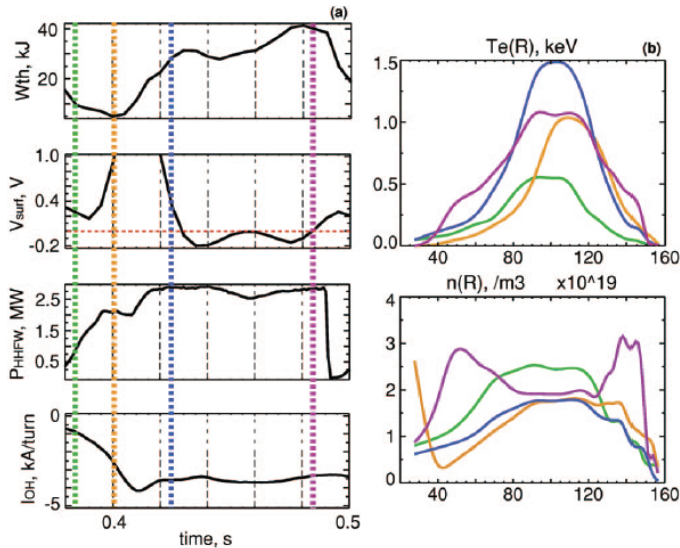


Figure 6.4.19: (a) Experimental time traces of the stored energy, surface voltage, injected HHFW power, and solenoid current during a segment of discharge 117605. (b) The electron temperature and density profiles as function of major radius at the time slices indicated on the time traces, 0.385 (green), 0.400 (yellow), 0.425 (blue), and 0.485 s (pink).

Experiments have begun to examine the HHFW heating and current drive at low  $I_p$ . Shown in Fig. 6.4.19 is a segment of a discharge where the plasma current was ramped up and maintained at 250 kA with the solenoid. Up to 2.8 MW of HHFW power was injected with  $k_{||}=14 \text{ m}^{-1}$  heating phase in an effort to drive the surface voltage to 0. The injection of power drives the stored energy up significantly and creates an H-mode confinement regime. The surface voltage is reduced to 0 or even slightly below, and the solenoid current becomes slightly inverted or flat indicating it is no

longer providing volt seconds to the plasma. Also shown in Fig. 6.4.19 are the electron temperature and density profiles at four time slices indicated on the time history plots. The starting profile shows the peak electron temperature of about 500eV, which rises to 1.0keV over the next 0.015 s from HHFW heating. This continues with the peak temperature reaching 1.5keV and an H-mode temperature pedestal beginning to form 0.040s later. Finally after 0.10s the electron temperature profile has broadened significantly generating high pedestal temperatures, and a lower peak temperature. This particular type of profile is ideal since it will generate a large bootstrap current, but keep the central temperature low enough to allow a reasonable  $I_p$  ramp rate. Unfortunately the HHFW power was unable to be sustained due to loading mismatches due to H-mode, but future upgrades to the HHFW system are planned for 2009-10 to increase the HHFW power and make the HHFW system more resilient to H-mode and ELMs.

Importantly, with the proposed major upgrades of NSTX (new center-stack and 2<sup>nd</sup> NBI), TSC

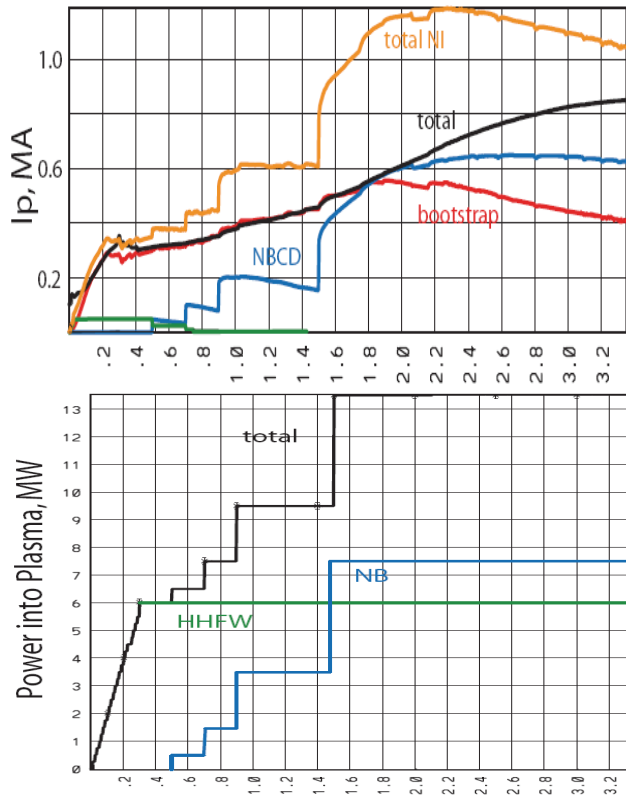


Figure 6.4.20: Current ramp up results from the TSC code at a toroidal field of 1T and with 7.7MW NBI and 6MW HHFW (plasma absorbed power)

simulations indicate that non-inductive plasma current ramp-up to higher plasma current approaching 1MA is possible. Shown in Figure 6.4.20 are results from preliminary (un-optimized) TSC simulations in which the toroidal field was increased to 1T in combination with increased NBI power and duration made possible by the addition of the second NBI source. As shown in the Figure, starting from 300ms with a plasma current level of 350kA, a constant HHFW power at 6MW is utilized to heat the target plasma and ramp the initial current non-inductively to a value where the NBI should begin to be absorbed efficiently. Starting at 500ms, the neutral beam power is increased in steps as for the simulations shown in Figure 6.4.18. Near the end of the simulations shown in Figure 6.4.20 the internal inductance begins to

increase and the central q and electron density are not yet stationary. Thus, although these simulations show the significant benefit of higher TF and NBI power for non-inductive ramp-up, additional work is needed to optimize the long-time-scale discharge evolution. Additional TRANSP simulations are also needed to ensure that NBI is adequately absorbed in the lowest current phase of the ramp-up. Finally, it is important to note that the current ramp-up to 800-850kA takes up to 3s in these simulations. Thus, the ability to sustain 1T toroidal field and 7-8MW NBI heating for at least 3s is essential to demonstrate ramp-up to currents in the ~1MA range, and these capabilities are only possible with the proposed major upgrades to NSTX.

**Plasma Current Ramp-up Research Plan for 2009 to 2013**

## **2008**

Conduct supporting experiments on heating deuterium discharges in NSTX to access H-mode and to understand HHFW coupling in deuterium plasmas.

## **2009-11**

In conjunction with TSC simulations, experimentally test and understand the minimum levels of plasma current required for current ramp-up using the higher power capability of HHFW. A FY10 HHFW milestone is to use higher power HHFW and ELM resilience to attempt  $I_p$  ramp-up from 200-250kA to 400-500kA using HHFW heating and current drive and bootstrap current drive.

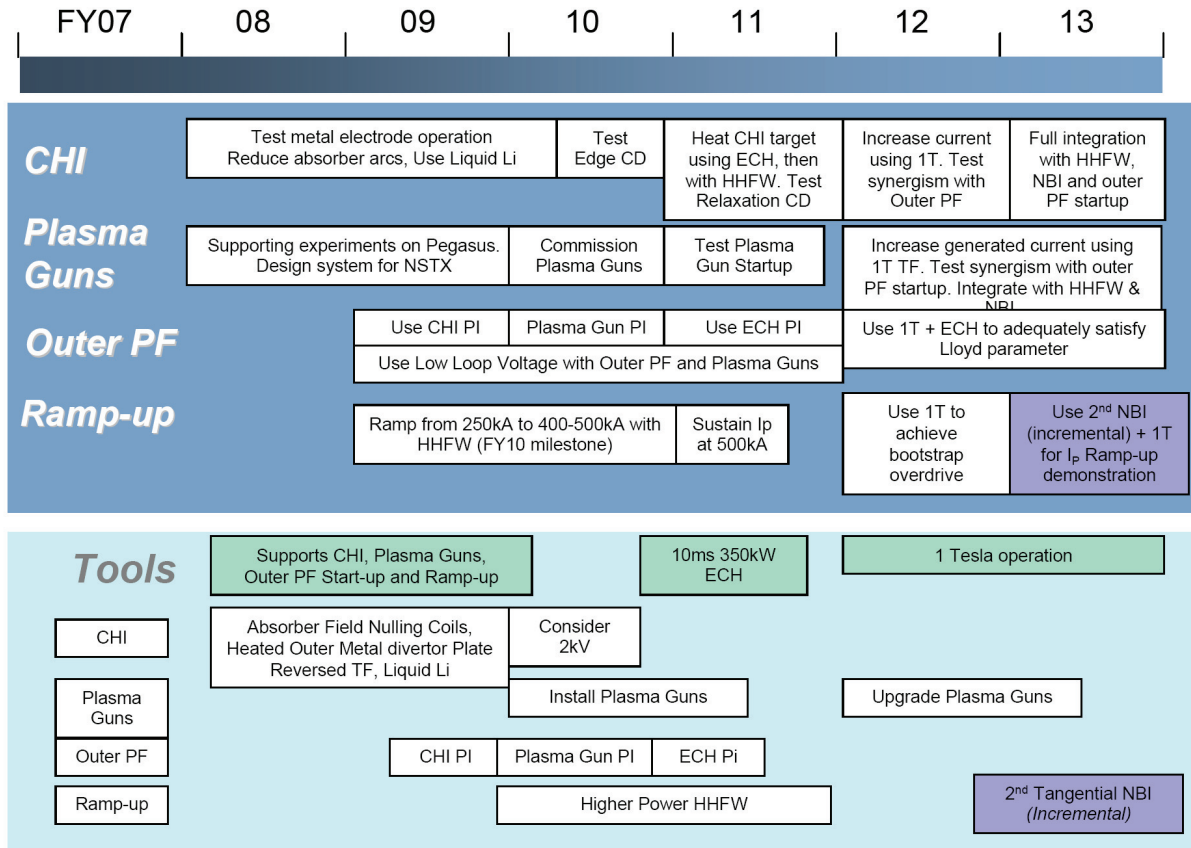
## **2012**

1T expected to reduce the normalized beta required to achieve high bootstrap fraction for overdrive, also expected to increase target  $T_e$  for increased HHFW absorption and higher CD efficiency. NBI also should become more effective at higher field and current.

## **2013**

Measure the extent of current ramp-up that is possible using a solenoid-free startup target and establish initial current startup requirements for full non-inductive ramp-up. (Incremental funding): Utilize 2<sup>nd</sup> NBI to increase absorbed NBI power and sustain high NBI power (7-8MW) to test solenoid-free ramp-up to ~800kA within 3-5s.

### 2009 – 2013 Timeline for Plasma Current Start-up and Ramp-up Research



## References

- [1] T.R. Jarboe, "Formation and steady state sustainment of a tokamak by Coaxial Helicity Injection," *Fusion Tech.* **15**, 7, (1989).
- [2] M. Ono and W. Choe, "Out-Board "Ohmic Induction" Coil for Low-Aspect-Ratio Toroidal Plasma Start-up", Princeton University Patent Disclosure 03-2003-1.
- [3] G.D. Garstka, *et al.*, "Attainment of High Normalized Current by Current Profile Manipulation in the Pegasus Toroidal Experiment," *Journal of Fusion Energy*, 27:20-27, DOI 10.1007/s10894-007-9094-1 (2008)
- [4] C.W. Barnes, T.R. Jarboe, *et al.*, "Spheromak Formation and Operation with Background Filling gas and a Solid Flux Conserver in CTIX," *Nuclear Fusion* **23**(3), 267 (2984).
- [5] M.J. Schaffer, *et al.*, "Increased divertor exhaust by electrical bias in DIII-D," *Nuclear Fusion*, **36**, 496 (1996).
- [6] Nelson, B.A., *et al.*, "Formation and sustainment of a low-aspect ratio tokamak by coaxial helicity injection," *Phys. Plasmas* **2** (1995) 2337.
- [7] Nagata, M., *et al.*, "Helicity injection current drive of spherical tokamaks and spheromak plasmas in HIST," 17th IAEA Fusion Energy Conference, Yokohama, IAEA-CN 69/EXP4/10 (1998).
- [8] Browning, P.K., *et al.*, "Injection and sustainment of plasma in a preexisting toroidal field using coaxial helicity injection," *Phys. Rev. Lett.* **68** (1992) 1722.
- [9] Jarboe, T.R., Raman, R, Nelson, B.A., *et al.*, "Current drive experiments on the HIT-II spherical torus," 17th IAEA Fusion Energy Conference, Yokohama, IAEA-CN 69/PDP/02 (1998).
- [10] R. Raman, T.R. Jarboe, B.A. Nelson, *et al.*, "Demonstration of plasma startup by coaxial helicity injection," *Phys Rev. Lett.* **90**, 075005-1 (2003).
- [11] R. Raman, B.A. Nelson, M.G. Bell, T.R. Jarboe, D. Mueller, T. Bigelow, B. LeBlanc, R. Maqueda, J. Menard, M. Ono, R. Wilson, Efficient generation of closed magnetic flux surfaces in a large spherical tokamak using coaxial helicity injection, *Phys Rev. Lett.*, **97**, 175002 (2006)
- [12] R. Raman, D. Mueller, *et al.*, "Non-inductive solenoid-less plasma current startup in NSTX using Transient CHI," *Nuclear Fusion*, **47** (8), 792 (2007).
- [13] R. Raman, T.R. Jarboe, B.A. Nelson, W.T. Hamp, V.A. Izzo, R.G. O'Neill, A.J. Redd, P.E. Sieck and R.J. Smith, "Experimental demonstration of plasma startup by coaxial helicity injection," *Phys Plasmas* **11**, 2565 (2004).
- [14] R. Raman, T.R. Jarboe, D. Mueller, D., *et al.*, "Non-inductive current generation in NSTX using coaxial helicity injection," *Nucl. Fusion* **41**, (2001) 1081.
- [15] T.R. Jarboe, R. Raman, B.A. Nelson, *et al.*, "Progress with helicity injection current drive," *19th IAEA Fusion Energy Conference*, Lyon, IAEA-IC/P 10 (2002).
- [16] R. Raman, T.R. Jarboe, D. Mueller, *et al.*, "Initial results from CHI experiments in NSTX," *Plasma Phys. Contrl. Fusion* **43**, 305 (2001).

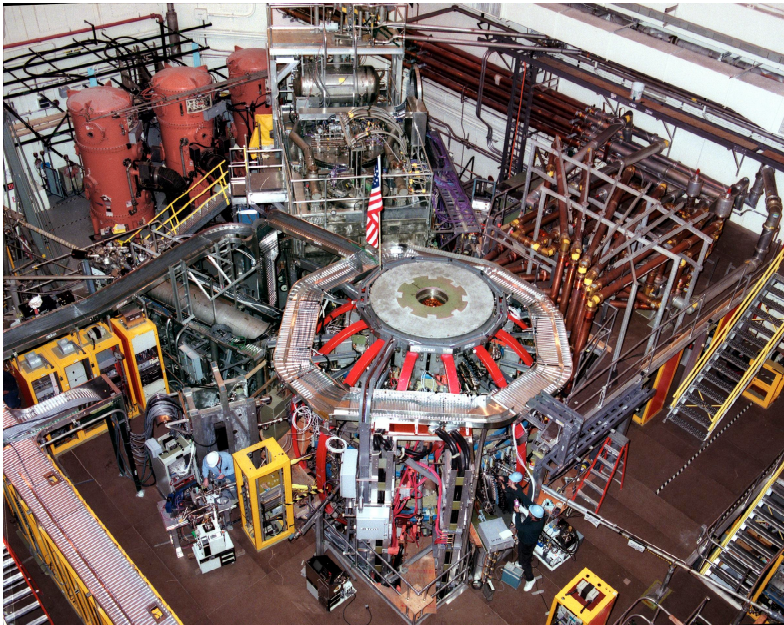
- [17] D. Mueller, R. Raman, T.R. Jarboe, et. al., “Coaxial Helicity Injection plasma plasma start-up coupled to inductively driven sustainment on NSTX,” Proc. 35<sup>th</sup> EPS Conference. Crete, Greece, 9-13 June (2008).
- [18] X.Z. Tang and A.H. Boozer, “Flux amplification in helicity injected spherical tori,” Phys. Plasmas 12, 042113 (2005).
- [19] X.Z. Tang and A.H. Boozer, “Scale-up of spherical tokamak solenoid-free startup by coaxial helicity injection,” Phys. Plasmas 14, 100704 (2007).
- [20] A. Sykes, “The spherical tokamak program at Culham,” Nuclear Fusion, **38**, No. 9Y, 1271 (1999).
- [21] Y. Takase, et. al., “Solenoidless startup in NSTX.” NSTX Research Forum, Nov 11 (2003), Princeton, NJ
- [22] J.E. Menard, “HHFW-assisted PF-only startup in NSTX,” NSTX Research Forum, Nov 10-11 (2003), Princeton, NJ
- [23] W. Choe, J. Kim, M. Ono, “Test of outer PF coil-only inductive plasma startup technique on NSTX,” NSTX Research Forum, Nov. 10-11 (2003), Princeton, NJ
- [24] J. Menard, et. al., NHTX information: [http://nstx.pppl.gov/DragNDrop/NHTX\\_Information/](http://nstx.pppl.gov/DragNDrop/NHTX_Information/)
- [25] Y-K.M. Peng, et al., “A component test facility based on the spherical tokamak,” Plasma Phys. Control. Fusion, **47** (2005) B263-B283
- [26] B. Lloyd, et al., “Low voltage Ohmic and Electron Cyclotron Heating assisted startup in DIII-D,” Nuclear Fusion 31, 2031 (1991)
- [27] J.E. Menard, “High harmonic fast wave coupling and heating experiments in the CDX-U spherical tokamak,” Ph.D. Thesis, Princeton University, June (1998).
- [28] S.C. Jardin, N. Pomphrey, N. GeLucia, “Dynamic modeling of transport and position control of tokamaks,” Journal of Computational Physics **66**, 481 (1986).
- [29] M. Ono, et al., “Steady-state tokamak discharge via DC helicity injection,” Phys. Rev. Lett., **44**, 393 (1980).
- [30] A.J. Redd, et al., “Non inductive plasma startup and current profile modification in Pegasus spherical torus discharges,” ICC Workshop, June 26 (2008), Reno, Nevada
- [31] A. Sontag, “DC helicity injection in Pegasus,” NSTX Research Forum, Nov 27 (2007), Princeton, NJ
- [32] C.E. Kessel, et al., “Long pulse high performance plasma scenario development for the National Spherical Torus Experiment,” Phys. Plasmas **13**, 056108 (2006)
- [33] S.C. Jardin, “Timescales for non-inductive current buildup in low aspect ratio toroidal geometry,” Nucl. Fusion **40**, 1101 (2000)

## **Chapter 7 - The NSTX National Fusion Facility Status and Upgrades**

<i>Abstract</i> .....	7.1
<i>7.1 Facility Overview</i> .....	7.2
<i>7.2 Facility Status and Plan</i> .....	7.4
<i>7.2.1 NSTX Facility Subsystems</i> .....	7.6
<i>7.2.2 Heating and Current Drive Systems</i> .....	7.10
<i>7.2.3 Macro-stability Tools</i> .....	7.13
<i>7.2.4 Boundary Physics</i> .....	7.16
<i>7.2.5 Start-up and Ramp-up</i> .....	7.20
<i>7.2.6 New Center Stack Upgrade</i> .....	7.22
<i>7.2.7 Second Neutral Beam Injection System Upgrade</i> .....	7.24
<i>7.3 NSTX Diagnostic System Status and Plans</i> .....	7.26
<i>7.3.1 Profile Diagnostics</i> .....	7.28
<i>7.3.2 MHD Diagnostics</i> .....	7.31
<i>7.3.3 Turbulence Diagnostics</i> .....	7.34
<i>7.3.4 Energetic Particle Diagnostics</i> .....	7.36
<i>7.3.5 Wave Diagnostics</i> .....	7.38
<i>7.3.6 Boundary Physics Diagnostics</i> .....	7.39
<i>7.4 NSTX Facility Utilization</i> .....	7.41
<i>References</i> .....	7.44

*This page intentionally left blank*





## Chapter 7

### The NSTX National Fusion Facility - Status and Upgrades

The National Spherical Torus Experiment (NSTX) is the world's leading spherical tokamak, combining an exceptionally wide plasma parameter space, a high degree of facility flexibility, and state-of-the-art diagnostic systems. Presently, the NSTX plasmas are heated by up to 7 MW of deuterium Neutral Beam Injection (NBI) and up to 6 MW High-Harmonic Fast Waves (HHFW). In addition to advanced plasma shaping capabilities, NSTX is equipped with a set of non-axisymmetric control coils to enhance plasma stability and is exploring and developing the use of lithium as a plasma facing material. Attracted by its unique capabilities, NSTX hosts a large number of national and international researchers (over 200 annually) with 55 institutions participating in the research program. Nationally, the team members are from 29 universities, national laboratories, and industries.

Major upgrades for 2009 include a liquid lithium divertor target to access lower collisionality, a modification to the HHFW antenna to double its power capability, and a Beam Emission Spectroscopy diagnostic to extend the localized measurements of plasma turbulence toward the ion gyro-radius scale. For the longer term, a new center stack is planned to enable operation at a magnetic field up to 1 T, plasma current 2 MA with a 5 s pulse length, along with a second neutral beam system for current profile control and a divertor upgrade to handle the expected heat-flux for the full pulse. These upgrades are aimed at achieving fully non-inductively sustained, long-pulse high-performance operation and exploring an expanded plasma parameter space in terms of higher plasma temperature and lower collisionality. The new physics regimes made accessible by these upgrades will significantly reduce the gap, and thus the uncertainty in extrapolating, from the present NSTX to projected next-step ST experiments.

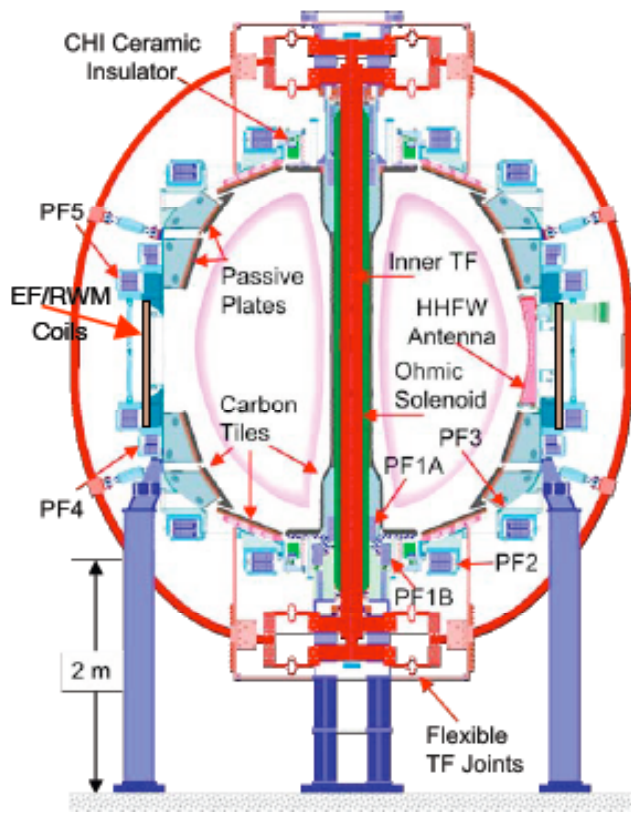


Fig. 7.1 NSTX Device Schematic

<u>Present Machine Capabilities</u>	
<b>Major Radius</b>	0.85 m
<b>Minor Radius</b>	0.68 m
<b>Elongation</b>	1.8 - 3.0
<b>Triangularity</b>	0.2 - 0.8
<b>Plasma Current</b>	1 MA (1.4 MA peak)
<b>Toroidal Field</b>	0.35 - 0.55 T
<b>Heating and CD</b>	7 MW NBI (2 sec) 5 MW NBI (5 sec) 6 MW HHFW (5 sec) 0.2 MA CHI
<b>Pulse Length</b>	~ 1 sec at 0.55 T ~ 2 sec at 0.38 T

Table 7.1 Facility Parameters

## 7.1 Facility Overview

NSTX is a major component of the restructured U.S. Fusion Energy Sciences Program, which encompasses both the investigation of innovative confinement concepts and the advancement of the underlying physics to strengthen the scientific basis for attractive fusion power. Operational since 1999 [7.1.1-3], the NSTX has been steadily building up its facility and diagnostic capabilities. To accomplish this mission, the NSTX facility, shown schematically in Fig. 7.1 and summarized in terms of major device parameters in Table 7.1, provides the following capabilities:

- Low aspect ratio,  $R/a \geq 1.27$ , and a strongly shaped plasma cross-section with nominal elongation  $\kappa \leq 3.0$  and triangularity  $\delta \leq 0.8$ ;
- Close-fitting conducting plates to stabilize pressure-driven instabilities at high plasma  $\beta$ ;
- Toroidal field (TF) coil operating routinely at up to 0.55 T;
- Plasma current  $I_p \sim 0.75$  MA for  $\sim 1.8$  s duration, limited by the TF coil pulse length, and up to 1.4 MA transiently, exceeding the toroidal magnet current;

- Neutral Beam Injection (7 MW) and High-Harmonic Fast-Wave system (6 MW) for heating, current drive, and current profile control;
- Transient Coaxial Helicity Injection (CHI) for solenoid-free startup current;
- Dual lithium evaporator system for ELM suppression, improved electron confinement, and improved HHFW and electron Bernstein wave coupling;
- Error Field Correction and Resistive Wall Mode feedback coils to stabilize MHD modes occurring at high plasma beta.

The NSTX national team members, many supported by competitive, peer-reviewed research grants, bring to NSTX highly valuable expertise, major plasma diagnostics, and computational tools, including data analysis packages and modeling codes. A number of research collaborators are directly supported by theory programs and the Virtual Laboratory for Technology (VLT). Internationally, there are collaborating researchers from 26 institutions in Japan, Korea, UK, Italy, France, Germany, Israel, the Czech Republic, Canada, Ukraine, and Russia. Most are researchers working on the ST concept in their respective countries but there are a number from tokamak and stellarator laboratories, such as LHD, KSTAR, and JT-60U. The collaboration with Japan is the largest, involving nine universities and two national laboratories because, while there are a number of small-scale ST research facilities in Japan, none is comparable with NSTX.

The NSTX engineering and technical support team brings valuable skills, knowledge, and experience in magnetic fusion engineering, experimental research, and plasma diagnostics. NSTX taps resources from rest of the Princeton Plasma Physics Laboratory including engineering designers, and versatile machine and electronic shops.

This NSTX Five Year Plan proposes significant facility upgrades, which together with the planned innovative diagnostic systems will provide the data needed to achieve the NSTX Five Year Plan Mission and in particular strengthen the database needed for the design of next-step ST facilities. Overview plans for these facility and diagnostic upgrades are summarized in Sec. 7.2 and 7.3. The proposed new center-stack(7.2.7) and the second NBI (7.2.8) are significant upgrades which will support all science topical areas of interest in NSTX. Accordingly they are discussed in greater detail in this plan. It should be noted that the schedule for their implementation is determined by the availability of the required funding.

## 7.2 NSTX Facility Status and Plans

The NSTX device is located in a well-shielded test cell at PPPL and utilizes many of the former TFTR facilities, notably the power systems which provide reliable operation of the magnets and auxiliary heating and current drive systems. The NSTX facility has commissioned all the major subsystems originally planned, and achieved or exceeded its original design capabilities. The innovative center-stack design (Fig. 7.1), together with a state-of-the-art plasma control system has yielded plasma elongations up to 3.0 transiently and 2.7 sustained, and the highest shaping factor  $q_{95}(I_p/aB_T) \approx 42 \text{ MA/m}\cdot\text{T}$  of any toroidal device. This extended operating space has produced a world record toroidal beta of  $\sim 40\%$  in a high temperature plasma. The NSTX plasma current has reached 1.5 MA, well above the original design value of 1 MA. The plasma current has exceeded the total toroidal field coil current, demonstrating the efficient magnetic field utilization of the ST configuration. The NBI system has delivered up to 7 MW total power by increasing the acceleration voltage of some sources to 100 kV. The energy confinement time in NSTX has exceeded 100 ms, and the plasma stored energy has reached 400 kJ.

Since its first plasma in 1999, NSTX has achieved its facility and operational milestones, except in 2003 when a joint in the toroidal field (TF) coil failed, causing a loss of 8 run weeks. A new center conductor bundle for the TF coil incorporating improvements to the joints was installed before the 2004 run. [7.2.1] The TF coil joints have since operated reliably and within design specifications for over 9000 pulses, routinely accessing its upper  $B_T$  range of 5.5 kG.

The NSTX plasma is surrounded by closely-fitting conducting plates (shown in Fig. 7.1), which passively stabilize pressure-driven modes, provided the plasma toroidal rotation exceeds a critical frequency. As a result, NSTX routinely produces plasmas with total pressure above that which cause MHD instability in the absence of the conducting wall, the so-called “no-wall beta limit”. To explore plasma operation with beta above the no-wall limit and approaching the limit for stabilization even by an ideal conducting wall, the “ideal-wall limit”, a fast feedback coil system, known as the Error Field and Resistive Wall Mode (EF/RWM) system, was commissioned at the start of the 2005 experimental run. The NSTX EF/RWM coil system has been highly effective in exploring and extending the stable high beta regimes. Furthermore it is contributing to the design of the system for ITER, since the NSTX coil locations are similar to those proposed for ITER and, in ITER, the tritium blanket modules on the outboard side will slow down the instability growth similarly to the NSTX passive plates. NSTX EF/RWM research benefits from a comprehensive array of magnetic sensors, the data from which can be processed in real time to generate time-varying corrections of both intrinsic and plasma-generated field perturbations.

The NSTX plasma is highly accessible due to the large number and size of diagnostic access ports. A comprehensive suite of diagnostics is now operational, many of them unique in their capabilities, providing physics information with excellent accuracy and resolution. Because the large mid-plane ports are close to the plasma and because of the compact outer TF coils, NSTX provides tangential access for a wide range of diagnostics. The strong toroidicity and excellent diagnostics make NSTX an excellent test bed for toroidal plasma theory and modeling to increase our confidence in the predicted performance of devices such as ITER and a Component Test Facility.

In the following subsections, we will describe the status and upgrade plans for several critical subsystems which provide support for the whole research program or are linked to specific research topics within that program. A timeline for the implementation of several important upgrades to the facility is provided in Fig. 7.2.

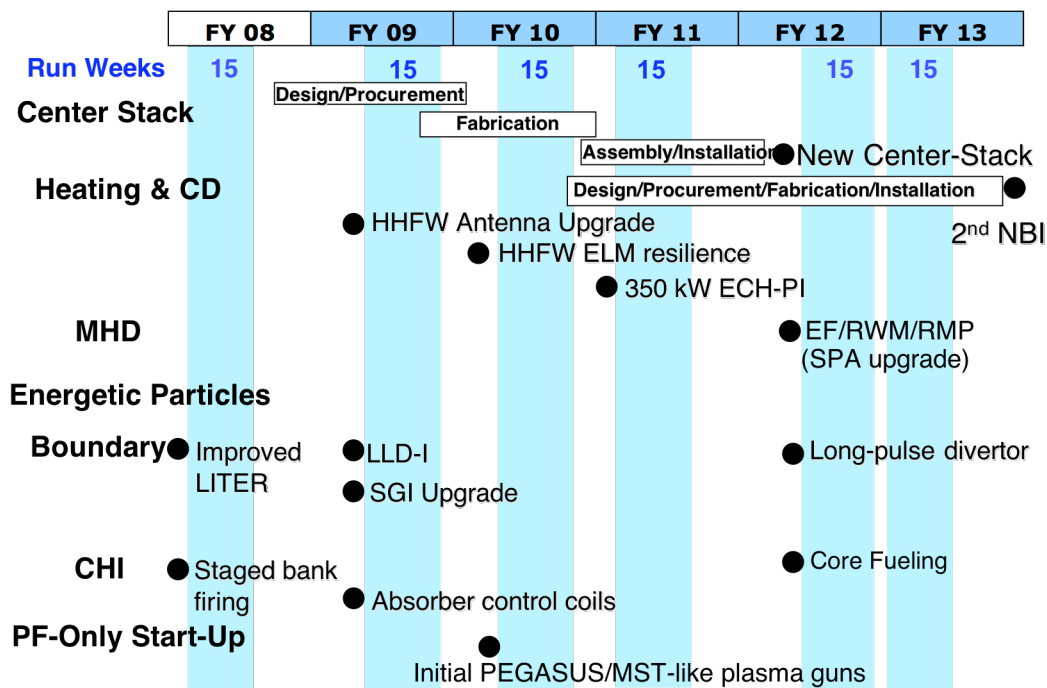


Fig. 7.2 Facility 5 Year Base Upgrade Plan. The shaded box indicates a range of implementation period determined by programmatic priorities.

## 7.2.1 NSTX Facility Subsystems

**Magnet Systems: Status** - The NSTX magnet systems are composed of the coils contained in the center-stack assembly, namely the inner TF, ohmic heating (OH) solenoid, top and bottom PF1A coils and the bottom PF1B coil, and those outside, namely the outer TF bundles, and top and bottom outer PF coils 2, 3, 4, & 5 as shown in Fig. 7.1. [7.1.3, 7.2.2] The inner coils are encased in, and thermally insulated from, an inconel vacuum casing on which are mounted the graphite tiles which form the inner plasma-facing surface. The entire center-stack assembly is fully demountable by removing the TF, OH, and PF1A connections. The demountable design provides opportunities for maintenance, repair, and upgrade as shown in Fig. 7.3. The magnets are powered by phase-controlled rectifier supplies; a motor generator provides the peak feed power (27 kA, 6 kV, 5 s) needed for operation. The TF magnet is operated routinely up to 0.55 T (nominal design limit 0.6 T) at the nominal vessel center  $R = 0.86$  m.



Fig. 7.3 Center-stack being installed

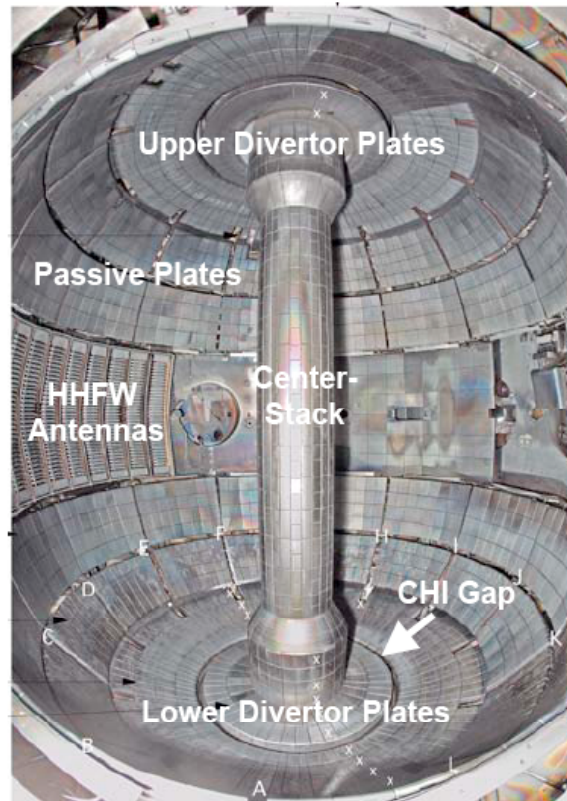


Fig. 7.4 Vacuum vessel internal components

**Plans** - A new center stack with 1 T, 5 s capability is planned. The new center stack is expected to include top and bottom PF1A and 1B coils for improved divertor and plasma shaping control. The power supply for the TF magnet and support structures will be upgraded for the 1T operation (see Sec. 7.2.7 for the new center stack details).

**Vacuum Systems – Status** -The NSTX vacuum vessel is roughly a spherical shape, 3 m tall and 3.5 m in diameter, with volume of about 30 m<sup>3</sup>. A view of vacuum vessel interior is shown in Fig. 7.4. The plasma facing surfaces are covered by graphite tiles. The volume available to the plasma is ~15 m<sup>3</sup>. The vacuum chamber provides very good plasma access with 12 major ports at the mid-plane between 12 outer TF coil sets. There are two NBI compatible rectangular ports 0.84 m (height) x 0.74 m (width); one is currently used for the existing NBI. The other, which is presently occupied by diagnostics, will be used for the proposed second NBI. Three port sections are occupied by the 12 element HHFW antenna systems and one port is dedicated for the vacuum pump duct which presently has two 1600 l/s turbo-molecular pumps. The remaining six sections each with a 0.60 m diameter circular port are mainly utilized for diagnostics. In addition, there are eleven medium size vertical-viewing ports and six smaller ports (horizontal-viewing toward the divertor regions) located on each of the upper and lower dome sections. There are gas feeds installed at three outboard mid-plane locations, one in-board at the mid-plane, one in-board at the “shoulder” where the center-stack case expands to accommodate the PF1A coils, and one in the CHI injector chamber.

**Plans** - The installation of the liquid lithium divertor in FY 2009 (see Sec. 7.2.5) will involve modifications of some plasma facing components on the lower divertor and their supports. A relocation and rearrangement of some diagnostics will accompany the planned installation of the second neutral beam injector system in FY 2013. Apart from these, no significant changes are planned to the main vacuum vessel.

**Plasma Control System:** Plasma control is an important aspect of achieving the improved performance associated with advanced plasma regimes. In particular, performance optimization involves approaching as near as possible to operating boundaries while avoiding deleterious plasma instabilities that can degrade or even terminate the plasma discharge. The approach taken to achieve the goals of plasma control is to use high speed computing combined with state of the art digital data acquisition and transmission to calculate accurate representations of the plasma state and to use this information in feedback loops to control plasma parameters

**Status** - The NSTX plasma control system (PCS) has been entirely digital from the outset. [7.2.4] It uses a dedicated fiber-optic communication network to bring real-time digitized data from diagnostics and other sensors to a central computer which analyzes important characteristics of the plasma equilibrium, compares them to desired values and generates feedback commands to the power supplies for the coils and other plasma actuators, such as the heating power and the gas fueling. The NSTX PCS was developed in collaboration with General Atomics, and uses the real-time equilibrium reconstruction code rtEFIT to control the plasma boundary. In particular, the PCS uses the real-time implementation of the EFIT (rtEFIT) solution to the Grad-Shafranov equation to control the position (radial and axial) and the cross-sectional shape of the axisymmetric MHD equilibrium. [7.2.5] The plasma control system has been continuously expanded and improved during the lifetime of NSTX. To facilitate creation of these highly shaped plasmas, two poloidal field coils, the PF1A upper and lower coils, were replaced by shorter bundles before the 2005 run. The rtEFIT/isoflux control capability of the NSTX plasma control system was extended to strongly shaped plasmas by the inclusion of additional magnetic measurements in the upper and lower divertor regions. These modifications led to the simultaneous achievement of a world record plasma elongation  $\kappa \sim 3$  at very high triangularity. The use of rtEFIT/isoflux control has led to excellent reproducibility in the strongly shaped regime and is now the predominant control scheme on NSTX.

In addition to axisymmetric shape control, NSTX has been developing non-axisymmetric control for error field correction and resistive wall mode (RWM) feedback. This involves the control of the six EF/RWM coils powered by 3 independent high speed power supplies. Data is taken using an array of large area magnetic sensors measuring both the radial and vertical magnetic field at 12 toroidal and 2 poloidal locations for a total of 48 measurements. These measurements have been used to determine the optimal error field correction as well as for direct RWM feedback. Use of these control techniques has led to a significant increase in the achievable pulse length.

In 2007 the NSTX plasma control system (PCS) was upgraded and now uses a high speed server with 8 2.2GHz processors using a version of the Linux operating system that has been modified to support the needs of real-time operation. Data is acquired over a modular high-speed (1Gb/s) data network based on the Front Panel Data Port (FPDP) standard. The PCS currently acquires 432 channels of data at a 5kHz rate. The data acquired includes coil currents, magnetic field measurements, gas valve status and plenum pressures, RF loading, and neutral beam power. The PCS currently controls all the NSTX magnetic field supplies and the gas valves used for fuelling. For 2008 the hardware capability for controlling the neutral beam source timing and measuring the neutral beam power has been added. Initially the control will mimic the preprogrammed control that is currently in use. This new capability will be demonstrated at the end of the 2008 run.



**Plans** - The NSTX PCS is a flexible system which will be upgraded and improved with the availability of new plasma real time diagnostic information to control the actuators (such as NBI, HHFW, fueling, feedback coils). In 2009 the capability to control the neutral beam power will be used in conjunction with rtEFIT to control the plasma pressure. rtEFIT will be used to predict the plasma pressure using magnetics measurements. An algorithm will be developed and employed that modulates the neutral beam source power to maintain a specified time history for the plasma  $\beta$ . This capability should allow the pressure to be held closer to the operational limits without going over them. In addition, the existing capability to measure the RF loading will be used to see if feedback on the loading can help maintain RF coupling during H-mode transitions. Experiments will be performed to see if signals suitable for real time control of the plasma position can be developed based on the loading measurements. This capability could help the RF systems to avoid trips caused by sudden changes in loading observed during H-mode transitions. In 2010, the capability to measure the real-time rotation will be added. Development of a real-time signal that is a reasonable representation of the existing charge exchange recombination spectroscopy (CHERS) rotation measurement will feed into the capability to control plasma rotation profiles in the 2011 run. Significant diagnostic development is required in order to make the CHERS measurement compatible with real-time. In 2011 the newly added capability to measure rotation in real-time will be combined with the existing capability to control the neutral beam power and the ability to apply  $n=3$  non-axisymmetric fields to control the rotation profiles. Algorithms will be developed that will generate control commands for the power supplies that control the  $n=3$  fields such that the combination of these fields and the torque from the neutral beams maintains the rotation at a specified location in the plasma at a specified value throughout the discharge. This capability could add significantly to the ability to do experiments that investigate the correlation between the plasma rotation speed and both plasma stability and plasma confinement. Starting at the end of the 2010 run, hardware modifications to the PCS will be made to support the implementation of real-time measurements of the motional-Stark effect polarimetry measurement of the magnetic field pitch angle. This capability would be available by the end of the run in 2011. This will support implementation of real-time equilibrium reconstructions with  $q$ -profiles constrained by internal measurements for the 2012 run. This capability would be directly support control of the current profile or with neutral beam current drive in future run years.

## 7.2.2 Heating and Current Drive Systems

The two main heating and current drive systems on NSTX are Neutral Beam Injection (NBI) and High-Harmonic Fast-Wave (HHFW) RF power. A heating and current system based on the electron Bernstein wave (EBW) is also being considered.

**Neutral Beam Injection System: Status** - The NSTX NBI system utilizes parts of the unsurpassed TFTR system. [7.2.5] The NSTX NBI system has delivered up to 7 MW at an acceleration voltage up to 100 kV. The beam system is the workhorse of the NSTX high- $\beta$  plasma research program, providing not only reliable plasma heating but also other important functions: imparting toroidal momentum to induce toroidal plasma rotation of up to  $\sim 300$  km/s; driving plasma current (in addition to the bootstrap current) of up to  $\sim 200$  kA; providing an energetic ion population for simulating alpha-particles (Ch. 4); and enabling plasma profile diagnostics such as the charge-exchange recombination spectroscopy (CHERS) and motional Stark-effect (MSE) systems (Sec. 7.3.)

**Plans** - With the increased toroidal field and current available with the proposed center stack upgrade, a second NBI system injecting more tangentially is planned to provide higher heating and current drive power as well as an improved NBI current profile control capability. Section 7.2.8 will present more detail on the second NBI upgrade.

### High Harmonic Fast Wave System:

**Status** – The NSTX HHFW system heats electrons and drives plasma currents for non-inductive current ramp-up and sustainment. It has also been used for pre-ionization during experiments to start the plasma using only the outer PF coils. A twelve-element-antenna system, shown in Fig. 7.5(a), is driven by six power amplifiers operating at 30 MHz with delivered power of up to 6 MW. [7.2.6] The antenna array utilizes an RF matching network developed by ORNL to vary the phase of the RF current in the six pairs of current straps in real-time to control the parallel wavenumber  $k_{\parallel}$  of the plasma waves for driving current and optimizing the wave absorption as the discharge evolves. This capability is required to track the plasma evolution from a few 100eV in OH plasmas at the start-up to a few keV in the heated phase. The HHFW has heated the core electrons from the few hundred eV typical in the ohmic phase to typically 2 – 3 keV and as high as 5 keV. The HHFW heating efficiency has been found to have a strong positive dependence on the toroidal magnetic field and an inverse dependence on the edge plasma density. Lithium coating of the plasma facing components, which decreases the edge density and recycling, has been shown to

improve the HHFW heating performance. Experiments to study HHFW current drive have shown a significant change in the loop voltage as the direction of the driven current was varied, consistent with the theoretical expectations. However, the experiments have also suggested that parasitic absorption of the HHFW by thermal and fast ions may limit the current drive efficiency of HHFW. This physics is now being investigated using the MSE diagnostic to measure the effects on the local current density.

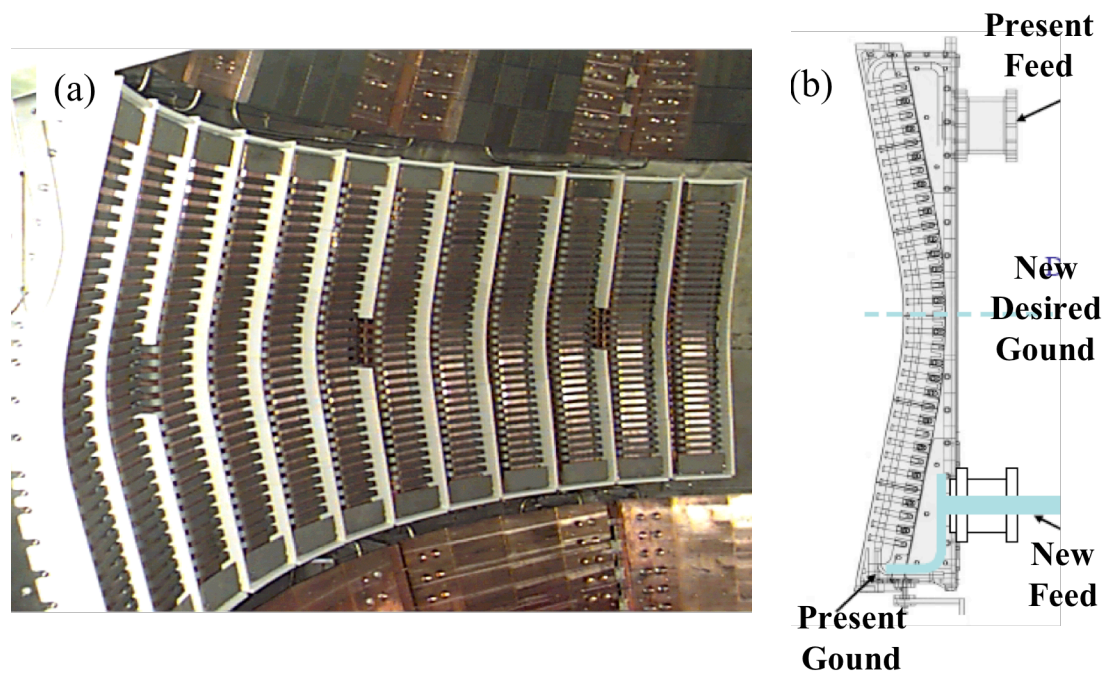


**Fig. 7.5 HHFW Antenna Upgrade. (a) HHFW Antenna View (b) Antenna upgrade schematic**

**Plans** - The HHFW power coupled to H-mode plasmas needs to be improved for planned experiments. The observed break-down voltage across the insulators in the RF feed-throughs is considerably lower in NSTX than TFTR, probably caused by increased cross-field particle diffusion into the feed-through assembly as a result of the lower toroidal field of NSTX. A solution is to upgrade the antenna to a symmetric-feed configuration which will increase the coupled power level by a factor of two for a given feed-through voltage. A schematic view of the modification which will be implemented in FY 2009, is shown in Fig. 7.5(b). This HHFW

antenna upgrade should double its power handling capability and optimize the antenna radiation pattern by locating the virtual antenna ground to the antenna mid-plane. In 2010, to reduce the antenna impedance changes during the H-mode ELM activity, an HHFW ELM resilience capability will be implemented for H-mode plasmas in collaboration with ORNL.

**Electron Bernstein Wave System: Status** - Electron Bernstein Waves (EBW) are a promising tool to drive localized off-axis current needed for sustained operation in advanced ST modes. The current is driven via the Ohkawa effect, in which a part of the electron thermal distribution which resonates with the wave is accelerated from co-passing to trapped orbits, thereby suppressing their counter-directed parallel electron current. Modeling predicts high current drive efficiency for this scheme, two to three times greater than conventional Fisch-Boozer electron-cyclotron current drive. However, the EBW current-drive scheme depends on converting externally launched electromagnetic waves into the EBW which can only propagate inside the plasma. Measurements in NSTX of the inverse process, that is mode conversion of thermally excited EBW inside the plasma to electromagnetic emission from the plasma show the possibility of achieving adequate coupling efficiencies for the viability of this current drive scheme. With lithium evaporation onto the NSTX divertor, good coupling to H-mode plasmas has been recently demonstrated. However, the physics of the EBW coupling is still not yet fully understood so research will continue in this area.

**Plans** - In view of recent encouraging results, research on the fundamental physics of EBW coupling and absorption will continue on NSTX. A medium power ECH/EBW system (350 – 700 kW at 28 GHz) is being considered for NSTX. [7.2.7] This system, which is being developed as a collaboration between PPPL and ORNL, would become available in FY 2011. It could also benefit plasma start-up research on NSTX by providing conventional ECH heating for the low-density plasmas created by CHI or the outer-PF coil startup scheme, which will be discussed in Sec. 7.2.6. The ECH heating would not only reduce the plasma resistivity but also could heat the plasma to higher electron temperature  $\sim 100$  eV where HHFW heating becomes effective. An active collaboration on EBW physics will be pursued with the MAST experiment at the UKAEA Culham Laboratory where a medium EBW power system will become available in the near term.

### 7.2.3 Macro-stability Tools

The possibility of achieving high plasma pressure at modest magnetic field, *i.e.* high plasma  $\beta$ , is a primary motivation for investigating the ST concept. NSTX is exploring two main avenues to maximizing the sustainable  $\beta$ : optimization of the axisymmetric equilibrium configuration and suppression or control of the growth of non-axisymmetric pressure-driven instabilities.

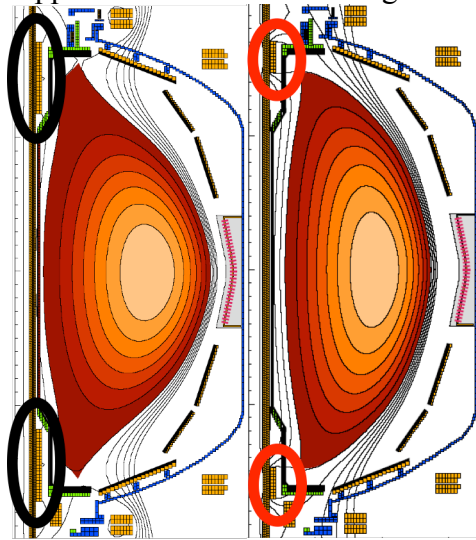


**Fig. 7.6** Cross-section of NSTX showing the PF1A coils (circled) and typical plasma configurations available in 2004 (left) and 2005 (right) and the Error Field and Resistive Wall Mode (EF/RWM) coils.

*In* experiments conducted on NSTX in 2004 with the original PF coils, encouraging results, in terms of higher achievable plasma current and thus lower normalized plasma beta  $\beta_N = \beta_T a B_T / I_p$ , were obtained with high elongation plasmas. However, MHD stability calculations suggested that further improvements in the stable  $\beta_N$  could be made if the plasma cross-section conformed more closely to the passively stabilizing conducting plates on the large major radius side. Because the NSTX center-stack is removable, ready access is available to any part of the device. This enabled the installation of a new set of upper and lower inner PF1A coils in early 2005 to achieve high-elongation, high-triangularity. In recent experiments, the new shaping coils produced plasmas with high elongation,  $\kappa = 3.0$  transiently and 2.7 sustained, and triangularity,  $\delta \approx 0.8$ . Examples of the plasma shapes obtained with the old and new coil sets are shown in Fig.

7.6.

As the plasma  $\beta$  increases above the level at which a surrounding conducting wall is necessary for MHD stability to pressure-driven modes, the so-called “no-wall  $\beta$ -limit”, it is important to have methods to control mode growth on the timescale for resistive decay of currents induced in the wall. Two approaches are being tested on NSTX: maintaining sufficient toroidal rotation and applying non-axisymmetric magnetic field perturbations to sustain plasma rotation and counteract mode growth.

A nearby conducting wall can stabilize the ideal pressure-driven MHD kink/ballooning mode, provided that sufficient plasma rotation is maintained. However, below a critical rotation rate, the resistive wall mode (RWM), a kink mode modified by the presence of a conducting wall, can

become unstable and grow, leading to rapid rotation damping and, ultimately,  $\beta$  collapse on the timescale of the decay of wall eddy currents. Such unstable modes appear to grow preferentially from perturbations caused by the intrinsic error fields in the plasma region which act as the “seeds”. In 2002, the maximum normalized plasma beta  $\beta_N$  was improved significantly by reducing the intrinsic error fields by realigning the PF5 coils. With sufficient plasma rotation maintained by the momentum imparted by the NBI, the  $\beta$  limit of NSTX plasmas has significantly exceeded the no-wall limit for many resistive wall times, demonstrating the effectiveness of wall stabilization. The second approach of applying non-axisymmetric magnetic field perturbations is discussed in the following section.

**Error Field/Resistive Wall Mode Coils – Status** - To explore plasma operation with beta above the no-wall limit and approaching the limit for stabilization by an ideal, perfectly conducting wall, the “ideal-wall limit”, three pairs of non-axisymmetric coils have been installed on NSTX to produce controllable radial magnetic field perturbations as shown in Fig. 7.7. [7.2.8] The individual coils are nearly rectangular “picture frames” of two turns each, centered on the mid-plane and mounted just outside the vacuum vessel wall. The three pairs of diametrically opposite coils are powered by a three-channel Switching Power Amplifier (SPA) with the capability for driving multi-kiloamp currents at frequencies up to 1 kHz. The individual coil polarities can be changed at a patch panel to provide controllable perturbations with dominantly odd ( $n = 1, 3$ ) or even ( $n = 2$ ) toroidal harmonics. The complete system was commissioned at the start of the 2005

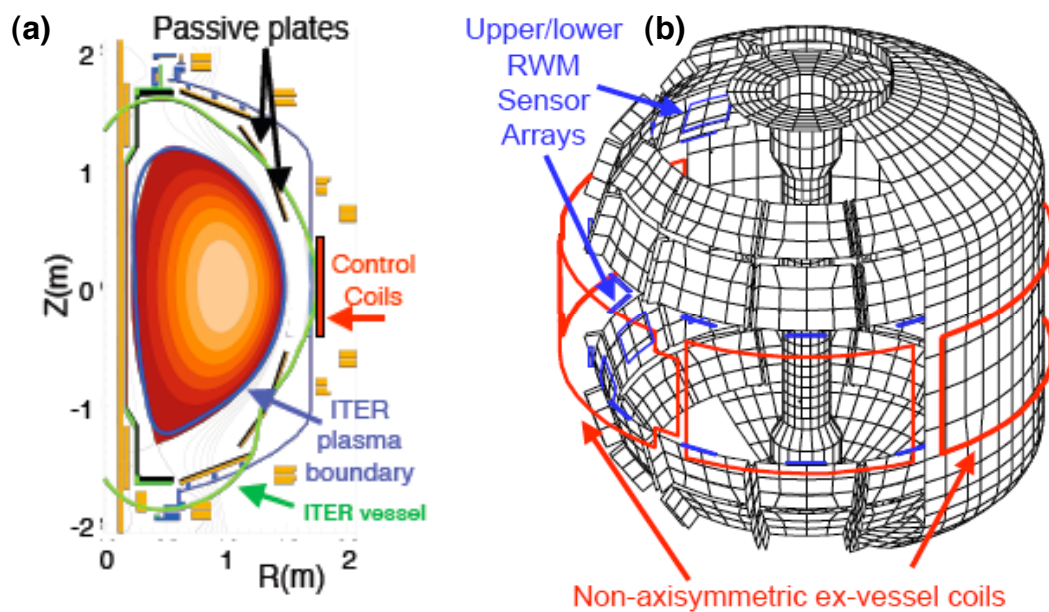


Fig. 7.7 EF/RWM/RMP Coil Schematics (a) Cross-sectional view. (b) 3-D view

experimental run. Experience with the NSTX EF/RWM coil system will contribute to the system proposed for ITER, since the NSTX coil locations are similar to those proposed for ITER and, in ITER, the tritium blanket modules on the outboard side will slow down the instability growth similarly to the NSTX passive plates as illustrated in Fig. 7.7 (a). NSTX EF/RWM research benefits from a comprehensive array of magnetic sensors, the data from which can be processed in real time to generate time-varying corrections of both intrinsic and plasma-generated field perturbations as shown in Fig. 7.7 (b). [7.2.9] Use of the EF/RWM coils has enabled sustained high beta operation in NSTX, even at low plasma rotation rates relevant to those expected in ITER and ST-Demo where the momentum input from NBI heating will be much lower. More recently the feedback coil system was used to test ELM stabilization and controllable destabilization using the Resonant Magnetic Perturbation (RMP) concept in support of the ITER design activity.

**Plans** – The present SPA provides three independent controllable currents to the EF/RWM coil set. These coils are generally configured through hardwired connections at a patch panel to provide either the odd ( $n = 1, 3$ ) or even ( $n = 2$ ) perturbations, although other “exotic” configurations which include higher field harmonics are possible, such as simulating the “missing” control coil of one set of such coils proposed for ITER. However, maximum flexibility would be achieved by installing an additional 3-channel SPA so that each coil would be separately powered, allowing simultaneous control of the full range of field harmonics. An assessment is being made to determine the need for this upgrade. Design studies are also being performed to assess the desirability of installing a second set of non-axisymmetric control coils inside the vacuum vessel and located symmetrically above and below the midplane. These coils would provide faster reaction to the evolution of MHD perturbations and better capability to counteract mode growth due to the very high pitch of the field lines at the outboard side of high- $\beta$  ST plasmas. Depending on the results of these assessments and design studies which are based on both theory and the results of ongoing experiments, one or both of these upgrades would be undertaken in FY 2011 to be available in FY 2012.

## 7.2.4 Boundary Physics Facility Tools

The achievement of good vacuum and surface conditions on the plasma-facing components (PFCs) in NSTX has been crucial to the progress in its plasma performance. NSTX employs state-of-the-art wall conditioning capabilities, including 350°C bake out of PFCs, periodic boronization, and between-shots helium glow discharge cleaning (HeGDC), to control the impurity influxes and the hydrogenic loading of the PFCs. This combination of methods both suppresses oxygen impurities and reduces the ratio of the hydrogen to deuterium concentrations to below 0.05 in plasmas with deuterium fueling.

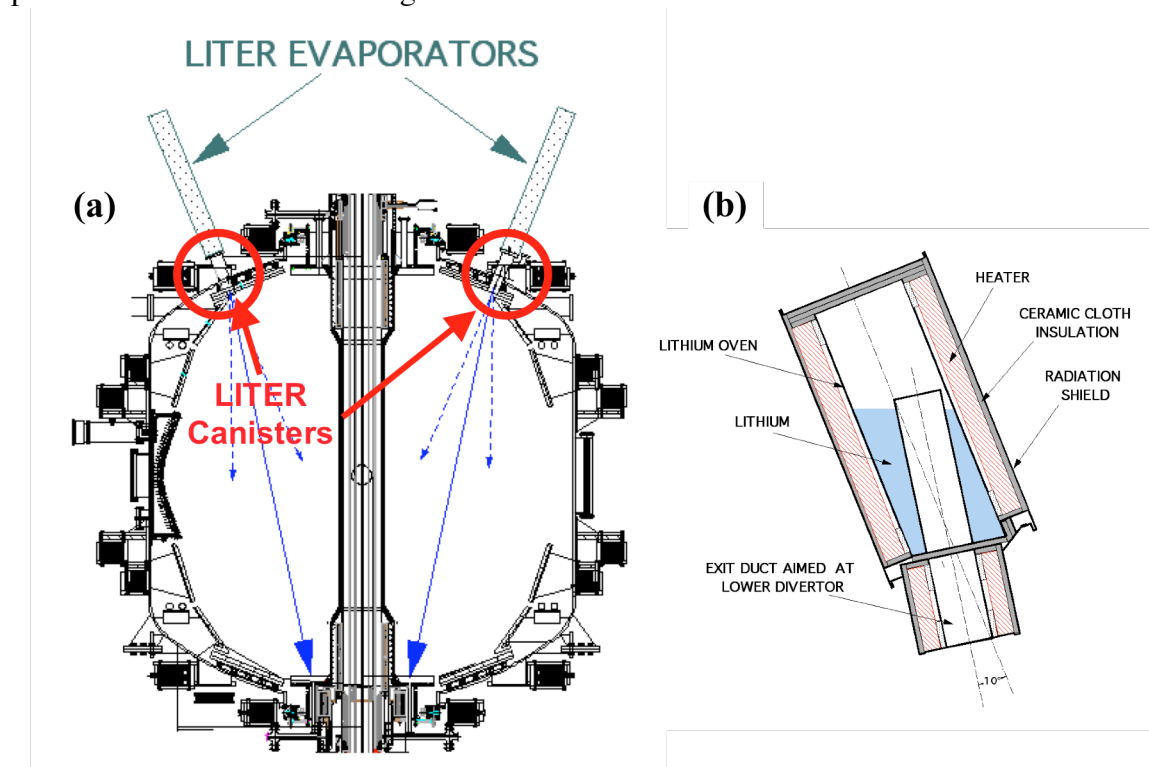


Fig. 7.8 NSTX “LITER” lithium evaporators (a) positioning, (b) canister schematic

**Lithium Evaporator for Coating Divertor Surfaces: Status** - A lithium evaporator, dubbed “LITER”, had been developed, installed on NSTX since 2006 and used in a variety of experiments which had shown several benefits for plasma operation. [7.2.10] In 2006, when a total of 10 g of lithium was evaporated during the run period, some promising indications of reduced recycling and impurity levels were measured. For the FY 2007 experiments, the LITER was upgraded by installing more robust radiant heaters, increasing the capacity of the lithium reservoir, enlarging the diameter of the exit duct and angling it to direct the lithium vapor stream towards the lower



divertor plate. With these changes, the maximum evaporation rate was increased by a factor of 3 to about 60 mg/min and the peak local deposition rate of lithium on the lower divertor was increased by a factor 3. A total of over 90 g of lithium was evaporated in the entire campaign with LITER in FY 2007 producing clear benefits in H-mode plasmas, including improved confinement, particularly of the electrons, and ELM-free periods. For FY 2008 experiments, a second LITER was installed at another upper port, separated 150° toroidally from the first, to complete coverage of the lower divertor target. The location of the LITER evaporators in 2008 and a schematic cross-section showing features of the evaporators are shown in Fig. 7.8. Shutters were installed in front of both LITERS to prevent lithium entering the plasma region both during the plasma pulse (to prevent lithium deposition on diagnostic windows while their protective shutters were open) and during any subsequent period of helium glow-discharge cleaning (to prevent the entrapment of helium in the deposited lithium layer). The LITER system can be refilled with about 100 g of lithium in about a half day. The effects of the lithium coating on the plasmas will be described in the section on Research Accomplishments to follow. The dual LITER system has contributed strongly to the NSTX research program in 2008 in numerous ways, including improving the plasma confinement, stabilizing ELMs, improving the HHFW heating efficiency, particularly in deuterium plasmas, and improving the EBW coupling in H-mode plasmas.

**Plans** - The LITERS now provide a mature, reliable lithium delivery system. In 2009, after the installation of the liquid lithium divertor target (described below), the LITERS will be used as its primary lithium delivery method, although they can also continue to be used in their present mode of operation.

### **Liquid Lithium Divertor Target:**

**Status** - Following the success of the lithium evaporator development and experiments, the NSTX team is focusing its effort on a liquid lithium divertor (LLD) target. [7.2.11] This initiative is a collaboration between PPPL and a team at Sandia National Laboratory (SNL). As shown in Fig. 7.9, the LLD will be located at the bottom of the vessel in the outer divertor strike point region. It will consist of a set of temperature-controlled, molybdenum-coated stainless-steel plates forming an almost continuous conical annular ring in the lower outboard divertor. When coated with lithium and heated above its melting point the plates will provide about 7000 cm<sup>2</sup> of active pumping surface area in contact with the outboard scrape-off layer of the plasma. The dual LITER system presently installed on NSTX will be used to deposit and resupply the layer of lithium onto the heated LLD surface. The liquid lithium limiter experiment on CDX-U was quite encouraging in terms of drastically reducing the oxygen level and the particle recycling while

handling high heat flux, but this experience was limited to ohmically heated L-mode plasmas. The NSTX system will be unique in the world to test the effectiveness of liquid lithium as the plasma contact surface for H-mode plasmas with significant auxiliary heating power. A liquid lithium divertor target has the potential to be a much more attractive option than a cryo-pump system because it can manage the intense heat flux as well as controlling particle recycling in the steady-state conditions expected in future devices such as CTF and Demo.

**Plans** – The design of the LLD system is complete and the components are currently being procured and fabricated. Ongoing R&D activities at PPPL and SNL are assessing and developing coating techniques. The LLD system is scheduled to be installed on NSTX in the fall of 2008 and will be available for experiment in FY 2009. Based on results of continuing laboratory tests and the initial LLD results, the LLD will be improved in FY 2010 (LLD-II) to increase its pumping and power handling capability sufficient to meet the demands of high-performance discharges extended to the limits of the NSTX magnets. One possibility being explored to increase the capacity is a mesh-based system, which can retain a larger volume of liquid lithium for long-pulse operation. A prototype mesh system is being developed and tested in collaboration with SNL. Another possibility for LLD-II is a second plate system located on the inboard side of the lower divertor to augment the pumping capability for high-triangularity discharges. An assessment will be made of the LLD performance after the FY 2009 run to decide on the long-pulse high-power divertor design including a possible transition to a cryo-based system in FY 2011.

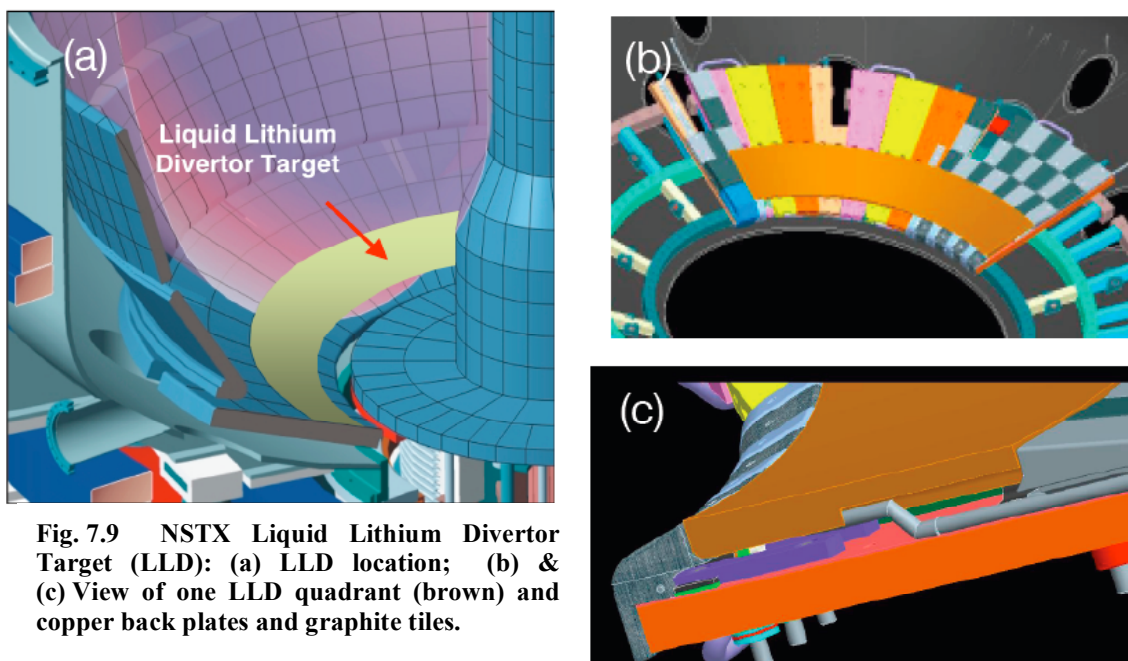


**Fig. 7.9** NSTX Liquid Lithium Divertor Target (LLD): (a) LLD location; (b) & (c) View of one LLD quadrant (brown) and copper back plates and graphite tiles.

**Fueling Tools: Status** - The capabilities for gas fueling the NSTX plasma have been steadily enhanced with gas injectors in several locations, including the outer mid-plane, inboard mid-plane, “upper shoulder” and divertor regions. [7.2.12] Experiments have shown that puffing deuterium into the private flux region or close to the outer strike point of the lower divertor can produce partial detachment of the outer divertor and a substantial reduction of the heat flux to the divertor surface without degrading the H-mode energy confinement. A supersonic gas injector (SGI) has been installed which introduces deuterium gas at a velocity up to 2.4 km/s into the plasma near the mid-plane on the outside. [7.2.13] High-speed camera images have confirmed that a collimated stream of deuterium enters the plasma from the nozzle. The fueling efficiency of the SGI is a factor 2 – 5 higher than conventional deuterium gas injectors and the H-mode threshold power is lower with SGI fueling.

**Plans** - The NSTX plan for core fueling includes both a frozen deuterium pellet injector and a compact toroid (CT) injector. [7.2.14] Interestingly, high beta plasmas on NSTX present a minimum-B target for outside-launch pellet injection, with the gradient of the total magnetic field pointing radially outwards a few centimeters inside the plasma edge, thereby presenting the possibility of inward transport of the pellet fuel even with the technically simpler outside launch. The NSTX field structure is also well suited to test controlled fuel deposition by the CT injector. A CT injector developed for a tested on the Tokamak de Varennes in the 1990s is available to NSTX although some refurbishment would be necessary and, if initial indications are favorable, an upgrade to the capacitor banks and their associated power supplies would be needed to provide the capability for multiple CT injections during a single NSTX discharge. The ITPA steady-state team has expressed interest in an investigation in NSTX of CT injection, which has reactor-relevant potential for particle fueling and radial deposition control.

### 7.2.5 Start-up and Ramp-up

In order to develop attractive ST power plants, a practical technique must be developed to start up the toroidal plasma current needed for confinement without reliance on induction from a central solenoid. Designs for ST reactors such as CTF and ARIES-ST assume no ohmic solenoid and even advanced tokamak reactors such as ARIES-AT also dispense with an ohmic solenoid. Solenoid-free start-up is therefore an important component of NSTX research. The main approach investigated to date in NSTX is coaxial helicity injection (CHI). This technique has been investigated previously in smaller devices including HIT/HIT-II (U. Washington). NSTX has also investigated techniques to start the plasma using only the outer PF coils; initial experiments have shown promise.

**Coaxial Helicity Injection: Status** – Coaxial Helicity Injection (CHI) involves generating a poloidal current between electrodes on the inner and outer parts of the vacuum vessel which are electrically isolated. [7.2.15] In the early NSTX experiments which used a rectifier supply to produce the discharge, CHI generated up to 400 kA of toroidal current and a current multiplication factor (the ratio of the toroidal plasma current to the injected current) up to 14 was obtained. However, it was difficult to assess how much of the toroidal current was actually flowing on closed toroidal flux surfaces. Recently on HIT-II, a new technique called a “transient” CHI was developed which produced substantial toroidal current flowing on closed flux surfaces after the injector current had been terminated. [7.2.16] By utilizing relatively short injection pulses, it was found to be possible to “detach” the plasma current ring from the injector to create flux closure. By initiating the plasma with the transient CHI technique, the performance of the plasma in HIT-II during a subsequent inductive phase was significantly improved, reducing the inductive volt-seconds needed and producing significantly higher final plasma current. On NSTX, a capacitor bank was commissioned in 2004 to test this method. Initial experimental results were encouraging, producing about 150 kA of toroidal plasma current with only a few kA of injected current, yielding current multiplication factors of as high as 40. For the 2005 experiments, direct gas-feed into the injector region was implemented to allow breakdown with reduced gas input to the main chamber. In 2008, staged firing of the CHI capacitor was implemented to provide control of the CHI current during the critical expansion of the discharge into the main plasma region. A successful transition from CHI initiation to inductive ramp-up of the plasma current has now been demonstrated.

**Plans** – The coupling of a discharge initiated by CHI to induction will be further optimized to minimize the requirements for inductive flux to reach the full operating current. Such a

demonstration is needed to validate the designs for the ST-CTF and ST-Demo where only limited inductive flux can be provided.

**PF-Only Start-Up: Status** - In parallel to the research on CHI, the NSTX team is pursuing another approach utilizing the outer PF coils. There are several variants of the outer-PF-only plasma start-up approach. On the JT-60U and TST-2 devices, significant plasma currents of up to 150 kA were generated by the simple vertical field swing in the presence of strong ECH heating. In addition to the TST-2/JT-60U technique, a merging plasma ring approach developed on TS3/4 has been successfully demonstrated on the MAST device recently. A poloidal flux / field-null optimized scenario is also being developed for STs. On NSTX, a scheme for outer-PF-only plasma start-up was tested in 2004. Using HHFW as a pre-ionization source, a successful start-up was demonstrated producing ~20 kA of toroidal current, but only when a very good field-null condition was satisfied. A high power ECH preionization and pre-heating source could relax the field-null requirements, as was demonstrated in TST-2 and JT-60U.

**Plans** - A medium power ECH system with power level of 350 -700 kW is planned in collaboration with ORNL which should improve the initial breakdown condition. Other alternatives, including a plasma gun and CT injection, are being considered to provide a suitable target plasma for the start-up. The goal is similar to that for CHI start-up, that is to reach full plasma current with minimum use of induction.

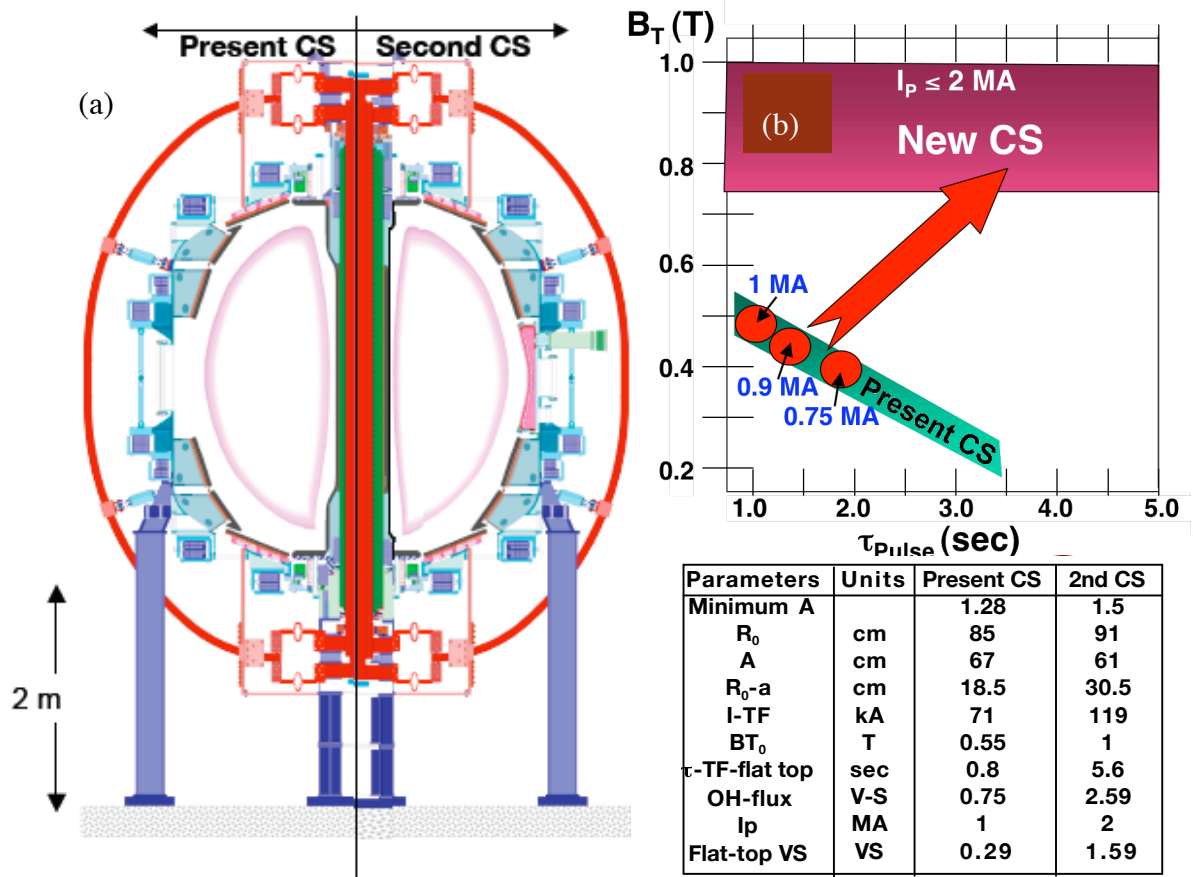


Fig. 7.10(a) The cross section of the present and second center-stack.  
 (b) Accessible  $B$ ,  $I_p$ , and  $\tau$ -pulse space for the present and second center-stack.

Table 7.2 The base parameters of the present and second center-stack

### 7.2.6 New Center-Stack Upgrade

**Status** - This upgrade involves a replacement of the slender central column of NSTX, which holds some of the magnet conductors, with a slightly wider column, capable of 2x higher magnetic fields for 5x longer pulses. This would raise the magnetic fields in NSTX half-way to those of the next-step devices and expand the accessible magnetic field range by a factor of 3.

The new center-stack is a logical step for the NSTX facility which was designed originally to be able to accommodate a replacement. The center-stack can be removed relatively easily by removing the 72 flexible joints (36 top and 36 bottom) of the TF coil as shown in Fig. 7.10 (a).

The removable/replaceable center-stack design facilitates the maintenance and repair of the center-stack which is the most stressed and complex component on NSTX. During the eight years of operation to date, the center-stack has been removed three times for maintenance, repair and improvements. The new center-stack will have the same vacuum sealing surfaces to the flexible elements of the vacuum vessel boundary so that it can be installed during a normal annual outage period (typically a period of few months.) A comparison of the present and the second center-stack cross sections and accessible parameter space are shown in Fig. 7.10 (a) and (b). Some of the basic parameter is listed in Table 7.2. The two designs are similar except that the new center-stack is about 12 cm larger in major radius as shown in the Table 7.2. In fact, it would be possible to use the two assemblies interchangeably if it made good programmatic sense. In addition to the TF and OH coils, the new center-stack will also include top and bottom PF 1A and 1B coils to retain divertor and plasma shaping flexibility. The present center-stack has symmetric top and bottom PF 1A coils but only a bottom PF 1B without a corresponding top PF 1B coil. Due to larger conductor sizes and larger radial build, the stresses in the upgraded TF and OH magnets are similar to those in the present center-stack. Similarly, the TF joint current density and the magnetic field at the joint are similar. So the overall design and the manufacturing processes for the TF, OH magnets and the TF joints should remain similar to those used for the present center-stack with some improvements. The overall forces (e.g., vertical lifting force at the TF joints and overturning force) will be larger due to the higher toroidal and poloidal fields so appropriate support structure enhancements will be implemented. The outer PF coils (PF 2, 3, 4, 5) as well as the outer TF coils are sufficient to support the higher field operation. The power system for the new center-stack will require doubling of the toroidal field coil current. This will be done by reconfiguring the available TFTR power supplies. The existing OH and PF power supplies are adequate for the projected plasma current of 2 MA, for a 5 s pulse. The new center-stack will cause relatively minor difficulties for most diagnostic systems although the laser path for the multi-point Thomson scattering system will need to be shifted outward by about 10 cm.

**Plans** - The design of the center-stack will be finalized in FY 2009 while starting the procurement of the long-lead items. In FY 2010 - 2011, component fabrication and installation will be completed to be ready to support the FY 2012 run.

## 7.2.7 Second Neutral Beam Injection System Upgrade

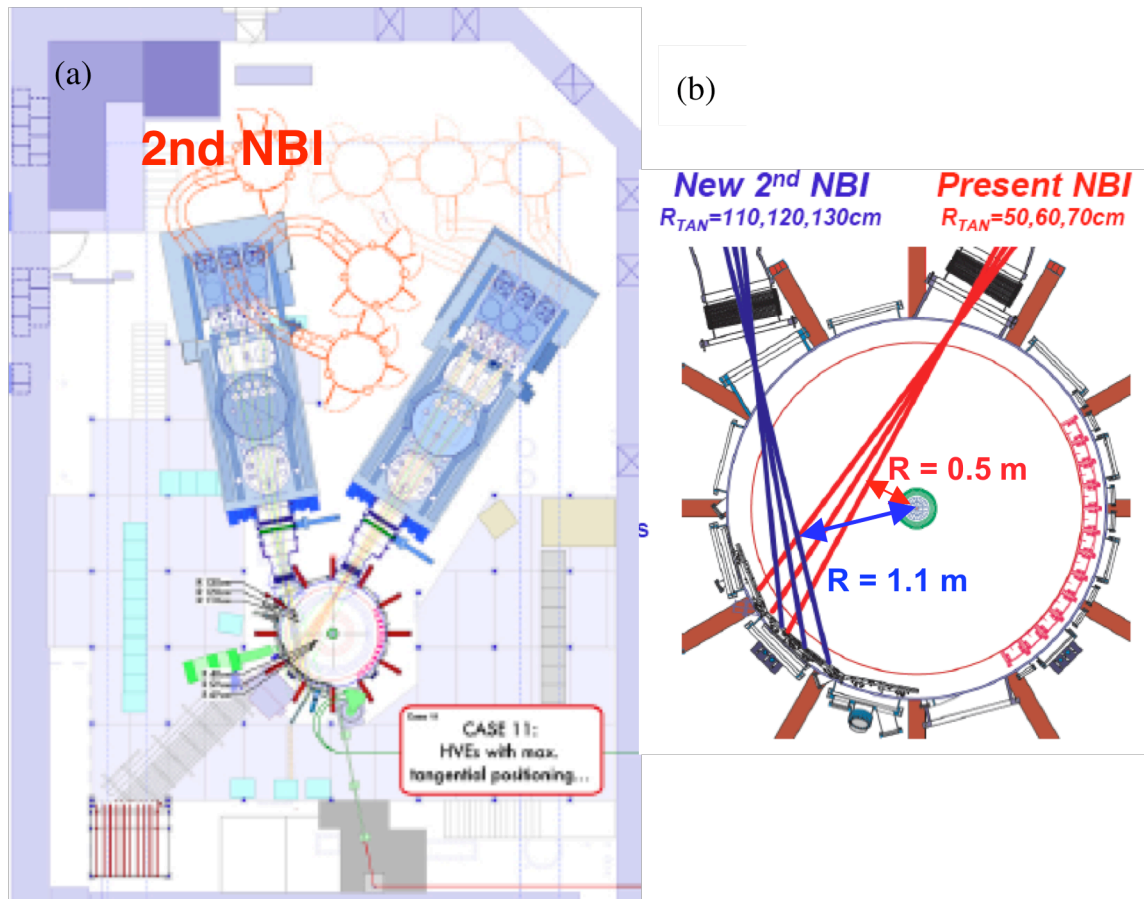


**Fig. 7.11** Second NBI Upgrade (a) NBI systems in the NSTX Test Cell. (b) NBI beam trajectories showing more tangential injection for the second NBI (in blue).

**Plans** - A second TFTR Neutral Beam Injection system with three sources will be refurbished and moved to NSTX, thereby doubling its neutral beam power. Provision for a second NBI system was made in the original design of the device which includes a second specialized NBI port (at Bay K). Space is available in the NSTX test cell for the second beamline and its high-voltage power supplies. The second beamline is shown in the NSTX Test Cell in Fig. 7.11. The second NBI system will have more tangential aiming, with tangency radii  $R_{TAN} = 1.10, 1.20, 1.30 \text{ m}$ , compared to the present NBI radii  $R_{TAN} = 0.50, 0.60, 0.70 \text{ m}$ . The work to accomplish this upgrade should be similar to that for installation of the first NBI, although the second beam box from TFTR



remains tritium contaminated and therefore requires decontamination process which may involve the replacement of some internal components. NSTX already uses ion sources from TFTR which have undergone a well-established decontamination process. There will be a relocation of the diagnostics and the pumping port.

The second NBI installation not expected until FY 2014 due to the resources required. It is planned to utilize a modest effort to perform some tests on the beam box to assess the decontamination work scope and the need for replacement of the internal components. It is also desirable to perform the engineering design up front to tighten the cost and schedule. If the resources were to become available, the second NBI could be accelerated by one year for the FY 2013 run in the incremental plan.

### 7.3 NSTX Diagnostic System Status and Plans

In addition to providing the capabilities to produce and control high  $\beta$  plasmas, it is crucial to have appropriate plasma diagnostics in order to develop our understanding of the physical processes governing plasmas through the comparison of data with theory and modeling. NSTX has been continuously implementing modern plasma diagnostic systems in key research areas. In this section, we will describe briefly some of the recent diagnostic additions and planned upgrades. A complete list of major diagnostics currently installed and operating on NSTX is shown in Table 7.3. The implementation of diagnostics on NSTX has benefited greatly from collaborations with many national and international institutions: more than half of the diagnostics listed (highlighted in italicized red in Table 7.3) are either collaborator-led or have a strong collaboration component. In the Appendix, those collaborative NSTX diagnostics and upgrades plans are described as an important part of the collaboration activities and plans.

#### MHD/Magnetics/Reconstruction

Magnetics for *equilibrium reconstruction*  
 Diamagnetic flux measurement  
 Halo current detectors  
 High- $n$  and high-frequency Mirnov arrays  
 Locked-mode detectors  
 RWM sensors ( $n = 1, 2, \text{ and } 3$ )

#### Profile Diagnostics

Multi-pulse Thomson scattering (30 ch, 60 Hz)  
 T-CHERS:  $T_i(R)$  and  $V_i(r)$  (51 ch)  
 P-CHERS:  $V_a(r)$  (51 ch)  
*MSE-CIF (15<sup>o</sup> ch)*  
*FIReTIP interferometer (119mm, 6 ch)*  
 Midplane tangential bolometer array (16 ch)

#### Turbulence/Modes Diagnostics

*Tangential microwave high- $k$  scattering*  
*Microwave reflectometers*  
*Ultra-soft x-ray arrays – tomography (4 arrays)*  
*Fast X-ray tangential camera (2ms)*

#### Energetic Particle Diagnostics

Neutral particle analyzer (2D scanning)  
 SSNPA  
 Fast lost-ion probe (energy/pitch angle resolving)  
 Neutron measurements  
*Fast Ion  $D_\alpha$  profile measurement*

#### • Collaboration contributions

#### Edge Divertor Physics

*Reciprocating Edge Probe*  
*Gas-puff Imaging (2ms)*  
*Fixed Langmuir probes (24)*  
 Edge Rotation Diagnostics ( $T_i, V_i, V_{pol}$ )  
*1-D CCD  $H_\alpha$  cameras (divertor, midplane)*  
*2-D divertor fast visible camera*  
 Divertor bolometer (12 ch)  
*IR cameras (30Hz) (3)*  
 Tile temperature thermocouple array  
 Dust detector  
*Scrape-off layer reflectometer*  
*Edge neutral pressure gauges*

#### Plasma Monitoring

*Fast visible cameras*  
 Visible bremsstrahlung radiometer  
 Visible survey spectrometer  
 UV survey spectrometer  
*VUV transmission grating spectrometer*  
*Visible filterscopes*  
*Wall coupon analysis*  
*X-ray crystal spectrometer (astrophysics)*

Table 7.3. Major Diagnostic Systems Installed on NSTX

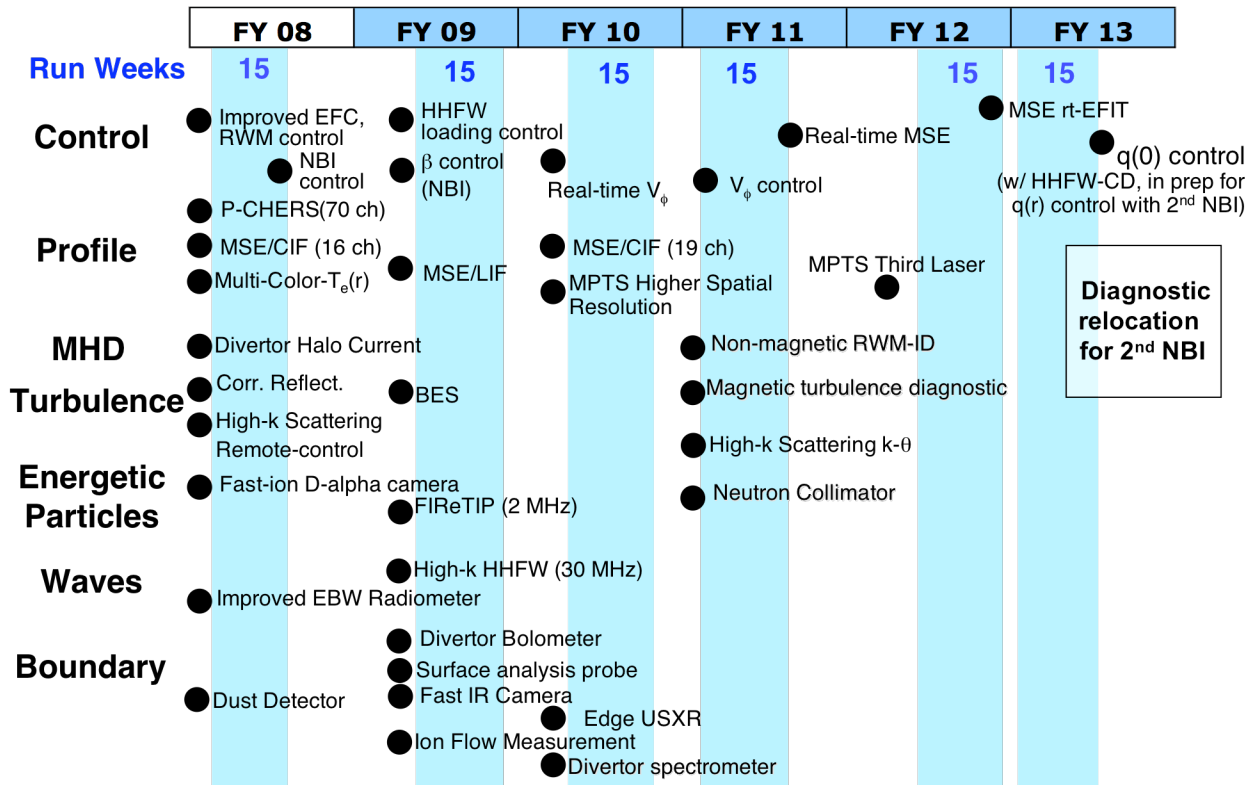
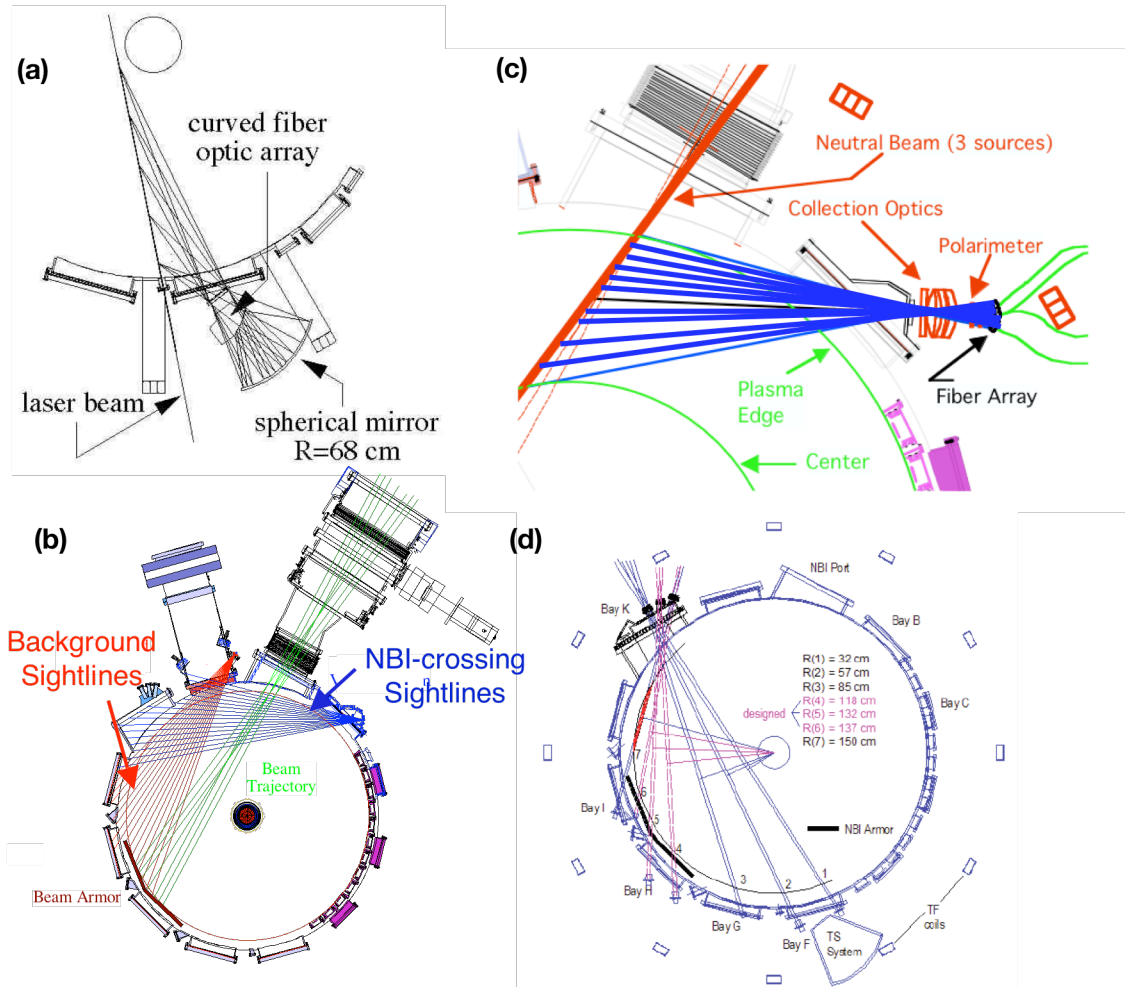


Fig. 7.11 NSTX 5 Year Diagnostic Upgrade Plan

Fig. 7.11 shows an overview of the diagnostic upgrade plan to support the NSTX Five Year Research Plan. The implementation of specific diagnostics depends on the available budget and programmatic priorities. This diagnostic upgrade plan is based on the projected available budget profile.

### 7.3.1 Profile Diagnostics:



**Fig. 7.12 Present NSTX profile diagnostics taking advantage of excellent tangential access. (a) 30 channel, 60 Hz Multi-Pulse Thomson Scattering System. (b) 51 Channel Toroidal CHRS system with both NBI and background views. (c) 16 channel Motional Stark Effect using Collisionally-Induced Florescence current profile diagnostic system. (d) 6 channel Far-infrared Tangential Interferometer.**

For transport studies, NSTX has developed an excellent set of plasma profile diagnostics which measure profiles near the plasma mid-plane to facilitate rapid data analyses. Through a combination of state-of-the-art profile and turbulence diagnostics with advanced theory and modeling, NSTX is contributing to the fundamental understanding of plasma transport and stability which is needed to develop predictive capability for ITER and future STs.

**Multi-pulse Thomson Scattering System: *Status*** - The large vacuum window and light collection mirror allow the multi-pulse Thomson scattering (MPTS) system to measure plasma density and temperature with excellent accuracy at a rate of 60 profiles per second and at 30 spatial points to resolve the structure of the H-mode edge pedestal and internal transport barriers. [7.3.1, 2] A schematic of the MPTS system is shown in Fig. 7.12 (a). ***Plans*** - The MPTS system is designed to be upgraded to 45 spatial channels and 3 lasers for 90 Hz operation. The MPTS system will be upgraded as the resources become available and according to programmatic needs.

**Toroidal Charge Exchange Recombination Spectroscopy (TCHERS): *Status*** - This system provides detailed ion temperature, plasma toroidal rotation and carbon density profiles as a function of time at 51 spatial locations across the outer half of the plasma region. [7.3.3] As shown in Fig. 7.12 (b), the NSTX TCHERS system involves viewing chord fans both crossing and outside the NBI path to achieve separation of the charge-exchange light from carbon impurities (C-VI line at 529 nm wavelength) in the center from the intrinsic (thermally excited) emission near the edge of the plasma. The emission from each sightline is transported along optical fibers to

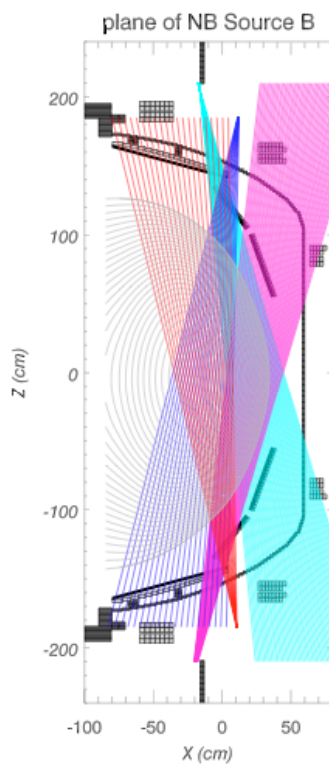


**Fig. 7.13 Poloidal CHERS system schematic.**

high resolution spectrometers. Charge-coupled device (CCD) cameras record the spectra in the image plane of the spectrometers with a time resolution of 10 ms. In the H-mode pedestal region, the spatial accuracy is comparable to the local ion gyro radius which is a unique NSTX capability. With a lithium filter and different diffraction gratings, the TCHERS system can be also used to measure the lithium density profiles. ***Plans*** - The present TCHERS system is state-of-the-art and further upgrades are not currently planned for the next 5 years. However, a real-time capability for its data acquisition and analysis within the plasma control system will be installed in 2011. This will enable real-time control of the rotation profile using the NBI and non-resonant magnetic braking as the actuators.

**Poloidal Charge-Exchange Recombination Spectroscopy (PCHERS): *Status*** - An interim version of the PCHERS system was installed and commissioned in FY 2007 and the full 75-channel PCHERS system, shown schematically in Fig. 7.13, was commissioned in FY 2008. This NSTX PCHERS system is a follow-on system from the TFTR PCHERS system. [7.3.4] This diagnostic, which also analyzes C-VI emission, measures the

spatial profile of the poloidal plasma flow across the entire outboard minor radius with ion gyro-radius spatial resolution. In the PCHERS system, 75 pairs of complementary sightlines view the plasma from above and below where the heating neutral beam passes through the plasma. There are additional top and bottom views of the plasma which do not intersect the beam; the emission on these sightlines is used to remove the background emission from the edge of the plasma where the carbon is not fully ionized. Because the neutral beams in NSTX are relatively tall compared to the plasma cross section, the centrally viewing chords collect light from an extended region inside the plasma, so an Abel inversion of the data from all the sightlines is needed to produce the local poloidal flow velocity. This poloidal flow contributes to the total plasma “shearing rate” and thus plays a role in the suppression of large-scale turbulence. This intrinsic suppression in the ST configuration is believed to be responsible for the good ion confinement in NSTX. The poloidal flow measurements will also be used to refine the interpretation of the MSE data for accurate determination of the q-profile and MHD stability of plasmas. **Plans** - The NSTX PCHERS system is fully implemented and there is no plan for further upgrade.

**Far-infrared Tangential Interferometer and Polarimeter: Status** - Taking advantage of the excellent tangential access, the tangential far-infrared laser system (FIRETIP) simultaneously measures density and polarimetry profiles with microsecond time resolution, a unique capability as shown in Fig. 7.12 (d). [7.3.5] The FIRETIP system has also yielded important information on the movement of ELMs around the torus. **Plans** - The FIRETIP system will be upgraded to detect higher frequency few MHz range to measure the high frequency energetic particle modes such as CAEs and GAEs.

**Motional Stark Effect using Collisionally-Induced Florescence (MSF-CIF): Status** – This diagnostic was successfully introduced to NSTX in 2004 to measure the plasma current profile which is crucial for advanced ST operation. [7.3.6] A schematic of the present 16 channel MSE system is shown in Fig. 7.12 (c). The sensitivity to the field-line pitch angle is excellent even in the relatively low field NSTX plasmas. Indeed, the NSTX MSE-CIF system has achieved a factor of 12 improvement in optical throughput over earlier high field systems through the development of an advanced spectroscopic filter and geometric optimization. In addition, higher quantum efficiency detectors provide a further factor of 3.3 improvement in sensitivity, resulting in an overall factor of ~40 improvement relative to the system in TFTR, for example. The MSE data are now routinely incorporated into the equilibrium analysis for NSTX. The measured q profiles have, for example, revealed deeply reversed-shear profiles in some conditions, confirming earlier inferences based on the ultra-soft x-ray and external magnetic data. Some of the MSE channels have now also been equipped with higher sensitivity detectors to improve their time resolution to detect magnetic fluctuations. **Plans** - The MSE system will be upgraded toward the full 19

channel system originally planned in the near future. The more sensitive detectors for magnetic fluctuation measurements will be also installed on additional channels as needed.

**Motional Stark Emission Diagnostic Using Laser-Induced Fluorescence (MSE-LIF): *Status*** – This diagnostic has been under development by Nova Photonics Inc. under an OFES Advanced Diagnostic Initiative Grant. [7.3.7] The MSE-LIF diagnostic will view the plasma on a midplane radial sightline. The combination its data with that from the existing MSE-CIF system will determine the profiles of both the magnetic field line pitch and the radial electric field, which are both needed for plasma transport research. The MSE-LIF system will also measure the radial profile of the total magnetic field inside the plasma, providing for the first time a direct measurement of the total plasma pressure profile. By subtracting the thermal pressure profiles measured by the diagnostics discussed above, the fast-ion pressure profile can be inferred. These profiles will be compared to the predictions of classical thermalization processes to determine the influence of Alfvén Eigenmodes and other MHD activity on fast-ion confinement. ***Plans*** - The MSE-LIF system is now funded by an OFES Advanced Diagnostic Initiative Grant to be implemented on NSTX in 2009-2010. Following a successful implementation of MSE-LIF (together with its other profile diagnostic), NSTX will be in a unique position to obtain a complete plasma profile information needed for rapid data analyses and comprehensive plasma transport modeling code validation.

**Other Profile Diagnostics** - The NSTX density profiles are also measured by the microwave reflectometers in the edge and core region.[7.3.8, 9] To complement the TCHERS system, an Edge Rotation Diagnostic (ERD) was implemented on NSTX using impurity lines from the plasma edge region where the intrinsic emission is sufficiently strong. ERD can measure both poloidal and toroidal rotation velocities and temperatures.[7.3.10] A strong wave-particle interaction was observed which produces significant (~400 eV) perpendicular ion heating and rotation at the edge during application of high harmonic fast wave (HHFW) power. The radiated power loss profile (and total radiated power) from the plasma are monitored by the 16 channel mid-plane tangential core bolometer system. [7.3.11] The impurity profiles are being monitored by the newly commissioned VUV transmission grating spectrometer (TGS). [7.3.12]

### 7.3.2 MHD Diagnostics

**Magnetics and between-shots EFIT equilibrium reconstruction: *Status*** - Accurate reconstruction of the plasma MHD equilibrium is crucial for investigating and optimizing plasma stability. Utilizing the extensive external magnetic data together with the plasma internal profile information, the plasma reconstruction code “EFIT”, extended and adapted to NSTX plasma conditions, provides detailed information on the basic plasma properties with time resolution

typically down to 1 ms. A hierarchy of successively more sophisticated analysis steps has been developed with EFIT to provide experimenters first with immediate feedback on their experiments and then for detailed analysis of the results afterwards. [7.3.13] These analyses which use more extensive diagnostic data and an increasingly comprehensive model for the plasma have been added as the capabilities and breadth of the NSTX diagnostics have improved over the years, and are routinely applied as time increases after a shot and the input data is analyzed and becomes available. For example, the first level of EFIT analysis uses the measured coil currents and external magnetic measurements; this analysis is available for the entire shot duration 2 – 3 minutes after a shot. The next level includes the diamagnetic measurement and the electron pressure profile measured by the multi-point, multi-pulse Thomson scattering diagnostic to constrain the total pressure profile shape. Thereafter, on a timescale typically of hours, data from measurements of the ion rotation profile measured spectroscopically and the internal magnetic field structure measured by the motional-Stark-effect (MSE) diagnostic are included. The EFIT analysis incorporating MSE data is already yielding important and exciting data on magnetic shear reversal in NSTX discharges. The EFIT code has also been linked to the plasma MHD stability analysis code DCON for rapid between-shots evaluation of plasma MHD stability. **Plans** - The NSTX magnetics and EFIT analysis system will continue to be improved and optimized as the additional magnetic sensors and profile information and the analysis codes becomes available.

#### **Soft X-ray MHD diagnostics:**

**Status** - The poloidal Ultra-soft X-ray (USXR) arrays have been serving as the primary diagnostic tool for the localization and imaging of internal MHD mode activity on NSTX. [7.3.14] A set of selectable filters allows for discrimination of the SXR contributions from the edge, bulk, and core of the plasma. With a mode frequency capability from DC to >100kHz, the arrays have been used to study a broad range of MHD behavior from the plasma edge to the core including  $n = 1$  modes, NTMs, ELMs, and energetic particles modes. An identification of tearing mode activity provided, for example, the first indication that electron transport barriers were generated in reversed shear NSTX plasmas, later confirmed by MSE in 2004. The multi-energy or ‘multicolor’ SXR (ME-SXR) array simultaneously views the same plasma through a set of three SXR filters. The ratios of the filtered emission are used to provide fast  $T_e$  profiles on timescales of  $\geq 0.1$  ms, using normalization from intermittent MPTS measurements. [7.3.15] Continuous  $T_e$  profiles have been obtained during MHD activity such the ELM and the RWM. The fast profiles have also been used to study core electron temperature perturbations, initiated both by ELMs (2007) and by pellet injection (2006). The perturbative studies confirmed rapid electron transport in the central plasma, possibly linked to shear Alfvén MHD activity (2008). In 2004, a fast tangential soft x-ray camera



for 2-D view of core MHD activity with a time resolution down to 2 ms was installed. [7.3.16] The core soft-x-ray (1–5 keV) signal is converted into visible light by a fast phosphor deposited on fiber-optic faceplate. The resulting image is captured by a CCD camera with 64 x 64 pixels with frame rates up to 500 kHz for 300 frames. Such a camera is a powerful tool to investigate the 2-D MHD mode dynamics including the sawtooth crash.

**Plans** - The Soft X-ray diagnostic upgrade plan includes (i) *A high resolution ME-USXR/ME-VUV tangential array* for fast measurements of the edge plasma profiles and (ii) *Two toroidally displaced, high resolution ME-SXR tangential arrays* for non-magnetic identification and measurement of low-frequency MHD modes (RWM, ELMs and disruptions). The edge multi-energy USXR/multi-energy VUV tangential array will cover the plasma from  $0.8 < r/a < 1.1$  and it will be a ‘hybrid’ device, incorporating together with a low-energy USXR filter set, also a VUV Transmission Grating (TG) dispersive and imaging element. The edge hybrid array will pave the path towards the implementation of a 2-D USXR/VUV tomographic array for divertor diagnostic in the 2011-2013 timeframe. Using a multi-energy technique that will include line emission in addition to the continuum, the device will aim to measure with high resolution ( $\geq 1$  cm) and speed ( $\geq 1$  ms) the edge  $T_e$  and  $n_e n_z$  profiles, together with their MHD perturbations. The two toroidally displaced ME-SXR tangential arrays will cover the plasma from  $0 < r/a < 0.9$  and will serve to identify and discriminate between toroidally symmetric profile perturbations, such as from the ELM, and between toroidally asymmetric perturbations, such as from the  $n=1$  RWM. In addition, through comparison with predictions, the two arrays will provide unique information about the internal structure of low frequency MHD phenomena, such as the RWM or the disruption. These diagnostics also project into the research plans beyond 2011. The system of  $n=1$  toroidally displaced ME-SXR arrays will be upgraded in the same period for the identification and diagnostic of low frequency MHD with  $n > 1$ . In addition, this system can be used to test the possibility of active control of the RWM and the ELM using ME-SXR feedback, instead of magnetic feedback. Lastly, following verification of if a connection between shear Alfvén activity and electron transport in NSTX is confirmed, an Extreme Ultraviolet BES (XUV-BES) system for the imaging of fast Alfvén modes such as the GAEs, in the central NSTX plasma ( $r/a \leq 0.4$ ) can be developed. The system will use focusing multilayer mirrors or Zone Plates to image with very high speed, few cm-sized perturbations in the heating or diagnostic beam XUV emission. It should be noted that the NSTX soft x-ray diagnostics plan is mainly carried out by the John Hopkins University collaboration. For more detail, their plan is described in the Appendix.

### 7.3.3 Turbulence Diagnostics

To investigate the sources of anomalous plasma transport, a set of core fluctuation diagnostics has been and continues to be developed in NSTX. The first element is a microwave reflectometer, operational since 2004, to measure longer wavelength fluctuations in the plasma core. Far-infrared interferometry with the FIRETIP diagnostic system is being used to measure the edge density fluctuations in NSTX. A powerful addition to the NSTX turbulence diagnostics is a tangential microwave high-k

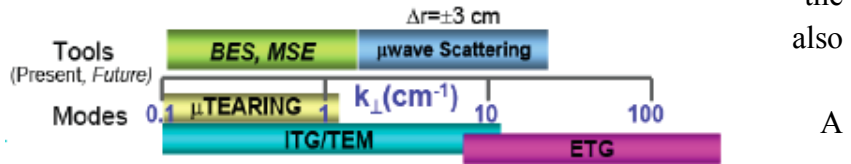


**Fig. 7.14 NSTX turbulence diagnostics and expected wave number range of transport relevant fluctuations.**

scattering system installed in 2005 to measure the electron-transport-relevant short-wavelength modes including, possibly, Electron-Temperature-Gradient Modes (ETGs). This system has already yielded extensive electron transport relevant fluctuation data under a variety of plasma conditions including H-mode, reversed shear, and strongly electron heated HHFW plasmas. A proposed addition is Beam Emission Spectroscopy (BES) to complete the measurement of local turbulent fluctuations across the relevant range of wave-numbers to test turbulence transport models. A summary of the existing and planned fluctuation diagnostics for NSTX appears in Fig. 7.14.

**High-k Microwave Scattering System: Status** - The NSTX “high-k” turbulence diagnostic is a coherent low-angle scattering system that can measure simultaneously turbulent fluctuations of the plasma density at five different wave-vectors perpendicular to the local magnetic field in the range  $1 < k_{\perp} < 20 \text{ cm}^{-1}$ . [7.3.17] Due to the relatively low magnetic field in NSTX, the fluctuations at the upper end of the k-range approach the spatial scale of the electron gyro-motion, i.e.  $k_{\perp} \rho_e \sim 1$ , where  $\rho_e$  is the typical local electron gyro-radius. The system, illustrated in Fig. 7.15, takes advantage of the large curvature of the magnetic field lines in the ST geometry to achieve a radial resolution  $\Delta R \sim 6 \text{ cm}$  of the measurements. By moving the launching and collection mirrors, the scattering volume can be positioned throughout the out-board plasma radius. Wave vectors of these fluctuations are mainly perpendicular to magnetic surfaces, but also have small components along the plasma diamagnetic velocity and the toroidal plasma current that could be used for determining the phase velocity of fluctuations. Measuring plasma fluctuations on this scale can provide insight into the long-standing mystery of anomalous electron thermal transport. Indeed the high-k scattering has been highly productive in providing the data for the electron gyro-scale turbulence in the recent years. **Plans** - Due to its importance to the study of electron transport which is central to this Five Year Plan, upgrades to the high-k scattering system are underway and planned. The system is currently being modified for remote control of its launching and collection mirrors to provide between-shots spatial scanning of the scattering volume. Over the 2008 summer outage, the 1mm microwave source will be upgraded to a solid state diode. Next, the

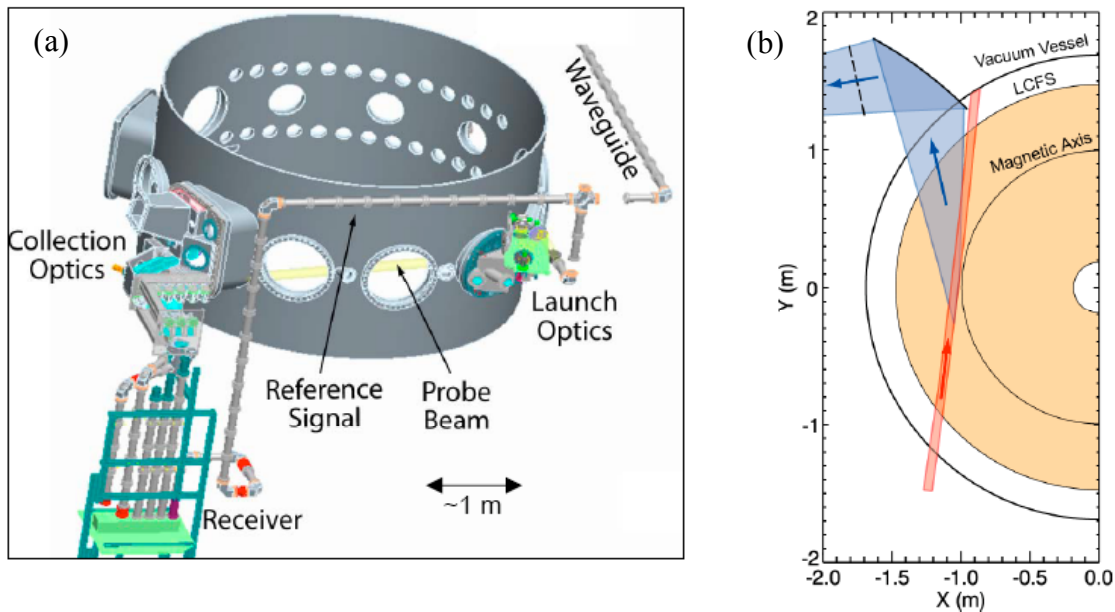


Fig. 7.15 NSTX High-k Scattering system. (a) Layout of the system; (b) Tangential scattering geometry.

system will be upgraded to measure the  $k_0$  component of the turbulence in addition to  $k_r$  information currently obtained.

**Beam Emission Spectroscopy (BES) System: Status** - A BES diagnostic developed by the University of Wisconsin under an OFES Innovative Diagnostic Initiative has been successfully deployed on DIII-D. [7.3.18] The BES system proposed for NSTX will enable direct measurements of longer wavelength density fluctuations in the plasma core providing valuable insights into the suppression of ion turbulence and attainment of the near-neoclassical ion confinement observed on NSTX. The BES diagnostic together with the existing microwave tangential scattering diagnostic (which measures medium to short wavelength turbulence) will provide the most comprehensive turbulence diagnostic set of any ST in the world. The BES diagnostic should also enhance the determination of the spatial structure of fast-ion-driven instabilities such as the TAE and BAAE observed on NSTX. **Plans** - A 32-channel BES system for NSTX, illustrated in Fig. 7.16, is being designed with guidance from the University of Wisconsin group. In 2009, a prototype two-view BES system will be installed on NSTX with the first light expected during the 2009 plasma operation. The system is expected to achieve its full 32 channel capability by 2010.

### 7.3.4 Energetic Particle Diagnostics

Fast-ion confinement in STs is an important issue, due to the large ratio of their gyro-radius to

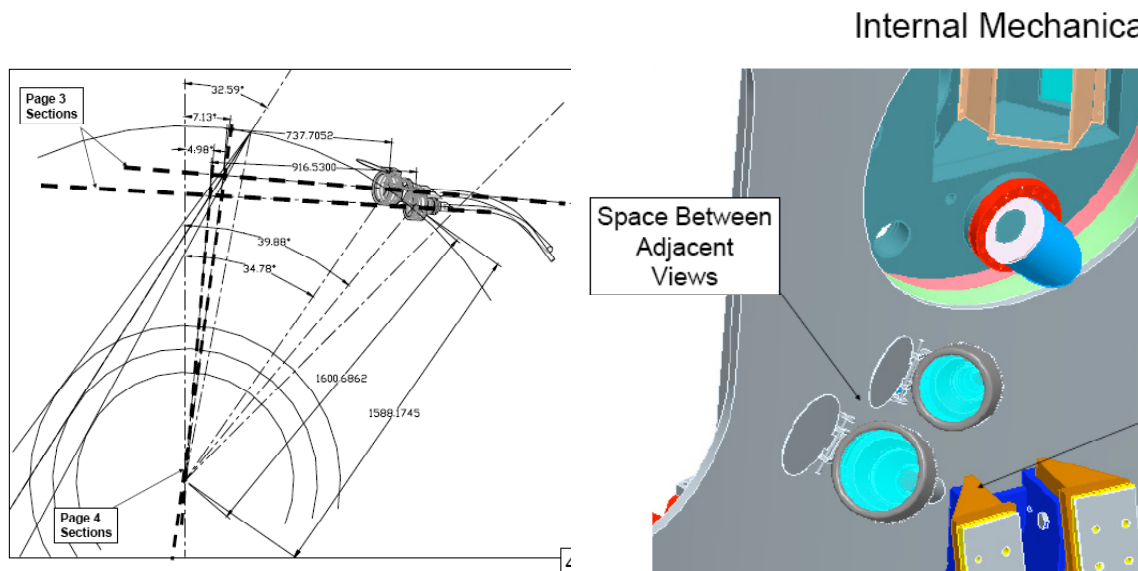


Fig. 7.16 BES diagnostic being developed for NSTX (a) viewing geometry; (b) Schematic of internal optical system providing two viewing cones

plasma minor radius. NSTX is also uniquely positioned to investigate ITER-relevant energetic-particle instabilities and their consequences. In NSTX high- $\beta$  plasmas produced by neutral beam injection, there is a substantial population of energetic ions whose velocity exceeds the local Alfvén velocity, similar to the energetic alpha-particle population expected in ignited plasmas in ITER. Such fast ions can excite many types of instabilities which have been and will continue to be studied with a comprehensive set of plasma diagnostics, including several specialized diagnostics, described below, plus MSE for the  $j(r)$  profile, high-frequency magnetic pick-up coils, correlation reflectometers, the tangential FIR interferometer array, the ultra-fast x-ray camera, and soft x-ray tomography.

**Energetic Ion Diagnostics: Status** - Fast-ion diagnostics on NSTX include a set of neutron detectors, a scanning energetic neutral-particle analyzer (NPA), a multi-sightline solid state detector NPA (SSNPA), and a scintillator-based fast lost-ion probe (sFLIP). [7.3.19] Since the DD fusion neutron rate in NSTX is dominated by beam-target reactions, the neutron measurements provide a global measure of beam ion confinement. The detectors include two absolutely-calibrated fission chambers and four scintillator detectors capable of resolving fluctuations in the neutron rate up to 100 kHz. The neutron response produced by short neutral beam pulses has shown classically-expected beam ion confinement in quiescent plasmas. The NPA can measure fast neutrals with energies up to 120 keV with an energy resolution of  $\sim 1$  keV, and can be scanned horizontally and vertically on a shot-to-shot basis. [7.3.20] The NPA measures the fast ion population at the point of charge exchange and its ability to probe the fast ion population in the core of the plasma is greatly enhanced by the NBI providing the source of neutrals. The SSNPA has four fixed sightlines in the mid-plane with  $\sim 10$  keV energy resolution and is designed to measure radial redistribution of neutral beam ions arising from MHD activity. [7.3.23] The sFLIP measures the energy and pitch angle of the escaping fast ions entering the detector, allowing determination of the orbits that are lost. Initial sFLIP measurements also appear consistent with classically-expected confinement in quiescent plasmas. However, MHD activity has been seen by the NPA to deplete the confined beam ion population and result in loss to the vessel wall of orbits with high pitch angle. The newest addition to the complement of fast ion diagnostics is the fast ion D-alpha (FIDA) line emission camera, illustrated in Fig. 7.17, which was successfully implemented in 2008 to measure light emitted by fast ions in the plasma which undergo charge exchange with injected beam neutrals. [7.3.21] **Plans** - A neutron collimator system is being designed to quantify the fast ion population in the plasma core region to complement the existing FIDA and NPA diagnostics.

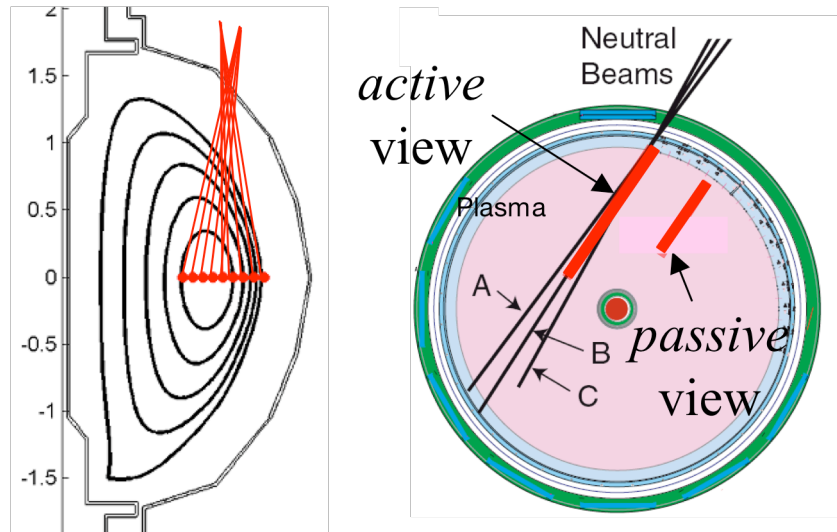


Fig. 7.17 FIDA diagnostic on NSTX (a) Poloidal cross sectional view; (b) Top view showing active and passive views.

**Energetic-Particle-Driven Mode Diagnostics: *Status*** - For studying the MHD activity driven by energetic particles, high frequency magnetic sensors with up to 5 MHz response are operational on NSTX. [7.3.22] The high-frequency MHD instabilities typically observed include Toroidal Alfvén Eigenmodes (TAEs) and Compressional Alfvén Eigenmodes (CAEs). These observed modes were reproduced by the kinetic high frequency MHD codes HYM, Nova-K and M3D-k. At present, the microwave reflectometer system and the poloidal Ultra-soft X-ray (USXR) arrays provide localized internal measurements of the mode amplitudes, with the FIRETIP and high-k systems providing complementary data extending further into the plasma core. ***Plans*** - The planned 32 channel BES system in 2009-2010 time frame will be a powerful addition to the energetic particle mode diagnostic.

### 7.3.5 Wave Diagnostics

**HHFW-related diagnostics: *Status*** - Several diagnostics are used to understand the physics of HHFW coupling. An edge reflectometer has been used to measure the electrostatic waves generated by the edge parametric decay instabilities. Three RF pickup probes are placed around the torus to measure the RF wave fields in the plasma edge region. The core reflectometer system has been used to measure the core HHFW density fluctuations. ***Plans*** - Additional diagnostic to measure directly the HHFW fluctuations in the core will be implemented to assess the wave propagation to the core. The existing high-k tangential scattering system will be upgraded to

cover the 30 MHz range of the HHFW and FIRETIP will be also upgraded to measure the core HHFW density fluctuations.

**EBW Radiometer system: Status** - To assess the EBW conversion (coupling) efficiency, two microwave radiometers were installed and commissioned on NSTX in 2006. [7.3.23] These radiometers measure thermal EBW emission in the plasma mode converted from EBW through X-mode and finally to O-mode radiation in the bands 8 – 18 GHz and 18 – 40 GHz. Each radiometer views the plasma from the midplane obliquely at toroidal and poloidal angles of 20 – 40° approximately and measures radiation in two orthogonal polarizations using a quad-ridged antenna. **Plans** - The EBW radiometer will be utilized on NSTX to monitor the EBW emission under a variety of plasma condition. The system will be refurbished and improved as needed.

### 7.3.6 Boundary Physics Diagnostics

**Status** - The NSTX boundary physics diagnostic set has been developed to support and strengthen the on-going research in scrape-off layer transport and turbulence, experiments with lithium coatings, and ELM and pedestal physics. A good access to plasma through diagnostic ports and good port coverage of important plasma regions on NSTX enabled a number of unique and important measurements. A schematic summarizing NSTX boundary physics diagnostics is shown in Fig. 7.18. Scrape-off layer parameters in the inner and outer midplane locations are measured by the fast reciprocating probe [7.3.24], fast reflectometers [7.3.25], VUV and UV-visible spectrometers [7.3.26] and cameras [7.3.27-30] that are spectrally filtered for deuterium and impurity line emission. Unique turbulence measurements in the midplane and divertor are provided by several fast cameras in combination with the gas puff imaging system [7.3.31,32]. A comprehensive set of divertor diagnostics includes infrared [7.3.33] and visible cameras for heat flux, recycling and impurity emission measurements, tile Langmuir probes, a 4-channel divertor bolometer system [7.3.11], a UV-visible spectrometer, and neutral pressure gauges [7.3.34]. ELM and pedestal measurements are addressed by the Multi-point Thomson Scattering system, the CHERS system, the

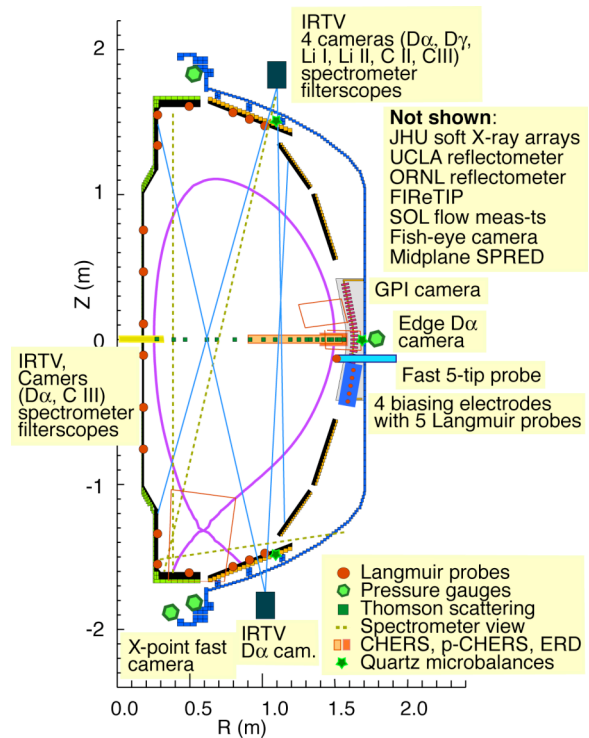
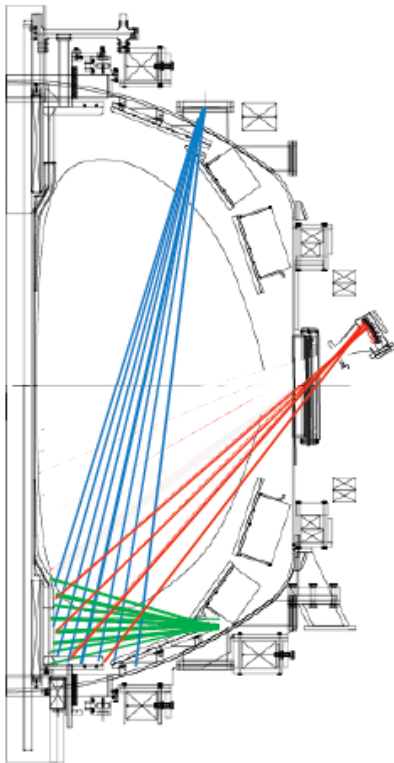


Figure 7.18 NSTX Boundary Physics diagnostics

the edge rotation diagnostic, and fast cameras. Measurements of plasma-wall interaction are achieved with unique surface deposition monitors [7.3.35], dust detectors [7.3.36] and dust-tracking system [7.3.37].

**Plans** - To support the Boundary Physics program and the planned facility upgrades in 2008-2013, a number of new diagnostics and diagnostic upgrades are planned. To understand the liquid lithium divertor performance and its effects on plasma, measurements of particle and heat fluxes in the challenging lithium environment will be developed. To this end, additional thermocouples



**Fig. 7.19 Three-view divertor bolometer system**

and Langmuir probes embedded in “smart” diagnostic tiles, two-color IR measurements, Ly- $\alpha$  diode arrays, an imaging UV-visible divertor spectrometer, and a surface analysis probe will be implemented in 2008-2010. Additional MPTS channels will be commissioned to improve  $T_e$ ,  $n_e$  profile resolution in the pedestal and scrape-off layer regions in 2010-2011. Further improvements are planned to the ongoing developments of a unique scrape-off layer flow measurement system based on filtered camera imaging. To improve our understanding of the SOL and divertor power balance, a staged upgrade of the divertor bolometer system is planned in 2008-2009 to include a full coverage of the divertor. Together with the existing mid-plane bolometer system, the new 20-channel system should enable a tomographic reconstruction of 2D radiated power patterns in the divertor. A fast IR camera will be also implemented in 2008-2009 to measure the large heat fluxes due to transient events and ELMs. To measure ELM parameter evolution on the fast scale, new high-resolution soft X-ray arrays are planned in 2012-2013. Also in 2012 or sooner, if resources become available, a divertor Thomson scattering system and an X-point reciprocating probe are planned.

and Langmuir probes embedded in “smart” diagnostic tiles, two-color IR measurements, Ly- $\alpha$  diode arrays, an imaging UV-visible divertor spectrometer, and a surface analysis probe will be implemented in 2008-2010. Additional MPTS channels will be commissioned to improve  $T_e$ ,  $n_e$  profile resolution in the pedestal and scrape-off layer regions in 2010-2011. Further improvements are planned to the ongoing developments of a unique scrape-off layer flow measurement system based on filtered camera imaging. To improve our understanding of the SOL and divertor power balance, a staged upgrade of the divertor bolometer system is planned in 2008-2009 to include a full coverage of the divertor. Together with the existing mid-plane bolometer system, the new 20-channel system should enable a tomographic reconstruction of 2D radiated power patterns in the divertor. A fast IR camera will be also implemented in 2008-2009 to measure the large heat fluxes due to transient events and ELMs. To measure ELM parameter evolution on the fast scale, new high-resolution soft X-ray arrays are planned in 2012-2013. Also in 2012 or sooner, if resources become available, a divertor Thomson scattering system and an X-point reciprocating probe are planned.



## 7.4 NSTX Facility Utilization

**Facility Operations Summary** - The NSTX facility utilization for the preceding five year period (FY 2004- 2008) is summarized in Table 7.4. The NSTX facility has met or exceeded the planned run weeks for all five years. The facility operational efficiency has increased significantly over those years. One measure of operational efficiency is the number of plasma shots per run week (defined as 40 hours of operation). The total number of plasma shots is also directly related to the productivity of experimental research. As shown in the Table 7.4, the number of plasma shots per week has increased steadily by about 33% over the five year period from 117 plasma shots per week in FY 2004 to 155 plasma shots per week FY 2008. In fact, in 2008, the facility has produced a record number of plasma shots of 2571 in just 16.6 run week compared to 2460 plasma shots in 21 run weeks in 2004. This increased efficiency is attributable to many factors including the maturing of the facility, the increased experience of the operations team, the improvements in the real time plasma control system, and general improvements of plasma conditions resulting from the development and use of tools such as the lithium evaporator.

	<b>FY 2004</b>	<b>FY 2005</b>	<b>FY 2006</b>	<b>FY 2007</b>	<b>FY 2008</b>
Run weeks planned / achieved	20/21	17/18	11/12.7	12/12.6	15/16.6
Hours of operation planned / achieved	800/844	680/720	440/508	480/504	600/664
Total Plasma Shots	2460	2221	1617	1879	2571
Plasma Shots per Run Week	117	123	128	149	155

***Table 7.4 FY 2004-2008 Facility Operations Summary***

**Facility Users Summary** - Table 7.5 lists the research users from PPPL/Princeton University and non-PPPL institutions which include national as well as international collaborating researchers. Over 200 researchers have participated in the NSTX research in FY 2007. The number has been relatively steady over the years. However, it should be noted that participation by younger researchers (post-doc, graduate students) is rising, more than doubling from 18 in 2004 to 42 in 2007.

	<i>PPPL</i>	<i>non-PPPL</i>
<i>Researchers</i>	<i>57</i>	<i>145**</i>
<i>Post Doc.</i>	<i>1</i>	<i>10</i>
<i>Grad. Students</i>	<i>9</i>	<i>12</i>
<i>Undergrad. Students</i>	<i>1</i>	<i>10</i>

\*\* There are over 41 overseas collaborating researchers from countries including Canada, China, Czech Republic, France, Germany, Israel, Italy, Japan, Korea, Russia, and UK, during FY 2006-2007.

**Table 7.5 Participating Research Personnel Summary**

**Facility Operations Plan** - The NSTX facility utilization plan for the next Five Year Period (FY 2009- 2013) is summarized in Table 7.6. The NSTX facility 20 weeks per year will enable the NSTX research team to make a satisfactory progress on the proposed NSTX Five Year Plan while implementing the necessary upgrade including the new Center Stack to be installed prior to the FY 2012 run. The reduced run weeks in FY 2013 is to allow the second NBI to be installed on NSTX.

**Planned Facility Base Plasma Operations**

	<b>FY 2009</b>	<b>FY 2010</b>	<b>FY 2011</b>	<b>FY 2012</b>	<b>FY 2013</b>
Run weeks planned	15	15	15	15	15
Hours of operation planned	600	600	600	600	600

**Planned Facility Incremental Plasma Operations**

	<b>FY 2009</b>	<b>FY 2010</b>	<b>FY 2011</b>	<b>FY 2012</b>	<b>FY 2013</b>
Run weeks planned	20	20	20	15	15
Hours of operation planned	800	800	800	600	600

**Table 7.6 FY 2009-2013 Facility Utilization Plan**

## References:

- 7.1.1 M. Ono, et al., Nucl. Fusion **40**, 557 (2000).
- 7.1.2 S. Kaye, et al., Fusion Technology, **36**, 16 (1999).
- 7.1.3 C. Neumeyer et al., the IEEE SOFE Conference, 99CH3050 (1999).
- 7.2.1 C. Neumeyer et al., in Proceedings of the 23rd Symposium on Fusion Technology (SOFT), Venice, Italy, 20-24 September 2004.
- 7.2.2 J. Chrzanowski, et al., the IEEE SOFE Conference, 99CH3050 (1999).
- 7.2.3 D. A. Gates, et al., "Status of the control system on the National Spherical Torus Experiment (NSTX)", Fus. Eng. And Design, **81** (2006) 1911.
- 7.2.4 J. R. Ferron, M. L. Walker, L. L. Lao, et al., Nucl. Fusion **38** 1055 (1998).
- 7.2.5 T. Stevenson, et al., "A Neutral Beam Injector Upgrade for NSTX ", Princeton Plasma Physics Laboratory Report number 3651, (2002).
- 7.2.6 J. Hosea, et al., Phys. Plasmas **15**, 056104 (2008).
- 7.2.7 G. Taylor et al., Phys. Plasmas **12**, 052511 (2005).
- 7.2.8 S. A. Sabbagh, R. E. Bell, J. E. Menard, et al., Phys. Rev. Lett. **97**, 045004 (2006).
- 7.2.9 A. C. Sontag, S. A. Sabbagh, W. Zhu, et al., Phys. Plasmas **12**, 056112 (2005).
- 7.2.10 H.W. Kugel, *et al.*, Physics of Plasmas **15**, 056118 (2008).
- 7.2.11 H. W. Kugel, et al., "Physics Design Requirements for the National Spherical Torus Experiment Liquid Lithium Divertor," Proceedings of the "25th Symposium on Fusion Technology", 15-19 September 2008, Rostock, Germany.
- 7.2.12 H.W.Kugel, et al., "NSTX High Field Side Gas Fueling System", Proceedings of the 20th IEEE/NPSS Symposium on Fusion Engineering, Oct. 2003, San Diego CA.
- 7.2.13 V. A. Soukhanovskii, et al., "High pressure supersonic gas jet fueling on NSTX", Proceedings of the 22nd IEEE/NPSS Symposium on Fusion Engineering (SOFE07), 17-21 June 2007, Albuquerque, New Mexico.
- 7.2.14 R. Raman et al., "Experimental demonstration of tokamak fueling by CT injection," Nuclear Fusion **37**, 967 (1997).
- 7.2.15 T.R. Jarboe, "Formation and steady state sustainment of a tokamak by Coaxial Helicity Injection," Fusion Tech. **15**, 7, (1989).
- 7.2.16 R. Raman, et al., "Efficient generation of closed magnetic flux surfaces in a large spherical tokamak using coaxial helicity injection," Phys Rev. Lett., **97**, 175002 (2006).
- 7.3.1 B.P. LeBlanc et al, Rev. Sci. Instrum. **74**, 1659 (2003).
- 7.3.2 B. LeBlanc, "Thomson scattering density calibration by Rayleigh and Rotational Raman scattering on NSTX," accepted for publication in the HTPD Conference issue of Review of Scientific Instruments, 2008.
- 7.3.3 R.E. Bell, et al., "Carbon ion plume emission produced by charge exchange with neutral beams on National Spherical Torus Experiment", Rev. Sci. Instr. **77** 10E902 (2006).
- 7.3.4 R.E. Bell "Tokamak fusion test reactor poloidal rotation diagnostic", Rev. Sci. Instr. Vol. 70 No.1, 821 (1999).
- 7.3.5 K. C. Lee, C. W. Domier, M. Johnson, and N. C. Luhmann, Jr. H. Park, "FIR laser Tangential Interferometry/Polarimetry on NSTX", IEEE transaction on plasma science Vol. 32 No.4, 1721 (2004).

- 7.3.6 F. Levinton et al., "The Motional Stark Effect (MSE) Diagnostic on the National Spherical Torus Experiment (NSTX)," accepted for publication in the HTPD Conference issue of Review of Scientific Instruments.
- 7.3.7 E. L. Foley and F. M. Levinton, "Progress on the motional Stark effect with laser-induced fluorescence diagnostic (invited), Rev. Sci. Instr. 77 10E311 (2006)
- 7.3.8 J. B. Wilgen, et al, "Reflectometer sensing of rf waves in front of the high harmonic fast wave antenna on NSTX" *Rev. Sci. Instrum.* **77**, 10E933 (2006).
- 7.3.9 S. Kubota et al., *Rev. Sci. Instrum.* **74**, 1477 (2003).
- 7.3.10 T. M. Biewer, et al., *Rev. Sci. Instrum.* , **75**, 650-654 (2004).
- 7.3.11 S. F. Paul, R. Maingi, V. Soukhanovskii, et al., "Accounting of the power balance for neutral-beam heated H-mode plasmas in NSTX", *J. Nucl. Mater.*, 337-39, 251-255, (2005)
- 7.3.12 D. Stutman, G. Caravelli, M. Finkenthal, G. Wright, et al., *J. Appl. Phys.* 103, 93307 (2007).
- 7.3.13 S. Sabbagh, et al., *Nuclear Fusion* **41**, 1601 (2001).
- 7.3.14 D. Stutman, et al., *Rev. Sci. Instrum.* **70**, 572 (1999).
- 7.3.15 L. Delgado, D. Stutman, K. Tritz, M. Finkenthal, et al., *J. Appl. Phys.* 102, 073304 (2007)
- 7.3.16 C. Bush et al., "Fast soft x-ray camera images of MHD phenomena in NSTX," accepted for publication in the HTPD Conference issue of Review of Scientific Instruments.
- 7.3.17 D.R. Smith et al. "Status of High-k Scattering System on NSTX", *Bull. of Am. Phys. Soc.*, **49**, 301 (2004).
- 7.3.18 G. R. McKee, et al., "High sensitivity beam emission spectroscopy for core plasma imaging," *Rev. Sci. Instrum.*, vol. 77, page 10F104-1 (2006).
- 7.3.19 D. Darrow, "Pitch angle resolved measurements of neutral beam ion loss from NSTX," *Bull. of Am. Phys. Soc.*, **49**, 301 (2004).
- 7.3.20 S. S. Medley, et al., *Rev. Sci. Instrum.* 75, 3625 (2004).
- 7.3.21 M. Podesta et al., "The NSTX fast-ion D-alpha diagnostic, accepted for publication in the HTPD Conference issue of Review of Scientific Instruments, 2008.
- 7.3.22 E. D. Fredrickson et al., "Beta suppression of Alfvén Cascade Modes in the National Spherical Torus Experiment" *Phys. of Plasmas* 14 (2007) 102510.
- 7.3.23 S. Diem et al., "Electron Bernstein Wave Emission and Mode Conversion Physics on NSTX (invited)," accepted for publication in the HTPD Conference issue of Review of Scientific Instruments.
- 7.3.24 J.A. Boedo, et al., "Particle and Energy Transport in the SOL of DIII-D and NSTX", *Proceedings of the 21st IAEA Conference, IAEA-CN-149*, pp EX/P4-2, Chengdu, China, 2006.
- 7.3.25 Lee, KC; Domier, CW; Johnson, M; Luhmann, NC; Park, H; Soukhanovskii, VA. "Survey of diagnostic systems for the study of gyrocenter shifts on National Spherical Torus Experiment", *Rev. Sci. Instrum.* 77, (2006).
- 7.3.26 Soukhanovskii, VA; Johnson, DW; Kaita, R; Roquemore, AL. "Electron density measurements in the National Spherical Torus Experiment detached divertor region using Stark broadening of deuterium infrared Paschen emission lines", *Rev. Sci. Instrum.*, 77, 10F127, (2006).
- 7.3.27 A. L. Roquemore, T. Biewer, et al., "NSTX tangential divertor camera", *Rev. Sci. Instrum.*, 75, 4190-4192, (2004).
- 7.3.28 V. A. Soukhanovskii, A. L. Roquemore, C. H. Skinner, et al., *Rev. Sci. Instrum.* 74, 2094 (2003).
- 7.3.29 N. Nishino et al., "NSTX boundary plasma measurement by fast camera and interpretations", 21st IEEE/NPSS Symposium on Fusion Engineering. SOFE 05 (IEEE Cat. No.05CH37764), 2007, p 6S.J. Zweben et al, *Phys. Plasmas* **13**, 056114 (2006).

- 7.3.30 R. J. Maqueda, et al., "Structure of MARFES and ELMs in NSTX" , Journal of Nuclear Materials, v 363-365, 15 June 2007, p 1000-5.
- 7.3.31 R.J. Maqueda, G. A. Wurden, G.A.; S. Zweben, et al., "Edge turbulence measurements in NSTX by gas puff imaging," Review of Scientific Instruments, v 72, n 1, pt.1-2, Jan. 2001, p 931-4.
- 7.3.32 S. J. Zweben, et al., "High-speed imaging of edge turbulence in NSTX", Nuclear Fusion, v 44, n 1, Jan. 2004, p 134-53.
- 7.3.33 R. Maingi, et al., Journal of Nuclear Materials 313-316, 1005 (2003).
- 7.3.34 R. Raman, H. W. Kugel, et al., "Fast neutral pressure gauges in NSTX", Rev. Sci. Instrum., 75, 4347-4349, (2004).
- 7.3.35 C. H. Skinner, et al., "Time resolved deposition measurements in NSTX", Journal of Nuclear Materials, v 337-339, n 1-3 SPEC. ISS., Mar 1, 2005, p 129-133.
- 7.3.36 C. H. Skinner, R. Hensley, A. L. Roquemore, "Large aperture electrostatic dust detector", Journal of Nuclear Materials, v 376, n 1, May 15, 2008, p 29-32
- 7.3.37 A. L. Roquemore, et al., "Imaging of high-speed dust particle trajectories on NSTX", Review of Scientific Instruments, v 77, n 10, 2006, p 10E526.

## **Appendix - NSTX Collaboration Research Plans**

A.1 Introduction.....	A.1
A.2 NSTX National Collaboration Research Capabilities and Plans.....	A.2
A-1. Columbia University (S.A. Sabbagh).....	A.4
A-2. General Atomics (R.J. La Haye).....	A.12
A-3. Johns Hopkins University (M. Finkenthal) .....	A.14
A-4. Lawrence Livermore National Laboratory (V. Soukhanovskii) .....	A.19
A-5. Lodestar Research Corporation (J.R. Myra) .....	A.24
A-6. Los Alamos National Laboratory (X. Tang) .....	A.27
A-7. Los Alamos National Laboratory (G. Wurden, J. Wang) .....	A.30
A-8. Massachusetts Institute of Technology (P.T. Bonoli) .....	A.32
A-9. Nova Photonics, Inc. (F.M. Levinton) .....	A.36
A-10. Oak Ridge National Laboratory (D.L. Hillis) .....	A.39
A-11. Purdue University (J.P. Allain) .....	A.46
A-12. Purdue University (A. Hassanein) .....	A.51
A-13. Sandia National Laboratory (R.E. Nygren) .....	A.55
A-14. University of California at Davis (N.C. Luhmann, Jr.) .....	A.58
A-15. University of California at Irvine (W. Heidbrink) .....	A.62
A-16. University of California at Los Angeles (T. Peebles) .....	A.65
A-17. University of California at San Diego (J. Boedo) .....	A.73
A-18. University of California at San Diego (A. Pigarov) .....	A.77
A-19. University of Colorado at Boulder (T. Munsat) .....	A.80
A-20. University of Illinois at Urbana-Champaign (D.N. Ruzic) .....	A.82
A-21. University of Tulsa (D.P. Brennan) .....	A.86
A-22. University of Washington at Seattle (T.R. Jarboe, R. Raman) .....	A.92

*This page intentionally left blank*



## Appendix - NSTX Collaboration Research Plans

*The NSTX National Research Program is carried out by a broadly based research team which has greatly advanced the understanding and performance of spherical torus plasmas since the start of NSTX experimental operations in FY2000. NSTX research collaborations have made substantial contributions to the long term goals of the OFES program: Configuration Optimization and developing a Predictive Capability for Burning Plasmas. This collaboration will continue to grow in breadth and effectiveness.*

### **A.1 - Introduction**

Research on NSTX is carried out by a National Team of research groups from 19 universities, national laboratories (including PPPL), and private industry, many of which participated in the team building effort since FY1998, obtaining direct collaboration funding from DOE. Approximately 40% of the NSTX scientific staff in full time equivalent (FTE) and 59% of the personnel are from these collaborating institutions. The contributions of all collaborating institutions, including foreign cooperation not funded by DOE, have been extensive, as can be seen in the overview and plan sections of this 5-year plan. The work plans of the collaborating research by the institutions other than PPPL are briefly described in this appendix to provide supporting information to the overall NSTX 5-year plan. These plans include those already funded by DOE for durations up to 3 years, and new ideas that extend the work to FY 2013. The extended collaborative research plans will require timely discussions within the NSTX research team, before formal proposals are submitted to DOE for peer review and approval. It is expected that, during FY 2009-2013 period the NSTX research efforts by the collaborating institutions will increase at a proportional rate equal to or faster than the NSTX research efforts by PPPL.

Among the 189 active research users of NSTX including graduate students and post doctoral researchers, 87 are from these collaborating institutions, 59 are from PPPL, and 43 are from fusion institutions of other countries. PPPL engineers and technicians carried out the operation, maintenance, upgrade of the NSTX facility, and the interface, installation, and maintenance of diagnostic systems including those provided by the collaborating researchers, at an effort level of 80 FTEs. The entire NSTX research and facility operations team have worked together effectively to enable rapid progress toward the proof-of-principle mission of NSTX, since the beginning of experimental research in FY2000.

## **A.2 - NSTX National Collaboration Research Capabilities and Plans**

The success of the NSTX national research team is ensured by an effective integration of these broad and exceptional capabilities and expertise into a research force aimed toward achieving the NSTX research goals. NSTX collaborators play an essential role in leading the NSTX scientific program as indicated by Table 1.8.1 in Chapter 1 which indicates that nearly half (6 of 14) of the topical science group leadership, deputy leadership, and run coordination support is provided by non-PPPL researchers. Working together, the NSTX national research team is effectively meeting the challenge of producing an expanded scientific knowledge base for practical fusion energy based on the ST concept.

The capabilities and plans of the NSTX national collaboration research are organized by the list of collaborating institutions, principal investigators, and research topics are provided below:

### **A-1. Columbia University (S.A. Sabbagh)**

*Study of MHD Stability and Active Mode Control in NSTX*

### **A-2. General Atomics (R.J. La Haye)**

*Plasma Control, H-mode pedestal stability, and ELM control with RMP*

### **A-3. Johns Hopkins University (M. Finkenthal)**

*USXR Measurements of Core and Edge Transport and MHD*

### **A-4. Lawrence Livermore National Laboratory (V. Soukhanovskii)**

*Integrated Measurements and Modeling of Edge Transport and Turbulence*

### **A-5. Lodestar Research Corporation (J.R. Myra)**

*Edge and Scrape-off-Layer Physics for NSTX*

### **A-6. Los Alamos National Laboratory (X. Tang)**

*Predictive Modeling of Helicity Injection Startup*

### **A-7. Los Alamos National Laboratory (G. Wurden, J. Wang)**

*Hypervelocity Dust Injection/ Dust Studies*

### **A-8. Massachusetts Institute of Technology (P.T. Bonoli)**

*Full-wave Studies of High Harmonic Fast Wave heating*

**A-9. Nova Photonics, Inc. (F.M. Levinton)**

*Radially resolved internal measurements of  $\mathbf{B}$  and  $E_r$  for reconstruction of  $q$  and  $p$*

**A-10. Oak Ridge National Laboratory (D.L. Hillis)**

*Boundary Physics, Heating, and Current Drive Program for NSTX*

**A-11. Purdue University (J.P. Allain)**

*Elemental & Chemical Characterization of D-Recycling on Lithiated Graphitic Surfaces*

**A-12. Purdue University (A. Hassanein)**

*Impact of Disruptions and ELMs on Liquid Lithium Surfaces in NSTX*

**A-13. Sandia National Laboratory (R.E. Nygren)**

*Liquid Lithium Divertor Experiments and Preparation for NHTX*

**A-14. University of California at Davis (N.C. Luhmann, Jr.)**

*Millimeter-Wave Fluctuation Diagnostics for NSTX and KSTAR*

**A-15. University of California at Irvine (W. Heidbrink)**

*Energetic Particle Physics*

**A-16. University of California at Los Angeles (T. Peebles)**

*The Study of Alfvén Mode Physics and Turbulent Transport in NSTX*

**A-17. University of California at San Diego (J. Boedo)**

*Heat and Particle Transport (radial and parallel) and divertor physics*

**A-18. University of California at San Diego (A. Pigarov)**

*Simulations of Synergy of Li-Coating, Non-diffusive Anomalous Transport and Drifts*

**A-19. University of Colorado at Boulder (T. Munsat)**

*Evaluation of Edge Turbulence & Convective Transport through Velocity Field Analysis*

**A-20. University of Illinois at Urbana-Champaign (D.N. Ruzic)**

*LLD and SOL Interactions on NSTX*

**A-21. University of Tulsa (D.P. Brennan)**

*Energetic Particle and Flow Shear Effects in Resistive MHD Instabilities*

**A-22. University of Washington at Seattle (T.R. Jarboe, R. Raman)**

*Solenoid-free Startup using CHI, Deep Fuelling and Momentum Injection using CT Fuelling*

## A-1. Columbia University Collaboration

Research Topic: **Study of MHD Stability and Active Mode Control in NSTX**

Principal, Co-Principal Investigators: Steven A. Sabbagh (PI/PD), G. A. Navratil (Co-I.)

Participating Researchers: S. A. Sabbagh, J.M. Bialek, J.W. Berkery, O. Katsuro-Hopkins (NSTX analysis in relation to KSTAR research).

Funded under DOE Grant: DE-FG02-99ER54524

### Introduction

The spherical torus (ST) magnetic fusion concept uses strong geometric alteration of the magnetic field to produce stable plasmas at relatively low toroidal field, and hence high toroidal beta,  $\beta_t$ . Practical understanding of this magnetic confinement device has been significantly increased by the study of an expanded ST database of plasmas with high  $\beta_t \equiv 2\mu_0\langle p \rangle / B_0^2$  up to 39%, high  $\beta_N \equiv 10^8 \langle \beta_t \rangle a B_0 / I_p$  up to 7.2, high energy confinement ( $\tau_E / \tau_{E \text{ ITER-89P}} > 2.5$ ), and  $\beta_N$  to internal inductance ratio,  $\beta_N / l_i$  exceeding 11 in NSTX. With high toroidal and normalized beta, wall-stabilized operation established, the Columbia University group proposes to continue, as part of the NSTX Research Team, research on macroscopic stability aimed directly at the long-term goal of this topical area: demonstration of sustained plasma operation in the wall-stabilized high  $\beta$  state, with high reliability, at or near the highest  $\beta_N$  produced in the device. This research also aims to address the two long-term OFES goals of Configuration Optimization (development of the spherical torus toward a spherical torus component test facility, ST-CTF) and Predictive Capability for Burning Plasmas (development of stability physics understanding applicable to tokamaks in general including ITER, leveraged by the unique low aspect ratio,  $A$ , and high beta operational regime of NSTX). One of the critical questions that must be addressed in the development of the ST concept for fusion energy and for toroidal magnetic fusion devices in general: what is the level of  $\beta_N$  that can be reliably sustained at high bootstrap current fraction and high  $\beta_t$ . Addressing this question through a careful research plan has brought, and will

continue to bring to fruition goals of passive and active stabilization research envisioned since the creation of first plasma in NSTX, as well as critical physics understanding applicable to advanced tokamak operation in general.

### Current research contributions to NSTX

Columbia group research has contributed to NSTX since the conceptual design of the device. A long-term experimental research plan over the past several years spanned the creation of the original equilibrium in the device and their reconstructions [1] to the significant milestone of the first active stabilization of the resistive wall mode (RWM) at low aspect ratio, and at reduced plasma rotation applicable to ITER [2]. The characteristics of the unstable RWM at low A were documented in NSTX by the Columbia group. Early work determined that the RWM eigenfunction is ballooning in nature with the largest perturbation on the outboard side and that the mode effectively couples to the passive stabilizing plates. This investigation included a physics design of an active stabilization control system for the device [3] (which was constructed and implemented by PPPL engineering). The presence of large error fields in early device operation resulted in unstable RWM growth soon after  $\beta_N$  exceeded  $\beta_N^{\text{no-wall}}$ , indicating reduced passive stabilization in this condition [4]. Subsequent error field reduction resulted in a much larger stabilized operating space with  $\beta_N/\beta_N^{\text{no-wall}}$  up to 1.5 at the highest  $\beta_N$  values reached in the device [5]. Here,  $\beta_N^{\text{no-wall}} = \beta_{N(n=1)}^{\text{no-wall}}$  is the  $\beta_N$  value above which ideal  $n = 1$  MHD kink-ballooning modes are computed without the stabilizing effect of nearby conducting structure. Here,  $n$  is the toroidal mode number. Maintaining high toroidal rotation across the entire profile leads to passive RWM stability [6]. Unstable RWMs with toroidal mode number up to three were observed in NSTX for the first time in a tokamak experiment [5]. Resonant field amplification (RFA) with  $n = 1$  was also observed [5], and increases with increasing  $\beta_N$  as observed in DIII-D. These experiments also led to an important new branch of research addressed by the Columbia group on NSTX – the physics of plasma viscosity induced by non-axisymmetric fields. A multi-year experiment led to the observation of neoclassical toroidal viscosity [7] (NTV) in NSTX due

primarily to non-resonant fields [8]. An essential component of all research mentioned above has been the ready availability of accurate, between-shots experimental kinetic equilibrium reconstructions with the NSTX EFIT code [1,9], which now can include toroidal rotation, flux-isotherm constraint (using Te data), and internal magnetic constraints (utilizing motional Stark effect data)) that allows between-shots MHD stability analysis (using the DCON code [10]) as required. The Columbia group has provided this capability for NSTX for several years (since sufficient diagnostic data became available).

### **Summary of proposed research plan for 2009-13**

Progress accomplished to date in the study of global MHD mode stability and active RWM control in NSTX sets the stage for the Columbia group to propose a 3 year program of study, leading research in several key areas to support the maintenance of high beta plasmas created in the device. The research applies to NSTX, the future development path of the ST, and will provide key physics understanding for advanced tokamak operation and future burning plasma devices.

The elements of our plan displayed in a timeline are:

#### **Timeline**

##### **2009-2010:**

- \* Continue experimentation and analysis of plasmas above the present NSTX ideal no-wall beta limit with the goal of firmly understanding the physics of the instabilities setting the beta limit under passive and active stabilization and maintaining the high beta state. (applies to all years).
- \* Continue experimentation to determine superior feedback control settings and sensor combinations for RWM active stabilization (continues into second year).
- \* Compare VALEN model of RWM active stabilization in NSTX with experimental RWM active stabilization results, including real geometry and positions of sensors

- and the influence of plasma rotation. Use results to guide control system improvements (applies to all years).
- \* Continue the study of RWM mode rigidity and unstable  $n$  spectrum during  $n = 1$  RWM active stabilization (applies to all years).
  - \* Begin investigation of multi-mode model as a suitable hypothesis to explain RFA and RWM characteristics.
  - \* Develop multi-mode VALEN code and begin initial tests.
  - \* Begin assessment of advanced RWM control algorithms in conjunction with RWM control algorithm design studies for KSTAR.
  - \* Begin analysis to support design of non-magnetic RWM sensors for NSTX in collaboration with JHU (continues into second year).
  - \* Continue to investigate the role of ion collisionality, plasma rotation magnitude and profile in RWM active and passive stabilization; if approved, perform a second joint experiment with DIII-D to examine aspect ratio effects on RWM stabilization and differences based on different plasma rotation profile shapes and magnitude.
  - \* Conduct MARS-F code stability analysis in collaboration with Y. Liu (including toroidal rotation, dissipation, kinetic effects) to evaluate the role of Alfvén and sound wave continuum damping physics in support of the RWM passive stabilization physics study (applies to all years).
  - \* Conduct analysis of trapped particle precession drift stabilization on NSTX plasmas at low plasma rotation in collaboration with B. Hu and R. Betti in support of the RWM passive stabilization physics study (applies to all years).
  - \* Examine the role of increased applied non-axisymmetric field (resonant and non-resonant) on RWM stabilization.
  - \* Continue to test the theory of neoclassical toroidal viscosity, especially the dependence of ion collisionality (ITER relevant); if approved, perform a joint experiment on DIII-D proposed for 2008 in this regard.

- \* Begin experiments to determine the role of island-induced NTV during observed resonant magnetic braking or tearing mode activity.
- \* Continue to distribute equilibrium reconstructions to the NSTX Research Team in a common public database format (applies to all years).
- \* Continue to provide supporting work and analysis for the NSTX real-time EFIT plasma control system, implemented by Dr. David Gates and Dr. John Ferron. (applies to all years).
- \* Initiate and lead a collaboration of NSTX physicists, engineers and design technicians on a practical and effective design of the new non-axisymmetric control coil (NCC) proposed for NSTX (applies to all years).

**2010-2011:**

- \* Use present RWM coil to dynamically suppress resonant field amplification, addressing the present amplitude modulation of the RFA observed.
- \* Make comparison between experimental observations of RWM amplitude modulation and multi-mode VALEN calculations using experimental equilibria.
- \* Continue investigation of multi-mode model as a suitable hypothesis to explain poloidal deformation of RWM during stabilization by comparing to multi-mode VALEN calculations.
- \* Determine the effect of varying latency in sensor feedback on RWM active stabilization (ITER application) as control system software upgrades allow.
- \* Begin steps to implement advanced RWM control algorithms in conjunction with RWM control design studies for KSTAR.
- \* Reach 2009 NSTX RWM milestone by drawing conclusions regarding physics models of RWM stabilization that support experimental results.
- \* Investigate a combined model of torque on the plasma due to both resonant and non-resonant NTV by comparing theory to experiment.



- \* Support NSTX plasma rotation control design effort by performing NTV calculations as needed.
- \* Compute stability of resistive MHD modes using resistive DCON (when available) on NSTX equilibrium reconstructions. Compare theory to experiment to develop the capability for future predictive use (extends into year 3).
- \* Incorporate conclusions reached in Year 2 into the continued NCC design
- \* Examine NCC design implications of enabling the increase of plasma rotation by non-resonant rotating fields.

**2011-2012:**

- \* Support  $n = 1$  RWM active stabilization system modifications and its use as a general tool for NSTX experiments.
- \* Determine needs for  $n > 1$  RFA suppression and active stabilization and apply to the NCC design.
- \* Determine needs for suppression of poloidal deformation of RWM and apply to NCC design.
- \* Continue comparison of multi-mode RWM behavior between experiments and VALEN theory model to establish the latter as a design tool for future devices.
- \* Provide physics support for implementation of non-magnetic RWM sensors by JHU group and design for future use in RWM feedback loop.
- \* Implement advanced RWM control algorithms to establish the first experimental tests (supports KSTAR and ITER).
- \* Implement results from plasma viscosity model due to non-axisymmetric fields into NCC design for plasma rotation control.

**2012-2013:**

- \* Upgrade existing between-shots EFIT reconstruction to support operation with new center stack and associated machine alterations.
- \* Perform experiments and associated theoretical analysis to examine RWM control and to gain physics understanding of passive stabilization at significantly lower (order of magnitude) ion collisionality with new center stack upgrade than in present NSTX plasmas.
- \* Determine how well the high  $\beta_N$  state can be maintained against RWM instability through the combination of LLD operation, plasma rotation control, and  $n = 1$  RWM control.
- \* Examine RWM measurement with non-magnetic sensors and compare to standard measurement with magnetic sensors. Determine the role of  $n > 1$  RWM activity during  $n = 1$  stabilization and expand study to higher power and increased  $q_0$  when additional NBI power capability becomes available.
- \* Conduct RWM stabilization and NTV rotation damping experiments using the NCC (incremental). Compare stabilization performance with design expectations and viscous torque profile with theory.
- \* Determine a reliable physics model to confidently predict RWM stabilization as a function of rotation and ion collisionality. Test this model against equilibria created with the second neutral beam when available (further variation of  $V_\phi$  and  $q$  profiles).
- \* Perform experiments and associated theoretical analysis to determine the scaling of neoclassical toroidal viscosity at significantly lower (order of magnitude) ion collisionality. This is especially important as the scaling of NTV between the present NSTX operating space and that predicted for operation with the new center stack upgrade is not well understood.

**Contributions to the NSTX 2009-13 Five Year Plan:**

S.A. Sabbagh is the present leader of the NSTX Macroscopic Stability Topical Science Group and is responsible for overseeing the NSTX Five Year Plan. The plan was defined in a process carried out over CY2007-08 in coordination with the NSTX Research Team. The research defined above contributes heavily to the plan.

**References**

- [1] S.A. Sabbagh, S. M. Kaye, J. Menard, *et al.*, Nuclear Fusion **41** (2001) 1601.
- [2] S.A. Sabbagh, R.E. Bell, J.E. Menard, *et al.*, Phys. Rev. Lett. **97** (2006) 045004.
- [3] S.A. Sabbagh, R.E. Bell, M.G. Bell, *et al.*, Phys. Plasmas **9** (2002) 2085.
- [4] S.A. Sabbagh, J.M. Bialek, R.E. Bell, *et al.*, Nucl. Fusion **44** (2004) 560.
- [5] S.A. Sabbagh, A.C. Sontag, J.M. Bialek, *et al.*, Nucl. Fusion **46** (2006) 635.
- [6] A.C. Sontag, S.A. Sabbagh, W. Zhu, *et al.*, Phys. Plasmas **12** (2005) 056112.
- [7] K.C. Shaing, S.P. Hirschman, and J.D. Callen, Phys. Fluids **29** (1986) 521.
- [8] W. Zhu, S.A. Sabbagh, R.E. Bell, *et al.*, Phys. Rev. Lett. **96** (2006) 225002.
- [9] L.L. Lao, *et al.*, Nucl. Fusion **25** (1985) 1611.
- [10] A.H. Glasser and M.C. Chance, Bull Am. Phys. Soc. **42** (1997) 1848.

## **A-2. General Atomics**

Research Topic: **5 year plans for NSTX**

Principal, Co-Principal Investigators: Robert J La Haye, Todd E Evans, Thomas H Osborne and David A Humphreys

Participating Researchers: John R Ferron, Lang L Lao, Anthony W Leonard, James A Leuer, Benjamin G Penaflor, Philip B Snyder, Alan D Turnbull, Michael L Walker, and Anders Welander

Funded under DOE Grant: GRANT00351261 (March 1, 2008 – March 1 2011)

### **Introduction**

General Atomics is participating in the NSTX research program in three topical areas: (1) plasma control, (2) H-mode edge pedestal character and stability, and (3) ELM stabilization using resonant magnetic perturbations (RMP). General Atomics has played a strong role in development of the NSTX plasma control system that is providing capability for production of the quality discharges required for the experimental research program. We are continuing to support the existing plasma control software that has already been provided. In addition, we are implementing the advanced model-based shape control algorithms which have been under development during the previous grant period. These algorithms will be particularly useful for the precise control of the strike point location required by the liquid lithium divertor research program. We are continuing participation in experiments and analysis to improve understanding of the H-mode edge pedestal and edge localized modes in NSTX. As part of work in the previous grant period, a large set of General Atomics developed data analysis tools specially designed for this type of research was adapted for use at NSTX and applied to preliminary analysis of NSTX H-mode pedestal data. These tools will continue to be exploited for analysis of the extensive set of NSTX pedestal data that is becoming available. In addition, the ELITE stability code will be used for analysis of medium toroidal mode number instabilities in the edge region, and other codes such as NIMROD will be tested for pedestal simulations. The use of magnetic perturbations primarily located in the H-mode edge pedestal region has shown great promise for the stabilization of ELMs. The General Atomics team has extensive experience in this type of research, including the design of the optimized coil set to produce the necessary magnetic fields. We are collaborating with the NSTX team in the modeling and design optimization of a new resonant magnetic perturbation (RMP) coil set to be installed in NSTX. We are also continuing

participation in experiments exploiting the existing set of non-axisymmetric coils to study the effect of resonant magnetic perturbations on ELMs in NSTX.

### **Current research contributions to NSTX**

We provide support on control, H-mode edge pedestal physics, and design of a new resonant magnetic perturbation coil for edge control; details are given in the grant proposal [1]. Work on the physics of neoclassical tearing modes and the effects of error fields on their stability is ongoing and a continuation of the previous 3 year grant (March 1, 2005 – March 1, 2008).

### **Summary of proposed research plan for 2009-13**

Details through March 2011 are given in (1); this will be coordinated with the NSTX staff on an ongoing basis. It is anticipated that the conceptual design of a new RMP coil to be done under the existing grant will lead to an engineering design, fabrication, and installation with participation by GA under a grant renewal for the years after March 1, 2011. Collaborations not in the grant are anticipated on the physics of NTMs, error fields, resistive wall modes, and MHD stability in general on a year-to-year basis through proposals at annual research opportunity forums.

### **References**

- 1 GACP 20000318 National Spherical Torus Experiment Research Participation, October 11, 2007, General Atomics

## A-3. Johns Hopkins University

Research Topic: **Ultrasoft X-ray diagnostics and measurements of transport and MHD activity in the core and edge NSTX plasma**

Principal, Co-Principal Investigators: M. Finkenthal, D. Stutman

Participating Researchers: K. Tritz, L. Delgado-Aparicio, G. Caravelli (graduate student)

Funded under DOE Grant: DE-FG02-99ER5452

### Introduction

The role of the ST in the US fusion program is to provide the basis for a volumetric neutron source for a Nuclear Testing Facility or, possibly, hybrid fusion-fission energy applications. Since the ST neutron source will be in good part a ‘beam-plasma’ device, it is essential that it maintains a high electron temperature, so that the fast beam ion population is not quickly degraded in energy. Understanding the highly anomalous electron transport observed in NSTX is thus of fundamental importance for the ST future. Neoclassical effects such as collisional impurity penetration through the edge H-mode barrier can also be important in a ST volumetric neutron source. In addition, non-magnetic identification of MHD instabilities during operation in an extreme radiation environment will be another critical issue. The current and proposed JHU research at NSTX addresses all these topics.

### Current research contributions to NSTX

Our current research at NSTX has two main directions:

- (i) The application of soft X-ray diagnostics and techniques for measurements of particle and electron thermal transport and of MHD activity
- (ii) Identifying the physical mechanisms behind the highly anomalous electron transport in the region of low  $T_e$  gradient inside  $r/a \leq 0.4$ .

In the area of particle and electron thermal transport our contributions are based on a recently developed *multi-energy SXR* (ME-SXR) technique and diagnostic. The technique consists in simultaneously imaging the plasma in multiple energy bands and using the SXR profiles to constrain the

evolution of the  $T_e$  and  $n_e n_z$  profiles. This enables to interpolate with high temporal and spatial resolution between the Thomson scattering  $T_e$  profiles, as well as to measure with accuracy the penetration of injected impurities. The diagnostic we built to implement this technique on NSTX is a tangential three-energy ‘optical’ array that measures the core plasma inside  $r/a < 0.8$  [1].

Our recent contributions can be summarized as follows:

- identification and study of electron transport barriers in beam L-mode plasmas [2]
- perturbative electron transport studies that established unusually rapid electron transport in the central plasma of high beam power H-modes [3]
- impurity transport measurements indicating that particle transport is around neoclassical levels in the core of high beam power NSTX H-modes [4]
- study of the correlation between large ELMs and the perturbed electron thermal transport, showing that the electron transport accompanying the ELM is consistent with critical gradient ETG activity in the peripheral plasma [5]
- proposal for a possible correlation between rapid electron transport in the central plasma of high beam power H-modes and the shear Alfvén (GAE) activity [6]

In addition, several diagnostics of interest for the future ST and Burning Plasma research have or are being demonstrated at NSTX under the Advanced Diagnostic DoE Program:

- USXR BES Telescope for measurement of low-k core fluctuations [7]
- Imaging XUV spectrometer using free-standing Transmission Gratings (TG) [8]
- ‘Hybrid’ ME-SXR/ME-XUV array combining multi-energy SXR with multi-energy XUV imaging for line and continuum emission measurements

The JHU contributions to MHD diagnostic and measurement are based on a system of poloidal USXR arrays that image the internal MHD activity. A set of selectable filters allows for discrimination of the SXR emission from the edge, mid-radius, and central plasma, respectively. With a mode frequency capability from DC to  $> 100$  kHz the arrays have been used to study a broad range of MHD phenomena:

- imaging of low-frequency RWM activity showed differences in internal mode structure between stabilized and un-stabilized modes [9]
- identification of double tearing mode activity provided first indication that electron transport barriers in NSTX are associated with reversed magnetic shear [2]
- imaging of tearing mode position and growth was applied to NTM beta threshold studies (ongoing DIII-D collaboration)

- SXR imaging of internal MHD contributed to the study of kink-mode dynamics and other internal MHD of high beta plasmas [10]
- measurement of ELM filaments in the USXR data led to the discovery of the small, Type V ELMs in high performance NSTX discharges [11]
- imaging of energetic particle modes has been used to localize and identify the eigenmode of bursting, ‘fishbone-like’ MHD activity and contributed to the identification and localization of the global BAAE, recently discovered at NSTX [12]

### **Summary of proposed research plan for 2009-13**

For the period 2009-2013 we propose to *continue and expand* the above lines of research, as well as to begin exploring *a new direction*, the control of fusion plasmas using ME-SXR feedback.

In the diagnostic area, will continue to maintain and operate the poloidal USXR system. In addition, we propose to develop and implement several new diagnostic systems. In the 2009-2011 timeframe, we plan implementing:

- (i) A *high spatial resolution ME-USXR/ME-XUV tangential array* for fast measurements of the edge plasma profiles
- (ii) *Two toroidally displaced, high resolution ME-SXR tangential arrays* for non-magnetic identification and measurement of low-frequency core MHD (RWM, ELMs and disruptions)

The edge ME-USXR/ME-XUV tangential array will be a ‘hybrid’ device, incorporating together with multiple low-energy USXR filters also an XUV TG dispersive and imaging element. The array will cover the plasma at  $0.8 \leq r/a \leq 1.1$  and will measure with high spatial ( $\geq 1$  cm) and temporal resolution ( $\geq 1$  ms) the edge line and continuum emission profiles, together with their MHD perturbations. Using normalization to the temporally and radially sparser Thomson profiles, we aim to obtain higher resolution  $T_e$ ,  $n_e$ , and  $n_z$  profiles. These in turn will be instrumental for many of the edge studies planned at NSTX, such as pedestal stability, ELM physics and mitigation, as well as studies of Li effects on the plasma.

The two toroidally displaced ME-SXR tangential arrays will cover the plasma from  $0 \leq r/a \leq 0.9$  and will serve to identify and discriminate between toroidally symmetric profile changes, such as those associated with the ELMs, and toroidally asymmetric perturbations, such as those arising from the RWM. The aim is to provide higher sensitivity in low frequency MHD detection than possible with magnetic sensors. In addition, the two arrays will provide unique information about the internal structure of low



frequency MHD phenomena, such as the  $n=1$  RWM or the modes leading to disruption. The edge ME-USXR array and one of the ME-SXR arrays will be integrated in a single tangential enclosure in order to save port space.

The above diagnostics also project into our NSTX research in the 2012-2013 timeframe. The hybrid edge array will pave the way towards the implementation of a 2-D ME-XUV tomographic diagnostics for the NSTX divertor. The system of  $n=1$  toroidally displaced ME-SXR arrays can be upgraded in the same period for the identification and diagnostic of low frequency MHD with  $n>1$ . In addition, this system will be used to assess the possibility of active RWM and ELM control using non-magnetic ME-SXR sensing [13].

Lastly, pending verification of our hypothesis on a connection between shear Alfvén activity and electron transport in NSTX, we will consider developing in the 2012-2013 timeframe a XUV BES system for the imaging of fast Alfvén modes, such as the GAEs, in the central NSTX plasma ( $r/a \leq 0.4$ ).

As in our previous work, the diagnostic implementation will be accompanied by physics studies. The main topics we plan to investigate are:

- the possible connection between electron transport and Alfvén MHD activity
- SXR signatures of stochastic/ $\mu$ -tearing electron transport in the core and edge plasma during heating/cooling transients
- study of the role of neoclassical impurity transport in the formation of the NSTX pedestal
- effects of active RWM stabilization and of ELM mitigation on the internal MHD activity

### Timeline

**2009-2010:** Construction of edge ME-USXR/ME-XUV hybrid array

**2010-2011:** Implementation and operation of edge hybrid array and construction of  $n=1$  toroidally displaced ME-SXR arrays

**2011-2012:** Implementation and operation of toroidally displaced arrays

**2012-2013:** XUV-BES GAE diagnostic

**2013:** 2-D ME-XUV divertor diagnostic, ME-SXR  $n>1$  RWM, ELM detection

### References

- [1] L. Delgado, D. Stutman, K. Tritz, M. Finkenthal, *et al.*, J. Appl. Phys. **102**, 073304 (2007)
- [2] D. Stutman, M. Finkenthal, K. Tritz, M. H. Redi, *et al.*, Phys. Plasmas **13**, 092511 (2006)

- [3] D. Stutman, K. Tritz, L. Delgado, M. Finkenthal et al., Proc. 33rd EPS, Rome, 2006, P5.120
- [4] L. Delgado, D. Stutman, K. Tritz, M. Finkenthal, *et al.*, PPCF **49**, 1245 (2007)
- [5] K. Tritz, S. Kaye, R. Maingi, S. Sabbagh, *et al.*, Phys. Plasmas **15**, 056119 (2008)
- [6] D. Stutman, L. Delgado, K. Tritz, M. Finkenthal  
[http://nstx.pppl.gov/DragNDrop/Topical\\_Science\\_Groups/Meetings/transport\\_turbulence/2008/5-22-08/JHU\\_Joint\\_Meeting\\_v1.pdf](http://nstx.pppl.gov/DragNDrop/Topical_Science_Groups/Meetings/transport_turbulence/2008/5-22-08/JHU_Joint_Meeting_v1.pdf)
- [7] D. Stutman, K. Tritz, L. Delgado, M. Finkenthal, *et al.*, Rev. Sci. Instrum. **77**, 10F330 (2006)
- [8] D. Stutman, G. Caravelli, M. Finkenthal, G. Wright, *et al.*, J. Appl. Phys. **103**, 93307 (2007)
- [9] S. Sabbagh, R. Bell, J. Menard, D. Gates, *et al.*, Phys. Rev. Lett. **97**, 045004 (2006)
- [10] J. Menard, R. Bell, E. Fredrickson, D. Gates, *et al.*, Nucl. Fus. **45** (7), 539 (2005)
- [11] R. Maingi, K. Tritz, E. D. Fredrickson, J. E. Menard, *et al.*, Nucl. Fus. **45** (4), 264 (2005)
- [12] N. Gorelenkov, H. Berk, N. Crocker, E. Fredrickson, *et al.*, PPCF **49**, B371 (2007)
- [13] D. Stutman and M. Finkenthal, <http://www.psfc.mit.edu/~g/spp/WhitePapers/Stutman-sensors-control.pdf>

## **A-4. Lawrence Livermore National Laboratory**

Research Topic: **The Study of Edge Transport and Turbulence - An Integrated Measurements and Modeling approach**

Principal Investigator: Vsevolod Soukhanovskii

Participating Researchers: new postdoctoral staff

Funded under DOE Contract DE-AC52-07NA27344

### **Introduction**

The goal of the present LLNL research effort on NSTX is to develop an experiment-based understanding and a predictive computational capability of the edge (pedestal and scrape-off layer) parallel and perpendicular heat and particle transport and plasma-wall interactions in the spherical torus (ST) magnetic geometry, to enable extrapolations to future high power density ST-based devices.

### **Current research contributions to NSTX**

The present LLNL collaboration on NSTX includes both the experiment and modeling, and takes advantage of the PI located on site at PPPL. The PI is involved in all aspects of the NSTX Research Program. The PI served as a Boundary Physics Experimental Task Group Deputy Leader in 2006, a Leader in 2007, and is now serving as a Boundary Physics Topical Science Group Leader. The LLNL Collaboration has been responsible for maintaining and operating five edge spectrally filtered CCD arrays, one spectrometer, and about 30 edge spectrally filtered detectors (“filterscopes”), as well as the supersonic gas injector. The LLNL research program in the Boundary Physics area focused on the divertor physics studies and the development of novel fueling techniques, while providing experimental and modeling contributions to many NSTX research efforts. In the divertor area, we studied divertor transport regimes and access to detachment in a range of H-mode plasma configurations, with the emphasis on ST SOL geometry effects. We demonstrated experimentally for the first time in a high power density ST the possibility of significant divertor peak heat flux reduction in the high flux expansion radiative divertor with simultaneous good core H-mode confinement. In the fueling area, we have designed and built in collaboration with PPPL researchers the novel high-pressure supersonic gas injector (SGI). The SGI demonstrated high fueling efficiency, and was used in H-mode fueling optimization

experiments, complemented by particle balance and ionization source studies. In the modeling area, LLNL supported radiative divertor experiments and LLD modeling efforts with the UEDGE code, and edge turbulence studies with the BOUT code.

### **Summary of proposed research plan for 2009-13**

The proposed continuation of LLNL research collaboration is well aligned with the NSTX priorities and takes a full advantage of the LLNL Boundary Physics experimental and modeling expertise. We propose an expansion in the scope of collaboration toward a “full service” (experiment, diagnostics, and modeling) effort. A modest increase in funding (1+ FTE) would allow LLNL to implement unique ST divertor measurements and strengthen the corresponding edge transport and turbulence modeling.

The proposed effort will focus on

- 1) Further studies of divertor heat flux mitigation using novel high flux expansion divertors and radiative solutions at reduced plasma collisionality
- 2) Experimental characterization of NSTX divertor heat and particle transport and particle sources with active recycling control provided by the lithium coatings and liquid lithium divertor (LLD)
- 3) Further optimization of the supersonic gas jet fueling for density control in long pulse discharges with the complementary pumping by lithium coatings
- 4) Further development of the two-dimensional multi-fluid UEDGE and three-dimensional turbulence BOUT computational models in support of LLD and SOL width research

To support these experimental activities and modeling, we propose a staged diagnostic development effort: new Lyman- $\alpha$  diode arrays, a new multichannel divertor spectrometer, and a divertor Thomson scattering (DTS) system. In particular, the proposed DTS system would be implemented by a new staff member, and could possibly take advantage of the legacy Thomson scattering hardware from the completed Sustained Spheromak Physics Experiment at LLNL, providing significant cost and effort savings for NSTX. In combination with the planned midplane SOL Thomson scattering channels, the DTS system would provide unique two-dimensional SOL  $T_e$  and  $n_e$  measurements that would allow critical tests of SOL heat and particle transport models.

## **Timeline**

### **2009-2010:**

- Experiments aimed at initial characterization of SOL regimes in the presence of LLD: characterization of LLD pumping capability, fueling and impurity sources, and access to radiative and partially detached divertor regimes
- H-mode fueling optimization using SGI for fueling and LLD for pumping
- Laboratory studies of advanced supersonic nozzles and cryogenic SGI for enhanced deuterium jet penetration
- In support of the above, an implementation of Lyman- $\alpha$  AXUV diode arrays for recycling measurements in the presence of highly-reflective liquid lithium surfaces
- In support of the above, installation of the new imaging divertor spectrometer to study 1) divertor deuterium, lithium and carbon sources 2) role of molecular sources in the divertor 3) private flux region transport
- Modeling of the above experiments with UEDGE multi-fluid transport code
- Systematic analysis of NSTX turbulence data with BOUT code in support of SOL width studies
- Design and installation of the new divertor Thomson scattering system

### **2010-2012:**

- Experiments aimed at optimization and control of partially detached divertor regime with impurity and deuterium injections at high power and reduced density (with new center stack and active pumping), and integration with long-pulse H-mode scenarios
- Development and characterization of novel divertor flux expansion configurations with existing or new magnetic coils
- SOL transport studies with DTS: general divertor heat transport studies, SOL kinetic effects, ELM divertor impact studies
- Modeling of the above experiments with UEDGE multi-fluid transport code

### **2012-2013:**

- Continuation of SOL transport studies with DTS: general divertor heat transport studies, SOL kinetic effects, ELM divertor impact studies
- Contribute to the design of the upgraded divertor and diagnostics for its characterization

**Contributions to the NSTX 2009-13 Five Year Plan:**

PI wrote two sections (“ST divertor physics and heat flux control” and “Fueling”) for the Boundary Physics Chapter. This work also contributes to chapters on “Plasma start-up and sustainment” and “Advanced Scenarios and Control”.

**References**

Refereed Journal Articles:

V. A. Soukhanovskii, R. E. Bell, C. Bush, R. Kaita, et al. "A study of the role of particle sources in secular density rises in NBI-heated H-mode plasma in NSTX", *J. Nucl. Mater.*, (2008).

V. A. Soukhanovskii. "Near Infrared Spectroscopy for Burning Plasma Diagnostic Applications", *Rev. Sci. Instrum.*, (2008).

Soukhanovskii, VA; Maingi, R; Bush, CE, et al. "Divertor heat flux reduction and detachment experiments in NSTX", *J. Nucl. Mater.*, 363, 432-436, (2007).

Soukhanovskii, VA; Johnson, DW; Kaita, R, et al. "Electron density measurements in the National Spherical Torus Experiment detached divertor region using Stark broadening of deuterium infrared Paschen emission lines", *Rev. Sci. Instrum.*, 77, (2006).

Soukhanovskii, VA; Maingi, R; Roquemore, AL, et al. "Divertor regimes in NSTX", *J. Nucl. Mater.*, 337-39, 475-479, (2005).

Soukhanovskii, VA; Kugel, HW; Kaita, R, et al. "Supersonic gas injector for fueling and diagnostic applications on the National Spherical Torus Experiment", *Rev. Sci. Instrum.*, 75, 4320-4323, (2004).

Published Conference Proceedings:

V. A. Soukhanovskii, M. G. Bell, R. E. Bell, D. A. Gates, et al. "H-mode fueling optimization with the supersonic deuterium jet in NSTX", 35th EPS Conference on Plasma Phys. Warsaw, 2 - 6 July 2007 ECA Vol.31F, P-2.023 (2007), (Hersonissos, Greece, 06/09/2008-06/13/2007), *Europhys. Conf. Abstr.*, NA, pp 2.109.

V. A. Soukhanovskii, R. Maingi, D. A. Gates, J. E. Menard, R. Raman, R. E. Bell, C. E. Bush, R. Kaita, H. W. Kugel, B. P. LeBlanc, S. F. Paul, A. L. Roquemore, and the NSTX Team. "Divertor heat flux amelioration in highly-shaped plasmas in NSTX", 34th EPS Conference on Plasma Phys. Warsaw, 2 - 6 July 2007 ECA Vol.31F, P-2.023 (2007), (Warsaw, Poland, 07/02/2007-07/06/2007), Europhys. Conf. Abstr., 31F, pp 2.023.

Soukhanovskii, VA; Bell, MG; Blanchard, WR, et al. "High pressure supersonic gas jet fueling on NSTX", 22nd IEEE/NPSS Symposium on Fusion Engineering, (Albuquerque, NM, 06/17/2007-06/21/2007), pp 183-186.

V.A. Soukhanovskii, R. Maingi, R. Raman, R. E. Bell, et al. "Divertor Heat Flux Reduction and Detachment in NSTX", 21st IAEA Fusion Energy Conference, (Chengdu, China, 10/ /2006), Fusion Energy 2006, Proceedings of the 21st IAEA Conference, IAEA-CN-149, pp EX/P4-28.

V. A. Soukhanovskii, H. W. Kugel, R. Kaita, et al. "Supersonic gas injector for plasma fueling", SOFE05, 21st IEEE/NPSS Symposium on Fusion Engineering, (Knoxville, TN, 09/ /2005), Proc. 21st IEEE/NPSS Symposium on Fusion Engineering (SOFE05).

V. A. Soukhanovskii, R. Maingi, C. J. Lasnier, A. L. Roquemore, R. E. Bell, C. Bush, R. Kaita, H. W. Kugel, B. P. LeBlanc, J. Menard, D. Mueller, S. F. Paul, R. Raman, S. Sabbagh, and NSTX Research Team. "Particle and power exhaust in NBI-heated plasmas in NSTX", 32nd EPS Plasma Physics Conference, (Tarragona, Spain, 06/ /2005), Europhys. Conf. Abstr., 29C, pp P4.016.

V.A. Soukhanovskii, H.W. Kugel, R. Kaita, R. Majeski, A.L. Roquemore, D.P. Stotler. "Supersonic Gas Jet for Fueling Experiments on NSTX", 31st EPS Conference on Plasma Physics, (London, United Kingdom, 06/ /2004), Europhys. Conf. Abstr., 28G, pp P-2.190.

#### Invited Talks:

"Divertor Heat Flux Reduction and Detachment in NSTX", APS DPP, Orlando, Florida, 11/2007.

## **A-5. Lodestar Research Corporation**

Research Topic: **Edge and Scrape-off-Layer Physics for NSTX**

Principal, Co-Principal Investigators: James R. Myra, Daniel A. D'Ippolito and David A. Russell

Participating Researchers: Stewart Zweben (PPPL), Daren Stotler (PPPL), Ricky Maqueda (Nova Photonics), Vlad Soukhanovskii (LLNL), Jose Boedo (UCSD), Tobin Munsat (CU Boulder)

Funded under DOE Grant: DE-FG02-02ER54678

### **Introduction**

An improved understanding of edge and scrape-off-layer (SOL) physics is essential to the goals of NSTX, future spherical tokamaks (STs), and to ITER. The work carried out under this project will address critical physics associated with boundary plasma turbulence: the origin and propagation of blob-filaments, the role of convective plasma transport in defining the SOL plasma, scaling of SOL characteristics with experimental control parameters, and the relation of experimental control parameters to the dimensionless control parameters in the latest theoretical models of edge turbulence and blob-filament propagation.

### **Current research contributions to NSTX**

In ongoing work, we are exploring the dynamics of SOL blob-filaments and comparing observation, primarily from gas-puff-imaging (GPI) data, with theory. We carried out GPI analysis and interpretation, testing theoretical predictions for the magnitude and scaling of blob velocity. The work [1, 2] showed that the data obeyed bounds associated with theoretical predicted regimes, but did not obey a deterministic scaling. Statistical variations within a shot could mask expected differences between shots. We conducted a birth zone analysis, and showed that blobs are born in a zone associated with maximum linear instability. Blobs convect plasma with density and temperature characteristic of the birth zone. We introduced a dimensionless parameter space [2] in which to analyze blob velocities and showed that NSTX data lay within the expected region. The same parameter space was applied to understand inter-machine blob characterization (task ITPA-DSOL-15) [3].



### **Summary of proposed research plan for 2009-13**

The proposed research for the next five years falls into three broad categories

1. Baseline topics addressing key SOL issues for NSTX, STs and ITER
2. Fundamental physics studies of blob-filaments
3. Novel topics

Our main project consists of several closely related studies under Category 1, which build on work discussed in the preceding. Here we seek to understand the origin of blobs (i.e. the turbulent creation zone, and the resulting level of blob activity) in terms of experimental and machine parameters. This important, but so far elusive, goal for the fusion community is key to eventually obtaining a predictive capability for heat and particle transport in the SOL. Lodestar will apply our 2D SOLT (Scrape-off-Layer Turbulence) simulation code in comparison with existing and/or new GPI experimental datasets to make progress in this area. The first step, already proceeding well, is to obtain quantitative agreement on SOL turbulence metrics (describing e.g. fluctuation levels, blob statistics, blob velocity distributions and dynamics) between the SOLT code and GPI data for a best case. This comparison invokes a simulated GPI diagnostic in SOLT that takes into account atomic radiation physics using models described in Refs. [2, 4]. In the next step, we will investigate the effect of parameter (code and machine) variations.

Research topics under Category 2 address the blob interaction with the magnetic geometry of the torus, and its influence on blob propagation and dynamical evolution, and on the heat and particle flux footprints on the divertor. We have proposed that increased blob speeds (and hence broader SOL widths) could be achieved if the more collisional (“disconnected”) blob transport regime could be accessed. Experiments to test this in partially detached plasmas are being carried out. Our analytical and numerical models will assist in the interpretation of these ongoing and proposed experiments on NSTX. This work will also address the parallel structure of blob-filaments, relevant to their interaction with the divertor. Finally, as time permits, a novel area of exploration will be considered under Category 3, viz. the interaction of ion-cyclotron radio frequency waves (ICRF) in the edge plasma with edge turbulence and its possible use as a means of edge control.

There is significant synergy of the proposed work with other presently funded research: Lodestar’s theory grant under which the blob and turbulence simulation models were developed, and an rf-SciDAC grant under which Lodestar is studying some related aspects of rf edge propagation and rf-sheath formation.

## **Timeline**

### **2009-2010:**

Carry out detailed comparison studies between the SOLT code and experimental data (GPI and other diagnostics such as probes) for a base case.

### **2010-2011:**

Extend the base-case studies to examine the variation of SOL turbulence with the SOLT turbulence code and machine (plasma) parameters.

### **2011-2012:**

Attempt to construct SOL turbulence scaling laws from 2010 studies. Begin work on one or more of: (i) blob speed in disconnected/detached plasmas, (ii) parallel blob-filament structure in the presence of X-points, (iii) ICRF interaction with edge turbulence.

### **2012-2013:**

Continue work on previous year studies. As warranted, work with NSTX team to design possible critical experiments to further test and/or explore scalings.

### **2013:**

Analyze available additional experimental data from previous year and assess the implications of all the work for future STs and ITER.

## **Contributions to the NSTX 2009-13 Five Year Plan:**

Contributed to the writing of Chapter 5 on boundary physics. This work also contributes to Chapter 6 on sustainment with regard to heat flux issues for long-pulse operation.

## **References**

- 2 J. R. Myra, D. A. D'Ippolito, D. P. Stotler, S. J. Zweben, B. P. LeBlanc, J. E. Menard, R. J. Maqueda, and J. Boedo, *Phys. Plasmas* **13**, 092509 (2006).
- 3 J.R. Myra, J. Boedo, B. Coppi, D.A. D'Ippolito, S.I. Krasheninnikov, B.P. LeBlanc, M. Lontano, R. Maqueda, D.A. Russell, D.P. Stotler, M.C. Varischetti, S.J. Zweben, and the NSTX Team, 21st IAEA Fusion Energy Conference, October 16-21, 2006, Chengdu, China, paper TH/P6-21.
- 4 B. Lipschultz et al., *Nucl. Fusion* **47**, 1189 (2007).
- 5 D. P. Stotler, et al., *Contrib. Plasma Phys.* **44**, 300 (2004).

## **A-6. Los Alamos National Laboratory**

Research Topic: **Predictive Modeling of Non-inductive Startup by Helicity Injection on NSTX**

Principal Investigator: Xianzhu Tang

Participating Researcher: Allen Boozer (Columbia University)

Funded under DOE Grant: C52-06NA25396

### **Introduction**

For the spherical tokamak (ST) to be a viable option for Component Test Facility (CTF) and DEMO, NSTX must demonstrate a way that enables mostly solenoid-free startup because of the intrinsic limitation on the physical size of the center stack. Furthermore, the solenoid-free startup scheme must scale up to an ST-based reactor and CTF. The leading candidate scheme that has been investigated experimentally on NSTX, which also has the highest performance to date, is the so-called transient co-axial helicity injection (CHI). This collaborative effort develops the theoretical basis and provides modeling support of current and future NSTX CHI experiments.

### **Current research contributions to NSTX**

We have made substantial progress in understanding the equilibrium [1], stability [2], and nonlinear relaxation [3] of a co-axial helicity injection plasma. Our recent publications on flux amplification in an ST-CHI plasma [4] and its reactor scalability [5] have laid out the theoretical and quantitative bases for future CHI experiments and design optimization on NSTX and future ST devices. The fundamental advances in the theory of magnetic self-organization via linear [6, 7, 8] and nonlinear [9] resonant coupling between the driven plasma and the helicity injector, in addition to applications in ST-CHI for solenoid-free startup, also find important applications in spheromak reactor [10] and astrophysical radio lobes [11].

### **Summary of proposed research plan for 2009-13**

We propose to continue our investigation of NSTX solenoid-free startup by helicity injection in support of the current experiments and to develop the physics bases for a new transient helicity injection startup

scheme that can be scaled up to spherical tokamak-based (ST) Component Test Facility (CTF). These research objectives will be accomplished by combining (1) analytical theory; (2) numerical calculation of spherical tokamak co-axial helicity injection (ST-CHI) equilibria; and (3) full torus 3D nonlinear MHD simulation of full cycle ST-CHI discharges. The programmatic goal will be achieved by working closely with NSTX experimentalists in formulating an experimental strategy to carry out the proposed new operational mode on NSTX and the post-run data analysis and physics interpretation. We will also continue our support of the current fast transient CHI startup campaign on NSTX and explore the feasibility of non-inductive startup via plasma gun helicity injection. The specific research tasks that will be carried out include: (1) further improving our understanding of how spherical tokamak plasma under co-axial helicity injection relax under sustained external drive, and correlating it to flux amplification and current multiplication; (2) understanding the physics that governs the flux amplification and current multiplication in a spherical tokamak plasma under helicity injection; (3) specifying the requirements on co-axial helicity injection in terms of flux amplification and current multiplication for spherical tokamak reactor and CTF applications, and demonstrating that the relaxed transient co-axial helicity injection scheme has the scalability to enable solenoid-free startup of the ST-based CTF. The proposed research is built upon a number of recent theoretical breakthroughs and computational advances that were made possible by previous NSTX collaboration support. If the proposed research is carried out with the required support, it promises a solenoid-free startup scheme that would overcome a primary obstacle in the ST path toward controlled fusion energy.

**Contributions to the NSTX 2009-13 Five Year Plan:**

Contributed CHI theory for Chapter 6, Section 4.

**References**

- [1] X.Z. Tang and A.H. Boozer, "Equilibrium and resistive steady state of an axisymmetric CHI plasma," *Physics of Plasmas* 10, 3661 (2003).
- [2] X.Z. Tang and A.H. Boozer, "Numerical studies of a steady state axisymmetric CHI plasma," *Physics of Plasmas* 11, 171 (2004).
- [3] X.Z. Tang and A.H. Boozer, "Current drive by CHI in a spherical torus," *Physics of Plasmas* 11, 2679 (2004).

- [4] X.Z. Tang and A.H. Boozer, “Flux amplification in helicity injected spherical tori,” *Physics of Plasmas* 12, 042113 (2005).
- [5] X.Z. Tang and A.H. Boozer, “Scale-up of spherical tokamak solenoid-free startup by co-axial helicity injection,” *Physics of Plasmas* 14, 100704 (2007).
- [6] X.Z. Tang and A.H. Boozer, “Force-free magnetic relaxation in driven plasmas,” *Phys. Rev. Lett.* 94, 225004 (2005).
- [7] X.Z. Tang and A.H. Boozer, “Constrained resonance in magnetic self-organization,” *Phys. Rev. Lett.* 95, 155002 (2005).
- [8] X.Z. Tang and A.H. Boozer, “Chandrasekhar-Kendall modes and Taylor relaxation in an axisymmetric torus,” *Physics of Plasmas* 12, 102102 (2005).
- [9] X.Z. Tang, “Driven resonance in partially relaxed plasmas,” *Phys. Rev. Lett.* 98, 175001 (2007).
- [10] X.Z. Tang and A.H. Boozer, “Reactor prospect of spheromak concept by electrostatic helicity injection,” *Physics of Plasmas* 15, (2008).
- [11] X.Z. Tang, “Self-organization of radio lobe magnetic fields by driven relaxation,” *Astrophysical Journal* 679, 1000 (2008).

## **A-7. Los Alamos National Laboratory**

Research Topic: **Hypervelocity Dust Injection/ Dust Studies**

Principal, Co-Principal Investigators: Glen Wurden, Jeff Wang

Participating Researchers: TBD

Funded under DOE Grant: Will propose to be restarted

### **Introduction**

In FY07, our Marshall gun/ high-speed dust injector collaboration on NSTX was discontinued. We propose restarting our experimental collaboration for this 5 year NSTX plan. Dust in plasmas is an interesting and exciting area of research. Studying dust interactions has value for ITER (dust can be an unwanted problem), and yet also other possible benefits as a way to inject neutrals across the plasma separatrix. Depending on the dust speed, (for example if launched at 5-10 km/sec), it may penetrate deeply. Previously (1-3), we developed a high speed dust injector, which utilizes a high speed (but cold) deuterium plasma to accelerate dusts to high velocities, and more recently, LANL has published a PRL on dust acceleration [4] physics.

### **Current research contributions to NSTX**

Presently, the piezoelectric dust dropper system (from our hypervelocity hardware), operated very successfully dropping lithium dust into NSTX for 2 days during the FY08 run. It was loaned to PPPL/NSTX (D. Mansfield) by Los Alamos in the fall of 2007.

### **Summary of proposed research plan for 2009-13**

We propose to install our hypervelocity dust injector, which can also inject slow speed dust, onto NSTX. The previously planned port is occupied by other diagnostics, so interfacing has to be re-organized, taking into account sightlines from various imaging systems already on NSTX. We also know that helium used at PPPL to inject Lithium pellets was problematic for good NSTX plasma operations.

- Gas load measurements at LANL, selection of port at NSTX, reconfigure hardware
- Install equipment at NSTX, conduct initial tests with carbon, and lithium dusts.

- Compare to dust ablation codes, look for diagnostic uses of dust in high temperature plasma

### Timeline

#### 2009-2010:

Restart the project. Make gas load measurements at LANL. Prepare interfaces to NSTX.

#### 2010-2011:

Install hypervelocity dust injector system at NSTX. Make initial measurements by piggybacking.


#### 2011-2012:

Compare with dust ablation/penetration models. Vary the types/size/speed of dust

#### 2012-2013:

With higher resolution imaging, study dust ablation cloud for possible B-field measurements

### References

- 1). Zhehui Wang and G. A. Wurden "[Hypervelocity dust beam injection for internal magnetic field mapping](#)" . Rev. Sci. Instrum. 74(3), 1887 (2003).
- 2). Ticos, CM; Wang, Z; Dorf, LA; Wurden, GA, **Plasma dynamic hypervelocity dust injector for the national spherical torus experiment**. Source: Review of Scientific Instruments; vol.77, no.10, 304 (2006).
- 3). Dorf, LA; Roquemore, AL; Wurden, GA; Ticos, CM; Wang, Z, **Imaging system for hypervelocity dust injection diagnostic on NSTX**, Review of Scientific Instruments; vol.77, no.10, 517 (2006).
- 4). C. M. Ticos, Zhehui Wang, G. A. Wurden, J. L. Kline, D. S. Montgomery, L. A. Dorf, and P. K. Shukla, **Experimental Demonstration of Plasma-Drag Acceleration of a Dust Cloud to Hypervelocities**, Phys. Rev. Lett. **100**, 155002 (2008).

## **A-8. Massachusetts Institute of Technology**

Research Topic: **Full-wave studies of high harmonic heating in NSTX**

Principal Investigator: Paul T. Bonoli

Co-Principal Investigator: John C. Wright

Participating Researchers (at PPPL): Cynthia K. Phillips, Joel Hosea, Stanley Kaye, Douglas McCune

Funded under DOE Grant: DE-FG02-99ER54525

### **Introduction**

In order to accurately assess the role of high harmonic fast wave (HHFW) heating in the NSTX device it is important to have a predictive calculation for the wave propagation, absorption, coupling and current drive. A full-wave electromagnetic field solver is generally the best approach to this type of calculation because effects due to toroidal geometry, focusing, diffraction, antenna geometry, nonthermal particles, and the edge scrape off layer (SOL) can all be included in such a calculation. These effects are all of great importance in NSTX as the device is low aspect ratio, employs a twelve strap antenna to couple ICRF power to the plasma, contains a population of fast ions due to neutral beam injection (NBI), and is characterized by a tenuous scrape-off-layer density that extends out to and beyond the antenna launching structures.

### **Current research contributions to NSTX**

One of the primary research contributions of this collaborative proposal is application of the high harmonic fast wave (HHFW) version of the TORIC full-wave ICRF field solver [1] to transport analysis studies of HHFW experiments in the NSTX device. This work consists of implementation of a “standalone” version of the solver on the PPPL computing clusters (PETREL, VIZ, and MHD) as well as an identical implementation of the solver in TRANSP. This implementation was accomplished by setting up a CVS repository for TORIC at MIT, which allows upgrades and improvements in the code to be immediately available to collaborators at PPPL (Drs. Cynthia Phillips and Dr. Ernie Valeo). This CVS version of TORIC is kept consistent with an SVN version that resides at the IPP in Garching, Germany.



Although TRANSP simulations have yet been performed, the HHFW version of the TORIC solver was successfully installed in TRANSP and we are now ready to begin these studies.

Concurrent with code development activities we have worked with Dr. Cynthia Phillips (PPPL) on studies of the dependence of electron heating on antenna phase in NSTX [2] using the MARSHALL computing cluster at MIT. We also worked with Dr. Phillips on high resolution TORIC simulations aimed at trying to understand the improvement in HHFW electron heating in NSTX at higher parallel wavenumber ( $k_{\parallel} = 7 \text{ m}^{-1}$ ) and magnetic field ( $B_0 = 0.55\text{T}$ ) [3]. These simulations show coupling of the HH fast wave to a short wavelength mode that has tentatively been identified as a slow wave with dispersion relation given by  $n_{\perp}^2 \sim -K_{zz} (n_{\parallel}^2 - S)/S$ , where  $K_{zz}$  and  $S$  are elements of the dielectric tensor in the Stix notation. This mode is usually evanescent but can propagate under conditions where  $\zeta_{oe} = (\omega / k_{\parallel} v_{te}) < 1$ , that is at higher  $k_{\parallel}$  and low frequency ( $\omega$ ), both of which occur in NSTX. Initial studies with TORIC indicate the coupling to this mode can be strong but the simulations we did were plagued by poor power balance, particularly at the highest poloidal mode resolution.

### **Summary of proposed research plan for 2009-13**

The objective of this collaborative proposal is to use the TORIC full-wave field solver [1] for analysis of HHFW experiments in NSTX in the following four areas:

- Analysis of HHFW surface wave excitation, motivated by recent experimental observations of the edge density affecting the core heating efficiency in NSTX.
- Analysis of parasitic HHFW – fast NBI ion interaction and HHFW-background ion (hydrogen) interaction in NSTX experiments.
- Time dependent and stationary (in time) transport analysis and RF analysis of NSTX discharges with HHFW heating (and current drive), including the possible use of HHFW electron heating in NSTX start up scenarios.

- Computational and theoretical support for PPPL program studies of slow wave mode conversion in the HHFW regime and simulations of Compressional Alfvén Eigenmodes (CAE's) and related RF-driven eigenmodes.

## **Timeline**

### **2009-2010:**

Finish standalone HHFW TORIC simulations to demonstrate surface wave excitation for relevant experimental parameters in NSTX, (that is, the measured density profile and parallel wave number).

Perform parametric scans to determine under which conditions (density, magnetic field, and parallel wave number) surface waves are excited and can be avoided.

### **2010-2011:**

Use standalone HHFW TORIC solver to investigate parasitic HHFW interaction with fast NBI ions and with background hydrogen, using relevant NSTX parameters.

Execute and test the HHFW TORIC solver within TRANSP for an NSTX discharge with HHFW electron heating.

### **2011-2012:**

Continue simulations of HHFW slow wave mode conversion in NSTX.

Perform TRANSP simulation of HHFW – fast ion interaction using an effective beam temperature from TRANSP.

### **2012-2013:**

Execute and test the HHFW TORIC solver within TRANSP for an NSTX discharge with HHFW current drive.

Perform time dependent TRANSP simulations of HHFW electron heating and current drive to demonstrate non-inductive plasma start-up for access to high performance

**Contributions to the NSTX 2009-13 Five Year Plan:**

The work described in each of these areas is closely aligned with the following two NSTX scientific priority areas:

Exploit improved coupling efficiency of launched fast waves at high ion cyclotron harmonic frequencies ( $n=10-15$ ), with emphasis on simulating and enhancing plasma performance in advanced operating scenarios.

Develop scenarios for solenoid-free ramp-up to substantial plasma currents by neutral beam injection and high harmonic fast wave.

**References**

[1] M. Brambilla, *Plasma Physics and Controlled Fusion* **44**, 2423 (2002).

[2] C.K. Phillips, S. Bernabei, J. Hosea, B. LeBlanc, J.R. Wilson, P.T. Bonoli, J.C. Wright, E.F. Jaeger, P. Ryan, D. Swain, “Full Wave Modeling of High Harmonic Fast Wave Heating in NSTX”, *Bulletin of the American Physical Society* **49**, 223 (2004).

[3] C. K. Phillips, S. Bernabei, E. Frederickson *et al*, “Full-Wave Modeling of Wave-Plasma Interactions in NSTX”, *Bulletin of the American Physical Society* **51**, 235 (2006).

## A-9. Nova Photonics, Inc.

Research Topic: **Radially resolved internal measurements of magnetic field magnitude and direction, radial electric field, and use of these for reconstruction of q-profiles and total pressure profiles**

Principal, Co-Principal Investigators: Fred M. Levinton

Participating Researchers: Howard Yuh & Jill Foley

Funded under DOE Grant: DE-FG02-99ER54520 & DE-FG02-01ER54616

### Introduction

The primary goal of our critically important research is to provide magnetic field pitch angle profiles. The MSE-CIF diagnostic system is currently operational with 16 sightlines. The data is routinely incorporated into LRDFIT to obtain q-profile and current profiles.

The new Motional Stark Effect with Laser-Induced Fluorescence (MSE-LIF) diagnostic<sup>1</sup> will allow radially resolved, high-precision measurements of magnetic field magnitude as well as pitch angle. The installation and use of the MSE-LIF diagnostic on NSTX will enable new physics studies in several topical areas, including fast ion instabilities from a unique measurement of the non-thermal ion population, rf heating and current drive as well as non-inductive startup and current drive through the ability to make MSE measurements in the absence of heating beams, effects of radial electric fields through the ability to measure them via the combination of the existing MSE-CIF system with the new MSE-LIF, and a contribution to ITER via a unique opportunity to directly compare the utility of two proposed types of MSE measurement that have been proposed for ITER equilibrium reconstruction. Because the MSE-LIF is based on the use of a diagnostic neutral beam, MSE measurements can be made in the absence of heating beams, which will contribute to studies of HHFW heating and current drive, as well as CHI methods of non-inductive startup and current drive.

All MSE systems are potentially sensitive to radial electric fields, and as such can be used to determine them given two independent measurements. In the NSTX case, the MSE-LIF system has a near-radial beam injection angle, and is minimally sensitive to radial electric fields, but the existing MSE-CIF system is sensitive to radial electric fields. Hence, the combination of MSE-CIF and MSE-LIF data can be used

to subtract out the purely magnetic aspects of the measurement to give radial electric field measurements when both MSE systems are operated in conjunction.

### **Current research contributions to NSTX**

The MSE-CIF diagnostic system is currently operational with 16 sightlines. The data is routinely incorporated into LRDFIT to obtain q-profile and current profiles. We have been actively engaged in transport analysis that has investigated the effects of magnetic shear on ion and electron transport. This has resulted in a publication and invited APS talk<sup>2</sup> and recently an invited talk to be presented at the APD-DPP 2008 conference, to be given by H. Yuh.

### **Summary of proposed research plan for 2009-13**

Magnetic field magnitude measurements in the MSE-LIF approach are achieved through a spectroscopic measurement of the line spacing in the MSE spectrum, and the use of this measurement for equilibrium reconstruction we refer to as MSE-LS for MSE with line shifts. In contrast, the traditional MSE measurement which relies on line polarization is termed MSE-LP. The MSE-LIF system will be capable of providing both MSE-LS (magnetic field magnitude) and MSE-LP (magnetic field pitch angle) measurements. The MSE-LIF diagnostic is presently funded through 2010 under a diagnostic development grant. During this time period, installation of the diagnostic on NSTX and initial data collection are planned. Though MSE-LIF is capable of both MSE-LS and MSE-LP measurements, the unique capability of MSE-LIF on NSTX is the magnetic field magnitude measurement, as the existing system provides reliable pitch angle data. Thus, the magnetic field magnitude measurements will be emphasized earlier in the research program plan.

The MSE-CIF diagnostic will complete the optics upgrade to improve sensitivity for magnetic fluctuation measurements and, if funded, will provide real-time MSE q-profiles. Research activities will probably focus on electron transport in the reversed shear regime developed on NSTX. We also plan to investigate Er corrections based on using the new MSE-LIF system as well as poloidal CHERS.

## Timeline

### 2009-2010:

MSE-LIF: Install diagnostic beam, laser, collection optics and fibers in NSTX test cell, detectors in mezzanine. Perform initial tests of alignment/operation of all components, plan to collect ‘first light’ from beam in NSTX plasma.

MSE-CIF: Complete upgrade of filter optics. Operate 16 channels.

### 2010-2011:

MSE-LIF: Operate four channels in MSE-LS configuration. Shakedown of system. Write new grant proposal.

MSE-CIF: Operate 16 channels.

### 2011-2012:

MSE-LIF: Upgrade system to include 12 channels. Use MSE-LIF data to perform reconstructions of q-profile and pressure. Demonstration of this ability relevant to ITER MSE system design. Use of system will contribute to NSTX research program in areas of non-inductive startup and current drive, fast ion instability studies, and radial electric fields.

MSE-CIF: Operate 16 channels. Add real-time MSE. Write new grant proposal. Design modifications of MSE-CIF for higher field operation.

### 2012-2013:

MSE-LIF: Installation of polarization rotation to achieve MSE-LP measurements with MSE-LIF system. Continued operation of MSE-LIF, further studies of phenomena related to non-inductive startup and current drive, fast ion instability studies, and radial electric fields.

MSE-CIF: Operate 16 channels. Install modification for higher toroidal field operation.

### 2013:

MSE-LIF/MSE-CIF: Operate 16 channels, further studies of phenomena related to non-inductive startup and current drive, fast ion instability studies, transport, and radial electric fields.

## References

1. E. L. Foley and F. M. Levinton, “Progress on the Motional Stark Effect with Laser-Induced Fluorescence Diagnostic (Invited)”, *Rev. Sci. Instrum.* **77**, 10F311 (2006).
2. F. M. Levinton et al., *Phys. Plasmas* **14**, 056119 (2007).

## **A-10. Oak Ridge National Laboratory**

Research Topic: **ORNL Boundary Physics, Heating, and Current Drive Program for NSTX**

Principal Investigators: D. L. Hillis, R. Maingi, D. A. Rasmussen, P. M. Ryan

Participating Researchers: T. Biewer, T. S. Bigelow, J. Canik, J. B. O. Caughman, S. Diem, E. F. Jaeger,  
A. Sontag, J. Wilgen and 1 post-doc(TBD)

Funded under DOE Grant: ORNL FWP (ERAT 308)

### **Introduction**

This document details the participation of staff members from the Oak Ridge National Laboratory (ORNL) in the physics program of the National Spherical Torus Experiment (NSTX) for the period 2009 - 2013. The scope of work is divided into the areas of Boundary Physics and RF Heating and Current drive.

The boundary physics research has two primary components: (a) execution and analysis of experiments, including physics analysis support with detailed modeling, and (b) operation and installation/upgrading of diagnostics.

The topics discussed in this plan are:

1. H-mode pedestal, ELM, and power threshold physics,
2. Scrape-off layer and divertor optimization for long pulse plasmas, including modeling and analysis with the SOLPS 2-D fluid code package
3. Boundary studies to enable improved RF coupling efficiency, and
4. Support for density control experiments, as well as density profile control enabled via pellet fueling.

These elements largely reflect a continuation of the existing ORNL leadership of and contribution to the NSTX program. The three main goals of these research lines are: 1) to develop the scientific basis for extrapolation to larger spherical tori, including a low aspect ratio Component Test Facility, 2) to test

theories used for higher aspect ratio designs, such as the International Thermonuclear Experimental Reactor (ITER), and 3) to optimize NSTX long pulse discharges. It is noted that ORNL staff presently serve as the Boundary Physics Experimental Task (ET) Group Deputy leader.

Progress toward research goals relies both on existing measurements and a few new diagnostics. Thus, ORNL's participation in the NSTX program relies on the conduct and analysis of experiments, as well as diagnostic operation of infrared cameras, reflectometry, and filterscopes. Looking forward, ORNL staff may support operation of the Edge Rotation Diagnostic and associated upgrades.

The proposed RF research is intended to advance the progress toward the IPPA-FESAC 5-10 year goals for the Spherical Torus concept of fully non-inductive operation and solenoid-free plasma current ramp-up to high beta operation. The combination of ECH/HHFW/EBW will be used to initiate plasma pre-ionization, ramp up low current coaxial helicity injection (CHI) plasmas to the currents and densities needed for neutral beam application, and to further reduce volt-second consumption for long pulse operation at high beta.

The RF research can be divided into High Harmonic Fast Wave (HHFW) and Electron Bernstein Wave (EBW) activities. The HHFW program is a natural continuation and extension of ongoing research:

1. Understanding and improving the HHFW power deposition, heating, and current drive efficiency.
2. Understanding and improving the power propagation through the edge plasma and its deposition in the core.
3. Increasing the HHFW power and reliability.
4. Providing heating power to transition from non-inductive startup plasmas to NBI target plasmas.

RF theory support will assist in the understanding of power flow, deposition, and loss channels by using the AORSA 1D and 2D codes to study wave propagation in the plasma edge, excitation of parametric decay instabilities and edge ion heating, and the damping of HHFW on the fast ion tails from neutral beam injection.

The EBW program is intended to provide off-axis electron heating and current drive for NSTX, as well as for ECH plasma startup and ramp up. We will continue EBW emission measurements to understand and



optimize mode conversion mechanisms, and we will develop, install, and operate a high power (~200 kW) EBW/ECH system at 15.3/28 GHz. The system will use existing equipment to minimize hardware and installation cost. It will provide sufficient power for proof of principle experiments on a reasonable schedule yet be easily upgradeable to higher power in the future. During the first year of operation, the system is expected to deliver a 0.5 s pulse at 300 kW for 28 GHz and 150 kW at 15.3 GHz; the power will double in the next year with the addition of a second gyrotron.

### **Current research contributions to NSTX**

ORNL staff leads research in the areas of H-mode pedestal and ELM physics and edge stability issues. We also contribute to the experimental test of Lithium as a divertor PFC. Finally we lead the effort on heat flux scaling, including peak heat fluxes and SOL widths. We also conduct 2-D modeling of ST plasmas for projection toward future STs, including NHTX and ST-CTF.

ORNL staff operates 2 slow IR cameras, a fast filterscope array on NSTX and the fast SOL microwave reflectometer for a variety of studies. In addition we are in the process of commissioning a fast IR camera for transient heat pulse studies, starting in 2009.

ORNL historically provides manpower and support for HHFW system design, equipment operation, and experimental implementation and analysis, as well as theory assistance through rf/plasma modeling. The ORNL reflectometer mentioned above and other edge diagnostics provide crucial information for the optimization of the power coupling and performance of the HHFW/EBW systems. The edge profile data is also needed to benchmark the modeling codes in order to better understand and interpret the experimental results.

### **Summary of proposed research plan for 2009-13**

The boundary physics program will carry out research in the following areas:

- H-mode pedestal – analyze dependencies on external parameters and determine explicit role of aspect ratio in setting heights, widths, and gradients

- ELMs – assess role of ideal and resistive MHD stability as the trigger for large and small ELMs, and extrapolate toward next step STs
- L-H Power threshold – assess role of shape in setting the power threshold in STs
- SOL and divertor physics – investigate underlying physics of SOL power flux peaks and widths (steady and transient), e.g. role of gyro-radius, collisionality, and beta, and participate in design efforts of novel divertors for improved power flux control
- Assess role of neutrals in edge RF coupling, and develop small/no ELM scenarios for improved coupling
- Lithium program – contribute to assessment of Lithium as a particle control and power control tool, including design of LLD module upgrades, and commission a pellet injector to enable core fueling

The HHFW research program will concentrate on four areas of activity:

- Understanding and improving the HHFW core propagation and absorption, heating, and current drive efficiency.
- Understanding and improving the power propagation through the edge plasma and its deposition in the core.
- Increasing the HHFW power and reliability
- Providing heating power to transition from non-inductive startup plasmas to NBI target plasmas.

ORNL will also provide theory support to the HHFW effort:

- HHFW coupling to fast ions: develop full time-dependent energetic tail evolution including radial diffusion and finite orbit effects and incorporate a second non-Maxwellian ion species.
- Excitation of parametric decay instability: develop resonant 3-wave interaction package to study “extended pump”.
- Collisionally enhanced absorption (AORSA-1D).
- Employ the full wave 3D power propagation capabilities of AORSA to study edge losses and far field sheaths.

The ECH/EBW program will provide off-axis electron heating and current drive for NSTX, as well as for ECH plasma startup and ramp up. ORNL will provide gyrotrons, each with a nominal 350 kW output power at 28 GHz, for installation on NSTX and will assist in the design of the launchers and operation of ECH/EBW experiments.

## **Timeline**

### **2009:**

#### Boundary Physics:

- Commission fast IR camera for steady and transient heat pulse studies
- Resolve common features of small ELM regimes between NSTX and other devices, i.e. MAST and Alcator C-Mod
- Assess role of aspect ratio in pedestal similarity experiments with MAST and DIII-D
- Measure dependence of L-H threshold on a few shape parameters (X-point height, connection length, elongation, triangularity)
- Assess impact of LLD on plasma parameters

#### HHFW:

- Complete the upgrade of the current straps to center-grounded operation for improved power delivery and reliability, including the re-tuning of the decouplers and the optimization of the power matching and distribution system.
- Optimize heating and CD operation with NBI; begin HHFW coupling optimization into plasma startup/ramp-up.

#### ECH/EBW:

- Optimize EBW emission coupling in H-mode with Li evaporation.

### **2010-2011:**

#### Boundary Physics:

- Commission 2-color IR system for measuring heat flux in Lithium environment for FY2010 multi-machine Joule milestone
- Use enhanced edge diagnostics in NSTX 5 year plan to better assess ideal MHD stability of large ELMs and resistive MHD stability of small ELMs

- Commission pellet injector for core fueling experiments
- Develop small/no ELM scenarios for RF experiments using LLD
- Participate in design of upgraded LLD, cryopump for installation in 2012
- Participate in design of X-divertor or Super X-divertor for installation in FY 2012

HHFW:

- Divide the 12-strap array into three sections to test competing ELM-resilient matching technologies under consideration for ITER. Design a “Conjugate-T” matching system for four of the straps and an “ELM-dump” matching system for four other straps, leaving four straps as an unmodified reference standard.
- Further optimize H-mode heating and CD operation with this system.
- Compare the ELM-resilient techniques and subsequently convert the full array to employ the most successful approach.
- HHFW coupling into ramp-up combined with 28 GHz ECH-assisted non-inductive startup

EBW:

- Complete installation of 350 kW, 28 GHz gyrotron system, study ECH-assisted startup using fixed horn launcher.

**2012-2013:**

Boundary Physics:

- Commission and study impact of upgraded LLD or cryopump on plasma
- Commission and study impact of X-div/Super X-div on plasma
- Pellet upgrade if needed for core fueling

HHFW/EBW:

- Assess high power long pulse HHFW at high B-field, support very long pulse scenario.
- Install second 350 kW, 28 GHz gyrotron and locally-steered O-X-B launcher.
- Combine ECH/EBW to provide fully non-inductive plasma startup and ramp-up.
- Upgrade to remotely-steered O-X-B launcher; benchmark deposition codes with 700 kW core and off-axis heating studies.

### Contributions to the NSTX 2009-13 Five Year Plan:

Lead authorship of Chapter 5 (Boundary Physics). Major contributor to the writing of Chapter 4 (Waves and Energetic Particles), sections 4.0, 4.1, and 4.2.

### Appendix – list of ORNL first-author NSTX-related refereed journal articles (FY 2004-2008)

1. T.M. Biewer, R. E. Bell, R. Feder, et. al., “An Edge Rotation and Temperature Diagnostic on NSTX”, *Rev. Sci. Instr.* **75** (2004) 650.
2. R. Maingi, C.S. Chang, S. Ku, T. Biewer, R. Maqueda, et. al., “Effect of Gas Fueling Location on H-mode Access in NSTX”, *Plasma Phys. Contr. Fusion* **46** (2004) A305.
3. T.M. Biewer, R. E. Bell, S. J. Diem, et. al., “Edge ion heating by launched high harmonic fast wave in the National Spherical Torus Experiment”, *Phys. Plasma* **12** (2005) #056108
4. R. Maingi, S.A. Sabbagh, C.E. Bush, E.D. Fredrickson, J.E. Menard, et. al., “ELMs and the H-mode Pedestal in NSTX”, *J. Nucl. Mater.* **337-339** (2005) 727.
5. R. Maingi, K. Tritz, E.D. Fredrickson, J.E. Menard, S.A. Sabbagh, et. al., “Observation of a High Performance Operating Regime with Small Edge-Localized Modes in the National Spherical Torus Experiment”, *Nucl. Fusion* **45** (2005) 264.
6. R. Maingi, C.E. Bush, E.D. Fredrickson, D.A. Gates, S.M. Kaye, et. al., “H-mode Pedestal, ELM, and Power Threshold Studies in NSTX”, *Nucl. Fusion* **45** (2005) 1066.
7. R. Maingi, M.G. Bell, E.D. Fredrickson, K.C. Lee, R.J. Maqueda, et. al., “Characterization of Small, Type V ELMs in the National Spherical Torus Experiment”, *Phys. Plasma* **13** (2006) #092510.
8. R. Maingi, C.E. Bush, R. Kaita, H.W. Kugel, A.L. Roquemore, et. al., “Divertor Heat Flux Scaling with Heating Power and Plasma Current in H-mode Discharges in the National Spherical Torus Experiment”, *J. Nucl. Mater.* 363-365 (2007) 196.
9. R. Maingi, R.E. Bell, B.P. LeBlanc, et. al., “The Enhanced Pedestal H-mode in NSTX”, *J. Nucl. Mater.* submitted 5/08.
10. J.M. Canik, R. Maingi, L.W. Owen, et. al., “2-D Divertor design calculations for NHTX”, *J. Nucl. Mater.* submitted 5/08.

## A-11. Purdue University

Research Topic: **In-Situ Elemental and Chemical Characterization of D-Recycling on Lithiated Graphitic Surfaces With Applications to NSTX**

Principal, Co-Principal Investigators: J.P. Allain

Participating Researchers: Dmitry Zemlyanov, Chase Taylor (graduate student), Dimitris Tsarouhas (graduate student)

Funded under DOE Grant: DE-FG02-08ER54990

### Introduction

This project consists of designing and conducting laboratory experiments that elucidate the effect of lithiated graphite and liquid lithium (Li) surfaces on deuterium recycling in NSTX Li evaporation and liquid Li experiments (e.g. liquid lithium divertor). In particular this work seeks to undertake systematic studies of energetic particle-surface interactions that can guide understanding of how lithium-based systems affect the plasma-material interface in NSTX. This understanding can further help to develop strategies to optimize particle density control and plasma performance in advanced NSTX plasma operation. This work is particularly important since lithium wall conditioning and proposed LLD will provide a unique approach to control hydrogen recycling and enhanced performance under high heat flux conditions. In addition, ELM suppression has been found to be associated with lithium wall conditioning in NSTX and thus laboratory experiments proposed here could help understand possible mechanisms behind this phenomenon.

Little is known about how long the Li layers remain on the substrate surface and how deuterium is pumped by a lithium-graphite mixed surface [1]. Questions that arise are for example: is it elemental lithium that is responsible for deuterium pumping or is it lithium in the presence of a compound (e.g. lithium carbide or lithium carbonate) that is responsible for D pumping? What is the effect of lithiated graphite plasma-wetted surface on the LLD in NSTX and are there conditioning scenarios that can be designed based on laboratory studies?

At Purdue University we conduct state-of-the art *in-situ* surface characterization techniques capable of monitoring lithium-based surfaces during particle irradiation. We can in principle, measure how the surface and near-surface is affected by energetic D particle irradiation during exposure ultimately elucidating on the D-pumping characteristics of lithium-treated surfaces. We can in addition measure the chemical evolution of the surface as a function of depth, which is important in determining the chemical state of the lithium atoms once deposited on a given matrix.

Our research supports the following key experimental areas in NSTX:

- 1) D pumping and particle density control
- 2) High-power particle handling
- 3) ELM suppression by lithium conditioning

### **Current research contributions to NSTX**

At Purdue University the PRIHSM, IMPACT and Omicron Cluster experimental laboratory facilities are being used to measure surface performance properties of lithiated graphite and liquid lithium surfaces simulating scenarios in NSTX [2,3]. In this project we address several critical questions that challenge our understanding of the plasma-lithium surface interface in NSTX:

- How long does the Li layer remain on the substrate surface?
- How does the layer evolve at elevated temperatures and what is the impact on D recycling?
- What is the state of Li during this time? Is there a change in the surface chemical state over time?
- What is the amount of Li atoms available to pump D?
- How is D bound to the lithium-graphite system? Is elemental lithium responsible for pumping D or is it Li in the presence of a compound (e.g. lithium carbide), which is responsible for pumping?
- What is the impact of lithium-graphite surface chemistry on D recycling in NSTX?
- What is the impact of liquid Li on D recycling under NSTX-relevant conditions?

This project started just recently in May 2008 and work is currently investigating the hydrogen pumping capabilities of lithiated ATJ graphite. Advanced particle-beam facilities are designed to determine the response of mixed and multi-species surfaces under energetic particle irradiation. These facilities consist of three main experiments: PRIHSM, IMPACT and the Omicron Cluster system. Each system uses complementary surface-sensitive techniques including: direct recoil spectroscopy (to measure impurity levels in the film) and angle-resolved X-ray photoelectron spectroscopy during irradiation of the surface with low-energy deuterium. The facility is equipped with in-situ ultra-sensitive dual microbalance unit measuring total erosion yields and these are coupled to two separate mass spectrometry systems capable of measuring chemical sputtering of hydrocarbon species formed during irradiation.

In addition to laboratory experiments at Purdue University, an in-situ surface analysis facility will be designed by Purdue University and delivered to NSTX as a plasma-facing surface diagnostic. The facility will study erosion/redeposition properties of lithiated graphite in NSTX and its impact on the LLD system performance. This will be accomplished by coupling erosion/redeposition data from this probe with computational edge modeling by the PI and collaborators (J.N. Brooks, et al.).

### **Summary of proposed research plan for 2009-13**

We propose to elucidate the hydrogen pumping mechanisms in lithium-based surfaces to optimize particle-density control strategies during lithium wall conditioning coupled to the LLD in NSTX. The primary elements of our plan are:

- Conduct laboratory experiments to understand the underlying mechanisms behind hydrogen pumping by lithium-based surfaces under simulated NSTX plasma conditions
- Design, proposed and execute experimental runs in NSTX plasmas that utilize recipes guided by laboratory experiments on optimized methods to pump hydrogen
- Design and install in-situ plasma-surface interaction probe to study erosion/redeposition mechanisms in NSTX plasmas dominated by lithiated graphite and LLD



## Timeline

### 2009-2010:

- Develop strategies for laboratory experiments based on recent NSTX lithium wall conditioning runs
- Li exposure on ATJ graphite calibrated to NSTX 2007 run conditions (high vs low Li vapor flux) to study effects on Li-C chemical state as function of Li flux and temperature
- Li exposure on SS (as a control) calibrated to NSTX 2007 run conditions (high vs low Li vapor flux)
- Exposure of Li/graphite with exposure to low-energy D to measure effect on particle sputtering (C, D and  $C_xD_y$ ). Impact energies and angles will be varied and validated with surface response codes and serve as input to subtask #5 below
- Design and construct plasma-surface interaction probe for erosion/redeposition measurements

### 2010-2011:

- Subsequent TDS (thermal desorption spectrometry) tests to assess D uptake and chemistry
- Install plasma-surface interaction probe in NSTX and conduct in-situ experiments to understand erosion/redeposition mechanisms with lithiated graphite and LLD
- Couple experimental laboratory data to erosion/redeposition modeling codes modeling the NSTX divertor floor in collaboration with J. Brooks
- He trapping in solid lithium and liquid lithium surfaces studies and He treatment of lithiated surfaces to study effect on D uptake

### 2011-2012:

- Experiments to measure the Li surface diffusivity on candidate substrates as a function of impact energy for species (D, He, Li) on: ATJ graphite, Mo, SS using LEISS, XPS and EUPS. Refer to appendix for details on techniques.
- Exposure to *both* D and He energetic beams to study their synergy and effect on surface Li coating properties (e.g. D pumping, erosion, etc...)

- Address the role of thin vs thick liquid Li coatings on D recycling.

**2012-2013:**

- Conduct experiments that measure D-retention from static free liquid Li surfaces on various substrates and couple to surface response modeling as function of temperature.
- Assess the role of impurities on liquid Li to D recycling properties as a function of temperature.
- Couple experimental laboratory data to erosion/redeposition modeling codes modeling the NSTX divertor floor in collaboration with J. Brooks (Argonne), R. Maingi (ORNL) and D. Stotler (PPPL)

**Contributions to the NSTX 2009-13 Five Year Plan:**

The primary contributions of the experimental work in this project address NSTX plans focused on “Operation at High Heat Flux in NSTX with applications to ITER and Beyond” by means of lithium conditioning strategies in NSTX.

**References**

1. J.P. Allain and D.N. Ruzic, “Deuterium treatment effects on lithium and tin-lithium sputtering in solid and liquid phase”, in NATO Science Series: Hydrogen and Helium Recycling at Plasma Facing Materials, ed. A. Hassanein (Kluwer Academic Publishers, Dordrecht, 2002) Vol. 54, 73.
2. J.P. Allain, et al., “IMPACT: a facility to study the interaction of low-energy intense charged particle beams with dynamic heterogeneous surfaces” Review of Scientific Instruments, 78 (2007) 113105.
3. J.P. Allain, M.D. Coventry, D.N. Ruzic. “Non-linear sputtering of D-treated liquid lithium under light-particle, low-energy bombardment” Phys. Rev. B, 76 (2007) 205434.

## A-12. Purdue University

Research Topic: **Impact of Disruptions and ELMs on Liquid Lithium Surfaces in NSTX and Mitigation/Extrapolation to ITER Relevant Conditions**

Principal, Co-Principal Investigators: Ahmed Hassanein

Participating Researchers: V. Sizyuk, G. Miloshevsky, and Graduate Students

Funded under DOE Grant: **DE-PS02-07ER07-29**

### Introduction

The primary goal of our critically important research is to:

- (1) Characterize the H-mode pedestal, scrape-off layer, and divertor plasma at low pedestal collisionality with ITER-level heat fluxes and relevance to CTF, and*
- (2) Model and assess experimentally the impact of off-normal events (disruptions, ELMs) on liquid lithium surfaces in the divertor.*

### Current research contributions to NSTX

1. Update physical and mathematical models in HEIGHTS of plasma particles motion (both ions and electrons) and interaction with the lithium divertor plate during plasma disruptions and ELMs using for NSTX conditions.
2. Upgrade HEIGHTS to NSTX divertor geometry for the full 3-D simulation. This will include calculation of plasma energy deposition in target material, heat conduction in bulk, debris vapor evolution, vapor-plasma heating, photon generation and transport, with taking into account detail local magnetic fields direction and magnitude. This will include performing full resistive 3-D MHD calculations for eroded materials.
3. Integrate HEIGHTS for ELMs modeling that include models from core plasma, SOL, and divertor response using two-fluid model. Unlike disruptions, the two-fluid model is important in this case where the evaporated Li material is comparable with incoming plasma particles.

## **Summary of proposed research plan for 2009-13**

We propose to calculate:

### **A. Lithium evolution dynamics in NSTX during Disruptions and ELMs**

1. Benchmark disruption and ELMs data for Li with NSTX conditions against numerical simulation of HEIGHTS.
2. Compare results of similar Li disruption experiments performed at TRINITY and Red Star facilities.

### **B. Study plasma contamination during ELMs**

1. Help develop diagnostic methods for monitoring particle flux increase during ELMs in private flux region.
2. Benchmark data for Li back diffusion in NSTX private flux region against numerical simulation of HEIGHTS

## **Summary of proposed research plan for 2010**

We continue to evaluate:

### **A. Lithium evolution dynamics in NSTX during Disruptions and ELMs**

1. Benchmark and compare various ELMs data for Li with different NSTX scenarios against numerical simulation of HEIGHTS.
2. Evaluate various Li erosion mechanisms during disruption and ELMs and compare to various models to identify dominant mechanisms.
3. Predict erosion behavior in ITER like conditions of melted Be and W materials under disruptions and giant ELMs.

### **B. Study plasma contamination during ELMs**

1. Develop techniques to diagnose X-point radiation enhancements during ELMs with the help of graduate students.
2. Continue to benchmark data for Li back diffusion in NSTX private flux region against numerical simulation of HEIGHTS at different ELM conditions.
3. Extrapolate conditions to ITER device and predict impurity diffusion to the X-point following ELMs. Predict the behavior of the impurity flux reaching the X-point and possible cause of disruptions during each giant ELM in ITER conditions.

### **C. Study SOL characteristics and behavior during ELMs**

1. Continue to benchmark the SOL parameters during NSTX normal and ELMs operations at mid-plane during different ELM conditions.
2. Continue to benchmark and compare the SOL parameters during NSTX different ELMs operations and conditions to verify the numerical models.
3. Extrapolate conditions to ITER device and recommend the anticipated behavior of stronger ELMs and SOL parameters and predict ion energies arriving at the divertor plate. Evaluate the effect of much higher particle flux and energies during ELMs in ITER and predict if runaway sputtering-erosion can occur.

### **Summary of proposed research plan for 2011-2013**

1. Continue to extrapolate conditions to ITER device and recommend and predict anticipated behavior of stronger ELMs and SOL parameters and predict ion energies arriving at the divertor plate.
2. Continue to evaluate the effect of much higher particle flux and energies during ELMs in ITER and predict if runaway sputtering-erosion can occur from various operating scenarios.

3. Define safe operating windows for plasma instabilities for ITER relevant conditions based on comprehensive understanding of ELMs and disruptions in NSTX conditions.

## References

1. A. Hassanein and I. Konkashbaev, *Fusion Eng. Des.* 51-52 (2000) 681.
2. A. Hassanein, *Fusion Technol.* 30 (1996) 713.
3. A. Hassanein, G. Federici, et al., *Fusion Eng. Des.* 39-40 (1998) 201.
4. A. Hassanein and I. Konkashbaev, *J. Nucl. Mater.* 273 (2000) 326.
5. A. Hassanein and I. Konkashbaev, "Physics of collisionless scrape-off-layer plasma during normal and off-normal tokamak operating conditions," Argonne National Laboratory Report ANL/FPP/TM-296 (March 1999).
6. L. L. Lengyel, V. A. Rozhansky, and J. Yu. Veselova, "Drift motion in the scrape-off-layer during hard disruptions," Proc. 24<sup>th</sup> European Physical Society Conf. on Contr. Fus. and Plasma Phys., (Berchtesgaden, Germany, 1997), Ed. Eur. Phys. Soc., Geneva, Vol. 21A - part 4 (1997) 1549.
7. V. Sizyuk, A. Hassanein, V. Morozov, and T. Sizyuk, Argonne National Laboratory Report ANL-MCS-CPH-06/56, Argonne, IL, 2006.
8. G.V. Miloshevsky, V.A. Sizyuk, M.B. Partenskii, A. Hassanein, and P.C. Jordan, *J. Comp. Phys.*, Vol. 212, (2006) 25.
9. A. Hassanein, *Fusion Technol.* 15 (1989) 513.
10. A. Hassanein, *Fusion Eng. & Des.* 60 (2002) 527.
11. M. E. Fenstermacher, "ELM Electron and Ion Particle and Energy transport in Tokamak SOLs and Divertors," EU-US TTF Workshop, Cordoba, Spain, September 9-12, 2002.

## A-13. Sandia National Laboratory

Research Topic: **Liquid Lithium Divertor Experiments and Preparation for NHTX**

Principal Investigators: Richard E. Nygren

Participating Researchers: Dennis Youchison, Henry Kugel, NSTX Team

Funded under DOE Grant: Current Grant

### Introduction

The general objective of this proposal is to supply NSTX with divertor hardware so that the outer strike point of a single null plasma will contact a liquid lithium surface. This objective stems from the strong affect of a lithium surface in reducing particle recycling that has been observed in experiments in both NSTX and TFTR that produced “super-shots” with lithium pellets, CDXU, T-11 and FTU and supports physics investigations identified in the NSTX Research Priorities for FY 2007-2009, i.e., item III-1. *Characterize effects of lithium wall coating on recycling and particle control* under area III. Plasma Boundary Interfaces - interface between fusion plasma and its lower temperature plasma-facing material surroundings.

Important considerations in the preparation of hardware for a liquid lithium divertor are:

- (1) a heating system for the lithium container(s)
- (2) the initial distribution and wetting of the surfaces by lithium, and mitigation as necessary of the potential subsequent spread of lithium by capillary action
- (3) thermal management of the lithium and container(s) during shots and plasma disruptions  
diagnostics for control, safe operation of the equipment and appropriate data to complement the ongoing experiments, e.g., temperature of the lithium surface.

Sandia began working in 2006 with the NSTX Team on the Liquid Lithium Divertor and received funding for a three year NSTX-Laboratory Grant in the winter of 2007 to develop a lithium tray system to install in the NSTX divertor. The system has electrical heaters and helium lines to control heat loss between shots and will be filled using the rebuilt LITER evaporators.

Sandia is providing the LLD plates, cabling for heater leads and thermocouple extensions to connection panels on the inside of the vessel, and the rack for heater controls, thermocouple signal processing and gas (helium) flow controls.

### **Current research contributions to NSTX**

During 2007 options for the LLD design and related thermal analyses were considered by Sandia and the NSTX Team. During this time Sandia built equipment for a lithium wetting test, performed thermal analyses, procured a mockup of an open Mo mesh as a candidate technology as the lithium bearing host for the LLD and performed thermal tests on this mesh. In late 2007 and early 2008, two options for the LLD design were refined and analyzed by Sandia and the NSTX Team. The simpler design with a copper plate clad with stainless steel and covered with a flame-sprayed coating was adopted as the reference design and PPPL generated detailed drawings for the procurement of the LLD parts, which is now underway. During this same period, the specifications for the heater controls were refined and Sandia procured a three-heater copper mockup of the LLD and has started work on a new vacuum vessel for thermal tests of the mockup. This testing is extremely important for benchmarking the LLD thermal model. The results from this thermal modeling will be the basis for the thermal control program for LLD and guidance to the NSTX operators on the acceptable duration of shots for various anticipated plasmas in LLD experiments. We expect to complete installation of the LLD late in calendar 2008.

### **Summary of proposed research plan for 2009-13**

We look forward to participating in experiments with the LLD in 2009. With appropriate funding, either through a subsequent NSTX-Laboratory Grant for 2010-2012 or new funding in Sandia's base program, we will continue to participate in LLD experiments and work with NSTX on the design of a follow-on LLD and designs for applications in NHTX. The primary elements of an extended plan are:

- Operation of the control rack, guidance on thermal control during operation of the LLD, and interpretation of IR data, and thermal analysis of the LLD for selected shots.
- Development of a follow-on design for an upgraded LLD that has a lithium reservoir, active replenishment of the lithium-covered surface by capillary forces and thermal control and heat removal adequate to maintain steady state cooling for some plasmas.



- Operation of the control rack, guidance on thermal control during operation of the LLD, and interpretation of IR data, and thermal analysis of the updated LLD for selected shots.
- Development of a liquid lithium divertor for NHTX and projections of performance based upon experience with an upgraded LLD in NHTX.

### **Timeline**

#### **2009-2010:**

Operate the control rack, provide guidance on thermal control during operation of the LLD, and interpret IR data based on thermal analysis of the LLD for selected shots during the first LLD campaign. Begin developing a design for an LLD upgrade. (Participation based on current grant would end at the end for FY2009.)

#### **2010-2011:**

Operate the control rack, provide guidance on thermal control during operation of the LLD, and interpret IR data based on thermal analysis of the LLD for selected shots during the second LLD campaign. Develop a follow-on design for an upgraded LLD that has a lithium reservoir, active replenishment of the lithium-covered surface by capillary forces and thermal control and heat removal adequate to maintain steady state cooling for some plasmas. Assist the NSTX Team in the specification and procurement of parts for an upgraded LLD. Begin developing a design of options for an NHTX.

#### **2011-2013:**

Continue participation in LLD experiments (operate the control rack, provide guidance on thermal control during operation of the LLD, and interpret IR data based on thermal analysis of the LLD for selected shots). Develop and participate in operation of an upgraded LLD in NSTX and use performance characteristics to assist design of NHTX Lithium options. Characterize LLD thermal performance with longer pulse duration enabled by centerstack upgrade and possible heat-flux increases (if 2<sup>nd</sup> NBI upgrade is present).

## **A-14. University of California at Davis**

Research Topic: **Millimeter-Wave Fluctuation Diagnostics for NSTX and KSTAR**

Principal Investigator: N.C. Luhmann, Jr.

Participating Researchers: K.C. Lee, C.W. Domier, D.R. Smith (PPPL), E. Mazzucato (PPPL),  
H.K. Park (POSTECH), W.C. Lee (POSTECH), J.H. Kim (POSTECH)

Funded under DOE Grant: DE-FG02-99ER54518

### **Introduction**

UC Davis, in collaboration with researchers from PPPL and POSTECH, addresses the critical issue of kinetic instabilities through a multi-pronged program of millimeter-wave diagnostics on NSTX. The focus is on the full range of MHD activity as well as ion and electron turbulence through the development of a unique suite of diagnostics. This work consists of upgrading, maintaining, and operating two diagnostic instruments on NSTX (the Far Infrared Tangential Interferometer/Polarimeter (FIReTIP) and the high-k 280 GHz collective scattering system), as well as the design and development of two new diagnostics: a 119  $\mu\text{m}$  poloidal scattering system to complement the high-k toroidal scattering system, and a 3-D microwave imaging reflectometry (MIR) system to image microturbulence and internal MHD modes.

### **Current research contributions to NSTX**

The FIReTIP system was upgraded from four-channel operation to five-channel operation for the FY07 campaign, with a sixth channel now under test in FY08. New electronics are being developed to increase the interferometry bandwidth from  $\sim 250$  kHz to  $\sim 4$  MHz. The ability of FIReTIP to study high harmonic fast wave (HHFW) heating will also be explored by the addition of new electronics to downconvert the  $\sim 30$  MHz HHFW fluctuation signals to  $< 1$  MHz for digitization and analysis. Even in its current form, however, FIReTIP continues to provide essential density fluctuation data for numerous physics studies.

In the area of NSTX boundary physics studies, FIReTIP data has provided strong supporting evidence for the theory of gyrocenter shift which explains the mechanism of radial electric field formation at the

tokamak boundary in L/H transitions [1-3]. FIRETIP measurements of energetic particle instabilities and toroidal Alfvén eigenmodes (TAEs) have proven extremely valuable [4]; the ongoing bandwidth upgrade to ~4 MHz will allow FIRETIP to make similar measurements of higher frequency modes including compressional Alfvén eigenmodes (CAEs) and global Alfvén eigenmode (GAEs). The high time resolution of FIRETIP measurements has proven extremely useful in the study of edge localized modes (ELMs), and has allowed the identification of small (type V) ELMs which rotate toroidally in a direction opposite to the plasma current [5].

The NSTX high-k scattering system was successfully operated in the FY07 campaign, and was central to a key NSTX milestone (to study the variation of high-k turbulence with plasma conditions). In comparing L- and H-mode plasmas, a monotonically decreasing power spectra was observed during the L-mode phase and a non-monotonic power spectra during the H-mode phase. A reduction in fluctuation amplitude for upper ITG/TEM modes and moderate changes for ETG modes is observed during H-mode plasmas as indicated from electron thermal diffusivity profiles. The ion transport is close to neo-classical in the H-mode ion thermal diffusivity profiles, while the high-k scattering data reveals that the electron transport is reduced from L- to H-mode. RF-induced fluctuations were also studied with the high-k scattering system. The scattered frequency spectrum showed significant broadening during the RF heating phase where  $T_e$  is peaked at ~3 keV while  $T_i$  is ~1 keV; in cases where  $T_e$  is comparable to  $T_i$  (such as during RF and NBI heating), no spectral broadening was detected.

Modifications to the high-k scattering system electronics in May 2007 have increased the video bandwidth from 650 kHz to ~3 MHz, and have allowed the system to examine a wide range of kinetic instabilities on NSTX. Alfvén eigenmodes observed during with the upgraded high-k scattering system include an electrostatic component named Beta-induced Alfvén Acoustic Eigenmode (BAAE). Plans are underway to increase the video bandwidth still further to 5 MHz for the FY09 campaign.

### **Summary of proposed research plan for 2009-13**

FIRETIP and the high-k scattering system will continue to be employed in the study of turbulence and transport, for which the upgraded electronics with their enhanced video bandwidths should prove

extremely helpful. A new component of both systems over the next 5 years will be to study HHFW-induced density fluctuations using upgraded electronics to be installed later this year.

We propose to implement two additional fluctuation diagnostics on NSTX during this time period. The first is a poloidal scattering system, similar to the high-k toroidal scattering system except in the choice of wavelength and scattering geometry. The poloidal system would employ a pair of 119  $\mu\text{m}$  optically-pumped lasers similar to the lasers used in the FIRETIP system, and would considerably enhance planned turbulence physics studies by providing a measurement of the  $k_\theta$ -spectrum of ETG and ITG modes. The second is a 3-D microwave imaging reflectometer (MIR) system [6,7], which would image ITG and internal MHD modes. The MIR system complements the poloidal scattering system in that each covers a different range of the  $k_\theta$ -spectrum; the scattering system is more sensitive to higher wavenumbers while the imaging reflectometer is more sensitive to the lower wavenumbers.

### **Timeline**

#### **2009-2010:**

Continue maintaining and operating the FIRETIP and high-k toroidal scattering systems on NSTX, and supporting NSTX physics studies. Get renewed funding.

#### **2010-2011:**

Continue maintaining and operating the FIRETIP and high-k toroidal scattering systems, and supporting NSTX physics studies. Undergo design reviews for the poloidal scattering diagnostic concepts.

#### **2011-2012:**

Upgrade the FIRETIP and high-k scattering systems to support the planned center stack upgrade and increased 5 second discharge length. Install and commission the poloidal scattering diagnostic on NSTX. Undergo design reviews for the 3-D MIR system.

#### **2012-2013:**

Operate the FIRETIP and toroidal/poloidal scattering systems on NSTX, and support NSTX physics studies with these diagnostics in the new center stack configuration. Install and commission the 3-D MIR system on NSTX.

## References

- 1 K.C. Lee, *Phys. Rev. Lett.* **99**, 065003 (2007).
- 2 K.C. Lee, *Phys. Plasmas* **13**, 062505 (2006).
- 3 K.C. Lee, C.W. Domier, M. Johnson, N.C. Luhmann, Jr., H. Park, V.A. Soukhanovskii, *Rev. Sci. Instrum.* **77**, 10F505 (2006).
- 4 K.C. Lee, C.W. Domier, M. Johnson, N.C. Luhmann, Jr., H. Park, *Rev. Sci. Instrum.* **75**, 3433(2004).
- 5 R. Maingi *et al.*, *Phys. Plasmas* **13**, 092510 (2006).
- 6 H. Park *et al*, *Rev. Sci. Instrum.* **74**, 4239 (2003).
- 7 H. Park *et al*, *Rev. Sci. Instrum.* **75**, 3787 (2004).

## **A-15. University of California at Irvine**

Research Topic: **Energetic Particle Physics**

Principal Investigator: William Heidbrink

Participating Researchers: Emil Ruskov, Mario Podesta (postdoc), Deyong Liu (graduate student)

Funded under DOE Grants: DE-FG02-06ER54867 and DE-FG03-02ER54681

### **Introduction**

The proposed work contributes to the study of fast-ion instabilities on NSTX. Energetic particle physics is an emphasis of the NSTX program for several reasons. First, fast-ion driven instabilities are observed on most beam-heated NSTX discharges. Through changes in the heat deposition, torque, and neutral-beam current profile, redistribution of the fast ions impacts the plasma performance or evolution of the discharge on virtually every high-performance shot. Second, because the beam ions are super-Alfvenic, NSTX data can play an important role in validating codes that will predict alpha-particle driven instabilities in ITER and other burning plasmas. Third, the ratio of beam-ion gyroradius to machine size in NSTX is comparable to the ratio of alpha-particle gyroradius to machine size anticipated in a spherical tokamak (ST) D-T reactor. Thus, beam-ion studies help assess the viability of the ST reactor concept.

### **Current research contributions to NSTX**

We are responsible for the solid-state neutral particle analyzer (SSNPA) [1] and the fast-ion D-alpha (FIDA) [2] diagnostics. We regularly lead experiments in the Wave-Particle Interaction topical group and also provide diagnostic support and analysis for experiments led by our collaborators. Overall, Irvine personnel have authored five NSTX refereed journal publications and have made significant contributions to five others.

### **Summary of proposed research plan for 2009-13**

The NSTX Energetic Particle research program strives to validate theoretical models of fast-ion instabilities and to develop the means to control their effects. The emphasis in the next five years will be on validation. The NSTX program is positioned to make a major contribution to the international effort to provide high-quality data that rigorously tests theoretical models and simulation codes. In

collaboration with theoretical efforts worldwide, our goal is to develop validated codes that can predict fast-ion instabilities and their consequences in ITER. In control, our goal in the next five years is to lay the groundwork for an ambitious program that begins near the end of the five-year period.

Several instabilities are important. Attention will focus on the various Alfvén instabilities, such as the toroidicity-induced Alfvén eigenmode (TAE) and reversed shear Alfvén eigenmode (RSAE).

The NSTX program will supply data that will test specific energetic particle (EP) physics models. The process of validation must address *all* levels of the models, including the most fundamental ones. The physics models build upon a hierarchical construction (sometimes called the “primacy hierarchy”) that begins with fundamental constituents and results in fast-ion transport predictions. The elements of this hierarchy are listed in Table 1. At the lowest level are the linear wave properties of the instabilities under study. These include the polarization, frequency, spatial structure, and stability threshold. Next are the mechanisms that determine the ultimate mode amplitude, which include both wave-wave and wave-particle interactions. The wave electric and magnetic fields modify the EP distribution function (DF) and cause fast-ion transport. If these phenomena are understood for a particular case, the next level of validation testing is parametric scaling. The final validation stage is agreement with trends across multiple devices.

	Fundamental constituents $\Rightarrow$			Derived Observables	
Primacy hierarchy	Linear wave properties	Nonlinear saturation	Transport	Scaling Trend	Statistics
Observables	Polarization, structure, frequency, threshold	Spectral intensity, bispectra, zonal flows/fields	EP DF & transport	Similarity experiments	ITPA database
Agent/mechanism	EP spatial gradient, velocity anisotropy	Wave-wave, wave-particle interaction	Cross-phase, relaxation	Dimensionless scaling	Inter-machine

**Table 1.** Primary hierarchy for validation of EP turbulence and transport predictions.

Although the Irvine team will participate in validation at all levels, leadership will occur in two main areas. One leadership area is measurement and interpretation of the transport of confined fast ions. Another leadership area is inter-machine comparisons. Professor Heidbrink previously led two Alfvén-mode similarity experiments between NSTX and DIII-D [3]. With the improvement of both fluctuation and fast-ion diagnostics on both devices, further experiments of this sort will be a major area of emphasis.

### **Timeline**

#### **2009-2010:**

Complete the first set of papers containing FIDA data. Papers on acceleration of fast ions during HHFW and on fast-ion transport by various instabilities are anticipated. Conduct similarity experiments with DIII-D.

#### **2010-2011:**

Analyze the data from the similarity experiments. Propose new experiments based on discrepancies found through detailed comparisons with the theoretical codes that are being developed through the SciDAC Energetic Particle projects. Propose upgrades to the FIDA diagnostic.

#### **2011-2012:**

Complete much of the validation work. Begin exploring tools that can alter the linear stability or nonlinear dynamics of the fast-ion driven instabilities. Upgrade FIDA.

### **Contributions to the NSTX 2009-13 Five Year Plan:**

UCI contributed to writing the energetic particle section of chapter 4.

### **References**

- [1] D. Liu, W.W. Heidbrink et al., Rev. Sci. Instrum. **77** (2006) 10F113.
- [2] M. Podesta et al., Rev. Sci. Instrum. **79** (2008) in press.
- [3] W.W. Heidbrink et al., Plasma Phys. Cont. Fusion **45** (2003) 983 ; Nucl. Fusion **46** (2006) 324.



## **A-16. University of California at Los Angeles**

Research Topic: **The Study of Alfvén Mode Physics and Turbulent Transport in NSTX**

Principal, Co-Principal Investigators: P.I. - Dr. Tony Peebles, Co-P.I.s - Prof. T Carter, Dr. D.L. Brower

Participating Researchers: Dr. Shige Kubota, Dr. Neal Crocker, Mr. Jon Hillesheim (graduate student)

Funded under DOE Grant: DE-FG03-99 ER54527

### **Introduction**

The National Spherical Torus eXperiment (NSTX) has opened up a wide range of exciting new physics research avenues within the overall US Fusion Energy Science Program. In particular, the study of a high-beta, high-performance plasmas in the magnetic geometry of a spherical torus (ST) has begun to provide significant new insight into Alfvén wave physics and transport/confinement research, which benefits not only the ST concept but fusion science overall. UCLA, as an active NSTX team member, has contributed to both the understanding and operation of the NSTX plasma. Application of innovative, cross-cutting measurement techniques have contributed across a broad range of research topics. A primary focus on NSTX has been the collaborative study of the plethora of Alfvén modes and their role in modifying fast-ion transport. A complementary interest is the understanding of the role that turbulence plays in governing anomalous transport in the spherical torus, and identifying the relationship to turbulent transport in other fusion plasma confinement configurations, such as the reversed field pinch and tokamak. UCLA has active research programs in both these areas on other fusion configurations (MST: RFP and DIII-D: tokamak) and is therefore well-positioned to help make these connections. During the next five years UCLA plans to play a major role in ensuring that the cross-cutting physics in Alfvén wave and turbulent transport research are clearly identified so that the overall U.S. Fusion Energy Sciences Program together with NSTX fully benefit. As a final note, in addition to the above research activities, UCLA has also contributed to NSTX operations by providing density profile information via reflectometry and line-integrated density measurement via a sensitive 1mm interferometer. The 5-year plan calls for significant upgrades to these systems, which will further enhance UCLA contributions to NSTX operations.

**Current research contributions to NSTX**

Alfvén Mode Studies

NSTX exhibits a wide variety of fast-ion driven modes such as compressional Alfvén modes at high frequency and energetic particle modes, such as fishbones, at low frequency. Such modes are of intrinsic interest for understanding wave particle interactions, as well as the more important concern of how such interactions impact fusion performance. Such modes can perturb fast ion orbits and, if they grow to sufficiently large amplitude, such ions may be lost to the wall or transported from the plasma. Understanding their stability, spatial structure, saturation and nonlinear interactions in existing experiments is critical in establishing a predictive capability for future burning plasma experiments. The interaction of fast ions with plasmas is also a topic of significant general interest not only in fusion plasmas, but also in the magnetosphere, ionosphere and solar wind. UCLA, as an institution, has great interest in this area of research. Understanding the wave dynamics is critical in revealing their role in fast ion confinement.

One area that received little attention was the interaction of such modes with each other through nonlinear three-wave coupling. Such interactions transfer energy between different spatial/time scales, potentially playing a significant role in mode damping, saturation, and even excitation. UCLA has performed unique

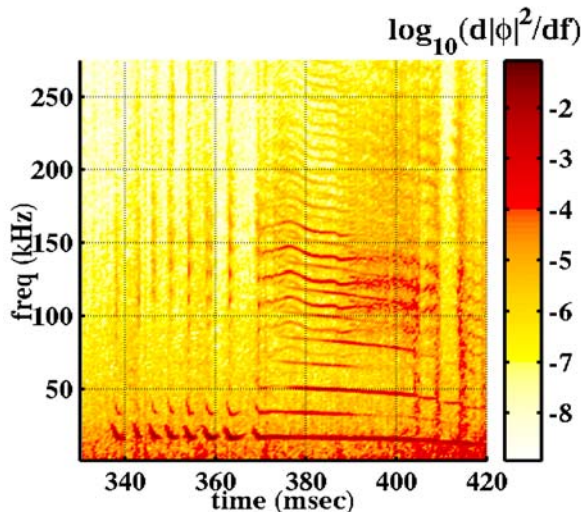


**Figure 1.** Power spectra of phase fluctuations of a 50GHz O-mode reflectometer localized in the core of an L-mode NBI NSTX plasma

local (reflectometry), and global (magnetics) measurements of nonlinear interactions via three-wave coupling between fast ion driven modes of two distinct types (see [PRL](#), 97, 045002, July 2006). **Figure 1** illustrates the power spectra of reflectometer phase fluctuations (proportional to density fluctuations) obtained from a 50 GHz (cutoff density  $\sim 3 \times 10^{13} \text{cm}^{-3}$ ) O-mode quadrature reflectometry measurement localized to the core of a beam-heated NSTX plasma. As can be seen there is a rich variety of mode activity. A large amplitude, low frequency mode ( $\sim 20$  kHz) together with numerous harmonics are observed interspaced

with a dominantly high-frequency mode (~120 kHz) that possesses a distinctly different temporal evolution. Careful analysis (including bicoherence calculations) has established unambiguously that pairs of these high frequency modes together with a low frequency mode frequency interact nonlinearly in a three-wave coupling process. Note also that around 390ms the high frequency mode appears to mode split and take on a more “chaotic” character. As mentioned above, such nonlinear processes can transfer energy to different spatial and temporal scales and therefore improved understanding is critical in order to assess their impact on fast ion confinement – especially in next-step devices.

More recently the UCLA focus has moved towards mode structure measurement and comparison to NOVA-K predictions. Multi-channel, simultaneous reflectometry measurements have significantly helped in revealing Alfvén mode structure. These results together with a description of the beta dependence of Alfvén cascades were presented in an **Invited Talk** by Dr. Neal Crocker (UCLA) at the 2007 APS Conference in Orlando, Florida. A list of publications in this research area, where UCLA has made major contributions, is provided at the end of this section. Future plans call for a significant increase in reflectometry spatial coverage by providing 13 simultaneous channels including coverage of high-density plasmas up to  $8 \times 10^{19} \text{m}^{-3}$ . A novel “comb-frequency” generator, recently successfully tested at DIII-D, will be employed so that data is obtained using the same launch and receive antennae. This upgrade will allow the temporal evolution of the *detailed radial structure* of various Alfvén modes to be monitored and rigorously compared with theoretical predictions. Quadrature reflectometry also provides a local measure of the absolute *density fluctuation* levels associated with these modes (e.g. the low frequency EPM in Figure 1 has an amplitude of ~2%).

As mentioned earlier it is also critically important to establish the *magnetic fluctuation* levels to assess their potential in generating fast-ion loss. UCLA, therefore, plans to add a radially-viewing polarimetry (Faraday rotation) capability to provide a measurement of the magnetic field fluctuations associated with these coherent modes. When combined with line-integrated interferometry, multichannel reflectometry and Mirnov coil data, this will provide a complete picture of the mode structure and amplitude, which can then be compared with theoretical/simulation predictions. Detailed comparison with theory will lead to improvement in predictive capability so essential for future studies.

As mentioned earlier, UCLA is interested in making cross-cutting comparisons with Alfvén wave studies in other plasma configurations. UCLA is in a unique position to pursue this avenue of research. UCLA has already made significant contributions to the study of “the sea of Alfvén modes” in DIII-D (Terry

Rhodes, Anne White) as well as to the measurement of magnetic fluctuations in MST (Co-P.I.: Dave Brower, Weixing Ding). MST is also moving quickly towards significant auxiliary heating and current drive, and is concerned about the potential role of fast-ion modes. Very little has been published about Alfvén eigenmodes in RFPs. An interesting point is that there are some significant differences between STs and RFPs that would influence the fast-ion mode spectrum, not the least of which is the  $q$  profile. There's a great deal of existing fast-ion mode theory developed for tokamaks that could be applied to RFPs, so there's a lot of theory-experiment comparison that could be performed starting with just a few relatively straightforward measurements. UCLA will play a lead role in facilitating such cross-cutting research which should aid greatly in improving understanding in this important research area.

It should also be noted that at UCLA there is also an active Alfvén mode “fusion campaign” on the Basic Plasma Science Facility (<http://plasma.physics.ucla.edu/bapsf/index.html> Director: Professor Walter Geikelman). The detailed goals and team members of the campaign can be found at <http://plasma.physics.ucla.edu/bapsf/pages/current.html> . The campaign is highly collaborative and is headed by Professor William Heidbrink (UC Irvine) who is also an active participant at both NSTX and DIII-D. The primary goal is to improve basic understanding of Alfvén waves through a collaborative theoretical/experimental research. The research will investigate Alfvén waves in a periodic mirror (providing a spectral gap similar to that found in tokamak magnetic fields) and the interaction between fast particles and Alfvén waves. Modification of a test ion beam by pre-existing Alfvén waves will be studied as well as the generation of Alfvén waves by fast particles. An intense ion beam will be injected at a variety of pitch angles into the LAPD plasma. The beam, which will spiral along the magnetic field, will match the phase velocity of Alfvén waves in the background LAPD plasma. The waves are expected to be generated by Cherenkov emission from the fast-ions. The goal is to create an analogue of TAE modes and study them in great detail. Participants include William Heidbrink, Roger McWilliams, Boris Breizman, Sergei Shaparov, Roddy Vann, Co-P.I. Troy Carter and Neal Cocker. Co-P.I., Professor Carter is also actively involved in a separate study of nonlinear interactions between colliding Alfvén waves. This research couples well to the UCLA focus at NSTX and will help in providing intellectual breadth to both efforts.

UCLA plans to more actively leverage UCLA involvement in these broad Alfvén wave/fast-ion research efforts and identify areas strongly cross-coupled to NSTX. Experimental time on the various facilities

would then be pursued and results correlated to improve our overall understanding of the physics and role of Alfvén waves in hot fusion plasmas, and particularly in the spherical torus configuration.

### Turbulence & Transport

Historically, long wavelength turbulence was thought to play a *secondary* role in the transport properties of NSTX discharges. For example, an early paper by Rewoldt *et al.* indicated that linear growth rates reduced dramatically for both the trapped electron  $\eta_i$  mode (low beta considered) and kinetic ballooning mode (high beta considered) as aspect ratio was reduced. This result was thought to be primarily due to the reduction in bad curvature available to drive such modes. Note, however, that this effect is mitigated as you penetrate deeper in to the core plasma. (i.e. the effect of aspect ratio would be much weaker at  $r/a = 0.5$  than  $r/a \sim 0.8$ ) as was shown by Rewoldt. Gyrokinetic calculations have indicated that linear growth rates are extremely sensitive to a wide range of parameters including electron to ion temperature ratios, ExB flow shear, magnetic shear, temperature and density gradients, beta, beta-prime, aspect ratio, etc. Using actual NSTX profiles linear growth rates for long wavelength ITG-like turbulence are found to be much lower than for shorter wavelength ETG-like modes. In addition, ExB shear flow suppression is generally predicted to be effective for ITG-like modes in NBI heated plasmas while ineffective to the shortest wavelength ETG modes.

To date UCLA has focused attention on longer wavelength turbulence measurements. For example, UCLA has installed a tunable correlation reflectometer to measure turbulent correlation lengths in the core NSTX plasma. In addition, local quadrature reflectometry measurements in the core plasma have allowed determination of local turbulent spectra and estimates of fluctuation levels. Turbulent correlation lengths are found to increase significantly from the edge to the core plasma. The values in the outer plasma ( $\rho \sim 0.8$ ) when normalized to the gyroradius  $\rho_s$  are similar to those observed in DIII-D – approximately  $5\rho_s$ . However, deeper in the core plasma ( $\rho \sim 0.6$ ) the normalized correlation lengths rise to normalized values significantly larger ( $\sim 17\rho_s$ ) than seen for example in DIII-D. This is surprising. UCLA has spent considerable effort in confirming that these long correlation lengths are not related to the presence of global modes in the NSTX plasmas. Data taken in Ohmic plasmas, stable Helium conditioning and RF only plasmas - devoid of MHD activity - are also found to have similar correlation length characteristics. The source of these long correlation lengths remains unknown and is under active study. New information has recently come to light with an upgrade of the fast sweep density profile

reflectometer. The system now generates phase delay versus position (rf frequency) information every  $10\mu\text{s}$ . This can be used to determine correlation length as well as density profiles with high temporal resolution. Recent analysis indicates that there is some evidence that the turbulent correlation length is intermittent. Long correlation lengths are still seen but interspersed are periods when shorter correlation lengths are observed. This is potentially a very interesting observation. In order to confirm, or not, this possibility UCLA plans to install a multichannel (13 channels) “comb frequency” reflectometry system to study the temporal evolution of correlation length. If the correlation is intermittent this will be clearly confirmed by this new system. This system, with suitable antenna modifications, can also be utilized as a Doppler backscattering system to locally probe intermediate-k (TEM-scale) turbulence and ExB flow. Turbulence data can also be obtained at DIII-D to cross-check and confirm any differences in correlation length scaling, flows, intermediate-k response, etc.

It should be noted that the recently upgraded fast sweep ( $10\mu\text{s}$ ) profile reflectometer will also be able to contribute to boundary physics studies such as the study of ELMs, ELM suppression and the L-H transition. When the toroidal field is increased to 10 kG this will significantly enhance the profile measurement capability. High resolution density profiles would then be available all the way from the core to the vessel wall. This will aid significantly in analysis of HHFW coupling to the edge plasma. Currently the low toroidal field limits measurements down to densities above  $2 \times 10^{12} \text{cm}^{-3}$ . This compromises accurate profile inversion in the very edge plasma. The FM system will also be upgraded in frequency in order to access higher core densities.

On the longer timescale UCLA plans to install a multichannel 600 GHz ( $\lambda \sim 0.5 \text{mm}$ ) Faraday rotation radial view measurement system. The primary goal of this system will be to provide magnetic fluctuation measurements in similar fashion to that demonstrated by UCLA (Co-P.I., David Brower, Weixing Ding) at MST. The system will contribute to both the study of Alfvén instabilities as well as magnetic turbulence. The system will also provide high bandwidth (40 MHz), high-resolution interferometry data which will be able to *directly probe* the fast waves (electrostatic component) generated by the HHFW.

## **Summary of proposed research plan for 2009-13.**

### **2009-2010:**

Install multichannel “comb-frequency” quadrature reflectometer system (13 channels: 8 widely spaced channels and 5 closely spaced channels with tunable center frequency) for detailed study of Alfvén wave mode structure, time resolved turbulent correlation length. Perform cross-cutting comparison experiments with DIII-D (e.g. check correlation length scaling using identical system hardware). Separately it is planned to upgrade the operating frequency range of the FM density profile reflectometer to access higher density plasmas.

### **2010-2011:**

Modify launch/receive antennas to optimize for multichannel Doppler backscattering measurement of intermediate-k turbulence and ExB flow. Perform core measurements of low and intermediate-k turbulence at L-H transition. On DIII-D, turbulence reductions are observed at the L-H transition even in the core plasma. Investigate other cross-machine comparisons. Begin design and fabrication of multichannel, radially-viewing 600GHz Faraday rotation (i.e. polarimetry) system for magnetic fluctuation measurements.

### **2011-2012:**

Install multichannel Faraday rotation system. This system will be capable of directly measuring magnetic fluctuation levels associated with Alfvén waves, as well as tearing modes, and potentially magnetic turbulence. The system will also provide large bandwidth (40MHz) high-sensitivity line averaged (along a midplane radial view) interferometry data which will allow direct probing of the strength of HHFW generated fast waves toroidally away from the launch antenna. This will be important in correlating with fast wave current drive efficiency. After installation of the new center stack, the existing high-k backscattering system will become fully operational. Higher-field operation (10 kG) will create an extremely effective internal beam dump (to absorb forward scattered light from large scale fluctuations) at the  $2f_{ce}$  resonance. Currently, at 5.5kG, this is located close to inside wall and is therefore ineffective.

### **2012-2013:**

Bring Faraday and high-k backscattering systems into operation to complement multichannel low- and intermediate-k density turbulence measurements. Investigate cross-cutting research with tokamak

(DIII-D) and RFP (MST) community especially in Alfvén wave research areas and the role that magnetic fluctuations, including tearing modes, play in these varying fusion plasma configurations.

## References

1. N. A. Crocker, W. A. Peebles and S. Kubota, E. D. Fredrickson, S. M. Kaye, B. P. LeBlanc and J. E. Menard, “Three-wave interactions between fast-ion modes in the National Spherical Torus Experiment” Physical Review Letters, 97, 045002, July 2006
2. E. D. Fredrickson, R. E. Bell, D. S. Darrow, G. Y. Fu, N. N. Gorelenkov, B. P. LeBlanc, S. S. Medley, J. E. Menard, H. Park, and A. L. Roquemore W. W. Heidbrink S. A. Sabbagh D. Stutman, K. Tritz, N. A. Crocker, S. Kubota, W. Peebles K. C. Lee F. M. Levinton, “Collective fast-ion instability-induced losses in National Spherical Tokamak Experiment” Phys. of Plasmas 13, 056109 (2006)
3. N.N. Gorelenkov, E.D. Fredrickson, W.W. Heidbrink, N.A. Crocker, S. Kubota and W.A. Peebles, “Discrete compressional Alfvén eigenmode spectrum in tokamaks” Nuclear Fusion, vol.46, no 10 2006, S933–S941
4. E.D. Fredrickson, N.N. Gorelenkov, R.E. Bell, J.E. Menard, A.L. Roquemore, S. Kubota, N.A. Crocker and W. Peebles, “Fast-ion loss in a ‘sea-of-TAE’” Nuclear Fusion, vol.46, no 10 2006, S926–S932
5. N N Gorelenkov, H L Berk, N A Crocker, E D Fredrickson, S Kaye, S Kubota, H Park, W Peebles, S A Sabbagh, S E Sharapov, D Stutmat, K Tritz, F M Levinton, H Yuh, the NSTX Team and JET EFDA Contributors, “Predictions and observations of global beta-induced Alfvén–acoustic modes in JET and NSTX” Plasma Physics & Controlled Fusion, 49 B371–B383, (2007)
6. “ $\beta$  suppression of Alfvén cascade modes in the National Spherical Torus Experiment”, E. D. Fredrickson, N. A. Crocker, N. N. Gorelenkov, W. W. Heidbrink, S. Kubota, F. M. Levinton, H. Yuh, J. E. Menard, and R. E. Bell, Phys. Plasmas 14, 102510 (2007)
7. “Alfvén Cascade modes at high  $\beta$  in the National Spherical Torus Experiment”, Crocker NA, E.D. Fredrickson, N.N. Gorelenkov, G.J. Kramer, D.S. Darrow, W.W. Heidbrink, S. Kubota, F.M. Levinton, H. Yuh, J.E. Menard, B.P. LeBlanc, R.E. Bell, submitted to PoP, June 2008



## A-17. University of California at San Diego

Research Topic: **Edge Heat and Particle Transport (radial and parallel) and divertor physics**

Principal, Co-Principal Investigators: J. Boedo (PI)

Participating Researchers: J-W Ahn, J. Boedo, S. Mueller, G. Tynan, D. Rudakov, H. Ji, S Zweben

Funded under DOE Grant: DE-FG02-03ER54731

### Introduction

Power loads to the divertor are a critical element of the development of the tokamak concept as a fusion power plant and due to the small aspect ratio, the ST concept is particularly sensitive to the power deposition in the walls. Additionally, particle exhaust, wall erosion and impurity generation and transport are crucial items in any tokamak, but even more in a ST due to tight tolerances. Therefore UCSD proposes a 5 year program that makes contributions to studying most, if not all, the processes involved in controlling or mediating particle and heat transport in the boundary/SOL. NSTX has several activities in it's 5 year plan to study and eventually manipulate heat loads in the divertor and they include divertor detachment and the Liquid Lithium Divertor (LLD). UCSD will therefore contribute by studying both particle and heat turbulent radial transport, blob generation and dynamics, ELM dynamics and parallel transport. Among the contributions to NSTX, UCSD will install a second reciprocating probe in the divertor region to enable divertor parameter studies during detachment and operation of the LLD. Development of magnetic sensors has been completed to study electromagnetic turbulence, thought to be relevant at high beta, and fast Te and possibly Ti diagnostics are in development. The probe has capabilities to measure Reynolds stress, a mechanism argued to be involved in the L-H transition in generating self-organized flows.

### Current research contributions to NSTX

UCSD has built, installed and commissioned a fast scanning probe for boundary physics studies, the probe capabilities are summarized below. There are NSTX needs for a second probe in the divertor region for LLD and detachment studies and the expected capabilities are also summarized below.

$n_e, T_e, V_{fl}, I_{sat}, E_\theta$  profiles. With 1 ms time resolution and 1.5 mm spatial resolution. So far, one

plunge per discharge. Profiles obtained in 60 ms. These are used for profile studies, decay length studies, perpendicular and parallel transport model validation. Also DC (low freq) convective cells studies. Relevant edge physics and divertor physics.

$V_{fl}$ ,  $I_{sat}$ ,  $\tilde{E}_\theta$ ,  $\tilde{\Gamma}_r$  profiles with 1 MHz time resolution, 1.5 mm spatial resolution. Profiles obtained in 60 ms. Plans to add  $\tilde{T}_e$  measurement with 400 kHz time resolution and 1.5 spatial resolution. These are used for turbulent particle and heat transport evaluation and to determine the conduction and convection heat channels, which have applications for edge physics, L-H transition physics, turbulent transport physics, intermittency. Relevant for L-H transition physics, edge physics and divertor physics.

We recently added 3 magnetic coils to add  $\tilde{A}_r$ ,  $\tilde{A}_\theta$  measurements to evaluate the importance of electromagnetic turbulence on particle and heat transport in an ST. Relevant since these channels will emerge at high beta. Relevant for L-H transition physics, edge physics and divertor physics. The data is being evaluated in the framework of a collaboration with Korea.

### Summary of proposed research plan for 2009-13

We propose to contribute to the NSTX program by measuring edge/SOL profiles in order to increase understanding of perpendicular particle and heat transport and their connection to the divertor parameters, understand ELM-mediated transport and parallel heat and particle transport. Will also install a divertor probe to aid divertor detachment and LLD work. Some of these venues of research are ongoing and the primary elements of our plan are:

- Runtime to be discussed, but of the order of 1 day per campaign
- Need boundary simulation capability
- Will build, commission and install X-point probe
- Will develop and install fast Te diagnostic for heat flux studies
- Will develop a Ti diagnostic for the boundary (either RFA or new diagnostic)

## Timeline

### 2009-2010:

Install new shaft and head with expanded capabilities. Continue work on parallel heat conductivity. Complete intermittency-mediated transport and SOL scaling work and comparison to DIII-D. Help characterize plate-based LLD. Design and build divertor probe. Start electromagnetic transport studies with new set of coils. Finish construction of fast Te diagnostic.

### 2010-2011:

Install, commission fast Te diagnostic, perform first heat conduction measurement. Continue LLD support. Evaluate scaling of EM transport using optimized set of coils. Contribute to SOL width studies by using new capabilities. R&D on Ti measurement should be completed. Focus on one concept.

### 2011-2012:

Install X-point probe at NSTX. Commission and make first measurements:

$n_e, T_e, V_{fl}, I_{sat}, E_\theta$  profiles. With 1 ms time resolution and 1.5 mm spatial resolution. So far, one plunge per discharge. Profiles obtained in 60 ms. These are used for profile studies, decay length studies, perpendicular and parallel transport model validation. Also DC (low freq) convective cells studies. Relevant edge physics and divertor physics.

$V_{fl}, I_{sat}, \tilde{E}_\theta, \tilde{\Gamma}_r$  profiles with 1 MHz time resolution, 1.5 mm spatial resolution. Profiles obtained in 60 ms. Plans to add  $\tilde{T}_e$  measurement with 400 kHz time resolution and 1.5 mm spatial resolution. These are used for turbulent particle and heat transport evaluation and to determine the conduction and convection heat channels, which have applications for edge physics, L-H transition physics, turbulent transport physics, intermittency. Relevant for L-H transition physics, edge physics and divertor physics.

Mach profiles in the divertor. Heat flux driven by large flows account for most of the

divertor heat flux in detached discharges. Compare lithium and carbon divertor. Study poloidal asymmetries and the physics of blob detachment and its influence on decay lengths. Study X-point driven turbulence as a possible tool to manipulate SOL decay length. Continue Ti diagnostic construction.

**2012-2013:**

Ti diagnostic installation and commissioning, first measurements. Continue LLD studies. Work on active SOL decay length control by using biasing and electrical blob detachment. Continue poloidal asymmetries work and electromagnetic transport work.

**Contributions to the NSTX 2009-13 Five Year Plan:**

Contributed to Section 3.5.1.3 for the SOL turbulence and width program.

**References**

*“The role of parallel heat transport in the relation between upstream SOL widths and target heat flux width in NSTX H-mode plasmas”*, J-W.Ahn, J.A.Boedo, R.Maingi, and V.Soukhanovskii, submitted to Physics of Plasmas (April 2008)

*“Dependence of SOL widths on plasma current and density in NSTX H-mode plasmas”*, J-W.Ahn, R.Maingi, J.A.Boedo, and V.Soukhanovskii, submitted to Journal of Nuclear Materials (May 2008)

## A-18. University of California at San Diego

Research Topic: **Edge Plasma Simulations in NSTX and CTF: Synergy of Lithium-Coating, Non-diffusive Anomalous Transport and Drifts**

Principal, Co-Principal Investigators: A.Yu. Pigarov (PI), S.I. Krasheninnikov (co-PI)

Participating Researchers: A.Yu. Pigarov, graduate student (TBN), S.I. Krasheninnikov

Funded under DOE Grant: DE-FG02-08ER54989

### Introduction

In the Lithium Wall concept [1-3] for fusion devices, the usage of lithium as plasma facing components allows the handling of frequent transient high heat power loads and the active control of plasma density and hydrogen isotope retention. Lithium Wall (LW) can also improve the core plasma performance and increase fusion power [1]. As has been shown very recently on NSTX, lithium coatings can reduce the particle recycling [4,5] and even eliminate the ELM activity [5,6]. The LW concept can be studied on NSTX with Liquid Lithium Divertor module planned for installation and on the next-step NHTX and CTF tokamaks.

Although a number of experiments related to the application of lithium technology in fusion devices increases year-to-year and there was significant progress in understanding the possible impact of lithium coatings/liquid on tokamak plasma performance, there are many issues in the LW concept that remain to be understood in detail. The physical processes of lithium-plasma interaction (e.g., lithium sputtering, evaporation, and hydrogen isotope retention) depend largely on plasma conditions and more work is needed for their characterization. Moreover, the behavior of edge plasma, radial gradients of edge plasma parameters and electric field, parallel plasma flows, and properties of intermittent non-diffusive cross-field transport have not been investigated yet for the low-recycling regimes envisaged to occur in the tokamaks with large area of plasma facing components covered with lithium. In addition, we see that engineering, plasma-lithium interaction, and plasma physics issues are strongly coupled. We

highlight that numerical simulation based on edge-plasma transport code UEDGE is a powerful tool to consider these issues together and to perform multi-parameter analysis for Lithium Wall.

### **Summary of proposed research plan for 2009-13**

We will work on sophisticated edge-plasma transport modeling in NSTX to develop a better understanding of basic boundary-plasma physics, in particular, in the low-recycling regimes expected in the presence of lithium coating/liquid and we will work closely with NSTX team on simulation of experimental data.

The main goal of the proposed theory research is to study the synergy of lithium coating/liquid, asymmetric ballooning-like anomalous non-diffusive cross-field transport, and classical plasma drifts. These are three main ingredients affecting the edge plasma transport and strong synergistic effects are expected in many aspects of basic edge-plasma physics. We will analyze the resulting plasma flow patterns, material migration, and impurity penetration into the core for NSTX. We will provide a support in modeling for experiments with Lithium Liquid Divertor (LLD) module planned on NSTX, in particular, the contributions will be made to assessment of edge plasma parameters in the low-recycling regimes, estimation of heating and net erosion of lithium components, and evaluation of hydrogen pumping/retention in lithium.

For the next step tokamaks, NHTX and CTF, we plan to analyze the hydrogen pumping, plasma contamination with lithium impurities, and power handling capabilities in the Lithium Wall concept. For NHTX and/or CTF, we intend to compare the plasma performance in conventional operation regime with all-carbon wall and in alternative regime with Lithium Wall.

In the period FY09-11 covered by the DoE grant DE-FG02-08ER54989, we will use the multi-fluid, multi-ion species, two-dimensional code UEDGE to simulate transport of plasma, neutrals, and impurities in the edge, scrape-off layer, and divertor for NSTX, NHTX and CTF tokamaks. This code has existing capabilities that suit our research. Improvements will be made in UEDGE mainly for better description of lithium impurity sources and hydrogen recycling which depend on surface temperature, thermostat temperature, irradiation dose, and liquid flow speed.

We have also developed the Wall and Plasma Surface Interaction (WallPSI) code which is the 1-D multi-scale multi-species code for particle and heat transport inside plasma-facing

components [7]. The code is in the process of benchmarking against vast experimental data on hydrogen retention, permeation, and erosion rates for major fusion related materials. WallPSI is a part of ongoing SciDAC project on Framework Application for Core-Edge Transport Simulations (FACETS) [8]. Initially this work includes coupling of core plasma codes, 2-D edge-plasma code UEDGE, and WallPSI. The coupling of WallPSI to UEDGE will be through assigning an instance of WallPSI to each wall facing cell of UEDGE. The project goal is to provide detailed core to wall transport modeling of tokamak fusion reactors. In the period FY11-13, we plan to modify and validate WallPSI code in a way necessary to model discharges with LW and use the coupled WallPSI/UEdge codes for further studies of the Lithium Wall concept.

**Contributions to the NSTX 2009-13 Five Year Plan:**

This work also contributes to chapter 5 on boundary physics.

**References**

- 1 S.I. Krasheninnikov, L.E. Zakharov, G.V. Pereverzev, “On lithium walls and the performance of magnetic fusion devices”, *Physics of Plasmas* 10, 1678 (2003).
- 2 APEX team, Interim report, “On the Exploration of Innovative Concept for Fusion Chamber Technology”, available at <http://www.fusion.ucla.edu/APEX/>
- 3 R.F. Mattas, J.P. Allain, M. Bastasz, J.N. Brooks, et al., “ALPS-advanced limiter-divertor plasma-facing system”, *Fusion Engineering and Design* 49-50, 127 (2000).
- 4 R. Kaita, R. Majeski, T. Gray, H. Kugel, et al., “Low recycling and high power density handling physics in the Current Drive Experiment-Uprade with lithium plasma-facing components”, *Physics of Plasmas* 14, 056111 (2007).
- 5 H. Kugel et al., Proceedings of the 18<sup>th</sup> Int. Conference on Plasma Surface Interaction in Fusion Devices (Toledo, Spain, May 2008), submitted to *J. Nucl. Materials*.
- 6 D.K. Mansfield, et al., “Suppression of Large Type-1 ELM Activity by the Deposition of Lithium on the NSTX Graphite Divertor Surfaces”, Proceedings of the 18<sup>th</sup> Int. Conference on Plasma Surface Interaction in Fusion Devices (Toledo, Spain, May 2008), submitted to *J. Nuclear Materials*.
- 7 A.Yu. Pigarov, S.I. Krasheninnikov, “Coupled plasma-wall modeling”, Proceedings of 18<sup>th</sup> Int. Conf. on Plasma-Surface Interactions (Spain, May 2008), submitted to *J. Nuclear Materials*.
- 8 J.R. Cary et al, *Journal of Physics* **78** (2007) 012086.

## **A-19. University of Colorado at Boulder**

Research Topic: **Evaluation of Edge Turbulence and Convective Transport through Velocity Field Analysis**

Principal Investigator: Tobin Munsat

Funded under DOE Grant: 1R01GM083953-01

### **Introduction**

The goal of this project is to perform analysis on data from the NSTX Gas Puff Imaging (GPI) diagnostic in a twofold effort to (a) quantitatively characterize the convective “blob” transport in the NSTX edge and (b) assess the existence and characteristics of sheared and zonal flows as visible in the viewing window of the GPI instrument. Analysis of this type and advanced understanding of the topics in this proposal is critical to the evaluation the plasma-boundary interface in fusion plasmas, and can have significant impact on next-step devices.

### **Current research contributions to NSTX**

This collaboration has just been funded, but draws upon the development (complete) of the HOP-V code, written by the Principal Investigator for this purpose [1]. We have already created an extensive library (>400 shots) of derived velocity fields for use in this study.

### **Summary of proposed research plan for 2009-13**

The research objectives will be achieved through the derivation of detailed velocity maps of cross-field plasma motion, resolved in both space and time, using the HOP-V (Hybrid Optical-flow Pattern-correlation Velocimetry) code, specifically written by the principal investigator for this purpose. Statistical analysis of the derived velocity fields will enable the identification of a wide variety of flow properties, including flow shear, the relationship between flow evolution and H-mode



behavior, the connection between flow, filament birth and evolution, and NSTX operating parameters/regimes, and the identification of zonal flows, among others. Furthermore, the evolution of the velocity fields can be used to assess convective edge transport, which can then be compared over a range of conditions to theoretical models and computed predictions. Indeed, a series of theoretical predictions of blob behavior already exist or are in the development stage, and the derivation of velocity maps from the GPI measurements is the key to connecting these models to the experimental observations.

The HOP-V velocimetry code developed for this project uses a hybrid optical-flow / direct-pattern-correlation technique which overcomes the limitations of many common velocimetry approaches. Advantages include the freedom from a-priori knowledge of any aspect of the velocity behavior, freedom from the “aperture effect” which limits many algorithms to deriving velocity only along density gradients, and freedom from imposed (arbitrary) definition of identifiable structures. The hybrid code derives “dense” velocity fields at the spatial and temporal resolution of the underlying image frames, which in this case is 64x64 pixels, 300 timepoints, taken at 4  $\mu$ s per frame at a spatial resolution of  $\sim$ 4 mm.

The Principal Investigator has established contacts with both S. Zweben, who heads the GPI project and coordinates many of the associated efforts, and with Lodestar Research, Inc., who are responsible for many of the most relevant theoretical models of convective blob transport in the plasma scrape-off layer.

There are no explicit run-time requirements for the initial funded three-year span of the project, for which data is already in hand. Additional image data will be collected by the on-site GPI team, with which we have close contact, and may evolve as the analysis is completed.

## References

- 1 T. Munsat and S.J. Zweben, Rev. Sci. Instrum. 77, 103501 (2006).

## A-20. University of Illinois at Urbana-Champaign

Research Topic: **LLD and SOL Interactions on NSTX**

Principal, Co-Principal Investigators: David N. Ruzic

Participating Researchers: M. A. Jaworski (post-doctoral researcher)

Funded under DOE Grant: DE-PS02-07ER07-29

### Introduction

The implementation of the Liquid Lithium Divertor (LLD) in NSTX presents unique opportunities in plasma-material interactions studies. The addition of a large area pumping surface provides the possibility of improved density control and new machine operating regimes. Lithium's high evaporation rates at relatively low temperatures presents a challenge to successful implementation and directly influences the particle pumping capabilities of the LLD. It is expected that as the temperature of the LLD increases, a transition between low and high recycling will occur impacting power deposition and particle fluxes. Due to the numerous temperature dependent properties of lithium (e.g. sputtering, ion-burial, and evaporation), the LLD-SOL interactions are expected to be complicated and represent a coupling at the plasma-wall interface.

To accomplish the stated goal of a quantitative understanding of plasma-LLD interactions, a comprehensive set of diagnostics will be utilized. Available NSTX diagnostics will be used such as the  $D_\alpha$  camera to view  $D_\alpha$  light emissions that correlate to the wall recycling of the LLD. Other diagnostics of use will be bolometers and a fast-framing camera to measure the radiated power of the plasma and any bulk motion in the LLD lithium surface respectively. In addition to the large set of diagnostics already on NSTX, this proposal seeks first to provide input into the design of a diagnostic array to be installed at one of the toroidal breaks in the LLD. The array is being fabricated by PPPL, and will consist of graphite armor with embedded, flush mounted Langmuir probes (LP's) spaced radially to monitor edge plasma density and temperature. To measure these parameters, the group at the University of Illinois at Urbana-Champaign (UIUC) has specified that the LP's be installed in sets of three at each radial location, so they can be operated in a "triple probe" configuration. Embedded thermocouples will provide feedback on the heat load experienced at the LLD radial position during each NSTX discharge.

Measurement of the lithium and deuterium flux at the interface between the LLD and the plasma will be provided by an array of photodiodes. A set already exists with a view perpendicular to the surface of the LLD, and a tangential array will eventually be added. A measurement of the deuterium and lithium fluxes will provide a detailed understanding of the recycling coefficient of the LLD during each discharge as a function of the incident heat flux as measured by the embedded thermocouples. These data will help calibrate infrared measurements of the LLD, which will be difficult due to lithium's reflectivity and chemical interactions with impurities. Together, these measurements will lead to a greater understanding of edge plasma behavior and its influence on the gross performance of the machine as a whole.

### **Current research contributions to NSTX**

At present, UIUC personnel provide design consulting for the LLD diagnostic module to be installed during the summer of FY08. This consultation covers the implementation of the divertor tile Langmuir probes, data acquisition and probe biasing, as well as thermocouple implementation. Beginning in FY09, UIUC will station a post-doctoral researcher at PPPL to participate in the operation of the diagnostic module, data collection and analysis with a focus on the proposed research plan.

### **Summary of proposed research plan for 2009-13**

The primary UIUC research interest is the interaction between the SOL plasmas produced in NSTX and the LLD. The UIUC group will fabricate and install the signal detection and biasing electronics for the dense "triple probe" array of edge LP's embedded between the LLD segments. The density and temperature data obtained with this array will be used to quantify the SOL-LLD plasmas at the divertor edge, using "state-of-the-art" SOL models. With the proposed machine upgrades, scaling studies will be carried out comparing current NSTX level fields (0.5T) to the upgraded levels (1T) with the goal of extrapolation to a Next-Step ST system. The data and analysis obtained with the LLD on NSTX, while most applicable to the ST system, will provide key experience on the performance of liquid lithium PFCs applicable to other confinement schemes.

## **Timeline**

### **2009-2010:**

Operation of the edge diagnostics will begin in this run campaign. Extensive data collection will occur during the NSTX run campaign and edge characterization will take place while model development and extension occurs of the LLD-SOL interface.

### **2010-2011:**

Following the initial model development describing LLD-SOL interface, dedicated XPs will be proposed for this run campaign testing the limits of the model and pumping ability, as well as temperature limitations of the liquid lithium surfaces. Model refinement and extension will be carried out based on this data. Pertinent information for the second iteration of the LLD will be provided based on the model to date. Diagnostic upgrades will be proposed for the following research campaign based on present experience.

### **2011-2012:**

With the introduction of an LLD that potentially includes flowing lithium for active cooling, the SOL-LLD plasma and models will be tested for such a module design. Characterization of the new SOL parameters will be necessary for future scaling studies at higher toroidal field and plasma currents after the planned center stack (CS) upgrade. XPs will be proposed to test the power handling limits of the new LLD design.

### **2012-2013:**

Analysis of the new plasma parameters and machine operation will occur this year after the planned CS upgrade. The ability to extrapolate the model developed in the previous years will be tested during operation at higher fields and plasma currents. Additionally, power handling will again be tested while the edge is characterized for various LLD temperatures. This model development will be applied with special focus to increased power handling for the proposed NBI upgrade.

**2013:**

After several years of research on the LLD-SOL interactions on NSTX with and without the proposed upgrades, a model will have been developed describing the pumping capabilities of the active lithium surfaces of the LLD over a range of magnetic fields and plasma currents. The impact of these models toward scaling to a Next-Step ST design will be assessed and the feasibility of liquid lithium in these scenarios evaluated from a firm experimental basis.

**Summary of Additional Off-site Research Activities**

In addition to the research undertaken at NSTX, UIUC is home to an active research group which can contribute to the NSTX mission. Two experiments in particular, the Ion-Interaction Experiment (IIAX) and the Solid/Liquid Lithium Divertor Experiment (SLiDE) will provide a laboratory basis for relevant parameters. The IIAX experiment has a long history of making fundamental sputtering yield measurements from exotic surfaces, including liquid lithium and lithiated graphite. The SLiDE machine utilizes an electron beam to mimic divertor heat fluxes onto a liquid lithium tray for studies of lithium behavior and power handling in fusion relevant conditions. Experimental results from both of these machines will support the NSTX mission and Next-Step ST designs.

## **A-21. The University of Tulsa**

Research Topic: **Energetic Particle and Flow Shear Effects in Resistive MHD Instabilities**

Principal, Co-Principal Investigators: Dylan P. Brennan

Participating Researchers: Ryoji Takahashi, 2 graduate students

Funded under DOE Grants: DE-FG02-08ER54950 and DE-FG02-07ER54931

### **Introduction**

The main thrust of our research plan is to simultaneously address linear dispersion relation analyses, modified Rutherford equation modeling, and nonlinear evolution computations for the onset and evolution of resistive MHD instabilities in comparison to cases selected from the NSTX and DIII-D experiments. The specific sub-topics we are currently focused on are the effects energetic particles and toroidal flow shear have on this physics.

One part of the work will focus on the use of the PEST-III code to compute the ideal MHD outer region solution for multiple rational surfaces using model equilibria based on experimental equilibrium reconstructions, and the subsequent use of the PEST-III results both in linear dispersion relation solutions including coupled modes, and modified Rutherford modeling for a single island evolution through to saturation. The ideal MHD outer region solution from the PEST-III code will be computationally matched to the resistive inner layer solutions[1] at each rational surface to determine the stability of both tearing and interchange resistive mode parities. An effort is underway to develop the energetic particle effects and toroidal flow shear into the PEST-III and inner layer computations. The tearing parity solutions ( $\Delta'$ ) will also be used within the modified Rutherford equation to study the evolution of resistive modes to saturation [2,3] in comparison to experiment and simulation.

Another part of the work will employ the NIMROD code [4] for nonlinear numerical studies of coupled resistive mode evolution. NIMROD currently has complete handling of energetic particle and toroidal flow shear effects.

Recent studies [5,6,7] have found that in DIII-D discharges where the  $\beta_N$  approaches the ideal kink limit for the  $n=1$ , the free energy available to the tearing mode, or the linear stability index  $\Delta'$ , increased rapidly causing the  $m/n=2/1$  tearing mode to onset. This mechanism was shown to operate even in the presence of coupling between multiple modes [6,2]. Most recently, in a high  $\beta_N$  DIII-D discharge, a strong, but non-resonant  $m/n=1/1$  perturbation was found to be dominant in the core and coupled to the  $2/1$  mode, which was driven unstable by the approach to  $1/1$  resonance [7].

Obtaining a clear and accurate understanding of the physics of onset and evolution of resistive MHD modes in NSTX is especially important considering the planned increase to magnetic field and current in the experiment. To date, stability analyses of the level of accuracy described above have not been performed with NSTX equilibria. It is an open and important question whether similar mechanisms are operating in NSTX discharges, and how their influence on the mode onset and evolution compares with those at higher aspect ratio. This is even more important when considering the added physics involved with toroidal flow shear and energetic particles.

### **Current research contributions to NSTX**

Only the initial stages of the NSTX specific research has begun, with an increasing amount of such research expected over the coming years. A single equilibrium reconstruction from NSTX shot 123970 from the LRDFIT code has been adapted for use in PEST-III, NIMROD, etc. in late 2007. This discharge developed a  $2/1$  NTM shortly after the time of this reconstruction. The effort has begun to generate an appropriate series of model equilibria based on this and other reconstructions.

Equilibria which model the state of the experimental discharges after the proposed upgrade to the experiment, including higher field and current, are also being considered.

## **Summary of proposed research plan for 2009-13**

We propose to study the effects of toroidal flow shear and energetic particles on low order rational MHD modes in NSTX and DIII-D equilibria.

Experimental discharges from NSTX that exemplify the physics of energetic particle and flow shear effects in the onset and evolution of resistive MHD instabilities will be studied and compared with results from simulation and modeling. Analyses with NIMROD can be complimented with a coupled rational surface analysis of the linear mode onset physics, and the modified Rutherford equation analyses described above, to clarify the effect aspect ratio has as the system evolves to instability. A thorough theoretical and computational analysis of how these effects depend on aspect ratio will give us insight to further develop our theoretical description of the physics of these instabilities.

Recently, results have been published showing numerical computation of mode onset and evolution which include flow shear as measured in DIII-D experimental discharges [2]. Systematic studies of flow shear effects on coupled resistive MHD modes have also recently been presented at EPS 2008 [8]. In these cases case a  $n=1$  mode is dominant in the core and drives an  $n=2$  mode through nonlinear coupling. Here the growth rates of the  $n=1$  and  $n=2$  modes are both increased with flow, but the relative amount of drive to the  $n=2$  mode is decreased. The increased growth rates with increased flow is due to inner layer effects, while the toroidal coupling is reduced with flow, and thus the relative amount of flux driven in the  $n=2$  is reduced. Even for moderate toroidal flow shear, the inner layer solutions can be affected, the relative rotation between rational surfaces can significantly affect the coupling, and the resultant nonlinear state will not be well described by linear models.

The combined application of these tools in comparison to the onset of resistive instabilities in DIII-D and NSTX will be extremely fruitful in our efforts to better understand this physics, and what to expect from future experiments. In particular, the results presented at EPS showed that toroidicity strongly affected behavior of the poloidal spectra of the  $n=1$  and 2 modes in this nonlinear evolution when compared with a standard large aspect ratio expansion model in cylindrical geometry. Furthermore, recent experiments on NSTX [9] have shown that a  $1/1$  mode component interacts with the  $2/1$  mode in what may be a similar mechanism to that detailed in DIII-D hybrid discharges [7]. How the rotational shear modifies the onset



in the NSTX experiments, within the context of the influence of this coupling, and how the lower aspect ratio affects this physics in comparison to DIII-D, will be addressed in this research.

Another part of the work will focus on the application of the delta-f and PIC methods already developed into the NIMROD code [10] to analyses of energetic particle effects on resistive mode onset and evolution in NSTX and DIII-D discharges. Assuming a low density of energetic particles ( $n_h \ll n_0$ ) and quasineutrality, the modification made to the MHD equations to include the energetic particle effects is to include an energetic particle pressure tensor into the momentum equation:

$$\rho \frac{\partial \mathcal{V}}{\partial t} + V \cdot \nabla V = J \times B - \nabla \cdot p_b - \nabla \cdot p_h$$

where  $p_b$  is the background pressure tensor,  $p_h$  is the "hot" particle pressure tensor that is assembled from a PIC  $\delta f$  method. Here  $f$  is the velocity distribution function over the computational grid and  $f = f_{eq} + \delta f$  where  $f_{eq}$  is the equilibrium or steady state distribution and at each timestep  $p_h = p_{h0} + \delta p$  where  $\delta p = \int m(v - V_h)^2 \delta f(r, v) d^3v$  is integrated over the volume. The  $\delta f$  evolves along the phase space characteristics (or trajectories) using the Vlasov equation. This is similar to a Monte-Carlo method in that statistics are used to calculate the moments of the distribution function.

The NIMROD PIC code has been successfully benchmarked against both the NOVA-K and M3D codes for the transition of an  $m/n=1/1$  internal kink mode to the Fishbone instability, which has a complex eigenvalue, as the fraction of energetic particle  $\beta$  to the total  $\beta$  is increased. With this formulation we can impose hot particle distribution functions on the resistive single fluid and two fluid MHD computations, calculate the effects, and compare with simple model described above for the effect on the outer ideal MHD region of a linear resistive MHD calculation. The combined application of these tools in the analyses of the onset and evolution of resistive instabilities in NSTX and DIII-D will be extremely fruitful in our efforts to better understand this physics. The addition of the kinetic effects of a non-Maxwellian distribution in the linear resistive stability codes will provide the basis for the study of a series of experimentally relevant cases. The accompanying inclusion of the hot particle effects in linear and nonlinear computations with NIMROD for the same cases will produce important scientific results and contribute to our understanding of what to expect from future burning plasma experiments.

The primary elements of our plan are:

- PEST-III / Inner Layer analyses of model NSTX equilibria and (possibly) equilibrium reconstructions.
- Quasilinear modified Rutherford analyses of mode onset and evolution.
- Nonlinear initial value computations of coupled mode evolution using NIMROD.

**Timeline**

**2008-2009:**

Begin applications of the  $\delta f$  code developed into NIMROD on model equilibria. Develop an analysis of resistive mode onset in selected NSTX cases, possibly including accurate equilibrium reconstructions and linear analyses. Begin linear analyses of flow inclusive equilibria with NIMROD in comparison to results from PEST-III.

**2008-2009:**

Extend the previous analyses to focus on aspect ratio effects using model equilibria in comparison with experimental cases. Study the nonlinear coupling between modes in nonlinear simulations.

**2010-2013:**

Study linear onset and nonlinear evolution of resistive modes in tokamaks, in comparison to experimental cases, including kinetic effects of energetic particles and flow shear effects, using reduced analytic models, linear codes, and NIMROD.

**Contributions to the NSTX 2009-13 Five Year Plan:**

Contributed to Section 2.1.1 Tearing Mode / NTM Physics

## References

1. S.A. Galkin, A.D. Turnbull, J.M. Greene and D.P. Brennan, Phys. Plasmas **9**, 3969 (2002).
2. D.P. Brennan, S.E. Kruger, T.A. Gianakon and D.D. Schnack, Nucl. Fusion **45**, 1178 (2005).
3. R.J. La Haye, P.A. Politzer and D.P. Brennan, General Atomics Report 25707, to be published Nucl. Fusion (2007).
4. C.R. Sovinec, A.H. Glasser, T.A. Gianakon *et al.*, J. Comp. Phys. **195**, 355 (2004).
5. D.P. Brennan, E.J. Strait, A.D. Turnbull, M.S. Chu, R.J. La Haye, T.C. Luce, S.E. Kruger and A. Pletzer, Phys. Plasmas **9**, 2998 (2002).
6. D.P. Brennan, R.J. La Haye, A.D. Turnbull *et al.*, Phys. Plasmas **10**, 1643 (2003).
7. D.P. Brennan, A.D. Turnbull, M.S. Chu, R.J. La Haye, L.L. Lao, T.H. Osborne and S.A. Galkin, Phys. Plasmas, **14** 056108 (2007).
8. D.P. Brennan, S.E. Kruger and R.J. La Haye, Proceedings of the 35<sup>th</sup> European Physical Society Plasma Physics Conference, Crete, Greece, June 2008.
9. S. Gerhardt, private communication, 2/2008.
10. C. C. Kim, C. R. Sovinec, S. E. Parker, and the NIMROD Team, Comp. Phys. Comm. **164**, 448 (2004).

## A-22. University of Washington at Seattle

Research Topic: **A) Solenoid-free Plasma Startup using Coaxial Helicity Injection, B) Deep Fuelling and Momentum Injection using Compact Toroid Fuelling**

Principal for CHI (Co-Pi for CT - Thomas R. Jarboe), Co-Principal Investigator (Principal for CT - Roger Raman)

Participating Researchers: Brian A. Nelson, Dennis Mueller, Henry W. Kugel, Steve Jardin, Michael Bell and others from PPPL, LLNL, ORNL

Funded under DOE Grants: DE-FG02-99ER54519 AM08 & DE-FG02-04ER54779

### Introduction

The primary goal of our research is (1) to incorporate CHI started discharges for integration with non-inductively driven discharges so that nearly full non-inductive startup and ramp-up current can be demonstrated on NSTX, (2) Demonstrate deep localized fuelling using Compact Toroid Injection with simultaneous momentum injection for eventual use in low wall recycling discharges.

### Current research contributions to NSTX

CHI research in NSTX has made considerable progress in developing transient CHI as a viable method for solenoid-free plasma start-up. These are (a) the generation of closed flux current in HIT-II and the very successful coupling of this current to induction from the central solenoid including CHI current generation with a pre-charged central solenoid [1], (b) the generation of 100kA closed flux current in HIT-II and demonstration of CHI plasma quality similar to that produced inductively [2,3], (c) the successful CHI generation of a record 160kA of closed flux current in NSTX demonstrating the high current capability of this method in a large ST [4,5,6] and (d) Successful coupling of CHI started discharges to induction from the central solenoid with the discharge transitioning to an H-mode demonstrating compatibility of this startup method with high-performance plasma operation [7]. The 160kA result was recently accomplished using the transient CHI method, first developed on the HIT-II ST [8].

In the area of Compact Toroid Injection we have informed the ST community through several presentations and two recent journal papers that describes the need for this advanced fuelling system for steady-state ST operation. The first paper [9] describes the importance of feed-back controlled density profile control and momentum injection benefits for sustaining high-bootstrap current fraction discharges under steady state operation. The second paper [10] describes the improved tritium usage and reduced tritium losses to the walls that could be realized as a consequence of CT fuelling.

### **Summary of proposed research plan for 2009-13**

#### **(A) Coaxial Helicity Injection:**

- (1) In this approach a transient CHI equilibrium will be produced and induction from the central solenoid will be added to this startup plasma to demonstrate compatibility of the CHI discharge with plasmas conventionally produced using the inductive method. In subsequent experiments, the CHI-started plasma will be driven inductively using a combination of outer poloidal field coils in conjunction with RF and NBI to ramp the initial startup current to a level where it can be non-inductively driven by neutral beams and by High Harmonic Fast Waves.
- (2) The CHI process initially drives current in the edge, whereas other non-inductive methods drive current in the interior of the plasma. This unique capability of CHI will be used to drive steady-state current at the edge of a pre-formed inductive discharge in NSTX for the purpose of improving the edge current profile and controlling edge SOL flows for the purpose of altering the SOL density.
- (3) Recent work on HIT-II has shown poloidal flux amplification when CHI is operated at low toroidal field. In dedicated experiments the physics of relaxation current drive will be studied as this has the potential of increasing the CHI produced current beyond what is possible using transient CHI.

***Coupling to OH:*** Work conducted during 2008 in NSTX has conclusively demonstrated the coupling of CHI started discharges to inductive drive from the central solenoid. The remaining steps are (1) to increase the magnitude of this current to about 500kA, using higher voltage capability and higher TF of up to 1T (2) to heat the CHI started discharge with 350kW of ECH so that the electron temperature is increased above 200eV, 3) at this temperature, HHFW should be able to further increase the temperature to about 1keV, 4) At 500kA NBI should be able to ramp the current up to several hundred kA and to sustain it noninductively.

***Coupling to a pre-charged OH coil:*** During 2008, preliminary work with a pre-charged solenoid showed a CHI discharge could be initiated under conditions when the OH introduces fringing error fields. These discharges will be improved to enable start up under this condition.

***Edge current drive for a high beta NSTX discharge:*** The goals are to determine the magnitude of edge current that can be added without confinement degradation. Since CHI current drive is applied to the edge region, it is possible that this current drive method can be used to modify the bootstrap current drive profile by providing current drive in regions where conventional methods cannot provide current drive. Initial experiments will use the transient CHI capacitor bank to apply voltage to the lower divertor legs of a reference inductive discharge. The purpose is to try to duplicate the experiments conducted on HIT-II, but with much improved diagnostics. The next step will be to reproduce these experiments using the DC power supply so that the duration of the edge current can be prolonged. Another purpose of these experiments is to alter the SOL flows to control the SOL plasma density. In a related experiment, the capability of the CHI system to be able to bias the SOL of a pre-formed LSN discharge will be used to control edge particle flows. Previous experiments in other machines have clearly shown that edge biasing can be used to favorably improve edge flows and possibly control the particle content in the closed flux region. For example, in NSTX high performance H-mode discharges, it is well known that the electron density continues to increase, until MHD eventually terminates the discharge. From previous experiments in tokamaks, it is well known that anti-CHI biasing of the lower divertor electrodes can result in pumping of the SOL as the  $E \times B$  flows are directed into the divertor region. Reducing the SOL density has the potential to increase the edge pedestal temperature during H-mode discharges.

***Steady-state CHI for poloidal flux amplification:*** This study is needed to investigate the high current potential of CHI under steady state operation. Experimental data produced as part of this work is needed in conjunction with computational modeling work carried out by X. Tang of LANL and C. Sovenic of the University of Wisconsin to develop an understanding of relaxation current drive physics. Steady state CHI experiments thus far have succeed in attaining 390kA of CHI generated toroidal current in 330ms discharges using about 28kA of injector current. CHI discharges have been obtained without relying on the central solenoid. These discharges will provide data for a more complete understanding of dynamo current drive physics, which was described in the previous section. The edge plasma in these discharges

will also be diagnosed in detail using the edge dynamo probe, ion Doppler spectroscopy and edge fluctuation measurements.

**(B) Compact Toroid Injection:**

The first year will be spent preparing the injector, which is currently in storage at PPPL, for installation on NSTX. After that the injector will be re-commissioned and the CT injector – NSTX control interfaces implemented.

The primary objective during the second and third years after installation on NSTX will be to develop tools needed for the non-inductive sustained operation phase. This involves:

- Demonstration of localized deep fueling.
- Demonstration of the ability to alter the fuel mass and deposition location.
- Demonstration of the ability to fuel advanced confinement mode discharges by injecting CTs into H-mode discharges.
- Measure momentum injected by the CT by configuring it for tangential injection in NSTX.
- After initial results on pulsed power system requirements are obtained, we will design the pulsed power system for a high repetition rate CT injector for NSTX. These would be used to conduct multi-pulse CT injection experiments.

**Timeline**

**2009 – 2010:**

- CHI: Use Lithium to improve CHI performance. Improve CHI voltage capability to 2kV.

**2010 – 2011:**

- CHI: Using the 350kW ECH system, the absorber field null capability and the full 2kV capability we will increase the magnitude of the CHI started currents. Test edge current drive.
- CT: Off-line testing of the CT injector.

**2011 – 2012:**

- CHI: Operate at 1T. Couple to HHFW and then to NBI. Use metal divertor plates to improve CHI current startup capability. Test relaxation current drive.
- CT: Demonstration of momentum injection.

**2012 – 2013:**

- CHI: Maximize solenoid-free startup currents using synergism with outer PF coil startup.
- CT: Test of localized core fuelling.

**2013:**

- CHI: Use CHI startup for full integration with nearly full non-inductive operation, which includes startup with CHI, reaching  $I_p \sim 500\text{kA}$  with or without HHFW current boost followed by ramp-up with NBI to currents levels where it is non-inductively sustained.
- CT: Initial test of multi-pulse operation for the eventual goal of fuelling low recycling discharges.

**Contributions to the NSTX 2009-13 Five Year Plan:**

We wrote the section on Solenoid-Free startup of (Chapter 6.4) in the NSTX 5yr plan document. This work also contributes to the chapters on boundary physics and Integrated operations.

**References**

- [1] R. Raman, T.R. Jarboe, B.A. Nelson, et al., *Physics of Plasmas*, **11**, 2565 (2004).
- [2] R. Raman, T.R. Jarboe, et al., *Nuclear Fusion* **45**, L15-L19 (2005).
- [3] R. Raman, T.R. Jarboe, D. Mueller, et al., *Physics of Plasmas* **14**, 056106 (2007).
- [4] R. Raman, B.A. Nelson, M.G. Bell, et al., *Phys. Rev. Lett.* **97**, 175002 (2006).
- [5] R. Raman, T. R. Jarboe, W.T. Hamp, *Physics of Plasmas* **14**, 022504 (2007).
- [6] R. Raman, D. Mueller, T.R. Jarboe, et al., *Nuclear Fusion*, **47**, 792 (2007).
- [7] D. Mueller, R. Raman, T.R. Jarboe, et al, *Proc. 2008 EPS Conf. Crete, Greece*
- [8] R. Raman, B.A. Nelson, M.G. Bell, et al., *Phys. Rev. Letters*, **97**, 175002 (2006).
- [9] R. Raman, *Fusion Sci. Technol.* Vol **50**, 84 (2006).
- [10] R. Raman, *Fusion Sci. Technol.* (2008) [accepted for publication].